bulletin 57

Shear and punching shear in RC and FRC elements

Workshop 15-16 October 2010, Salò (Italy)

technical report

Shear and punching shear in RC and FRC elements

Technical report

Proceedings of a workshop held on
15-16 October 2010, in Salò,
Lake Garda, Italy

October 2010

Subject to priorities defined by the Technical Council and the Presidium, the results of *fib*'s work in Commissions and Task Groups are published in a continuously numbered series of technical publications called 'Bulletins'. The following categories are used:	
category	**minimum approval procedure required prior to publication**
Technical Report	approved by a Task Group and the Chairpersons of the Commission
State-of-Art Report	approved by a Commission
Manual, Guide (to good practice) or Recommendation	approved by the Technical Council of *fib*
Model Code	approved by the General Assembly of *fib*
Any publication not having met the above requirements will be clearly identified as preliminary draft. This Bulletin N° 57 is a collection of individual contributions to a workshop. Their content is believed to be of general interest to *fib* members and especially helpful in the finalization of the new Model Code; therefore the *fib* Presidium decided to publish these contributions as a Technical Report in *fib*'s series of Bulletins.	

On behalf of Task Group 4.2 (convener: V. Sigrist, TU Hamburg-Harburg, Germany) and Commission 4 (chair: S. Foster, Univ. of New South Wales, Australia), the workshop was organized and the papers edited by F. Minelli and G. Plizzari (Univ. of Brescia, Italy).

Further contributors to the workshop:
G.L. Balázs (Budapest Univ. of Technology and Economics, Hungary), P. Bamonte (Politecnico Milano, Italy), B. Belletti (Univ. of Parma, Italy), E. Bentz (Univ. of Toronto, Canada), M.-Y. Cheng (National Taiwan Univ. of Science and Technology), M. P. Collins (Univ. of Toronto, Canada), C. Damoni (Delft Univ. of Technology, The Netherlands), M. di Prisco (Politecnico di Milano, Italy), H. H. Dinh (Moffatt and Nichol, USA), R. Felicetti (Politecnico Milano, Italy), M. Fernández Ruiz (EPF Lausanne, Switzerland), P. G. Gambarova (Politecnico Milano, Italy), E. Giuriani (Univ. di Brescia, Italy), B. Hackbarth (TU Hamburg-Harburg, Germany), M. Hendriks (Delft Univ. of Technology, The Netherlands), K.S. Kim (Univ. of Seoul, S. Korea), D. Kuchma (Univ. of Illinois, USA), A. Muttoni (EPF Lausanne, Switzerland), T. Nagle (Nagle Signs Inc., USA), G. J. Parra Montesinos (Univ. of Michigan, USA), J. Rots (Delft Univ. of Technology, The Netherlands), S. Sun (Parsons, USA), J. Susetyo (Hatch Mott McDonald Ltd, Canada), L. Vandewalle (Katholieke Univ. Leuven, Belgium), F. J. Vecchio (Univ. of Toronto, Canada), J. Walraven (Delft Univ. of Technology, The Netherlands), J. K. Wight (Univ. of Michigan, USA)

Cover image: Shear test on a 1.5 m deep beam containing 50 kg/m^3 of steel fibers. Experiment carried out at the University of Brescia in July 2010.

First published in 2010 by the International Federation for Structural Concrete (*fib*)
Postal address: Case Postale 88, CH-1015 Lausanne, Switzerland
Street address: Federal Institute of Technology Lausanne – EPFL, Section Génie Civil
Tel +41 21 693 2747 • Fax +41 21 693 6245
fib@epfl.ch • www.fib-international.org

ISSN 1562-3610
ISBN 978-2-88394-097-0

Printed by DCC Document Competence Center Siegmar Kästl e.K., Germany

Preface

Shear is one of a few areas of research into fundamentals of the behaviour of concrete structures where contention remains amongst researchers about the mechanisms that enable the force flow through a concrete member and across cracks. There is no more evidence for this than the continuing debate between researchers emanating from a structures perspective and those from a materials or fracture mechanics perspective.

Since the early days of concrete construction, researchers have been looking for models and methods to describe and determine the resistance of members in shear. Different from other materials, concrete exhibits a cracking behaviour that is, on the one hand, complex and difficult to predict and, on the other, essential for the functioning of the composite material. Inspired by crack patterns typically observed in beam tests, Ritter and Mörsch had the idea to visualise the flow of forces with the help of truss models and to clearly assign tension and compression forces to reinforcing steel ties and concrete struts. This model is easy to understand and has ever since been used as the starting point for the development of design models. Nevertheless, shear remains an open problem and our understanding is clearly incomplete.

Important progress has been made in the last fifty years when, within the framework of the theory of plasticity, the truss model concept was extended and systematised. Following this, compression field approaches were developed that complement the truss model approach by incorporating compatibility considerations as well as more general material properties. Additionally, the models are expanded for the whole range of members; from those that are unreinforced in shear to those that are heavily reinforced and from low strength concrete to ultra-high strength concrete, as well as for newer materials such as Fibre Reinforced Concrete (FRC). Finally, calculation procedures are adjusted to more accurately predict the shear resistance, especially for the evaluation of existing structures. At the same time, it is realised that these developments lead to elaborate computations that are not always suitable for practical design and, therefore, researchers have put some effort in simplifying their models for use in structural design codes and standards.

One of the ongoing projects of *fib* Task Group 4.2 “Ultimate Limit State Models” is to compile and discuss the most relevant design methods for shear and punching available today. This work led to the preparation of the relevant sections of the “New Model Code” draft being elaborated under the auspices of *fib* Special Activity Group 5. In 2009, a Working Group was formed within Task Group 4.2 consisting of Evan Bentz, Miguel Fernández Ruiz, Stephen Foster, Aurelio Muttoni and Viktor Sigrist (Chair). The challenge of the group was to harmonise different ideas about design procedures for shear and punching and - as documented in the Draft Model Code 2010 - the group was partly successful. There are three major outcomes of the work. The first is the concept of “Level of Approximation”, which was introduced to differentiate engineering tasks with respect to effort and required modelling accuracy. The second, a decision in principle to use an approach that is similar for beam shear and punching shear and, in general, fully reveals the reinforcement as well as the concrete contribution. The third, not yet entirely realised, is to adjust related code provisions such as “torsion”, “strut and tie modelling” and “fibre reinforced concrete” to be consistent in both approach and modelling to that presented for shear.

An important result of the above developments was that experts and practitioners began a discussion to scrutinise the shear and punching provisions of the Draft Model Code. Motivated by this, Fausto Minelli and Giovanni Plizzari, concerned with questions on shear design as well as on fibre reinforced concrete, proposed to have a workshop where different view-points could be explained and open questions addressed. The resonance on this proposal was encouraging and an elite group of researchers, experts in the field of shear in concrete structures, gathered in Salò, at Lake Garda in Italy. During the workshop 18 lectures were given by invited experts in the field of shear and FRC. A total of 72 participants attended the workshop, coming from three different continents and 12 countries: Australia, Belgium, Canada, Czech Republic, Germany, Hungary, Italy, Portugal, Spain, Switzerland, The Netherlands, UK and USA.

Without question the workshop was an outstanding success and the written contributions from this conference are compiled in this *fib* Bulletin. These as well as the lively and fruitful discussions held in Salò will influence the further development of the Model Code provisions and - more importantly - should inspire future research in the field of shear. At the end of the workshop all participants agreed that shear will remain one of the key issues of research in structural concrete for some years to come and, while the models presented represent the best of the current state of knowledge today, there is no doubt that the story of shear in concrete structures is still an incomplete one.

Viktor Sigrist
Convener of Task Group 4.2

Fausto Minelli
Member of TG 4.2 and organiser of the Workshop in Salò

Giovanni Plizzari
Member of TG 8.3 and organizer of the Workshop in Salò

Stephen Foster
Chairman of Commission 4

Contents

PART III: Recent advancements in shear and punching shear of FRC structures

1 A historical review of shear

György L. Balázs

Prof. Dr., Budapest University of Technology and Economics

Abstract: Herein we go back to the early works by Ritter, Mörsch, Kupfer, Walther, Kani, Leonhardt, Thürlimann, Walraven, Collins and Vecchio to trace the development of understanding and treatment of shear behaviour in reinforced and prestressed concrete. Additionally, our own recent test results are presented showing the advantageous influence of steel fibres on shear behaviour and shear capacity. The experimental results indicated that steel fibres may reduce the amount of stirrups and congestion of reinforcement in high shear regions.

1.1 Introduction

The purpose of this contribution is to give a short historical review about the most important components of shear behaviour, extended with recent test results on the shear behaviour of steel fibre reinforced concrete beams (prestress or non-prestressed). All these intend to contribute to the best possible formulation of the Model Code 2010.

1.2 Hennebique and Ritter – Steel strips as stirrups

The search for an effective type of stirrup reinforcement goes back to the end of 19th century. Ritter presented in his publication in the Schweizerische Bauzeitung (Ritter, 1989) Hennebique's construction method that was patented in Switzerland in 1985 and 1987. In contrary to the Monier method, he used steel strips as stirrup reinforcement in beams. The proposed width of steel strips was 30 to 60 mm with thickness of 2 to 4 mm. The stirrups were running around the longitudinal bars one by one and remained open at the top. The anchorage of stirrups was provided by bending the ends of the stirrups by 90 degrees. Both the longitudinal reinforcement and the stirrups had to be completely embedded into the concrete.

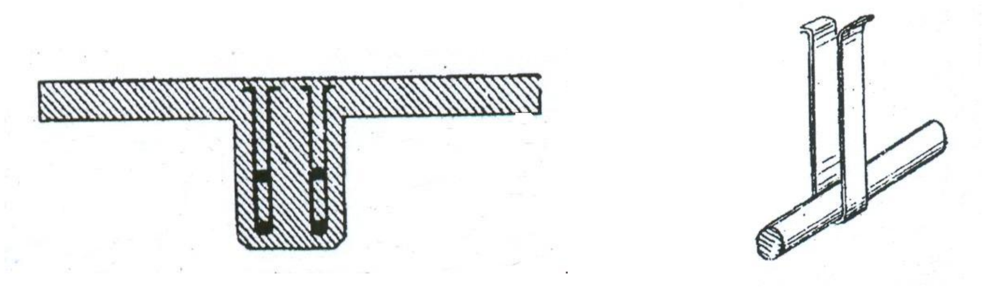

Fig. 1.1: Shape of stirrups at end of 19th century (Ritter, 1899)

In the early publication of Ritter (1899) we can find important details also on bond and anchorage capacities. He assumes the allowable bond stress of 1 N/mm^2 based on bond test results by Bauschinger that resulted in 4.0 to 4.7 N/mm^2 bond strength values.

The anchorage length to 100 N/mm^2 steel stress was simply obtained by using the equation $100 \cdot \frac{1}{4} \cdot \pi \cdot \varnothing^2 = 1.0 \cdot \pi \cdot \varnothing \cdot l$ and expressing the anchorage length it gives $l = 25 \cdot \varnothing$. Hooks had to be applied if this length was not available. It is suggested to improve the bond capacity of bars by cement milk applied on the surface of the bars.

Steel strips as stirrups were also used for a period of time at the beginning of 20th century. Fig. 1.2 shows the main reinforcement of a beam around which is a stirrup in the form of a steel strip that was constructed in 1905 at the Budapest University of Technology.

Fig. 1.2: Stirrup reinforcement in the form of a steel strip from 1905 at the Budapest University of Technology (opened during a reconstruction work, photo: courtesy of Tamás Lichter and Piroska Arany)

During a large part of the 20th century in most of the countries closed stirrups made of small diameters reinforcing bars (not opened and not in strip form) were used. For technological reasons open stirrups again became important some decades ago. Industrialization of reinforcement required (even in form of wire fabric) opening of stirrups from the top to enable easy placement of longitudinal bars into the formwork. Adequate anchorage capacity of the open ends of the stirrups had always to be provided by hooks or by welded cross bars.

1.3 Mörsch – Simple or double truss systems

An important part of the early textbook by Mörsch (1908) also deals with shear behaviour and shear capacity. This is actually the third edition of his book, published first in 1905 in Neustadt and then in Zürich, that were extended with new test results and applications. Several shear test results are presented and compared, including bent-up bars or stirrups or both. In most of the experiments stirrups had the same form as presented in Fig. 1.1 by Ritter:

opened at the top and covering every longitudinal reinforcement separately. In some other tests the open stirrups covered all of the longitudinal tensile reinforcements not one by one. In some of these early tests the number and distance of bent-up bars were also experimentally studied.

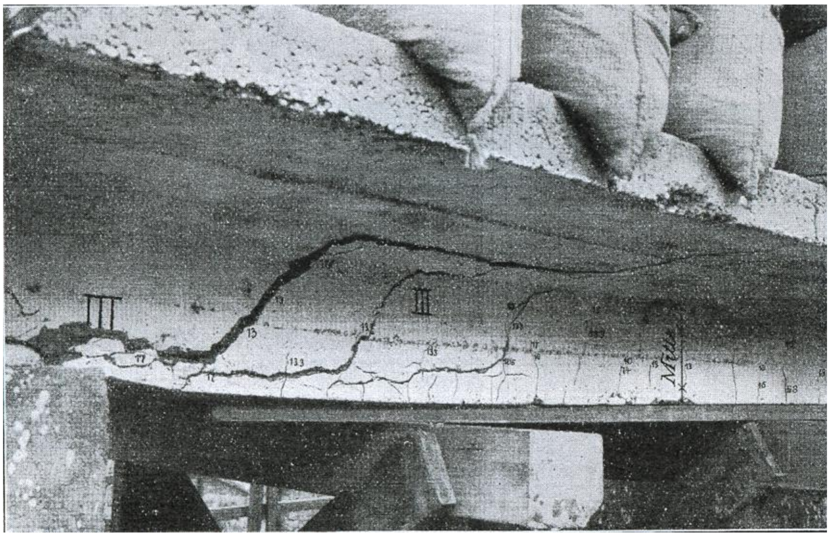

Fig.1.3: Failure pattern of a T beam without stirrups. Test result by company Wayβ & Freytag AG. (Mörsch, 1908)

The experimental result in Fig. 1.3 indicates a classic shear failure of a T beam without shear reinforcement. The failure crack starts horizontally at the support following the longitudinal tensile reinforcement, then goes up to the compressed flange at about 45 degrees and terminates by reaching the position of the load.

Mörsch (1908) explains that the reinforced concrete beam can be treated as a simple or multiple truss system (Fig. 1.4) where the shaded concrete strips represent the compressed struts and stirrups or bent-up bars act as tensile members. The tensile forces in the shear reinforcement are then obtained by the analysis of the truss itself. This approach is often referred to as truss analogy and it provided the basis of shear design.

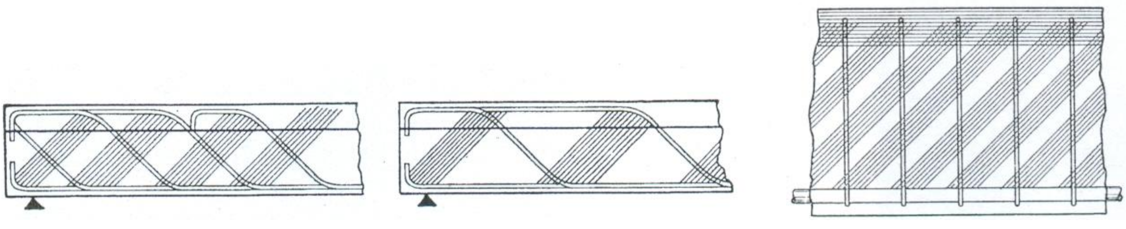

Fig. 1.4: Simple or multiple truss systems with bent-up bars and with stirrups (Mörsch, 1908)

1.4 Kupfer – Variable inclination of struts

Kupfer (1962) in his presentation for the Shear Colloquium in Stuttgart proposed a modification of the Mörsch truss analogy by allowing the compressive strut inclination even smaller than 45 degrees within the following limits:

$$0.25 \leq \mathrm{tg}\alpha \leq 1.0 \tag{1.1}$$

where α is the inclination of compressive strut to the axis of the member (Fig. 1.5).

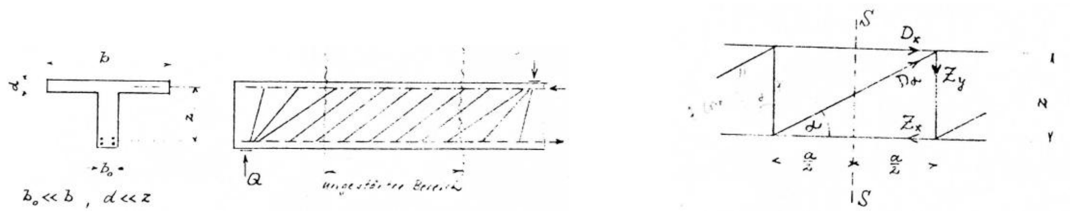

Fig.1.5: Variable strut inclination (Kupfer, 1962)

Kupfer (1962) proposed to select the shear reinforcement with simultaneous yielding of longitudinal reinforcement and suggested to define the inclination of the strut by using the principle of minimum deformation work.

1.5 Walther – Shear failure theory based on Mohr circles

Walther (1962) developed a generalized design theory using Mohr circles (Fig. 1.6). In Fig. 1.6 line (1) represents the envelope curve to Mohr, (2) is the stress Mohr circle (with $\sigma_y = 0$) and (3) means the failure criterion of a biaxial stress state with $\sigma_y = 0$.

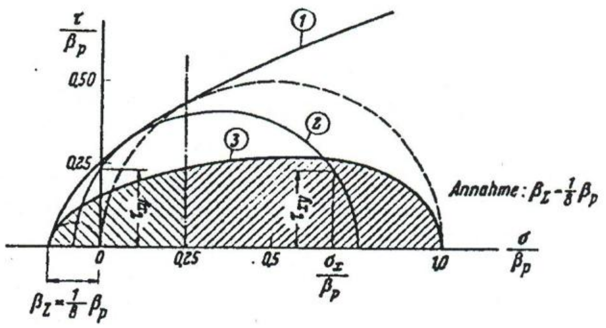

Fig. 1.6: Background of the model by Walther (1962) ($\beta_Z = f_{ct}$, $\beta_p = f_{c,pr}$)

Walther (1962) obtained the following equation for the maximum compressive strength in shear as a function of the concrete prism strength and the moment-shear ratio (M/(V·d)):

$$\frac{f_{c,pr}}{1+3.2\left(\frac{V\cdot d}{M}\right)^2} \tag{1.2}$$

In this theory the ratio of concrete tensile strength (f_{ct}) to prism strength $f_{c,pr}$ was supposed to be $f_{ct}/f_{c,pr} \approx 1/8$. The vertical stresses in the beam were neglected ($\sigma_y = 0$).

1.6 Kani – The riddle of shear failure

Kani (1964) supposed the following mechanism of a reinforced concrete beam. The formation of flexural cracks transforms the reinforced concrete beam into a comb-like structure (Fig. 1.7). The compression zone of the beam is the backbone of the comb, while the tensile zone of the concrete teeth, separated from each other by flexural cracks, represent the teeth of the comb. As long as the capacity of the concrete teeth is not exceeded the comb-like behaviour governs. After the resistance of the concrete teeth has been destroyed, the tied arch, having quite different proportions, remains (Kani, 1964).

Kani (1964) explained that the main obstacle to the shear problem is the large number of parameters involved, some of which may not be known.

Kani (1964) presented the critical moment by failure of concrete teeth (M_{cr}) related to the flexural capacity versus the a/d ration i.e. the shear arm ratio. In this representation he showed a valley with a local minimum at a/d ratio of 2.5 (Fig. 1.7). This valley is referred to as the *riddle of shear failure*.

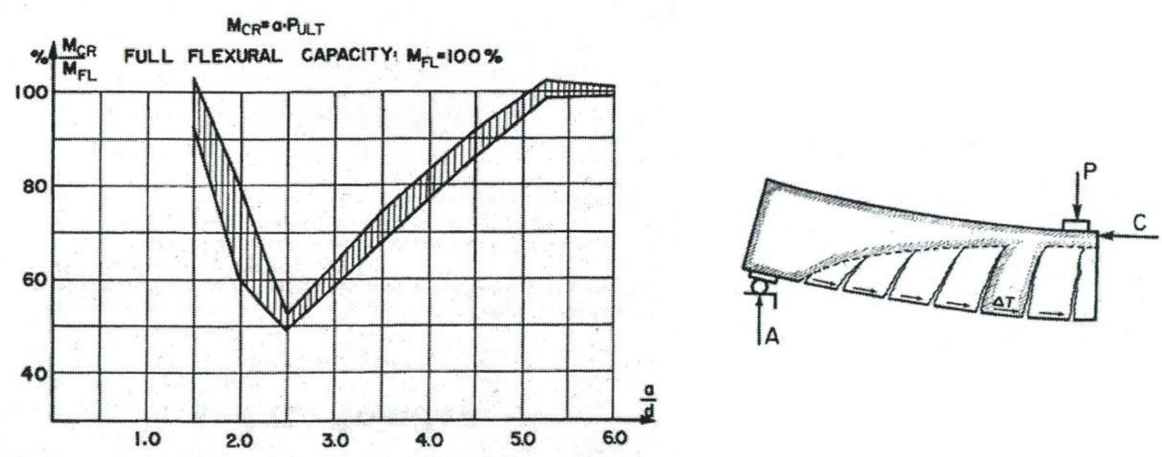

Fig. 1.7: Riddle of shear failure (beam capacity versus a/d ratio) and comb-like model by Kani (1964)

1.7 Leonhardt et. al – Web compression failure

Leonhardt and Mönig (1973) published a textbook on *Lectures about reinforced concrete (Vorlesungen über Massivbau)* which became very well known in several universities. This book gives details on the so-called classic truss analogy by Mörsch with 45 degree struts as well as an improved truss analogy.

Fig. 1.8 indicates test results on beams with the same concrete section and same amount of longitudinal reinforcement but different amounts of shear reinforcement. Crack patterns in Fig. 1.8 indicate the influence of the amount of stirrup reinforcement on the inclination of cracks. With a lower amount of shear reinforcement the inclination of cracks was reduced in the shear span.

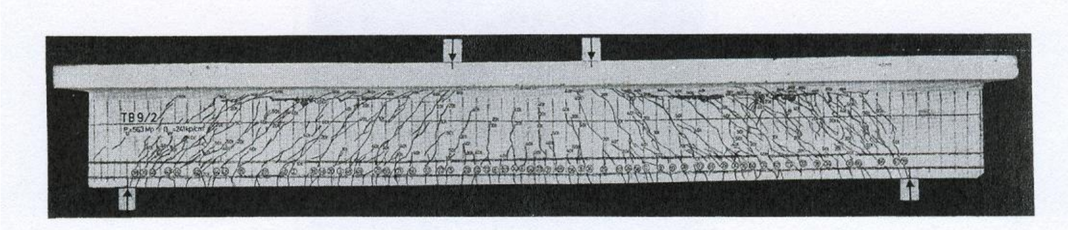

a) Shear reinforcement ratio: $\eta = 0.93$

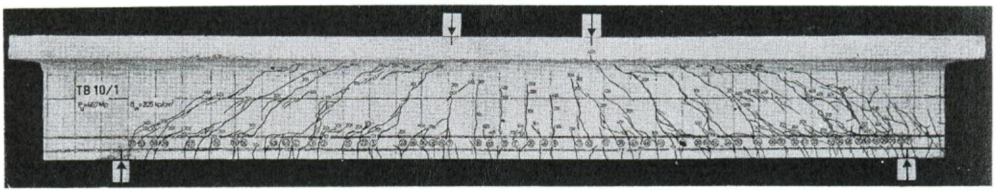

b) Shear reinforcement ratio: $\eta = 0.38$

Fig. 1.8: Crack patterns of T beams with very different amounts of shear reinforcements (Leonhardt and Mönnig, 1973)

Special attention was directed to the possible failure of compressive concrete struts. In I sections with large flanges and large amount of web reinforcement as well as relatively thin webs the compressive struts may suddenly fail between inclined cracks, even before the web reinforcement yields (Fig. 1.9). The web compression failure gives the upper limit of shear resistance (Leonhardt and Mönig, 1973).

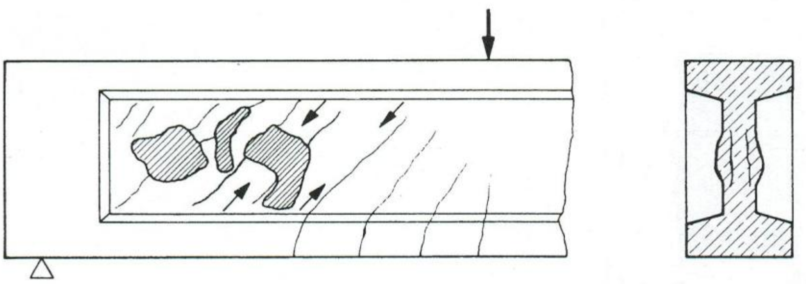

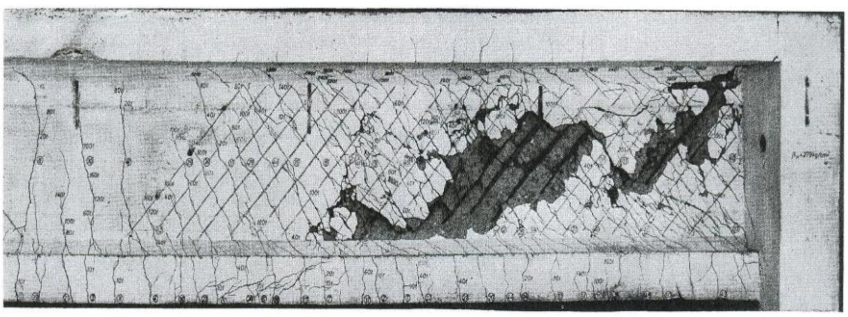

Fig. 1.9: Sudden web compression failure in case of large amount of web reinforcements (Leonhardt and Mönnig, 1973)

Leonhard, Rostásy and Koch (1973) experimentally showed not only the existence of the V_c term (shear resistance provided by the compressed concrete flange) but also the further increase of shear capacity in case of prestressing (Fig. 1.10). The increase of shear capacity in Fig. 1.10 is indicated by the decrease of stirrup stresses.

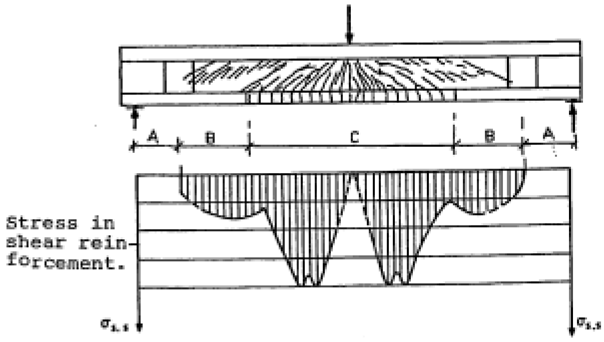

Fig. 1.10: Shear in fully prestressed member (Leonhardt, Rostásy and Koch, 1973) (cited from CEB bull 180, 1987)

1.8 Thürlimann et. al – Influence of degree of prestressing

Thürlimann experimentally showed that the positive influence of prestressing on the shear capacity depends on the level of prestressing. Contribution of prestressing to shear capacity increases by increasing the level of prestressing. Fig. 1.11 indicates the stirrup forces versus the acting shear force including the cases of non-prestressed, practically prestressed and fully prestressed members. In this series of tests the degree of prestressing varied between 0 and 100%.

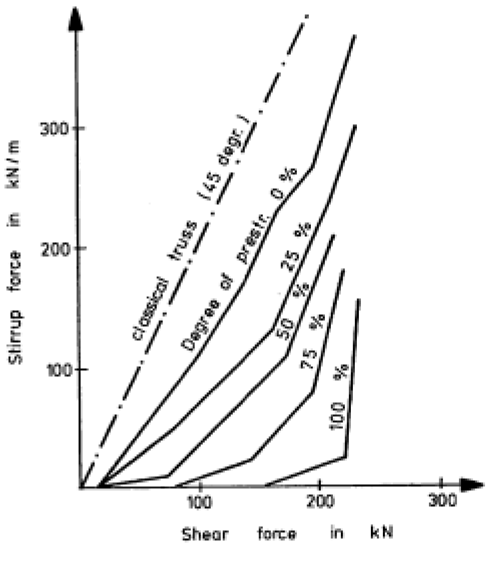

Fig. 1.11: Influence of degree of prestressing on stirrup forces (Thürlimann et. al, 1978) (cited from CEB Bull 180, 1987)

1.9 Walraven – Shear in prestressed concrete members

Walraven (1983) carried out a series of experiments on beams with the same amount of shear reinforcement but different compositions of tensile reinforcement *beam 1*: A_s = 1005 mm^2 + A_p = 1; *beam 2*: A_s = 534 mm^2 + A_p = 93 mm^2 and *beam 3*: A_s = 101 mm^2 + A_p = 186 mm^2. The stirrup stresses are presented as a function of actual force (V) in Fig. 1.12. It indicates a decreasing axial compressive force leads to on earlier activation of the stirrups. After yielding of the stirrups has started, still a considerable increase of the load is possible (Walraven, 1983).

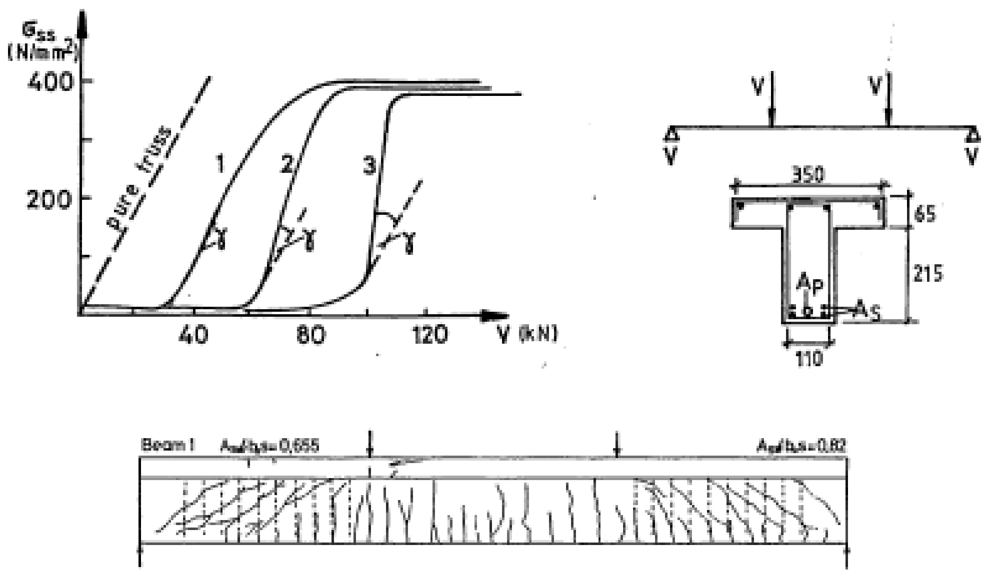

Fig. 1.12: Measured stirrup stresses in partially prestressed concrete beams with varying A_s/ A_p ratios (Walraven, 1983)

1.10 Collins and Vecchio – Modified compression field theory

Vecchio and Collins (1986) developed the modified compression field theory for reinforced concrete elements subjected to shear which was calibrated to the so-called Toronto large panel tests. Further details of the theory are not given here because it is presented in another chapter of this bulletin.

1.11 MC78 – MC90 – MC2010

fib is working to find the best possible procedure for shear design based on the earlier experiences with MC78, MC90 as well as new test results. The Workshop on “Recent development on shear and punching shear in RC and PC elements” in Salò was a major contribution in finalizing the MC2010 text.

1.12 Influence of fibre reinforcement on shear

At the end of this review on shear behaviour, we have to mention that steel fibres in concrete can also considerably influence shear behaviour and shear capacity (Fig. 1.13). Fibres can reduce the amount of stirrups and congestion of reinforcement in high shear regions. Fibres do not only increase shear capacity but also provide substantial post-peak resistance and ductility. Moreover, by the use of steel fibres in plain concrete substantial decrease of crack width can be achieved. Experimental evidence is presented in this Section.

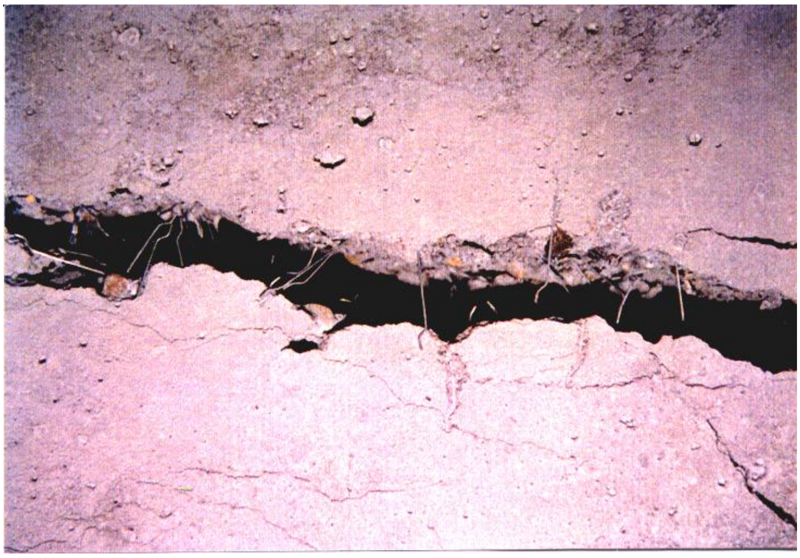

Fig. 1.13: Fibres across cracks

The main purpose of the research at the Budapest University of Technology (Kovács and Balázs, 2003; Balázs, 2006) was to study the shear behaviour of prestressed and reinforced concrete beams provided with the same amount of longitudinal reinforcement but with various fibre contents (0, 0.5 V%, 1.0 V%), amount of stirrups and type of fibres (hooked-end and crimped). Investigated parameters included load-deflection behaviour, cracking behaviour, failure load and type of failure (shear or bending). First the results of prestressed concrete beams are reported and then the results of reinforced concrete beams.

Concrete mix was made of 460 kg/m^3 Portland cement, 220 l/m^3 water, 0.063/4 mm river sand (62 %) and 4/8 mm gravel (38 %) with a grading curve between A and B limiting curves to DIN 1045. Steel fibres were added after mixing the concrete conventionally. Two types of fibres were used, hooked-end DRAMIX ZC 30/.5 fibres and crimped D&D ~ 30/.5 fibres. Average concrete cube strength was for all these tests 41.9 N/mm^2.

1.12.1 Prestressed concrete beams with various amounts of steel fibres

Three prestressed pretensioned concrete beams of 80×120 mm cross-section and 2 m length were prestressed by a simple seven-wire strand (∅12,9 mm, f_{ptk}=1770 N/mm^2, $f_{p,0.1}$=1550 N/mm^2, A_p=100 mm^2) at the core point of the section (Fig. 1). Specimens were prestressed simultaneously along a single strand. Specimens did not contain any other non-prestressed reinforcement (not even stirrups) except the prestressing strand. Prestressing force was released gradually by hydraulic jacks. DRAMIX ZC 30/.5 hooked-end fibres were applied in 0 V%, 0.5 V% and 1.0 V% fibre contents.

Four-point bending tests were carried out on the prestressed pretensioned concrete beams. Failure loads and failure modes are presented in Fig. 1.14. As results of the flexural tests indicate, fibre content affects the failure mode and the failure loads. Increasing fibre content resulted higher failure loads in addition to the changing of the failure mode from shear through combined shear + bending to clear bending. The change of the crack pattern was very remarkable. Failure of the beam without fibre reinforcement was very brittle and explosive.

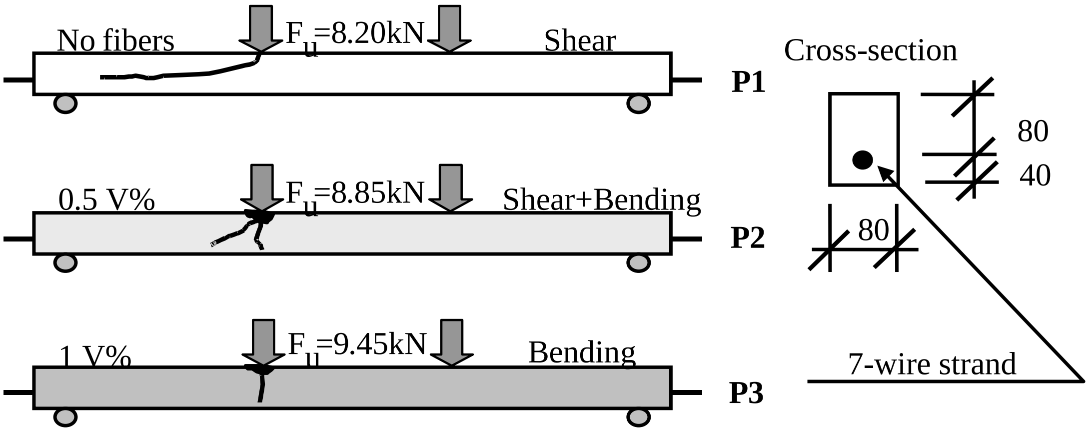

Fig. 1.14: Failure modes of prestressed pretensioned fibre reinforced concrete beams (fibre reinforcement: Dramix ZC 30/.5) (Kovács and Balázs, 2003; Balázs, 2006)

1.12.2 Reinforced concrete beams with various amounts of steel fibres

2 m long (span 1.8 m) fibre reinforced concrete beams with 100×150 mm of cross-section were tested in four-point bending. The longitudinal reinforcement was the same for each beam (2∅16 bars in the tension zone and 2∅6 bars in the compressed zone) (Fig. 1.15). In each loading step the crack pattern, the crack propagation and the crack widths were detected at the level of the main longitudinal reinforcement.

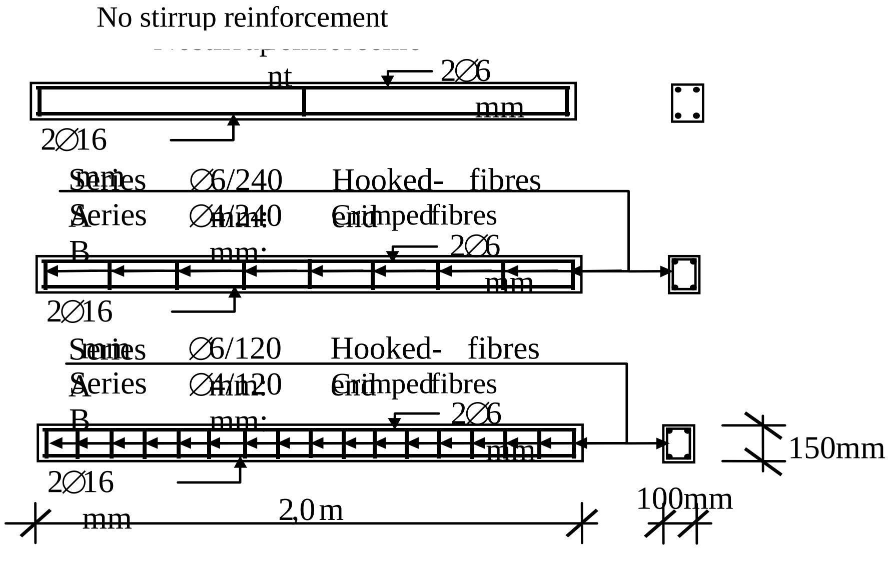

Fig. 1.15: Reinforcing details to tests with steel fibre reinforced concrete beams (Kovács and Balázs, 2003; Balázs, 2006)

Significant influence of the fibre reinforcement was detected in the shear resistance of fibre reinforced concrete beams (Fig. 1.16). Due to the increasing fibre content, considerable improvement of the failure load was observed in beams without stirrup reinforcement independently of the type of the steel fibres (B1…B3). On the other hand, the failure mode changed from shear (B1 and B2) to simultaneous shear + bending failure for the beam containing 1.0 V% crimped fibres and no stirrup (B3). Considering stirrup reinforcement ∅4/240 mm, the shear capacity improved by applying crimped fibres (B4…B6). *In this case the higher fibre content led to changing of the failure mode, from shear failure to clear bending failure.*

0.5 V% crimped fibres showed higher shear capacity (B8: 46.6 kN) than the beam made with only stirrup reinforcement (B7: 35.2 kN). Moreover, 1.0 V% crimped fibres resulted bending failure since the increasing fibre content was able to carry the increasing shear forces in the member (B9).

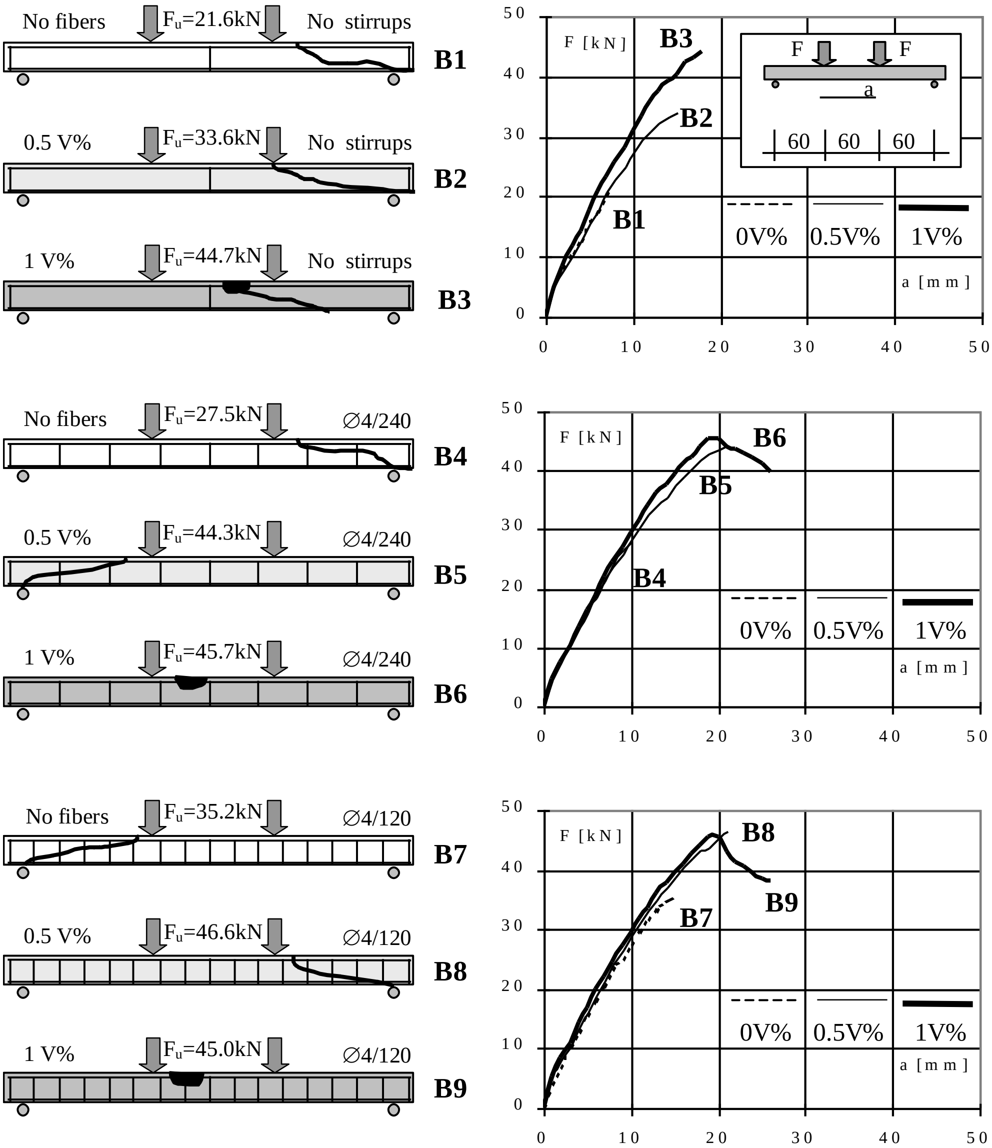

Fig. 1.16: Four point bending tests on SFRC beams (fibres: D&D~30/.5 crimped fibres)
a) Failure loads and failure modes b) Load vs. mid-span deflections
(Kovács and Balázs, 2003; Balázs, 2006)

Steel fibre reinforcement is commonly used for increasing toughness and energy absorption in concrete as well as to distribute cracks. During our tests full crack mapping was carried out in each load step. Fig. 1.17 indicates the crack distribution of the beams on the service load level at F = 20 kN jacking force. Heights of column in Fig. 1.17 indicate the widths of the cracks and positions of the columns indicate the place of the cracks along the beam. On the right hand side of Fig. 1.17, tables summarise the number of cracks, the sum and the average widths of the cracks, as well as the mean crack spacing. Presented test results indicate that in case of application of steel fibres: (i) maximum crack width decreased, (ii) average crack width decreased from 0.066 mm (0 V%) to 0.034 mm (1.0 V%), (iii) average crack spacing decreased from 82 mm (0 V%) to 60 mm (1.0 V%). Fibres were more effective in the middle portion of the beam where (B) the bending moment is constant than over the shear span (S).

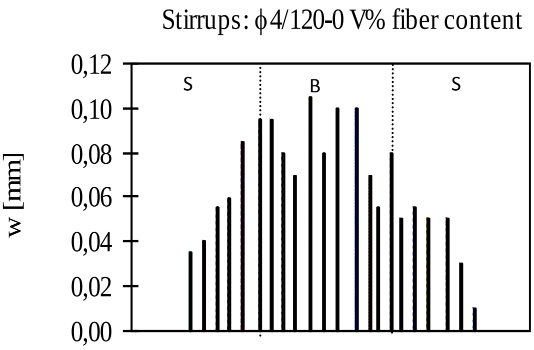

Cracks

	S+B	B	S
No.	22	9	13
Σw [mm]	1.45	0.74	0.71
w_m [mm]	0.066	0.082	0.055
s_w [mm]	82	67	92

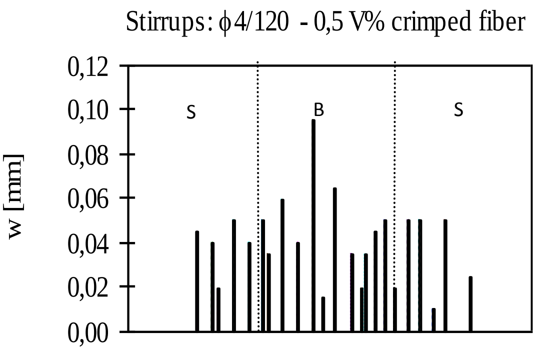

Cracks

	S+B	B	S+B
No.	23	9	14
Σw [mm]	0.945	0.445	0.500
w_m [mm]	0.041	0.049	0.036
s_w [mm]	78	67	86

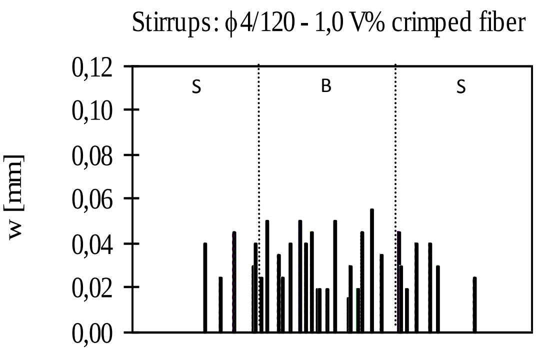

Cracks

	S+B	B	S
No.	30	17	13
Σw [mm]	1.030	0.585	0.445
w_m [mm]	0.034	0.034	0.034
s_w [mm]	60	35	92

Fig. 1.17: *Crack distribution in beams having crimped fibres and Ø4/120 shear reinforcement measured at F=20 kN jacking force (S+B: shear and bending region = whole beam, B: bending (middle) portion, S: shear (outer) portion). The horizontal axes of the diagrams give the position of the crack. (Kovács and Balázs, 2003; Balázs, 2006)*

1.13 References

Balázs, L. G. (2006), Increase of shear and flexural capacities in steel fibre reinforced concrete, Proceedings of 2nd Int. Conf. of Asian Concrete Federation, 20-21 Nov. 2006, Bali, Indonesia pp. 104-112.

CEB (1987), Shear in prestressed concrete members, CEB Bulletin d' Information 180

Kani, G. N. J. (1964), The Riddle of Shear Failure and Its Solution, ACI Journal, April 1964, pp. 441-465.

Kovács, I., Balázs, G. L. (2003), "Structural behaviour of steel fibre reinforced concrete", *Journal of Structural Concrete*, pp. 57-63.

Kupfer, H. (1962), *Extension of truss model by Mörsch by using the principle of minimal work of deformations (Erweiterung der Mörsch' schen Fachwerkanalogie mit Hilfe des Prinzips vom Minimum der Formäderungarbeit),* Schear-Colloquium Stuttgart, Manuscript

Leonhardt, F., Rostásy, F. Koch, R, (1973), *Shear tests on prestressed concrete beams (Schubversuche an Spannbetontraegern),* Deutscher Ausschuss für Stahlbeton, Heft 227, Berlin

Leonhardt, F., Mönnig, E. (1973), *Lectures about reinforced concrete (Vorlesungen über Massivbau)*, Part 2, Springer, pp. 175-217.

Mörsch, E. (1908), *Reinforced concrete – Theory and application (Der Eisenbetonbau – Seine Theorie und Anwendung)*, Verlag von Konrad Wittwer, Stuttgart, pp. 146-215.

Ritter, W. (1899), *Construction method of Hennebique (Die Bauweise Hennebique), Schweizerische Bauzeitung*, February 1899, pp. 41-61.

Thürlimann, B., Bachmann, H., Kraus, R., Caflisch, R., Heimgartner, E., (1978), *Shear tests on partially prestressed beams (Schubversuche an teilweise vorgespannten Balken),* Institut für Bautechnik ETH Zürich, Report Nr. 6504-2, 6504-3, 6504-5, 6504-6

Vecchio, F., Collins, M. P. (1986), The modified compression field theory for reinforced concrete elements subjected to shear, *ACI Journal*, March-April 1986, pp. 219-231.

Walraven, J., Mercks, P. (1983), *The bearing capacity of prestressed hollow core slabs,* Heron, Vol. 28, No. 3, Nov. 1983

Walther, R. (1965), About the calculation of shear capacity of reinforced and prestressed concrete beams (Über die Berechnung der Schubtragfaehigkeit von Stahl- und Spannbetonbalken - Schubtheorie), *Beton- und Stahlbetonbau*, 11/1965, pp. 261-268.

1.14 Acknowledgements

fib appreciates that Fausto Minelli and Giovanni Plizzari (from the University of Brescia) as well as Lucie Vandewalle (from the Catholic University of Leuven) together with Viktor Sigrist (Convener of ***fib*** Task Group "Ultimate Limit States" from the Technical University of Hamburg-Harburg) and Stephen Foster (Chairman of ***fib*** Commission 4 "Modelling of Structural behaviour and design" from the University of New South Wales) took the initiative to organize the Workshop on "Recent development on shear and punching shear in RC and PC elements" on 15-16 Oct. 2010 in Salò.

Intensive discussions with Andor Windisch on shear behaviour and shear design are gratefully acknowledged.

Special thanks also go to *Beton-Star Ltd.* for the financial support of studies on shear reinforced and prestressed concrete members with or without fibres.

2 MC2010: Shear strength of beams and implications of the new approaches

Evan C. Bentz

Associate Professor, Department of Civil Engineering
University of Toronto, Toronto, Canada

Abstract: The *fib* draft Model Code 2010 has introduced a new set of shear design equations for reinforced and prestressed concrete structures. The equations have been defined with a basic structure that requires two calculated parameters that relate to the angle of inclination of the stress field, θ, and a coefficient for a concrete contribution k_v. The code provides three levels of approximation to calculate these terms with the first and third based on the Modified Compression Field Theory and the second based on a strain-modified form of plasticity. As the level of approximation is increased, the quality of the predictions improves, but at the cost of more complex calculations. This paper shows the derivation of the methods and compares them to a large set of experimental data. A sample design for Level III is included. Overall it is found that the quality of predictions, and computational effort increases as the level of approximation is increased.

2.1 Introduction

The *fib* draft Model Code 2010 includes a new set of shear design methods that are intended to give the engineer flexibility in selecting a balance between complexity and accuracy for new designs and for evaluation or verification of existing designs. For shear a total of four "Levels of Approximation" (LoA) are included in the code with Level I providing the simplest analysis method though it is also the most conservative method. Level II is intermediate in complexity and accuracy, while Level III provides the most accurate and general predictions, though at the cost of more computational complexity. A Level IV analysis option is also included which allows the use of tools such as nonlinear finite element analysis or generalized stress-field approaches. This document explains the basic structure of Levels of Approximation I to III and provides a brief derivation of the method in Level III. It also provides a database comparison to a large set of over 2250 published shear tests where it is shown that the accuracies of the methods vary with LoA but that all methods provide safe shear designs that can be used in practice.

2.2 Basic structure of provisions

The shear provisions are all provided in a consistent format with only two parameters being defined by the different LoA values: θ to represent the angle of principal compressive stresses in the web of the member and k_v to represent a coefficient for the concrete contribution. Equations (2.1) to (2.4) present these basic equations. Note that these equations are intended to predict the shear strength of the web of a member of reinforced or prestressed concrete and thus are equally applicable for shear and torsion analyses. The same equations apply to all member webs whether or not they contain stirrups, and whether or not they are subjected to axial load or prestressing.

The limit states equation states that:

$$V_{Rd} = V_{Rd,c} + V_{Rd,s} \geq V_{Ed} \tag{2.1}$$

Where V_{Rd} is the reliable shear strength, $V_{Rd,c}$ is the estimate of the reliable concrete contribution and $V_{Rd,s}$ is the estimate of the reliable stirrup contribution. The value of V_{Rd} cannot exceed the crushing capacity of the concrete calculated as:

$$V_{Rd} \leq V_{Rd,\max} = 0.6\left(\frac{30}{f_{ck}}\right)^{1/3} f_{cd} b_w z \frac{\cot\theta + \cot\alpha}{1+\cot^2\theta} \tag{2.2}$$

Where θ is the first parameter defined by the different levels of approximation and indicates the angle of principal compressive stress in the web while α is the angle of the stirrups from the beam axis. Note that the concrete strength term in the brackets cannot exceed 1.0. Instead of the value 0.55 given in the draft code a factor of 0.6 is used in Equation (2.2) as in recent discussions such a change was considered. For members not controlled by this web crushing equation, the following two equations apply:

$$V_{Rd,s} = \frac{A_{sw}}{s_w} z f_{ywd} \left(\cot\theta + \cot\alpha\right)\sin\alpha \tag{2.3}$$

$$V_{Rd,c} = k_v \frac{\sqrt{f_{ck}}}{\gamma_c} b_w z \tag{2.4}$$

Where k_v is the second parameter defined by the level of approximation and indicates the ability of the web to resist aggregate interlock stresses which provide the concrete contribution to shear strength.

The shear provisions presented in the Model Code represent a combination of state-of-the-art methods from around the world developed over many years. Key contributions have been made by M.P. Nielson (1971), Collins (1978) and Thürlimann (1979) and others that have further developed the ideas (e.g. Muttoni (1989), Sigrist (1995)), with many of the concepts introduced into earlier international and model codes. The Draft Model Code 2010 provisions are partly an attempt to harmonize these different approaches.

To use the shear equations of the Draft Model Code, the parameters θ and k_v must be defined, and three Levels of Approximation (LoA) to determine these values are provided. The first two are appropriate for initial member sizing and general member design when a potentially conservative design is acceptable, though within their own ranges of optimal applicability, they provide strength estimates of similar quality to the general Level III analyses. The third LoA requires the most computational effort, but also provides the most accurate predictions. This third method will be explained in this paper in some detail as it is also the basis of the Level I Approximation.

2.2.1 Level of Approximation I

The first Level of Approximation is based on a simplified form of the Level III approximation and both are based on the Modified Compression Field Theory [Vecchio and Collins 1986]. This method may only be used for members with a concrete strength f_{ck} not in excess of 64 MPa, and steel with f_{yk} not in excess of 500 MPa, and with maximum coarse aggregate size of at least 10 mm. For such cases:

$$\theta = 36° \tag{2.5}$$

$$k_v = \begin{cases} = \dfrac{200}{(1000+1.3z)} & \text{if } \rho_w = 0 \\ = 0.15 & \text{if } \rho_w \geq 0.08\sqrt{f_{ck}}\,/\,f_{yk} \end{cases} \tag{2.6}$$

Note for this LoA that there are no terms in the above equations that require additional calculations; they are all available to the engineer at design time. The two different k_v relationships are to account for the size effect for members without stirrups. This method has similarities to the Canadian simplified and the American ACI shear provisions.

2.2.2 Level of Approximation II

The second Level of Approximation is based on the principles of plasticity modified with a strain term to better model the behaviour of heavily reinforced members. For this method, no concrete contribution is included and the angle of principal compression, θ, can be selected by the engineer to lie within the range provided below:

$$20° + 10{,}000\varepsilon_x \quad \leq \quad \theta \quad \leq \quad 45° \tag{2.7}$$

$$k_v = 0 \tag{2.8}$$

Where ε_x is the calculated longitudinal strain at the mid-depth of the member calculated with a plane sections analysis ignoring tension stiffening, or based on the following equation that results from a simple truss model of a beam subjected to bending shear and axial load:

$$\varepsilon_x = \frac{M_{Ed}\,/\,z + 0.5V_{Ed}\cot\theta + 0.5N_{Ed} - A_p f_{po}}{2(E_s A_s + E_p A_p)} \tag{2.9}$$

Where M_{Ed}, V_{Ed}, and N_{Ed}, are the factored design forces or, for shear strength evaluation, are the calculated forces themselves. The term f_{p0} is taken as the stress in the prestressing strands when the strain in the resulting concrete is zero. Note that unlike Level I, this method requires (if theta is not taken well above the lower limit in Eq. (2.7)) that the engineer calculates an intermediate term, ε_x, and to iterate to convergence on that strain for shear strength evaluation, though this is not difficult with a spreadsheet. By ignoring the concrete component and allowing a selection in the angle of compression, this method corresponds to the conventional European plasticity-based shear design provisions. In general, design comprises the determination of the stirrup reinforcement A_{sw} on the basis of Equation (2.3), the control of the web width b_w with help of Equation (2.2) and if appropriate, an adjustment of the latter.

2.2.3 Level of Approximation III

The third level of Approximation is based directly on the equations of the Modified Compression Field Theory (MCFT). The two parameters for the basic model can be calculated as:

$$\theta = 29° + 7000\,\varepsilon_x \tag{2.10}$$

$$k_v = \begin{cases} = \dfrac{0.4}{(1+1500\varepsilon_x)} \cdot \dfrac{1300}{(1000+0.7k_{dg}z)} & \text{if } \rho_w = 0 \\ = \dfrac{0.4}{(1+1500\varepsilon_x)} & \text{if } \rho_w \geq 0.08\sqrt{f_{ck}}\,/\,f_{yk} \end{cases} \tag{2.11}$$

Where the strain ε_x is calculated using Eq. (2.9) though here it is recommended that the term 0.5cotθ in that equation be replaced by 1.0 as θ depends on ε_x. The term k_{dg} is a measure of the roughness of the cracks, and is also used in the punching shear chapter. It is calculated as:

$$k_{dg} = \frac{48}{16+d_g} \geq 1.15 \tag{2.12}$$

Where d_g is the maximum specified coarse aggregate size. Note that in the use of the above equations, there are a series of limitations and special restrictions that are not explained in this paper but which must be satisfied. This method of shear evaluation is similar to that in the 2004 Canadian shear provisions, and the 2008 AASHTO LRFD shear provisions from the United States.

2.3 Sample strength evaluation by Level III

As the Level III analysis method is perhaps the least familiar, its use will be demonstrated so the reader can better understand how to use it. Consider the beam shown in Fig. 2.1, a test modelling highway bridges in Oregon, USA, by Higgins et al. [2004].

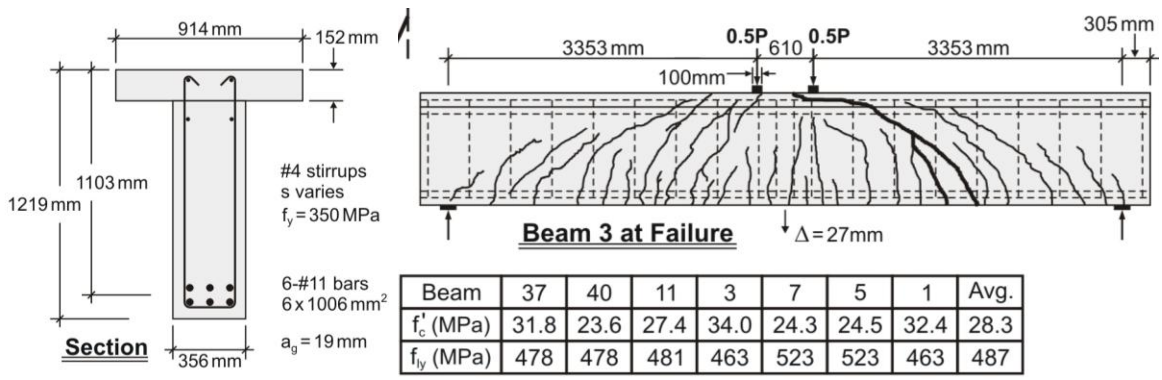

Beam	37	40	11	3	7	5	1	Avg.
f'_c (MPa)	31.8	23.6	27.4	34.0	24.3	24.5	32.4	28.3
f_{ly} (MPa)	478	478	481	463	523	523	463	487

Fig. 2.1: Sample beam for demonstration of Level III analysis [Higgins et al. 2004]

Of the beams listed in the table, Beam 3 will be considered. It was constructed with 34 MPa concrete and had US#4 stirrups (A_{sw} = 258 mm^2) spaced at 457 mm. As this member contained sufficient stirrups, the size effect term does not apply and thus the k_{dg} term need not be evaluated. The calculation will be performed at the critical control section for shear, a distance z (= 0.9d = 993 mm) away from the edge of the loading plate where the longitudinal strain ε_x will be highest and thus the shear strength the lowest. At this location, the M/V ratio, from the bending moment and shear force diagrams, will be (3353-100/2-993) = 2310 mm, meaning that for each kN of shear force, there will be a corresponding moment of 2.31 kNm.

If it is initially assumed that the beam will fail when ε_x equals 0.001, or approximately at first flexural yield, Eq. (2.10) produces a k_v of 0.160 and from Eq. (2.4), $V_{Rd,c}$ would equal 329 kN if all safety factors were ignored. Eq. (2.10) indicates that θ=36º and thus Eq. (2.3) produces $V_{Rd,s}$ = 270 kN. Combining these produces a first estimate of V_{Rd} of 599 kN. This shear force would be associated with a moment of 599*2.31 = 3183 kNm, and these values are directly substituted into Eq. (2.9) producing a calculated ε_x of $0.825\text{x}10^{-3}$ using the simplification that 0.5cotθ =1.0 as noted above. Thus the initial assumption of the strain was slightly off, and a second iteration is required. Convergence is achieved when the strain is calculated as $0.875\text{x}10^{-3}$, and the shear strength is calculated as 635 kN. The experiment failed at a shear force of 755 kN, for a test to predicted ratio of 1.19, a typical level of conservativeness for this method. Additional checks that the longitudinal reinforcement was not overstressed have not been shown in this document.

2.4 Theoretical background of Level III analysis

As the MCFT analysis is the basis of Levels I and III analyses, it will be explained in some detail here. With the MCFT, the concrete contribution is predicted to be carried by aggregate interlock. The ability of a crack to resist these stresses was observed by Walraven (1978) to decrease with decreasing concrete strength; decreasing maximum specified coarse aggregate size, representing crack roughness; and increasing absolute crack width. The suggestion that wider cracks are less able to resist sliding shear stresses is hopefully intuitive. To estimate a crack width, w, the following relationship can be used:

$$w = \varepsilon \cdot s \tag{2.13}$$

where s is the crack spacing and ε is the average strain perpendicular to the crack. As wider cracks will be associated with lower aggregate interlock strength, anything that increases the value of w can be expected to result in decreased shear capacity. Thus if the crack spacing increases due to, say, the construction of a larger member, it can be expected that the shear strength will decrease. This is called the size effect in shear and is an important part of the behaviour of members without stirrups. Secondly, if the average strain in the cracked concrete, ε, increases due to, say, applied tension then the shear strength is also predicted to drop. This is called the strain effect in shear and is less well known than the size effect, though it is of comparable importance.

Overall, then, a size effect and a strain effect are predicted to be important aspects of the concrete component of shear strength of members. Experiments show that these are indeed the two most important aspects influencing shear stress at failure and should be included in any state of the art shear provisions.

The full derivation of the method is given elsewhere [Bentz and Collins 2006, Bentz et al. 2006], but the important concepts are summarized here. Determining shear strength will depend on the terms s and ε in Eq. (2.13). The value of the crack spacing, s, will depend largely on the size of the member. The crack spacing in the longitudinal direction is taken as the inner lever arm $z = 0.9d$ if no stirrups are provided and 20 mm aggregate is used, that is, the term $0.7k_{dg}z$ term in Eq. (2.11) reduces approximately to z if 20 mm aggregate is used. To account for other aggregate sizes and for consistency with the punching shear relationships, the variable k_{dg} is used. For high strength concrete, the aggregate fractures and does not contribute to crack roughness. To account for this, take $d_g = 0$ for $f_{ck} > 70$ MPa. To avoid a discontinuity, linearly interpolate d_g from the specified value at f_{ck}= 64 MPa down to zero at f_{ck} = 74 MPa. For members with stirrups, the stirrups will control the crack spacing and the term $0.7k_{dg}z$ may be simply taken as 300 mm though this value need not be taken as larger than z.

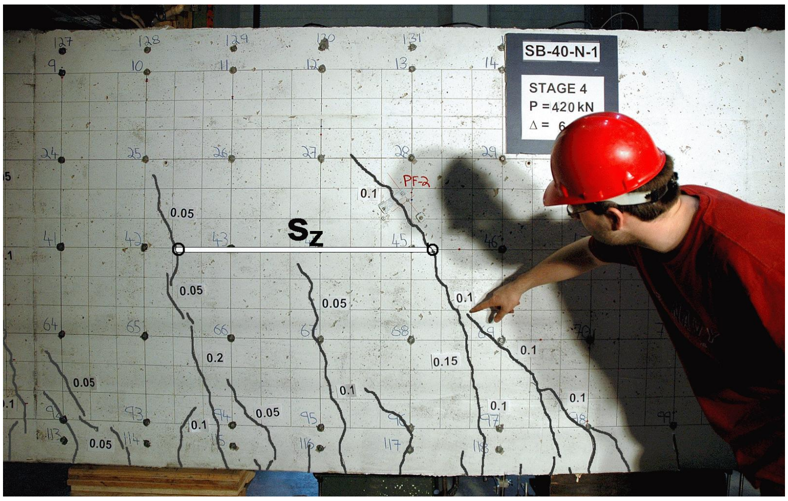

Fig. 2.2: 1500 mm deep slab strip with shear cracks near failure.

Figure 2.2 shows the test of a 300 mm wide slab strip of a 1500 mm thick one-way slab. It can be seen that the spacing of the cracks at the mid-depth of the member is much greater than the spacing of the cracks at the flexural tension face. The crack spacing term in Eq. (2.10), $0.7k_{dg}z$ refers to the longitudinal spacing of the cracks at mid-depth of the member where the shear stress is generally critical.

The value of ε is slightly more complex to determine compared to the effective crack spacing as it depends on the currently applied load level, the amount of prestress, material properties of the flexural reinforcement, etc. Consider that a given amount of applied load will be associated with a given strain in the longitudinal reinforcement based on a free body diagram such as that on the left of Fig. 2.3. This value of strain will be present in the reinforcement, whereas Eq. (2.13) requires the strain at 90º to the diagonal crack. As such, the equations of the MCFT are employed to derive a relationship between the width of a diagonal crack, for a given crack spacing, at shear failure given that the longitudinal strain is a known quantity. This involves the simultaneous solution of 15 nonlinear equations and is described elsewhere [Bentz and Collins, 2005].

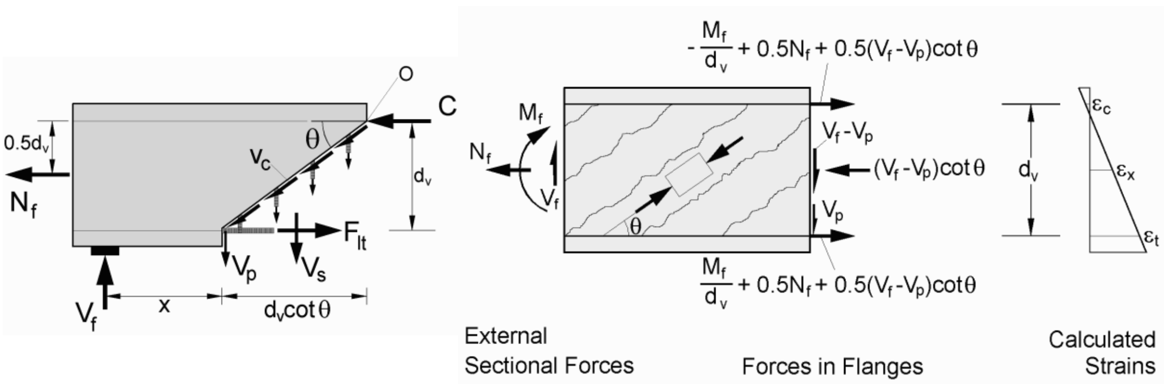

Fig. 2.3: Free body diagrams of beam section.

Figure 2.4 shows the results of the calculation of diagonal crack width for various longitudinal strains by the MCFT. As the longitudinal strain increases, the critical crack width also increases. The analysis results are nonlinear, but a simplified equation is also shown on the figure that conservatively approximates the nonlinear behaviour. This equation is intentionally selected to provide a good match to the MCFT nonlinear results for mid-depth strains that are expected for a member reinforced with 500 MPa flexural reinforcement. If a member is to be subjected to larger longitudinal strains, say with FRP reinforcement, these provisions should be conservative as the crack width will be overestimated by the simplified equation.

When the simplified equation in the figure is substituted into the MCFT equation for aggregate interlock, and a size effect terms is also added [Bentz and Collins 2005], Eq. (2.11) is obtained for the value of k_v which defines the concrete contribution based on the MCFT. The first term in the general equation accounts for the strain effect whereby members with smaller longitudinal strains are stronger in shear. The second term accounts for the size effect which reduces to unity for members with at least minimum stirrups (i.e. $0.7k_{dg}z$ ~ 300 mm). The estimation of the other term in the equation, ε_x, will be discussed below.

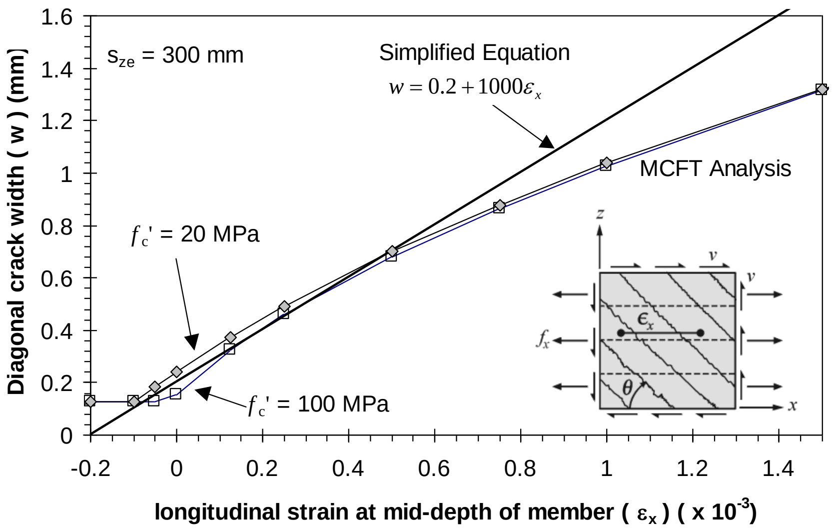

Fig. 2.4: Calculation of diagonal crack width from MCFT

Members with at least a minimum quantity of well-anchored stirrups are predicted to fail in shear not by sliding on the critical shear crack, but by yielding of the stirrups and eventual crushing of the concrete in the web. In the Level II approximation, which allows the engineer to select the value of θ, equations are provided to ensure that the concrete does not crush before reaching the design shear strength, which provides a lower limit on θ, while an upper limit could be calculated to ensure that the stirrups will yield at design shear failure. At low applied shear forces, that is, small values of ε_x, the range over which the value of θ can be selected is large, but as shear stresses increases, the range became more restrictive. For the Level III analysis, it was decided to select the value of θ to be valid at the higher shear limit where the range of potential values is more restrictive and then apply this value to all levels of shear loading so a single deterministic equation could be provided, Eq. (2.10).

Figure 2.5 shows the limits on allowable angle of principal compression, θ, based on the MCFT for members heavily loaded in shear and for different strains in the member at mid-depth (ε_x). As can be seen, the predicted range of allowable angles to select from at this high shear loading is rather narrow. Members designed based on angles in the upper shaded region would be expected to fail in shear before yielding of the transverse steel making the use of Eq. (2.3) unconservative. Members designed based on angles from the lower shaded region would also be unconservative as here the member would be predicted to fail by crushing of the concrete in diagonal compression before achieving the design shear strength. Only within the unshaded region would such a member be predicted to be able to resist the applied shear force and thus Eq. (2.10) was chosen for this range.

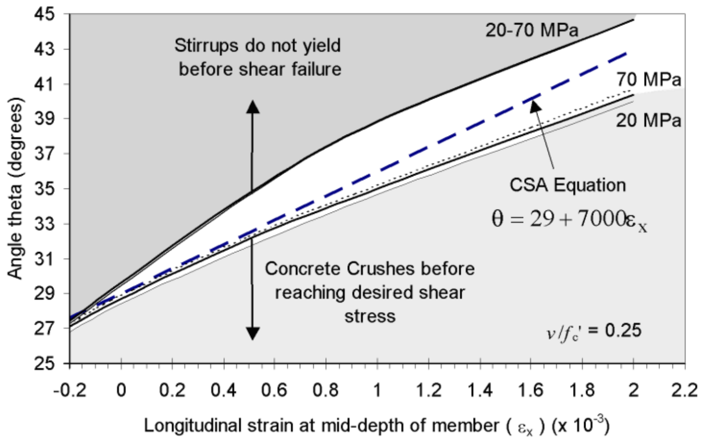

Fig. 2.5: Selection of theta equation for level III analysis

Embedded in Eqns. (2.10) and (2.11) as well as in the Level II method equations, is the strain term ε_x which represents the average longitudinal strain in the member at the mid-depth. For general reinforced concrete members subjected only arbitrary loading, the second free body diagram in Fig. 2.3 can be resolved to produce the equation for ε_x given as Eq. (2.9). Note the conservative assumption that the strain in flexural compression may be neglected such that ε_x is equal to half of ε_t, the tension chord strain. In the use of this equation, the values of moment and shear are always taken as positive. The numerator of the equation estimates the force that must be resisted in the flexural reinforcement of a member including the shear-moment interaction. The denominator converts this force to a strain in the tension reinforcement by dividing by the quantity and stiffness of flexural reinforcement. As a final simplification, the strain at mid-depth of the member, ε_x, is simply taken as one half of the value in the flexural tension reinforcement. For prestressed concrete or members subjected to axial loads, additional terms will lower or raise the terms in the numerator of the equation.

2.4.1 Level of Approximation I

The discussion above summarizes the development of the k_c and θ terms used in the basic shear strength equations of the Model Code Level III. The most important behavioural aspects are the size effect for members without stirrups, and the strain effect which applies to all member types. Given that the strain effect predicts lower shear strengths for members with higher strains, it becomes possible to develop a simplified form of the Level III analyses that removes the requirement of calculating the longitudinal strain ε_x. If it can be assumed that the strain in the longitudinal reinforcement is near that associated with flexural yield, a "lower bound" equation can be derived. Accounting for some of the conservativeness in the method, it can be assumed that at predicted shear failure, the strain in the longitudinal reinforcement will be, about 85% of the flexural yield value. Thus the value of ε_x used to derive the Level I relationships was taken as $0.85f_{yk}/(2E_s)$ or 1.06×10^{-3}. That is, if this strain is substituted into the Equations from Level III, the Level I equations are produced. It can thus be expected that the Level I equations should produce good quality predictions for members with reinforcement stresses near flexural yield. It is also therefore necessary to provide limits to the Level I method such that ε_x does not exceed the assumed value ($f_{yk} \leq 500$ MPa), and that the equivalent crack spacing is appropriately calculated ($f_{ck} < 64$ MPa, $d_g > 10$ mm). If for a given project these rules may be violated, it would be appropriate to recalculate the Level I equations with the new limitations that apply for that particular project.

2.4.2 Level of Approximation II

The Level II shear equations were developed by Sigrist as an extension of the conventional European plasticity-based methods, but with an additional strain restriction to prevent unconservative designs being produced. The equation for the selection of theta will be explained in more detail in a forthcoming paper.

Note that the descriptions given above for Levels I, II, and III do not include all the aspects of the shear design provisions in the Draft Model Code. Additional important aspects include the impact of the shear on the longitudinal reinforcement, limitations on the use of the ε_x equation, amongst others. This document provides only a summary of these rules, but the statistical comparisons that follow were performed with all checks implemented though the minimum shear reinforcement ratio was relaxed, and the longitudinal yield strength equation was not checked as it was desired to determine the predicted shear capacity, not the flexure-shear interaction capacity.

2.5 Experimental validation of Levels I, II, and III shear analyses

For a direct comparison between the predictions of Level I, Level II, and Level III, the beam series tested by Higgins and shown in Fig. 2.1 will be considered. These beams represented sections of highway girders designed in the 1950's in the United States as part of the original Interstate highway system. Since that time, it has become clear that shear provisions of that era were less conservative than they should have been, and thus some of these beams contain less shear reinforcement than would be required today. This comparison thus represents a shear evaluation scenario of members with light amounts of transverse reinforcement. This comparison is therefore likely to show that the Level II analysis, which neglects the influence of a concrete contribution, will be conservative, and this should not be considered as a weakness of Level II as it is optimized to be used for other situations.

The cross sections of the girders is shown in Fig. 2.1 and this geometry applied for all beams except the one without transverse reinforcement which contained only 3 longitudinal bars rather than the 6 that the other beams contained. The quantity of shear reinforcement was varied by the spacing of the stirrups. To provide a comparison of what is possible using a relatively complex Level IV nonlinear computer analysis, the results from the program Response-2000 written by the author and based on the MCFT [Bentz 2000] is also shown.

As can be seen in Figure 2.6, the Level I method provides a prediction of all members including the one without stirrups. As this member is 1.2 metres deep, it will demonstrate a significant size effect, and this can be seen to modelled in an appropriate way. Level II provides a range of potential strengths depending on the angle θ selected by the engineer and does not provide a prediction for the shear strength of the member without transverse reinforcement. As expected, the Level II predictions are conservative as they are intended for design of members that have much higher shear stresses than these particular members. The Level III analyses provide slightly better predictions than the Level I though the calculations they were more complex to perform. The best predictions come from the computer program Response-2000 and it is included largely to indicate that these tests can be predicted with surprisingly good accuracy if all the cross sectional properties and material characteristics are available. Figure 2.7 compares the statistics of this small set of tests, and it can be seen that the predictions for these beams are generally good and account for the influence of the quantity of transverse reinforcement well. The Level II method can be seen to provide better predictions as the level of stirrups is increased as expected.

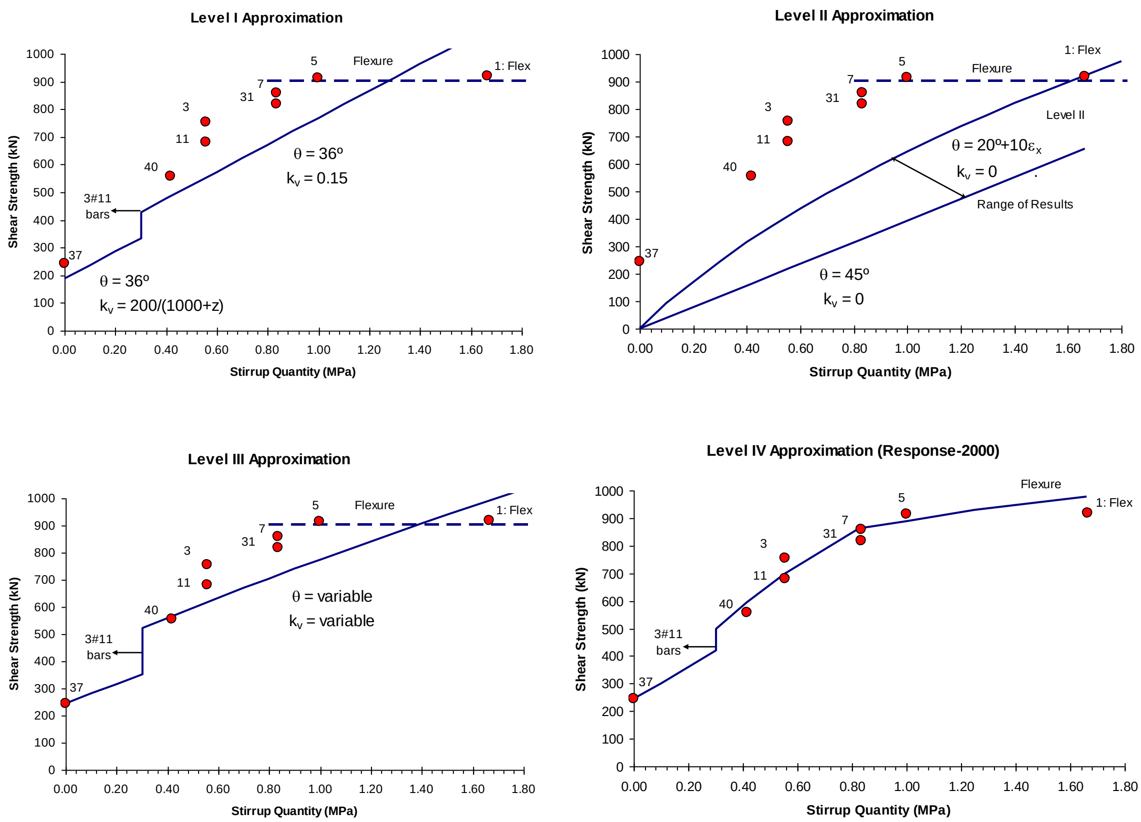

Figure 2.6: Quality of shear predictions of four Levels of Approximation for Oregon beams.

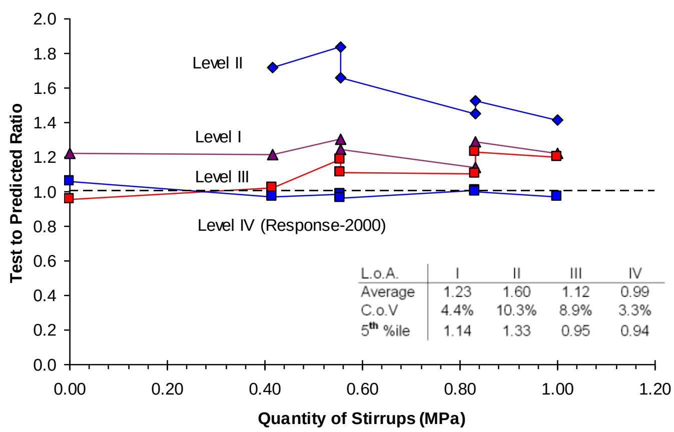

Fig. 2.7: Statistical comparison of Oregon beams

While Figs 2.6 and 2.7 demonstrate good performance for a given test series performed in a given lab, a larger dataset comparison is required to determine if the provisions in the Draft Model Code provide safe predictions of shear strength. To do this, comparisons have been made to a large dataset. For members without stirrups, the database of Collins et al. (2008) will be used, while for members with transverse reinforcement, the database of Bentz (2000) will be used. The former is a large database including essentially all shear tests published in the ACI Structural Journal since 1948 plus additional tests from other journals, test reports and sources. The database for members with stirrups is smaller, and only includes members that were unlikely to fail with a strut-and-tie mechanism. Both databases include continuous members as well as simply supported members. For members without stirrups, uniform loads are considered while for the members with stirrups, only point loads are included. All members were reported to fail in shear with no anchorage failures. For members with stirrups, members with axial tension, axial compression, and prestressed beams were also included.

The comparisons will be made first for the most complex analysis method, Level III. Considering first members without stirrups, i.e. slabs, Fig. 2.8 shows the ability to predict the shear strength of 1921 published experimental shear failures with respect to a number of variables. The first plot in Fig. 2.8 shows the impact of the a/d ratio demonstrating that the Level III predictions are safe if they are applied to members that would be classified as "deep beams" and analyzed by the strut-and-tie method. Note that no strut-and-tie calculations were done for the results in this paper and thus very conservative results occur for those tests. To avoid these tests being distracting on the figures, the specimens with a/d ratios less than 2.7 were removed from the following figures, though they are included in the statistical comparisons which follow.

The second graph in Fig. 2.8 compares the ability of a Level III analysis to model the strain effect in terms of the percentage of reinforcement. The deep beams that are predicted conservatively by the method are now spread across the range of the graph and it is the bottom trend of the data, i.e. the unconservative part, that should be considered. As can be seen, good results are obtained even for members with very high reinforcement ratios. Note that some of these high reinforcement ratios are associated with large a/d ratios, and thus actually represent high strain states and lower shear strengths rather than higher strengths. Thus methods which take shear strength as a function only of the percentage of reinforcement and neglect the influence of the corresponding demand on that reinforcement often require cumbersome limits like the 2% limit on the EC2 shear strength equation for members without stirrups.

The third plot in Fig. 2.8 shows that the size effect is accurately modelled by the Level III equations. Note the single test at a depth of 3000 mm, the largest shear test ever, performed in Japan. The next plot shows that the predictions are equally good independently of the concrete strength. The 2nd last plot shows good predictions independently of the strength of the reinforcement. Finally the last plot shows that the strain effect concept is well modelled.

If the same experiments are compared to the Level I analysis method and plotted with respect to ε_x, Fig. 2.9 is obtained. This shows that generally the Level I predictions are more conservative for lower strains, as expected from the strain effect, potentially very much so. This is compensated for, however, by the simplicity of the equation, also shown on the plot. If members with a flexural steel stress at shear failure within the range of 300 to 550 MPa are defined as "practical," the quality of the predictions can be seen to be much better in this region. That is, good quality results are obtained from the Level I methods if the members are expected to fail by flexural yielding, as they are for reinforced concrete slabs and transfer girders for example.

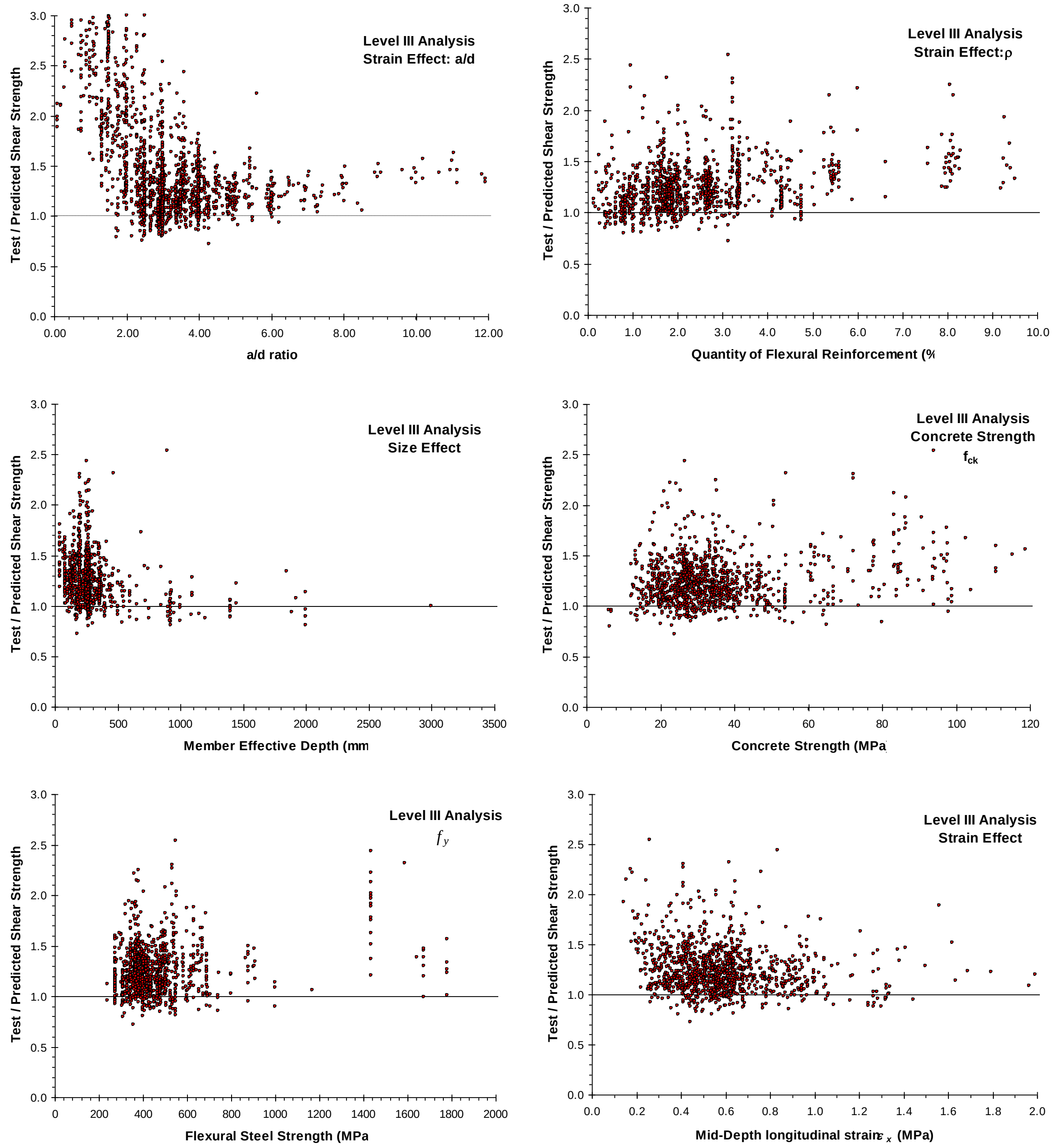

Fig. 2.8: Quality of Level III predictions for members without stirrups

Turning to members with stirrups, Figure 2.10 shows the ability of the Level III analysis method to predict the influence of a range of variables. As can be seen, the quality of prediction is of similar quality across the range of the quantity of stirrups. The second plot shows that the size effect is appropriately accounted for, in the sense that it is confirmed to be safe to ignore it for members with stirrups. Rather than showing separate plots for a/d and ρ effects, the combined strain effect plots shows that the predictions are of uniform quality independently of the calculated strain. Note the negative strains in the strain effect plot indicating members that had sufficient axial load or sufficient prestress that they were predicted to still be in net longitudinal compression on the cross section at shear failure. Recall that a compressive ε_x does not necessarily indicate a zero diagonal crack width, see Fig. 2.4.

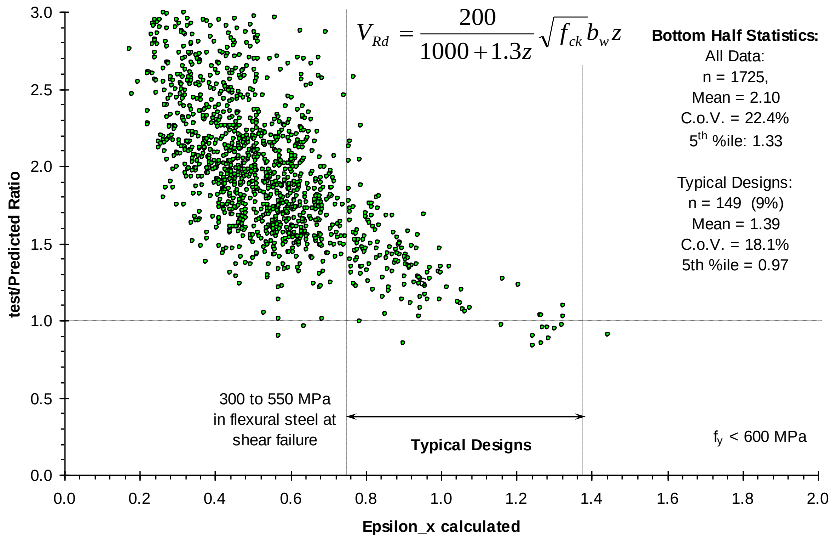

Fig. 2.9: Quality of Level I predictions for members without stirrups

Figure 2.11 shows the Level I comparison on the left in a similar way to Fig. 2.9. Again the tests within the "practical region" are seen to be better modelled than those with lower strains. The right plot in Fig. 2.11 shows the quality of the Level II predictions with respect to quantity of stirrups and shows a very clear trend. As expected, the predictions are best for members with sufficient stirrup quantity that they are failing by crushing the concrete. Note that the Oregon beam results from Fig. 2.7 fall right in the data cloud for lower strains. For compatibility with the Level I comparisons, in this paper a stirrups index $\rho_v f_y/f_{ck}$ between 0.10 and 0.25 will be defined as a "practical" test for a level II analysis though those particular limits are somewhat arbitrary.

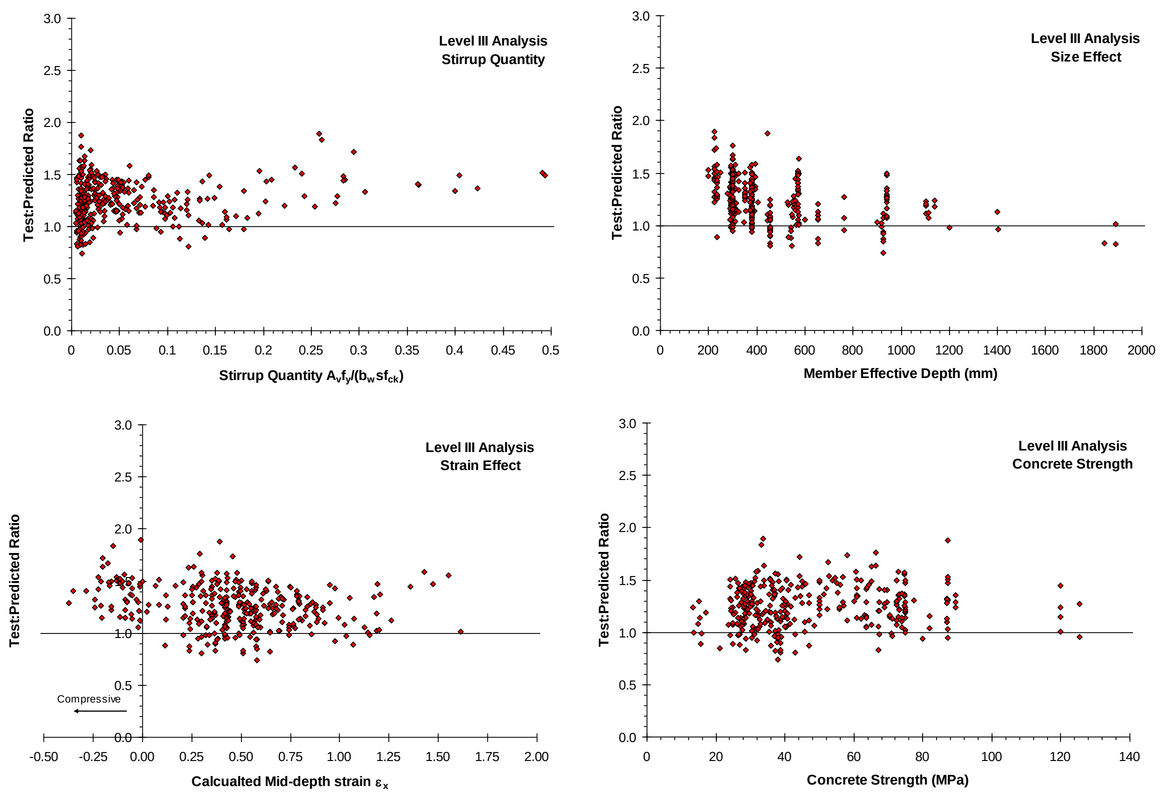

Fig. 2.10: Quality of Level III predictions for members with stirrups

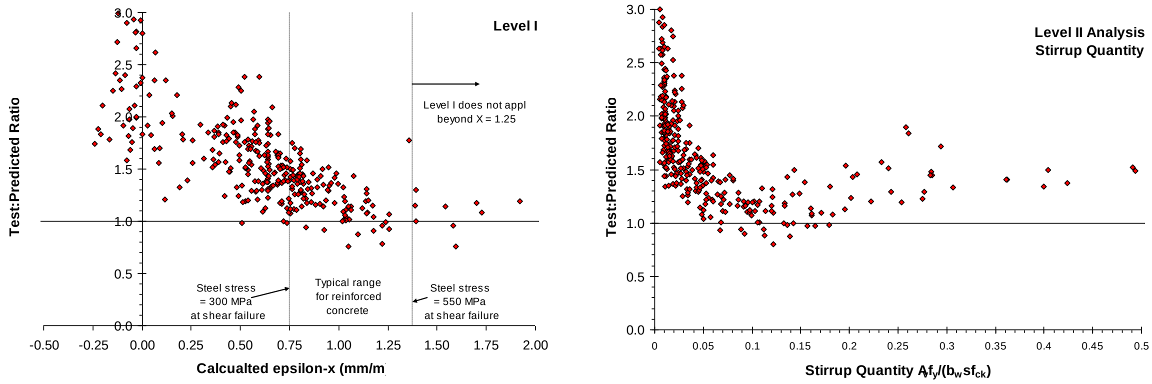

Fig. 2.11: Quality of Level I and Level II predictions for members with stirrups

Level of Approximation		Data Subset	Observed / Predicted Shear Strength Ratios # of Tests	Mean	C.o.V.	5th %ile
Level I	With stirrups	All	334	1.48	19.1%	1.02
		Practical	107	1.28	16.5%	0.93
	No stirrups	All	1725	2.10	22.4%	1.33
		Practical	149	1.39	18.1%	0.97
	All Members	All	**2059**	**1.97**	**23.5%**	**1.21**
	All Practical	Practical	**252**	**1.34**	**17.6%**	**0.95**
Level II	Stirrups only	All stirrups	**334**	**1.54**	**19.7%**	**1.04**
		Practical	**54**	**1.18**	**14.3%**	**0.91**
Level III	With stirrups	All	334	1.24	15.5%	0.93
	No stirrups	All	1921	1.27	15.1%	0.96
	All Members	All	**2255**	**1.27**	**15.1%**	**0.95**

Notes:
Statistical properties calculated based on a normal curve-fit to the least conservative half of the data
All a/d ratios are included for members without stirrups, a/d ratios > 2.5 for members with stirrups
Uniformly loaded members included for members without stirrups, point loads only for stirrups
Continuous members included in both datasets, Axial load and prestress for members with stirrups
For Level I, 600 MPa limit on fy applied. Code limit = 500 MPa
For Level I, aggregate size limit and concrte strength limit were ignored
For Level I, Practical tests have between 350 and 550 MPa in flexural steel at predicted shear failure
For Level II, Practical tests have a stirrup reinforcement index between 0.10 and 0.25

Table 2.1: Summary of statistical comparisons

Table 2.1 shows all of the statistical results combined into a single table. As can be seen, the 5th percentile values of all the subsets are sufficiently close to 1.0 to merit the designation of safe predictions. In general the coefficient of variations and means are larger for the lower Levels of Approximation and are lower for the higher levels of Approximation. Coupling these results with those from Response-2000 representing a Level IV analysis, Figure 2.12 is obtained. The graph on the left of the figure shows that when all tests in the database are compared, as the Level of Approximation is increased, the mean test to predicted ratio approaches 1.0. It is also shown that the 5th percentile value is also close to being uniform across this range and at a value of about 1.0. Of course, for a Level IV analysis, it is usually intended that average behaviour will result, and thus the 5th percentile for that case can be expected to be lower than unity. If only the “practical tests” are included in the comparison, it can be seen that all 4 Levels of Approximation provide good shear designs on the right side plot of Fig. 2.12. To reiterate, for Level I, the practical members are defined as members that are expected to fail in shear with between 300 and 550 MPa in the longitudinal reinforcement independently of the quantity of stirrup reinforcement. For Level II, the practical tests are those with high levels of stirrup reinforcement independently of the demand on the longitudinal reinforcement. For Level III, the results are excellent for all input parameters compared.

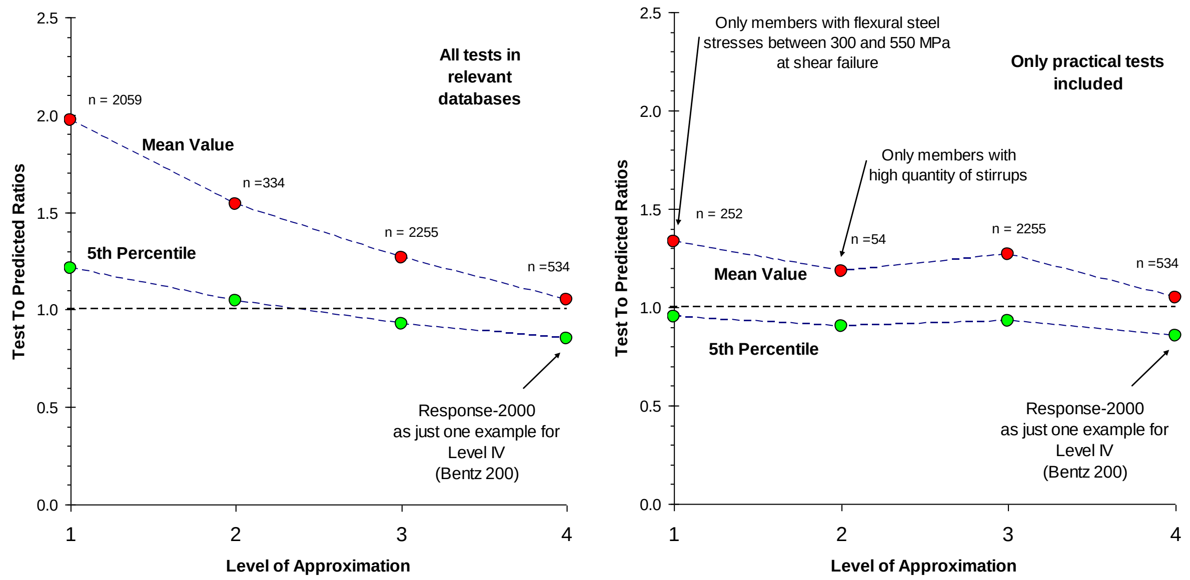

Figure 2.12: Comparison of different Levels of Approximation

2.6 Conclusions

This paper has summarized the background and use of the shear equations in the 2010 Draft Model Code. The concept of the Level of Approximation has been presented, and the equations for each level of approximation were shown. The concept of the Level of Approximation for shear essentially defines how the values of θ and k_v are to be determined, the two key parameters for the stirrup component to shear strength, and the concrete component to shear strength respectively. With a Level I approximation, these two values are constants for members with stirrups, and are a function of the member size for members without stirrups to capture the size effect in shear. For Level II analyses, k_v is taken as zero meaning that this method is only applicable to predict the strength of members with stirrups. The θ value must fall within a range that depends on the longitudinal strain at mid-depth, ε_x making this method a modified-plasticity approach. For Level III designs, the two parameters are both a function of the strain, and generally they must be solved for in a spreadsheet or computer program. A Level IV analysis would generally require a computer program.

The Levels of Approximation are not only in the order they are due to the quality of the predictions they produce, See Fig. 2.12, but also due to the complexity of applying the methods. Level I requires no intermediate calculations by the engineer. For Level II, the engineer must confirm that the angle θ is selected within a range that is a function of strain, and thus this strain must be calculated. For level III, the strain is required to produce any predictions, and thus this method requires the most computational effort to calculate. Overall, excellent shear strength predictions can be obtained, perhaps even rivalling those obtained from flexural calculations.

2.7 References

AASHTO 2010. LRFD Bridge Design Specifications and Commentary, Third Ed. with updates, American Association of State Highway Transportation Officials, Washington, D.C.

Bentz, E.C., 2000, "Sectional Analysis of Reinforced Concrete Members," PhD Thesis, Department of Civil Engineering, University of Toronto, Canada, 210 pp. http://www.ecf.utoronto.ca/~bentz

Bentz, E.C., and Collins, M.P., 2006 "Development of the 2004 CSA A23.3 Shear Provisions for Reinforced Concrete," Canadian Journal of Civil Engineering, 33(5), pp.521-534.

Bentz, E.C., Vecchio, F.J., and Collins, M.P., 2006, "The Simplified MCFT for Calculating the Shear Strength of Reinforced Concrete Elements", ACI Struct J, 103(4), pp.614-624.

Collins, M.P., 1978, "Towards a Rational Theory for Reinforced Concrete Members in Shear," Journal of the Structural Division, ASCE, 104(4), pp. 649-666.

Collins, M.P., Bentz, E.C., and Sherwood, E.G., 2008, "Where is Shear Reinforcement Required? Review of Research Results and Design Procedures", ACI Journal, 105(5), pp. 590-600.

CSA Committee A23.3, 2004, "Design of Concrete Structures (CSA A23.3-04)," Canadian Standards Association, Mississauga, 214 pp.

fédération internationale du béton (*fib*), 2010. *fib* Bulletin 55, Model Code 2010 – First complete draft, Volume 1, 318 pp.

fédération internationale du béton (*fib*), 2010. *fib* Bulletin 56, Model Code 2010 – First complete draft, Volume 2, 312 pp.

Higgins, C., Potisuk, T., Farrow, W.C., Robelo, M., McAuliffe, T.K., Nicholas, B.S., 2007, "Tests of RC Deck Girders with 1950s Vintage Details," ASCE Jrnl of Bridge Eng., 12(5), pp. 621-631.

Muttoni, A., 1989, The applicability of the theory of plasticity in the design of RC (in German, Die Andwendbarkeit der Plastizitätstheorie in der Bemessung von Stahlbeton), IBK 176, ETH Zürich, 159 p.

Nielsen M. P., 1971, "On the Strength of Reinforced Concrete Discs," Acta Polytechnica Scandinavica, Civil Engineering and Building Construction Series No. 70, Copenhagen, Denmark, 261 p.

Sigrist V., 1995, On the deformation capacity of reinforced concrete girders, (German: Zum Verformungsvermögen von Stahlbetonträgern), Diss., IBK, ETH Zürich, Switzerland, 160 pp.

Thurlimann B., 1979, "Shear Strength of Reinforced and Prestressed Concrete-CEB Approach," ACI, Special publication, Volume 59, pp. 93-116.

Vecchio, F.J. and Collins, M.P., 1986 "The Modified Compression Field Theory for Reinforced Concrete Elements Subjected to Shear," ACI Journal, 83(2), 219-231.

Walraven, J.C., 1981, "Fundamental Analysis of Aggregate Interlock," Journal of the Structural Division, ASCE, 107(ST11), pp 2245-2270.

3 MC2010: The Critical Shear Crack Theory as a mechanical model for punching shear design and its application to code provisions

Aurelio Muttoni[1] and Miguel Fernández Ruiz[2]

[1] Prof. Dr., École Polytechnique Fédérale de Lausanne, Switzerland
[2] Dr., École Polytechnique Fédérale de Lausanne, Switzerland

Abstract: This chapter presents the fundamentals of the Critical Shear Crack Theory. This theory is based on a mechanical model and grounds the punching shear provisions of the first complete draft of Model Code 2010. The chapter discusses its main hypotheses and mechanical parameter and compares its results to experimental data, providing confirmation of its accuracy and generality. The chapter also shows how the theory can consistently be used to a number of different applications by suitably evaluating the various mechanical parameters of the model in each case. Reference to a design example using the punching shear provisions of the draft of Model Code 2010 is also provided.

3.1 Introduction

The strength and deformation capacity of flat slabs supported by columns is typically governed by their punching shear strength. Failures in punching can be very brittle (for slabs without transverse reinforcement and with moderate to large amounts of flexural reinforcement) and their limited capacity for redistribution of internal forces can lead to the progressive collapse of the structure [Muttoni et al. (2008b)].

Due to the significance of this failure mode, punching shear has been the object of intense experimental and theoretical efforts since the 1950's. In the past, several approaches have been developed (an extensive review on the most significant approaches can be found in [*fib* (2001), Pollak et al. (2005)]). These methods are either based on empirical approaches (fitting to experimental evidence) or on mechanical models (based on physical theories). Although mechanical models are more consistent and provide the engineer with an understanding of the physical phenomenon of punching shear, a number of current design codes [EC-2 (2004), ACI 318 (2008)] are still based on empirical models for simplicity reasons.

The Model Code 90 [CEB (1993)] was also based on an empirical model with reference to punching shear design. The provisions for the new Model Code 2010 [*fib* (2010a,b)] have however been significantly modified in order to ground the code provisions on a physical model, the Critical Shear Crack Theory (CSCT). This theory allows considering shear and punching shear behaviour in members with and without transverse reinforcement and its use for design has shown to be simple and to provide accurate results (even more than empirical models [Muttoni (2008)]).

The basic principles of the CSCT were introduced for the first time in the Draft code proposal of the Swiss code for structural concrete SIA 162 [Muttoni (1985)]. These theoretical findings [Muttoni and Schwartz (1991)] were the basis of the approach for slabs without transverse reinforcement in the Swiss code SIA 162 [SIA (1993)]. Further improvements of the theory for shear in one- and two-way slabs [Muttoni (2003)] were also included into the new version of the Swiss code for structural concrete SIA 262 [SIA (2003)], which can be considered to be fully based on this theory with respect to shear design of members without stirrups. A series of recent experimental and theoretical works have provided justification of its mechanical model [Muttoni (2008), Muttoni and Fernández Ruiz (2008), Guidotti (2010)] and have also extended its use to members failing in shear after development of plastic strains in the flexural reinforcement [Guandalini et al. (2009), Vaz Rodrigues et al. (2010)], shear-reinforced slabs [Fernández Ruiz and Muttoni (2009), Fernández Ruiz et al. (2010)], punching of bridge deck slabs [Vaz Rodrigues et al. (2008)], punching of slab-column joints under high column loads [Guidotti et al. (2010)], punching under non axis-symmetric conditions [Sagaseta et al. (2010)] or prestessed slabs [Clément and Muttoni (2010)].

It is interesting to note that, since the theory is based on a physical model, the accuracy on the strength estimate depends on the level of approximation of the hypotheses applied to the mechanical model. Taking advantage of this fact, the CSCT has been implemented into the new Model Code draft following a levels-of-approximation approach, see Figure 3.1.

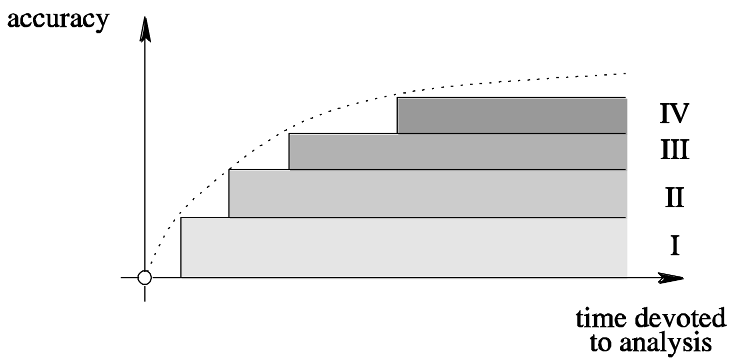

Fig. 3.1: Expected accuracy as a function of time devoted to analysis [Schertenleib et al. (2003)]

Such approach [Schertenleib et al. (2003), Muttoni and Fernández Ruiz (2010)] proposes to adopt simplified and safe hypotheses for design of new structures. This allows one obtaining safe (but sufficiently accurate) designs with a low effort of calculation. For the assessment of existing structures or in some cases for design of complex structures, the accuracy of the strength estimate can be gradually increased by refining the hypotheses on the mechanical model. This requires devoting more time to the analysis, but allows increasing the accuracy of the estimate of the strength and may avoid expensive strengthening or retrofitting.

The results of the CSCT have been checked against tests found in the literature as well as 146 punching shear tests specifically performed at École Polytechnique Fédérale de Lausanne over the past 10 years. These tests have been carried on specimens with size and loading conditions similar to those of actual flat slabs (typical specimen size of 3.0×3.0×0.25 m). Thanks to these test campaigns, the main hypotheses of the theory have been validated and some behaviours predicted by the theory (as the slenderness effect or the activation of the shear reinforcement in flat slabs) have been confirmed.

In this paper, the mechanical model of the CSCT is thoroughly explained and justified as well as the main hypotheses typically adopted for design of new structures. On that basis, it is explained how the theory can also be consistently used for non conventional cases, by accounting for the peculiarities of each situation in the mechanical parameters of the model. The paper also discusses the applications of the theory to design of practical cases (a detailed example can be found in [Lips et al. (2010)]).

3.2 The fundamentals of the Critical Shear Crack Theory and its application to punching of flat slabs

3.2.1 Shear strength on the basis of a physical model

The critical shear crack theory was based on the assumption that the shear strength in members without transverse reinforcement is governed by the width and by the roughness of a shear crack which develops through the inclined compression strut carrying shear [Muttoni (2008), Muttoni and Fernández Ruiz (2008)], see Figure 3.2.

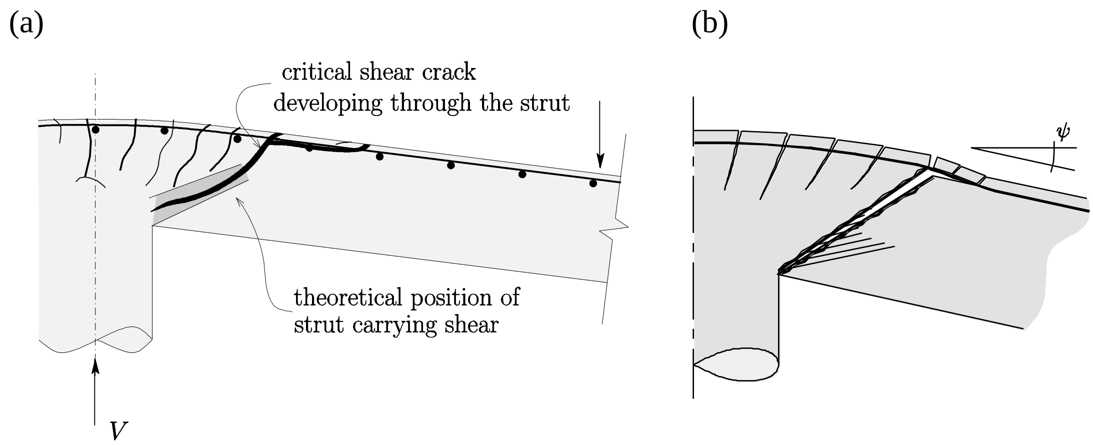

Fig. 3.2: Critical shear crack developing through the compression strut: (a) position of the strut and of the critical shear crack according to Muttoni (2008); and (b) analysis of the direction and load carried by the compression strut according to Guidotti (2010)

The shear strength under this assumption can be calculated by assuming a free-body with kinematics at failure characterized by the rotation of the slab (developed in agreement to test measurements, [Guidotti (2010)]), see Figs. 3.2b and 3.3a. Assuming such kinematics, not only tensile stresses but also stresses due to aggregate interlocking (relative slip between the lips of the crack) develop along the critical shear crack. The shear strength can thus be calculated by integrating both contributions (concrete in tension and aggregate interlock) along the failure surface. It can be noted that dowel action is neglected due to spalling of the concrete cover of the flexural reinforcement (Fig. 3.3a).

As Figs. 3.3c,d show, the contribution of concrete in tension is significant only for limited rotations (Fig. 3.3c), the behaviour being dominated by aggregate interlocking thereafter (Fig. 3.3d). The punching shear strength calculated using this procedure is plotted as a function of the rotation of the slab for a wide range of cases in Fig. 3.4 [Guidotti (2010)]. The plot is normalized in both axes to account for support region size, concrete compressive strength, depth of the member and aggregate size. It can be noted that the punching shear strength decreases for increasing rotations (opening of the critical shear crack). This is logical since wider cracks reduce both the concrete in tension and aggregate interlock contributions. It is also interesting to note that, in Fig. 3.4, failures occur in a well-defined and rather narrow band for all cases [Muttoni (1985)].

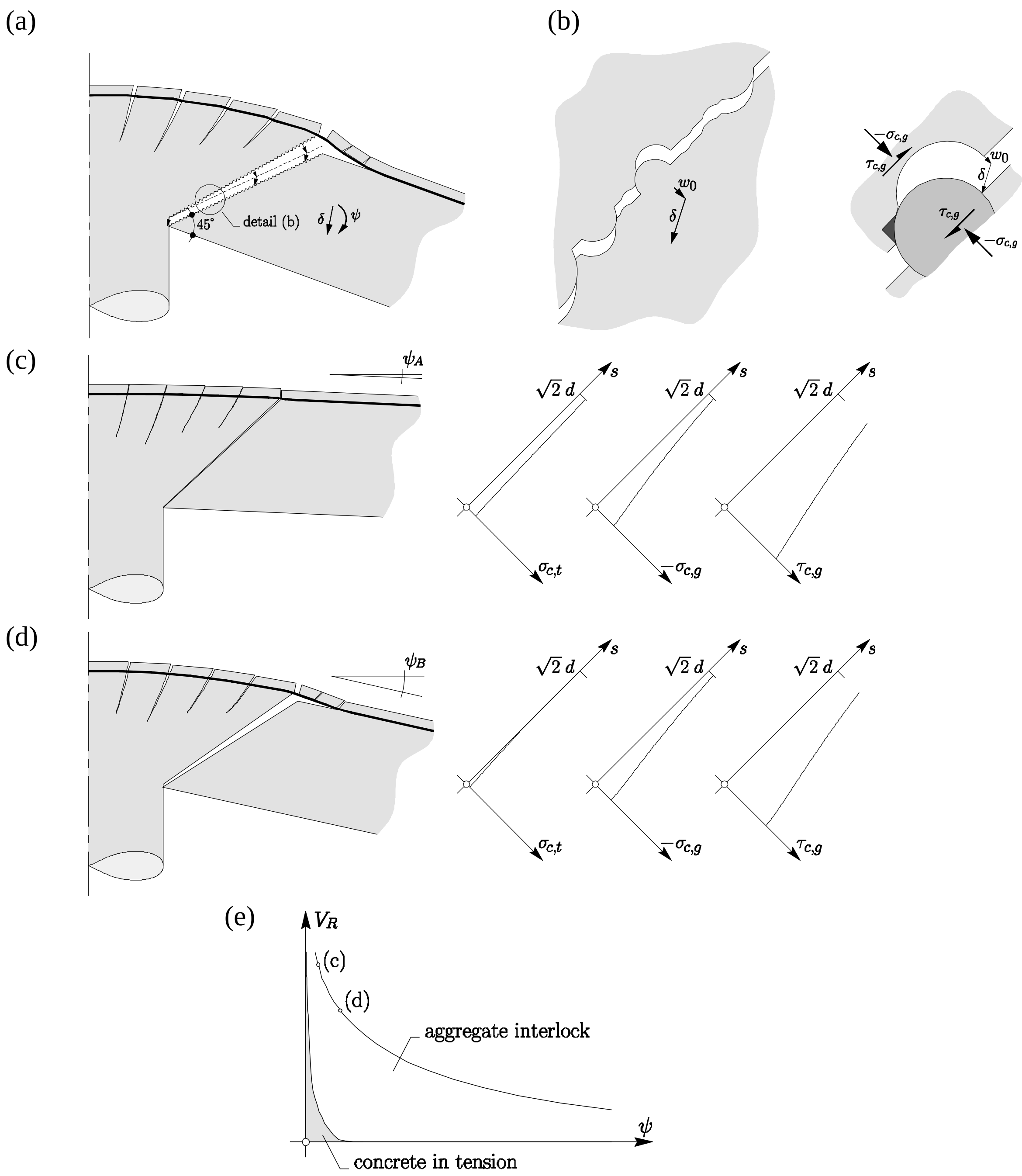

Fig. 3.3: Theoretical derivation of the punching shear strength: (a) free-body and assumed kinematics at failure; (b) aggregate interlock activation; (c) concrete in tension and aggregate interlock contributions for small rotations; (d) concrete in tension and aggregate interlock contributions for large rotations; and (e) punching shear strength and shear-carrying contributions of aggregate interlock and concrete in tension for cases (c) and (d) as a function of the rotation of the slab

For design purposes, and accounting for the narrow width of the failure band, the general calculation of the failure envelopes through the integration of concrete in tension and aggregate interlock contributions is not necessary. For these cases, a simplified failure criterion was proposed by Muttoni (2003,2008). It assumes that the punching shear strength (traditionally correlated to the square root of the concrete compressive strength after the works of Moody et al. (1954)) is a function of the width and of the roughness of a shear crack as justified by the previous mechanical model:

$$\frac{V_R}{b_0 \cdot d_v} = \sqrt{f_c} \cdot f\left(w, d_g\right) \tag{3.1}$$

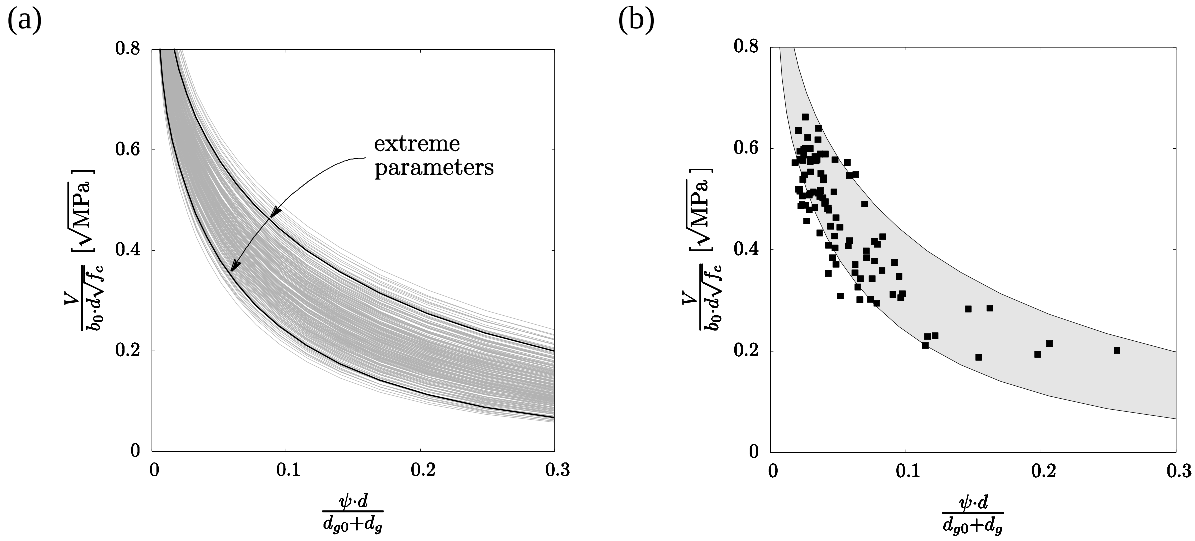

Fig. 3.4: Failure envelopes for reinforced concrete slabs as a function of the slab rotation: (a) results for specimens with effective depth ranging 95–450 mm (h=100–500 mm), flexural reinforcement ratio ranging 0.4–1.6%, concrete strength ranging 15–60 MPa, aggregate size ranging 8–32 mm and column diameter ranging, 100–200 mm; and (b) comparison of failure band to test results on 99 punching shear tests (data from [Muttoni (2008)])

In this expression V_R is the shear strength, b_0 is a control perimeter (set at $d/2$ of the edge of the support region for punching shear), d_v is the shear-resisting effective depth of the member (distance between the centroid of the flexural reinforcement and the surface at which the slab is supported), f_c is the compressive strength of the concrete, w is the width of the critical shear crack and d_g is the maximum size of the aggregate (accounting for the roughness of the lips of the cracks). In order to evaluate the width of the critical shear crack (w), [Muttoni (1991)] assumes it to be proportional to the slab rotation (ψ) times the effective depth of the member (see Fig. 3.5):

$$w \propto \psi \cdot d \tag{3.2}$$

Based on these assumptions, the following failure criterion was proposed by Muttoni (2003, 2008) for members without stirrups:

$$\frac{V_R}{b_0 \cdot d_v \cdot \sqrt{f_c}} = \frac{3/4}{1+15 \dfrac{\psi \cdot d}{d_{g0}+d_g}} \tag{3.3}$$

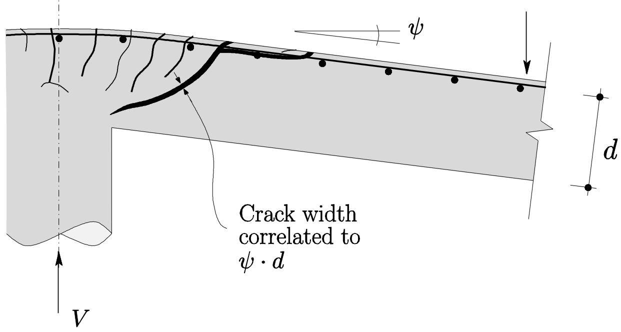

Fig. 3.5: Opening of critical shear crack as a function of slab rotation and effective depth of the member

where d_{g0} is a reference aggregate size equal to 16 mm. Eq. (3.3) is compared in Fig. 3.6a to the failure band calculated on the basis of the mechanical model, showing good agreement. A comparison of the simplified failure criterion to the test results of 99 punching tests on slabs [Muttoni (2008)] is also given in Figure 3.6b. For design purposes a characteristic failure criterion has to be adopted (target 5% fractile, refer to Muttoni (2008), and Model Code 2010 Eq. (7.3-41) [*fib* (2010b)]).

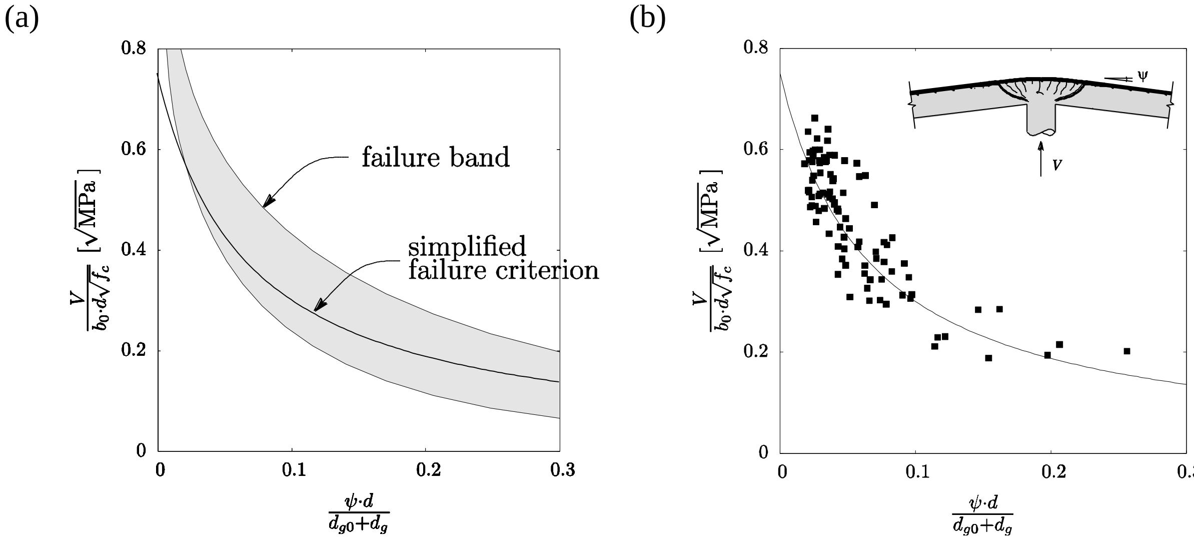

Fig. 3.6: Simplified failure criterion of CSCT: (a) failure band and simplified design criterion; and (b) comparison of failure criterion to 99 tests (data according to Muttoni (2008))

The comparison shows an excellent correlation between theory and experiments, with a very small coefficient of variation. These results are typically better than those obtained with some codes of practice [ACI 318 (2008), EC2 (2004)] as shown by Muttoni (2008).

3.2.2 Applications to slabs without shear reinforcement

The punching shear strength of a slab without shear reinforcement can be directly calculated using the CSCT failure criterion (Eq. 3.3). To do so, the intersection between the failure criterion and the actual behaviour of the slab (characterised by its load-rotation curve) has to be calculated, refer to point A in Fig. 3.7.

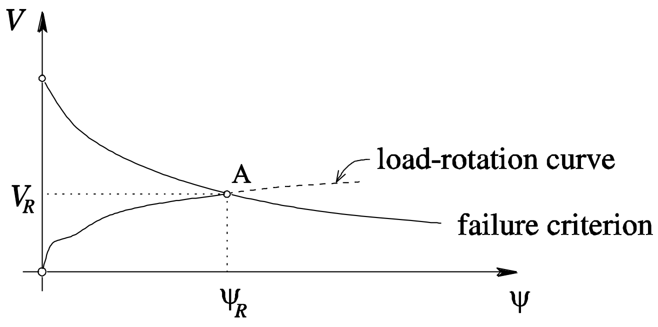

Fig. 3.7: Calculation of punching shear strength for members without shear reinforcement

It can be noted that following this procedure allows one to calculate not only the punching strength but also to estimate the deformation capacity (rotation) at failure. This provides valuable information to the designer on the behaviour of the structure (ductility, brittleness). Moreover, the rotation (as an estimate of the shear crack opening) can be used to calculate the activation of the transverse reinforcement for shear-reinforced slabs or to estimate the contribution of fibres to the punching shear strength. These topics will be discussed later in this paper.

Various methods can be used to estimate the load-rotation behaviour:

- Formulas based on an analytical integration of the moment-curvature law of the slab [Muttoni (2008)]
- Simplified formulas derived on the basis of the analytical formulas [Muttoni (2008)]
- Integration of moment-curvature laws by numerical procedures (finite differences [Guandalini (2005)] or finite elements [Vaz Rodrigues (2007)]

These methods have different scopes and applications. Simplified formulas typically provide safe estimates of the actual behaviour and are thus mostly used for design. In the draft document of the new model code, the following expression according to Muttoni (2008) has been adopted:

$$\psi = 1.5 \cdot \frac{r_s}{d} \frac{f_{yd}}{E_s} \cdot \left(\frac{m_{sd}}{m_{Rd}} \right)^{1.5} \tag{3.4}$$

where r_s refers to the distance from the column axis to the line of contraflexure of radial bending moments (approximately equal to 0.22 times the span length for regular flat slabs), f_{yd} is the yield strength of the flexural reinforcement, E_s is the value of the modulus of elasticity of steel, m_{sd} is the average moment per unit length for calculation of the flexural reinforcement in the support strip and m_{Rd} is the average flexural strength per unit length in the support strip. The ratio between measured-to-calculated punching shear strength for the tests of Fig. 3.6b results for the simplified load-rotation relationship equal to 1.07 with a CoV of 9% (significantly better than most design codes, Muttoni (2008)).

Numerical procedures provide more accurate results but require a certain level of experience and are usually rather time-consuming. Their use is thus normally restraint to the assessment of existing structures (where a more refined analysis can help in avoiding or reducing strengthening of the structure). It can be noted that developing suitable moment-curvature and axial force-in plane strains provides a general frame to investigate some phenomena like the increase of the punching shear strength in slabs with restricted horizontal expansion ([Guandalini (2005)], Fig. 3.8a), the behaviour and strength of flat slabs under fire conditions ([Guandalini (2005)], Fig. 3.8b) or the increase of the punching shear strength for slabs transferring large column loads [Guidotti (2010)].

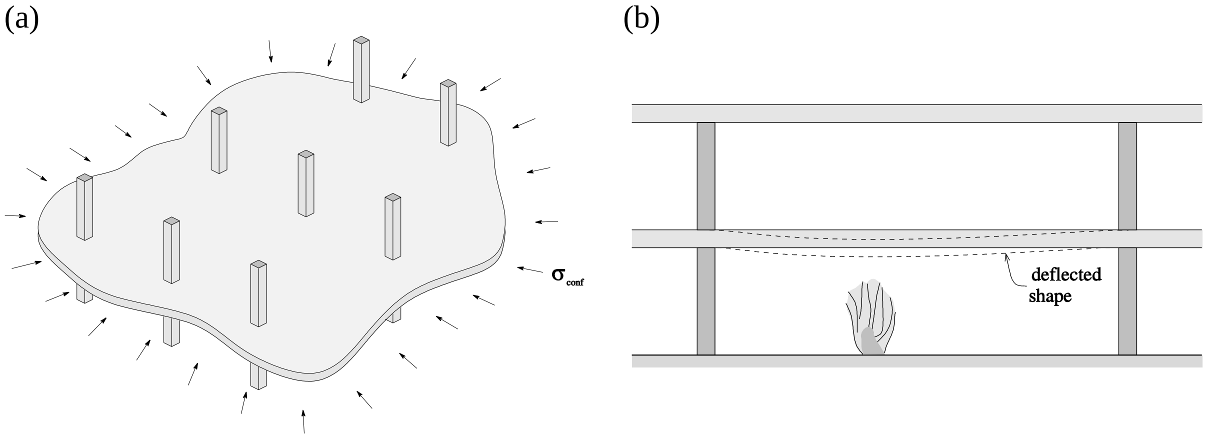

Fig. 3.8: Examples of complex structures investigated through numerical integration of moment-curvature laws [Guandalini (2005)]: (a) in-plane confinement; and (b) slab exposed to fire

3.2.3 Applications to slabs with shear reinforcement

The CSCT can also be used for members with transverse reinforcement [Fernández Ruiz and Muttoni (2009)]. To do so, the various potential failures modes need to be investigated (refer to Fig. 3.9):

- crushing of the concrete struts near the support region
- punching with development of a shear crack within the shear-reinforced zone and activation of the shear reinforcement
- punching outside the shear-reinforced zone

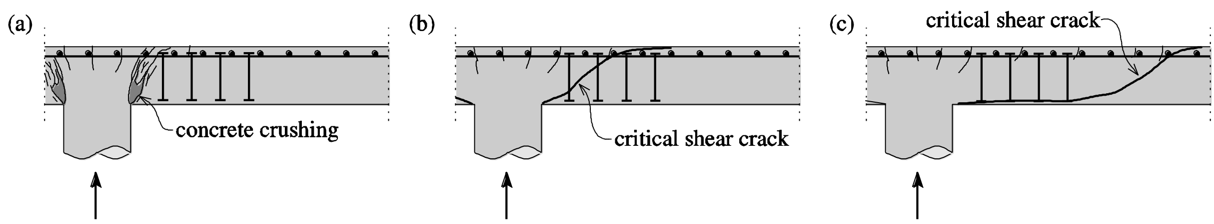

Fig. 3.9: Potential failure modes for shear-reinforced slabs: (a) crushing of concrete struts near the support region; (b) punching within the shear-rienforced zone; and (c) punching outside the shear-reinforced zone

In addition, other potential failure modes may be governing (delamination of concrete core, pull-out of shear reinforcement anchorages, flexural capacity…). They can however be treated within the same approach [Fernández Ruiz and Muttoni (2009), Fernández Ruiz et al. (2010)].

3.2.3.1 Punching outside the shear-reinforced zone

For large amounts of shear reinforcement concentrated in the immediate vicinity of the support region, punching may develop outside the shear-reinforced zone. This happens with development of a single crack localizing strains. The approach of the CSCT for members without shear reinforcement is thus applicable and Eq. (3.3) remains valid. It should be noted that the shear-resisting effective depth (d_v) depends on the geometry and anchorage conditions of the shear reinforcement, see Figure 3.10 and may significantly influence the shear strength.

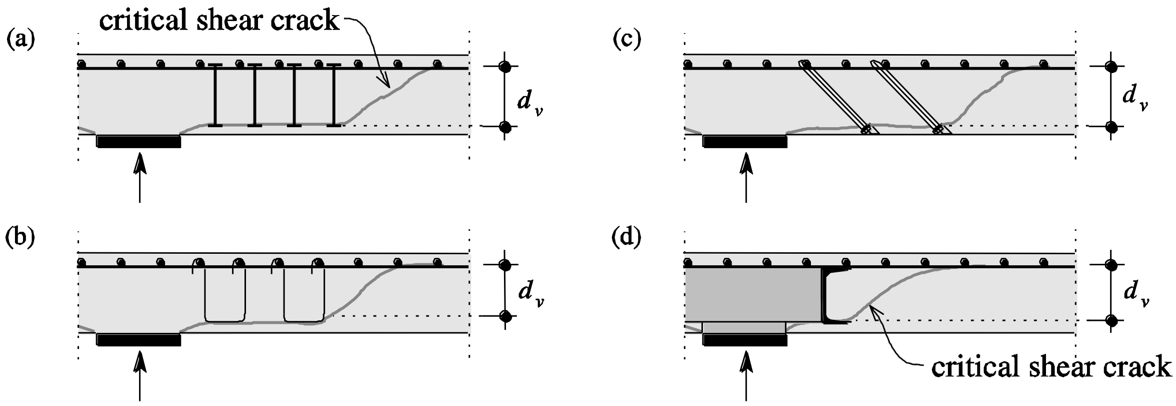

Fig. 3.10: Effective depth outside the shear-reinforced zone as a function of the punching shear reinforcing system: (a) studs; (b) stirrups; (c) bonded reinforcement with anchorage plates; and (d) shearheads

3.2.3.2 Punching within the shear-reinforced zone

For moderate or low amounts of shear reinforcement, punching within the shear-reinforced zone due to localization of strains in a single crack becomes governing. Along the failure surface, shear is carried not only by concrete but also by the shear reinforcement, see Fig. 3.11.

Thus, the punching shear strength can be calculated as the sum of the concrete ($V_{Rd,c}$) and shear reinforcement ($V_{Rd,s}$) contributions, see Fig. 3.11b:

$$V_{Rd} = V_{Rd,c} + V_{Rd,s} \tag{3.5}$$

It is interesting to note, see Fig. 3.11c, that the contribution of concrete decreases with respect to that of a member without punching shear reinforcement ($V_{Rd,c0}$). This is logical because, as the punching strength increases, the deformation capacity (rotation) also increases, leading to wider cracks at ultimate and to a smaller shear capacity of concrete. Codes of practice based on empirical models (EC-2 (2004) or ACI 318 (2008)) also acknowledge this effect which they quantify with a constant reduction on the concrete contribution (25% and 50% respectively for EC-2 (2004) and ACI 318 (2008)). According to the CSCT, however, such decrease on the concrete contribution is not constant and depends on the amount of shear reinforcement and on its activation law. This leads to more accurate results and avoids adopting potentially unsafe (too low) decreases on the concrete shear-carrying capacity [Fernández Ruiz and Muttoni (2009)].

With respect to the contribution of the shear reinforcement ($V_{Rd,s}$) it results:

$$V_{Rd,s} = \sum A_{sw} k_e \sigma_{swd} \sin\alpha \tag{3.6}$$

where ΣA_{sw} is the sum of the cross-sectional area of all shear reinforcement suitably developed and intersected by the potential failure surface (where reinforcement closer than 0.35 d_v to the edge of the support region should not be accounted), α is the angle of the shear reinforcement with respect to the reference surface of the slab and σ_{swd} is the stress that can be mobilized in the shear reinforcement (coefficient k_e refers to eccentric loading and will be explained later in the paper).

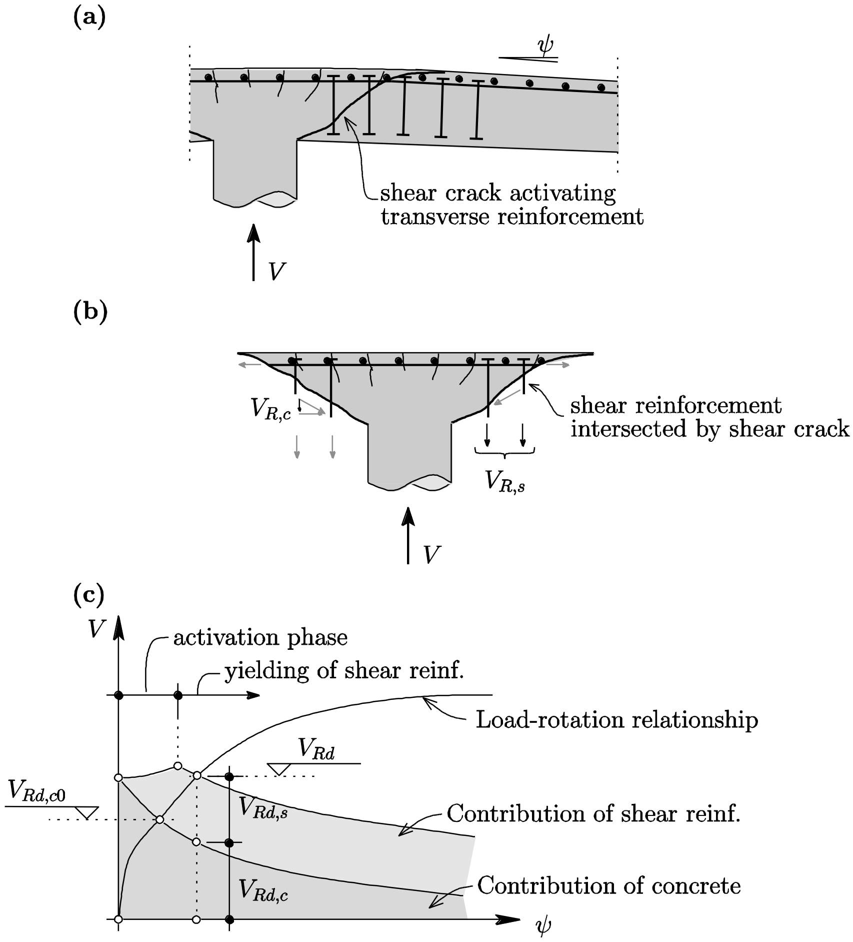

Fig. 3.11: Slabs with transverse reinforcement: (a) activation of shear reinforcement by a shear crack; (b) concrete and shear reinforcement contributions; and (c)

The calculation of σ_{sw} depends on the rotations of the slab and on the development conditions of the shear reinforcement. For increasing rotations, cracks become wider and the shear reinforcement increases its stress and shear-carrying capacity, refer to Fig. 3.11c. According to Fernández Ruiz and Muttoni (2009), the following relationship can be adopted for design:

$$w(\psi, h_i) = \kappa \cdot \psi \cdot h_i \tag{3.7}$$

where w refers to the opening of the critical shear crack at a height h_i from the distance from the soffit of the slab and κ is a coefficient relating total rotation and critical crack width opening (that can be chosen equal to 0.5 for design purposes [Fernández Ruiz and Muttoni (2009)]).

The maximum capacity of the shear reinforcement is limited by its yield strength or by the anchorage efficiency in some cases [Fernández Ruiz et al. (2010)]. According to Fernández Ruiz and Muttoni (2009), if bond between the shear reinforcement and the concrete is neglected (safe assumption for design), the contribution of the shear reinforcement can be estimated as:

$$\sigma_{swd} = \frac{E_s \psi}{6} \leq f_{ywd} \tag{3.8}$$

It can be noted that, although for design of new structures this formula provides sufficient accuracy, it is possible to consider in the activation of the shear reinforcement any condition influencing it. Applications to systems with different bond conditions, pull-out of anchorages and prestressing of the shear reinforcement have already been developed and can be found elsewhere [Fernández Ruiz and Muttoni (2009), Fernández Ruiz et al. (2010)].

3.2.3.3 Crushing of concrete struts near the support region

For large amounts of shear reinforcement spread over a sufficiently wide area, crushing of concrete struts governs the punching shear strength. As shown by Vecchio and Collins (1986), the crushing strength of concrete is highly influenced by its transverse state of strains (opening of cracks in the shear-critical region). According to the hypothesis of the CSCT that the width of the shear cracks can be estimated as a function of the slab rotation (Eq. (3.2)), the crushing shear strength can also be calculated as a function of it. On the basis of this assumption, Fernández Ruiz and Muttoni (2009) proposed to estimate the crushing shear strength proportional to the punching shear strength as:

$$\frac{V_R}{b_0 \cdot d_v \cdot \sqrt{f_c}} = \lambda \frac{3/4}{1 + 15 \dfrac{\psi \cdot d}{d_{g0} + d_g}} \tag{3.9}$$

In this expression, parameter d_g (aggregate size) accounts for the width of the crushing zone where strains localize (shear band) and coefficient λ measures the performance of the shear reinforcing system to control crack widths in the shear-critical region. Coefficient λ depends much on the detailing rules and on the performance of the anchorage and bond conditions of the shear reinforcement system. According to Fernández Ruiz and Muttoni (2010), systems with almost perfect anchorage conditions can reach values of λ up to 3.0 or even more. On the contrary, systems with less performing anchorage conditions have values of λ typically ranging between 2 and 2.6. A comparison of the performance of various punching shear reinforcing systems for specimens failing by crushing of concrete struts is shown in Fig. 3.12. The figure shows that the punching shear strength can be increased by about 60% depending on the properties of the shear reinforcement of the systems investigated.

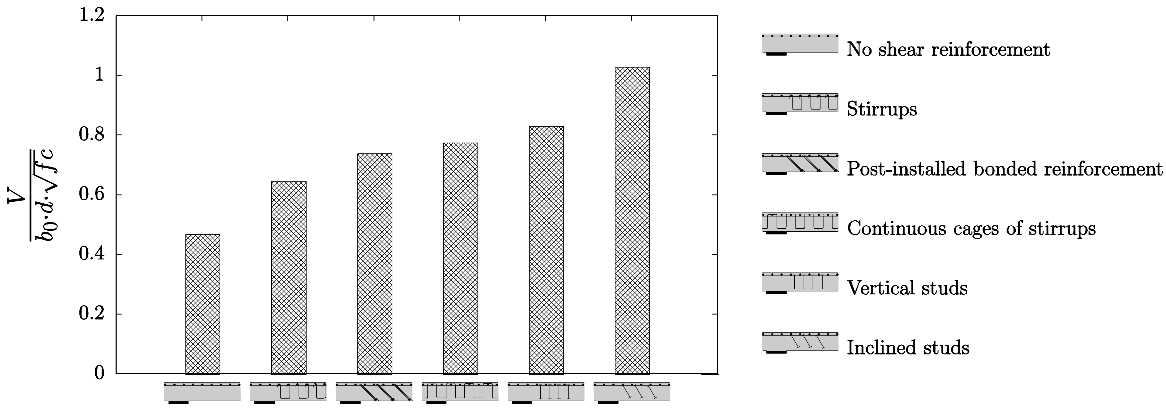

Fig. 3.12: Performance of punching shear reinforcing systems (test data according to Fernández Ruiz and Muttoni (2010))

The actual value of coefficient λ for a given punching shear reinforcing system can only be estimated accurately after evaluation of a number of test results [Fernández Ruiz and Muttoni (2010)]. In absence of experimental data, and for systems complying with the detailing rules provided in the model code draft, a safe estimate λ = 2.0 can be adopted for design.

3.2.3.4 Comparison to test results

Figure 3.13 shows a comparison of the CSCT to slabs with transverse reinforcement (according to the data presented in Fernández Ruiz and Muttoni (2009)). The predictions are very good, with a limited scatter (10% CoV) for a wide range of punching shear reinforcing systems and for all investigated failure modes. Further comparisons can be found in [Fernández Ruiz et al. (2010)].

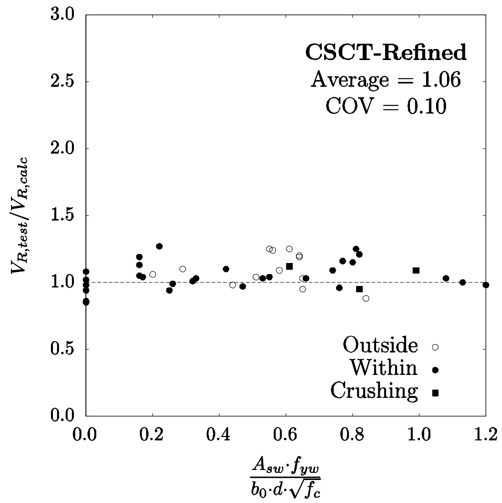

Fig. 3.13: Comparison of the CSCT to the tests presented in [Fernández Ruiz and Muttoni (2009)]

3.3 The use of the Critical Shear Crack Theory for non-symmetrical and for non-conventional cases

In section 3.2, the fundamentals of the theory have been presented and applied to inner columns without load eccentricity. However, since the approach is based on a physical model, it can be applied to general and rather complex problems. This can be consistently done by evaluating how the various mechanical parameters (critical crack width, reinforcement activation,…) are influenced in each situation. In the following, applications to a number of practical cases will be presented.

3.3.1 Columns with moment transfer, edge and corner columns

Although the theory has been presented for axisymmetric cases, its use for other loading or reinforcement conditions can be easily performed [Vaz Rodrigues et al. (2008), Sagaseta et al. (2010)]. Basically, when a moment is transferred from a column to a slab, this influences the punching shear strength with respect to two aspects:

- The distribution of shear forces around the support region is no longer constant. This fact is shown in Fig. 3.14, where the elastic shear fields for three tests performed by Kruger (1999) are shown. For the test with no load eccentricity (Fig. 3.14b) the distribution of the shear forces around the control perimeter is rather smooth and constant. On the contrary, as eccentricity increases, Figs. 3.14c,d, the shear field is no longer axisymmetric, and concentrations develop near the corners of the column.
- The distribution of bending moments, and thus of the width of the cracks potentially leading to a shear failure are also no longer constant along the control perimeter, and they increase on one side of the support region depending on the transferred moment, see Fig. 3.14e

The influence of non uniform distribution of shear forces around the basic control perimeter can be accounted for by reducing the basic control perimeter [*fib* (2010b)] to a shear-resisting control perimeter according to the following expression:

$$b_0 = \frac{V_d}{v_{perp,d,\max}} \tag{3.10}$$

where $v_{perp,d,max}$ refers to the maximum value of the projection of the shear force perpendicular to the basic control perimeter. Such reduction means performing design on the basis of the maximum shear force. This approach has proven to be safe but yet rather accurate [Vaz Rodrigues et al. (2009), Sagaseta et al. (2010)]. For design purposes, it is however sufficiently accurate [Muttoni et al. (2007)] to reduce the basic control perimeter by a coefficient (k_e) accounting for load eccentricity, whose value can be calculated as:

$$k_e = \frac{1}{1 + e_u / b_u} \tag{3.11}$$

where e_u is the load eccentricity with respect to the centroid of the basic control perimeter and b_u is the diameter of a circle with the same surface than the region inside the basic control perimeter.

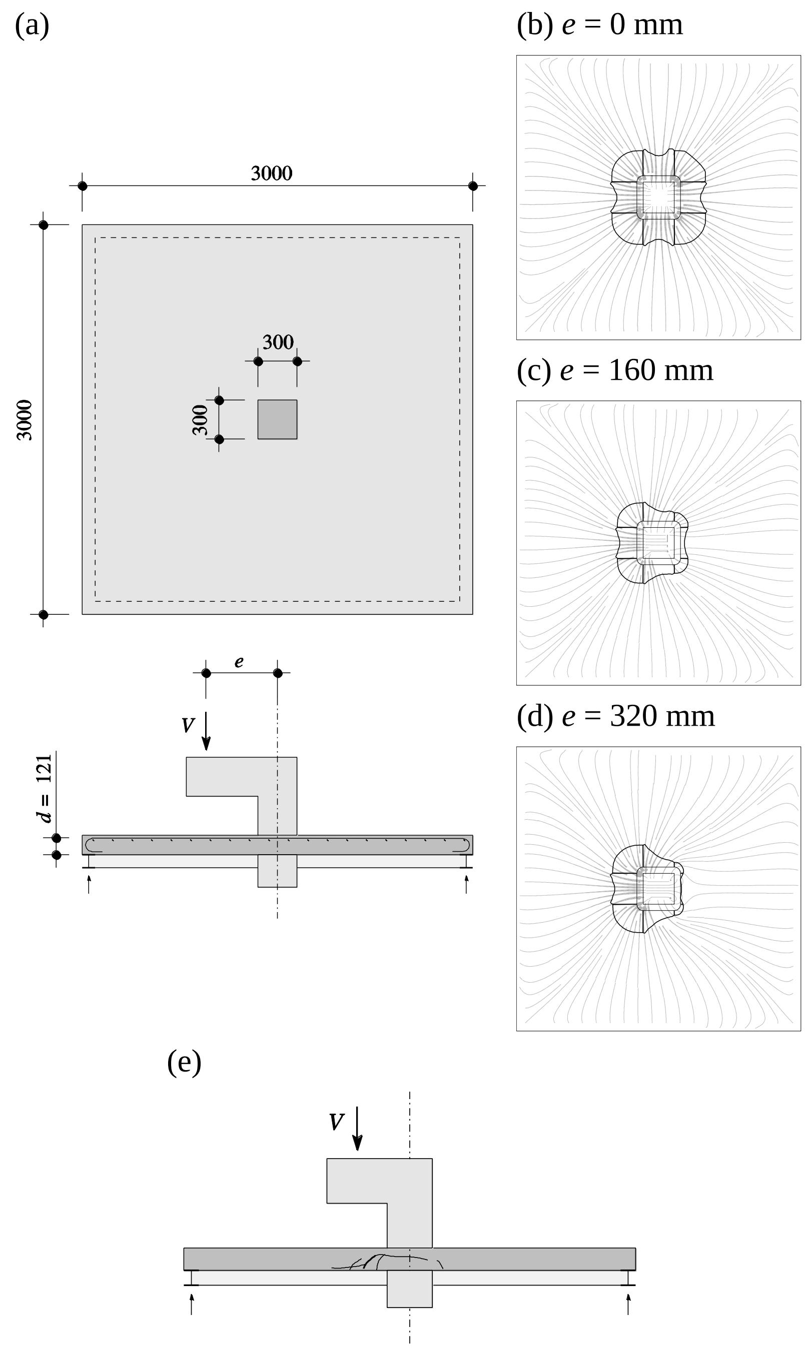

Fig. 3.14: Shear fields for slabs with inner columns with moment transfer: (a) geometry and loading conditions for tests from Kruger (1999); (b-d) shear fields and distribution of shear forces at the basic control perimeter for varying eccentricities (0, 160 mm and 320 mm respectively);and (e) saw cut of specimen P30A (e = 320 mm) after punching failure

The increase of the width of the cracks potentially leading to a shear failure is directly accounted for by the load-rotation relationship (Eq. (3.4)) as the term m_{sd} (average moment for calculation of flexural reinforcement at the support strip) increases for increasing transferred moments. This approach is equivalent to checking the punching shear strength with the maximum opening of the cracks developing at the shear-critical region. This assumption is safe and leads to rather accurate predictions [Sagaseta et al. (2010)]. More refined estimates accounting for shear and moment redistributions have been investigated elsewhere [Sagaseta et al. (2010)].

It can be noted that these effects (concentrations of the shear field and of the crack widths) also develop for corner and edge columns. A comparison of the CSCT with tests on slab specimens reproducing the geometry and loading conditions of inner columns with transferred moments, corner columns and edge columns is shown in figure 3.15. The results are given for levels two and three of approximation of Model Code's approach, and provide good and consistent agreement, significantly better than other design approaches such as EC-2, ACI 318 [Vocke (2002)].

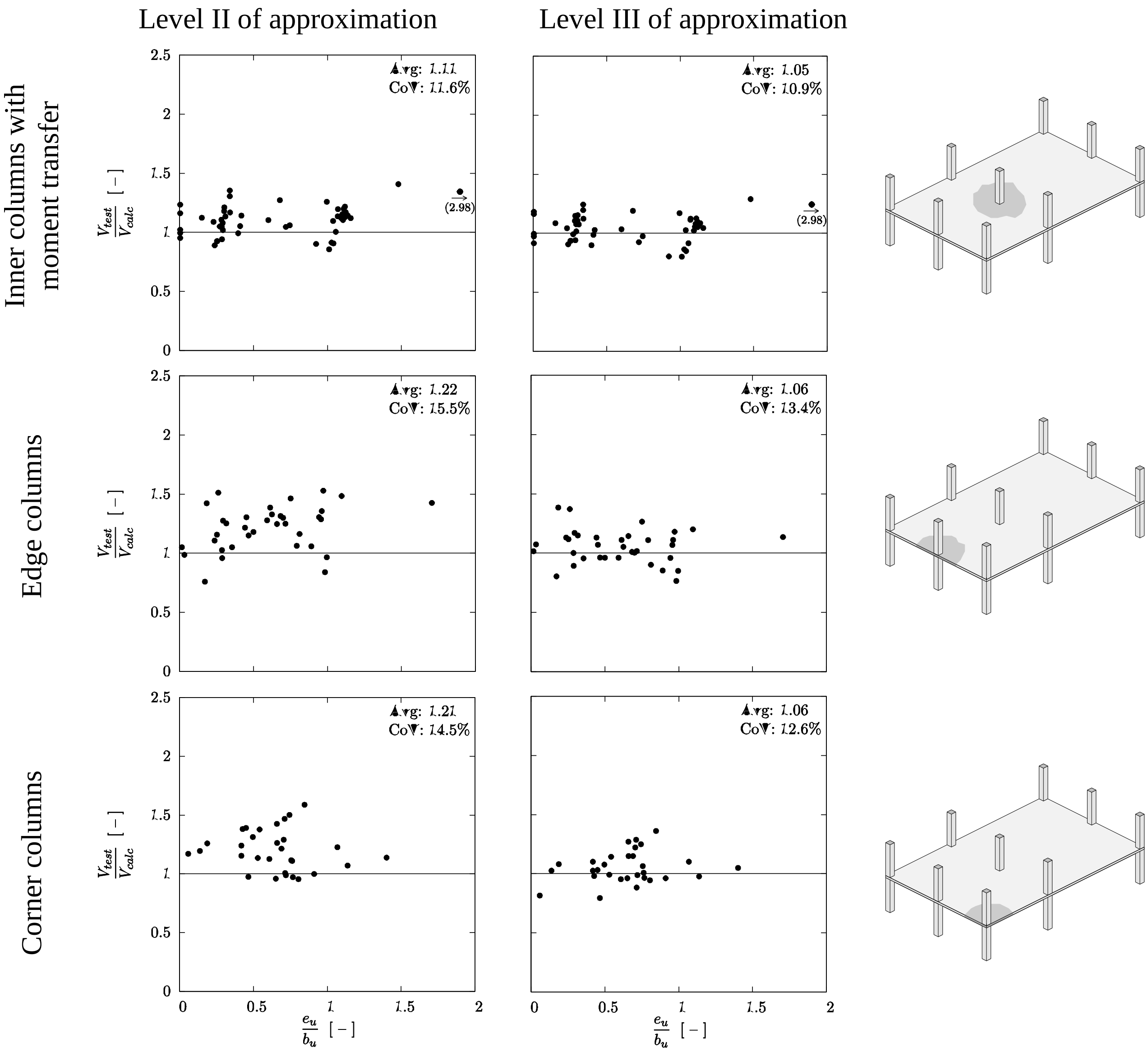

Fig. 3.15: Comparison of the CSCT with tests of flat slabs with varying moment transfer for inner, corner and edge columns. Tests on inner columns with moment transfer from Anis (1970), Elstner and Hognestad (1956), Hawkins et al. (1989), Kruger (1999) and Moe (1961). Tests on edge columns from Andersson (1966), Brändli (1985), Mortin and Ghali (1991), Narasimhan (1971), Regan et al. (1979), Sherif (1996), Sudarsana (2001), Hegger et al. (2006), Hegger and Tuchlinski (2006) and Kinnunen (1971). Tests on corner columns from Hammil and Ghali (1994),Regan et al. (1979), Sudarsana (2001), Vocke (2002), Zaghlool and Paiva (1973), Zaghlool et al. (1970), Ingvarsson (1974)

3.3.2 Applications to deck slabs of bridges

General applications of the CSCT can be performed to unusual geometries or loading conditions. This is for instance the case of the cantilever deck slab of bridges, where the shear field and developed rotations around the concentrated (wheel) loads differ notably from those of residential flat slabs supported by columns.

Some analytical relationships have been derived for determining the load-rotation curves in such cases [Fernández Ruiz et al. (2009)]. These are normally sufficient for design of new structures. For the assessment of critical existing bridges, however, it is preferable to follow the general approach based on the calculation of the nonlinear load-rotation relationship by integrating the moment-curvature behaviour of the slab. This procedure, which can be performed by using for instance the FEM, allows accounting for the influence of the various parameters such as the actual geometry (including the presence of kerbs) and the actual reinforcement in each direction and layer, see for instance Fig. 3.16 (Paudèze bridge, Switzerland, investigated in [Fernández Ruiz et al. (2009)]).

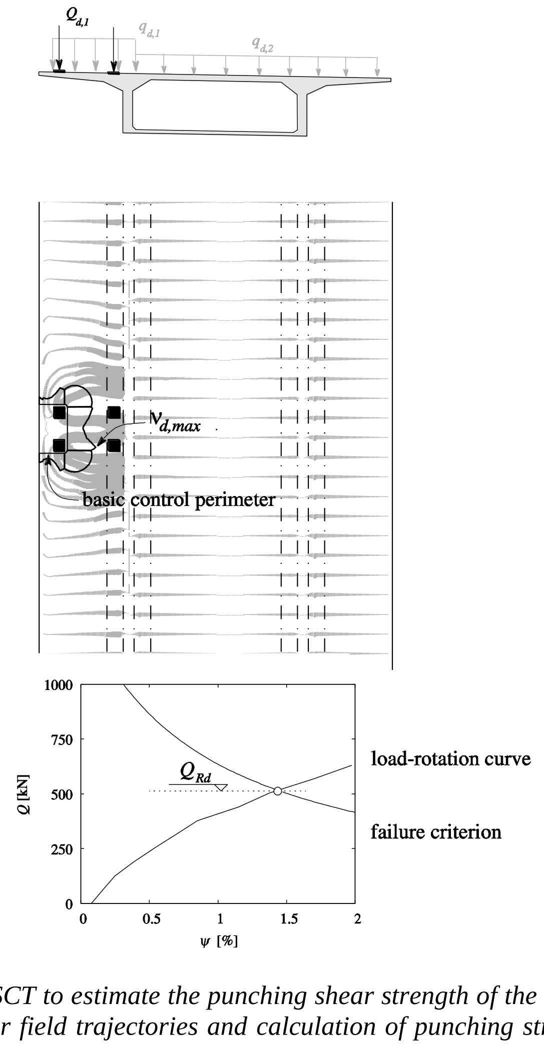

Fig. 3.16: Application of the CSCT to estimate the punching shear strength of the cantilever deck slab of an existing bridge: shear field trajectories and calculation of punching strength on the basis of the nonlinear load-rotation curve of the cantilever

The results of this approach have been verified experimentally on the basis of 6 tests performed on cantilever deck slabs subjected to concentrate loading [Vaz Rodrigues et al. (2007)]. All tests failed with the development of shear (inclined) failure surfaces (see side edge of slab in Fig. 3.17a), in a brittle manner and prior to reaching their flexural capacity, see Fig. 3.17b. A comparison of the CSCT approach to the test results of Vaz Rodrigues (2007) leads to good results in terms of deformation capacity and strength (average value of measured-to-calculated shear strength of 1.07 with a CoV of 13% using nonlinear analysis to determine the load-rotation curves).

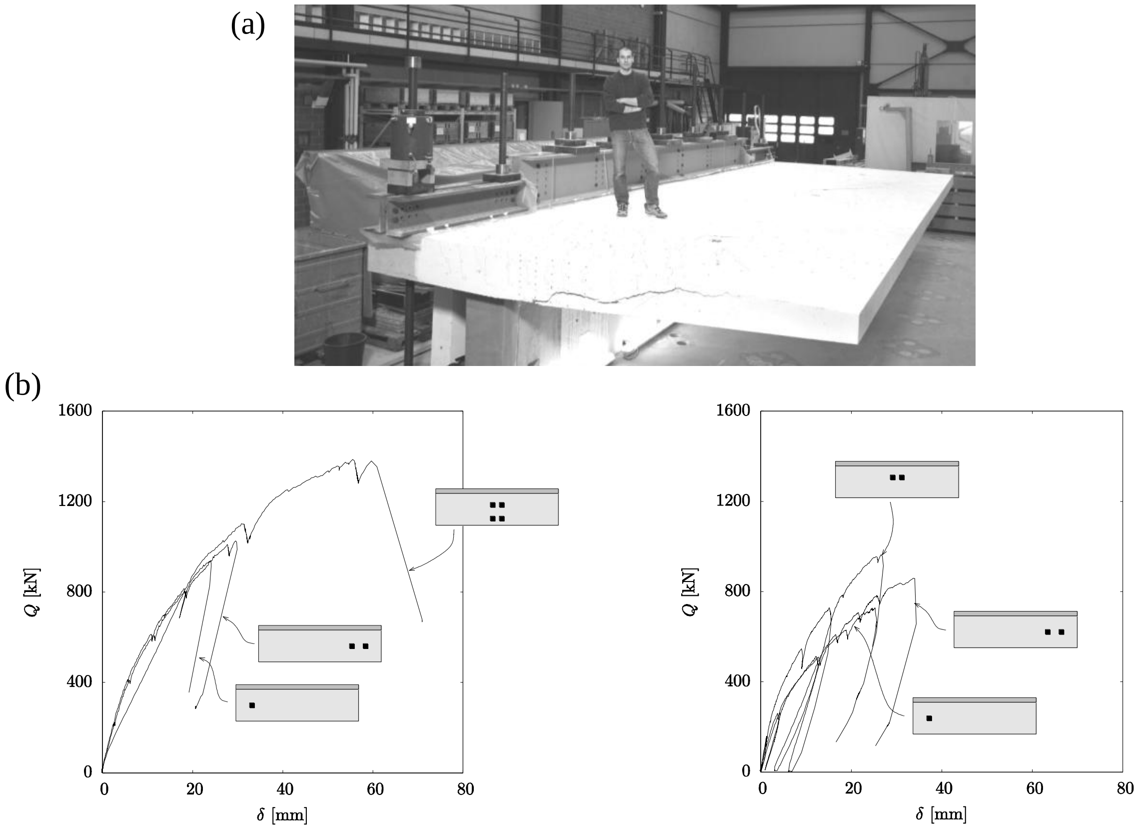

Fig. 3.17: Tests on cantilever deck slab of bridges at École Polytechnique Fédérale de Lausanne: (a) view of a specimen after failure (see shear crack at the side edge of the slab); and (b) load-deflection curves of cantilevers [Vaz Rodrigues (2007)]

3.3.3 Applications to non-conventional shear reinforcing systems

One of the main advantages of the physical model provided by the critical shear crack theory is that it allows extending its use to non conventional cases. As a practical application, Fig. 3.18a shows a post-installed shear reinforcement [Muttoni et al. (2008a), Fernández Ruiz et al. (2010)] used for strengthening of existing flat slabs against punching. The shear reinforcement is installed by drilling holes at 45° from the soffit of the existing slab, placing the shear reinforcement, sealing it with a high-performance mortar and installing the bottom anchorage nut.

The equation provided by the Model Code draft for the activation of the shear reinforcement (Eq. (3.8) of this paper) considers smooth bars (unbonded) with perfect anchorage conditions at their ends. This is rather different from the conditions of the system of Fig. 3.18, where the stresses in the shear reinforcement are governed by their bond conditions, refer to Fig. 3.18b. Additionally, other potential failure modes may develop, as pull-out cracks at the bottom anchorage, refer to Fig. 3.18c.

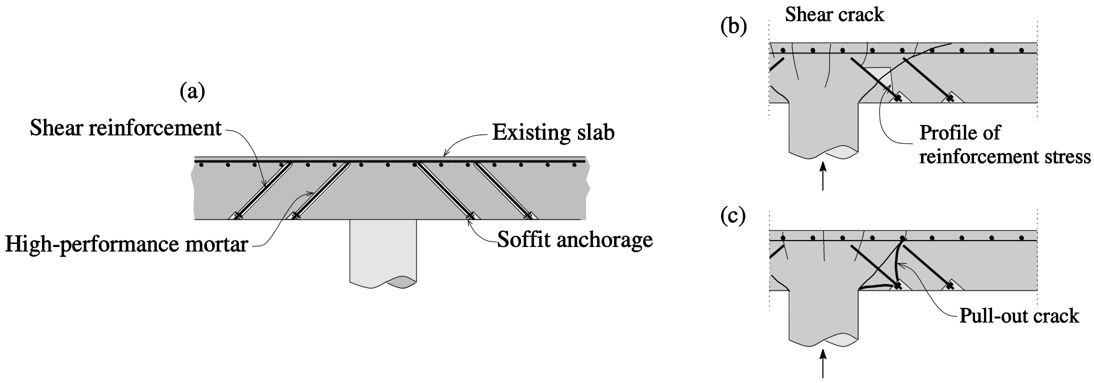

Fig. 3.18: Application of the CSCT to a post-installed shear reinforcement: (a) layout; (b) calculation of shear reinforcement stresses on the basis of bond conditions; and (c) pull-out of bottom anchorages

These considerations can however be easily considered for design by reworking the term σ_{sd} to include bond in the activation phase of the post-installed reinforcement and by limiting its strength to account for anchorage pull-out:

$$\sigma_{sw} = \min(\sigma_{s,el}; \sigma_{s,b}; \sigma_{s,p}; f_{yw}) \tag{3.12}$$

where $\sigma_{s,el}$ is the stress during the activation phase, $\sigma_{s,b}$ is the maximum stress that can be developed by bond, $\sigma_{s,p}$ is the maximum stress that can be developed by pull-out of the lower anchorages and f_{yw} is the yield strength of the steel. Assuming a rigid-plastic law for bond, $\sigma_{s,el}$ can be calculated prior to yielding as [Fernández Ruiz et al. (2010)]:

$$\sigma_{s,el} = \sqrt{\frac{4 \cdot \tau_b \cdot E_s \cdot w_b}{d_b}} \tag{3.13}$$

where τ_b refers to the bond strength of the mortar, d_b is the bar diameter, E_s is its modulus of elasticity and w_b is the opening of the critical shear crack at the level of the shear reinforcement (which can be calculated using the CSCT hypotheses, [Fernández Ruiz et al. (2010)]. With respect to the pull-out of bottom anchorages, their strength can be calculated on the basis of the concrete capacity design method [Fuchs et al. (1995)] but accounting for the size of the anchorage [Fernández Ruiz et al. (2010)].

A comparison of this approach against 12 tests performed on full-scale specimens (3.0 × 3.0 × 0.25 m) with post-installed reinforcement leads to excellent results (average value of the measured-to-calculated strength of 1.07 and a CoV of only 4%, [Fernández Ruiz et al. (2010)]). This example shows that adapting the CSCT to unusual cases (which are not covered by the design formulas of the code) can be performed in a simple and consistent way taking advantage of the mechanical model of the CSCT.

3.3.4 Strengthening of existing structures

The use the CSCT has revealed to be of particular interest for retrofitting of existing structures [Muttoni et al. (2008b)]. This is mostly due to the fact that the theory is based on a mechanical model that allows accounting for the behaviour of the slab at the moment of retrofitting and how this influences the behaviour and strength of the member after strengthening. Two examples are shown in Fig. 3.19, a slab retrofitted with bonded flexural reinforcement (Fig. 3.19a) and a slab retrofitted with post-installed shear reinforcement (Fig. 3.19b). For both cases, it is considered that the slab has a certain level of load at the moment of retrofitting (V_{SLS}, point A).

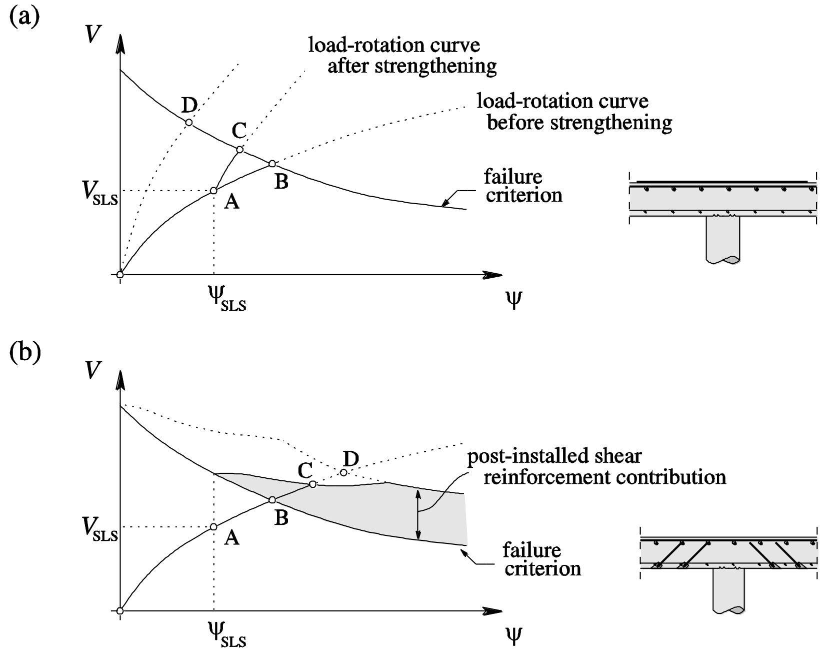

Fig. 3.19: Determination of strength and behaviour after strengthening: (a) flat slab reinforced with glued reinforcing strips; and (b) flat slab reinforced with post-installed shear reinforcement

With respect to the slab retrofitted with bonded flexural reinforcement (Fig. 3.19a), its load-rotation curve becomes stiffer after strengthening. Thus, with respect to the shear strength without strengthening (point B), the strength can be increased (point C). Such increase on the strength depends however significantly on the level of load on the slab at the moment of strengthening (being smaller in any case than that of a one of a new slab with the same amount of total flexural reinforcement, point D in Fig. 3.19a). It is also interesting to note that the behaviour of the slab will be more brittle (less rotation at failure at point C than at point B).

For slabs retrofitted with post-installed shear reinforcement (Fig. 3.19b) the load rotation curve after strengthening remains unchanged. However, a subsequent increase of the rotation of the member (opening more the shear crack) activates the post-installed reinforcement (shaded curve in Fig. 3.19b) thus increasing its punching shear strength (point C). Contrary to the previous case, the deformation capacity of the member increases with respect to a non-retrofitted member. It can further be noted that the increase of the punching shear strength depends again on the level of load at the moment of strengthening and that it may potentially be smaller than for a new member (point D). However, through the use of high-performance mortars, the required rotation for full activation of the reinforcement can be significantly reduced and the system may develop its full strength.

These two examples show that the use of the CSCT allows accounting for a series of physical phenomena on the behaviour and punching strength of flat slabs. This approach overcomes most limitations of empirical models and provides the engineer with an understanding on the response of the structural members.

3.3.5 Punching of fibre-reinforced concrete slabs

Fibre-reinforced concrete can be considered as a composite material composed of a cement matrix (concrete or mortar) and discrete fibres. Its behaviour after cracking, refer to Fig. 3.20a, depends both on the matrix and on the activation and strength of the fibres. Fibres are mostly used to improve serviceability behaviour (crack control) although for thin members they can partly or totally replace conventional reinforcement.

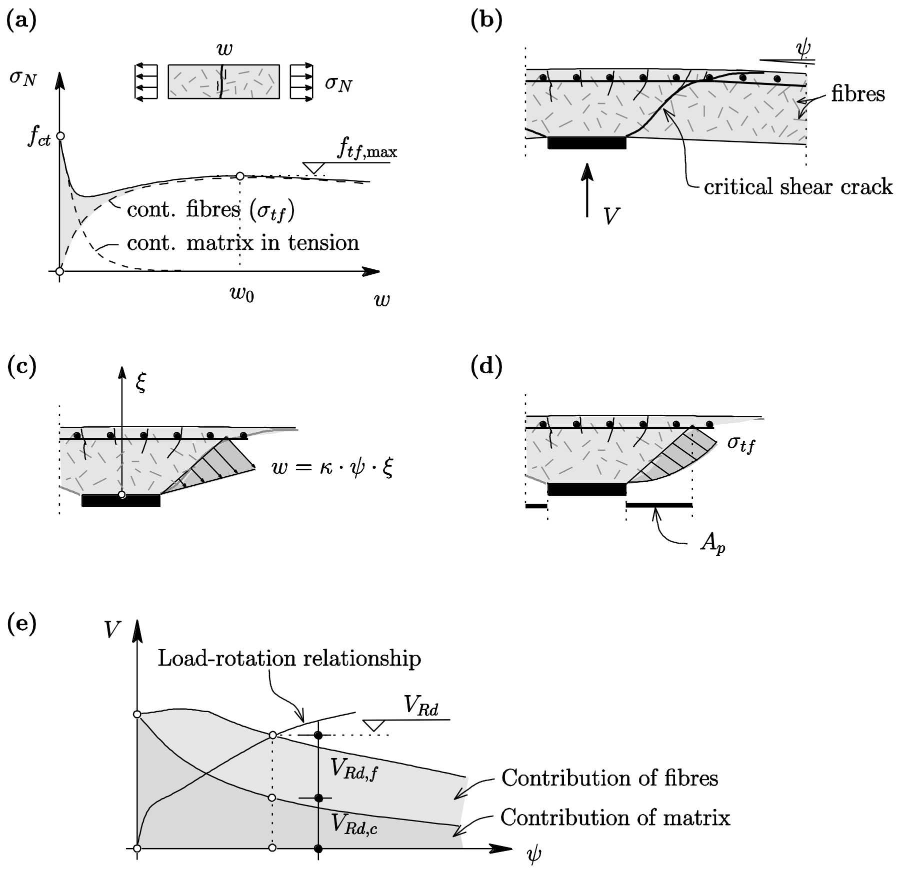

Fig. 3.20: Fibre-reinforced members: (a) behaviour of fibre-reinforced concrete after cracking; (b) critical shear crack in slabs; (c) assumed distribution of crack widths along the failure surface; (d) profile of fibre's stresses along the failure surface; and (e) matrix (concrete) and fibre contributions to punching shear strength

The punching shear behaviour of fibre-reinforced concrete can also be consistently investigated on the basis of the CSCT. This can be done (as for shear-reinforced slabs) by considering the contributions of the matrix (concrete in tension and aggregate interlock, $V_{Rd,c}$ refer to Eq. (3.3)) and of the fibres ($V_{Rd,f}$):

$$V_{Rd} = V_{Rd,c} + V_{Rd,f} \tag{3.14}$$

The contribution of the fibres can be calculated if a suitable crack opening–tensile stress relationship is provided ($\sigma_{tfd}(w)$). The new Model Code [*fib* (2010a)] proposes some simplified relationships to be calibrated on the basis of material testing. Analytical approaches providing rather accurate predictions of the activation phase are also available in the literature (as for instance the Variable Engagement Model by Voo and Foster (2004)). By using Eq. (3.7) of the CSCT, the tensile stress of the fibres can be calculated as function of the slab rotation and of the position of the fibres in the slab ($\sigma_{tfd}(\psi,\xi)$), refer to Fig. 3.20. By integrating such law at the failure surface, the shear-carrying capacity of fibres results:

$$V_{Rd,f} = \int_{A_p} \sigma_{tfd}(\psi,\xi) \cdot dA_p \tag{3.15}$$

where A_p refers to the horizontally projected area of the failure surface (Fig. 3.20d).

To calculate the punching shear strength, the failure criterion of the fibre-reinforced concrete has to be intersected by the load-rotation relationship of the slab (Fig. 3.20e). The latter can be estimated by means of Eq. (3.4), where the flexural strength (m_{Rd}) may account for fibre contribution to flexural strength (particularly significant for thin members).

The results of this approach are compared in Figure 3.21 to a number of test results taken from the scientific literature (for calculations, the fibre activation law proposed by Voo and Foster (2004) is adopted; detailed equations are given in Appendix 1 of this paper). The theory shows a very good agreement with test results, with an average measured-to-calculated strength of 1.09 and a CoV of 8%. This is notable since exactly the same assumptions as for ordinary concrete slabs with transverse reinforcement (kinematics at failure, opening of the shear crack with respect to slab rotation and angle of the failure surface) are adopted.

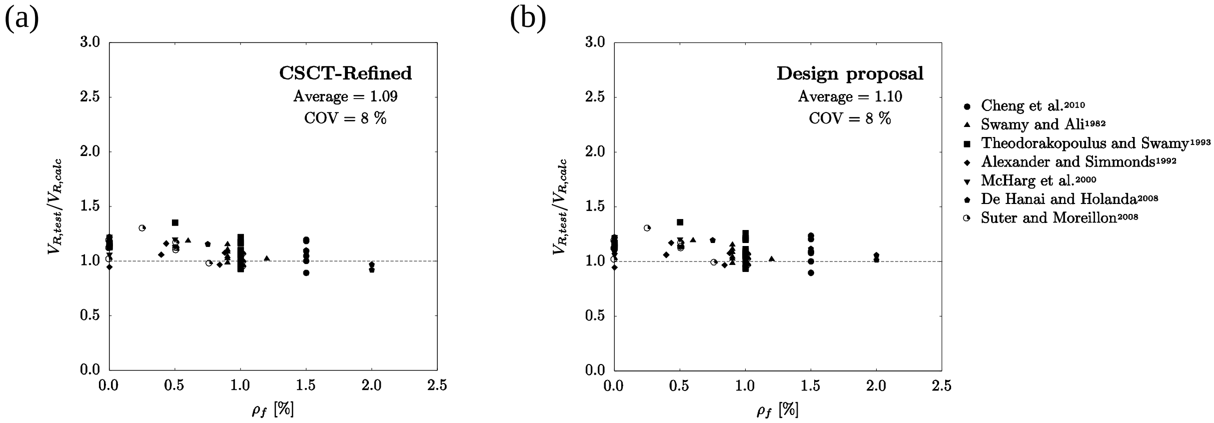

Fig. 3.21 Comparison of the CSCT results to punching tests on fibre-reinforced concrete slabs using the VEM mode [Voo and Foster (2004)] for fibre activation: (a) full-integration; and (b) design proposal (refer to Appendix 1)

3.4 Conclusions

In this paper, the main hypotheses of the Critical Shear Crack Theory (CSCT) and of its mechanical model are presented and justified. The meaning of the various physical parameters is explained as well as the way they can be evaluated for both simple and complex cases. The main conclusions of this paper are:

1) The CSCT is grounded on a consistent mechanical model, which allows estimating the shear strength accounting for the contribution of concrete in tension and the aggregate interlock developed at the shear failure surface.
2) For slabs where limited crack widths develop (very small depths, very large amounts of flexural reinforcement or prestressed slabs) the punching strength is mostly governed by the tensile strength of concrete. For large crack widths (usual depths and reinforcement ratios) aggregate interlocking becomes dominant.

3) If failures in punching are expressed in terms of its deformation capacity, they always develop within a narrow region (failure band). A simplified failure criterion can be used to approximate this band. This is convenient for its use in practical applications.
4) Failures in punching without transverse reinforcement can be calculated using the failure criterion in combination with a suitable load-rotation relationship. The accuracy of the load-rotation relationship can be progressively refined in various levels of approximation.
5) For design, safe and simple estimates of the load-rotation relationship are sufficient. For assessment of existing structures, however, it can be justified to perform more refined nonlinear numerical analysis if expensive strengthening can be avoided.
6) On the basis of the deformation capacity of the slab, the contribution of shear reinforcement can be consistently calculated accounting also for anchorage and bond conditions. The model shows that in some cases the shear reinforcement cannot be fully activated, even for usual yields strengths.
7) Punching shear design of fibre-reinforced slabs can also be performed using the CSCT by accounting for the same set of kinematical hypotheses adopted for slabs with shear reinforcement.
8) The CSCT can be applied to non-symmetrical or unusual cases, by accounting for the peculiarities of each situation in the mechanical parameters of the model.

3.5 References

Alexander S. D. B., Simmonds S. H., 1992, "Punching Shear Tests of Concrete Slab-Column Joints Containing Fiber Reinforcement", ACI Structural Journal, V. 89, No. 4, pp. 425-432

Andersson, J. L., 1966, "Punching of slabs supported on columns at free edges", Nordisk Betong 2, pp. 179-200.

Anis, N. N., 1970, "Shear strength of reinforced concrete flat slabs without shear reinforcement", PhD thesis, Faculty of Engineering of the University of London, 265 p.

ACI, 2008, Building Code Requirements for Structural Concrete (ACI 318-08) and Commentary (ACI 318R-08), American Concrete Institute, Farmington Hills, Mich., USA, 473 p.

Brändli, W., 1985, "Tests on RC and PC slabs for edge and corner columns" (in German: Bruchversuch an Stahlbeton–und Spannbetonplatten bei Rand–und Eckstützen), Nr. 146, Technical report, ETHZ - Institut für Baustatik und Konstruktion, 145 p.

Cheng M.-Y., Parra-Montesinos G.J., 2010, "Evaluation of Steel Fiber Reinforcement for Punching Shear Resistance in Slab-Column Connections— Part I: Monotonically Increased Load", ACI Structural Journal, Vol. 107, No 1, pp. 101-109

Clément T., Muttoni A., 2010, "Influence of a Prestressing Eccentricity on the Punching Shear Strength of Post-Tensionned Slab Bridges", Proceeding of the 8th *fib*-PhD Symposium, Copenhagen, Denmark, pp. 63-68,

Comité Euro-International du Béton (CEB-FIP), 1993, "Model code 90 for concrete structures", Lausanne, Switzerland, 460 p.

De Hanai J.B., Holanda K.M.A., 2008, "Similarities between punching and shear strength of steel fiber reinforced concrete (SFRC) slabs and beams", IBRACON, Volume 1, Number 1, pp. 1 – 16

Elstner, R. C., Hognestad, E., 1956, "Shearing Strength of Reinforced Concrete Slabs", ACI Materials Journal, Vol. 53, No 2, pp. 29-58

Eurocode 2, 2004, "Design of concrete structures - Part 1-1: General rules and rules for buildings", CEN, EN 1992-1-1, Brussels, Belgium, 225 p.

Fernández Ruiz, M., Muttoni, A., 2009, "Applications of the critical shear crack theory to punching of R/C slabs with transverse reinforcement", ACI Structural Journal, Vol. 106, No. 4, 2009, pp. 485-494

Fernández Ruiz, M., Vaz Rodrigues, R., Muttoni, A., 2009, "Design and assessment of deck slab of bridges (in French : Dimensionnement et vérification des dalles de roulement des ponts routiers)", Département fédéral des transports, des communications et de l'énergie, Office fédéral des routes, Rapport 636, Bern, Switzerland, 53 p.

Fernández Ruiz, M., Muttoni, A., Kunz, J., 2010, "Strengthening of flat slabs against punching shear using post-installed shear reinforcement", ACI Structural Journal, Vol. 107, No. 4, pp. 434-442

Fernández Ruiz, M., Muttoni, A., 2010, "Performance and design of punching shear reinforcing systems", 3rd International *fib* congress, Washington, USA, 15 p.

fédération internationale du béton (*fib*), 2001, "Punching of structural concrete slabs", *fib* Bulletin No 12, Lausanne, Switzerland, 314 p.

fédération internationale du béton (*fib*), 2010a, "Model Code 2010 - First complete draft, fédération internationale du béton", Bulletin 56, Lausanne, Switzerland, May 2010, Vol. 2, 312 p.

fédération internationale du béton (*fib*), 2010b, "Model Code 2010 - First complete draft, fédération internationale du béton", Bulletin 55, Lausanne, Switzerland, April 2010, Vol. 1, 318 p.

Fuchs, W, Eligehausen, R., Breen, J. E., 1995, "Concrete Capacity Design (CCD) Approach for Fastening to Concrete", ACI Structural Journal, Vol. 92, No 1, pp. 73-94

Guandalini S., Burdet O., Muttoni A., 2009, "Punching tests of slabs with low reinforcement ratios", ACI Structural Journal, V. 106, No1, pp. 87-95

Guandalini S. 2005. "Symmetric Punching in R/C slabs (in French: "Poinçonnement symétrique des dalles en béton armé")", PhD. thesis, École Polytechnique Fédérale de Lausanne, Switzerland, 289 p.

Guidotti, R., 2010, "Poinçonnement des planchers-dalles avec colonnes superposées fortement sollicitées", PhD. thesis, École Polytechnique Fédérale de Lausanne, Switzerland, 187 p.

Guidotti, R., Fernández Ruiz, M., Muttoni, A., 2010, "Punching of flat slabs subjected to large column loads (in German: Durchstanzen von Flachdecken bei hohen Stützenlasten)", Beton- und Stahlbetonbau, Ernst & Sohn - Wiley, Berlin, Vol. 105, No. 1, pp. 19-26

Hammil, N., Ghali, A., 1994, "Punching shear resistance of corner slab-column connections", ACI Structural Journal, Vol. 91, No 6, pp. 697-707.

Hawkins, N. M., Bao, A., Yamazaki, J., 1989, "Moment Transfer From Concrete Slabs To Columns, ACI Structural Journal", Vol. 86, No 6, pp. 705-716.

Hegger, J., Ricker, M., Häusler, F., 2006, "Research on punching and 3D shear failures for shear reinforced slabs near edge columns, (in German: Versuchsbericht zum Durshtanzen und Räumlichen Querkraftversagen von querkraftbewehrten Randstützen) ", Nr. 151, Technical report, RWTH Aachen, 129 p.

Hegger, J., Tuchlinski, D., 2006, "Punching of lfat slabs – influence of moment shear interaction and of prestressing (in German: Zum Durchstanzen von Flachdecken – Einfluß der Momenten–Querkraft Interaktion und der Vorspannung)", Beton–und Stahlbetonbau, Vol 101, No 10, pp. 742-752.

Ingvarsson, H., 1974, “Experimental investigation on reinforced concrete slabs near edge columns (in Swedish: Experimentellt Studium Av Beteongplattor Understödda Av Hörnpelare)”, No 33, Technical report, Institutionen für Byggnadsstatik, Kungl. Tekniska Hügskolan, Stockholm, 26 p.

Kinnunen, S., 1971, “Tests on Concrete Slabs Supported on Columns at Free Edges (R2:1971)”, Technical report, Statens institut for byggnadsforskning, Stockholm, (translated text in English), 103 p.

Krüger, G, 1999, “Résistance au poinçonnement excentré des planchers-dalles”. PhD. thesis, École Polytechnique Fédérale de Lausanne, Switzerland, 174 p.

Lips, S., Muttoni, A., Fernández Ruiz, M., 2010, “NMC2010 - Punching shear of flat slabs: Design example”, École Polytechnique Fédérale de Lausanne, Switzerland (this document can be downloaded from: http://ibeton.epfl.ch/MC2010Punching)

McHarg P.J., Cook W. F. , Mitchell D., Yoon Y.-S., 2000, “Benefits of Concentrated Slab Reinforcement and Steel Fibers on Performance of Slab-Column Connections”, ACI Structural Journal, V. 97, No. 2, pp. 225-235

Moe, J., 1961, “Shearing strength of reinforced concrete slabs and footings under concentrated loads, Technical report”, Portland Cement Association-Research and Development Laboratories, 72 p.

Moody, K. G., Viest, M., Elstner, R. C., and Hognestad, E., 1954, “Shear Strength of Reinforced Concrete Beams—Part 1: Tests of Simple Beams”, ACI Journal, Proceedings V. 51, No. 4, pp. 317-332.

Mortin, J. D., Ghali, A., 1991, “Connection of flat plates to edge columns”, ACI Structural Journal, Vol 88, No 2, pp. 191-198

Muttoni, A. 1985. “Punching shear – Draft code proposal, SIA 162”, Swiss Society of Engineers and Architects, Zürich, 15 p.

Muttoni A., Schwartz J. 1991. “Behaviour of Beams and Punching in Slabs without Shear Reinforcement”, IABSE Colloquium Stuttgart, Vol. 62, IABSE, Zurich, Switzerland, pp. 703-708.

Muttoni, A. 2003. “Shear and punching strength of slabs without shear reinforcement, (in German, “Schubfestigkeit und Durchstanzen von Platten ohne Querkraftbewehrung”)”, Beton- und Stahlbetonbau, Vol. 98, pp. 74-84.

Muttoni, A., Fernández Ruiz, M., Guandalini, S., 2007, “Punching of slab bridges (in French : Poinçonnement des ponts-dalles)”, 4. FBH / ASTRA - Studientagung "Neues aus der Brückenforschung, Doc. D0223 SIA, Societé suisse des ingénieurs et architects, Zürich, Switzerland, pp. 85-94.

Muttoni A., Fernández Ruiz M., 2008, “Shear strength of members without transverse reinforcement as function of critical shear crack width”, ACI Structural Journal, V. 105, No 2, pp. 163-172

Muttoni A., 2008, “Punching shear strength of reinforced concrete slabs without transverse reinforcement”, ACI Structural Journal, V. 105, No 4, pp. 440-450

Muttoni, A., Fernández Ruiz, M., Kunz, J., 2008a, “Post-installed shear reinforcement for strengthening of flat slabs (in German: Nachträgliche Durchstanzbewehrung zur Verstärkung von Stahlbetonflachdecken)”, Bauingenieur, Springer, VDI Verlag, Germany, Vol. 83, pp. 503-511

Muttoni, A. (Ed.), Fernández Ruiz, M., Fürst, A., Guandalini, S., Hunkeler, F., Moser, K., Seiler, H., 2008b, “Structural safety of parkin garages (in French: Sécurité structurale des parkings couverts)”, Doc. D 0226 SIA, Société Suisse des ingénieurs et des architectes, Zürich, Switzerland, 105 p.

Muttoni, A., Fernández Ruiz, M., 2010, “Design through an incremental approach: the Swiss experience”, 2010 Joint IABSE-*fib* Conference, Dubrovnik, Croatia, 8 p.

Narasimhan, N., 1971, “Shear reinforcement in reinforced concrete column heads”, PhD thesis, Faculty of Engineering of the University of London, 268 p.

Pollak, M.-A. and ACI comitee 445, 2005, “Punching Shear in Reinforced Concrete Slabs”, American Concrete Institute, SP-232, 298 p.

Regan, P. E.; Walker, P. R., Zakaria, K. A. A., 1979, “Tests of reinforced concrete flat slabs– CIRIA Project RP 220”, Technical report, Polytechnic Of Central London-School of the Environment, 171 p.

Sagaseta, J., Muttoni, A., Fernández Ruiz, M., Tassinari, L., 2010, “Non axis-symmetrical punching shear around internal columns of RC slabs without transverse reinforcement”, Magazine of Concrete Research, Thomas Telford Publishing Ltd., London, accepted for publication

Schertenleib P., Muttoni A., Schwartz J., 2003, “Column buckling (in French : Pièces comprimées)”, Documentation SIA, D 0182 Introduction à la norme SIA 262, Zürich, Switzerland, pp. 67-77

Sherif, A. G., 1996, “Behaviour of reinforced concrete flat slabs”, PhD thesis, Civil Engineering, University of Calgary, 425 p.

Sudarsana, I. K., 2001, “Punching shear in edge and corner column slab connections of flat plate structures”, PhD thesis, Department of civil engineering, University of Ottawa, 254 p.

Suter, R., Moreillon L., 2008, “High performance concrete reinforced with metallic fibres (in French: Bétons à hautes performances renforcés de fibres métalliques, poinçonnement de dalles minces)”, Test report, Ecole d'ingéniurs et architectes de Fribourg, Switzerland, 83 p.

SIA 2003. “Code 262 for Concrete Structures”, Swiss Society of Engineers and Architects, Zürich, Switzerland, 94 p.

Swamy, R. N., and Ali, S. A. R, 1982, “Punching Shear Behavior of Reinforced Slab-Column Connections Made with Steel Fiber Concrete”, ACI Journal, Proceedings V. 79, No. 5, pp. 392-406.

Theodorakopoulos D.D., Swamy N., 1993, “Contribution of Steel Fibers to the stregth Characteristics of Lightweight Concrete Slab-Column Connections Failing in Punching Shear”, ACI Structural Journal, V. 90, No. 4, pp. 342-355

Vaz Rodrigues, R. 2007. “Shear strength of reinforced concrete bridge deck slabs, PhD. thesis, École Polytechnique Fédérale de Lausanne, No. 3739, Lausanne, Switzerland, 114 p.

Vaz Rodrigues, R., Muttoni, A., and Fernández Ruiz, M., 2010, “Influence of Shear on Rotation Capacity of Reinforced Concrete Members Without Shear Reinforcement”, ACI Structural Journal, V. 107, No 5, pp. 516-525

Vaz Rodrigues, R., Fernández Ruiz, M., Muttoni, A., 2008, “Punching shear strength of R/C bridge cantilever slabs”, Engineering Structures, Elsevier, Vol. 30, No. 11, pp. 3024-3033

Vecchio, F. J. and Collins, M. P. 1986, “The modified compression field theory for reinforced concrete elements subjected to shear”, ACI Journal, 83, March-April, pp. 219-231

Vocke, H, 2002, “Punching of flat slabs near edge and corner columns (in German: Zum Durchstanzen von Flachdecken im Bereich von Rand- und Eckstützen)”, PhD. thesis, University of Stuttgart, 228 p.

Voo, J.Y.L. and Foster, S.J., 2004, “Tensile Fracture of Fibre Reinforced Concrete: Variable Engagement Model”, Sixth Rilem Symposium on Fibre Reinforced Concrete (FRC), Varenna, Italy, 20-22 September, pp. 875-884

Zaghlool, E. R. F., Paiva, H. A. R., 1973, “Tests of flat-plate corner column-slab connections”, Journal of the Structural Division, Vol 99, No 3, pp. 551-572.

Zaghlool, E. R. F., de Paiva, H. A. R., Glockner, P. G., 1970, “Tests of reinforced concrete flat plate floors”, Journal of the Structural Division, Vol. 96, No 3, pp. 487-507.

Appendix 1: Equations for punching shear behaviour in fibre-reinforced concrete

In this Appendix the necessary equations for evaluating the shear-carrying capacity of fibres in fibre-reinforced concrete are derived on the basis of the Voo and Foster (2004) Variable Engagement Model (VEM).

According to the VEM, the fibre stress (f_{tfd}) for a given crack opening (w) can be calculated according to the following expression:

$$\sigma_{tf}(w) = \frac{1}{\pi} \cdot \arctan\left(\frac{w}{\alpha_I \cdot l_f}\right) \cdot \left(1 - \frac{2 \cdot w}{l_f}\right)^2 \cdot \frac{l_f}{d_f} \cdot \rho_f \cdot \tau_b \tag{A1}$$

where l_f is the length of the fibres, d_f is their diameter, ρ_f is the volumetric ratio of fibres, α_I is the engagement parameter (typically $d_f/(3.5 l_f)$) and τ_b is the interfacial fibre/matrix bond strength ($\tau_b = 0.8 f_{cm}^{0.5}$ for hooked steel fibres, $0.6 f_{cm}^{0.5}$ for crimped steel fibres and $0.4 f_{cm}^{0.5}$ for straight steel fibres).

For the integration of the fibre contribution, it can be noted that the kinematic assumptions of the CSCT (Eq. (3.7)) can be used to estimate the crack opening for a segment of the failure surface at a distance ξ of the soffit of the slab, see Fig. 3.20c:

$$w(\psi, \xi) = \kappa \cdot \psi \cdot \xi \tag{A2}$$

Thus, the total shear carried by the fibres results (Eq. (3.15), assuming an angle of 45° for the failure surface in accordance to Fernández Ruiz and Muttoni (2009)):

$$\begin{aligned} V_{R,f} &= \int_{A_p} \sigma_{tf}(\psi, \xi) \cdot dA_p = \\ &= \int_{\theta=0}^{2\pi} \int_{\xi=0}^{d} \left(\frac{1}{\pi} \cdot \arctan\left(\frac{\kappa \cdot \psi \cdot \xi}{\alpha_I \cdot l_f}\right) \cdot \left(1 - \frac{2 \cdot \kappa \cdot \psi \cdot \xi}{l_f}\right)^2 \cdot \frac{l_f}{d_f} \cdot \rho_f \cdot \tau_b \right) \cdot (r_c + \xi) \cdot d\theta \cdot d\xi = \\ &= 2 \cdot \frac{l_f}{d_f} \cdot \rho_f \cdot \tau_b \cdot \int_{\xi=0}^{d} \arctan\left(\frac{\kappa \cdot \psi \cdot \xi}{\alpha_I \cdot l_f}\right) \cdot \left(1 - \frac{2 \cdot \kappa \cdot \psi \cdot \xi}{l_f}\right)^2 \cdot (r_c + \xi) \cdot d\xi \end{aligned} \tag{A3}$$

where θ refers to the angle with reference to the axis of the support region. This expression can be integrated leading to a closed-form solution. For clarity, the following notation will be used:

$$a = \frac{\kappa \cdot \psi}{\alpha_I \cdot l_f}; \quad b = \frac{2 \cdot \kappa \cdot \psi}{l_f}; \quad c = r_c \tag{A4}$$

Being thus $V_{R,f}$:

$$V_{R,f} = 2 \cdot \frac{l_f}{d_f} \cdot \rho_f \cdot \tau_b \cdot \frac{1}{12a^4} \cdot \left\{ \begin{array}{l} \arctan(a \cdot d) \cdot (a^4 \cdot d \cdot (4c \cdot (b^2 \cdot d^2 - 3b \cdot d + 3) + \\ + d(3b^2 \cdot d^2 - 8b \cdot d + 6)) + a^2 \left(6 - 12b \cdot c\right) - 3b^2) - \\ - a((6a^2 \cdot c - 2b^2 \cdot c + 4b) \cdot \log(a^2 \cdot d^2 + 1) + \\ + d \cdot (a^2 (b^2 \cdot d \cdot \left(2c + d\right) - 4b \cdot \left(3c + d\right) + 6) - 3b^2)) \end{array} \right\} \tag{A5}$$

This expression allows integrating the behaviour of fibres for any opening of the critical shear crack accounting for the behaviour of the fibres prior and after reaching their maximal strength.

The use of Eq. (A5) for practical applications is not necessary however. Instead of performing a full integration of the crack opening–fibre stress law, one can adopt an average value of the fibre's stress and multiply it by the whole failure surface:

$$V_{R,f} = \int_{A_p} \sigma_{tf}(\psi, \xi) \cdot dA_p = A_p \cdot \sigma_{tf}(\psi, h_c) \tag{A6}$$

where h_c refers to a control distance from the soffit of the slab at which the average stress is obtained. The position of h_c depends on the shape of the crack opening–fibre stress law and thus on the maximum opening of the crack. However, for typical fibre-reinforced slabs, crack widths remain below the crack opening at which the maximal fibre strength is reached (refer to w_0 in Fig. 3.20a) and a similar fibre's stress profile can thus be assumed. As a consequence, adopting a constant value for h_c is sufficiently accurate for usual cases. On this basis, the authors propose to adopt $h_c = d/3$ as a first estimate, leading to good agreement to test results (see Fig. 3.21b). This means that, on the basis of Eq. (A2), the average stress can be evaluated as:

$$V_{R,f} = A_p \cdot \sigma_{tf}\left(w = \frac{\psi \cdot d}{6} \right) \tag{A7}$$

For special members, where large rotations and significant crack widths are developed, it is on the contrary preferably to use the general expression (Eq. (A5), Fig. 3.21a or direct integration of an experimentally obtained law).

Design proposal

The previous approach for fibres can be used for design by calculating the design fibre's contribution ($V_{Rd,f}$) and introducing it into Eq. (3.14). Thus:

$$V_{Rd,f} = A_p \cdot \sigma_{tfd}\left(w = \frac{\psi \cdot d}{6} \right) \tag{A8}$$

To calculate σ_{tfd}, one can use the following design formula:

$$\sigma_{tfd}(w) = \frac{K_{ek}}{\gamma_f} \cdot \frac{1}{\pi} \cdot \arctan\left(\frac{w}{\alpha_I \cdot l_f} \right) \cdot \left(1 - \frac{2 \cdot w}{l_f} \right)^2 \cdot \frac{l_f}{d_f} \cdot \rho_f \cdot \tau_b \tag{A9}$$

where γ_f refers to the partial safety factor of fibre-reinforced concrete (γ_f = 1.5) and K_{ek} is a coefficient allowing to calculate characteristic (5% percentile) values of the fibre's stresses (Eq. (A1)). According to the new Model Code approach for fibre-reinforced concrete (2010a), material parameters of fibre-reinforced concrete need to be calibrated on the basis of test results. This can be done for instance for parameter K_{ek} by calculating the percentile 5% of the ratio $\sigma_{Nti}/\sigma_{Nci}$ for a number of crack widths (1, 2 and 3 mm, see Fig. A.1) and by equalling K_{ek} to the minimum value of them.

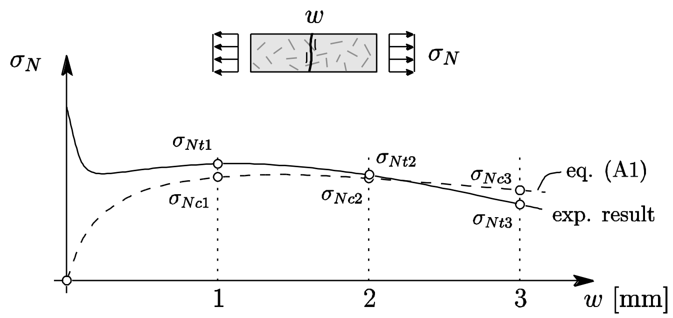

Fig. A.1: Calibration of factor K_{ek} on the basis of test results

Appendix 2: Notation

A_p	=	horizontal projection of failure surface
A_{sw}	=	cross-sectional area of a shear reinforcement
E_s	=	modulus of elasticity of the reinforcement
V	=	shear force
V_d	=	design shear force
V_R	=	punching shear strength
V_{Rd}	=	design punching shear strength
$V_{R,c}$	=	concrete contribution to punching shear strength
$V_{R,s}$	=	shear reinforcement contribution to punching shear strength
$V_{Rd,c}$	=	design concrete contribution to punching shear strength
$V_{Rd,c0}$	=	design punching shear strength of a slab without shear reinforcement
$V_{Rd,f}$	=	design fibre contribution to punching shear strength
$V_{Rd,s}$	=	design shear reinforcement contribution to punching shear strength
$V_{R,calc}$	=	calculated punching shear strength
$V_{R,test}$	=	measured punching shear strength
$V_{R,f}$	=	fibre contribution to punching shear strength
V_{SLS}	=	applied shear force at serviceability limit state
Q	=	applied load
Q_{Rd}	=	maximum load carried at design level
a,b,c	=	constants for integration
b_0	=	perimeter of the critical section
b_u	=	diameter of a circle with same surface than the basic control perimeter
d	=	effective depth
d_b	=	bar diameter
d_f	=	diameter of a fibre

d_v	=	shear-resisting effective depth
d_g	=	maximum diameter of the aggregate
d_{g0}	=	reference aggregate size (16 mm (0.63 in))
e	=	load eccentricity
e_u	=	load eccentricity with respect to the centroid of the basic control perimeter
f_c	=	average compressive strength of concrete (measured on cylinder)
f_{cm}	=	average compressive strength of concrete (measure on cylinder)
f_{tf}	=	stress in fibre
f_{tfd}	=	design stress in fibre
$f_{tf,\max}$	=	strength of fibres
f_{yd}	=	design yield strength of flexural reinforcement
f_{ywd}	=	design yield strength of shear reinforcement
h_i	=	distance from the soffit at which a reinforcement is crossed by the shear plane
k_e	=	coefficient of eccentricity
l_f	=	length of a fibre
m_{Rd}	=	average flexural strength per unit length in the support strip
m_{sd}	=	average moment per unit length (design of flex. reinforcement) in the strip
r_c	=	column radius
r_s	=	distance between the column and the line of contraflexure of moments
w	=	critical shear crack opening
w_0	=	crack opening at maximum fibre strength
w_b	=	opening of the critical shear crack at the level of the shear reinforcement
α	=	angle between the critical shear crack and the soffit of the slab
α_I	=	engagement parameter
δ	=	deflection
κ	=	coefficient relating total rotation and critical crack width opening
λ	=	coefficient to measure the crushing performance
$v_{d,max}$	=	maximum shear force
$v_{perp,d,max}$	=	maximum projected shear force perpendicular to the basic control perimeter
ψ	=	rotation of slab outside the column region
ψ_R	=	rotation of slab at failure
ψ_{SLS}	=	rotation of slab at serviceability limit state
θ	=	angle with reference to the axis of the support region (cylindrical coordinates)
ρ_f	=	fibre reinforcement ratio (in volume)
σ_{sw}	=	stress in shear reinforcement
σ_{swd}	=	design stress in shear reinforcement
$\sigma_{s,el}$	=	steel stress during elastic activation of shear reinforcement
$\sigma_{s,b}$	=	maximum shear reinforcement stress due to bond failure
$\sigma_{s,p}$	=	maximum shear reinforcement stress due to pull-out failure
τ_b	=	bond strength
ξ	=	distance (in vertical) of a point with respect to the soffit of a slab

4 MC2010: Overview on the shear provisions for FRC

Marco di Prisco[1], Giovanni Plizzari[2] and Lucie Vandewalle[3]

[1] Professor, Department of Structural Engineering, Politecnico di Milano, Italy
[2] Professor, Dept of Civil Eng., Architect., Land and Environm., Univ. of Brescia, Italy
[3] Professor, Department of Civil Engineering, K. U. Leuven, Belgium

Abstract: Although the use of Fibre Reinforced Concrete (FRC) for structural applications is continuously increasing, it is still limited with respect to its potentials mainly due to the lack of International Building Codes for FRC structural elements. The *fib* Model Code 2010 includes several innovations and addresses, among other topics, new materials for structural design, including FRC. The material requirements and design aspects for FRC structures were prepared by Technical Groups *fib* TG 8.3 " Fibre reinforced concrete" and TG 8.6 "Ultra high performance fibre reinforced concrete". This paper aims to briefly explain the main concepts behind the structural rules for shear design of FRC elements.

4.1 Introduction

Fibre Reinforced Concrete (FRC) is a composite material that is characterized by an enhanced post-cracking tensile residual strength, also defined toughness in the following, due to the capacity of fibres to bridge the crack faces. The enhanced toughness is mainly provided by high-modulus fibres in a suitable concrete matrix and, in structural applications of FRC, it allows to reduce the use of conventional reinforcement (rebars or welded mesh).

FRC is suitable for structures where diffused stresses are present. In structures where both localized and diffused stresses are present, which is the usual case, the reinforcement is better based on a combination of rebars and fibre reinforcement. In structures characterized by a high degree of redundancy, fibre reinforcement can totally substitute rebars; the possibility of saving the labour time necessary to place conventional reinforcement made FRC very attractive for practitioners.

Besides the structural resistance at ULS, a significant contribution can be provided by FRC at service conditions (SLS); in fact, fibre reinforcement may reduce the crack opening and the tension stiffening of concrete between cracks. Crack control is particularly important for durability issues. In structures with rebars, a reduced minimum concrete cover is expected when fibre reinforcement is present.

During the last three decades, a wide research has been performed on material properties of FRC, both at fresh and hardened state (Rossi & Chanvillard, 2000; di Prisco et al., 2004; Reinhardt & Naaman, 2007; Gettu, 2008). Research on structural response of FRC elements was mainly developed during the last fifteen years. Early design considerations were produced by ACI 544 (1996) and even in ACI 318 (2008) some new rules were just introduced with reference to minimum shear reinforcement; RILEM TC162-TDF produced pioneer design guidelines for typical structural elements (Vandewalle et al., 2002; 2003). Afterwards, design guidelines were produced by other Countries, as France (AFGC-SETRA, 2002), Sweden (Stälfiberbetong, 1995), Germany (DAfStb, 2007), Austria Richtlinie Faserbeton, 2002), Italy (CNR, 2006) and Spain (Task group EHE: Annex 18).

Due to a better knowledge of FRC and the recent developments worldwide of guidelines for structural design, the *fib* Special Activity Group 5 (SAG 5) introduced some Sections (5.6 and 7.7) on FRC in the new *fib* Model Code (2010); these sections were mainly prepared by *fib* TGs 8.3 - Fibre reinforced concrete and 8.6 - Ultra high performance fibre reinforced concrete (di Prisco et al., 2009).

This paper aims to present some principles governing structural design of FRC elements made of ordinary concrete, as included in the new *fib* Model Code (MC): the main concepts were derived from some national guidelines for FRC structural design (CNR, 2006; DAfStb, 2007) and from the guidelines proposed by RILEM TC162-TDF (Vandewalle et al., 2002; 2003). The principles discussed herein are mainly related to (post-cracking) softening "steel" FRCs in uniaxial tension (Fig. 4.1a), even though they can be extended to hardening materials (Fig. 4.1b). Special attention is devoted to shear design of FRC beams, with or without transverse reinforcement.

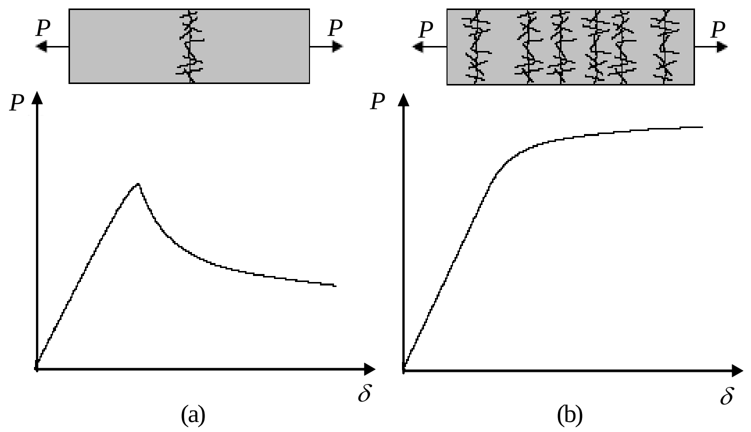

(a) Strain softening (b) Strain hardening

Fig. 4.1: Typical Load (P) - deformation (δ) curve for Fibre Reinforced Concrete: post-cracking softening (a) and hardening (b) behaviour

4.2 FRC classification

Classification is an important requirement for structural materials. When referring to ordinary concrete, designers choose its strength, workability or exposition classes that have to be provided by the concrete producer. When using FRC, compressive strength is not particularly influenced by the presence of fibres (up to a volume fraction of 1%) so that the classification for plain concrete can be adopted. It is well known that fibres reduce workability of fresh concrete but workability classes for plain concrete can be adopted for FRC as well. Some studies are still needed for exposition classes since fibres may reduce the crack opening (Vandewalle, 2000); therefore, for the exposition classes described in the EN 206 (2006), different rules may be adopted in FRC structures (i.e. smaller concrete covers, etc.).

Since fibre reinforcement activates after cracking of the concrete matrix, fibres are not effective in uncracked elements. Therefore, concrete tensile strength is related to the matrix strength and is not influenced by fibres (actually, fibres may slightly reduce tensile strength since they introduce new interfaces in the concrete matrix). The mechanical property that is significantly influenced by fibres is the residual (post-cracking) tensile strength that represents an important design parameter for FRC structures. Due to the well known difficulties in performing uniaxial tensile tests, standard methods generally require bending tests on small beams. However, it should be underlined that bending behaviour is markedly different from uniaxial-tension behaviour. It may happen that softening materials in tension evidence a hardening behaviour in bending (Naaman and Reinhardt, 2003; Fig. 4.2).

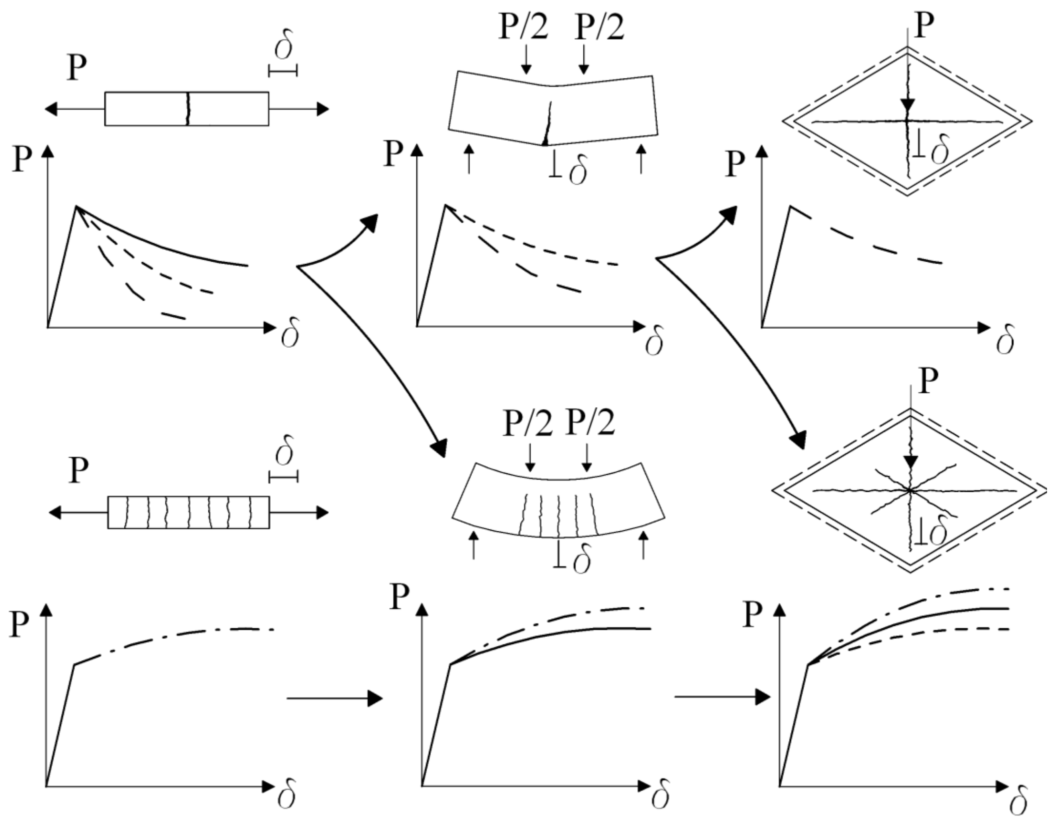

Fig. 4.2: Main differences between materials having softening or hardening behaviour from material to structural level (fib, 2010)

Material classification for FRC is based on nominal properties determined from bending tests on notched beams according to EN 14651 (2005). Other tests (either from beams or from plates) can be accepted, if correlation factors with the parameters of EN 14651 can be demonstrated. These tests directly provide properties of the composite that depend on the fibre, the matrix as well as their interface. When fibre orientation may occur due to a small thickness or to casting procedures, more realistic tests on "structural specimen", that better reproduce the real structural behaviour, should be performed.

Post-cracking strength in hardening or softening materials varies with the increasing deformation or crack opening. Since the residual strength varies during the test, at least two deformation values should be considered: the first one should be significant for service conditions (SLS), while the second one should be significant for Ultimate Limit States (ULS). Actually, European standard EN 14651 (2005) requires four different values of the residual strength (f_{R1}, f_{R2}, f_{R3}, f_{R4}; Fig. 4.3), corresponding to different values of the Crack Mouth Opening Displacement (CMOD = 0.5, 1.5, 2.5 and 3.5 mm, respectively) of the notched section. The two design parameters significant for SLS and ULS are f_{R1} (corresponding to $CMOD_1$=0.5 mm) and f_{R3} (corresponding to $CMOD_3$=2.5 mm), respectively.

In order to further simplify the classification, material behaviour at ULS can be related to the behaviour at SLS by means of the ratio f_{R3}/f_{R1}. With the previous assumptions, FRC toughness can be classified by using a couple of parameters: the first one is a number representing the f_{R1} class while the second one is a letter representing the ratio f_{R3}/f_{R1} (Fig. 4.4).

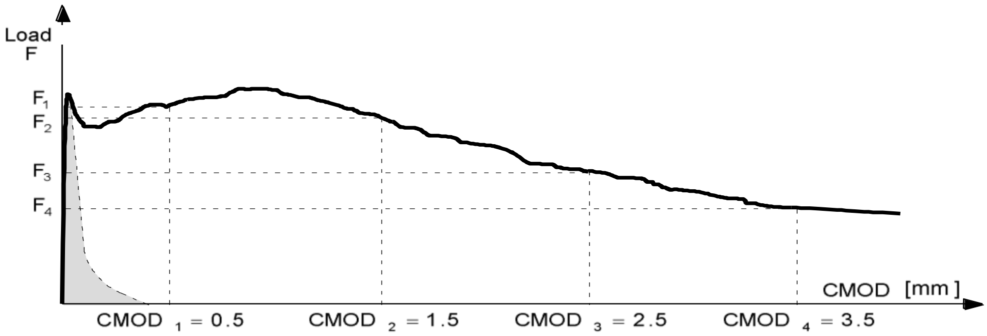

Fig. 4.3: Typical load curve F – CMOD for FRC

The strength interval for the characteristic value f_{R1k} is defined by two subsequent numbers in the following series (the lowest number of this interval is used for the classification.):

1.0; 1.5; 2.0; 2.5; 3.0; 4.0; 5.0; 6.0; 7.0; 8.0 [MPa]

The ratio f_{R3k}/f_{R1k} ratio can be represented with letters a, b, c, d, e, corresponding to the values:

“a” if $0.5 \leq f_{R3k}/f_{R1k} \leq 0.7$

“b” if $0.7 \leq f_{R3k}/f_{R1k} \leq 0.9$

“c” if $0.9 \leq f_{R3k}/f_{R1k} \leq 1.1$

“d” if $1.1 \leq f_{R3k}/f_{R1k} \leq 1.3$

“e” if $1.3 \leq f_{R3k}/f_{R1k}$

This classification properly represents the most common cases of softening FRCs (in tension), but it can also adopted for hardening FRCs. By using the proposed classification, a material having, for example, f_{R1k}=2.2 MPa and f_{R3k}=1.8 MPa is classified as “2b” (Fig. 4.4).

Since brittleness must be avoided in structural behaviour, fibre reinforcement can be used as substitution (even partially) of conventional reinforcement (at ULS), if the following relationships are both fulfilled:

$$f_{R1k}/f_{Lk} > 0.4 \tag{4.1}$$

$$f_{R3k}/f_{R1k} > 0.5 \tag{4.2}$$

where f_{Lk} is the characteristic value of the nominal strength, corresponding to the peak load (or the highest load value in the interval 0-0.05 mm) determined from the beam test (Fig. 4.3).

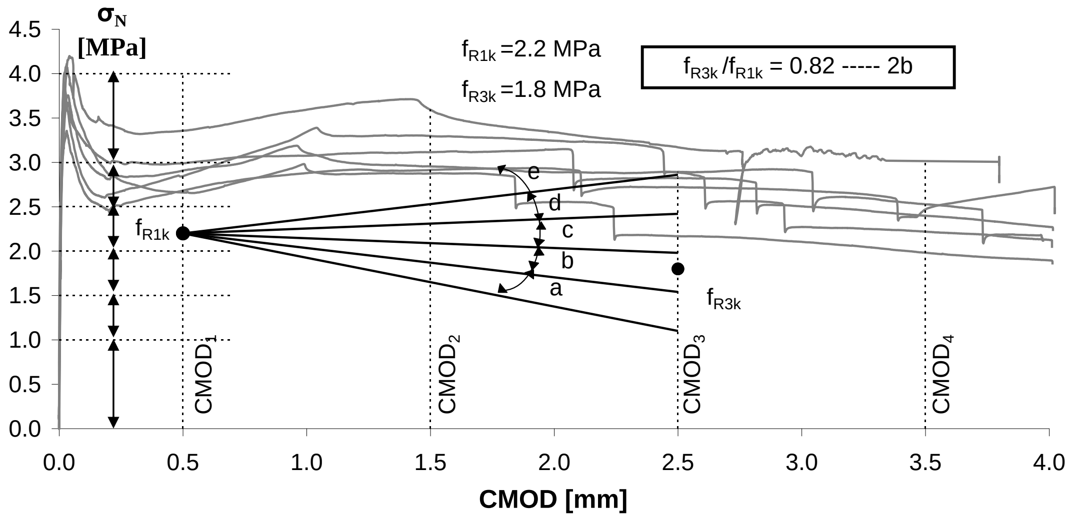

Fig. 4.4: Typical example of FRC classification

4.3 Partial safety factors

The substantial difference from conventional Reinforced Concrete (R.C.) is connected with the need of considering in FRC the residual strength which is mainly due to the fibre pull-out mechanism (Fig. 4.1a). The material is scantly homogeneous and isotropic because fibres location is random and depends mainly on casting procedure, formwork geometry and mix consistency affected by flowability, viscosity, filling ability. Therefore, the scattering of its response mainly depends on fibres number in the cracked section as well as on their location and orientation.

The main partial safety factor required by the *fib* MC for FRC structures are the following:

- FRC in compression: $\gamma c=1.5$
- FRC in tension: $\gamma_F=1.5$
- Rebars: $\gamma s=1.15$

A reduced safety factor $\gamma_F = 1.3$ may be adopted for improved control procedures.

4.4 Constitutive laws in uniaxial tension

The stress-crack opening law in uniaxial tension is defined (for the post-cracking range) as the main material property of FRC. Two simplified stress-crack opening constitutive laws may be deduced from the bending test results: a plastic-rigid or a linear post-cracking behaviour (hardening or softening), as schematically shown in Fig. 4.5 where f_{Fts} represents the serviceability residual strength and f_{Ftu} represents the residual strength significant for ULS. In Fig. 4.5 w_u is the crack opening corresponding to the ultimate limit state considered.

When considering softening materials, the definition of a stress-strain law is based on the identification of a crack width and on the corresponding structural characteristic length, l_{cs} , of the structural element. This basic concept was first introduced by Bazant with reference to plain concrete structures (Bazant & Oh, 1983; Bazant & Cedolin, 1983, di Prisco et. al., 2009). It is commonly used to make mesh-independent the computation by using finite element approaches or beam kinematic models (Kooiman, 2000; Ferrara & di Prisco, 2001; di Prisco et al., 2003; Barros et al., 2005). It represents a "bridge" to connect continuous mechanics governed by stress-strain (σ-ε) constitutive relationships and fracture mechanics governed by stress-crack opening (σ-w; Hillerborg et al., 1976).

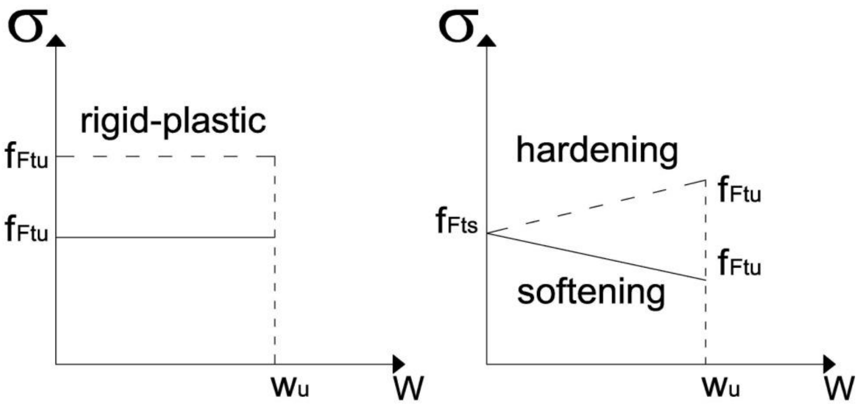

Fig. 4.5: Simplified constitutive laws: stress-crack opening (continuous and dashed lines refer to softening and hardening materials respectively)

The introduction of the characteristic length allows the designer to define the strain as:

$$\varepsilon = w / l_{cs} \tag{4.3}$$

In elements with conventional reinforcement (rebars), the characteristic length may be evaluated as:

$$l_{cs} = \min\{s_{rm}, y\} \tag{4.4}$$

where:

s_{rm} is the mean value of the crack spacing;

y is the distance between the neutral axis and the tensile side of the cross section, evaluated in the cracked phase, at SLS, by neglecting the tensile strength of FRC.

The ultimate tensile strength (f_{Ftu}) in the linear model depends on the required ductility that is related to the allowed crack width. The ultimate crack width can be calculated as:

$$w_u = l_{cs} * \varepsilon_{Fu} \tag{4.5}$$

where ε_{Fu} is assumed equal to 2% when the neutral axis crosses the cross section and 1% when the neutral axis is external to the cross section.

In sections without conventional reinforcement under bending (or under combined tensile – flexural and compressive – flexural forces, with resulting force external to the section), the simplified expression

$$y = h \tag{4.6}$$

can be assumed due to the very reduced extension of the compressed region. The same assumption can be taken for slabs.

For hardening materials in tension, multiple cracking occurs (JSCE, 2008); therefore, the identification of crack openings is not necessary, because a conventional stress-strain law may be directly determined from an uniaxial tensile test, by dividing the relative displacement for the gauge length.

4.4.1 Rigid-plastic model

The rigid-plastic model identifies a unique reference value, f_{Ftu}, based on the ultimate behaviour. The rigid-plastic model takes the static equivalence into account (Fig. 4.6a) and f_{FTu} results from the assumption that the whole compressive force is concentrated in the top fibre of the section.

$$f_{FTu} = \frac{f_{R3}}{3} \tag{4.7}$$

Equation (4.7) is obtained by rotational equilibrium at ULS, by assuming that w_u=$CMOD_3$, when a stress block in tension along the section is taken into account.

4.4.2 Linear post-cracking model

The linear post-cracking model identifies two reference values (f_{Fts} and f_{Ftu}) that have to be defined through residual values of flexural strength by using the following equations (di Prisco et al., 2004):

$$f_{FTs} = 0.45 f_{R1} \tag{4.8}$$

$$f_{FTu} = f_{Fts} - \frac{w_u}{CMOD_3}(f_{FTs} - 0.5 f_{R3} + 0.2 f_{R1}) \geq 0 \tag{4.9}$$

Equation (4.9) is valid for $\sigma = f_{FTu}$ and $w_u \neq CMOD_3$, and it is obtained by considering a linear constitutive law between points with abscissa $CMOD_1$ and $CMOD_3$, up to the point with abscissa w_u (Fig. 4.7).

The strength value corresponding to the crack opening $CMOD_1$ is determined from equilibrium, with the assumption that the compressive stress distribution is linear (Fig. 4.6b) and that the tensile behaviour is elasto-plastic until a crack opening displacement corresponding to the serviceability limit state (the variability introduced in the results by elastic modulus is considered as negligible and a common value is assumed):

$$M(CMOD_1) = \frac{f_{R1} b h_{sp}^{\ 2}}{6} \tag{4.10}$$

The stress value corresponding to the crack opening $CMOD_3$ is determined from equilibrium, with the assumption that the compressive stress resultant is applied on the extrados chord (Fig. 4.6c) and that the tensile behaviour is rigid-linear:

$$M(CMOD_3) = \frac{f_{R3} b h_{sp}^{\ 2}}{6} \tag{4.11}$$

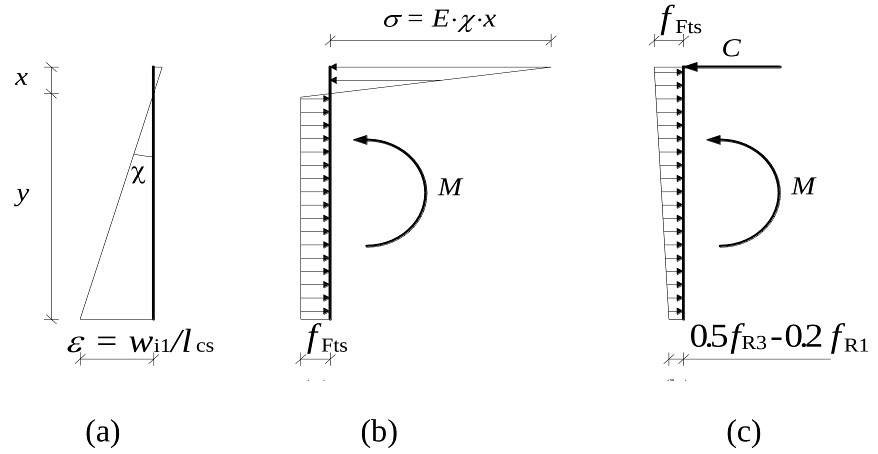

Fig. 4.6: Simplified models adopted to compute: (b) the tensile strength (f_{Fts}) by means of a elasto-plastic model; (c) f_{Ftu} for the linear model by means of a rigid-linear model

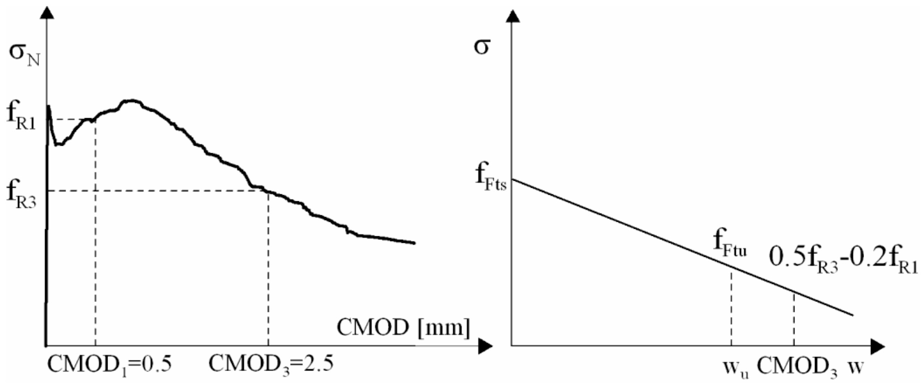

Fig. 4.7: (a) Typical results from a bending test on a softening material; (b) linear post-cracking constitutive law

Once the linear stress-crack opening relationship is identified, by introducing characteristic length it is possible to deduce the stress-strain -relationship.

4.5 Basic aspects for structural design

The residual strength of FRC becomes significant in structures characterized by a high degree of redundancy, where a remarkable stress redistribution occurs. For this reason, in structures without rebars, where fibres completely substitute conventional reinforcement, a minimum level of redundancy of the structural member is required. On the contrary, in structures with rebars, where fibres provide an additional reinforcement, ductility is generally provided by conventional reinforcement that plays a major contribution to the tensile strength. For hardening FRCs (in uniaxial tension), fibres can be used as the only reinforcement (without rebars) also in statically determined structural elements. In structures made of linear elements without traditional reinforcement, ductility requires that FRC has a hardening behaviour in tension.

Structural design must satisfy requirements for resistance and serviceability during the expected life of FRC elements. The ductility requirement in bending can be satisfied by minimum conventional reinforcement.

In all FRC structures without the minimum conventional reinforcement, one of the following conditions has to be satisfied (Fig. 4.8):

$$\delta_u \geq 20\ \delta_{SLS} \tag{4.12}$$

$$\delta_{peak} \geq 5\ \delta_{SLS} \tag{4.13}$$

where δ_u is the ultimate displacement of the structure, δ_{peak} is the displacement at the maximum load and δ_{SLS} is the displacement at service load computed by performing a linear elastic analysis with the assumptions of uncracked condition and initial elastic Young's modulus. Load P_u has always to be higher than P_{cr}.

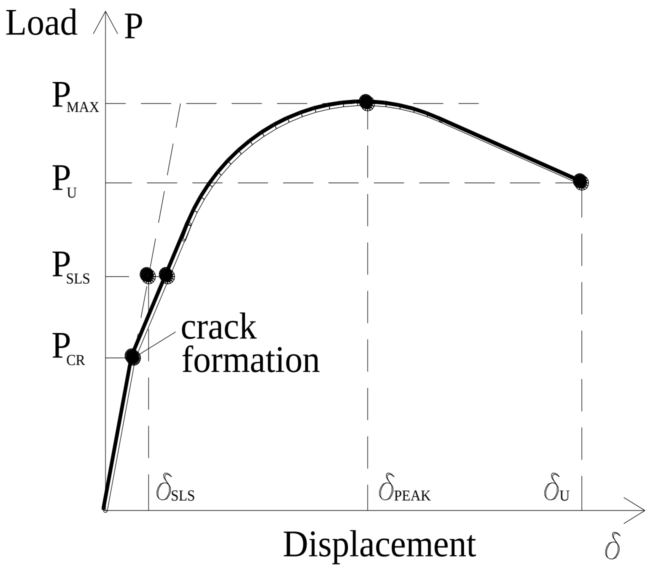

Fig. 4.8: Typical load (P) – displacement curve for a FRC structure

When the structure is able to significantly redistribute the applied loads at failure, a safety factor K_{Rd} ($\geq$ 1) that takes into account model uncertainties can be assumed. In fact, a high standard deviation from results on material tests does not correspond to a high standard deviation in the bearing capacity of structures with a high degree of redundancy. The main reason is due to the activation of a parallel system of each representative volume of the structure that makes the structural behaviour to be mainly related to the mean value of the material strength rather than to the characteristic value (di Prisco & Colombo, 2006; Dozio, 2008).

Factor K_{Rd} is mainly affected by two main parameters: 1) the ratio between the volume of the structure involved in the collapse mechanism at failure (V), and the volume involved in the collapse mechanism of the third point bending test (V_0) used in the identification of the post-cracking residual strengths, and 2) the ratio between the maximum load reached by the structure (P_{max}) and the first cracking load P_{cr} (Fig. 4.8; this ratio can be considered as a measure of the redistribution capability of the structure). Equations (4.14) underline that the dependence of the ultimate design load (P_{Rd}) and the material properties, as determined from standard tests (f_{Fd}), should take into account factor K_{Rd}.

$$P_{Rd} = K_{Rd}\, P(f_{Fd}) \tag{4.14a}$$

$$K_{Rd} = K_{Rd}\,(V/V_0,\ P_{max}/P_{cr}) \tag{4.14b}$$

4.6 Shear design

4.6.1 Minimum shear reinforcement

Fibres in a beam represent an additional distributed reinforcement that enhances shear resisting mechanisms both in elements with and without transverse reinforcement.

It is possible to prevent the use of the minimum amount of conventional shear reinforcement (stirrups), if the following condition is fulfilled (Minelli et al., 2007):

$$f_{\mathrm{Ftuk}} \geq \frac{\sqrt{f_{\mathrm{ck}}}}{20} \tag{4.15}$$

This limitation allows to reduce the development and the diffusion of the inclined cracking and, as a consequence, can ensure a sufficient member ductility. When a great amount of longitudinal reinforcement in the compressive zone is present, adequate stirrups reinforcement is better applied in order to avoid buckling of the compressed rebars.

4.6.2 Beams with and without shear reinforcement

The design equations for shear resistance proposed in the Model Code draft (2010) aimed to include concrete toughness (which is not negligible in FRC) in the EC2 equation for the evaluation of shear strength of a plain concrete beam without shear reinforcement.

Fibres improve this contribution mainly because of the additional strength exerted between the crack sides (di Prisco and Romero, 1996). Moreover, further shear-resistant mechanisms are also enhanced by fibre addition: an increase of the confinement in the aggregate interlock, an improved bending strength of the strut in connection with the compressive chord (which can be associated also to the improvement of the strength in the compressed chord subjected to compression and shear) as well as the increase of the dowel action of the longitudinal reinforcement at the bottom chord. To simplify as much as possible the design equation, only the main contribution due to pull-out mechanism was considered in the shear resistance. This contribution can be evaluated by using the stress- crack opening constitutive law identified by means of standard bending tests (EN 14651, 2007). When a rigid-plastic approach is assumed (Fig. 4.5), also a kinematic limit expressed in terms of crack opening has to be introduced in order to define the ultimate limit state condition. By associating the crack propagation in shear mainly to a mode I opening at crack onset and, eventually, to a mixed mode (mode I + mode II) opening, the value f_{Ftuk} (associated to the uniaxial tensile test) corresponding to a crack opening w_u = 1.5 mm was considered for remaining always on the safe side.

As a first approach, the equation suggested by Eurocode 2 to compute the shear contribution in concrete members without shear reinforcement, was modified to include FRC toughness. Since fibres represent a kind of a distributed reinforcement, it seems reasonable to model the shear contribution of fibres as a modifier of the longitudinal reinforcement ratio throughout a factor that includes the toughness properties of FRC; in doing so, the semi-empirical equation was rearranged by adding the term 7.5 f_{Ftuk}/f_{ctk} (in N):

$$V_{\mathrm{Rd,F}} = \left\{ \frac{0.18}{\gamma_{\mathrm{c}}} \cdot k \cdot \left[100 \cdot \rho_1 \cdot \left(1 + 7.5 \cdot \frac{f_{\mathrm{Ftuk}}}{f_{\mathrm{ctk}}} \right) \cdot f_{\mathrm{ck}} \right]^{1/3} + 0.15 \cdot \sigma_{\mathrm{cp}} \right\} \cdot b_{\mathrm{w}} \cdot d \tag{4.16}$$

where:

k is a factor that takes into account the size effect and it is equal to: $1+\sqrt{\frac{200}{d}} \leq 2.0$

d [mm] is the effective depth of the cross section

ρ_l is the reinforcement ratio for longitudinal reinforcement

f_{Ftuk} [MPa] is the characteristic value of the ultimate residual tensile strength for FRC, by considering $w_u = 1.5$ mm according to Eq. (4.9);

f_{ctk} [MPa] is the characteristic value of the tensile strength for the concrete matrix;

f_{ck} [MPa] is the characteristic value of cylindrical compressive strength;

$\sigma_{cp} = N_{Ed}/A_c < 0.2\ f_{cd}$ [MPa] is the average stress acting on the concrete cross section, A_c [mm^2], for an axial force N_{Ed} [N], due to loading or prestressing actions;

b_w [mm] is the smallest width of the cross-section in the tensile area.

Eq. (4.16) is a rather simple relationship and is already widely used for members made of plain concrete; therefore, it should be easily transferred into the design of FRC beams. Note that Eq. (4.16) applies in presence of shear diagonal failure ("beam behavior"), namely for a/d ratios greater than 2.5. In case of failure due to arch action, further studies have to be carried out.

The shear resistance ($V_{Rd,F}$) is assumed to be not smaller than a minimum value ($V_{Rd,Fmin}$) defined as:

$$V_{\mathrm{Rd,Fmin}} = \left(v_{\min} + 0.15 \cdot \sigma_{\mathrm{cp}}\right) \cdot b_{\mathrm{w}} \cdot d \tag{4.17}$$

where $v_{\min} = 0.035 \cdot k^{3/2} \cdot f_{\mathrm{ck}}^{\ 1/2}$

Once again, note that fibers were included into the concrete contribution, rather than with the definition of a separate addendum. This was done aiming at a more representative modeling of the actual effect of fibers, which basically make the concrete matrix tougher after cracking, improving both the transfer of residual tensile stresses and the aggregate interlock (the latter, by keeping cracks smaller).

Since shear cracking in FRC members proved to develop in a quite stable fashion, even for crack widths greater than 3 mm (Minelli, 2005; Minelli and Plizzari, 2006), the residual post-cracking strength related to the ultimate limit state (f_{Ftuk}) is considered. The ability of fibers in controlling the second branch of the shear-critical crack (even for big crack widths) is due to their capability of bridging the two crack faces. By keeping cracks stable, the shear capacity of members considerably increases till, eventually, the full flexural capacity is attained.

Eq. (4.16) could be modified by taking into account the new equation proposed in the Model Code draft, with reference to the same contribution in regions cracked in bending, as:

$$V_{Rd,c} = k_v \frac{\sqrt{f_{ck}}}{\gamma_c} z b_w \tag{4.18}$$

with $k_v = \begin{cases} \dfrac{200}{(1000 + 1.3z)} \leq 0.15 \cdots if \cdots \rho_w = 0 \\ = 0.15 \cdots if \cdots \rho_w \geq 0.08 \sqrt{f_{ck}} \big/ f_{yk} \end{cases}$

The term $V_{Rd,c}$ corresponds to $V_{Rd,F}$: it could be the same already presented (Eq. (4.16)) or, for a better consistency with Eq. (4.18), it could be computed as a function of a term $k_v = k_v (f_{Ftuk}, z)$ or directly by substituting the term $(f_{ck})^{1/2}/\gamma_c$ with the term f_{Ftuk} multiplied by a suitable calibrated coefficient k_θ depending on the inclination of the first macro-crack.

In the literature, even an additional term formulation is proposed like:

$$V_{Rd,F} = k_v \left(\frac{\sqrt{f_{ck}}}{\gamma_c} + k_\theta f_{Ftud} \right) z b_w \tag{4.19}$$

Fig. 4.9 compares the fitting of a wide experimental database between the proposed model (Minelli, 2005) and the well known RILEM formulation (Vandewalle et al., 2003) where fibre contribution is represented by an additional term (Eq. (4.19)). Note that the RILEM's model defines a separate contribution for fibers, to be added to that of concrete and that of transverse reinforcement, if provided. The first 43 beams in the plot come from a RILEM's database (Vandewalle et al., 2003), while the others refer to experimental tests carried out at the University of Brescia (Minelli, 2005). Predictions of the formulation proposed in MC are quite satisfactory for all beams, even though the fitting results are less promising when dealing with high strength concrete specimens or prestressed members. A similar response is seen for the RILEM model (they both result from an adaptation of the EC2 current design equation), which turned out to be a little more refined for small size elements than for deep beams. One should notice that the two formulations require toughness properties. The standard deviation for all 60 experiments considered turned out to be equal to 0.29 for the proposed model while is 0.31 for the RILEM's. Those values can be considered very high, but one should keep in mind that the scatter in doing shear tests is always high, due to the huge dispersion always related to phenomena strongly dependent on the tensile strength of concrete.

From a practical point of view, the interest in using FRC for shear resistance is mainly related to the possibility of replacing all transverse reinforcement. However, when stirrups are present in a FRC beam, an additive formulation that takes into account the shear contribution of FRC can be considered:

$$V_{Rd} = V_{Rd,F} + V_{Rd,s} \tag{4.20}$$

where the term $V_{Rd,F}$ is the same defined in Eq. (4.16) while the shear reinforcement term ($V_{Rd,s}$) is computed as:

$$V_{Rd,s} = \frac{A_{sw}}{s_w} z f_{ywd} (\cot \vartheta + \cot \alpha) \sin \alpha \tag{4.21}$$

The angle ϑ corresponds to the first cracking and can be computed according to the negative principal stress direction agent in the barycentre of the cross section.

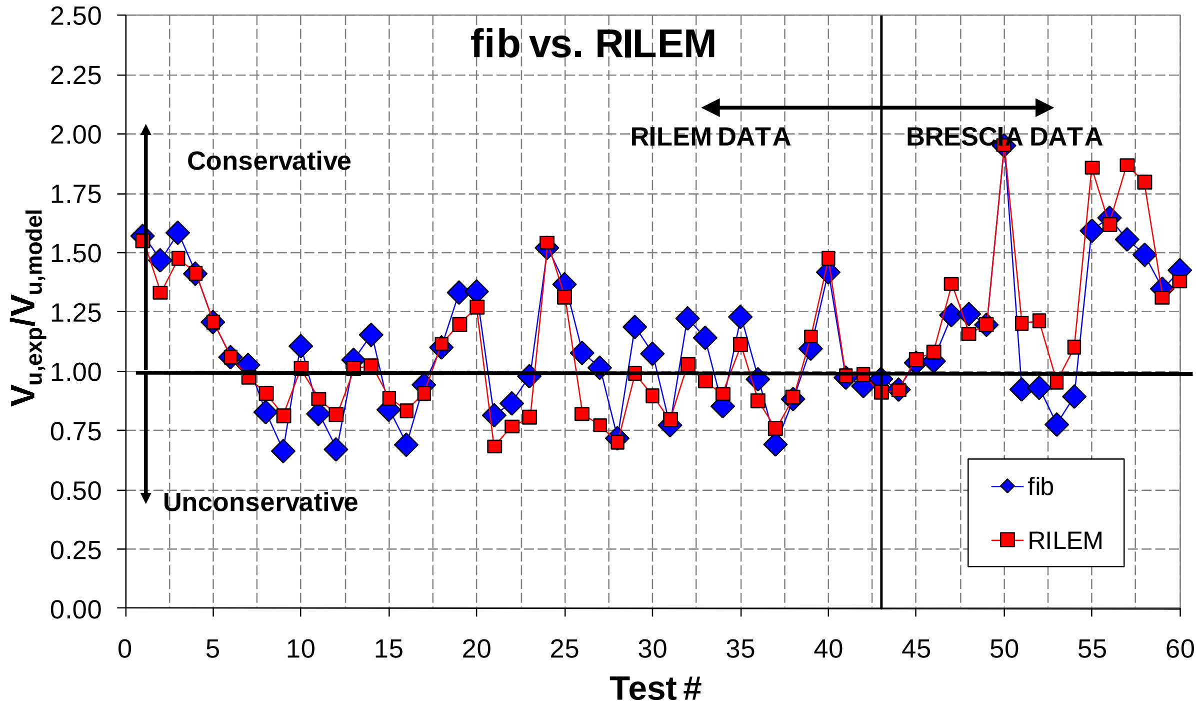

Fig. 4.9: Comparison between fib and RILEM models for more than 60 experiments (Minelli and Plizzari, 2006)

Also the level III approximation proposed for shear in MC 2010 draft can be introduced according to the σ(w) simplified constitutive model proposed. On the contrary, the level II approximation is not easy to be computed, because the diagonal compression field rotates in a different way with respect to the conventional R/C beam: it is clear that an ideal elasto-plastic behaviour in uniaxial tension guaranteed by a high volume fraction of fibres could even prevent the rotation due to its ability to conserve the orientation of tensile stresses.

When a hardening FRC material is considered (that means the cementitious composite shows a hardening behaviour in uniaxial tension up to a ε_{Fu} =1%), a beam without any reinforcement (neither longitudinal nor transverse) can be accepted if:

$$\sigma_I < f_{Ftud} \tag{4.22}$$

In the Model Code draft proposal, also a level IV is introduced, where Finite Element or other specific software can be adopted. The relative small experience accumulated in FRC structural analysis suggests to limit the increase of shear bearing capacity guaranteed by a level IV approach in relation to what computable according to level III.

4.7 Concluding remarks

A very important milestone for the practical use of Fibre Reinforced Concrete (FRC) is the introduction of this material in the new *fib* Model Code that, in the next future, will lead to a development of structural rules for FRC elements in Eurocodes and in many national codes. This will encourage designers to use FRC since new structural materials are easily accepted only when design rules are present in building codes.

From a mechanical point of view, FRC is a concrete with an enhanced toughness and, therefore, a distinction between fibre and matrix contribution can be helpful for fundamental research but not for practice where the mechanical properties are better determined from a fracture test directly performed on the composite; these properties also include the effects of the matrix and fibre (one or more types) characteristics and have to be specifically required by designers and guaranteed by the builders during construction.

Most of the research carried out on FRC was mainly related to steel fibres and, therefore, when other fibres are considered for structural use, a special attention is recommended for the long term behaviour when little results are available into the literature.

Fibres can be particularly useful at ULS for shear since they can totally substitute transverse reinforcement in many cases; the advantages from using fibres are not so relevant in beams with transverse reinforcement since the stirrup spacing is lightly reduced by fibre reinforcement; in this case the advantages from using fibres is mainly related to crack control in service conditions.

Although the level of knowledge on FRC tremendously increased during the last ten years, further research is needed to verify and optimize the design rules as well as to investigate the long term behaviour of different FRCs and other open issues. As far as shear behaviour is concerned, a first step should concern the harmonisation of shear design rules between RC and FRC by considering that material toughness of FRC is not negligible as in plain concrete.

4.8 Acknowledgements

A special acknowledgement goes to Prof. Joost Walraven for the fruitful discussions and to Prof. Falkner who shared its large design experience. The Authors are also grateful to all the members of *fib* Task Groups TG 8.3 and TG 8.6 for the constructive discussions during the several meetings where many ideas presented in this paper took a definitive shape. Finally the Authors would thank Prof. Fausto Minelli for contributing to the update of the literature framework.

4.9 References

ACI Committee 544, Design considerations for steel Fiber Reinforced Concrete, ACI 544.4R-88, American Concrete Institute, ACI Farmington Hills, MI, 1996.

ACI Committee 318, Building code and commentary, Report ACI 318-08/318R-08, American Concrete Institute, Farmington Hills, 2008.

AFGC-SETRA, Ultra High Performance Fibre-Reinforced Concretes, Interim Recommendations, AFGC Publication, France, 2002.

Barros, J.A.O., Cunha, V.M.C.F., Ribeiro, A.F., Antunes, J.A.B., “Post-Cracking Behaviour of Steel Fibre Reinforced Concrete", RILEM Materials and Structures Journal, 38(275), 2005, 47-56.

Bazant, Z.P. and Oh, B.H., Crack band theory for fracture of concrete, Materials and Structures, 16, 93, 1983, 155-177.

Bazant, Z.P. and Cedolin, L., Finite element modeling of crack band propagation, ASCE Journal of Structural Engineering, 109, 1, 1983, 69-92.

CNR-DT 204, Guidelines for design, construction and production control of fiber reinforced concrete structures, National Research Council of Italy, 2006.

Deutscher Ausschuss für Stahlbeton (DAfStb): Guidelines for steel fiber reinforced concrete– 23th Draft – richtlinie Stahlfaserbeton – DIN 1045 Annex parts 1 – 4, August 2007.

EN 14651, Test method for metallic fibre concrete – Measuring the flexural tensile strength (limit of proportionality, residual), 2005.

di Prisco, M., Plizzari, G., Vandewalle, L. (2009): “Fibre reinforced concrete: new design perspectives”, Materials and Structures. Vol. 42 N.9, pp. 1261-1281, ISSN: 1359-5997.

di Prisco, M., Romero, J., Diagonal Shear in Thin-Webbed Reinforced-Concrete Beams: Fiber and Stirrup Roles at Shear Collapse, Magazine of Concrete Research, Vol. 48(174), 1996, 1-18.

di Prisco, M., Iorio, F., Plizzari, G.: HPSFRC prestressed roof elements, in Test ad design methods for steel fibre reinforced concrete – Background and experiences -, B. Schnütgen and L. Vandewalle (Eds.), PRO 31, RILEM, 2003, 161-188.

di Prisco, M., Felicetti R. and Plizzari G. (eds.), Fibre-Reinforced Concrete, BEFIB 2004, Bagneux, France, RILEM Publications S.A.R.L., PRO39, 2004.

di Prisco, M., Felicetti, R., Lamperti, M. & Menotti, G., On size effect in tension of SFRC thin plates, in Fracture Mechanics of Concrete Structures, V.C. Li, et al. Eds., 2, B.L. Schmick and A.D.Pollington, USA, 2004, 1075-1082.

di Prisco, M., Ferrara, L., Colombo, M., Mauri, M., On the identification of SFRC costitutive law in uniaxial tension – in Fiber reinforced concrete, di Prisco, M. et al. (Eds.), Proc. of 6th Rilem Symp. BEFIB 04, Varenna (Italy), PRO 39, Bagneaux Rilem Publications S.a.r.l. (FRANCE), 2004, 827-836.

di Prisco M. and Colombo M., FRC and HPFRC Composites: from constitutive behaviour to structural applications, in Measuring, Monitoring, and Modelling Concrete Properties, Konsta-Gdoutos M.S. (Ed.), Proc. of the International Symposium dedicated to Prof. S. P. Shah, Alexandroupolis (Greece), Springer, Dordrecht, 2006, 59-68.

di Prisco, M., Plizzari, G. and Vandewalle, L., Fibre reinforced concrete: new design perspectives, Materials and Structures. Vol. 42 N.9, 2009, 1261-1281.

Dozio D., SFRC structures: identification of the uniaxial tension characteristic constitutive law, Department of Structural Engineering, Politecnico di Milano, 2008.

fédération internationale du béton (*fib*), “Model Code 2010 - First complete draft.” Bulletins 55 and 56, 2010.

Ferrara, L., di Prisco, M., Mode I fracture behaviour in concrete: non-local damage modeling, ASCE, Journal of Engineering Mechanics, 127(7), 2001, 678-692.

Gettu Ravindra (ed.), Fibre Reinforced Concrete: Design and Applications, BEFIB 2008, Bagneux, France, RILEM Publications S.A.R.L., PRO60, 2008.

Hillerborg, A., Modeer, M. and Peterson, P.E., 1976, Analysis of crack formation and crack growth by means of fracture mechanics and finite elements, Cement and Concrete Research, 6, 773-782.

JSCE, Recommendations for Design and Construction of High Performance Fiber Reinforced Cement Composites with Multiple Fine Cracks (HPFRCC), Rokugo K., (ed.) Concrete Engng. Series, 82, 2008.

Kooiman A.G. “Modelling steel fibre reinforced concrete for structural design, Ph.D. Thesis Technical University Delft., Optima Grafische Communicatie, Rotterdam, 2000.

Minelli, F, Plain and Fiber Reinforced Concrete Beams under Shear Loading: Structural Behavior and Design Aspects, Ph.D. Thesis, Department of Civil Engineering, University of Brescia, February 2005, Starrylink Editrice, Brescia, pp. 430. ISBN 88-89720-30-1.

Minelli, F., Plizzari, G.A., Steel Fibers as Shear Reinforcement for Beams, Proceedings of The Second Fib Congress, Naples, Italy, 5-8 June, 2006, abstract on page 282-283, full length paper available on accompanied CD, pp.12.

Minelli F, Plizzari G., Vecchio F.J., Influence of Steel Fibers on Full-Scale RC Beams under Shear Loading. In High performance concrete, brick-masonry and environmental aspects. Sixth international conference of fracture mechanics of concrete and concrete structures FRAMCOS6, ISBN/ISSN: 978-0-415-44617-4, London, Taylor & Francis Group (UK), Catania, 3, 2007, 1523-1531.

Naaman, A.E. and Reinhardt, H.W., High performance fiber reinforced cement composites – HPFRCC4,' RILEM Proc., PRO 30, RILEM Publications S.A.R.L., Bagneaux (France), 2003.

Richtlinie Faserbeton, Osterreichische Vereinigung für Beton-und Bautechnik, March 2002.

Reinhardt, H.W. & Naaman, A.E., (eds.), High Performance Fibre Reinforced Cement Composites (HPFRCC5), PRO 53, Rilem Publication S.A.R.L., 2007.

Rossi, P. and Chanvillard, G. (eds.), 5th RILEM Symp. on Fibre Reinforced Concretes (BEFIB 2000), RILEM Publications S.A.R.L., Cachan, France, 2000.

Stälfiberbetong, rekommendationer för konstruction, utförande och provning Betongrapport n.4 – Svenska Betongföreningen 1995.

Task group EHE: Annex 18- Fibre Reinforced Concrete. Version 10: 2.04.2007

Swamy, R.N. and Bahia, H.M., The effectiveness of steel fibres as shear reinforcement. Concr. Inst. Des. Constr., 1985, 7(3), 35-40.

UNI EN 206-1, Concrete - Part 1: Specification, performance, production and conformity, 2006.

Vandewalle, L. et al., 'Recommendation of Rilem TC162-TDF : Test and design methods for steel fibre reinforced concrete : Design of steel fibre reinforced concrete using the σ-w method : principles and applications', Materials and Structures Vol.35 (2002) 262-278.

Vandewalle L. et al., 'Recommendation of Rilem TC162-TDF: Test and design methods for steel fibre reinforced concrete : σ-ε-design method (final recommendation)', Materials and Structures Vol.36, 2003, 560-567.

Vandewalle, L., Cracking behaviour of concrete beams reinforced with a combination of ordinary reinforcement and steel fibres, Materials and Structures, 33 (227), 2000, 164-170.

5 Improving analytical models for shear design and evaluation of reinforced concrete structures

Michael P. Collins

University Professor and Bahen-Tanenbaum Professor, Department of Civil Engineering
University of Toronto, Toronto, Ontario, Canada

Abstract: After presenting a brief summary of analytical models for shear based on the Modified Compression Field Theory (MCFT), short descriptions are given on research related to the one-way shear strength of thick slabs, the shear behaviour of large members with small amounts of shear reinforcement, the shear behaviour of members with large amounts of shear reinforcement and, finally, a brief description is given of research related to the influence of the bond characteristics of the reinforcement on shear behaviour.

5.1 Introduction

Shear design and evaluation procedures which are based on rational models rather than empirical equations enable the engineer to develop a better understanding of actual structural behaviour and to more clearly appreciate situations where shear will be a critical safety issue. Deficiencies in the shear design of concrete structures are inherently more dangerous than deficiencies in flexural design because shear failures can occur without prior warning and with no possibility for redistribution of internal forces. While assessing the shear capacity of a reinforced concrete structure accurately is critically important for public safety, the traditional techniques available for this task are open to dispute. Developing more rational models for shear has been the objective of a long-term worldwide research effort and considerable progress has been made over the last twenty years. For example the current Canadian shear provisions have come some way towards achieving shear provisions comparable in rationality and generality with those used for flexure. This paper will concentrate on research performed at the University of Toronto which is currently being extended with the aim of further improving shear design and evaluation procedures.

5.2 Analytical models based on the MCFT

The modified compression field theory (MCFT) is a procedure to predict the load-deformation response of a reinforced concrete element subjected to bi-axial stresses f_x, f_z and v. Figure 5.1 shows the 15 equations of the MCFT. Across the width of the figure the equations are divided into three sets: five equilibrium equations, five geometric conditions and five stress-strain relationships. In the upper part of the figure the equations deal with average stresses, average strains and the relationships between average stresses and average strains. Average stresses (e.g. f_{sx}) and average strains (e.g. ε_x) correspond to stresses and strains averaged out over lengths long enough to damp out the local variations that occur at cracks and between cracks. The bottom five relationships in the figure are concerned with stresses at a crack (e.g. f_{sxcr}), the crack width and the maximum shear stress that can be transmitted across the crack. The term v_{ci} stands for shear stress transmitted across the crack interface. The two small inset stress-strain figures represent the standard bilinear stress-strain relationship assumed for reinforcing bars and the uniaxial compressive stress-compressive strain relationship obtained from a standard cylinder test. The average stress-average strain relationships for the cracked concrete given by Equation 13 and Equation 14 in Fig. 5.1 are the result of the panel testing and the early shell element testing program. The relationship used for determining the ability of the crack surfaces to transmit the interface shear stresses, Eq. 15 in Fig. 5.1, was derived from the aggregate interlock experiments of Walraven (1981). Note that this shear stress limit is a function of the crack width, w, the maximum aggregate size, a_g, and the concrete cylinder strength, f_c'.

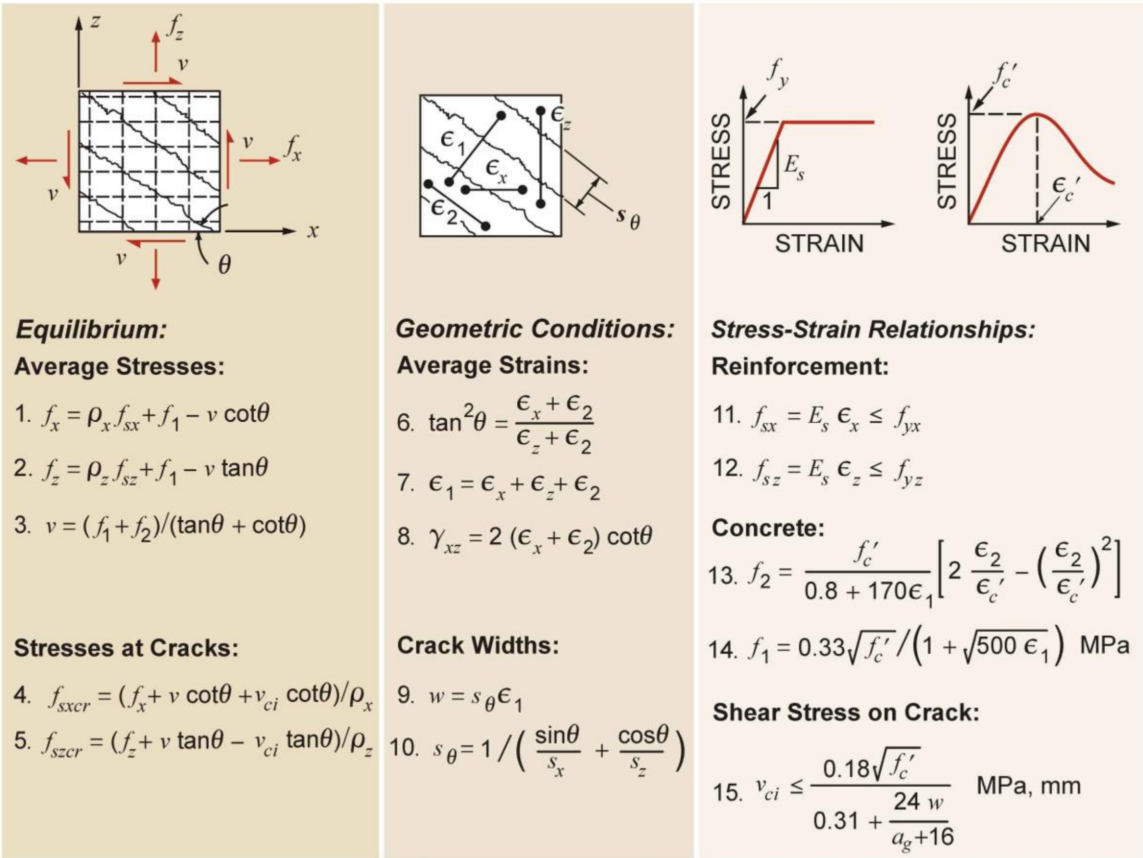

Fig. 5.1: The equations of the Modified Compression Field Theory

To use the theory to predict the load-deformation response of a reinforced concrete beam such as that shown in Fig. 5.2, the beam could be represented as a two dimensional grid of elements with the response of each element being predicted by the MCFT. This is the basis of non-linear finite element programs such as VecTor2 (Vecchio 1989, 2010) which have been developed at the University of Toronto over the past 25 years. If such a program is used to analyze the beam it will be found that in zones extending for a distance of about d away from the point loads and the reactions there will be significant vertical compressive stresses in the concrete. These clamping stresses will enhance the shear strength of the elements in these zones making it probable that the shear failure will occur outside of these zones. For beams with short shear spans the zones with significant clamping stresses will overlap and the shear strength of the beam will be considerably increased. It is important to recognize that in these "disturbed regions" the shear stress distribution over the depth of the beam is influenced by the distribution of the clamping stresses and near the loads and reactions, plane sections do not remain plane.

Outside of the disturbed regions discussed above it is appropriate to assume that plane sections remain plane and that the clamping stresses are negligible. With these two assumptions a beam cross-section can be modeled as a stack of biaxially stressed elements with the response of each element being predicted by the MCFT. This is the basis of program Response-2000 (Bentz 2000, 2010) which can be used to predict the shear stress distribution over the depth of the beam and the complete load-deformation response of concrete sections subjected to shear, flexure and axial load, see Fig. 5.2. If only the shear strength of a beam cross-section is required then the web of the beam can be approximated by just one biaxial element located at mid-depth and the shear stress on the element can be assumed to be $V/(b_w d_v)$ where b_w is the web width and d_v is the flexural lever arm which can be taken as $0.9d$. The longitudinal strain, ε_x, at mid-depth of the beam can be found from the calculated strain in the longitudinal flexural reinforcement and the assumption that plane sections remain plane. For a given value of ε_x the failure shear stress can then be calculated from the MCFT as the sum of two terms, V_c and V_s, see Fig. 5.2. The first term depends on the ability of the cracks to transmit shear stress, characterized by the coefficient β, while the second term is a function of the amount of shear reinforcement, $\rho_z f_y$, and the angle of inclination of the principal compressive stresses, θ. Both β and θ depend on the strain ε_x and the equivalent crack spacing s_{xe}. This MCFT-based sectional design model for shear is the method used in the current Canadian Standards Association (CSA) document “Design of Concrete Structures” A23.3-04.

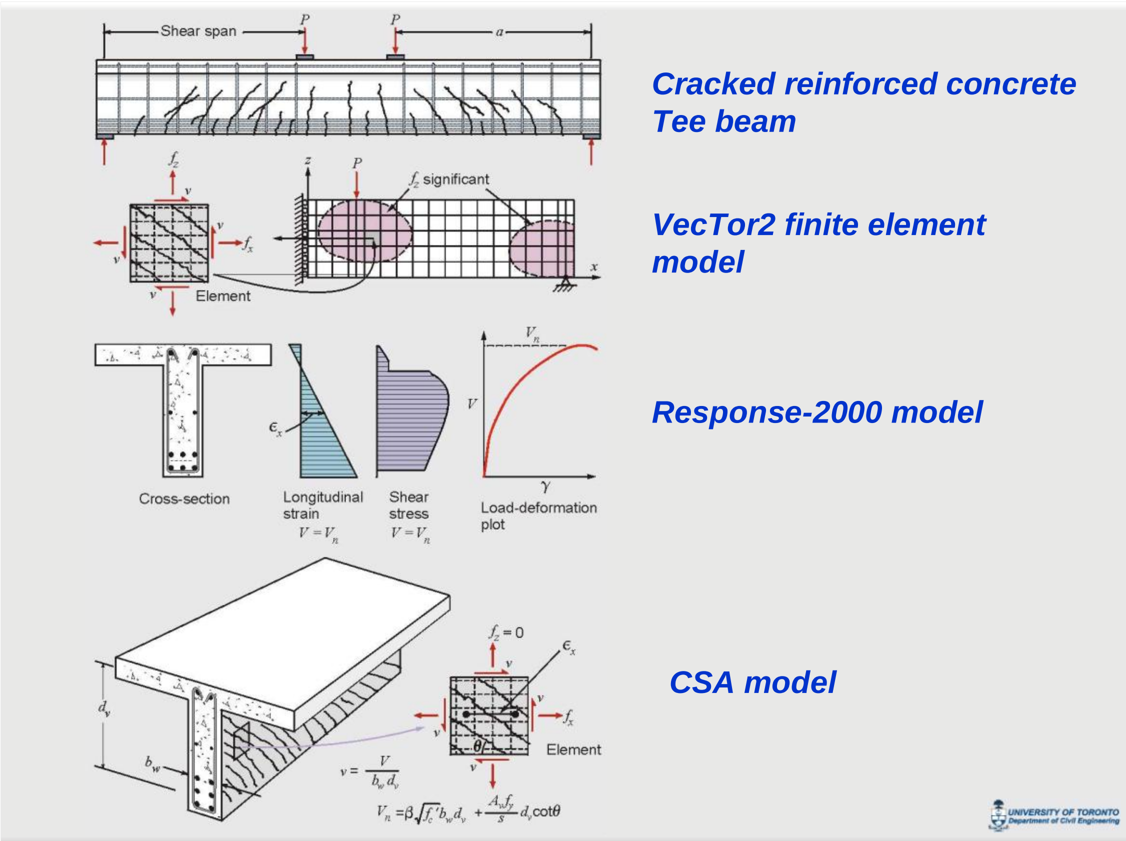

Fig. 5.2: Levels of Approximation in MCFT Analyses

5.3 One-way shear strength of thick slabs

Through much of the last decade the Toronto shear group have been studying specific types of concrete structures where the use of the traditional North American shear design procedures used in the design of existing concrete structures may have resulted in unacceptably high risks of shear failures. Thick, slender, one-way slabs such as those shown in Fig. 5.3 have been an area of particular concern.

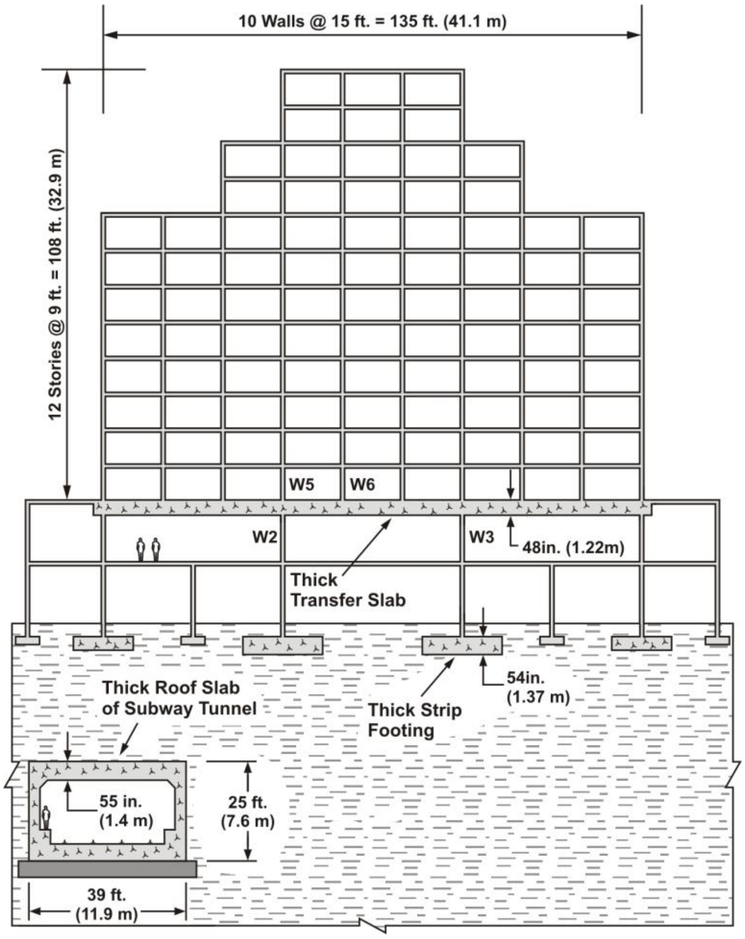

Fig. 5.3: Examples of shear critical thick one-way slabs

On September 30th 2006 in Laval, Quebec, a 35 year old, 1.25 metre thick reinforced concrete slab suddenly failed in shear resulting in the collapse of a major overpass and the death of five people, and serious injuries to seven more (Collins et al. 2008). After a major public inquiry into this failure and a detailed evaluation of 135 concrete slab bridges, the Government of Quebec identified 28 additional bridges for immediate demolition because of similar structural deficiencies and a further 25 that need substantial strengthening. The bridge slab which failed had a number of similarities to slab strip specimens which were tested at Toronto in 2004. See Fig. 5.4 in which the upper diagram is of the Laval bridge while the lower is the Toronto experiment. These slab strip tests were designed to investigate what was predicted to be a particularly dangerous combination of parameters. The 1970 Canadian bridge code specified that the Laval slab could be subjected to a service load shear stress of 0.48 MPa without needing shear reinforcement. Since 1963 the ACI Code has recommended that the failure shear stress, $V/(b_w d)$, of a beam or slab without shear reinforcement can be taken as $0.166\sqrt{f_c'}$, which for the 27.6 MPa concrete of the Laval bridge slab would be 0.87

MPa. Hence the designer of the Laval slab would have assumed that the factor of safety against a shear failure was at least 0.87/0.48 = 1.81. However the Toronto slab strip test failed at just 0.63 MPa indicating that the factor of safety against shear failure of this slab was only about 0.63/0.48 = 1.31 at the time the bridge was completed. Note that the ACI Code also gives a more complex expression for the failure shear stress which is a function of the stress in the longitudinal reinforcement. If this stress is very low the predicted failure shear stress can be as high as $0.29\sqrt{f_c'}$.

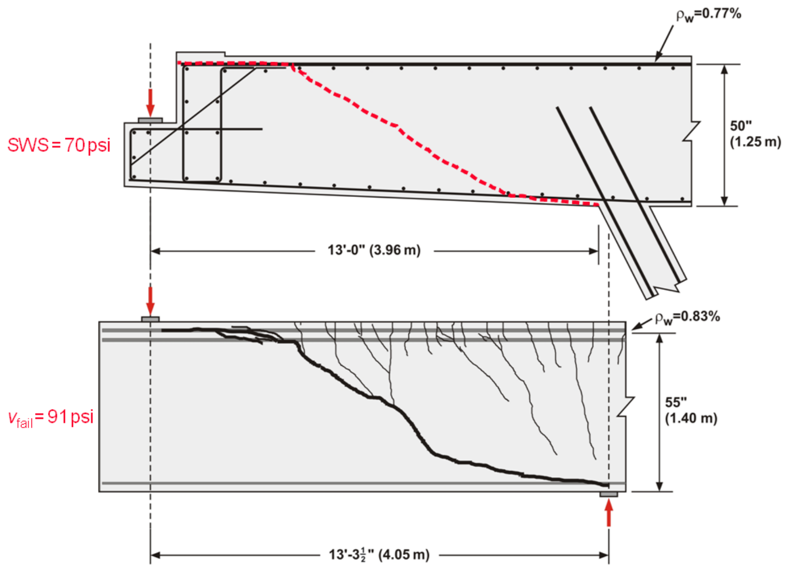

Fig. 5.4: Comparison of failed bridge slab and laboratory experiment

To understand why thick slabs such as those shown in Fig. 5.3 may fail at much lower shear stresses than the small laboratory beams which were used to establish the “safe” shear stress limits of the traditional shear provisions, it is useful to consider the somewhat simplified flexurally cracked beam shown in Fig. 5.5. The depth of the flexural compression zone is *kd* and the flexural lever arm is *jd*. Because the compressive stresses under the loading plate fan out into the beam the tensile force in the longitudinal reinforcement will remain about constant over a region about 2d long. Near the bottom face of the beam the spacing of the vertical cracks will be controlled by the bond characteristics of the reinforcement. On the other hand near mid-depth of the beam crack spacing will be controlled by the distance required for tensile stresses in the concrete to spread out from the reinforcement and from the stiff uncracked compression zone. Assuming that the dispersion angle is 45º, see Fig. 5.5, the horizontal spacing of the cracks in the upper region of the web will be about (1-*k*)*d*. Consider the free body diagram of the “tooth” of concrete defined by the neutral axis and two of these widely spaced cracks shown on the bottom left of Fig. 5.5 and labelled Case 1. Horizontal equilibrium requires that the average shear stress on the top horizontal plane is $V/(bjd)$. If the vertical cracks are narrow enough to be able to transmit this shear stress then the concrete in the tooth between the two vertical cracks will be in pure shear. This means there will be principal tensile stress also equal to $V/(bjd)$ which will cause a diagonal crack at an angle of 45º when $V/(bjd)$ equals the cracking stress of the concrete, f_{cr}. The ACI value (ACI 2008) for the principal tensile stress to cause diagonal cracking is $0.33\sqrt{f_c'}$.

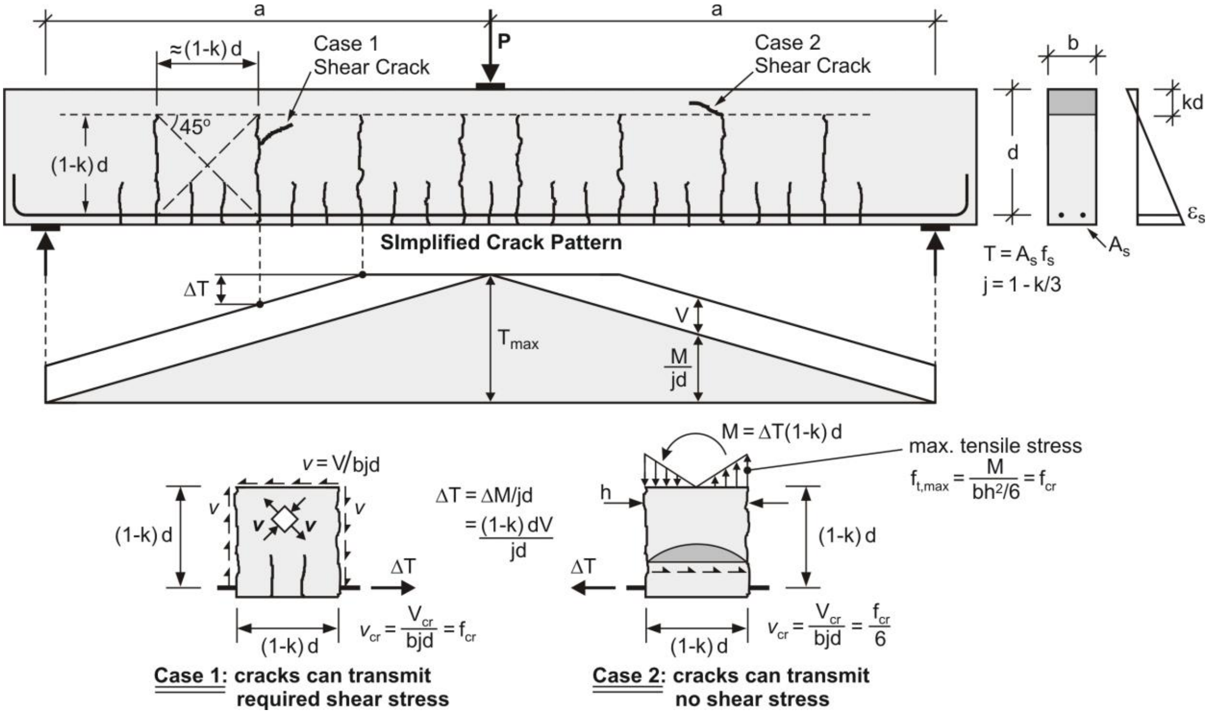

Fig. 5.5: Influence of aggregate interlock on diagonal cracking load of beam

Case 2 in Fig. 5.5 shows the situation for a beam where the cracks are so wide that no shear stresses can be transmitted across the cracks. Again horizontal equilibrium requires that the average shear stress on any horizontal plane across the tooth must equal $V/(bjd)$ but now these horizontal shear stresses must reduce to zero at the crack locations. In this case in order to change the force in the longitudinal reinforcement as required by beam action, bending moments causing vertical stresses must develop in the concrete tooth. The highest tensile stress in concrete tooth will occur at the top right corner and will equal $6V/(bjd)$. Thus, for Case 2, the concrete must resist a tensile stress 6 times higher than that for Case 1. In Case 2, a nearly horizontal inclined crack is predicted to form when the shear stress $V/(bjd)$ equals $0.055\sqrt{f_c'}$. Thus in terms of shear stresses expressed as $V/(bd)$ and assuming that jd is about $0.9d$, diagonal cracks are predicted to occur somewhere between $0.05\sqrt{f_c'}$ and $0.30\sqrt{f_c'}$ depending upon the width of the cracks. While the Case 1 upper limit is in close agreement with the ACI upper limit of $0.29\sqrt{f_c'}$ the Case 2 lower limit suggests that the traditional ACI lower limit of $0.166\sqrt{f_c'}$ may be out by a factor of about three for beams with very wide cracks. As crack width depends on crack spacing and as crack spacing in the upper region of the web is proportional to beam depth, it is to be expected that as beam depths increase the failure shear stresses will become closer to the $0.05\sqrt{f_c'}$ lower limit. This decrease in failure shear stress with increasing depth is called the size effect in shear.

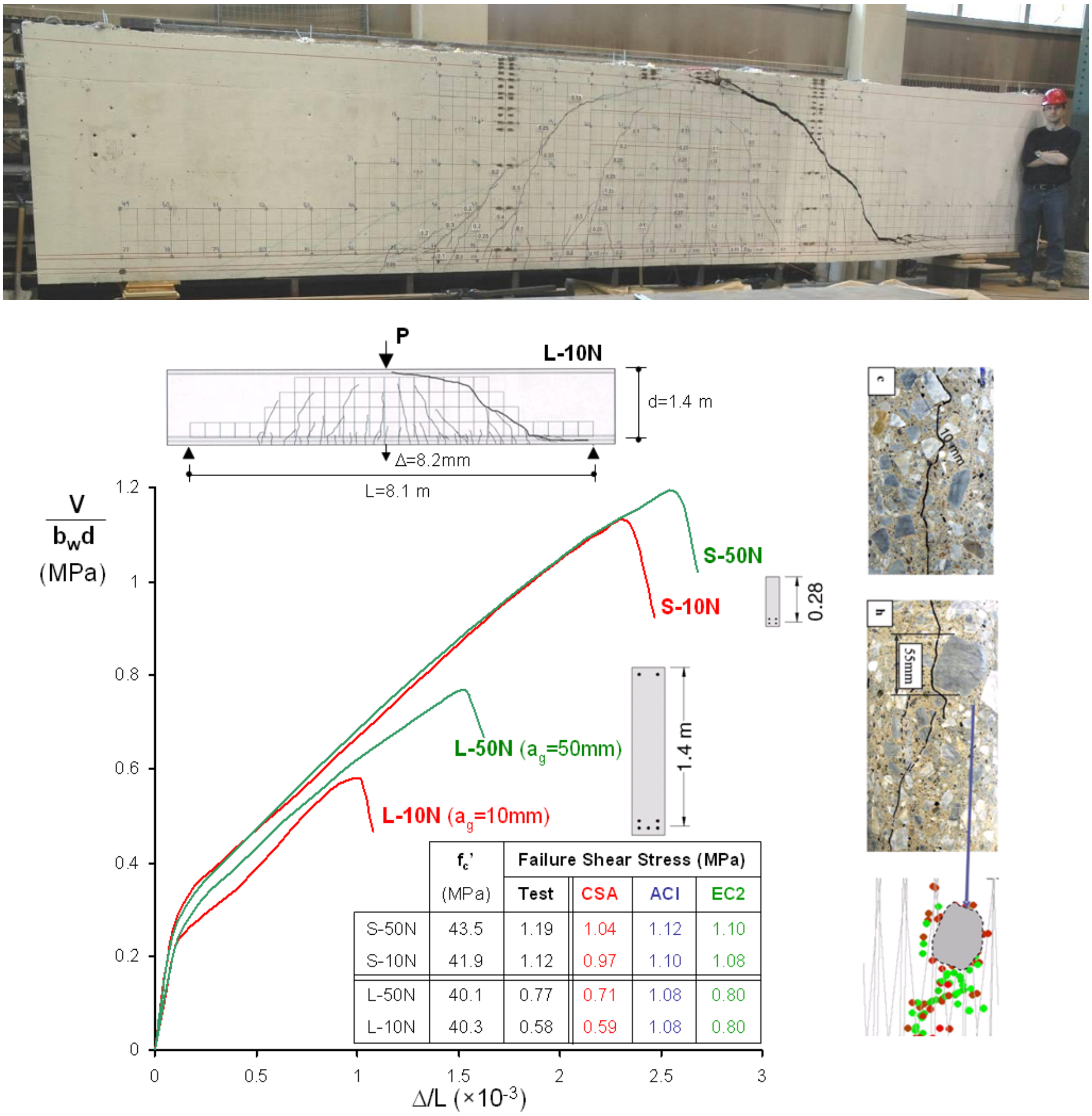

	f_c' (MPa)	Failure Shear Stress (MPa) Test	CSA	ACI	EC2
S-50N	43.5	1.19	1.04	1.12	1.10
S-10N	41.9	1.12	0.97	1.10	1.08
L-50N	40.1	0.77	0.71	1.08	0.80
L-10N	40.3	0.58	0.59	1.08	0.80

Fig.5.6: Effect of aggregate size and member depth on shear strength

In order to understand at a more fundamental level the mechanisms involved in the shear failure of critical members such as the transfer slab discussed above, ten large-scale and ten geometrically-similar, small-scale, shear-critical reinforced concrete slab-strip specimens were tested. The key results of this work were summarized in a 2007 ACI paper by Sherwood, Bentz and Collins titled "Effect of Aggregate Size on Beam-Shear Strength of Thick Slabs." Additional information on the acoustic emission imaging techniques that were used to track crack propagation in a number of the specimens is given in a 2007 paper by Katsaga, Sherwood, Collins and Young. The large-scale specimens had an effective depth of 1400 mm, which was large enough to permit very detailed measurements to be made. See Fig. 5.4. Apart from depth (d = 1400 mm or 280 mm) the prime variable was the maximum aggregate size (10, 20, 40 and 50 mm). Figure 5.6 shows that increasing the maximum aggregate size from 10 mm to 50 mm made the path of the shear crack rougher and increased the failure shear stress for the large specimens by 33%. The figure also shows that the CSA equations predict the failure shear stresses for all four specimens reasonably well. For the large specimen with small aggregate, both ACI and the 2004 Eurocode (EC2) give unconservative predictions.

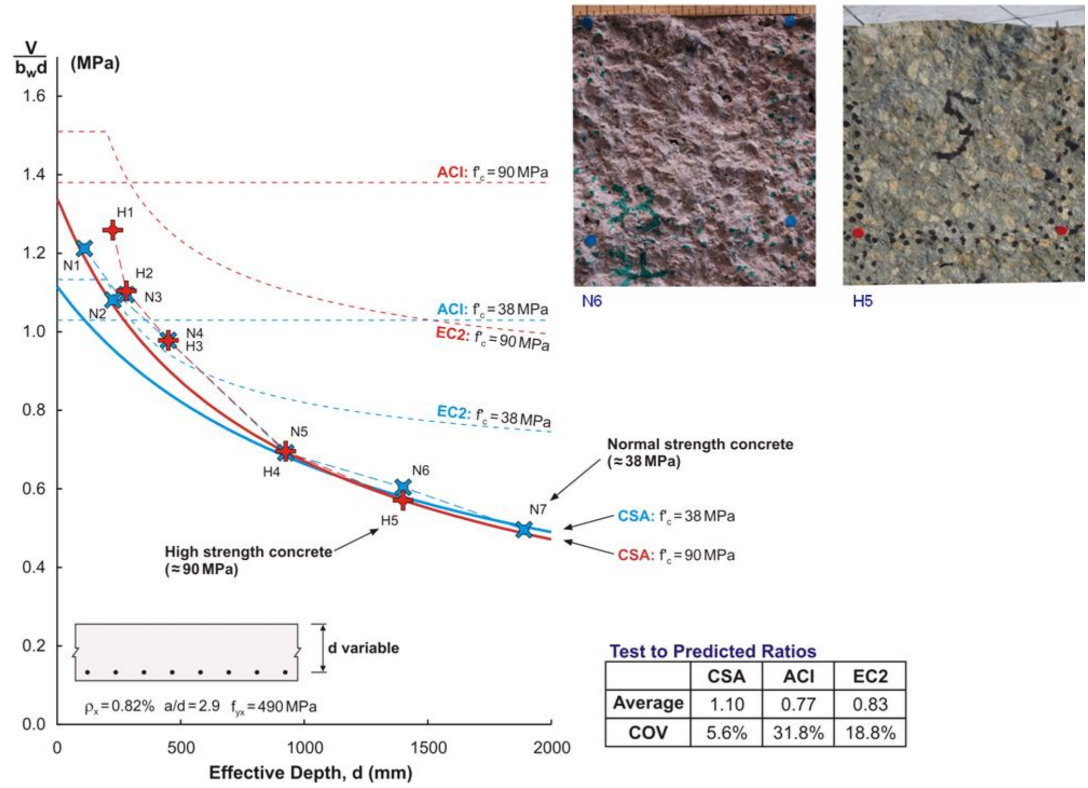

	CSA	ACI	EC2
Average	1.10	0.77	0.83
COV	5.6%	31.8%	18.8%

Fig. 5.7: Effect of member depth and concrete strength on shear strength

The specimens shown in Fig. 5.6 were designed so that the results could be compared with previous experiments conducted at Toronto. Figure 5.7 compares the failure shear stresses for specimens made from normal-strength concrete with the failure shear stresses for specimens made from high-strength concrete. It can be seen that, except for small specimens, no significant increase of shear strength results from the use of high-strength concrete for these members which do not have shear reinforcement. It can also be seen that the CSA standard predicts these results very well. The high-strength concrete members such as H5 have cracks which pass through the aggregate resulting in smoother crack surfaces less capable of transmitting shear stresses. While the CSA shear provisions predict the influence of size and concrete strength very well, the ACI provisions, which were formulated in the 1960's, and the EC2 provisions, which were formulated in the mid 1990's, do not account well for either the effect of size or the effect of concrete strength. Note that the deepest high strength concrete specimen, H5, failed at a shear stress of about $0.07\sqrt{f_c'}$ which is very close to the lower bound predicted by the analysis of the simplified crack pattern shown in Fig. 5.5.

5.4 Large members with small amounts of shear reinforcement.

It can be seen from Fig. 5.7 that the shear stress to cause failure for members without shear reinforcement decreases substantially as the member depth increases and that the magnitude of this size effect is predicted well by the CSA provisions. These provisions predict that if the amount of shear reinforcement, $\rho_z f_y$, in the member exceeds $0.06\sqrt{f_c'}$ the size effect will be negligible. While the ACI code does not directly account for the size effect in shear there are minimum shear reinforcement requirements which help to mitigate the consequences. These requirements state that a minimum amount of shear reinforcement, $0.062\sqrt{f_c'}$, shall be provided in all beams where the applied factored shear force is greater than half of factored shear capacity. Minimum shear reinforcement requirements were first introduced in the 1971 ACI code and hence many existing concrete structures designed prior to this date may contain amounts of shear reinforcement smaller than the current minimum. For example, shown in Fig. 5.8 is an actual beam in a major industrial facility which is about 5 metres deep and contains only about two thirds of the currently specified minimum quantity of shear reinforcement. Does this beam need to be strengthened in shear? Figure 5.8 compares this real beam with the largest shear specimen ever tested (Shioya 1989), along with some of the largest members tested at the University of Toronto which contained small amounts of transverse reinforcement. Also shown is the size of the traditional shear tests (6" x 12") upon which the design provisions used for the beam were based.

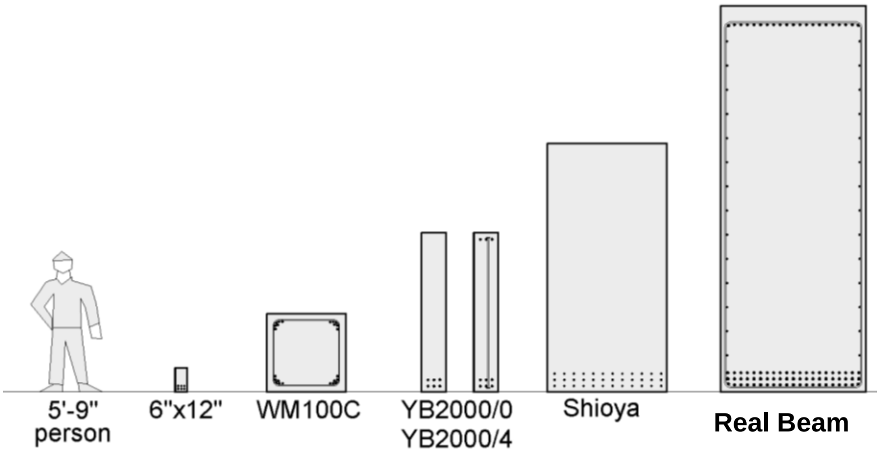

Fig. 5.8: Relative size of beams

Figure 5.9 compares the experimental results of beams containing less than the CSA specified minimum shear reinforcement with the predictions from the CSA code and Response-2000. It can be seen that while the code assumes no benefits of any shear reinforcement less than the minimum, the experiments and the MCFT predictions show that there can be significant increases in shear capacity even for very small quantities of shear reinforcement though there is, of course, still a significant size effect for these members. For the beam in question it was concluded that increasing the existing shear capacity was not required.

Two of the specimens shown in Fig. 5.8 and plotted in Fig. 5.9 were two metre thick slab strip specimens each 300 mm wide forming part of a four specimen series designed to investigate the influence of small quantities of shear reinforcement on the one-way shear behaviour of very thick slabs (Yoshida 2000). Specimen YB2000/0 contained no shear reinforcement while YB2000/4 contained single #4 T-headed bars (yield force 59.4 kN) spaced at 590 mm giving a $\rho_z f_y$ value of 0.336 MPa which is very close to the original required minimum amount of 50 psi. If an existing thick slab was deemed to be unsafe in shear and it was required to provide minimum shear reinforcement, drilling such a closely spaced array of holes would be impractical. Specimen YB2000/6 contained #6 T-headed bars (yield force 132.5 kN) spaced at 1350 mm which gave a $\rho_z f_y$ value of 0.327 MPa, while specimen YB2000/9 contained just one #9 T-headed bar (yield force 303 kN) in the shear span for an equivalent spacing of 2700 mm and a $\rho_z f_y$ value 0.374 MPa. From Fig. 5.9 it can be seen that the CSA provisions predict the shear capacity of YB2000/0 and YB2000/4 very well, but what about YB2000/6 and YB2000/9 which have shear reinforcement spacings that greatly exceed the CSA limits of $0.7d_v$ (1190mm) or 600 mm? The observed shear at failure was 255 kN for YB2000/0 which failed in shear and 674 kN for YB2000/4 which failed in flexure. The specimens with the widely spaced shear reinforcement failed at a shear of 550 kN for YB2000/6 (s/d = 0.71) and 472 kN for YB2000/9 (s/d = 1.43).

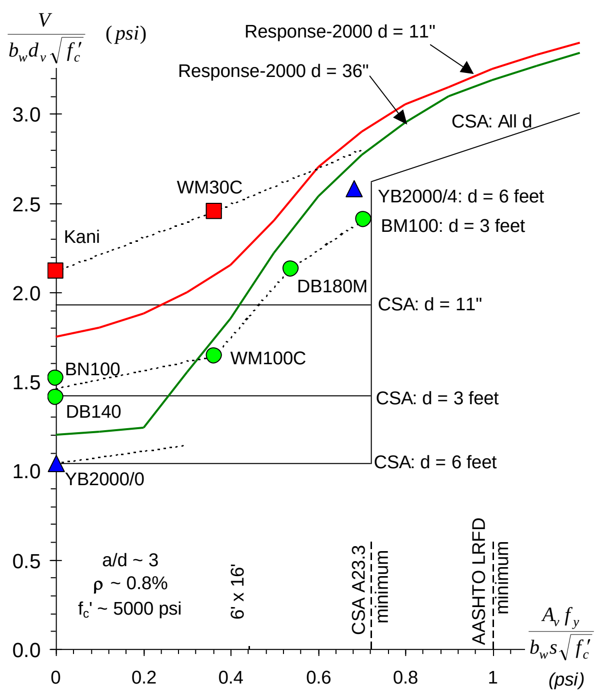

Fig. 5.9: Effect of small quantities of transverse reinforcement on size effect in shear

The observed load-deformation curves of the four YB specimens are shown in Fig. 5.10 while a photograph of YB2000/9 after failure is shown in Fig. 5.11. Note that the addition of just this one large bar halfway along the shear span increased the shear capacity by more than 80%. While the CSA sectional procedures can not predict this strength increase the CSA provisions for strut-and-tie models can be used to make a reasonably accurate estimate of the shear strength of this specimen. See Fig. 5.12.

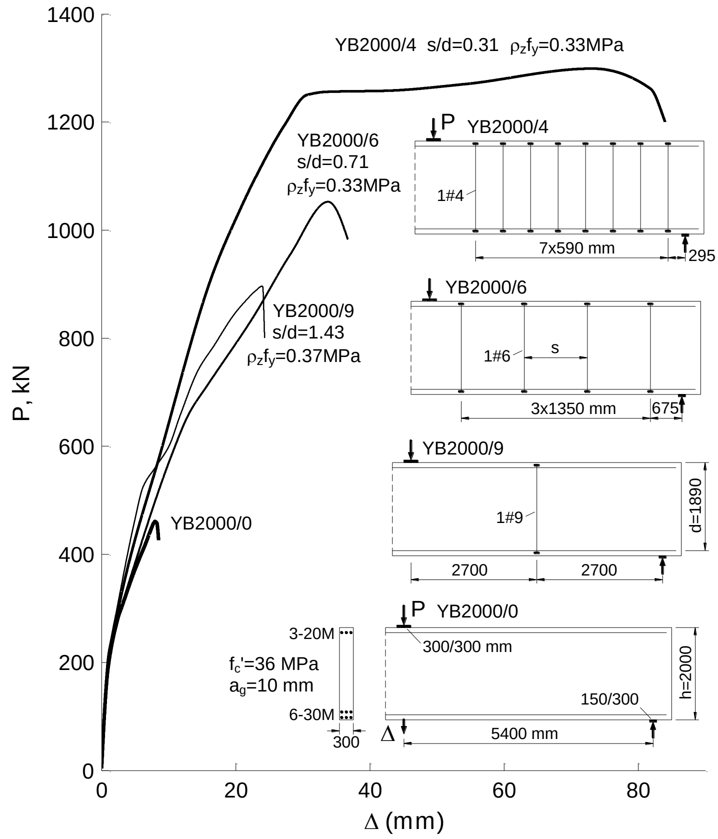

Fig. 5.10: Load-deformation response of slab strips

Fig. 5.11: Post-failure YB2000/9 left end with YB2000/0 on right end

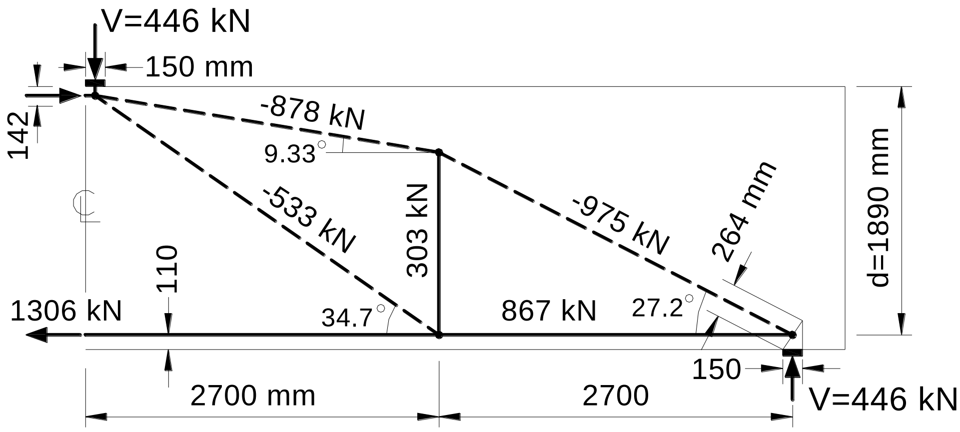

Fig. 5.12: Strut-and-tie model for YB2000/9 with calculated failure shear of 446 kN

5.5 Members with large amounts of shear reinforcement.

Based on the observation that beams with large amounts of shear reinforcement may fail by crushing of the concrete prior to yielding of the stirrups, the ACI-ASCE shear committee in 1963 recommended that the failure shear stress of a beam should not be taken as greater than $0.83\sqrt{f_c'}$. This conservative limit still governs the maximum shear capacity for typical beams designed by the ACI code. The 1984 CSA code introduced both a strut-and-tie model for shear design and a general sectional design method based on the compression field theory. In these methods concrete crushing was assumed to occur when the concrete compressive stress reached the value predicted by Equation 13 in Fig. 5.1 that is $f_c'/(0.8 + 170\varepsilon_1)$. These methods enabled beams to be designed to resist much higher shear stresses than those permitted by the ACI code and this had a considerable effect on the design of coupling beams and transfer girders in high rise buildings.

The photograph in Fig. 5.13 was taken during construction of specimens SA3 and SA4 used in the development of the Compression Field Theory (Collins 1978). The box beams were both loaded and supported by cross beams to reduce the vertical compressive stresses introduced at the load and reaction points. Loads were applied at the ends of the central cross beam and at the end of one of the cantilever overhangs so that the bending moment was zero midway between the cross beams. Considering the thin webs (152 mm) the members contain a large amount of shear reinforcement with the parameter $A_v f_y/(b_w s f_c')$ being equal to 0.116. The difference between the two test sections is that while SA3 had a concrete cover of close to zero SA4 had a clear cover over the stirrups of about 40 mm. Specimens SA1 and SA2 can be seen in the background. These two specimens had stirrups spaced at three times the spacing of SA3 and only contained only one third as much longitudinal reinforcement. SA1 was solid (b_w = 304 mm) while SA2 was hollow (b_w = 152 mm). The cover over the stirrups for both was close to zero. More details of these specimens are given in Fig. 5.14 which also compares the observed failure shears for these four specimens with the predictions of VecTor2, Response-2000, CSA general method (2004), ACI and a traditional 45° truss model. The observed shears at failure were 374 kN for SA1, 324 kN for SA2, 727 kN for SA3 and 531 kN for SA4.

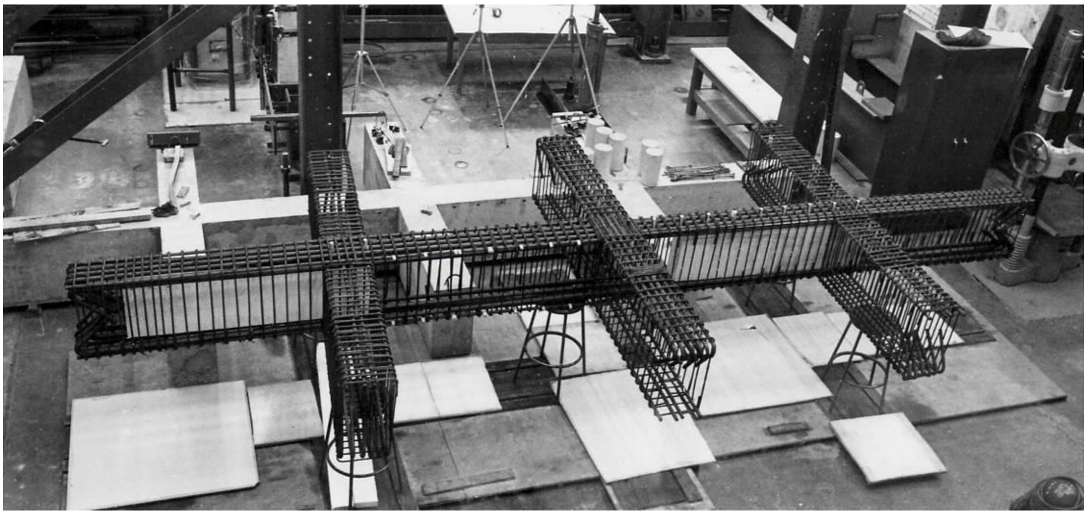

Fig. 5.13: Reinforcing cage for specimens SA3 (left) and SA4 (right) with thinner cage

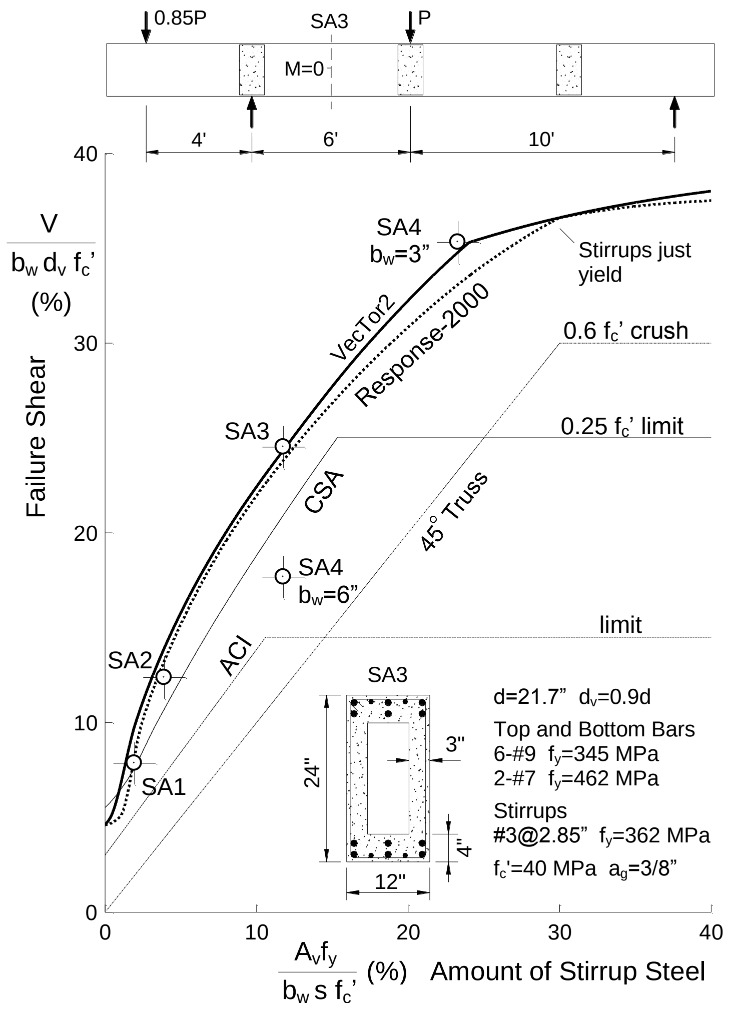

Fig. 5.14: Comparison of observed and predicted failure shears for SA series

Specimen SA4 failed at only 73% of the shear required to fail SA3. This was because the concrete cover in this highly reinforced specimen began to spall as the stirrups reached yield stress resulting in a substantial decrease in the effective web width of the member. In Fig. 5.15a, the splitting cracks that caused the concrete cover to spall can be seen on the top face of the beam close to the cross arms which applied the load. Figure 5.15b shows that this spalling propagated from the top face to the bottom face of the member. The photograph in Figure 5.15c was taken at a somewhat higher load and shows that the covers on both sides of the member have spalled off. Specimen SA4 was constructed in order to investigate if the cover spalling that had been observed in pure torsion tests, see Fig. 5.15d, would also occur in beams with unrestrained concrete covers subjected to high shear forces. As shown in Fig. 5.15, this spalling did indeed occur. If it is assumed that the web width of beam SA4 remains at its initial value of 6” (152 mm) then the experimentally observed failure shear is substantially below the predicted failure shears given by the CSA general method, Response-2000, and VecTor2, see Fig. 5.14. However, if it assumed that 1.5” (38 mm) of concrete cover has spalled off from each side, then b_w reduces to 3” (76 mm) and now the experimental failure shear is in very close agreement with the predictions of Response-2000 and VecTor2 and is considerably above the $0.25f_c'$ maximum shear limit of the CSA general method. Currently, experimental beams are under construction which are designed to investigate further the upper limit on shear strength and how this compares to predictions from both sectional and strut-and-tie models.

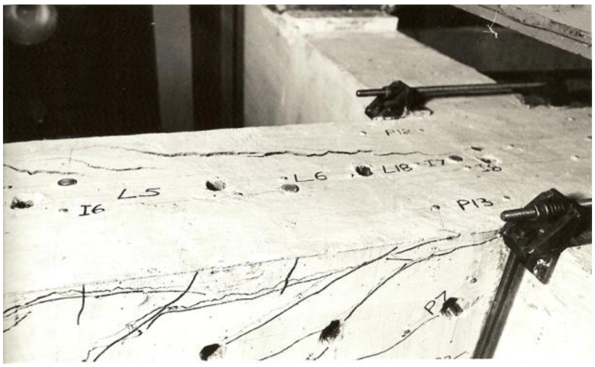

(a) View of cover spalling from above

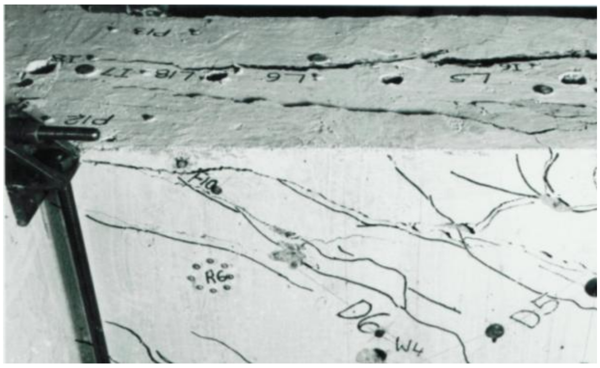

(c) View of cover spalling on both sides

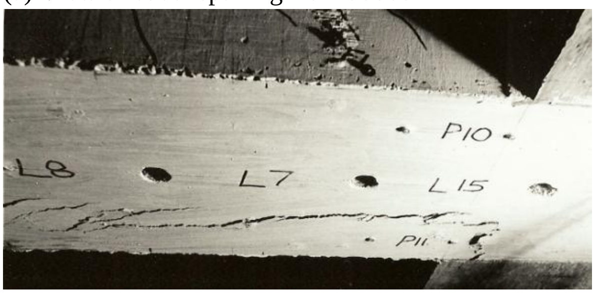

(b) View of cover spalling from below

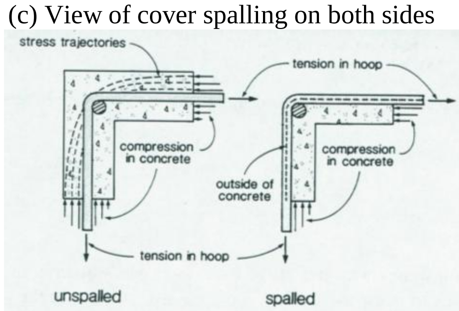

(d) spalling of cover in torsion tests

Fig. 5.15: Cover spalling in specimen SA4

5.6 Influence of reinforcement bond characteristics and bar cutoffs

A series of eight beams 450 mm wide, 750 mm deep, and on a 5.4 m span were loaded to failure in shear to investigate the influence of bond characteristics of the reinforcement and bar cutoffs (5 of the 10 longitudinal bars were cutoff at 1 metre from the centre of the support) (Masukawa 2011). To maintain consistency in the stress-strain properties of the reinforcement, the plain bars for the stirrups and the longitudinal reinforcement were manufactured by grinding the deformations off deformed bars. The stirrups consisted of US#3 bars spaced at 300 mm with a yield stress of 494 MPa ($\rho_v f_y$=0.52 MPa) while the longitudinal reinforcement consisted of 10-25M with a yield strength of 460 MPa (ρ = 1.7%). The average concrete strength was 37 MPa. It can be seen from Fig. 5.16 that the bar cutoffs reduced the shear strength by about 20% in the case of the members with deformed reinforcement and by about 28% for the beams with plain bars. For the beams without bar cutoffs, removing the deformations from the bars reduced the shear strength by about 10% while for beams with bar cutoffs removing the deformations reduced the shear strength by about 18%. While the Reponse-2000 predictions can account to some degree for the reductions in bond properties of the reinforcement by reducing the tension stiffening factor from 1.0 to 0.7, it is not capable of considering the effect of bar cutoffs. With respect to the CSA sectional method, an increase in ε_x by a factor of perhaps 1.5 will give a reasonable estimate of the reduction in shear capacity caused by bar cutoffs.

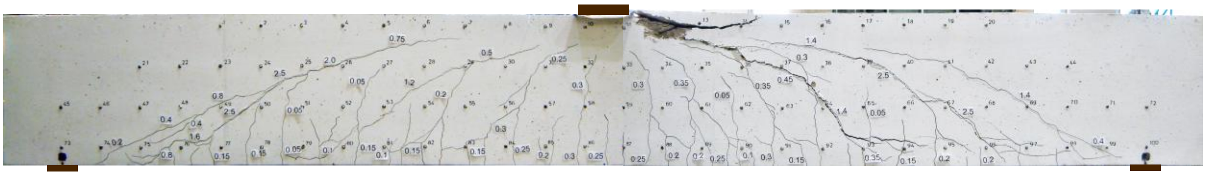

(a) JB1: Deformed bars with no bar cutoffs, Failure Load, P=913 kN

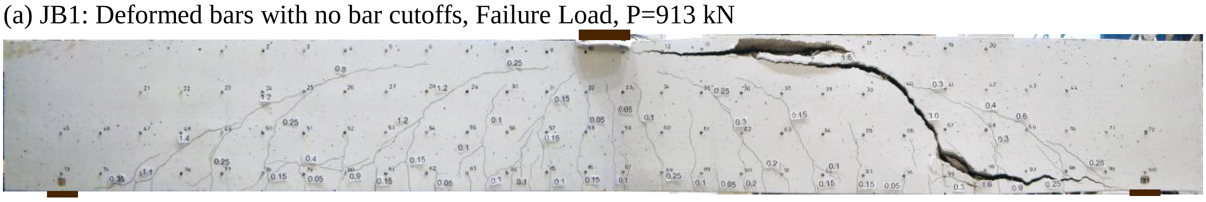

(b) JB5: Deformed bars with bar cutoffs, Failure Load, P=726 kN

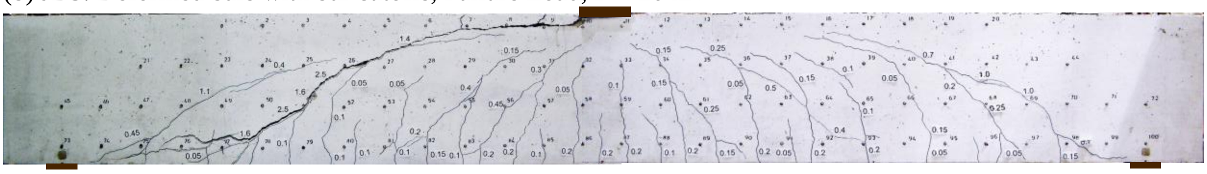

(c) JB3: Plain bars with no bar cutoffs, Failure Load, P=825 kN

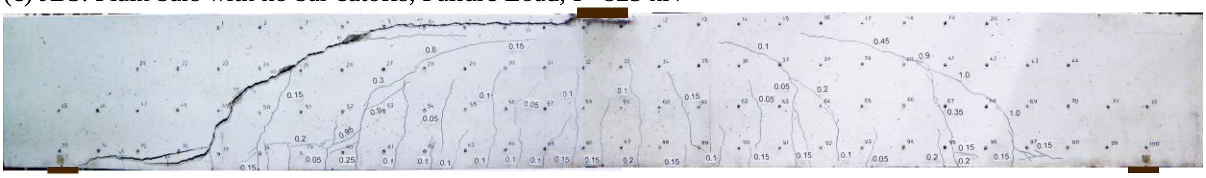

(d) JB7: Plain bars with bar cutoffs, Failure Load, P=593 kN

Fig. 5.16: Influence of bar type and bar cutoffs on failure crack patterns and loads

5.7 Concluding remarks

This paper has presented a brief overview of research conducted at the University of Toronto related to predicting the shear behaviour of reinforced concrete structures. Particular emphasis was placed on situations where the traditional shear design procedures resulted in structures now known to have inadequate factors of safety against shear failure.

5.8 References

ACI Committee 318, 2008, “Building Code Requirements for Reinforced Concrete (ACI 318-08) and Commentary (ACI 318 R-08),” American Concrete Institute, Detroit, 465 pp.

Bentz, E.C., 2000 “Sectional analysis of reinforced concrete members.” Ph.D. Thesis, Department of Civil Engineering, University of Toronto, 198 pp.

Bentz, E.C., 2010, http://www.ecf.utoronto.ca/~bentz/r2k.htm, Response-2000 webpage last accessed 2010/09/29.

Bentz, E.C., and Collins, M.P., 2006, “Development of the 2004 CSA A23.3 Shear Provisions for Reinforced Concrete,” Canadian Journal of Civil Engineering, 33(5), pp.521-534.

Canadian Standards Association, 2004, “CSA Standard A23.3-04: Design of Concrete Structures.” CSA, Mississauga, Ontario, 214 pp.

Collins, M.P., 1978, “Towards a Rational Theory for Reinforced Concrete Members in Shear,” Journal of the Structural Division, ASCE, 104(4), pp. 649-666.

Collins, M.P., Mitchell D., and Bentz E.C., 2008, “Shear Design of Concrete Structures,” The Structural Engineer, Vol. 86, No. 10, pp. 32-39.

European Committee for Standardization, CEN, EN 1992-1-1:2004 Eurocode 2: Design of Concrete Structures- Part 1-1: General rules and rules for buildings, Brussels, Belgium, 2004, 225 pp.

Katsaga, T., Sherwood, E.G., Collins, M.P., and Young, R.P., 2007, “Acoustic Emission Imaging of Shear Failure in Large Reinforced Concrete Structures”, International Journal of Fracture, Springer, Netherlands, 148(1), pp. 29-45.

Masukawa, J., 2011, “Degradation of Shear Performance of beams due to Bond Deterioration and Bar Cutoffs,” Ph.D. thesis, Civil Engineering, University of Toronto, in preparation.

Sherwood, E.G., Bentz, E.C., and Collins, M.P., 2007, “Effect of Aggregate Size on Beam-Shear Strength of Thick Slabs”, ACI Structural Journal, 104(2), pp 180-190.

Shioya, T., 1989, “Shear Properties of Large Reinforced Concrete Member,” Special Report of Institute of Technology, Shimizu Corporation, No. 25, 198 pp. (in Japanese)

Vecchio, F.J. 1989, “Nonlinear Finite Element Analysis of Reinforced Concrete Membranes,” ACI Structural Journal, 86(1), Jan.-Feb. 1989, pp. 26-35.

Vecchio, F.J. and Collins, M.P., 1986, “The Modified Compression Field Theory for Reinforced Concrete Elements Subjected to Shear,” ACI Journal, 83(2) pp. 219-231.

Vecchio, F.J., 2010, http://www.civ.utoronto.ca/vector, VecTor2, last accessed 2010/08/13

Walraven, J.C., 1981, “Fundamental Analysis of Aggregate Interlock,” Journal of the Structural Division, ASCE, 107(ST11), pp 2245-2270.

Yoshida, Y., 2000, “Shear Reinforcement for Large Lightly Reinforced Concrete Members,” M.A.Sc. thesis, Civil Eng, University of Toronto, 150 pp.

6 A structured approach to the design and analysis of beams in shear

Viktor Sigrist[1] and Britta Hackbarth[2]

[1] Professor, Institute of Concrete Structures
Hamburg University of Technology, Germany
[2] Research Assistant, Institute of Concrete Structures
Hamburg University of Technology, Germany

Abstract: Even after many years of in-depth research, the determination of shear strength of structural concrete beams still is in discussion. The reasons for that are, on the one hand, the complexity of the problem and, on the other hand, further developments of structural systems and building materials as well as new questions arising from the evaluation of existing structures. In this contribution a structured procedure including design, detailed analysis and elaborate assessment of structural concrete members subjected to shear is presented. The focus is on the Generalised Stress Field Approach which particularly enables a profound analysis and a general evaluation of a structure. As a rule, such calculations have to be performed iteratively but the equations given here may easily be used in engineering practice, nevertheless. Shear strengths calculated on the basis of this method are compared to experimental findings as well as to results according to *fib* Draft Model Code 2010 and Eurocode 2. It shows that the different methods are partially in good agreement but yield deviating strength values in certain ranges of reinforcement ratio.

6.1 Introduction

Stress field analysis and strut and tie models, respectively, permit visualisation of the force flow and proportioning of a member [Marti (1999)]. They indicate the necessary amount, the correct position, and the required detailing of the main reinforcement. Comprehensive contributions and monographs on these methods are available [Marti (1985), Schlaich and Schäfer (1987), Muttoni et al. (1997)]. The background of these developments is mainly formed by limit analysis methods as are well summarised in an IABSE state-of-the-art report (1979), in Thürlimann et al. (1983) and in Nielsen (1984). However, the problem of determining the shear strength remains open to discussion. In recent years, research has focused on the enhancement and refinement of the above mentioned methods and several compression field approaches which consider equilibrium as well as compatibility conditions and more general stress-strain relationships have been presented. As a rule, the application of such a refined approach requires specialised knowledge and computer programs and therefore, is not prevailing in engineering practice. For the design and analysis of a structural concrete member calculation procedures have to be easy to understand and to use, and the engineer should be able to give physical significance to the parameters involved and understand their importance [Bentz et al. (2006)].

In the present contribution a structured approach to the design, analysis and assessment of reinforced concrete members subjected to shear is described. First, the well known design procedure associated with limit analysis is expounded and next, the Generalised Stress Field Approach (GSFA) which is an extension of the former. Finally, the (modified) Cracked Membrane Model is briefly outlined and it is shown that it comprises the other two methods.

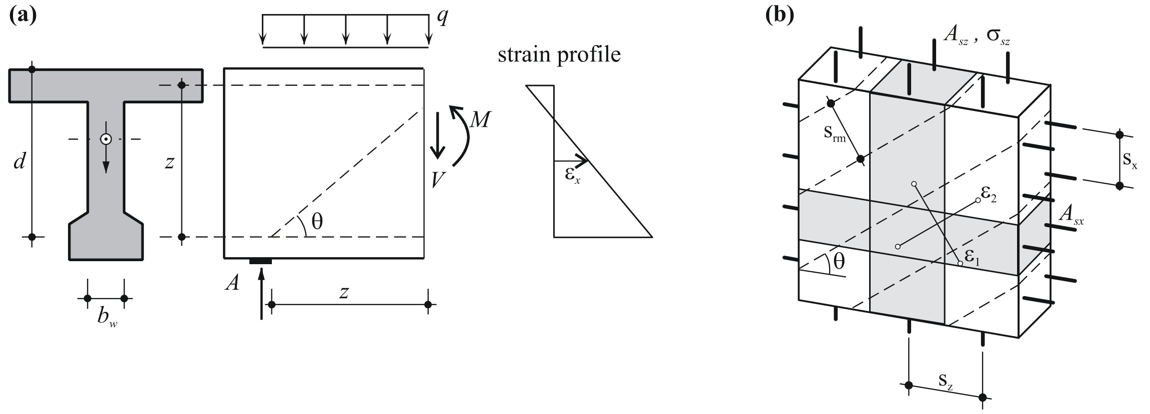

Fig. 6.1: Geometric definitions: (a) cross-section, control section and strain profile; (b) web element

Stress fields are models for describing the stress state within a structure at ultimate. Usually, in the analysis concrete stresses are assigned to nodal zones, fans, compression bands and chords whereas steel stresses refer to tension bands and chords. Fig. 6.1(a) shows the support region of a beam for which (as well as possibly for other locations) design for shear has to be carried out. As defined in several codes [e.g. *fib* (2010)] a control section at the distance z from the face of the support may be assumed, z denoting the effective shear depth and the distance between the top and the bottom chord axes, respectively. Shear forces are resisted by an internal load bearing system consisting of the steel bars (with cross-sectional areas A_{sz} and A_{sx}) and the inclined concrete struts, see Fig. 6.1(b). In webs of beams the forces in horizontal or x-direction are normally taken by the chords and hence, the horizontal reinforcement is of minor importance. For vertical stirrups and a given value of the stress field inclination θ equilibrium considerations yield the well known design equations

$$V_{R,s} = \frac{A_{sz}}{s_z} f_y z \cot\theta \qquad \text{and} \qquad V_{R,\max} = f_{ce} b_w z \sin\theta \cos\theta \qquad (6.1a)\ (6.1b)$$

$V_{R,s}$ denotes the shear resistance provided by the stirrup reinforcement, s_z the stirrup spacing and f_y the yield limit of the reinforcing steel. This resistance is limited to the strength of the concrete struts which is defined by Eq. (6.1b) or rather the effective concrete compressive strength f_{ce}. In the context of design the angle θ may be chosen whereas in the analysis of an existing member θ has to be computed. In any case minimum and maximum limits have to be respected, thus

$$\theta_{\min} \leq \theta \leq \theta_{\max} \qquad (6.2)$$

For $\theta_{\min}$ the resistance is defined by Eq. (6.1a), for higher θ values by $V_{R,s} = V_{R,\max}$ and for $\theta_{\max}$ by Eq. (6.1b). The reduction of the concrete compressive strength is due to strain effects as well as the brittle failure behaviour of concrete in compression:

$$f_{ce} = k_c\ f_c \qquad \text{with} \qquad k_c = \eta_c k_f \qquad (6.3a)\ (6.3b)$$

Analytical expressions for k_c, η_c and k_f are given in the following chapters.

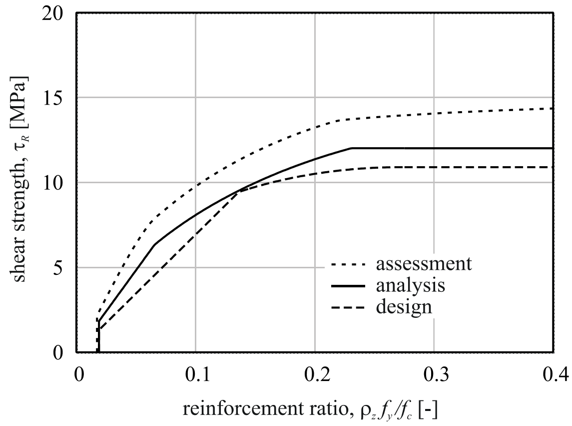

Fig. 6.2: Structured approach to design (limit analysis), detailed analysis (GSFA) and assessment (Cracked Membrane); results for f_c = 40 MPa (or $f_{cm} = f_c$ + 8 MPa for assessment), f_y = 500 MPa, $\varepsilon_x = 0.5 \cdot 10^{-3}$ and steel N (normal ductility)

The application of the above equations in the context of the models presented in the following chapters form a structured approach to design, analysis and assessment of members subjected to shear. The resulting systematics is exemplified in Fig. 6.2; the material strengths are f_c = 40 MPa and f_y = 500 MPa, the longitudinal strain at mid-depth of the web ε_x is $0.5 \cdot 10^{-3}$ and characteristics according to normal ductility steel (steel *N* with f_t/f_y = 1.08, $\varepsilon_{su} = 50 \cdot 10^{-3}$) are assumed. The diagram shows the shear strength $\tau_R = V_R/b_w z$ as a function of the mechanical reinforcement ratio $\rho_z f_y/f_c$ where ρ_z denotes $A_{sz}/b_w s_z$.

The three curves illustrate the idea of differentiating engineering tasks with respect to effort and expected or required precision. For the conception and the "design" of a new structure a procedure according to limit analysis can be used; the results are below those of more accurate calculations. Generally, in the design of structures not all information about material properties, loads and service conditions is available and therefore, a conservative strategy is advisable. However, for a complex design situation or a general evaluation of a structure a detailed "analysis" using the Generalised Stress Field Approach might be necessary; in these cases, more effort in procuring data and computing is reasonable. Eventually, for the elaborate "assessment" of a structure calculations on the basis of the Cracked Membrane Model may be carried out. For the application of this model, full particulars of material properties, structural geometry and loading states are required, but the highest precision is attained. Note that changes in concrete strength as well as in the strength and ductility characteristics of the reinforcing steel may be taken into account. Hence, as visualised in Fig. 6.2 with the choice of an increased concrete strength value, analysis and assessment do not depend on the same set of data.

6.2 Design, analysis and assessment

6.2.1 Design of members in shear

For the design of beams in shear it is reasonable to use a clear procedure which can be derived directly from limit analysis. The basis for this is the inclined stress field (see Fig. 6.1(b)) and the corresponding equilibrium equations. Even if compatibility of strains is not considered, the strength of the inclined stress field has to be reduced to the effective concrete compressive strength f_{ce}. A possible reduction, used in the Swiss design code SIA 262 (2003), is found by applying Eq. (6.3) in the following form:

$$f_{ce1} = 0.6 k_f f_c \qquad \text{with} \qquad k_f = \left(\frac{30}{f_c}\right)^{1/3} \leq 1.0 \qquad \text{[MPa]} \qquad \text{(6.4a) (6.4b)}$$

To account for strain effects, a constant reduction $\eta_c = 0.6$ is assumed. With the factor k_f the concrete compressive strength is diminished for $f_c > 30$ MPa; in this way, the more brittle behaviour of such concrete types is taken into account [Muttoni (1989)]. By considering the use of steel with limited ductility (see Chapter 6.2.2) the following limits for θ should be satisfied:

$$30° \leq \theta \leq 45° \qquad \text{(6.5)}$$

Within these constraints the inclination θ of the concrete struts can freely be chosen. Rearranging Equations (6.1a) and (6.1b) and using the expressions $\tau_R = V_R / b_w z$ and $\rho_z = A_{sz} / b_w s_z$ yields the following equations:

$$\tau_{R,s} = \rho_z f_y \cot \theta_{\min} \qquad \text{(6.6)}$$

$$\tau_R = \sqrt{\rho_z f_y (f_{ce} - \rho_z f_y)} \qquad \text{with} \qquad \tan\theta = \sqrt{\frac{\rho_z f_y}{f_{ce} - \rho_z f_y}} \qquad \text{(6.7a) (6.7b)}$$

$$\tau_{R\max} = f_{ce} \sin\theta_{\max} \cos\theta_{\max} \qquad \text{(6.8)}$$

In the context of limit analysis Eq. (6.7a) is termed as web crushing criterion [Braestrup (1976)]. Results from the above equations are shown in Fig. 6.3. Note that a minimum reinforcement ratio $\rho_{z,\min}$ of $0.12(f_c)^{1/2}/f_y$ [MPa] is presupposed in both cases. The three parts defined by Eqs. (6.6) to (6.8) can clearly be identified as a linear function for low, a curved line for medium and a horizontal branch for high reinforcement ratios. The corresponding stress field inclinations are depicted in Fig. 6.3(b); again, a slightly curved transition line from the lower limit $\theta_{\min}$ to the given maximum value $\theta_{\max}$ is visible.

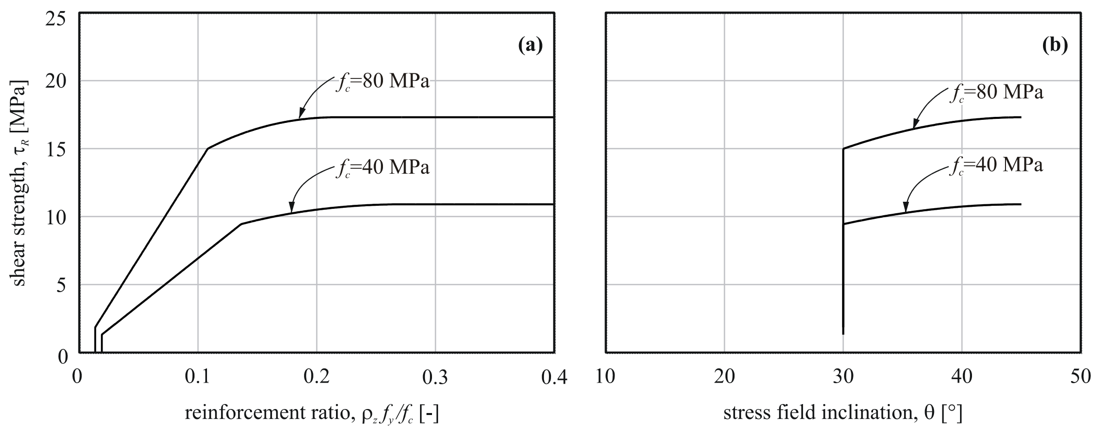

Fig. 6.3: Design of members on the basis of limit analysis: (a) shear strength for f_c = 40 MPa and f_c = 80 MPa, f_y = 500 MPa; (b) corresponding stress field inclinations

6.2.2 Analysis of members in shear

For a general evaluation of an existing structure or for treating a complex design situation some more effort and precision may be adequate. One possibility to increase the accuracy of the calculation is the use of the Generalised Stress Field Approach (GSFA). Fig. 6.4(b) shows a centred fan that is defined by the two inclined discontinuity lines and by the parallel chord axes. The uniformly distributed load q is equilibrated in vertical direction by the stirrup forces $\sigma_{sz} A_{sz} / s_z$ acting on either side of the fan. The concrete within the fan is uniaxially compressed along straight trajectories that intersect outside the beam; the stresses σ_2 vary hyperbolically along these lines. The highest value is found for the bottom right corner of the fan where the smallest angle θ as well as the shortest width occurs. A fan with $\theta = \theta_r$ becomes a stress field with parallel trajectories. In this case, the concrete stresses σ_2 are constant; for the assumptions $\sigma_{sz} = f_y$ and $-\sigma_2 = f_{ce}$ the Eqs. (6.6) to (6.8) are found.

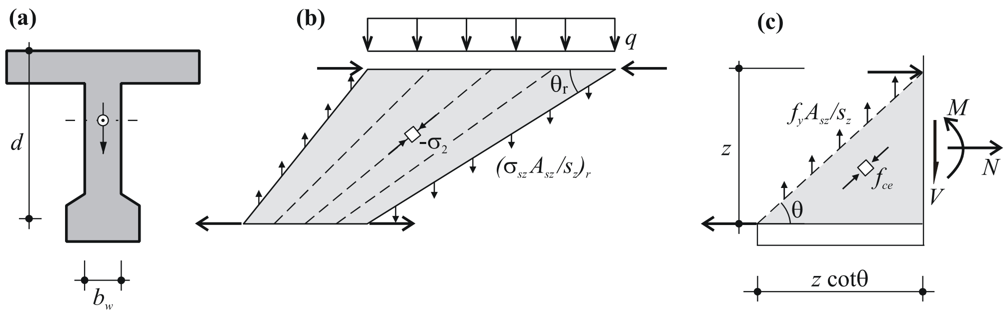

Fig. 6.4: Generalised Stress Field Approach: (a) cross-section; (b) free body diagram of centred fan; (c) beam segment with sectional forces

The generalization of the stress field analysis is accomplished by introducing special limits for the angle θ as well as by adopting a more general equation for determining the effective concrete compressive strength f_{ce}. For the latter, Eq. (6.3) can be used, but η_c has to be evaluated on the basis of experimental results. Kaufmann (1998) proposed a relationship for membrane elements that has been modified to include beam elements as well and adjusted to the notation used here [Sigrist and Hackbarth (2010a,b)]; this yields

$$f_{ce2} = \eta_c k_f f_c \qquad \text{with} \tag{6.9a}$$

$$\eta_c = \frac{1}{1.2 + 55\varepsilon_1} \qquad \text{and} \qquad k_f = \left(\frac{30}{f_c}\right)^{1/3} \leq 1.0 \qquad \text{[MPa]} \qquad (6.9b)\ (6.9c)$$

The principal strain ε_1 (as defined in Fig. 6.1(b)) is found with help of Mohr's circle of strains to $\varepsilon_1 = \varepsilon_x + (\varepsilon_x - \varepsilon_2) \cot^2\theta$. The principal strain ε_2 may be taken as the peak strain $-\varepsilon_{c0}$ at reaching f_{ce}. This value is affected by numerous influences, including the sequence of loading. Though, comparative calculations prove the relatively small implication of this parameter on the predicted strength and therefore, in good approximation a constant value $\varepsilon_{c0} = 0.002$ may be used. Note that longitudinal strains of webs vary linearly over the depth which results in slightly curved stress trajectories with somewhat flatter inclinations and hence, higher compressive stresses at the compression chord. However, the concrete rather crushes at the tension chord where the reduction of the concrete compressive strength is more pronounced. Incidentally, it can be shown that after the onset of yielding of the stirrups initially curved cracks become almost straight [Kaufmann (1998)] as assumed in the stress field analysis. For reasons of applicability, it is recommended to adopt the idea of taking the strain value ε_x at mid-depth of the web as being decisive (Fig. 6.1). This is an arbitrary definition, but it helps harmonizing design rules as well as the analysis of tests.

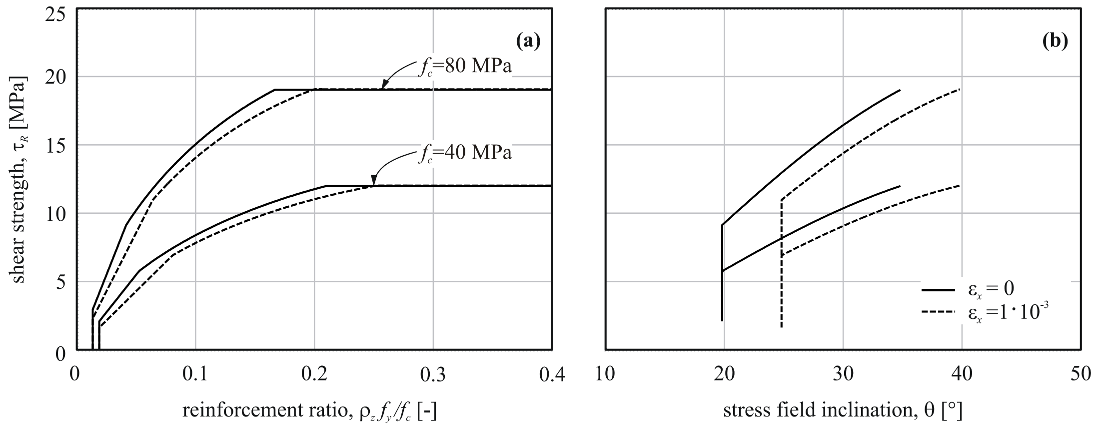

Fig. 6.5: Analysis of members with help of the Generalised Stress Field Approach (GSFA): (a) shear strength for f_c = 40 MPa and f_c = 80 MPa, f_y = 500 MPa, ε_x = 0 and $1.0 \cdot 10^{-3}$ and steel N (normal ductility); (b) corresponding stress field inclinations

Limits of the stress field inclination according to Eq. (6.2) can be determined on the basis of the kinematic condition for membrane elements [Baumann (1972), Collins and Mitchell (1980)]; from Mohr's circle of strains one finds

$$\tan^2\theta = \frac{\varepsilon_x - \varepsilon_2}{\varepsilon_z - \varepsilon_2} \qquad (6.10)$$

and by rearranging and inserting $-\varepsilon_2 = \varepsilon_{c0}$ and $\varepsilon_z = \varepsilon_{sm}$

$$\theta_{\min} = \arctan\left(\frac{\varepsilon_x + \varepsilon_{c0}}{\varepsilon_{smu} + \varepsilon_{c0}}\right)^{1/2} \quad \text{and} \quad \theta_{\max} = \arctan\left(\frac{\varepsilon_x + \varepsilon_{c0}}{\varepsilon_{smy} + \varepsilon_{c0}}\right)^{1/2} \qquad (6.11a)\ (6.11b)$$

By respecting $\theta_{\min}$ the average stirrup strains are limited to values below or at rupture of the steel, i.e. $\varepsilon_{smu} = \kappa_1\varepsilon_{su}$, and by complying with $\theta_{\max}$ to the onset of yielding, i.e. $\varepsilon_{smy} = \kappa_2\varepsilon_{sy}$. The relevant bond coefficients $\kappa = \varepsilon_{sm}/\varepsilon_{s\max}$ can be computed with the Tension Chord Model [Sigrist (1995), Marti et al. (1998)]; in a first approximation $\kappa_1 = 0.25$ and $\kappa_2 = 0.8$ may be taken, indicating that reduction of the steel strain due to tension stiffening is 75% at rupture and 20% at the onset of yielding. Equation (6.11) is rather inappropriate as long as bond coefficients and maximum steel strains are not known and therefore, a simplified expression might be helpful. Provided that the yield limit of the steel f_y is between 400 MPa and 550 MPa and that $-0.5 \cdot 10^{-3} \le \varepsilon_x \le 1.5 \cdot 10^{-3}$ the following limits are recommended:

$$20° + 5'000\,\varepsilon_x \le \theta \le 35° + 5'000\,\varepsilon_x \qquad \text{(steel } N\text{)} \qquad (6.12a)$$

$$16° + 4'000\,\varepsilon_x \le \theta \le 35° + 5'000\,\varepsilon_x \qquad \text{(steel } H\text{)} \qquad (6.12b)$$

Equations (6.12) correspond to linear approximations of Equation (6.11). In this contribution for steel *N* (normal ductility) the values $f_t/f_y = 1.08$ and $\varepsilon_{su} = 50\cdot10^{-3}$ are assumed and for steel *H* (high ductility) $f_t/f_y = 1.2$ and $\varepsilon_{su} = 100\cdot10^{-3}$. Note that for f_y different from the values given above, steel *L* (low ductility) and values $\varepsilon_x > 1.5\cdot10^{-3}$ Equation (6.11) has to be applied.

In Fig. 6.5 results from calculations according to the Generalised Stress Field Approach are shown, i.e. from applying Eqs. (6.6) to (6.8) and considering Eqs. (6.9) and (6.12); basically, this is an iterative procedure. The curves visualize the differences in shear strength τ_R for the strains $\varepsilon_x = 1\cdot10^{-3}$ and 0; these longitudinal strains comprise the most relevant range for beams in shear. A value $\varepsilon_x < 0$ refers to a compressed or prestressed member whereas $\varepsilon_x > 1\cdot10^{-3}$ signifies a member whose tension chord is at the onset of yielding; note that with Eq. (6.11) cases with higher strain values i.e. plastic hinge regions can be treated as well.

6.2.3 Structural assessment

The background of the Generalised Stress Field Approach is the Cracked Membrane Model. This model was presented by Kaufmann (1998) and Kaufmann and Marti (1998) and modified by Sigrist (2011). It is based on the Tension Chord Model which allows treating problems of crack formation and deformation capacity, and extends the concept to states of plain stress. For this purpose, the web of a beam is considered as a composition of membrane elements which are orthogonally reinforced (Fig. 6.1(b)) and subjected to in-plane stresses. In the course of the loading process cracks occur which, in a fully developed crack pattern, have an average spacing of s_{rm}. Assuming a stepped, perfectly plastic bond shear stress-slip relationship [Sigrist (1995)] and applying the general equilibrium equations for the cracked membrane as well as the kinematic condition (6.10) and adequate material properties s_{rm}, θ and τ_R can numerically be determined. Corresponding computations yield the shear strength diagrams plotted in Fig. 6.6.

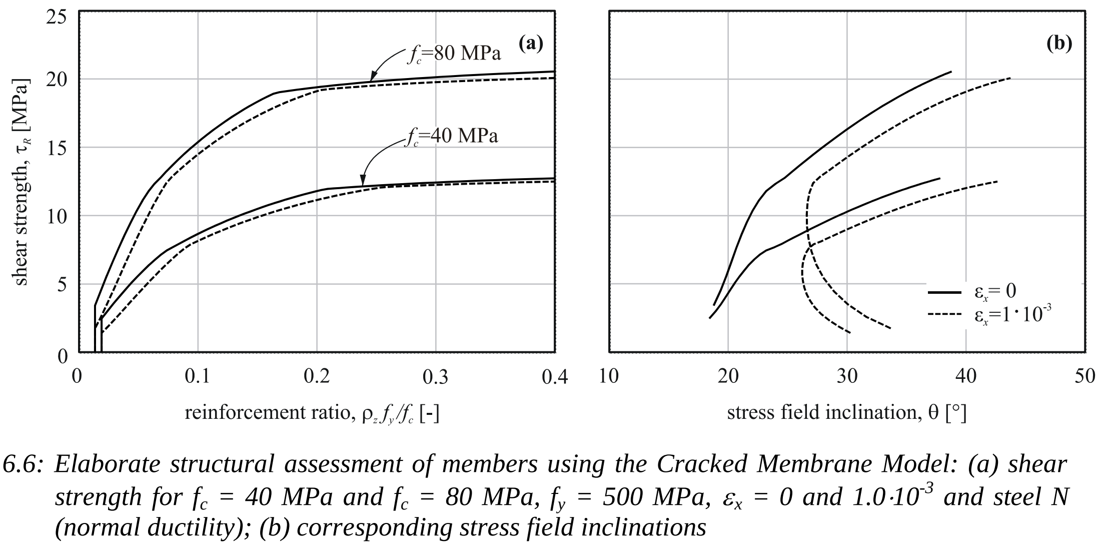

Fig. 6.6: Elaborate structural assessment of members using the Cracked Membrane Model: (a) shear strength for f_c = 40 MPa and f_c = 80 MPa, f_y = 500 MPa, ε_x = 0 and $1.0\cdot10^{-3}$ and steel N (normal ductility); (b) corresponding stress field inclinations

The assumptions described above imply that the directions of the principal stresses and strains coincide, i.e. crack faces are stress free, able to rotate, and perpendicular to the principal tensile direction of the average strains. Thus, θ is a variable rather than a fixed angle. In such a model other influences have to be considered through the definition of the effective concrete compressive strength; since there is good agreement with experimental evidence, in Sigrist (2011) it is proposed to use Eq. (6.9).

The results of Fig. 6.6 apply to elements with f_c = 40 MPa and 80 MPa, f_y = 500 MPa and steel *N* (normal ductility) and again, the two longitudinal strains $\varepsilon_x = 1\cdot10^{-3}$ and 0. The curves can be subdivided into three parts. For low reinforcement ratios rupture of the stirrups is decisive. For higher reinforcement ratios crushing of the concrete governs failure, where up to shear strengths of approximately 12 MPa and 19 MPa the stirrups are yielding. Eventually, for high mechanical reinforcement ratios the stirrups remain elastic. The two failure modes can be distinguished also in Fig. 6.6(b) where the corresponding angles θ are shown. It might be of particular interest that the values of θ quite strongly depend on the longitudinal strain and the ductility characteristics of the steel.

It has to be emphasised that a change of one or more of the input values has an influence on the results but does not bias the general findings. For computing the curves of Fig. 6.6 realistic (rather unfavourable) values are chosen so that the calculated strength values are typical for practical application; consequently, these curves can be used as reference. As the method is general, each value can be adjusted to the actual situation and effects like reduced strength or bond properties due to corrosion of the steel or degradation of the concrete may be taken into account. For the assessment of a structure such refinements are of special interest.

6.3 Comparison of results

6.3.1 Comparison to experimental data

The definitions of Eq. (6.9) rely on experimental data. In the course of a study presented in Sigrist (2011) 113 experiments, 56 of which are beam and 57 are panel tests, have been analysed with help of the Generalised Stress Field Approach. Only selected experiments are included in the evaluation. Beam tests with flexural or anchorage failures as well as panel tests with applied axial stresses or anchorage failures are excluded.

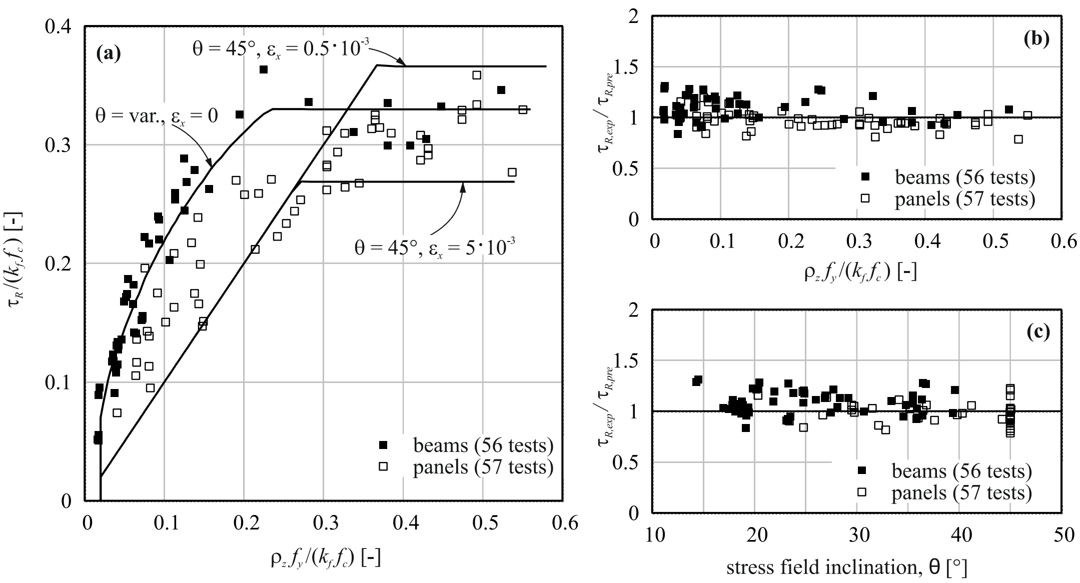

Fig. 6.7: Comparison of predicted and observed values: (a) observed shear strengths and approximated envelope of predictions; ratio of observed to predicted shear strengths as a function of (b) the reinforcement ratio and (c) the stress field inclination

Geometric data, material properties and failure loads are acquired from the reports and all the static key figures such as stresses and strains are computed on the basis of the equations given above. For the beam tests the longitudinal strains are found with the top and bottom chord forces

$$F = \mp \frac{M}{z} + \frac{|V|}{2} \cot \theta \qquad (6.13)$$

from which, by considering cross-sectional areas and stiffness of the chords, the strains ε_x can be approximated; in doing so, tension stiffening in the tension chord is taken into account.

In Fig. 6.7(a) the observed shear strengths are divided by $k_f\, f_c$ and plotted versus the normalised mechanical reinforcement ratio $\rho_z f_y /(k_f\, f_c)$; thus, the results are independent of the concrete compressive strength. In the beam tests the longitudinal strains ε_x are in the range of $0.1{\cdot}10^{-3}$ to $1.5{\cdot}10^{-3}$ (with one exception) and the calculated θ values are between 14.3° and 39.3°. Therefore, the curved line drawn in the diagram can be regarded as an upper boundary for all experiments with $\rho_z f_y /(k_f\, f_c) < 0.24$. In the panel tests the strain values are between $0.5{\cdot}10^{-3}$ and $43{\cdot}10^{-3}$ (maximum $5{\cdot}10^{-3}$ for high reinforcement ratios) with θ values in the range of 20.3° and 45°. For low and medium reinforcement ratios the straight line, corresponding to $\theta = 45°$, can be seen as a lower boundary. For values of approximately $\rho_z f_y /(k_f\, f_c) > 0.3$ upper and lower boundaries may be defined by $\varepsilon_x = 0.5{\cdot}10^{-3}$ and $5{\cdot}10^{-3}$. In all, the calculated lines of Fig. 6.7(a) represent the approximated envelope of predictions and impressively visualise the accuracy of the method.

However, it has to be noted that the experimental results are not uniformly distributed within the ranges of the parameters. In Fig. 6.7(b) the ratios of observed to predicted strength values are depicted. The reinforcement ratio $\rho_z f_y /(k_f\, f_c)$ varies widely but most of the experiments refer to values smaller than 0.2 and in this range the average of the strength-ratios reveal a less accurate prediction compared to the overall trend. The scatter of the plotted points suggests that especially for low reinforcement ratios additional factors contributing to the strength might be important, such as dowel action of the reinforcing bars or the resistance of the compression chord. As the calculation of the inclination of the stress field involves most of the parameters related to the shear problem it is of special interest to plot the shear strength ratios as a function of θ; the results are more or less uniformly distributed in this diagram which again supports the general findings. Overall, an average of the ratio $\tau_{R,exp}/\tau_{R,pre}$ of 1.03 and a coefficient of variation of 11.5% are found; the corresponding values for the beam tests are 1.09 and 10.6% and for the panel tests 0.98 and 9.8%.

As can be seen from the comparison to experimental data, the relationships given here cover a wide range of parameters and include the behaviour of beams as well as that of panels. On the one hand, this unification strongly supports the reliability of the method but on the other hand, it is debatable since the state of strain in panels in pure shear differs from that in beams subjected to flexure and shear. Nevertheless, good correlation of experimental data and the results from Equation (6.9) is obtained in both cases. Within the framework of research further differentiation might be made and some of the parameters should individually be accounted for; of special interest are concrete strength, member size and contributions of the chords.

6.3.2 Comparison to code equations

In Fig. 6.8 results from the Generalised Stress Field Approach (GSFA) are compared to those from Level I, II and III calculations according to *fib* Draft Model Code (2010) and from Eurocode 2 (2004) (EC2). Level I and III equations are based on the general idea that the shear resistance of a reinforced concrete member is provided by the shear reinforcement (stirrups) $V_{R,s}$ and the contribution of the concrete $V_{R,c}$ due to frictional forces transferred over the cracks; this results in

$$V_R = V_{R,s} + V_{R,c} \tag{6.14}$$

For given θ values $V_{R,s}$ can be calculated with help of Eq. (6.1a), and for $V_{R,c}$ the expression $k_v\ (f_c)^{1/2}\ b_w\ z$ is used; the factor k_v is defined as 0.15 for a Level I and as $0.4/(1+1'500\varepsilon_x)$ for a Level III Approximation. In applying these methods θ values of 36° and $(29°+7'000\varepsilon_x)$, respectively, have to be assumed. In a Level II Approximation k_v is set to 0, i.e. the contribution of the concrete is not considered explicitly. This method refers to limit analysis as described in Chapter 6.2.1, however, for the choice of θ the lower limit of (Eq. 6.5) is replaced by $(20°+10'000\varepsilon_x)$. In any method, the shear resistance is limited to the values of Eq. (6.1b) where according to *fib* Draft Model Code $k_c = 0.50k_f$ (Level I) and $0.55k_f$ (Levels II and III) have to be inserted.

Eurocode 2 (2004) is based on conventional limit analysis (Chapter 6.2.1) and Eqs. (6.1a) and (6.1b) apply. The limits for the stress field inclination are given to $21.8° \leq \theta \leq 45°$ and the reduced concrete compressive strength is defined as $0.6(1-f_c/250)\,f_c$. Note that for comparison purposes the results from Eurocode 2 have to be transformed to the control section, see Fig. 6.1 [Sigrist and Hackbarth (2010b)].

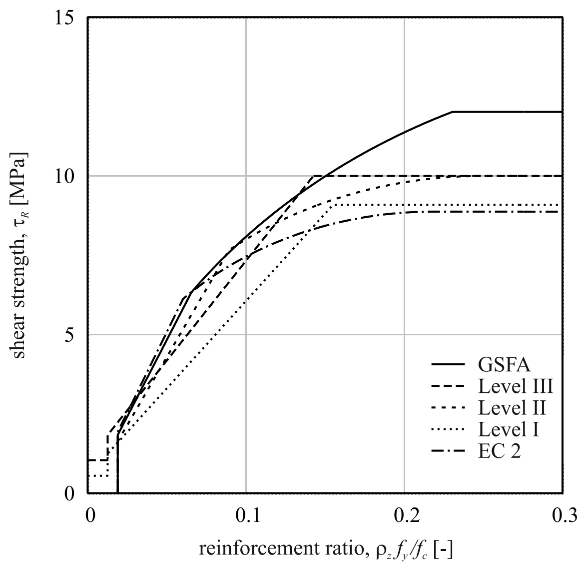

Fig. 6.8: Comparison of Generalised Stress Field Approach (GSFA) to Level I, II and III calculations according to fib Draft Model Code (2010) as well as to results from Eurocode 2 (2004) for f_c = 40 MPa, f_y = 500 MPa and $\varepsilon_x = 0.5\cdot10^{-3}$ and steel N (normal ductility)

In Fig. 6.8 it can be seen that the curve of the Generalised Stress Field Approach is close to or lies above the other lines in the entire range of reinforcement ratios. This finding is true for longitudinal strains ε_x higher than approximately $0.5 \cdot 10^{-3}$; for lower ε_x values the Level III results exceed the others. In a similar manner, the Level II results partly overlap those from Level III. This is due to the angle θ_{min} which is a model parameter in the methods based on limit analysis. For low reinforcement ratios this does not cause great problems, however, for medium and high reinforcement ratios as well as for high longitudinal strains Level I and III results seem to be somewhat conservative. Apart from that, as can be concluded from Fig. 6.8 it is appropriate to increase the upper limit (e.g. to $0.6 k_f f_c$) given by the *fib* Draft Model Code for high reinforcement ratios. Regarding Eurocode 2, it is evident that for low and medium reinforcement ratios results are rather high but basically do not contradict the ones from the Generalised Stress Field Approach. For high reinforcement ratios they agree well with the results from Level I analysis.

For members without shear reinforcement or with ratios below $\rho_{z,min}$ only Level I and III calculations yield a shear resistance which for the latter is given by

$$V_{R0} = \frac{0.4}{(1+1500\varepsilon_x)} \cdot \frac{1300}{(1000+0.7k_{dg}z)} \sqrt{f_c}\; b_w z \qquad \text{[MPa]} \tag{6.15}$$

where k_{dg} accounts for the influence of the aggregate size. This equation (or an equivalent expression) might be combined with the Generalised Stress Field Approach and with Level II Approximations, respectively. By doing so, the gap in the diagram of Fig. 6.8 could be closed and the respective procedures would be amended to cover all possible cases.

6.4 Conclusions

The structured approach presented in this contribution covers design, detailed analysis and elaborate structural assessment of beams in shear. The models involved are consistent and can be deduced from one another. Evidently, the effort in calculating the shear strength is low for designing and high for evaluating a member but accuracy is increased as well and moreover, insight in structural behaviour is significantly deepened.

The procedures discussed here are based on rational models, i.e. on models that reflect the physical background of structural behaviour. Such models do not (and never will) cover all aspects of the actual relations but enable - provided that parameters are chosen carefully - the safe design of structures. With respect to engineering practice, the strength of a rational model also lies in the possibility of extending it to new design problems apart from the few that are discussed in engineering text books.

6.5 References

Baumann, T. (1972). Zur Frage der Netzbewehrung von Flächentragwerken (On the Problem of Net Reinforcement of Surface Structures). *Bauingenieur*, Berlin, Vol. 47, No. 10, pp. 367-377.

Bentz, E.C., Vecchio, F.J., Collins, M.P. (2006). The Simplified MCFT for Calculating the Shear Strength of Reinforced Concrete Elements. *ACI Structural Journal*, V. 103, No. 4, pp. 614-624.

Braestrup, M.W. (1976). Plastic Analysis of Shear in Reinforced Concrete. *Magazine of Concrete Research*, Vol. 26, No. 89, Dec. 1974, pp. 221-228.

Collins, M.P., Mitchell, D. (1980). Shear and Torsion Design of Prestressed and Non-Prestressed Concrete Beams. *PCI Journal*, V. 25, No. 5, pp. 32-100.

Eurocode 2 (2004). EN 1992-1-1: Design of concrete structures - Part 1, General rules and rules for buildings. CEN - *European Standard*, 225 pp.

fib (2010). *Model Code for Concrete Structures - first complete draft*. *fib* Bulletin, No. 56, pp. 312.

IABSE (1979). Colloquium on Plasticity in Reinforced Concrete. Copenhagen, International Association for Bridge and Structural Engineering (IABSE), *Introductory Report* V. 28, 179 pp. and *Final Report* V. 29, 360 pp.

Kaufmann, W. (1998). Strength and Deformations of Structural Concrete Subjected to In-Plane Shear and Normal Forces. *Report*, Institute of Structural Engineering, ETH Zürich, No. 234, 147 pp.

Kaufmann, W., Marti, P. (1998). Structural Concrete: Cracked Membrane Model. *Journal of Structural Engineering*, ASCE, Vol. 124, No. 12, pp. 1467-1475.

Marti, P. (1985). Basic Tools of Reinforced Concrete Beam Design. *ACI Structural Journal*, V. 82, No. 1, pp. 46-56.

Marti, P., Alvarez, M., Kaufmann, W., Sigrist, V. (1998). Tension Chord Model for Structural Concrete. *Structural Engineering International*, V. 8, No. 4, pp. 287-298.

Marti, P. (1999). How to Treat Shear in Structural Concrete. *ACI Structural Journal*, V. 96, No. 3, pp. 408-414.

Muttoni, A. (1989). *Die Andwendbarkeit der Plastizitätstheorie in der Bemessung von Stahlbeton* (The Applicability of the Theory of Plasticity in the Design of Reinforced Concrete). Report, Institute of Structural Engineering, ETH Zürich, No. 176, 159 pp.

Muttoni, A., Schwartz, J., Thürlimann, B. (1997). *Design of Concrete Structures with Stress Fields*. Birkhäuser, 141 pp.

Nielsen, M.P. (1984). *Limit Analysis and Concrete Plasticity*. Prentice Hall, 420 pp.

Schlaich, J., Schäfer, K. (1987). Towards a Consistent Design of Structural Concrete. *PCI-Journal*, May-June 1987, pp. 75-150.

SIA 262 (2003). Concrete Structures. *Code*, Swiss Society of Engineers and Architects, Zürich, 90 pp.

Sigrist, V. (1995). Zum Verformungsvermögen von Stahlbetonträgern (On the Deformation Capacity of Structural Concrete Girders). *Report*, Institute of Structural Engineering, ETH Zürich, No. 210, 159 pp.

Sigrist, V., Hackbarth, B. (2010a). Stress Field Analysis of Structural Concrete Beams. *Proceedings*, 3rd International *fib* Congress 2010 and Annual **pci** Convention, Washington D.C., USA, May 29 - June 6.

Sigrist, V., Hackbarth, B. (2010b). Querkrafttragfähigkeit von Stahlbetonträgern - Bemessung, Überprüfung, Beurteilung (Shear Capacity of Structural Concrete Beams - Design, analysis, Assessment). *Beton- und Stahlbetonbau*, Wiley - Ernst & Sohn, V. 105, No. 11.

Sigrist, V. (2011). Generalized Stress Field Approach for the Analysis of Beams in Shear. *ACI Structural Journal*, accepted for publication 2011

Thürlimann, B. et al. (1983). *Die Anwendung der Plastizitätstheorie auf Stahlbeton* (Application of the Theory of Plasticity to Reinforced Concrete). Institute of Structural Engineering, ETH Zurich, Switzerland, 252 pp.

7 Shear in slabs and beams: should they be treated in the same way?

Aurelio Muttoni[1] and Miguel Fernández Ruiz[2]

[1]Prof. Dr., École Polytechnique Fédérale de Lausanne, Switzerland
[2]Dr., École Polytechnique Fédérale de Lausanne, Switzerland

Abstract: This chapter discusses the differences on the mechanical behaviour and strength of beams (one-way slabs) and two-way slabs with reference to their shear response with and without transverse reinforcement. This investigation evidences some fundamental differences on their governing failure modes and shear-carrying mechanisms. On the basis of such differences, the suitability of performing shear design using strain-based models or equilibrium-based models is discussed for the different members.

7.1 Introduction

Since the early developments of reinforced concrete, the construction of slabs has traditionally been performed without placing of any shear reinforcement or by placing it only in limited areas near concentrated loads or supports. On the contrary, beams and girders have typically been provided with shear reinforcement. Members with stirrups can carry relatively large shear forces and, provided with a minimal amount of transverse reinforcement, their behaviour is rather ductile. On the contrary, members without transverse reinforcement typically fail in a brittle manner by development of a shear crack localizing strains. As a consequence, shear design has traditionally been performed on the basis of different approaches for members with and without transverse reinforcement.

With respect to girders or beams with transverse reinforcement, the first consistent shear design methods were based on the truss analogy [Ritter (1899), Mörsch (1908)], see Figures 7.1a,b. This approach was based on an intuitive understanding of the experimental behaviour of reinforced concrete members and proposed to use equilibrium-based models (typically statically determinate trusses) to calculate the necessary shear reinforcement. This approach was later developed mostly in Germany during the 60’s by Leonhardt and his team (proposing truss models for design of complicated members on the basis of the elastic stress field in a member) and in the 80’s by Schlaich et al. (1987).

In parallel to these works, Drucker developed in 1961 a plastic stress field for design of a simply-supported beam. The work on the theory of plasticity of Drucker was later extended in Switzerland [Thürlimann et al. (1983), Muttoni et al. (1997), Marti et al. (1999)] and in Denmark [Braestrup (1974), Nielsen (1999)] leading to the development of the stress field method for design of concrete structures [Müller (1978), Muttoni et al. (1997)] which also provides a consistent basis for design of members in shear with transverse reinforcement.

The basic behaviour and failure mechanisms of beams without shear reinforcement were also early identified by Mörsch. Contrary to members with transverse reinforcement (where shear design was performed on the basis of a distributed compression field in the web, Figs. 7.1a,b), Mörsch (1929) acknowledged that for members without transverse reinforcement shear was carried by an inclined compression strut, whose strength was influenced by the inclined cracks developing through the web (Figs. 7.1c,d).

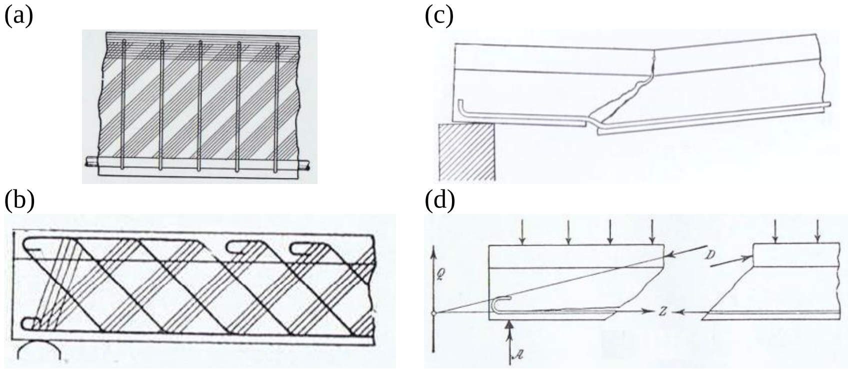

Fig. 7.1: Shear carrying-mechanisms according to Mörsch (1929): (a) compression field in the web of a beam with transverse reinforcement; (b) detail of compression struts near a support region; (c) shear crack leading to failure in a beam without transverse reinforcement; and (d) compression zone in the web (single strut) carrying shear

Although the basic principles leading to shear failures in members without transverse reinforcement were correctly observed by Mörsch, their design was mostly based on empirical models. The works of Moody et al. (1954) at Illinois clearly showed the influence of some parameters on the shear strength of simply supported beams (like the amount of longitudinal reinforcement, concrete compressive strength and shear span-to-depth ratio *a/d*). This work had a significant impact and influenced the design formulas in North-American codes. In 1968, Zsutty proposed an empirical approach on the basis of available test data (containing amongst others the tests by Moody et al. (1954)). Zsutty was professor at San Jose State College (USA) and was specialized in the use of probability theory and statistics. His work led to an empirical equation relating the shear strength to some mechanical and geometrical parameters such as concrete compressive strength, reinforcement ratio and beam span-to-depth ratio. His approach provided significantly more accurate estimates of the shear strength than the empirical formula considered in the ACI code of the time (ACI 318-63). Although the formula from Zsutty was fully empirical and in principle only applicable to simply supported beams subjected to point loading (the shear span-to-depth ratio *a/d* is for instance undefined for uniform loading), his work has been later refined to include the influence of other phenomena such as the size effect and adopted in many codes of practice, such as Model Code 90 [CEB (1993)] or Eurocode 2 (2004).

However, some approaches based on physical models have also been developed for members without transverse reinforcement. The first mechanical model with large significance was proposed by Kani (1955) (see a detailed summary in [Kani et al. (1979)]). More recently, some theories like the Modified Compression Field Theory [Vecchio and Collins (1986)] or the Critical Shear Crack Theory [Muttoni (2003), Muttoni and Fernández Ruiz (2008)] have provided a rational basis to calculate the shear strength of beams as a function of crack widths and the roughness of the cracks. The calculation of the shear strength in these theories relies on strain-based models (contrary to the equilibrium-based models of members with stirrups). Their accuracy, their consistency as well as their rather simple design expressions have recently led to their implementation into codes of practice (such as the Canadian code CSA (2004) and the Swiss code SIA 262 (2003)).

Regarding the behaviour and strength of slabs subjected to concentrated loads, failure in punching shear was early identified as one of the governing phenomena for design of flat slabs [Muttoni (2008)]. No significant mechanical model was available however until 1960, when the works of [Kinnunen and Nylander (1960)] led to the development of the first rational theory for punching shear design of members without transverse reinforcement. Their approach was based on the calculation of the strength of the inclined strut carrying shear near a concentrated load, which (according to Kinnunen and Nylander) was a function of the concrete tangential strains. The model provided consistent and rather accurate results. However, its practical application was rather cumbersome and it had limited impact on design codes, which remained mostly based on empirical models. Currently, consistent design approaches based on mechanical models and leading to compact design formulations are available [Broms (2006), Muttoni (2008)]. A discussion of the applications of the Critical Shear Crack Theory to punching shear design can be found on a companion paper in this bulletin [Muttoni and Fernández Ruiz (2010b)].

This paper presents a discussion of the differences between the shear behaviour of slabs and beams. They are treated in the perspective of the basic shear-carrying mechanisms and governing failure modes of members with and without shear reinforcement. On that basis, a justification of rational approaches for shear design in each case is presented.

7.2 Shear in slabs and in beams, phenomenological considerations

The design of many structural members is governed by shear. This is the typical case for slabs (usually without shear reinforcement or with shear reinforcement concentrated in limited zones) and for the webs of beams or girders (usually with shear reinforcement), see Figure 7.2.

7.2.1 Distribution of shear forces in slabs and linear members

In one-way slabs subjected to uniform distributed loading, the directions for transmission of the shear forces are parallel and correspond to perfect shear loading conditions (Figure 7.2a). In these cases, shear failures typically develop in a brittle manner without yielding of the flexural reinforcement. For statically redundant members (as the top slab of the earth-covered structure of Fig. 7.2a), failures in shear may also develop in plastic hinges, potentially limiting their rotation capacity and thus the strength of the member [Vaz Rodrigues et al. (2010)].

On the contrary, for slabs subjected to concentrated loads, the directions followed by shear forces are not parallel, see Figures 7.2b,c. In these cases, failures in shear may appear near linear supports (Fig. 7.2b), although, depending on the gradient of shear forces, punching shear failures may also develop near concentrated loads (refer to Figs. 7.2b,c). Contrary to failures in perfect shear conditions, failures in punching shear are associated with the development of significant rotations around the concentrated load (local yielding of the flexural reinforcement [Muttoni (2008)]). In these cases, determination of the governing shear force and of its associated failure mode requires combining shear field analysis with shear and punching shear strength models [Vaz Rodrigues et al. (2008)].

Due to the brittle failure nature of failures in shear without transverse reinforcement, shear design and assessment of slabs without transverse reinforcement is usually performed on the basis of the elastic shear field [Fernández Ruiz et al. (2009), Sagaseta et al. (2010)]. However, analyses accounting for redistributions in the shear field after cracking, yielding of flexural reinforcement or localized shear deformations are also possible, provided that shear failure does not necessarily lead to a sudden unstable propagation [Sagaseta et al. (2010)].

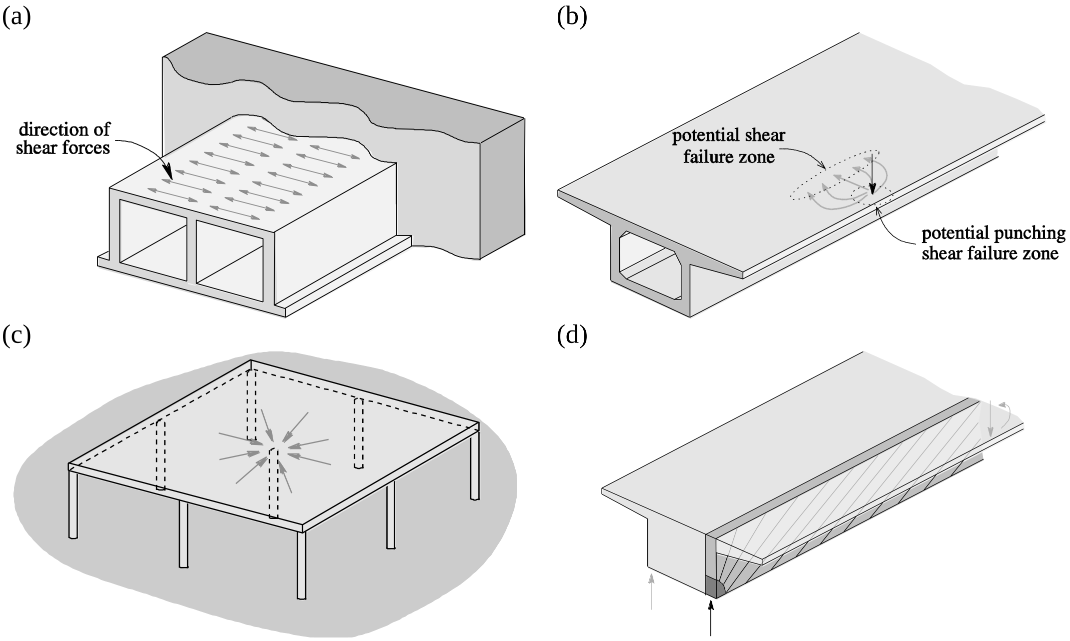

Fig. 7.2: Shear in slabs and beams: (a) top slab of an earth-covered structure; (b) deck slab of a bridge subjected to concentrated loading; (c) directions of shear forces near the inner column of a flat slab; and (d) stress field reproducing the struts in the web of a box-girder bridge near the supports.

The shear forces in girders or webs of beams (Fig. 7.2d) are carried in the direction of the web, and design shear has to be calculated accounting for shear forces and torsion (pure and warping) in the member. These members are usually provided with transverse reinforcement. Consequently, due to their rather ductile behaviour, the design shear force can be estimated on the basis of equilibrium-based models [Muttoni et al. (1997)]. This allows internal shear forces redistributions between webs if equilibrium conditions are respected.

7.2.2 Shear carrying-mechanisms

7.2.2.1 Shear in one-way slabs without transverse reinforcement

In members without transverse reinforcement, shear is carried essentially by concrete. Prior to cracking, shear is carried by the elastic (uncracked) stress field of the member, see Figure 7.3a.

After cracking, a number of shear-carrying mechanisms can develop allowing to carry shear [Muttoni and Fernández Ruiz (2008)]:

- Cantilever action. This mechanism was proposed by Kani (1955) who provided a mechanical model to assess its strength contribution (named the shear comb model). Cantilever action develops between two flexural cracks without the need of developing compression or tension forces through the flexural cracks and requires the compression chord to be inclined (see Figure 7.3b). Thus, for a cross-section where a flexural crack develops (refer to Fig. 7.3b), all shear is carried by the inclination of the force in the compression zone. According to Kani, the strength of the cantilever action is mostly governed by the strength of concrete in tension (inclined tension tie). When the tensile strength of concrete is reached for the tie (point “A” in Fig. 7.3b) the crack propagates horizontally, thus disabling the cantilever action.

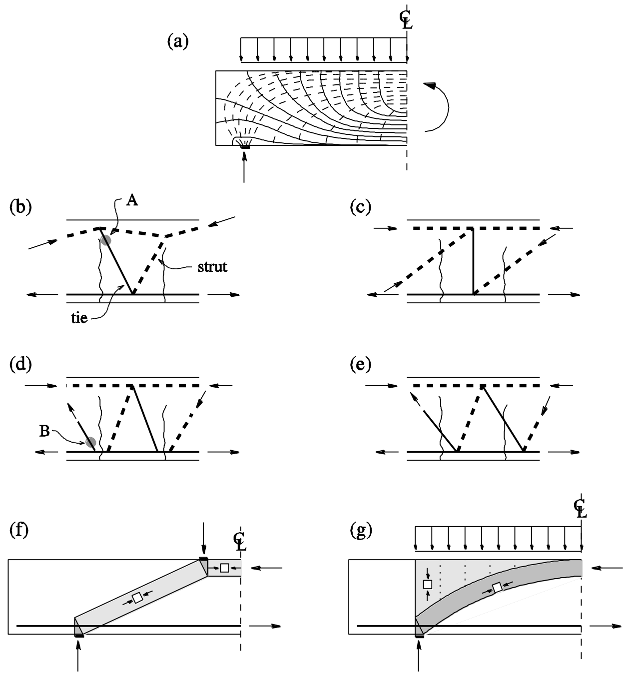

Fig. 7.3: Shear-carrying mechanisms in members without shear reinforcement: (a) elastic (uncracked) stress field; (b) cantilever action; (c) aggregate interlock; (d) dowel action; (e) concrete in tension; (f) arching action for a point load; and (g) arching action for a distributed load

- Aggregate interlock. As experimentally and theoretically demonstrated by Walraven (1981), cracked concrete has a significant capacity to transmit shear forces which depends on the opening and roughness of the cracks (Figure 7.3c). The activation of aggregate interlocking requires a relative slip between the lips of the cracks. Such sliding has been demonstrated by experimental measurements of the slip between lips of the shear cracks [Muttoni (1989)], mainly after failure of the cantilever action (propagation of the flexural crack beyond point “A” of fig. 7.3b) and even after yielding of the flexural reinforcement. This sliding is possible if the kinematics of a beam with a shear (curved) crack is investigated [Vaz Rodrigues et al. (2010)], see Figure 7.4a,b. For calculation of the aggregate interlock capacity, the roughness of the lips can be assumed to be correlated to the maximum aggregate size of the member [Muttoni and Fernández Ruiz (2008)], see Figure 7.4c.
- Dowel action. Another possible shear-carrying mechanism can be developed through the doweling action of the flexural reinforcement (Figure 7.3d). As experimentally verified [Muttoni and Fernández Ruiz (2008)], the very concentrated tensile stresses at the concrete cover (point “B” of Fig. 7.3d) lead however to the development of delamination cracks, which mostly cancels the shear-carrying capacity of this mechanism (the development of these cracks was already observed by Mörsch, refer to Fig. 7.1d).
- Concrete in tension. For very small crack widths (or near the tip of cracks), concrete has a residual capacity to carry tensile stresses (Figure 7.3e). The contribution of concrete in tension is thus only significant for members with small crack widths.

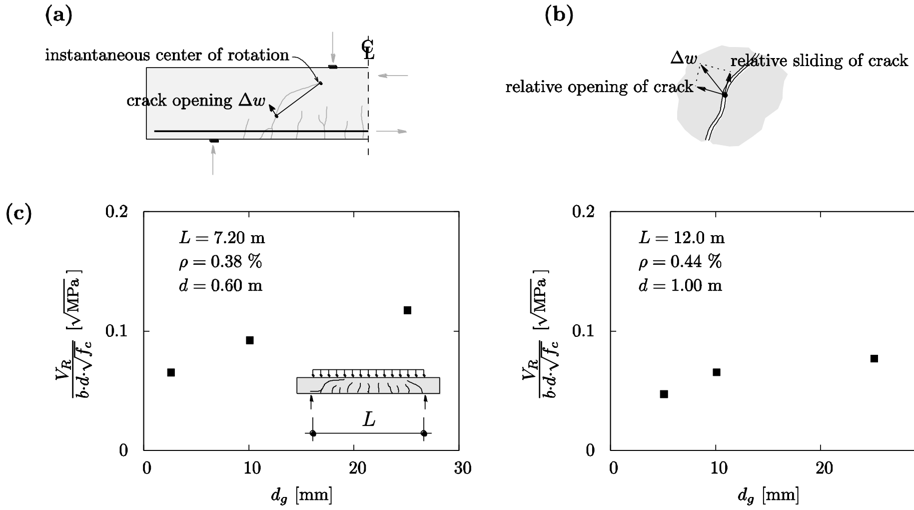

Fig. 7.4: Activation of aggregate interlock in shear: (a) kinematics at failure and opening of the critical shear crack; (b) relative opening and relative sliding of the lips of the crack; and (c) influence of aggregate size according to the tests of Shioya and Okada (1985)

It can be noted that the shear-carrying mechanisms presented above allow varying the force in the flexural reinforcement (a horizontal force has to be introduced at the level of the flexural reinforcement). This is why they are usually known as beam shear-carrying mechanisms. Except for aggregate interlock, the various beam shear-carrying mechanisms rely on the tensile strength of concrete and thus become less effective as cracking progresses. This fact is shown in Figure 7.5 where the typical flexural crack pattern of a beam (Fig. 7.5a) is shown. The regions subjected to tension due to the beam shear-carrying mechanisms (Fig. 7.5b, A: cantilever action; B: dowel action) force flexural cracks to progress with a curved shape. As a consequence, the shear-carrying capacity of these mechanisms (cantilever action and dowel action) is disabled and the shear strength is mostly controlled by aggregate interlocking (for members with very limited crack widths, however, the contribution of concrete in tension can also be governing for the shear strength).

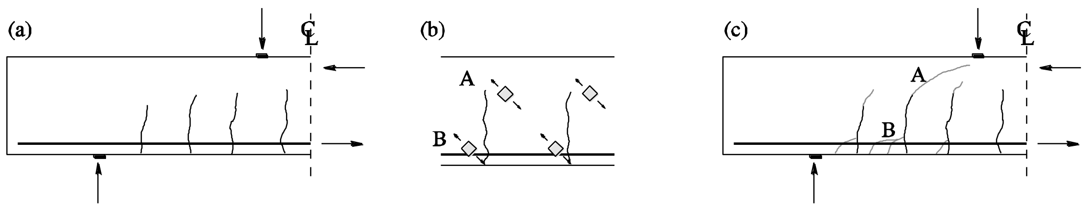

Fig. 7.5: Development of cracks according to beam shear-carrying mechanisms: (a) flexural cracks; (b) zones in tension; and (c) progression of flexural cracks

There is still another shear-carrying mechanism, as first observed by Mörsch (Fig. 7.1d) and later confirmed on the basis of the theory of plasticity by Drucker (1961), in which the force in the flexural reinforcement remains constant. This mechanism, sketched for a point load in Figure 7.3f and for a distributed load in Fig. 7.3g, is usually known as arching action. As experimentally observed, the shear strength predicted by the theory of plasticity may however be rather unsafe [Kani (1964)]. This is justified because inclined cracks (originating from flexural cracks, see Figure 7.5c) may develop through the compression strut and limit its strength. An alternative solution consists of an elbow-shaped strut (Fig. 7.6b) as proposed by Muttoni (1989). In reality, the load-carrying mechanism consists of a combination of the two (direct strut enabled by aggregate interlock and elbow-shaped strut enabled by the tensile strength of concrete) according to the stress field suggested by Muttoni and Fernández Ruiz (2008).

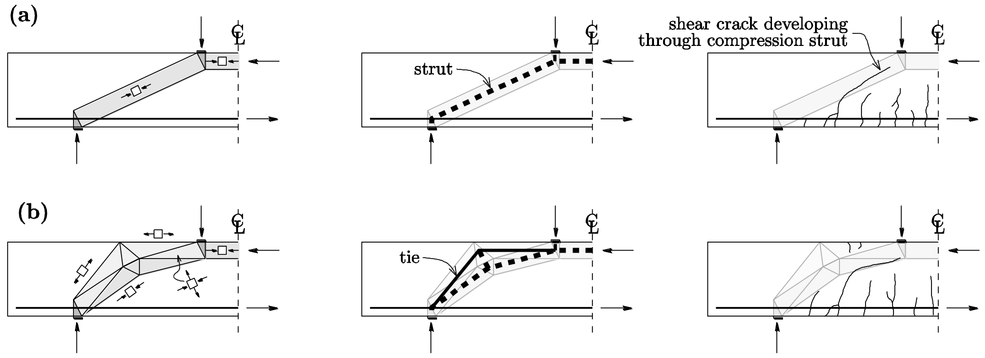

Fig. 7.6: Stress fields and strut-and-tie models for: (a) straight (non deviated) strut; and (b) elbow-shaped (deviated) strut [Muttoni and Fernández Ruiz (2008)]

The role of crack distribution (location) and opening on the shear strength has been recognized by different researchers. For instance, Figs. 7.7c show the normalized shear strength of two tests performed on geometrically identical beams, but where one specimen was cast with corrugated bars (Fig. 7.7a) whereas the other was cast with smooth bars (Fig. 7.7b). The difference in the crack pattern is notable. The specimen with corrugated bars developed several flexural cracks, one of which developed into the theoretical compression strut and severely limited the shear strength of the member. On the contrary, for the specimen with smooth bars, as bond stresses were rather limited, only a few flexural cracks developed (and mostly concentrated in the region between loads). Consequently, only a limited part of the theoretical compression strut was affected by these cracks, and the shear strength was significantly higher (the plastic solution was however not reached as the strut was somewhat influenced near the load introduction region). The influence of this phenomenon was also systematically investigated and confirmed by Kani (see [Kani et al. (1979)]). This was done on the basis of a test campaign on beam specimens where the bond properties between the flexural reinforcement and the concrete specimen were varied (thanks to the use of a vermiculite-cement core, refer to Fig. 7.7d). The results of Kani show that as the bond strength decreased, the shear strength increased, in accordance to the experiment of Leonhardt and Walther (1962).

Further experimental evidence of the influence of cracks developing through the compression struts was provided by Muttoni (1989), see Figure 7.8. Two specimens (BP0 and BP2) were used. They were geometrically identical, but one of them (BP2) contained a crack-control reinforcement in the shear-critical region (region were the unstable crack propagation develops). This reinforcement could not carry any shear as it was not enclosing the flexural reinforcement. As tests BP0 and BP2 were performed, both specimens exhibited a similar behaviour until beam BP0 failed due to the propagation of the critical shear crack through the compression strut. On the contrary, the shear crack widths remained controlled for specimen BP2, with more cracks appearing for higher levels of load. Thus, the load could be increased for specimen BP2 until the member failed in bending (with the applied load corresponding to the plastic strength of the beam).

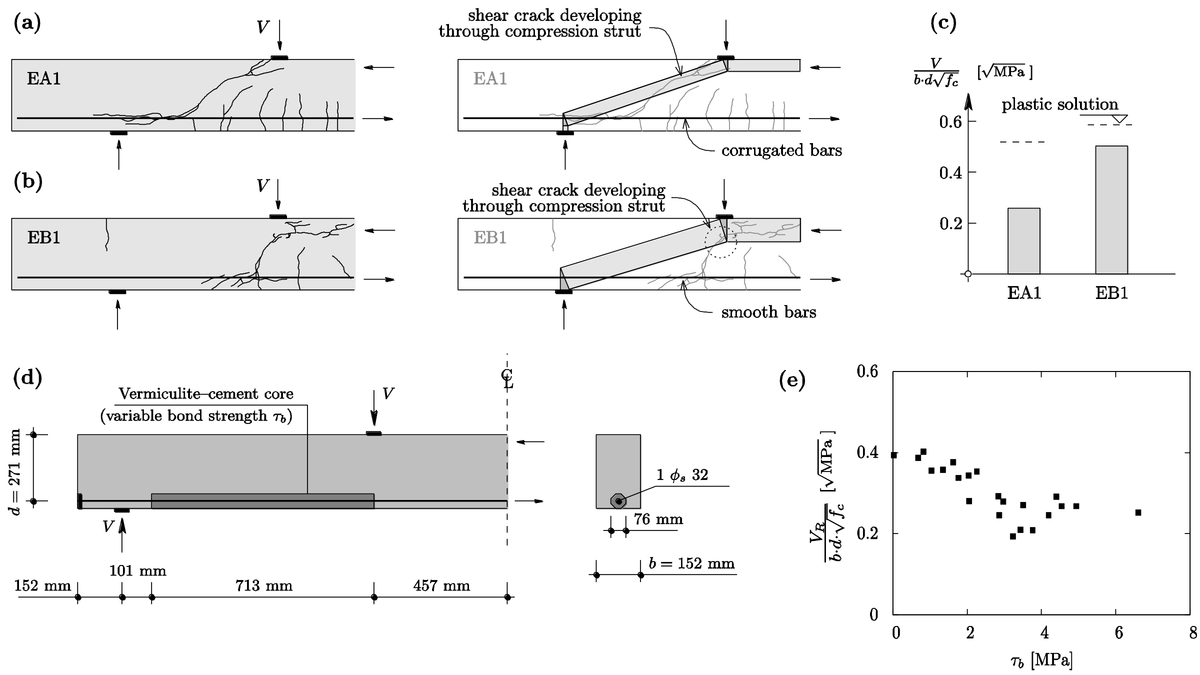

Fig. 7.7: Influence of cracking and bond on shear strength: (a) specimen EA1 with corrugated bars [Leonhardt and Walther (1962)]; (b) specimen EB1 with smooth bars [Leonhardt and Walther (1962)]; (c) comparison of shear strength for specimens EA1 and EB1; (d) beams with varying bond properties tested by Kani et al. (1979); and (e) shear strength of previous beams as a function of the bond strength of the vermiculite-cement core

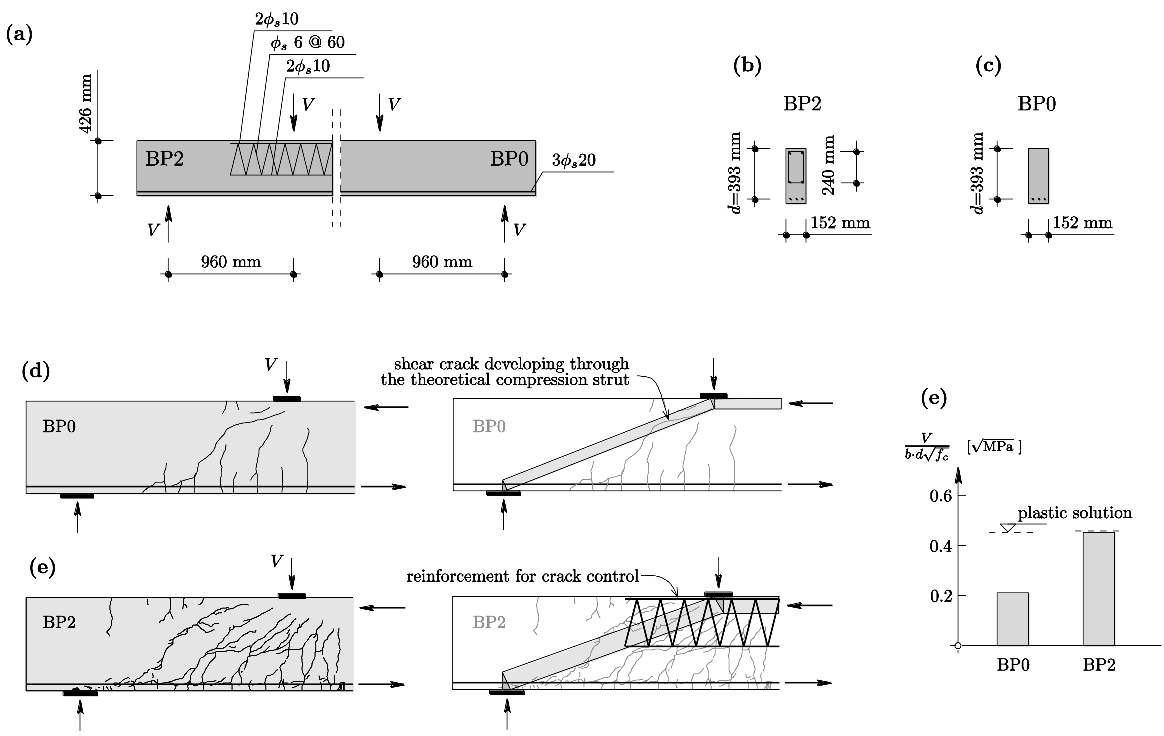

Fig. 7.8: Influence of crack width on shear strength: (a) specimens BP0 and BP2 of Muttoni (1989); (b) cross section at mid-span of specimen BP2; (c) cross-section at mid-span of specimen BP0; (d) crack patterns; and (e) shear strength of specimens

The total amount of shear carried by beam shear-carrying mechanisms and by arching action is mostly governed by the slenderness of the member. This phenomenon was investigated in depth by Leonhardt (1962) and also by Kani (1966). These authors showed that four regimes govern shear failures, see Figure 7.9:

- For very short-span beams, ($a/d \leq \alpha_1 \approx 1$), the strength of the member is controlled by yielding of the flexural reinforcement, as cracks almost do not disturb the compression strut.
- For rather short-span beams (a/d between α_1 and $\alpha_2 \approx 2.5$-3, refer to Fig. 7.9) arching action is dominant. In this regime, shear cracking (as shown in Fig. 7.5c) may progress in a stable manner. The load can thus be increased beyond the development of the first inclined (shear) crack. In this regime, the position of the shear crack developing through the compression strut is governing for the strength, and large scatter in test results has traditionally been reported for such members.
- For slender beams (a/d between α_2 and $\alpha_3 \approx 8$-13, refer to Fig. 7.9) failure develops due to the localization of the strains in a shear crack which limits the strength of the inclined compression strut carrying shear (aggregate interlock).
- For very slender beams ($a/d \geq \alpha_3$), yielding of the flexural reinforcement is again governing as beam shear-carrying mechanisms are capable of carrying loads larger than the one corresponding to the flexural strength.

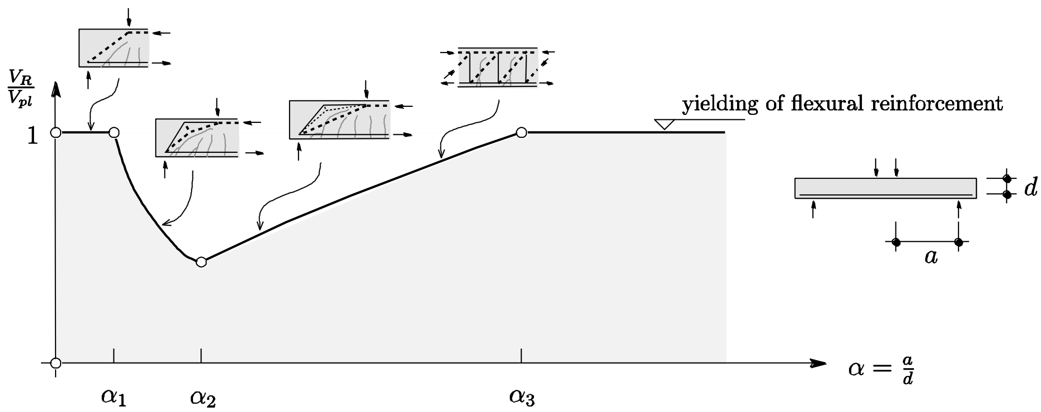

Fig. 7.9: Shear strength as a function of shear span-to-depth ratio ($\alpha = a/d$)

7.2.2.2 Shear in slabs subjected to concentrated loads

As previously discussed in section 7.2.1, when concentrated loads are applied to flat slabs, shear forces are transmitted in the radial direction (Figs. 7.2b,c). Consequently, a strong gradient in the unitary shear force (shear force per unit length) can be observed in these cases. This fact is sketched in Figs. 7.10a,b for a beam (or a one-way slab) and for a slab subjected to a point load. In the first case (Fig. 7.10a), the distribution of the unitary shear force is almost constant (if the influence of self weight can be neglected). On the contrary, for the slab (Fig. 7.10b) the distribution leads to large unitary shear forces in the region close to the concentrated load and to moderate or fairly low unitary shear forces in the rest of the slab.

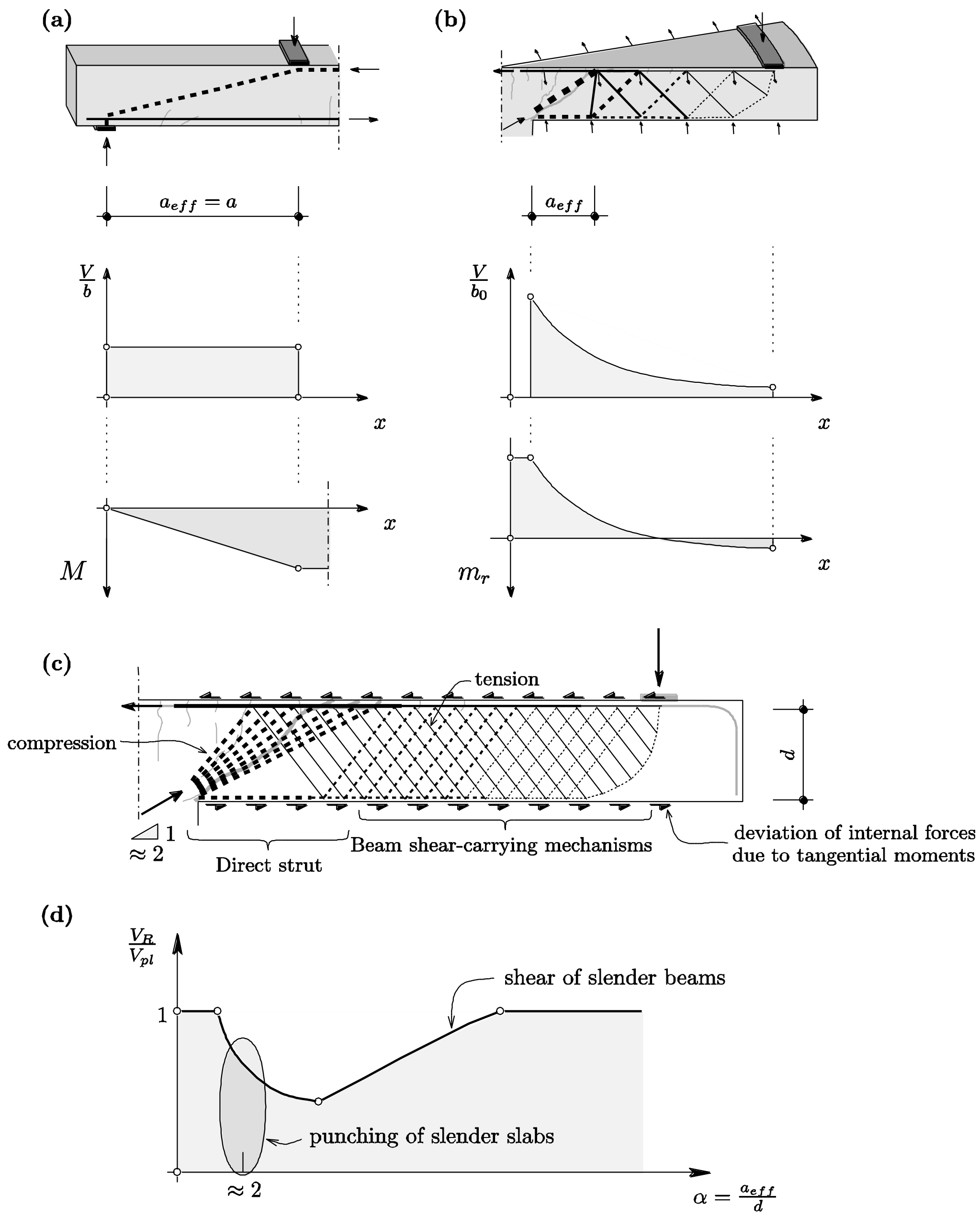

Fig. 7.10: Shear strength in slabs subjected to concentrated loads: (a) unitary shear force and bending moments for a beam or a one-way slab; (b) unitary shear force along a slab with concentrated forces; (c) regions of governing direct strut and beam shear-carrying mechanisms; and (d) comparison of shear strength as a function of the effective shear slenderness

In the regions where moderate shear forces develop, the beam shear-carrying mechanisms are sufficient to provide the shear strength (Fig. 7.10c). Close to the concentrated load, however, shear forces are carried by a small portion of the slab and thus direct strut action is required (Fig. 7.10c). As shown by Muttoni (2008), the development of a direct strut action is possible because, at a certain distance from the concentrated load, the beam shear-carrying mechanisms are sufficient to ensure shear strength (the concrete ties have sufficient surface and strength to carry the vertical component of the strut force). The direct strut thus develops starting at the concentrated load over that distance, defining an effective shear span (a_{eff}) as shown in Figs. 7.10b,c. The angle of the strut is consequently rather steep even for slender slabs, and yields to an effective span-to-effective depth ratio corresponding to that of short span beams, refer to Fig. 7.10d. On that basis, consistent shear design should account for considerably higher unitary shear strengths for two-way slabs (punching shear) than in one-way slabs, as acknowledged by ACI 318 ([2008] unitary punching shear strength double than unitary shear strength) or the draft of the new Model Code [*fib* (2010a,b)].

In addition, on the basis of the actual shear-carrying mechanism, it is also justified to adopt control perimeters close the concentrated load (at distances smaller than d), in order to account for realistic values of the shear actions, acting bending moments and concentrations on the shear field in the shear-critical region. It can be noted that empirical models such as EC-2 (2004) propose to adopt control perimeters at distances rather distant from the edge of the concentrated action ($2d$ in the case of EC-2). This choice is a consequence of the unitary shear strength considered (adopted to provide better fitting to test results) but it is inadequate to provide realistic values of the unitary shear forces acting in the shear-critical region or for loads applied within the nominal punching shear control perimeter (in case of transfer moments for instance).

7.2.2.3 Girders

Members with fairly low amounts of shear reinforcement (typically lower than approximately 0.1%) still fail by localization of the strains in a shear crack. The strength is somewhat increased (this increase is very dependent on the shape of the shear crack and on the amount of transverse reinforcement) but a rather brittle behaviour is still exhibited [Yoon et al. (1996)]. Control of the width and number of shear cracks is achieved as the transverse reinforcement amount is increased. In this case, the shear-carrying mechanisms as well as the behaviour are rather different and dominated by a compression field (as observed by Mörsch, Figs. 7.1a,b) with its strength limited by the opening of the shear cracks developing through it (in-plane failures) or by crushing in compression (out-of-plane failures).

The shear-carrying mechanisms of members with sufficient transverse reinforcement are significantly different to those of members without shear reinforcement. For instance, for a typical prestressed concrete girder (refer to Figure 7.11), shear on a vertical cross-section is carried by the following mechanisms:

- inclined compression field in the web (in equilibrium with the stirrups)
- inclination of prestressing tendons and of the tension chord
- inclination of the compression chord

Depending on the shape and properties of the structural member, the significance of each component may vary. In reinforced concrete beams with rectangular cross sections, almost all the shear force is carried by the inclined compression field and the stirrups. On the contrary, for prestressed girders, tendons as well as the inclination of the compression chord can carry a large fraction of the total shear force.

The behaviour after cracking of beams with sufficient transverse reinforcement is rather different of that of members without stirrups. This is due to the fact that a number of inclined cracks develop in the web and their width remains controlled by the transverse reinforcement. According to the theory of plasticity [Muttoni et al. (1997)], shear will thus not be carried by a single concentrated strut, but a compression field will develop in the web.

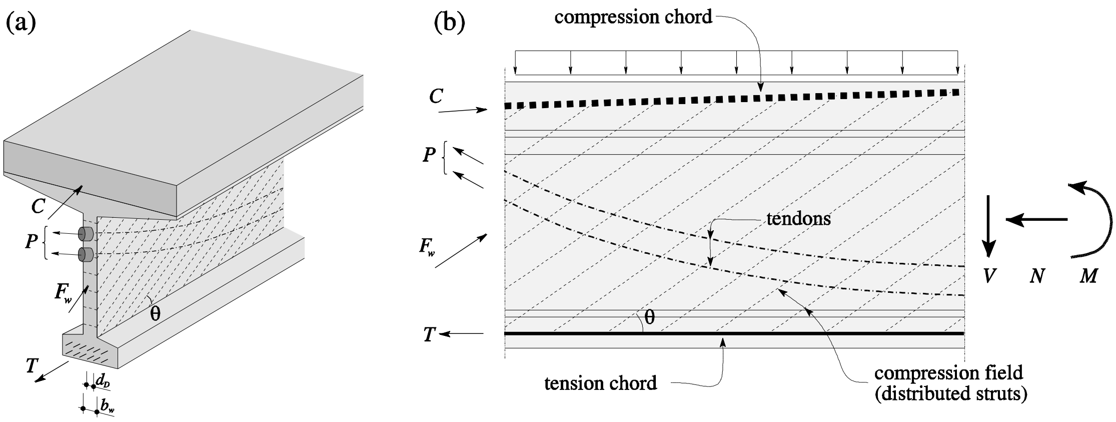

Fig. 7.11: Shear-carrying mechanisms of members with sufficient transverse reinforcement: (a) internal forces; and (b) equilibrium of forces

The angle of the compression field is governing for the shear strength of the web. Its value can be calculated accounting for the available stirrups and for the crushing strength of the compression field. For members with large amounts of shear reinforcement, the compression field will remain at values of approximately 45° (crushing of the web prior to stirrup yielding). However, for low amounts of shear reinforcement, the compression field will significantly reorientate, leading to flatter angles of the struts (and thus activating more shear reinforcement). Failure will in this case also develop when the stresses in the compression field after strut reorientation (and stirrup yielding) are such that the concrete crushes in compression (out of plane failure with cover spalling influenced by reinforcement strains [Fernández Ruiz et al. (2010)]).

The phenomenon of strut reorientation can be seen in Figure 7.12 for a prestressed concrete girder at different load levels (cross section as Fig. 7.11, see details in [Hars and Muttoni (2006)]). In Figure 7.12a, the recorded principal directions of the strain field are shown for a moderate load level (30% of failure load). The directions of the compression field in the web are rather steep, with angles larger than 45° near the tension flange and are deviated throughout the web (particularly at the level of the tendons), and are rather flat near the compression flange. As the load increases (Fig. 7.12b at 55% of failure load and Fig. 7.12c at failure), struts become flatter and the deviation of the compression field at the web becomes less significant. It is also significant to note that the principal directions in the compression chord (top flange) are not horizontal, but that they are inclined and can carry a certain fraction of the total shear force (they are on the contrary almost horizontal in the tension flange).

In addition to the plots of the principal strain directions, the reorientation of the struts can also be clearly appreciated in the crack pattern of the specimen. Fig. 7.13a shows the crack pattern at 55% of the failure load. The angles of the cracks are rather steep. Also, the cracks in the web are deviated at the level of the tendons. As load increases (Fig. 7.13b at failure load) new cracks appear. These cracks develop at flatter angles (near 20°), and the deviation of the compression struts at the level of the tendon is mostly negligible. Failure occurred by crushing of the concrete at the level of the tendons with spalling of the cover (out-of-plane failure) as shown in Fig. 7.13c.

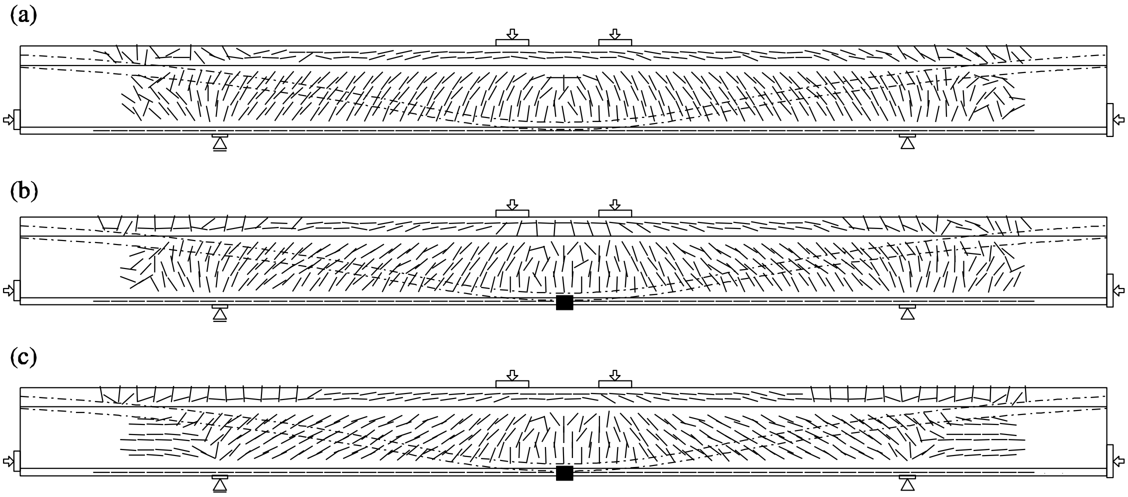

Fig. 7.12: Principal compressive strain directions in specimen SH3 [Hars and Muttoni (2006)]: (a) applied shear equal to 30% of failure load; (b) applied shear equal to 55% of failure load; and (c) at failure

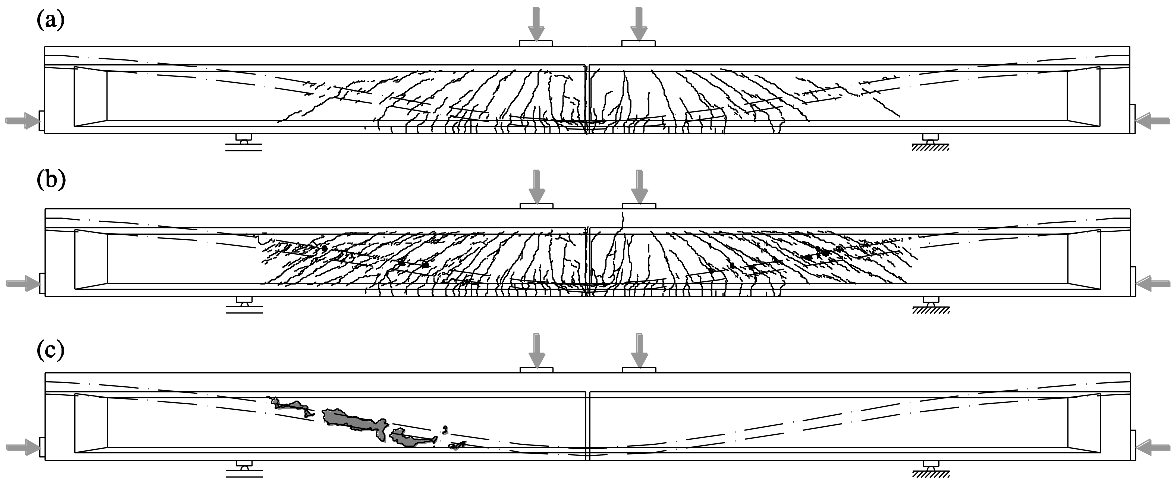

Fig. 7.13: Cracking pattern of test SH3 by Hars and Muttoni (2006): (a) crack pattern at 55% of failure load; (b) cracking pattern at failure load; and (c) concrete spalling at failure

As it can be noted, the strength of the compression field is governing for estimating the shear-carrying capacity of webs or for design of their thickness. Its strength depends on a series of factors [Fernández Ruiz and Muttoni (2008)], mainly:

- concrete strength and brittleness (compression softening)
- the transverse strains (width of the shear cracks developing through the compression field) decreasing the crushing strength [Vecchio and Collins (1986)] and leading to in-plane failures, but also the reinforcement strain leading to concrete spalling (out-of-plane failures [Fernández Ruiz et al. (2010)]), refer to Fig. 7.14
- the presence of tendon ducts, their material and injection properties [Muttoni et al. (2006)]

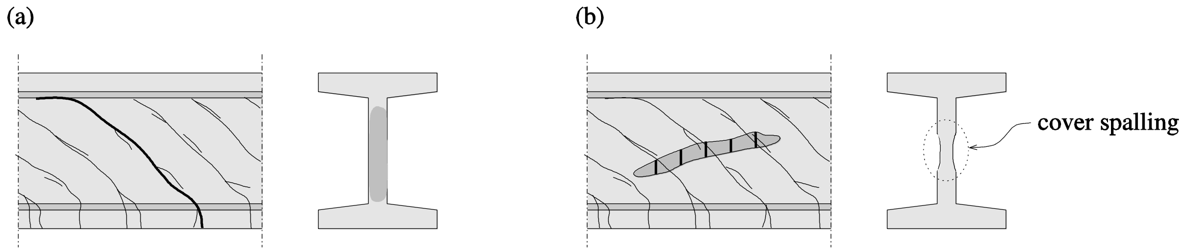

Fig. 7.14: Influence of transverse strains: (a) in-plane failures; and (b) out-of-plane failures

It can be noted that, contrary to girders, slabs with transverse reinforcement cannot develop out-of-plane failures since dilatancy in the transverse direction is restrained. Failure in these cases can only develop by in-plane failures with localization of strains in a critical shear crack or in a plastic shear band. Furthermore, in presence of concentrated loads, failures in slabs develop always close to the concentrated load due to the large strains and internal forces (shear and moment) in this region (refer to Fig. 7.10).

7.3 Design approaches

The shear design approaches for members with and without transverse reinforcement have traditionally been rather different as previously explained. A detailed and extensive summary of most significant approaches can be found elsewhere [ASCE-ACI (1998)].

On the basis of the shear-carrying mechanisms previously described, the shear strength of slender members without transverse reinforcement is mostly dependent on the opening and development of a critical shear crack (localization of strains). On the contrary, failure of the compression field (or distributed struts) is governing in girders. As a consequence, it is reasonable to perform shear design on the following basis:

- Using strain-based models for members without stirrups (typically slabs). This allows evaluating the width of the critical shear crack.
- Using equilibrium-based models for members with shear reinforcement (typically girders), introducing a reduction of the compressive strength of the compression field to account for the transverse cracking state in the web.

7.3.1 Strain-based models

The strain based models (such as the CSCT or the MCFT) allow determining the shear strength on the basis of the opening of the critical shear crack (shear crack leading to failure). They also normally account for the roughness of the lips of the cracks to account for aggregate interlock capacity (Fig. 7.4). For instance, the CSCT proposes to evaluate the shear strength as [Muttoni and Fernández Ruiz (2008)]:

$$\frac{V_R}{b \cdot d} = \sqrt{f_c} \cdot f(w, d_g) \tag{7.1}$$

where V_R is the shear strength, b is the width of the shear-carrying member, d is the effective depth, f_c is the compressive strength of the concrete (in [MPa]), w is the width of the shear critical crack and d_g is the maximum size of the aggregate (accounting for the roughness of the lips of the cracks). The accuracy of the model is thus based on the estimate of the opening of the critical shear crack (w). For members without shear reinforcement [Muttoni (2003)], it can be assumed proportional to a reference strain (ε, defined at a given depth and control section [Muttoni (2003), Muttoni and Fernández Ruiz (2008)]) times the effective depth of the member (d):

$$w \propto \varepsilon \cdot d \tag{7.2}$$

Similar approaches for the estimate of the critical shear crack width have also been adopted by other researchers (as the simplified version of the MCFT [Bentz et al. (2006)]). On the basis of these assumptions, a failure criterion, defining the maximum shear strength on the basis of the shear crack opening was proposed by Muttoni (2003):

$$\frac{V_R}{b_0 \cdot d \cdot \sqrt{f_c}} = \frac{1/3}{1+120\dfrac{\varepsilon \cdot d}{d_{g0}+d_g}} \tag{7.3}$$

This criterion leads to an excellent correlation with test data, see Figure 7.15. Simplifications on the estimate of the reference strain also leads to compact shear design formulas correlating the opening of the critical shear crack to the bending moments acting in the control section [Muttoni (2003), Muttoni and Fernández Ruiz (2008)] that can be refined with a levels-of-approximation approach [Muttoni and Fernández Ruiz (2010a)].

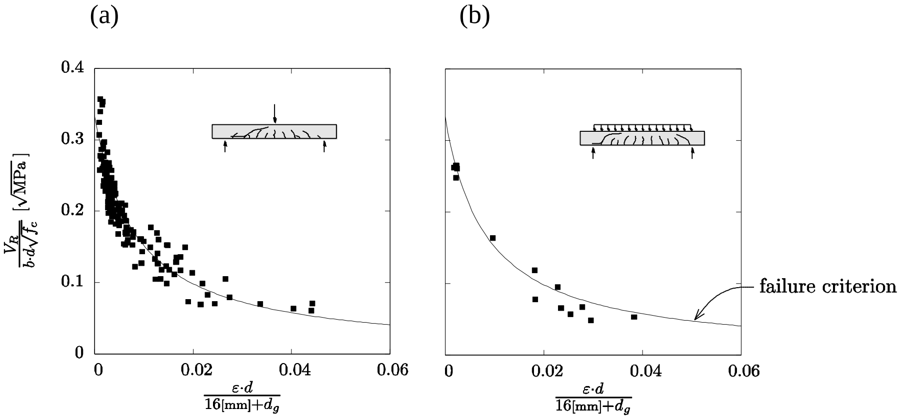

Fig. 7.15: Comparison of failure criterion of CSCT for beams in shear with 285 tests on beams with concentrated and uniform loading (test data from [Muttoni and Fernández Ruiz (2008)]): (a) point load; and (b) distributed load

It can be noted that for members subjected to distributed loading (Fig. 7.15b), the position of the shear critical section is not known *a priori*. Close to the supports, the shear force is high but the bending moments are low. This means that crack widths are limited and the shear strength is high. On the contrary, close to mid-span, the shear force is low but the bending moments are high (meaning limited shear strength). The shear critical section can thus be potentially located at any section of the beam. Design rules for these cases are discussed in [Muttoni and Fernández Ruiz (2008)].

With respect to slabs subjected to concentrated loads (punching shear), a similar approach than for one-way slabs can be adopted. According to Muttoni (2008), this can be done by correlating the width of the critical shear crack to the rotation of the slab, which leads to a failure criterion with decreasing shear strength for increasing rotations of the slab. Some fundamental differences however exist, as the governing parameters of the width of the critical shear crack (strain for one-way slabs and rotation for slabs subjected to concentrated loads) or the relationship between the applied load and the opening of the critical shear crack (mostly linear for one-way slabs and strongly nonlinear for slabs) are not the same. More details on this topic as well as on its applications to punching in slabs with transverse reinforcement are discussed in [Muttoni and Fernández Ruiz (2010b)].

7.3.2 Equilibrium-based models

Equilibrium-based models were used since the early development of reinforced concrete. They allow performing consistent and safe shear design and assessment provided that sufficient transverse reinforcement is available (avoiding shear crack localization) and that a suitable reduction of the strength of the compression field (or struts) is considered. As previously stated, the effective compressive strength in the web (f_{ce}) depends on the transverse state of cracking, concrete brittleness in compression and on the presence of ducts in the web [Fernández Ruiz and Muttoni (2007)]:

$$f_{ce} = \eta_{\varepsilon} \cdot \eta_{fc} \cdot \eta_{D} \cdot f_c \tag{7.4}$$

where η_{ε} is a strength reduction factor accounting for transverse cracking and reinforcement strain, η_{fc} is a strength reduction factor accounting for concrete brittleness in compression and η_D is a strength reduction factor accounting for the presence of ducts in the web.

A suitable value of η_{fc} was proposed by Muttoni (1989), accounting for the fact that as the strength of concrete increases, its softening behaviour in compression becomes more brittle:

$$\eta_{fc} = \left(\frac{f_{c0}}{f_c} \right)^{1/3} \leq 1.0 \tag{7.5}$$

The value of f_{c0} (compressive strength at which the strength has to be reduced accounting for brittleness) can be adopted at 30 MPa [Fernández Ruiz and Muttoni (2007)]. Other suitable values are discussed in [Kostic (2009)].

With respect to the strength reduction factor accounting for transverse cracking, η_{ε}, a lot of research has been performed on this topic [Vecchio and Collins (1986), Pang and Hsu (1996)]. Its value is typically evaluated as a function of the principal transverse strain in concrete (ε_1). For instance as proposed by Vecchio and Collins (1986):

$$\eta_{\varepsilon} = \frac{1}{0.8 + 170\varepsilon_1} \leq 1.0 \tag{7.6}$$

The presence of ducts can be considered by reducing the concrete compressive strength depending on the diameter (d_D) and number of ducts as well as on the properties of the duct:

$$\eta_D = 1 - k \sum \frac{d_D}{b_w} \tag{7.7}$$

where k depends on the material and injection properties of the duct (suitable values are discussed in [Muttoni et al. (2006)]). Alternatively, it is also possible to consider the influence of prestressing ducts as a reduction on the effective width of the web (b_w), leading to the same results [Fernández Ruiz and Muttoni (2008)].

For practical design purposes, it is usually sufficient to ensure equilibrium by means of simple stress fields or strut-and-tie models. The angle of the compression field in these cases is chosen to respect equilibrium with external loads and to avoid crushing of the web. At this level, it is sufficient to adopt a constant strength reduction factor η_ε equal to 0.60 [Fernández Ruiz and Muttoni (2007)]. For design of complicated members or for the assessment of critical existing structures, the accuracy on the estimate of the shear strength can be improved by progressively refining the hypotheses adopted in the stress field or strut-and-tie model. This can for instance be done by taking advantage of more complex load-carrying mechanisms [Fernández Ruiz and Muttoni (2008)] or by evaluating more precisely the reduction of the strength on the compression field by considering the local state of strains (typically requiring finite element-based analyses [Fernández Ruiz and Muttoni (2007)]). For instance, Fig. 7.16 shows a stress fields analysis of specimen SH3 (whose strain field and cracking pattern was shown in figures 7.12,13).

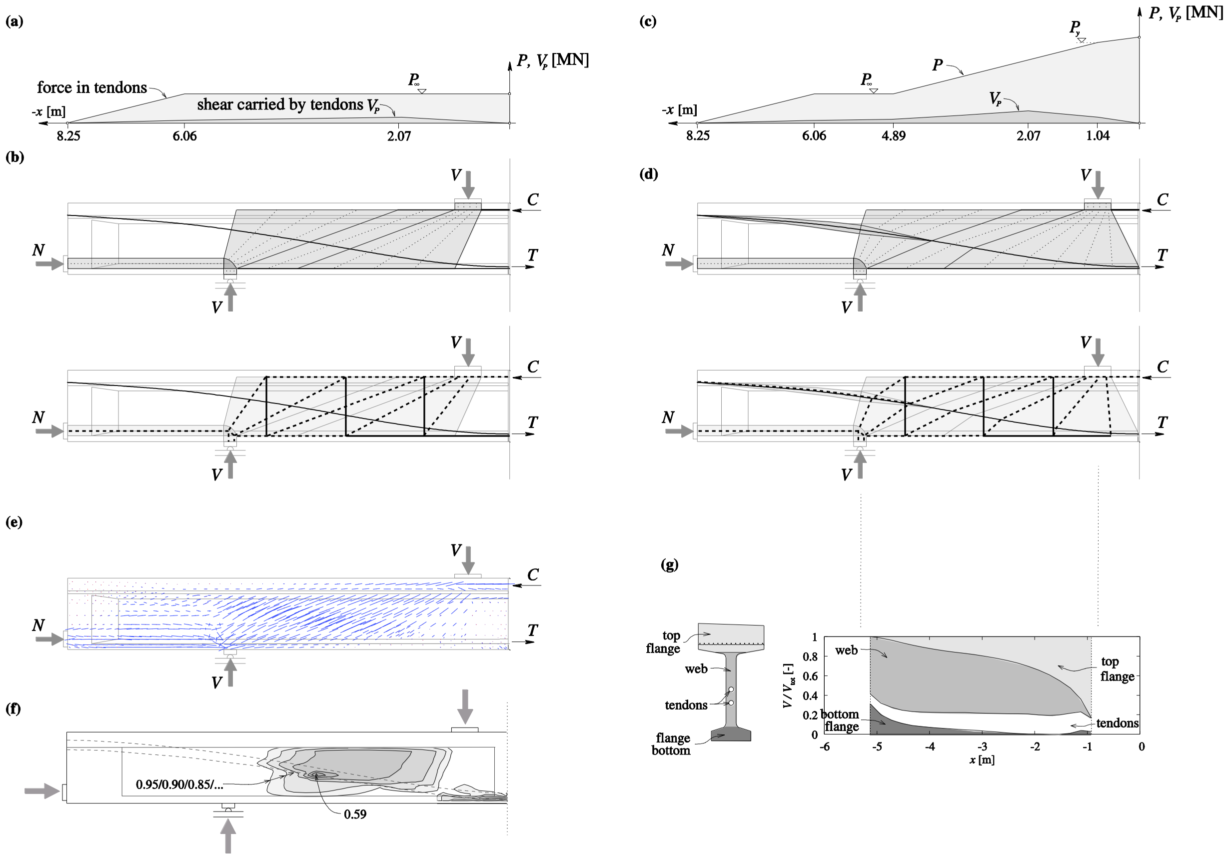

Fig. 7.16: Analysis of girder SH3 [Hars and Muttoni (2006)] using equilibrium-based models: (a) forces and shear carried by the tendons using non-deviated stress fields; (b) detail of the non-deviated stress field and corresponding truss model; (c) forces and shear carried by the tendons using deviated stress fields; (d) detail of the deviated stress field and corresponding truss model; (e) principal directions of compression field according to an elastic-plastic stress field analysis; (f) concrete strength reduction factor η_ε accounting for transverse strains; and (g) shear carried by the various parts of the section

The first stress field (Fig. 7.16b) corresponds to a non-deviated rigid-plastic stress field [Fernández Ruiz and Muttoni (2008)]. It can be noted that the force in the tendons remains constant (Fig. 7.16a). On the contrary, a refinement on the stress field (Fig. 7.16d) allows considering the potential increase in the force of the tendons by deviating the stress field at the level of the tendons (a phenomenon in agreement with test results, refer to Figs. 7.12,13) and thus to increase the shear-carrying capacity of the member. An evaluation of the measured-to-predicted strength for a test series on 6 girders (with same geometry as specimen SH3 but for various loading conditions) leads to an average value of 1.19 for non-deviated stress fields and of 1.09 for deviated stress fields, with a CoV of 14% and 13% respectively [Fernández Ruiz and Muttoni (2008)]. The accuracy of the strength prediction can be further increased if the strains in the web are calculated locally and the value of factor η_ε is thus obtained at each point of the girder. This can be for instance implemented by means of elastic-plastic stress fields [Fernández Ruiz and Muttoni (2007)] which satisfy equilibrium and allow considering compatibility conditions (strains and deformations). In so doing, accurate estimates of the strength, failure mode and failure region can be obtained. For instance, the elastic-plastic stress field corresponding to specimen SH3 is shown in Fig. 7.16e. It closely reproduces test measurements (Fig. 7.12) and allows determining accurate values of the strength reduction factor η_ε according to Eq. (7.6), see Fig. 7.16f. The failure zone and mode is also correctly estimated, with an average measured-to-predicted strength of 0.98 and a CoV of 5% for the complete test series on 6 specimens [Fernández Ruiz and Muttoni (2008)]. Furthermore, this type of analysis allows investigating the significance of the various shear carrying mechanisms, refer to Fig. 7.16g. In this case, it can be noted that the compression flange plays a significant role in carrying shear, especially near mid-span where compression forces in the top flange are largest.

The use of equilibrium-based models following this approach (from simple models with approximated considerations of the influence of transverse cracking up to refined analyses accounting for compatibility conditions) can be implemented following a levels-of-approximation approach [Muttoni and Fernández Ruiz (2010a)]. This means that refinements of the hypotheses can be introduced, increasing the accuracy of the estimate of the strength but requiring to devote more time to analyses.

7.3.3 Design for members with low shear reinforcement or for punching shear in slabs with transverse reinforcement

As previously discussed (section 7.3.1) members without shear reinforcement fail by development of a single crack localizing strains. Thus, design of such members has to be based on strain based models providing refined estimates of the critical shear crack width (basic parameter governing the strength of the shear-carrying mechanisms). On the contrary, for members with sufficient transverse reinforcement, cracks are distributed over the web avoiding strain localization. Such members can thus be designed on the basis of equilibrium based models (suitable stress fields) where the influence of the transverse strains on the strength of the compression field (η_ε) can be accounted by more or less refined methods (see section 7.3.2).

With respect to members with low amounts of shear reinforcement, localization of strains in a single crack still happen (refer to section 7.2.2.3). Consequently, design for these members needs to be performed on the basis of strain-based methods providing accurate estimates of the width of the critical shear crack and of its shear-carrying capacity. However, as the critical shear crack opens, it activates the transverse reinforcement which also contributes to the shear-carrying capacity of the member (failure in these cases can potentially develop prior to yielding of the transverse reinforcement). Thus, for members with low amounts of shear reinforcement, a combination of both models (strain-based and equilibrium-based) is required. This is the approach that has been privileged for shear design in current draft of Model Code 2010 [*fib* (2010b)].

A similar problem to the shear design of members with low shear reinforcement (crack localization with activation of transverse reinforcement) is the design of slabs with transverse reinforcement against punching shear. As shown by Fernández Ruiz and Muttoni (2009) the angle at which the shear failure surface develops in slabs with transverse reinforcement is roughly constant (about 45°, steeper angles can develop for crushing failures with large amounts of transverse reinforcement [Muttoni and Fernández Ruiz (2010b)]). This is due to the fact that, at a certain distance from the concentrated load, beam shear-carrying mechanisms are sufficient to ensure punching shear strength (Fig. 7.10c). Thus, reorientations of concrete struts after cracking (leading to flatter angles of the compression field) are significantly more limited than for beams in shear with sufficient transverse reinforcement (refer to Fig. 7.12). In addition, the stresses developed by the shear reinforcement are governed by the opening of a critical shear crack, localizing strains near the concentrated load, and in many cases remain below the yield strength of the reinforcement [Fernández Ruiz and Muttoni (2009)]. This behaviour is again rather different to that of beams with sufficient shear reinforcement, where the transverse reinforcement typically reaches its yield strength (leading to reorientation of the struts).

7.4 Conclusions

In this paper, the mechanical behaviour and design approaches for shear in slabs and beams (both for members with and without shear reinforcement) are presented and discussed. The main aspects summarizing the behaviour and governing mechanical parameters of shear strength are shown in Figure 7.17.

<table>
<tr><td></td><td>Girders
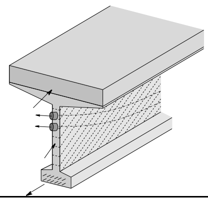</td><td>One-way slabs
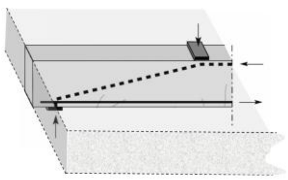</td><td>Punching shear
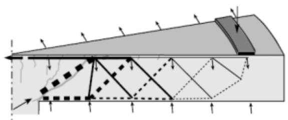</td></tr>
<tr><td rowspan="3">Without shear reinforcement</td><td colspan="3">In-plane failure with strain localization (critical shear crack)</td></tr>
<tr><td colspan="3">Failure criteria with strain, size, and aggregate effect</td></tr>
<tr><td colspan="2">Linear load-strain relationship</td><td>Non-linear load-rotation relationship</td></tr>
<tr><td rowspan="3">With small and medium amount of shear reinforcement</td><td colspan="3">Out-of plane failure (spalling)
In-plane failure with strain localization</td></tr>
<tr><td colspan="3">Concrete crushing with strain, but without size effect
Critical shear crack, failure criteria with strain, size and aggregate effect</td></tr>
<tr><td colspan="3">Yield strength in stirrups can usually be activated
Yield strength in transverse reinforcement cannot always be activated</td></tr>
<tr><td rowspan="2">With large amount of shear reinforcement</td><td colspan="3">Out of plane failure
In-plane failure due to concrete crushing with strain localization (thin crushing band)</td></tr>
<tr><td colspan="3">Concrete crushing, spalling without size effect
Failure criteria with strain, size and aggregate effect (size of thin crushing band related to aggregate size)</td></tr>
</table>

Fig. 7.17: Failure modes and governing parameters for shear strength in slabs and beams

According to these aspects, the following recommendations for shear design can be considered:

1) The strength of slabs without shear reinforcement failing in shear (one-way slabs) and in punching shear (two-way slabs) is governed by different shear-carrying mechanisms. Consistent shear design has thus to be performed accounting for different unitary shear strengths for shear and for punching shear.
2) For slabs failing in punching shear, a strong gradient in shear forces and bending moments develop, with very large values developing near the concentrated loads and with a significant localization of strains in this region (which becomes governing for the strength). For punching shear design, control perimeters have to be set close to concentrated loads to provide realistic estimates of the actions and deformations of the shear-critical region.
3) Members failing in shear without transverse reinforcement (such as one-way slabs) and with transverse reinforcement (typically girders) develop different state of stresses at failure associated to different failure modes (in-plane and out-of-plane failures respectively). For design purposes, it is advantageous to perform shear design on different bases (all shear carried by concrete for slabs and all shear carried by the transverse reinforcement for girders). This can be done by using strain-based models for members without shear reinforcement (allowing accurate estimates of the critical shear crack width and of its shear-carrying capacity) and equilibrium-based models for members with sufficient shear reinforcement (accounting for the influence of cracking on the strength of the compression field by means of more or less refined considerations).
4) However, for assessment of existing structures, for design of special members (such as beams with low shear reinforcement) or for design of transverse reinforcement against punching shear, both the contributions of concrete and of the transverse reinforcement have to be considered. This can be done accounting for equilibrium and strain conditions on the compression field (or struts) carrying shear, as proposed in the draft of Model Code 2010.

7.5 References

ACI, 2008, Building Code Requirements for Structural Concrete (ACI 318-08) and Commentary (ACI 318R-08), American Concrete Institute, Farmington Hills, Mich., USA, 473 p.

ASCE-ACI Committee 445 on Shear and Torsion, 1995, Recent approaches to shear design of structural concrete, ASCE Journal of Structural Eng., Vol. 124, no. 12, pp. 1375-1417.

Bentz, E. C., Vecchio, F. J., and Collins, M. P., 2006 , Simplified modified compression field theory for calculating shear strength of reinforced concrete elements, ACI Structural Journal, Vol. 103, No. 4, pp. 614-624.

Braestrup M. W., 1974, Plastic analysis of shear in reinforced concrete, Magazine of Concrete Research, Thomas Telford, Vol. 26, No. 89, pp. 221-228

Broms, C. E., 2006, Concrete flat slabs and footings : Design method for punching and detailing for ductility, Royal Institute of Technology, Stockholm, Sweden, 114 p.

CSA Committee A23.3, 2004, Design of Concrete Structures (CSA A23.3-04), Canadian Standards Association, Mississauga, 214 p.

Comité Euro-International du Béton (CEB-FIP), 1993, Model Code 90 for concrete structures, Lausanne, Switzerland, 460 p.

Drucker, D. C., 1961, On structural concrete and the theorems of limit analysis, Publications, International Association for Bridge and Structural Engineering, Vol. 21, Zürich, pp. 49-59.

Eurocode 2, 2004, Design of concrete structures - Part 1-1: General rules and rules for buildings, CEN, EN 1992-1-1, Brussels, Belgium, 225 p.

fédération internationale du béton (*fib*), 2010a, Model Code 2010 - First complete draft, fédération internationale du béton, Bulletin 56, Lausanne, Switzerland, May 2010, Vol. 2, 312 p.

fédération internationale du béton (*fib*), 2010b, Model Code 2010 - First complete draft, fédération internationale du béton, Bulletin 55, Lausanne, Switzerland, April 2010, Vol. 1, 318 p.

Fernández Ruiz, M., Muttoni, A., 2007, On development of suitable stress fields for structural concrete, American Concrete Institute, Structural Journal, Vol. 104, No. 4, pp. 495--502

Fernández Ruiz, M., Muttoni, A., 2008, Shear strength of thin-webbed post-tensioned beams, American Concrete Institute, Structural Journal, Vol. 105, No. 3, pp. 308-317

Fernández Ruiz, M., Muttoni, A., 2009, Applications of the critical shear crack theory to punching of R/C slabs with transverse reinforcement, ACI Structural Journal, Vol. 106, No. 4, 2009, pp. 485-494

Fernández Ruiz, M., Vaz Rodrigues, R., Muttoni, A., 2009, Design and assessment of reinforced concrete deck slabs (in French : Dimensionnement et vérification des dalles de roulement des ponts routiers), Département fédéral des transports, des communications et de l'énergie, Office fédéral des routes, Rapport 636, Bern, Switzerland, 53 p.

Fernández Ruiz, M., Plumey, S., Muttoni, A., 2010, Interaction between bond and deviation forces in spalling failures of arch-shaped members without transverse reinforcement}, American Concrete Institute, Structural Journal, Vol. 107, No. 3, pp. 346--354

Hars, E., and Muttoni, A., 2006, Shear tests on thin-webbed post-tensioned girders (in French : Essais à l'effort tranchant sur des poutres précontraintes à âme mince), Test Report, Ecole Polytechnique Fédérale de Lausanne, Lausanne, Switzerland, 108 p.

Kani, G. N. J., 1955, Prestressed concrete in design and construction (in German: Spannbeton in Entwurf und Ausführung), Verlag Konrad Wittwer, Stuttgart, pp. 501-531

Kani, G. N. J., 1964, The Riddle of Shear Failure and its Solution, ACI Journal Proceedings, Vol. 61, No. 4, pp. 441-468

Kani, G. N. J., 1966, Basic Facts Concerning Shear Failure, ACI Journal Proceedings, Vol. 63, No. 6, pp. 675-692

Kani, M. W., Huggins, M. W., and Wittkopp, R. R., 1979, Kani on shear in reinforced concrete, University of Toronto, Dept. of Civil Eng., 97 p.

Kinnunen S., Nylander H., 1960, Punching of Concrete Slabs Without Shear Reinforcement, Transactions of the Royal Institute of Technology, N° 158, 112 p.

Kostic N., 2009, Topology of stress fields for design of reinforced concrete structures (in French: Topologie des champs de contraintes pour le dimensionnement des structures en béton armé), École Polytechnique Fédérale de Lausanne, Switzerland, 235 p.

Leonhardt, F., and Walther, R., 1962, Shear tests on beams with and without shear reinforcement (in German, Schubversuche an einfeldrigen Stahlbetonbalken mit und ohne Schubbewehrung), Deutscher Ausschuss für Stahlbeton, Heft 151, 83 p.

Marti, P., Alvarez, M., Kaufmann, W., Sigrist, V., 1999, Structural behaviour of reinforced concrete (in German, "Tragverhalten von Stahlbeton"), Institut für Baustatik und Konstruction, Fortbildungskurs für Bauingenieure, ETH Zürich, 30.9./1.10.1999, 301 p.

Moody, K. G., Viest, M., Elstner, R. C., and Hognestad, E., 1954, Shear Strength of Reinforced Concrete Beams—Part 1: Tests of Simple Beams, ACI Journal, Proceedings V. 51, No. 4, pp. 317-332.

Mörsch, E., 1908, Reinforced concrete construction, theory and application (in German, "Der Eisenbetonbau, seine Theorie und Andwendung"), 3rd Edition, Verlag von Konrad Wittwer, 376 p.

Mörsch, E., 1929, Reinforced concrete construction, theory and application I-2, (in German, "Der Eisenbetonbau, seine Theorie und Andwendung"), 6th Edition, Verlag von Konrad Wittwer, 541 p.

Müller, P., 1978, Plastic analysis of reinfoced concrete shells and beams, (in German: Plastische Berechnung von Stahlbetonscheiben und –balken), Intitut für Baustatik und Konstruktion, ETH Zürich, Bericht 83, Birkhäuser Verlag, Basel-Stuttgart, 160 p.

Muttoni, A., 1989, The applicability of the theory of plasticity in the design of reinforced concrete, (in German, "Die Andwendbarkeit der Plastizitätstheorie in der Bemessung von Stahlbeton"), Institut für Baustatik und Konstruction, ETH Zürich, Bericht Nr. 176, Birkhäuser Verlag, Basel-Stuttgart, 159 p.

Muttoni, A., Schwartz, J., and Thürlimann, B., 1997, Design of concrete structures with stress fields, Birkhaüser, Basel, Boston and Berlin, 145 p.

Muttoni, A. 2003. Shear and punching strength of slabs with-out shear reinforcement, (in German, "Schubfestigkeit und Durchstanzen von Platten ohne Querkraftbewehrung"), Beton- und Stahlbetonbau, Vol. 98, pp. 74-84.

Muttoni A., Burdet O., Hars E., 2006, Effect of Duct Type on the Shear Strength of Thin Webs, ACI Structural Journal, Vol. 103, No.5, pp. 729-735

Muttoni A., 2008, Punching shear strength of reinforced concrete slabs without transverse reinforcement, ACI Structural Journal, V. 105, No 4, pp. 440-450

Muttoni A., Fernández Ruiz M., 2008, Shear strength of members without transverse reinforcement as function of critical shear crack width, ACI Structural Journal, V. 105, No 2, pp. 163-172

Muttoni, A., Fernández Ruiz, M., 2010a, Design through an incremental approach: the Swiss experience, 2010 Joint IABSE-*fib* Conference, Dubrovnik, Croatia, 8 p.

Muttoni, A., Fernández Ruiz, M., 2010b, The Critical Shear Crack Theory as a mechanical model for punching shear design and its application to code provisions, Shear workshop at Salò, Italy, companion paper in this *fib* bulletin, 33 p.

Nielsen, M. P., 1999, Limit analysis and concrete plasticity, 2nd Ed., CRC Press, 908 pp.

Pang, X-B, Hsu, T.T.C, 1996, Fixed Angle Softened Truss Model for Reinforced Concrete, ACI Structural Journal, Vol. 93, No. 2, pp. 197-207

Ritter, W., 1899, The Hennebique construction method (in German, "Die Bauweise Hennebique"), Schweizerische Bauzeitung, XXXIII, N° 7, pp. 41-61.

Sagaseta, J., Muttoni, A., Fernández Ruiz, M., Tassinari, L., 2010, Non axis-symmetrical punching shear around internal columns of RC slabs without transverse reinforcement, Magazine of Concrete Research, Thomas Telford Publishing Ltd., London, accepted for publication

Schlaich, J., Schäfer, K. And Jennewein, M., 1987, Toward a consistent design of structural concrete, Prestressed Concrete Institute Journal, May-June, pp. 75-150.

Shioya T., and Okada T., 1985, The Effect of the Maximum Aggregate Size on Shear Strength of Reinforced Concrete Beams, Japanese Concrete Institute, pp. 521-524.

SIA, 2003, Code 262 for Concrete Structures, Swiss Society of Engineers and Architects, Zürich, Switzerland, 94 p.

Thürlimann, B., Marti, P., Pralong, J., Ritz, P. and Zimmerli, B. 1983, Application of the plasticity theory to reinforced concrete (in German, Anwendung der Plastizitätstheorie auf Stahlbeton), Institut für Baustatik und Konstruction, ETH Zürich, 252 pp.

Vaz Rodrigues, R., Fernández Ruiz, M., Muttoni, A., 2008, Punching shear strength of R/C bridge cantilever slabs, Engineering Structures, Elsevier, Vol. 30, No. 11, pp. 3024-3033

Vaz Rodrigues, R., Muttoni, A., and Fernández Ruiz, M., 2010, Influence of Shear on Rotation Capacity of Reinforced Concrete Members Without Shear Reinforcement, ACI Structural Journal, V. 107, No 5, pp. 516-525

Vecchio, F. J. and Collins, M. P. 1986, The modified compression field theory for reinforced concrete elements subjected to shear, ACI Journal, 83, March-April, pp. 219-231

Walraven J.C. 1981, Fundamental Analysis of Aggregate Interlock, Journal of the Structural Division, Vol. 107, No. 11, pp. 2245 – 2270.

Yoon, Y-S, Cook, W.D. and Mitchell, D., 1996, Minimum Shear Reinforcement in Normal, Medium, and High-Strength Concrete Beams, ACI Structural Journal, Vol. 93, No. 5, pp. 576-584

Zsutty, T. C., 1968, Beam shear strength ptrediction by analysis of existing data, ACI Journal, November 1968, Vol. 65, No. 11, pp. 943-951

Appendix 1: Notation

C	=	compression force
F_w	=	compression force in the web
L	=	total span
M	=	bending moment
N	=	axial force
P	=	prestressing force
T	=	tendon force
V	=	shear force
V_R	=	shear strength
V_P	=	shear force carried by prestressing
V_{tot}	=	total shear force
a	=	shear span
b	=	beam width
b_0	=	length of control perimeter

b_w = web width
d = effective depth
d_D = duct diameter
d_g = maximum diameter of the aggregate
d_{g0} = reference aggregate size (16 mm (0.63 in))
f_c = average compressive strength of concrete (measured on cylinders)
f_{c0} = compressive strength to account for concrete brittleness
f_c = average compressive strength of concrete (measured on cylinders)
k = coefficient for reduction of web width
x = coordinate
w = critical shear crack opening
α = shear span-to-depth ratio (=a/d)
ε = reference strain
ε_1 = transverse strain
η_D = strength reduction factor accounting for post-tensioning ducts
η_ε = strength reduction factor accounting for transverse cracking
η_{fc} = strength reduction factor accounting for concrete brittleness
θ = compression field angle with reference to the axis of the support region
ρ = flexural reinforcement ratio
τ_b = bond strength

8 Residual shear bearing capacity of existing bridges

Joost Walraven

Professor of Concrete Structures, Delft University of Technology, The Netherlands

Abstract: Many bridges in The Netherlands are meanwhile 40-50 years old. These bridges were designed according to old design codes, which do not reflect the state of the art of today. Moreover, traffic loads have been increased substantially. If those bridges are recalculated according to modern design codes they often do not meet the safety standards, particularly with regard to the shear bearing capacity. In spite of that, most of these bridges do not show significant distress, which does not support the results of the analysis. Obviously there are hidden reserves in the bearing capacity. To determine the real bearing capacity, existing design rules, even those found in recent codes, are too conservative since they represent simplified lower bound models, basically suitable for the design of new structures. This paper deals with recent experiences in analyzing the real shear bearing capacity of existing bridges.

8.1 Introduction

Until quite recently, the design of reinforced concrete structures was only based on structural safety and serviceability. Experience with damage due to corrosion and doubtful concrete quality showed, however, that design for durability deserves to be put at the same level as design for safety and serviceability. In future codes design for service life should become a major design task. In this respect the development of a new Model Code for Concrete Structures should be noted. Figure 8.1 shows schematically the idea behind design for service life. At the vertical axis the capitals R and S represent Resistance (R = Resistance) and Load (S = Solicitation, Fr.) respectively. The dotted line with upward tendency represents the development of traffic load in time. The lower of the two declining dotted lines shows the decrease of average bearing capacity in time. Both the bearing capacity and the load are subjected to scatter. The condition $Z = R(t) - S(t) < 0$ means that the structure fails, which should be avoided with a specified degree of reliability. If the corresponding reliability index β is exceeded, the decision should be made to strengthen the structure. However, the real bearing capacity of structures might be higher than calculated by even recent design provisions, for various reasons. Taking this into account could lead to an increase of the bearing capacity, even to such an extent that retrofitting is unnecessary, or can be shifted to a later date. In this respect the shear bearing capacity turns out to be a dominating criterion. Searching for the real bearing capacity of existing bridges is therefore the aim of this paper. Detecting residual shear bearing resistance is important, since it might avoid unnecessary repair and strengthening investments, which could lead to large savings. In this paper it is demonstrated that determining the real shear bearing capacity should not be done with design equations, derived for new structures, as found in building codes. Other considerations are necessary, which should be implemented in future codes of practice. This is the more important, since dealing with existing structures will be a task for many design engineers in the near future.

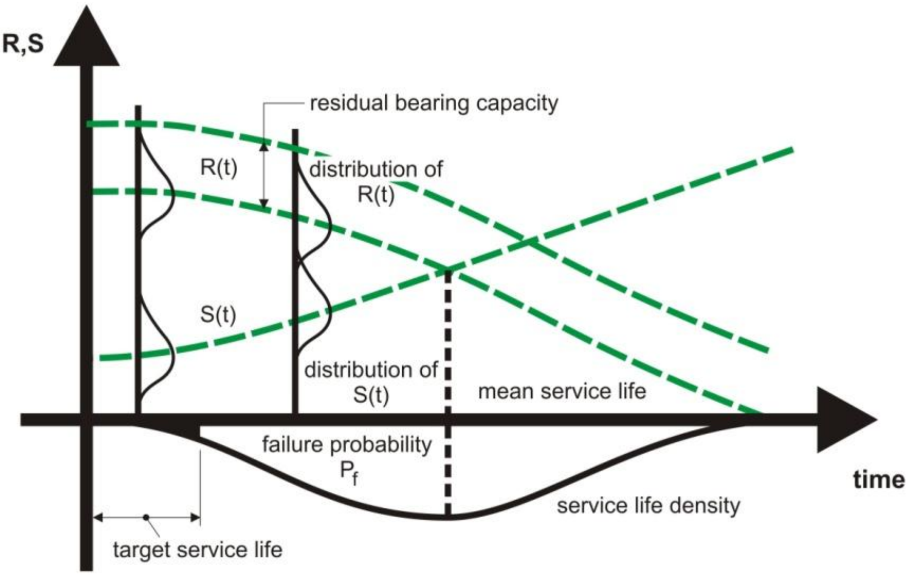

Fig. 8.1: Representation of increased traffic load against decreasing bearing capacity

8.2 Results of a "quick scan" investigation of the shear bearing capacity of existing bridges in The Netherlands

In the Netherlands the bearing capacity of many bridges, built in the period 1960-1970, was recently investigated. The results of "quick scans" carried out by design offices, showed a remarkable result. Table 8.1 shows a small selection of different bridge types. The assessment of the bearing capacity was carried out under the assumption of modern traffic loads and actual building codes, whereas for concrete and steel the original design strengths were used. The last column in Table 8.1 shows the so-called UC-values, where UC stands for "Unity Check". According to this analysis the safety values for the loads and the materials are removed: the UC-value is the ratio between the maximum load on the bridge in use and the shear bearing capacity, calculated on the basis of existing code rules. If the UC-value is larger than 1, this means theoretically that the shear bearing capacity is insufficient. The table shows unexpectedly high UC-values. In all cases the shear capacity apparently turns out to be largely insufficient. The highest UC values were found for T-beam decks and solid slab bridge decks, Fig. 8.2 and 8.3.

Bridge number	Categorie	Year	UC-Value
37E-122	Culvert	1996	1.89
37F-110	T-Beam deck	1970	2.43
38D-103	Solid slab	1936	4.53
38F-108	Subway	1966	1.61
38G-112	Subway	1961	1.18
38G-103	T-Beam deck	1959	3.13
39G-114	Straight solid slab	1959	2.85
52G-105	Skew solid slab	1969	3.53

Table 8.1: Results of quick scans for a selection of bridges.

Fig. 8.2: T-beam bridge deck

Fig. 8.3: Solid slab bridge deck

In spite of the alarming UC-values, however, inspections did not show signs that confirmed the expectation of a serious lack of shear bearing capacity. Obviously there is a substantial residual bearing capacity, which means that the real bearing capacity is significantly larger than calculated. Therefore in Fig. 8.1 a second declining line is shown: the vertical distance between the declining lines represents the hidden bearing capacity. It is clear that an accurate determination of this reserve bearing capacity is of large significance and should be regarded before any decision for retrofitting of the bridge is taken.

8.3 Hidden shear bearing capacities

8.3.1 Considerations with regard to the use of higher concrete strength

The first investigations of the bearing capacity of the bridges were carried out using the original design values for concrete and steel. The bridges had originally been built with concrete of strength class C20/25. However, after 28 days the strength of the concrete increases significantly, as a result of continuous hydration during decades. Tests on drilled cores, taken from the bridges, showed that the mean concrete strength is even in the range of 60-85 N/mm^2. Those high values can be explained by the fact that the cement particles used in those early days were relatively coarse, so that the hydration process will continue for a long time, delivering a substantial gain of strength. The compressive strength is an important factor, but not the most important. Especially with regard to the shear capacity the tensile strength plays an important role, especially in solid slabs which normally do not contain shear reinforcement. In most design codes, the shear bearing capacity is a direct, or an indirect, function of the concrete tensile strength. With regard to the concrete tensile strength, however, a remarkable observation was made. Tests on the drilled cylinders, mostly taken from the bottom of the slab, determining the spitting tensile strength and the uniaxial tensile strength showed that the splitting tensile strength was in the range 4-5 N/mm^2, whereas the uniaxial tensile strength was only in the range 1-2 N/mm^2 (Fig. 8.4). According to EC-2 the ratio uniaxial tensile strength to splitting tensile strength should be 0.9, whereas the Model Code 2010 proposes even a value 1.0. An important observation in Fig. 8.4 is that the scatter in the values of the splitting tensile strength and the uniaxial tensile strength is about the same. A possible explanation for the difference between splitting tensile strength and uniaxial tensile strength is given in Fig. 8.5. After casting the concrete and vibrating, under the coarse aggregate particles water layers are left behind due to bleeding, see Fig. 8.5 left. Especially the concrete of those days was sensitive to this type of phenomenon, since in those days no superplasticizers were applied yet, so that excess water was used for achieving the required workability. The concrete of those days showed generally a low concrete strength, which corresponds with the use of a surplus of water.

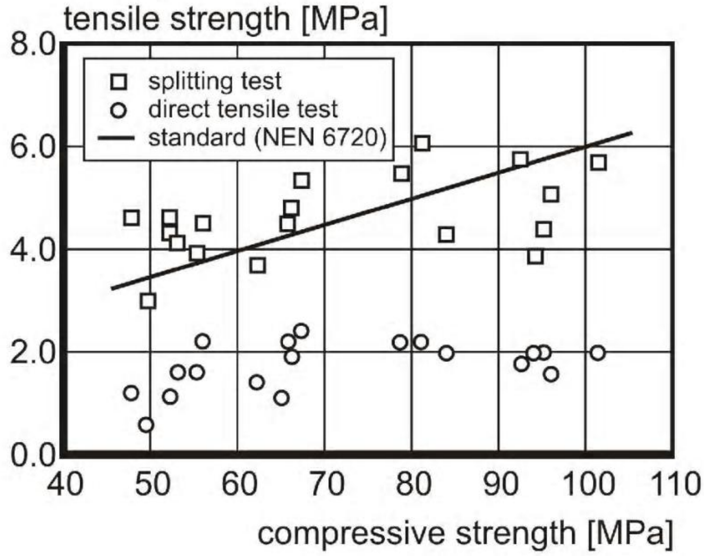

Fig. 8.4: Direct tensile strength and splitting tensile strength as a function of the concrete compressive strength, as determined on drilled cylinders taken from concrete bridges in The Netherlands.

Fig. 8.5: Drilled cylinder with visual flow under one of the large particles (weakened interface)

The weakened interfaces between the coarse aggregates explain the low axial tensile strength of the concrete. On the splitting strength the weak areas have no large influence, since they are not in the planes where cracks are expected to develop. The same holds true for the cylinder compressive strength. In beams and slabs loaded in shear at first bending cracks occur, in a direction perpendicular to the axis of gravity. Such cracks are not influenced by the weak interfaces. Only after the transition from bending cracks to inclined shear cracks there might be an influence, but this applies only to the stage in which the shear crack tends to bend to a low angle with the member axis, in which state the element is already near to shear failure. In order to verify this supposition, large beams were sawn out of existing slab bridges, showing the phenomenon described, and tested in analogy with similar, newly cast beams made of concrete with the same dimensions, the same reinforcement configuration and the same compressive strength, but much better workability. The tests showed that the behaviour of old and new beams was similar, which confirms that the weak interfaces under the course aggregates do not play a significant role with regard to the shear bearing behaviour. Therefore it was concluded that the shear capacity can be calculated with the usual equations, introducing the measured cylinder compressive strength (Yang et al., 2010).

The results of this investigation showed a similarity with the results of tests carried out some years ago at TU Delft. Fig. 8.6 shows a shear test carried out on a strip, sawn from an old slab bridge. This solid slab showed a large number of short horizontal cracks, which were due to the effect of the alcali silica reaction. The cracks were explained on the basis of the swelling of concrete under the influence of the ASR. In the horizontal direction a lot of reinforcement was available, both at top and bottom, which restrained the horizontal extension, and generated a type of axial prestressing. Therefore no vertical cracks occurred. In the vertical direction, however, the extension could occur freely, so that the crack formation was not suppressed. A considerable reduction of the shear bearing capacity was feared, because cylinders drilled from the bottom often showed a tensile strength equal to 0, caused by the horizontal cracks, intersecting the cylinders. The tests on severely damaged slab strips, however, showed only a slight reduction of the shear bearing capacity. The reduction was always smaller that 20% (den Uijl, 2000).

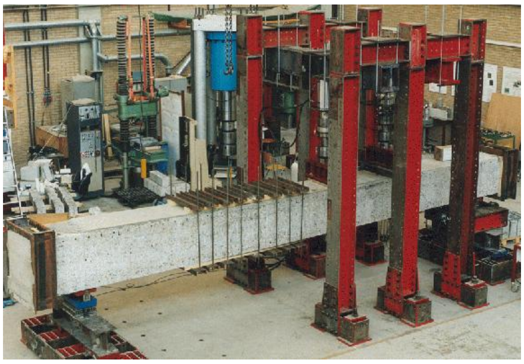

Fig. 8.6: Shear tests on beams damaged by short horizontal cracks due to alkali silica reaction (TU Delft)

8.3.2 Compressive membrane action in slabs

The design of solid slabs is carried out already for many years under the assumption that in case of a load perpendicular to the slab only bending and torsional moments occur. There is, however, another effect which is mostly ignored in design, but can significantly contribute to the bearing capacity. Already in 1955 Ockleston carried out tests on one of the inner slabs in a slab field in the Old Dental Hospital in Johannesburg (that was available for proof loading, since it was destined to be demolished anyhow). The inner decks failed at a load which was about twice the theoretical load according to the yield line theory. The increase of the bearing capacity was explained on the basis of compressive membrane action (dome effect). This mechanism occurs under the influence of restraint of lateral deformations, caused by the surrounding part of the slab. The mechanism is explained in Fig. 8.7. As a result of the development of cracks at midfield and at the edges, a mechanism occurs, in which the slab tries to expand in lateral direction. Since this lateral extension is restrained, a compressive arch forms, which is able to sustain significant forces. The increase of the bearing capacity depends on the degree of restraint. Already in the sixties it was demonstrated by tests (Tong, Batchelor, 1971) that the punching shear capacity is considerably increased by compressive membrane action. Canadian and New Zealander Building Recommendations allow the consideration of this effect in design. Although in these recommendations conservative values are given for the effect of compressive membrane action, considerable savings of reinforcement are possible. By considering compressive membrane action only a reinforcement ratio of about 0.5% is due, whereas without compressive membrane action about 1.7% is necessary.

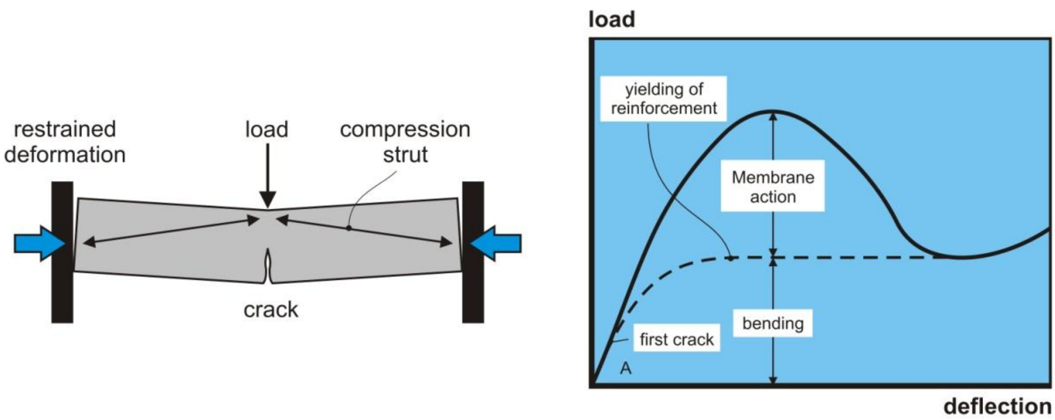

Fig. 8.7: Compressive membrane action in a bridge deck (left) and interaction between membrane action and bending (right).

The fact that up to now for the design of bridges in most countries compressive membrane action was not regarded means that there is still a considerable residual capacity with regard to bending and shear. Fig 8.7 shows a test by Tailor (2007), carried out recently on a bridge in Northern Ireland. The reinforcement in the deck was applied in the middle of the deck plate. The loads reached values of 3-5 times the theoretical values, calculated without compressive membrane action. In none of the twelve tests which were carried out failure occurred: the tests had to be stopped because the limit capacity of the testing equipment was reached.

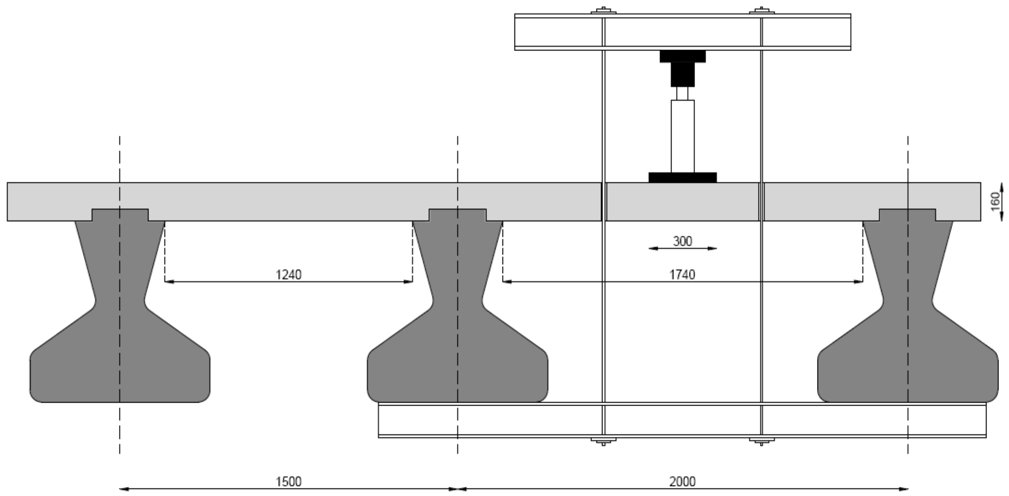

Fig. 8.8: Test carried out on a bridge deck by Tailor (2007), demonstrating the influence of compressive membrane action on the shear and punching bearing capacity.

8.3.3 Shear bearing capacity of slabs with loads near to line supports

From the control of the bearing capacity of solid slab bridges in The Netherlands it turned out that often the loads near to line supports, single or in combination, are governing for the shear bearing capacity, at least according to the design models. Herefore it was investigated whether the design practice in combination with the code requirements is not too conservative. According to those design methods the load is spread under angles of 45° to the support and then compared with the limit values for shear. Fig. 8.9 shows the test equipment for a solid end slab in a continuous statically indeterminate bridge (Landsoght, van der Veen, to be published). A concentrated load, simulating a large wheel load, is applied near the outer line-support. The effect of loads near supports was investigated both for end- and intermediate supports.

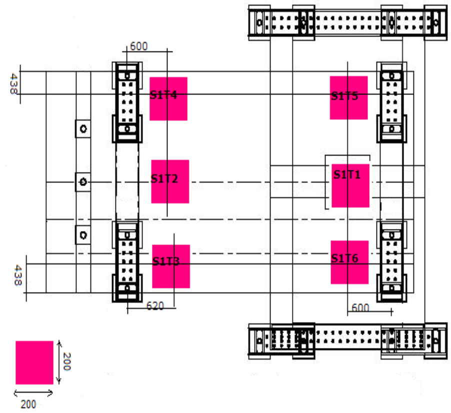

Fig. 8.9: Tests at TU Delft on solid slabs subjected to concentrated loads near supports (at the right side top view on slab with potential positions of the load).

Fig. 8.9, right, shows a top view on the slab with different possible positions of the load. The tests ST1, ST2 and ST3 were carried out with the load near to the linear end support (hinged support). The tests ST4-ST6 were carried out with the load near to the intermediate support. Table 8.2 shows that the bearing capacities found in these tests were considerably higher than obtained from a prediction based on the shear equations from the Dutch Building Code, assuming a 45° spreading of the load into the direction of the line support. This is due to the fact that the shear equations on the basis of the Dutch Code (and nearly all other codes) are obtained from tests on beams without shear reinforcement, whereas the results obtained on the slabs are influenced by considerable redistribution by virtue of the larger width of the slab and the effect of transverse reinforcement.

Test nr.	P_u (test) kN	P_u (Dutch Code)
S1T1	954	539
S1T2	1023	533
S1T3	758	491
S1T4	731	470
S1T5	851	501
S1T6	659	501

Table 8.2: Results of tests on slabs with concentrated loads near to supports: comparison between test results and theoretical results obtained with the equations from the Dutch Code.

8.4 Other methods to determine the shear bearing capacity

In order to find out whether a bridge has a sufficient bearing capacity very often nonlinear finite element calculations are used. From experiences with NLFEM calculations it is known that, up to now, this method has been particularly useful for the analysis of tests results obtained before calculating. However, it is much more difficult to predict the behaviour and a reliable value for the bearing capacity of existing bridges, without prior availability of test data, which could be used for calibration. Furthermore, for using nonlinear FEM calculations, there is a large choice with regard to element types, element size, calculation procedures and material parameters. A possibility to enhance the reliability of NLFEM calculations is to carry out calibrations on test results obtained for similar types of elements. Fig. 8.10 shows an example. In order to develop a basis for a reliable prediction of the behaviour of prestressed T- and I-beams, trial calculations and calibrations were carried out with the numerical programs DIANA and ATENA on the behaviour of long prestressed beams obtained from literature. This calibration on similar types of beams, the behaviour of which is well documented, is expected to increase the reliability of NLFEM predictions. Meanwhile a practitioner's guide for NLFEM analysis has been adopted in the Model Code 2010.

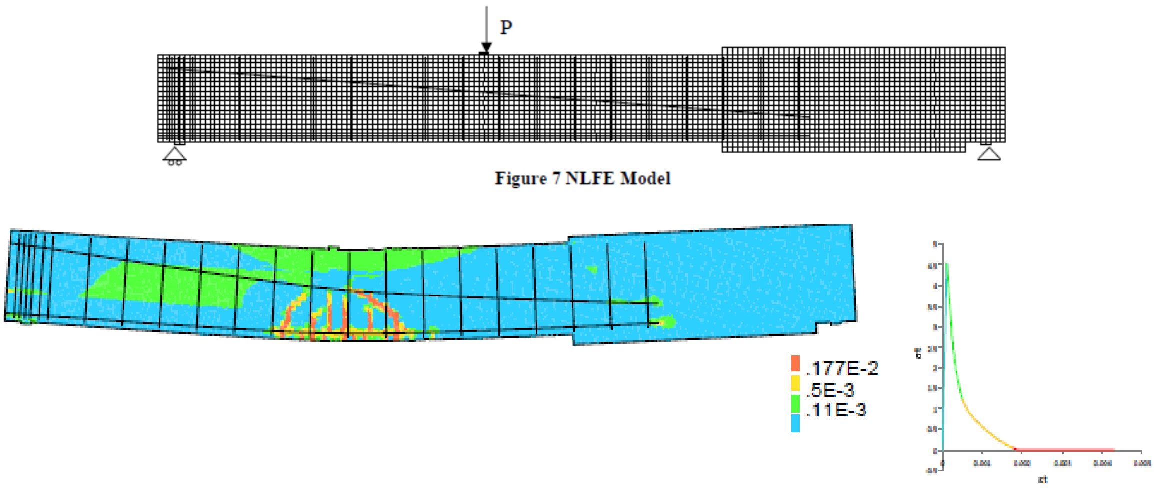

Fig. 8.10: NLFEM analysis of a beam under shear loading as a part of a research program to develop tailor-made finite element programs for particular types of beams.

Another way of optimizing the use of nonlinear programs for the reliable calculation of the bearing capacity of existing bridges is to combine them with proof loading and acoustic emission measurements. Fig. 8.11 shows the proof loading of a small bridge with the specially developed German vehicle BELFA (Belastung Fahrzeug = Loading Truck). In order to guide the testing, acoustic signals are registered. In future the combination of proof loading, acoustic emission and numerical analysis is seen as an important method for the estimation of the behaviour of existing bridges.

Fig. 8.11: Proof loading of an existing bridge with specially instrumented German Loading Truck (BELFA) in The Netherlands.

8.5 Conclusions

1) When old bridges are analyzed for the higher traffic loads of today, and the old design data are used for the analysis, the result is often that the shear bearing capacity is insufficient.
2) The bridges dispose of a considerable residual capacity as a consequence of higher concrete strength after decades of hydration, compressive membrane action and better redistribution of moments and shear forces than assumed in design.
3) Verification of the results of concrete strength on the basis of drilled cylinders should be done with utmost care.
4) Nonlinear FEM methods can be developed tailored to the prediction of the behaviour of particular types of bridge beams.
5) The combination of proof loading, numerical analysis and acoustic emission deserves further development, since it may become an important tool for future assessment of existing bridges.

8.6 References

Den Uijl, J.A., Kaptijn, N., Walraven, J.C., "Shear capacity of flat slab bridges affected by ASR", Proceedings of the 11th International Conference on ASR in Concrete, Quebec City, Canada, 2000, pp. 1129-1138.

fédération internationale du béton (*fib*), "Model Code 2010 - First complete draft." Bulletins 55 and 56, 2010.

Landsoght, E., van der Veen, C., Walraven, J.C. "Shear capacity of slabs with concentrated loads near to supports", to be published.

Ockleston, A.J., "Load tests on a three storey reinforced concrete building in Johannesburg", The Structural Engineer, October 1955, Vol. 33, pp 304-322,

Tailor, S.E., Rankin, B., Cleland, D.J., Kirkpatrick, J., "Serviceability of Bridge Deck Slabs with Arching Action", ACI Structural Journal, Jan-Feb 2007, pp. 39-48.

Tong, P.Y., Batchelor, B. de V. "Compressive membrane action enhancement in two way bridge slabs", Cracking, Deflection and the Ultimate Load of Concrete Slab Systems, SSP-30, ACI Detroit, 1971, pp. 271-286.

Yuang, Y., den Uijl, J.A., Dieteren, G., de Boer, A., “Analysis of 50 years old bridge decks", 3rd *fib* Congress, Washington, June 2010, Proceedings.

9 Development of Dutch guidelines for nonlinear finite element analyses of shear critical bridge and viaduct beams

Jan Rots[1], Beatrice Belletti[2], Cecilia Damoni[3] and Max Hendriks[4]

[1] Full Professor, Faculty of Civil Engineering and Geosciences, Delft University of Technology
[2] Assistant Professor at DICATeA, University of Parma
[3] Guest researcher, DICATeA, University of Parma- Faculty of Civil Engineering and Geosciences, Delft University of Technology
[4] Assistant Professor, Faculty of Civil Engineering and Geosciences, Delft University of Technology

Abstract: The Dutch Ministry of Transport, Public Works and Water Management initiated a project to re-evaluate the carrying capacity of existing bridges and viaducts due to the change in use and the increase of traffic in the last years. The structural assessment necessary can be done through the use of nonlinear finite element analyses, taking advantage of their capacity to take into account real material properties and hidden capacities of the structures. Numerical simulations of several cases studies taken from several experimental programs have therefore been performed in order to assess and criticize the finite element approaches and to propose guidelines for nonlinear finite element analyses. Through the guidelines it is possible to optimize the results obtained from numerical simulations and to reduce model and user factors. In this paper the main directions of the guidelines are presented for reinforced and pre-stressed concrete beams.

9.1 Introduction

The Dutch Ministry of Transport, Public Works and Water Management initiated a project to make structural assessment of existing structures through the use of nonlinear finite element analyses. The project comes from the need to re-evaluate the carrying capacity of existing bridges and viaducts in the whole country due to the increase of traffic and change in use in the last years. For a certain amount of those Dutch bridges and other infrastructures the safety verifications are not satisfied if the usual analytical procedures, proposed by the current norms, are adopted for the calculations. Nonlinear finite element analyses can offer refined modeling based on realistic material properties, leading to a proper estimation of structural safety taking into account hidden capacities of the structures, neglected by the current analytical formulations. Furthermore the methods of verifications proposed by the new Model Code [*fib* (2010)] (Global Safety Factor Method, Partial Safety Factor Method, Estimation of Coefficient of Variation of Resistance Method) allow the determination of safety levels, similar as for the analytical procedures. However, the power of nonlinear finite element simulations, which are more and more becoming an usual instrument of calculation in the daily design procedures, shouldn't be overestimated; appropriate checks must be done to verify the reliability of the results. It is well known indeed that the results of nonlinear finite element analyses strongly depend on the analysts modeling choices, e.g. type and dimension of the elements, mechanical model, constitutive model, etc.. As a consequence, a big scatter of the results obtained from the same structure analyzed by several analysts can be detected. This scatter usually increases with decreasing analysts skills.

For these reasons, the guidelines the Dutch Ministry of Transport initiated the development of guidelines for nonlinear finite element analyses. They hold instructions necessary to obtain reliable and at the same time safe results from nonlinear finite element analyses. The reliability of the results obtained has been assessed through several experimental programs. Several reinforced and pre-stressed beams and slabs failing in different modes have been tested in laboratory and the experimental results have been compared with the results obtained from numerical simulations. The safety level of the numerical results has also been compared with the analytical procedures proposed by the EC2 [EC2(2004)] and the new *fib* Model Code (2010). The new Model Code proposes three different analytical methods to calculate the design resistance of a structure. These methods are based on the definition of three different safety levels: Level I, II and III respectively; by increasing the safety level the complexity and precision of the calculation increases.

The guidelines not only contain indications on the modeling but also on the way to present the results in order to facilitate the preparation of technical reports and the reviewing by professionals. The guidelines can be used for nonlinear finite element analyses performed with any software in which basic crack models, such as total strain fixed or rotating crack models, are implemented. In order to allow the analyst, even if not fully experienced, to have the basic knowledge about the numerical procedures, and also to make the results less software dependent, relatively simple crack models are chosen. The aim is therefore to emphasize the analysts skills in order to control the results obtained from the nonlinear finite element analyses without “a priori” accepting these results.

In the following paragraphs the main directions of the guidelines regarding nonlinear finite element analyses of reinforced and pre-stressed beams are presented.

9.2 Finite element model

To perform nonlinear finite element analyses of reinforced and pre-stressed concrete beams, adopting plane stress conditions, quadratic quadrilateral elements with Gauss integration (3x3) are suggested for concrete. For the reinforcement embedded truss elements can be used. Perfect bond between steel and concrete is assumed.
Since the resulting crack models based on fracture mechanic and total strain depends on the element dimensions, it is better to avoid big elements that could produce snap back phenomena. For this reason, elements with a characteristic length h equal to $0.5 \cdot l_{ch}$ [Hillerborg (1983)] are suggested; l_{ch} is the process zone length defined by Eq. (9.1):

$$l_{ch} < \frac{E \cdot G_F}{f_t^2} \tag{9.1}$$

Usually, in commercial software, the characteristic length h depends only on the dimensions and the integration scheme of the elements. A more accurate estimation of the characteristic length should depend also on the crack orientation with respect to the local axis of the element. An accurate modeling of support and loading plates, with interface elements having “no-tension” behavior between the plates and the beam, is suggested.

In Fig. 9.1 an overview of the cases studies is presented: four reinforced beams, RB1 [Vecchio (2004)], RB2 [Collins (1999)], RB3 [Grace (2001)] and RB3A [Grace (2001)] and four pre-stressed beams, of which two pre-tensioned beams, MNDOT [Runzell (2007)] and NSEL [Sun & Kuchma (2007)] and two post-tensioned beams, PB1 [Leonhardt (1973)] and PB4 [Leonhardt (1973)] are shown.

The main geometrical and mechanical features of the cases are listed in Table 9.1 and the failure mode of each beam and the experimental ultimate load in *KN*, obtained from laboratory tests, are summarized in Table 9.2.

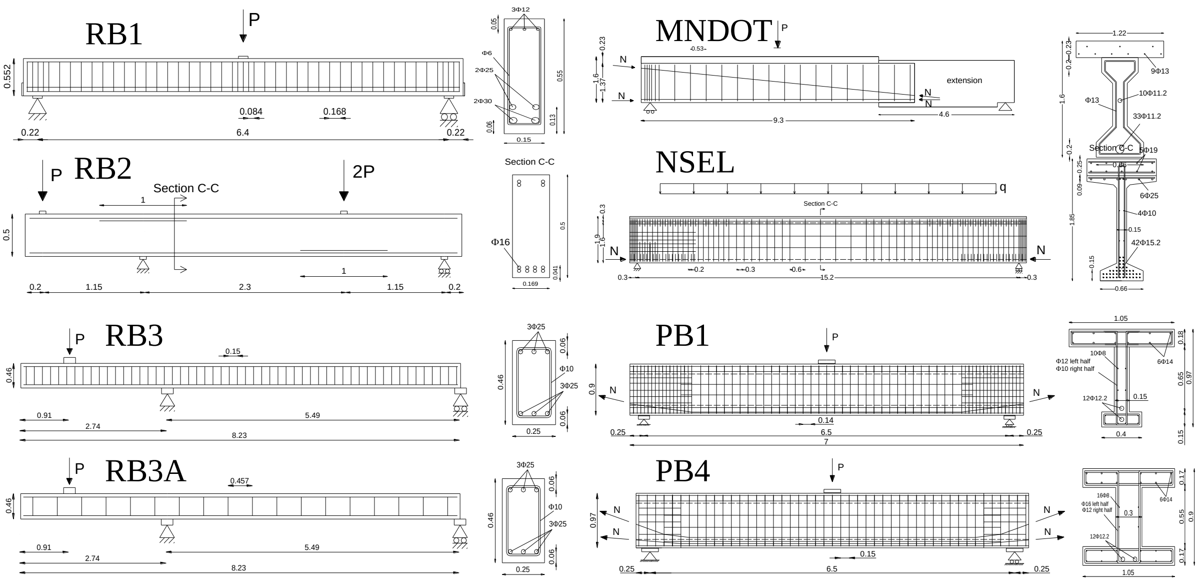

Fig. 9.1: Cases studies analyzed

	L (m)	h (m)	A_c (m^2)	A_{sl} (m^2)	A_p (m^2)	f_c (MPa)	E_c (MPa)	E_s (MPa)	f_{pe} (MPa)
RB1	6.84	0.552	0.084	0.0024	-	43.5	34195	200000	-
RB2	5.00	0.500	0.084	0.0008	-	53.0	36283	200000	-
RB3	8.23	0.457	0.114	0.0015	-	31.2	30950	200000	-
RB3A	8.23	0.457	0.114	0.0015	-	31.2	30950	200000	-
MNDOT	12.10	1.372	0.509	-	0.0042	69.84	34818	-	864
NSEL	15.85	1.854	0.460	0.0003	0.0061	109.6	52710	200000	1068
PB1	7.00	0.900	0.306	0.0008	0.0028	30.5	26675	197000	635
PB4	7.00	0.970	0.341	0.0005	0.0028	29.0	25977	197000	681

L = beam length; h = beam height; A_c = cross section of concrete; A_{sl} = cross section of longitudinal reinforcement in tension; A_p = cross section of prestressing strands; f_c = mean compressive strength of concrete; E_c = Young modulus of concrete; E_s = Young modulus of steel; f_{pe} = effective prestressing stress.

Table 9.1: Main geometrical and mechanical features of each beam

Reinforced beams	Failure mode	$P_{u,exp}$ (KN)	Pre-stressed beams	Failure mode	$P_{u,exp}$ (KN)
RB1	F	265	MNDOT	SC	2313
RB2	DT	69 81	NSEL	SC	6984
RB3	F	142	PB1	F	1897
RB3A	SC	156	PB4	SC	1491

F = bending failure; SC = shear-compression failure; DT= diagonal-tension failure; $P_{u,exp}$ = experimental ultimate load.

Table 9.2: Failure mode and experimental ultimate load of each beam

9.3 Constitutive models

The relationships of the parabolic law in compression and the exponential law in tension are reported below, Eq. (9.2):

$$\sigma = f_t \cdot exp\left(-\frac{\varepsilon}{\varepsilon_{ut}}\right) \qquad \text{when } \varepsilon > 0$$

$$\sigma = -f_c \cdot \frac{1}{3} \cdot \frac{\varepsilon}{\alpha_{c/3}} \qquad \text{when } \alpha_{c/3} < \varepsilon \leq 0$$

$$\sigma = -f_c \cdot \frac{1}{3} \cdot \left(1 + 4\left(\frac{\varepsilon - \alpha_{c/3}}{\alpha_c - \alpha_{c/3}}\right) - 2\left(\frac{\varepsilon - \alpha_{c/3}}{\alpha_c - \alpha_{c/3}}\right)^2\right) \qquad \text{when } \alpha_c < \varepsilon \leq \alpha_{c/3}$$

$$\sigma = -f_c \cdot \left(1 - \left(\frac{\varepsilon - \alpha_c}{\alpha_u - \alpha_c}\right)^2\right) \qquad \text{when } \alpha_u < \varepsilon \leq \alpha_c \tag{9.2}$$

where $\varepsilon_{ut} = G_F / (h \cdot f_t)$, h is the element characteristic length , f_t is the tensile strength, G_F the fracture energy in tension, $\alpha_{c/3} = -f_c/(3 \cdot E)$, f_c is the compressive strength, E is the Young modulus, $\alpha_c = -5\alpha_{c/3}$, $\alpha_u = \alpha_c - 3G_c/(2 \cdot h \cdot f_c)$, G_c is the fracture energy in compression, taken equal to $250 \cdot G_f$ [Nakamura (2001)].
In Fig. 9.2 the constitutive model used for concrete in tension and in compression is shown.

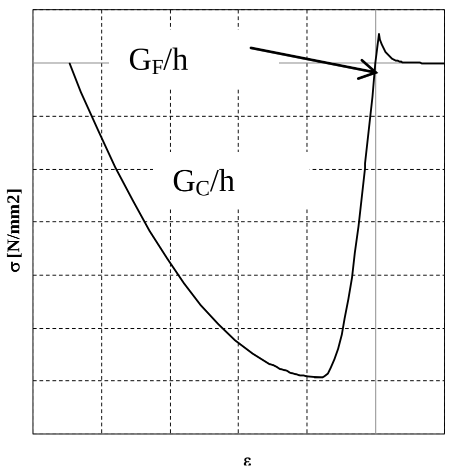

Fig. 9.2: Constitutive model of concrete

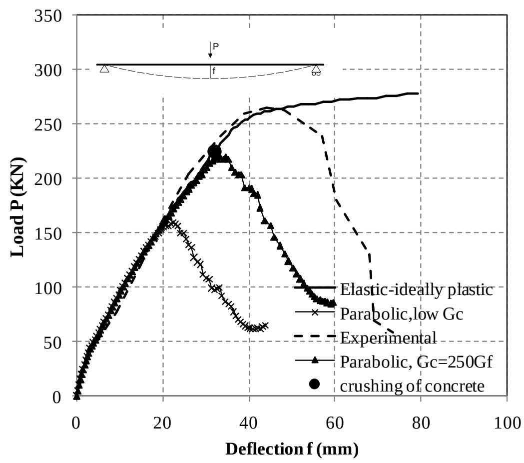

Fig. 9.3: Load-deflection curves of RB1 beam-comparison among different constitutive models

For the longitudinal reinforcement and the prestressing steel an elastic-plastic model with hardening is adopted.

The compressive behavior of concrete plays an important role in the structural response of beams and slabs. In Fig. 9.3 the load-deflection curves obtained with different constitutive models for RB1 beam [Vecchio (2004)], failing in bending due to crushing of concrete, are plotted. It can be noted that if an elastic-ideally plastic law in compression is adopted, a real peak load is not reached during the analysis, while if a parabolic law is used, the load-deflection curve reaches a peak load and a post-peak behavior, that depends on the value of the fracture energy in compression [Nakamura (2001)]. The constitutive relation in compression has therefore a big influence on the peak load value and on the choice of a suitable convergence criterion; for these reasons an elastic-ideally plastic law in compression for concrete is disqualified.

9.3.1 Multi-axial stress state

The concrete subjected to multi-axial stress states has an important influence on the general behavior of beam failing in shear due to crushing of concrete. The reduction of the compressive strength due to lateral cracking had been investigated and tested on reinforced concrete panels subjected to pure shear by Vecchio & Collins (1993).

The software DIANA [DIANA (2008)], used for the nonlinear finite element analyses performed, applies the reduction of the compressive strength according to the "Model B" proposed by Vecchio & Collins (1993). The constitutive model used in compression and the reduction of the compressive strength as a function of the lateral cracking are shown in Fig. 9.4.

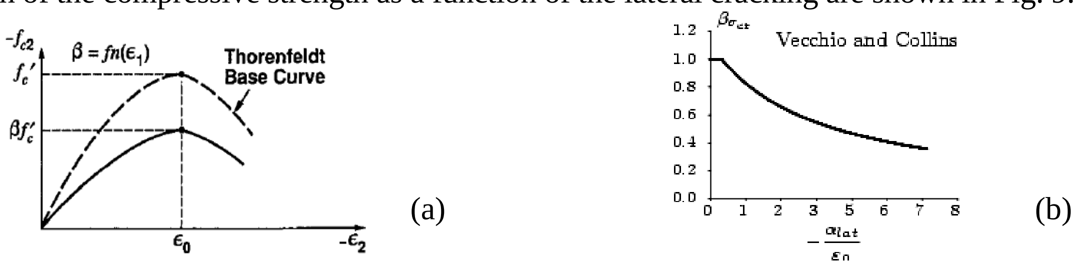

Fig. 9.4 a: Constitutive model, b: reduction of the compressive strength due to lateral cracking according to the "Model B" of Vecchio & Collins

Eq.(9.3) and Eq. (9.4) show the expressions of the strength reduction coefficient (β_σ) and the strain reduction coefficient (β_ε).

$$\beta_\sigma = \frac{f_{c,red}}{f_c} = \frac{1}{1+K_c} \tag{9.3}$$

$$\beta_\varepsilon = \frac{\varepsilon_{c,red}}{\varepsilon_c} = 1 \tag{9.4}$$

where $K_c = 0.27\left(\frac{\alpha_{lat}}{\varepsilon_0} - 0.37\right)$, α_{lat} is the tensile strain, ε_0 is the compressive peak strain.

From Fig. 9.4 it can be noted that the reduction of the compressive strength (Eq. (9.3)) without the simultaneous reduction of the peak strain (Eq. (9.4)) leads to a very high reduction of the Young modulus most of all for low strain values. It is therefore suggested to apply models, such as those proposed by Vecchio & Collins (1993) and Belarbi & Hsu (1991), that take into account both the reduction of the compressive stress and the reduction of the peak strain.

Checks are suggested to be made on simple models in order to investigate the way in which the software adopted considers the effect of multi-axial stress states. Hence, nonlinear finite element analyses have been carried out on a plane concrete element subjected, in a first load step, to a tensile strain leading to fully open cracks and, in a second load step, to a lateral compressive strain. In Fig. 9.5a the mechanical model of the concrete element is shown and in Fig. 9.5b the stress-strain curves in compression and the reduction of the compressive strength are plotted; each curve of Fig. 9.5b is characterized by a different ratio between the tensile and the compressive strain applied.

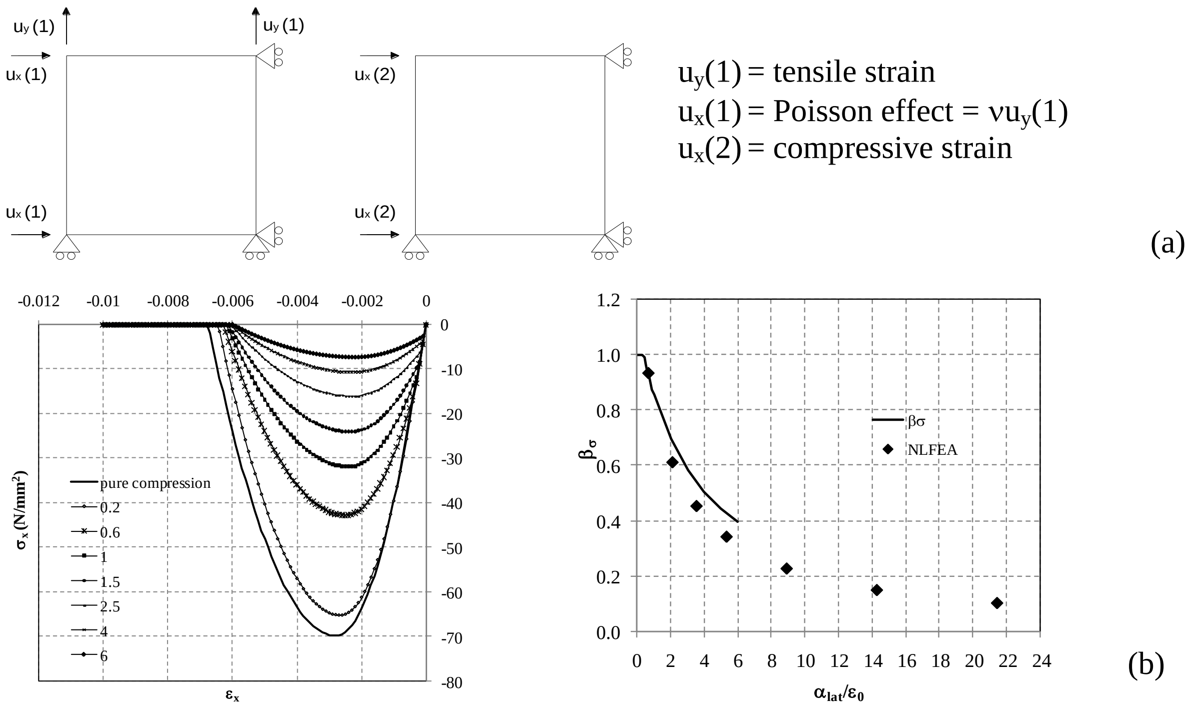

Fig. 9.5 a: Mechanical model of a plane concrete element, b: compressive stress-strain curves and reduction of the compressive strength of the concrete element

It can be noted that the software doesn't apply any limit to the reduction of the compressive strength which could therefore theoretically reach 100%, contrarily to the indications of Vecchio & Collins (1993) who limit the reduction at about 60% of the uni-axial compressive strength. From Fig. 9.6 (PB4 beam [Leonhardt (1973)]) it can be noted that the influence of the reduction of the compressive strength on the results can be substantial, most of all in terms of peak load reached.

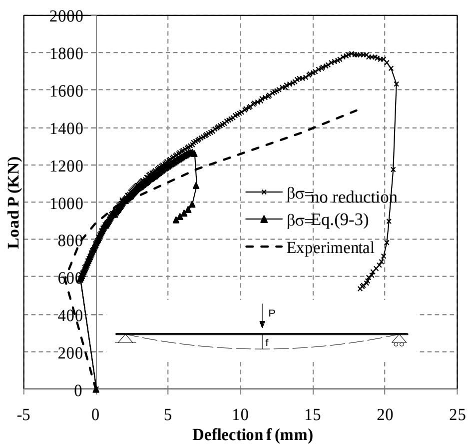

Fig. 9.6: Load-deflection curves of PB4 beam-influence of the reduction of the compressive strength

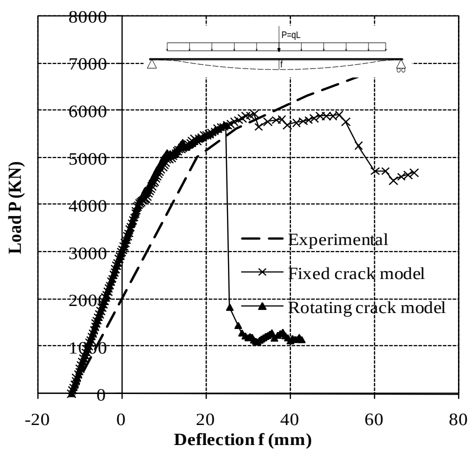

Fig. 9.7: Load-deflection curves of NSEL beam-comparison between fixed crack model and rotating crack model

9.4 Crack models

Among simple total strain crack models, two different approaches, denoted as rotating crack model and fixed crack model, have been proposed by several authors [e.g. Cervenka (1985), Vecchio & Collins (1986), Foster (1996), Hsu (2010)] and they are available in literature. The main features of the rotating and the fixed crack models are described below.

A total strain rotating crack model is suggested, basically for its effective simple theoretical characteristics. As proposed by Feenstra (1998), this crack model is based on the concept of co-axiality between stress and strain. For each load increment Δt the stress vector is updated according to Eq. (9.5):

$${}^{t+\Delta t}_{i+1}\varepsilon_{xy} = {}^{t}\varepsilon_{xy} + {}^{t+\Delta t}_{i+1}\Delta\varepsilon_{xy} \tag{9.5}$$

where x,y are the local axes and i is the current Newton-Raphson increment. The stress vector is evaluated in the ns coordinate system, where n represents the axis perpendicular to the primary cracking and s the parallel axis. A secondary cracking, perpendicular to the primary cracking, could develop orthogonally to s axis. The strain referred to ns coordinate system are calculated with Eq. (9.6):

$${}^{t+\Delta t}_{i+1}\varepsilon_{ns} = T\ {}^{t+\Delta t}_{i+1}\varepsilon_{xy} \tag{9.6}$$

where T represents the transformation matrix that depends on the current strain vector, Eq. (9.7):

$$T = T\left({}^{t+\Delta t}_{i+1}\varepsilon_{xy}\right) \tag{9.7}$$

The constitutive model is formulated in the ns coordinate system, Eq. (9.8):

$${}^{t+\Delta t}_{i+1}\sigma_{ns} = \sigma\left({}^{t+\Delta t}_{i+1}\varepsilon_{ns},\ {}^{t+\Delta t}_{i+1}\hat{\varepsilon}_{ns},\ {}^{t+\Delta t}_{i+1}\breve{\varepsilon}_{ns}\right) \tag{9.8}$$

where the second and the third argument represent respectively the maximum and minimum strain values during the loading history, Eq. (9.9):

$${}^{t+\Delta t}_{i+1}\hat{\varepsilon}_{ns} = \max_{(0,t+\Delta t)}\left({}^{t+\Delta t}_{i+1}\varepsilon_{ns}\right);\ {}^{t+\Delta t}_{i+1}\breve{\varepsilon}_{ns} = \min_{(0,t+\Delta t)}\left({}^{t+\Delta t}_{i+1}\varepsilon_{ns}\right) \tag{9.9}$$

The stress vector updated in xy coordinate system derives therefore from Eq. (9.10):

$${}^{t+\Delta t}_{i+1}\sigma_{ns} = T^{T}\ {}^{t+\Delta t}_{i+1}\Delta\sigma_{xy} \tag{9.10}$$

Now Eq. (9.8) can be written as Eq. (9.11):

$${}^{t+\Delta t}_{i+1}\sigma_{ns} = \sigma\left({}^{t+\Delta t}_{i+1}\tilde{\varepsilon}_{ns},\ {}^{t+\Delta t}_{i+1}\hat{\varepsilon}_{ns},\ {}^{t+\Delta t}_{i+1}\breve{\varepsilon}_{ns}\right) \tag{9.11}$$

where the strain ${}^{t+\Delta t}_{i+1}\varepsilon_{ns}$ is substituted by the equivalent uni-axial strain ${}^{t+\Delta t}_{i+1}\tilde{\varepsilon}_{ns}$ to take into account the lateral expansion due to the Poisson effect, Eq. (9.12):

$${}^{t+\Delta t}_{i+1}\tilde{\varepsilon}_{ns} = \begin{bmatrix} \dfrac{1-\nu}{(1+\nu)(1-2\nu)} & \dfrac{\nu}{(1+\nu)(1-2\nu)} \\ \dfrac{\nu}{(1+\nu)(1-2\nu)} & \dfrac{1-\nu}{(1+\nu)(1-2\nu)} \end{bmatrix} {}^{t+\Delta t}_{i+1}\varepsilon_{ns} \tag{9.12}$$

Besides the Poisson effect, the reduction of the compressive strength due to lateral cracking and its increase due to lateral confinement are taken into account (paragraph 9.3). Both multi-axial effects are implemented through an update of the stress vector for the individual *ns* directions. Two uni-axial relations are then left, Eq. (9.13):

$$ {}^{t+\Delta t}_{i+1}\sigma_n = \sigma\left({}^{t+\Delta t}_{i+1}\tilde{\varepsilon}_n\right);\ {}^{t+\Delta t}_{i+1}\sigma_s = \sigma\left({}^{t+\Delta t}_{i+1}\tilde{\varepsilon}_s\right) \tag{9.13} $$

Unlike the rotating crack model previously described, according to the fixed crack model the orthotropic material coordinate system *ns* remains fixed after the appearance of the primary cracking and the transformation matrix T (Eq. (9.7)) remains constant, so that shear stresses develop along the crack face. These shear stresses depend on the shear stiffness reduced by a coefficient called “shear retention factor” to take into account the cracking.

Below the stiffness matrix D used for the fixed crack model, matching stress and strain in case of plane stress state, is given, Eq. (9.14):

$$ D = \begin{bmatrix} \dfrac{E_n}{1-\nu_{ns}\nu_{sn}} & \dfrac{\nu_{sn}E_n}{1-\nu_{ns}\nu_{sn}} & 0 \\ \dfrac{\nu_{ns}E_s}{1-\nu_{ns}\nu_{sn}} & \dfrac{E_s}{1-\nu_{ns}\nu_{sn}} & 0 \\ 0 & 0 & G_{ns} \end{bmatrix} \tag{9.14} $$

where E_n ,E_s are the elasticity modules in the cracked phase, ν_{ns} e ν_{sn} are the Poisson’s ratios, $G_{ns} = \beta G$ where β is the shear retention factor that reduces the initial shear stiffness G .

Nonlinear finite element analyses performed with a fixed crack model can result more appropriate especially for shear critical beams, if the shear retention factor trend is properly evaluated by the implementation of adequate laws that take into account the aggregate interlock effect phenomena [Walraven (1981), Gambarova (1983)]. For this reason some cases studies have been analyzed using both a fixed crack model and a rotating crack model. In Fig. 9.7 the load-deflection curves of NSEL beam [Sun & Kuchma (2007)] obtained using a rotating crack model and a fixed crack model with a constant shear retention equal to 0.1 are plotted. From Fig. 9.7 it can be noted the scatter in terms of load-deflection curve due to the differences of the two models described above.

An important effect, most of all for beams failing in shear due to crushing of concrete, is covered by the Poisson’s ratio ν, Eq. (9.14). The software used for the analyses [DIANA (2008)] applies a constant Poisson’s ratio even after cracking; in this way the real physical behavior is not well caught and the effects due to secondary cracking are amplified.

In Fig. 9.8a the load-deflection curves of the NSEL beam [Sun & Kuchma (2007)] obtained applying a fixed crack model with a Poisson’s ratio equal to 0.2 and 0.0 are illustrated; in Fig. 9.8b the secondary cracking developed in both cases is plotted. It can be noted that the secondary cracking is much lower if the Poisson effect is neglected with a substantial effect on the ultimate load reached. Therefore, for the NSEL beam [Sun (2007)] a more realistic behavior of the Poisson’s ratio has been implemented, that linearly decreases from its real initial value in the elastic phase up to zero in the cracked phase of concrete.

In Fig. 9.9a the variable Poisson's ratio is plotted and in Fig. 9.9b the load-deflection curves for different values of the Poisson's ratio are shown. It can be noted that the load-deflection curve obtained with a variable Poisson's ratio is close to the curve obtained with a constant Poisson's ratio equal to zero.

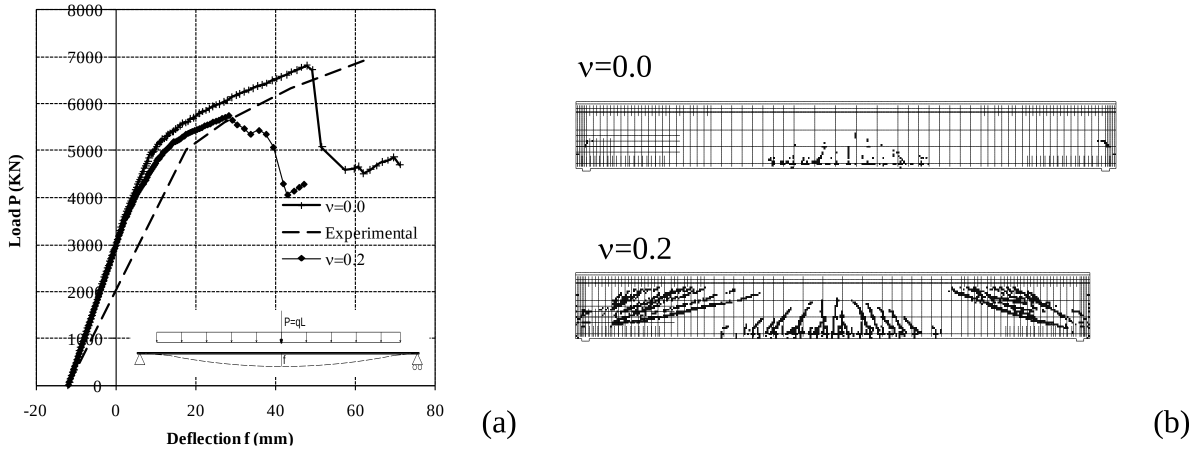

Fig. 9.8 a: Load-deflection curves of NSEL beam, b: secondary cracking developed due to Poisson effect

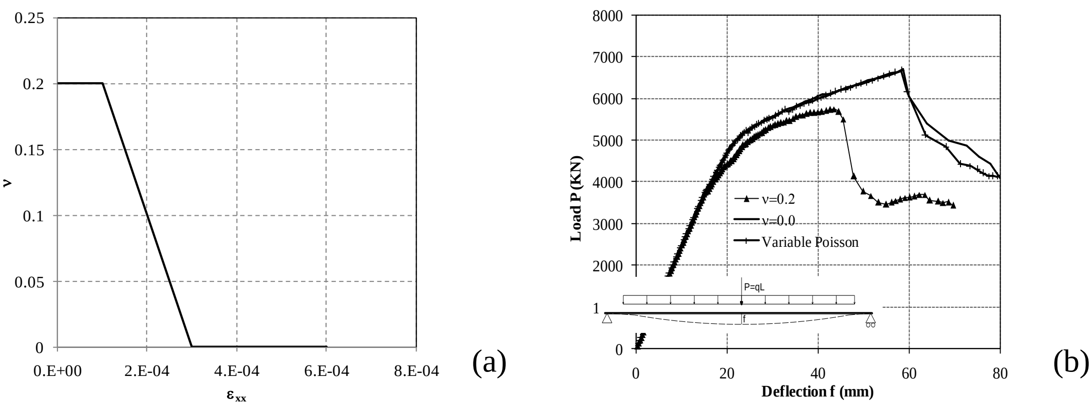

Fig. 9.9 a: Variable Poisson's ratio behavior, b: load-deflection curves of NSEL beam

9.5 Convergence parameters

Reliable results can be obtained from nonlinear finite element analyses if appropriate choices of the convergence parameters are made.

All the analyses have been carried out in load control with Newton-Raphson method and arc-length control monitoring the vertical displacement of a critical point of each beam. Some of the beam analyzed, especially the shear-critical beams, resulted to be very sensitive to the convergence parameters chosen.

In Fig. 9.10a the load-deflection curves of RB2 beam [Collins (1999), Belletti (2010)] obtained applying different convergence criteria are plotted and in Fig. 9.10b the convergence trend of one of the analyses is shown. The horizontal axis denotes the successive iterations of the successive load increments and the vertical axis denotes the convergence norm. The horizontal line indicates the tolerance chosen and the circle indicates the peak load of the analysis. Table 9.3 is the legend explanation used in Fig. 9.10.

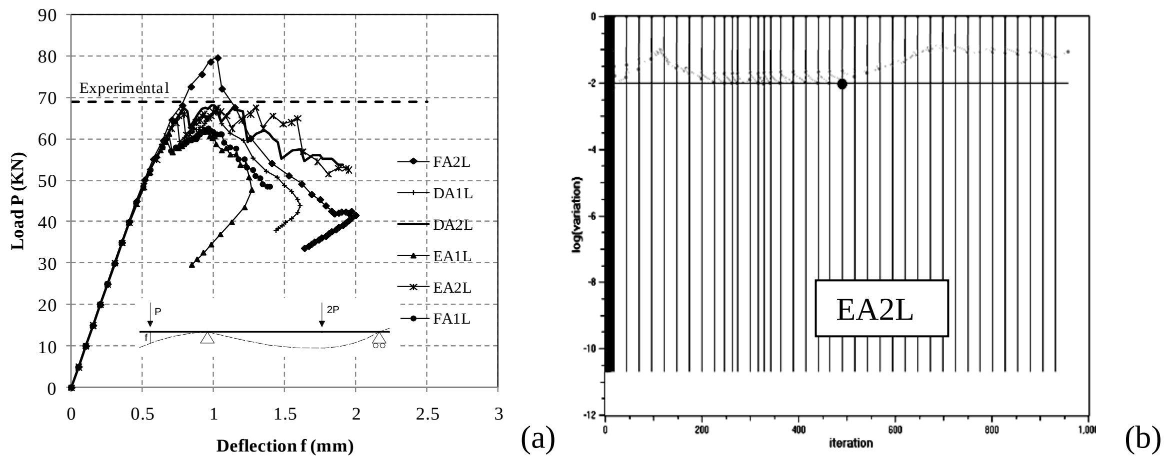

Fig. 9.10 a: Load-deflection curves of RB2 beam obtained with different convergence criteria, b: convergence trend of one of the analyses

Sometimes the peak load is reached without the full convergence of the analysis; for this reason the choice of the convergence parameters is very important to understand the reliability of the results obtained. The most robust and consistent criteria proved to be the energy based criterion with a tolerance of 10^{-4} or a force based criterion with a tolerance of 10^{-2}.

	Criterion	**Tolerance**
FA1L	Force	10^{-2}
FA2L	Force	$5\cdot10^{-2}$
EA1L	Energy	10^{-4}
EA2L	Energy	$5\cdot10^{-3}$
DA1L	Displacement	10^{-2}
DA2L	Displacement	$5\cdot10^{-2}$

Table 9.3: Legend explanation- analyses with different convergence criteria

9.6 Ultimate limit state verifications

Through nonlinear finite element analyses it is possible to perform ultimate limit state verifications, as requested by the current European standard [EC2 (2004)]. The ultimate limit state verifications concern the definition of a design resistance to be compared with the design load applied to the structure.

The new *fib* Model Code (2010) proposes three different methods to obtain the design resistance of a structure from a nonlinear finite element analysis: the Global Safety Factor Method (GSF), the Partial Safety Factor Method (PSF) and the Estimation of Coefficient of Variation of Resistance Method (ECOV).

Global Safety Factor Method (GSF)

According to this method the effect of the different uncertainties is integrated in a global design resistance and can be expressed by a global safety coefficient γ_{GL} taken equal to 1.27. Mean strength values of material, calculated from the characteristic strength values, are inputted in the NLFE analysis. For the numerical simulations of the experimental tests performed in this paper, measured strength values of material were available, so that it has been necessary to transform the measured strength values in characteristic strength values, according to the prescriptions of the EC2 (2004). This operation is not necessary if the characteristic strength values are available. Below the procedure followed for the calculation of mechanical properties of material is illustrated. First of all the characteristic strength is evaluated from the measured strength obtained from the experimental test, Eq. (9.15)-(9.17):

$$f_{ck} = f_{c,measured} - 8 \tag{9.15}$$

$$f_{ctk} = 0.7 \cdot f_{ct,measured} \tag{9.16}$$

$$f_{yk} = f_{y,measured} \tag{9.17}$$

From the characteristic compressive strength so obtained the fracture energy G_{fk} and the elastic modulus E_{ck} of concrete are derived, Eq. (9.18)-(9.19):

$$G_{fk} = G_{f0}\left(\frac{f_{ck}}{10}\right)^{0.7} \tag{9.18}$$

$$E_{ck} = 22000\left(\frac{f_{ck}}{10}\right)^{0.3} \tag{9.19}$$

From the characteristic mechanical properties, the corresponding mean properties are evaluated, Eq. (9.20)-(9.24):

$$f_{cm} = 0.85 \cdot f_{ck} \tag{9.20}$$

$$f_{ctm} = 0.85 \cdot f_{ctk} \tag{9.21}$$

$$G_{fm} = 0.85 \cdot G_{fk} \tag{9.22}$$

$$E_{cm} = 0.85 \cdot E_{ck} \tag{9.23}$$

$$f_{ym} = 1.1 \cdot f_{yk} \tag{9.24}$$

To obtain the design load, the ultimate load P_u obtained from the nonlinear finite element analysis must be reduced of γ_{GL}, Eq. (9.25):

$$P_d = \frac{P_u}{\gamma_{GL}} \tag{9.25}$$

Partial Safety Factor Method (PSF)

According to this method the effect of the various uncertainties is considered by assigning design values to the mechanical resistance. The design mechanical properties are directly inputted in the nonlinear finite element analysis. Below the procedure to transform the characteristic mechanical properties (estimated with Eq. (9.15)-(9.19)) in design mechanical properties of material is illustrated, Eq. (9.26)-(9.30):

$$f_{cd} = \frac{f_{ck}}{\gamma_{RD} \cdot \gamma_c} \tag{9.26}$$

$$f_{ctd} = \frac{f_{ctk}}{\gamma_{RD} \cdot \gamma_c} \tag{9.27}$$

$$f_{yd} = \frac{f_{yk}}{\gamma_{RD} \cdot \gamma_s} \tag{9.28}$$

$$G_{fd} = G_{f0}\left(\frac{f_{cd}}{10}\right)^{0.7} \tag{9.29}$$

$$E_{cd} = 22000\left(\frac{f_{cd}}{10}\right)^{0.3} \tag{9.30}$$

where $\gamma_c = 1.5, \gamma_s = 1.15$, $\gamma_{RD} = 1.06 =$ coefficient of uncertainty of the model. The ultimate load deriving from the NLFE analysis is already the design load, Eq. (9.31):

$$P_d = P_u \tag{9.31}$$

Estimation of Coefficient of Variation of Resistance Method (ECOV)

According to this method the random distribution of resistance can be described by a lognormal bi-parametric distribution; the two random parameters are the measured strength value and the coefficient of variation (V_R). It is therefore necessary to perform two nonlinear finite element analyses: one with measured mechanical properties as input data and the other one with characteristic mechanical properties as input data. The design resistance is then calculated with Eq. (9.32):

$$P_d = \frac{P_{u,measuerd}}{\gamma_{RD} \cdot \gamma_R} \tag{9.32}$$

where $P_{u,measured}$ is the ultimate load obtained from the NLFE analysis by inputting measured mechanical properties, $\gamma_R = e^{\alpha_R \cdot \beta \cdot V_R}$, $\alpha_R = 0.8$, $\beta = 3.8$, $V_R = \frac{1}{1.65} ln\left(\frac{P_{u,measuerd}}{P_{u,characteristic}}\right)$, $\gamma_{RD} = 1.06$, $P_{u,characteristic}$ is the ultimate load obtained from the NLFE analysis by inputting characteristic mechanical properties. In Fig. 9.11 the load-deflection curves of NSEL beam [Sun & Kuchma (2007)] obtained with different material properties are reported as example.

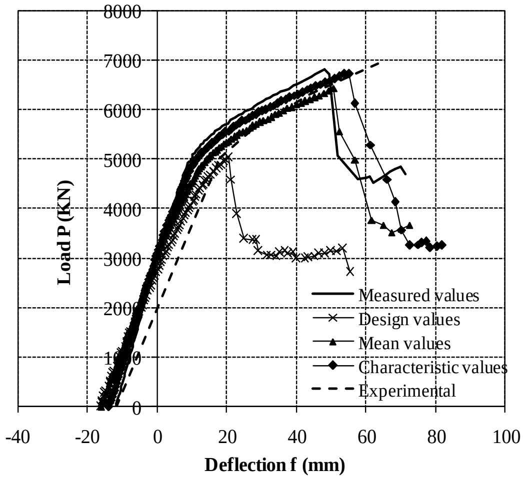

Fig. 9.11: Load-deflection curves of NSEL beam obtained with measured, characteristic and design values of material

<table>
<tr><th></th><th>Failure mode</th><th colspan="2">$P_{u,exp}$ (KN)</th><th colspan="2">$\%P_{d,GSF}/P_{u,exp}$</th><th colspan="2">$\%P_{d,PSF}/P_{u,exp}$</th><th colspan="2">$\%P_{d,ECOV}/P_{u,exp}$</th></tr>
<tr><td>RB1</td><td>F</td><td colspan="2">265</td><td colspan="2">67%</td><td colspan="2">66%</td><td colspan="2">75%</td></tr>
<tr><td>RB2</td><td>DT</td><td>69</td><td>81</td><td>62%</td><td>53%</td><td>68%</td><td>58%</td><td>72%</td><td>62%</td></tr>
<tr><td>RB3A</td><td>SC</td><td colspan="2">156</td><td colspan="2">51%</td><td colspan="2">65%</td><td colspan="2">53%</td></tr>
<tr><td>MNDOT</td><td>SC</td><td colspan="2">2313</td><td colspan="2">57%</td><td colspan="2">63%</td><td colspan="2">67%</td></tr>
<tr><td>NSEL</td><td>SC</td><td colspan="2">6984</td><td colspan="2">73%</td><td colspan="2">72%</td><td colspan="2">90%</td></tr>
<tr><td>PB1</td><td>F</td><td colspan="2">1897</td><td colspan="2">63%</td><td colspan="2">63%</td><td colspan="2">77%</td></tr>
<tr><td>PB4</td><td>SC</td><td colspan="2">1491</td><td colspan="2">44%</td><td colspan="2">42%</td><td colspan="2">45%</td></tr>
<tr><th></th><th>Failure mode</th><th colspan="2">$\%P_{d,EC2}/P_{u,exp}$</th><th colspan="2">$\%P_{d,MC,LevI}/P_{u,exp}$</th><th colspan="2">$\%P_{d,MC,LevII}/P_{u,exp}$</th><th colspan="2">$\%P_{d,MC,LevIII}/P_{u,exp}$</th></tr>
<tr><td>RB1</td><td>F</td><td colspan="2">-</td><td colspan="2">-</td><td colspan="2">-</td><td colspan="2">-</td></tr>
<tr><td>RB2</td><td>DT</td><td>117%</td><td>100%</td><td>59%</td><td>51%</td><td>-</td><td>-</td><td>106%</td><td>90%</td></tr>
<tr><td>RB3A</td><td>SC</td><td colspan="2">64%</td><td colspan="2">52%</td><td colspan="2">63%</td><td colspan="2">85%</td></tr>
<tr><td>MNDOT</td><td>SC</td><td colspan="2">44%</td><td colspan="2">32%</td><td colspan="2">38%</td><td colspan="2">69%</td></tr>
<tr><td>NSEL</td><td>SC</td><td colspan="2">49%</td><td colspan="2">33%</td><td colspan="2">49%</td><td colspan="2">54%</td></tr>
<tr><td>PB1</td><td>F</td><td colspan="2">-</td><td colspan="2">-</td><td colspan="2">-</td><td colspan="2">-</td></tr>
<tr><td>PB4</td><td>SC</td><td colspan="2">76%</td><td colspan="2">56%</td><td colspan="2">61%</td><td colspan="2">54%</td></tr>
</table>

F = bending failure; SC = shear-compression failure; DT= diagonal-tension failure; $P_{d,GSF}$= design resistance obtained with the GSF method; $P_{d,PSF}$ =design resistance obtained with the PSF method; $P_{d,ECOV}$= design resistance obtained with the ECOV method; $P_{d,EC2}$= design resistance obtained with the EC2; $P_{d,MC,LevI}$= design resistance obtained with the Model Code according to safety Level I; $P_{d,MC,LevII}$= design resistance obtained with the Model Code according to safety Level II; $P_{d,MC,LevIII}$= design resistance obtained with the Model Code according to safety Level III.

Table 9.4: Design resistance of different cases studies

In Table 9.4 the design resistance of the cases are reported; the design resistance are expressed as a percentage of the experimental load and they are obtained with the three methods described above proposed by the *fib* Model Code (2010). These resistances are compared in the same Table with the design resistance obtained with the analytical procedures proposed by the EC2 (2004) and the *fib* Model Code (2010) according to the three safety levels (paragraph 9.1) that differ in the way in which the concrete and steel contributions and the concrete strut inclination are taken into account [Bentz & Collins (2006)].

The design resistance evaluated both from the nonlinear finite element analyses and from the analytical procedures are lower than the experimental load, as they are calculated by adopting the appropriate safety coefficient proposed in the norms.

The results obtained from the nonlinear finite element analyses proved to be more on the safe side (or comparable with safety Level I and II) respect to the analytical results, except for the two pre-tensioned beams (MNDOT [Runzell (2007)] and NSEL [Sun & Kuchma (2007)]). Among the methods proposed by the *fib* Model Code (2010) the ECOV method gave always the highest design resistance except for RB3A beam [Grace (2001)].

9.7 Service limit state verifications

The current European norm [EC2 (2004)] requests service limit state verifications that can be also performed by nonlinear finite element analysis. The service limit state verifications developed in this paper refer to the crack width estimation, to be compared with limit values imposed by the current norms.

As already mentioned, all the cases were experimentally tested in laboratory by applying concentrated or distributed loads up to failure. For this reason a precise load value for the service limit state verification is not available. A reference load value for the service limit state (P_{SLS}) has therefore been calculated from the ultimate load as follow, Eq. (9.33):

$$P_{SLS} = \frac{P_u}{1.7} \tag{9.33}$$

Below different procedures for the calculation of the crack width in case of bending failure, shear failure and plane concrete are reported. In case of bending failure the crack width can be calculated according to Eq. (9.34):

$$w = s_{r,max} \cdot \overline{\varepsilon_s} \tag{9.34}$$

where $\overline{\varepsilon_s}$ is the average strain value of the longitudinal reinforcement in the cracked zone coming from the NLFE analysis, $s_{r,max}$ is the maximum crack spacing calculated according to the EC2 (2004), Eq. (9.35):

$$s_{r,max} = k_3 c + \frac{k_1 k_2 k_4 \phi_{eq}}{\rho_{p,eff}} \tag{9.35}$$

where $k_3 = 3.4$, c is the cover, $k_1 = 0.8$, $k_4 = 0.425$, $k_2 = 0.5$, ϕ_{eq} is the equivalent reinforcement diameter.
In case of shear failure the crack width can be calculated according to Eq. (9.36):

$$w = s_\theta \cdot \overline{\varepsilon_{stirrups}} \tag{9.36}$$

where $\overline{\varepsilon_{stirrups}}$ is the average strain value of the stirrups in the cracked zone coming from the NLFE analysis, s_θ is the spacing between inclined cracks calculated according to EC2 (2004), Eq. (9.37):

$$s_\theta = \frac{1}{\dfrac{cos\,\theta}{s_{r,max,y}} + \dfrac{sin\,\theta}{s_{r,max,z}}} \tag{9.37}$$

where $s_{r,max,y}$ and $s_{r,max,z}$ represent the crack spacing along y and z direction calculated according to Eq. (9.35), θ is the angle between the reinforcement along y direction and the principal tensile stress direction.
In case of plane concrete the crack width can be calculated according to Eq. (9.38):

$$w = \varepsilon_1 \cdot h \tag{9.38}$$

where ε_1 is the principal tensile strain coming from the NLFE analysis and h is the crack bandwidth value.

The software used for the analyses [DIANA (2008)] considers a crack bandwidth value equal to $\sqrt{2A}$ for 4-node elements and equal to $\sqrt{A}$ for 8-node elements, where A is the area of the single element. The crack bandwidth value is kept constant during the analysis, independently from the crack orientation.

In order to estimate the effect of the crack bandwidth value, several analyses on different cases have been performed by considering a crack bandwidth value equal to h, 0.5h and 2h.

It has been demonstrated that a value of crack bandwidth equal to *h* is appropriated for straight cracks while for inclined cracks a higher value should be considered. For this reason it is suggested to take into account a variable crack bandwidth value that varies with the crack orientation [Oliver (1989), Cervenka (1995)].

9.8 Conclusion

Software for nonlinear finite element analyses proved to be a useful instrument for a detailed investigation of the behavior of reinforced and pre-stressed concrete structures. It is however fundamental to check the choices made during the analysis in order to verify their suitability and the reliability of the results obtained. As already mentioned in the previous paragraphs, the checks to be done comprise the mesh adopted, the constitutive models, the crack models and the convergence parameters. It is also very important to control the results obtained from the nonlinear finite element analyses and integrate them with analytical procedures proposed by the current European norm [EC2 (2004)] and the *fib* Model Code (2010) in order to verify that the ultimate limit state and the service limit state verification imposed by the current European norm [EC2 (2004)] are satisfied.

Furthermore with help of the appropriate directions proposed in the guidelines, which aim to reduce the scatter of the results due to choices of the analysts, it is possible to obtain realistic and safe results.

In this paper it has been demonstrated that for simple structures, such as reinforced or pre-stressed beams, the results obtained from analytical procedures proposed by the current norms are equally appropriate in the determination of the carrying capacity, without the need of refined and complex finite element models.

However for more complex structures it is very difficult to govern the problem with simple analytical calculations. In this case the availability of reference guidelines for numerical simulations results helpful in finding correct predictions of the structural behavior.

9.9 Acknowledgement

The authors acknowledge the support of the Dutch Ministry of Transport, Public Works and Water Management that made the development of this research possible.

9.10 References

Belarbi A., Hsu T.T.C., “Constitutive laws of reinforced concrete in biaxial tension-compression”, Research Report UHCEE 91-2, University of Huston, 1991.

Belletti B., Hendriks M., den Uijl J.A., Damoni C., “Developing standardized guidelines for a safety assessment of shear-critical RC beams based on nonlinear a finite element modeling”, 3rd *fib* International Congress, Washington, 2010.

Bentz E.C., Collins M.P., “Development of the 2004 Canadian Standards Association (CSA) A23.3 shear provisions for reinforced concrete”, Canadian Journal of Civil Engineering, 33(5), pp.521–534, 2006.

Cervenka V., “Constitutive model for cracked reinforced concrete”, ACI Struct. Journal, 71, pp.396-408, 1985.

Cervenka V., “Mesh sensitivity effects in smeared finite element analysis of concrete fracture”, Framcos-2, 1995.

Collins M.P., Kuchma D., “How Safe Are Our Large, Lightly Reinforced Concrete Beams, Slabs, and Footings?”, ACI Struct. Journal, 96 (4), pp. 482-490, 1999.

DIANA Release 9.3, Latest Update: Nov.27 12:02:30, 2008.

Eurocode 2, “Design of concrete structures-Part 1-1: General rules and rules for buildings”, EN 1992-1-1:2004.

Feenstra P.H., Rots J.G., Arnesen A., Teigen J.G., Hϕiseth K.V., “A 3D constitutive model for concrete based on a co-rotational concept”, Computational Modelling of Structures, de Borst, Bicanic, Mang & Meschke (eds), Balkema, 1998.

Foster S.J., Budiono B., Gilbert R.I., “Rotating Crack Finite Element Model for Reinforced Concrete Structures”, International Journal of Computers & Structures, Vol. 58, No. 1, January, pp. 43-50, 1996.

Gambarova P.G., “Sulla trasmissione del taglio in elementi bi-dimensionali piani in c.a. fessurati” Proc., Giornate AICAP, pp.141-156, 1983, (in Italian).

Grace N.F., “Strengthening of Negative Moment Region of Reinforced Concrete Beams Using Carbon Fiber-Reinforced Polymer Strips”, ACI Struct. Journal, 98 (3), pp. 347-358, 2001.

Hillerborg A., “Examples of practical results achieved by means of the fictitious crack model”, In Preprints, Prager Symp. On Mechanics of Geomaterials: Rocks, Concrete, Soils, (editore Z.P. Bažant), Northwestern University, Evanston, pp. 611-614, 1983.

Hsu T.T.C., Mo Y.L., “Unified theory of concrete structures”, John Wiley and Sons, Ltd, Publication, 2010.

Leonhardt E.F., Kock R., Rostasy F. S., “Schubversuche an Spannbetontragern”, Deutscher Ausschuss fur Stahlbeton, 1973.

fédération internationale du béton (*fib*), “Model Code 2010 - First complete draft.” Bulletins 55 and 56, 2010.

Nakamura H., Higai T., “Compressive Fracture Energy and Fracture Zone Length of Concrete”, Benson P. Shing (editor), ASCE, pp. 471-487, 2001.

Oliver J., “A consistent characteristic length for smeared cracking models”, International Journal for numerical Methods in Engineering, vol.28, pp. 461-474, 1989.

Runzell B., Shield C., French C., “Shear capacity of prestressed beams”, Minnesota Department of transportation Research Services Section, 2007.

Sun S., Kuchma D., “Shear behaviour and capacity of large-scale prestressed high-strength concrete bulb-tee girders”, Department of Civil and Environment Engineering, University of Illinois at Urbana-Champaign, 2007.

Vecchio F.J., Collins M.P., “Compression response of cracked reinforced concrete”, J. Str. Eng., ASCE 119, pp. 3590-3610, 1993.

Vecchio F.J., Shim W., “Experimental and Analytical Reexamination of Classic Concrete Beam Tests”, J. Str. Eng., ASCE, 130 (3), pp. 460-469, 2004.

Vecchio F.J., Collins M.P., “The modified compression-field theory for reinforced concrete elements subjected to shear”, ACI Struct. Journal, 83(2), pp. 219-231, 1986.

Walraven J.C., “Fundamental analysis of aggregate interlock”, J. Str. Eng., ASCE, 107(11), pp.2245-2270, 1981.

10 Components of shear resistance in prestressed bulb-tee girders

Daniel Kuchma[1], Shaoyun Sun[2], Tom Nagle[3] and Kang Su Kim

[1] Associate Professor, University of Illinois
[2] Structural Engineer, Parsons, Chicago, Illinois
[3] Nagle Signs Inc., Waterloo, Iowa
[4] Assistant Professor, University of Seoul, Seoul, Korea

Abstract: The differences in shear design requirements between and within codes-of-practice are unacceptably large. Many of these differences are due to competing shear design philosophies, while others are due to a resistance to change that is motivated in good part by the satisfactory performance of most structures in the field. The inability to resolve technical differences in opinion is largely due to deficiencies in available test data. This is because the research community has focused on determining the shear capacity of members and thereby not gathered the data on performance that is needed to evaluate the accuracy of competing models for shear behaviour. This paper presents the results from a research project in which detailed data was collected on the shear response of large prestressed concrete bridge girders. A new method for data-visualization and analysis was developed to explore the test data and to quantify the contributing components to shear resistance. This testing identified a few concerns about the performance of members subjected to shear and the impact of sectional shape and end region behaviour on “shear” capacity. The paper presents many of the most significant observations from this research project

10.1 Introduction

For more than 100 years, the parallel chord truss model introduced by Ritter (1899) and Morsch (1920 & 1922), has been the globally accepted model for how shear is carried in structural concrete. As shown in Fig. 10.1, shear flows down a compression diagonal of a truss, is lifted up by stirrups, and then continues in this manner until it reaches the support.

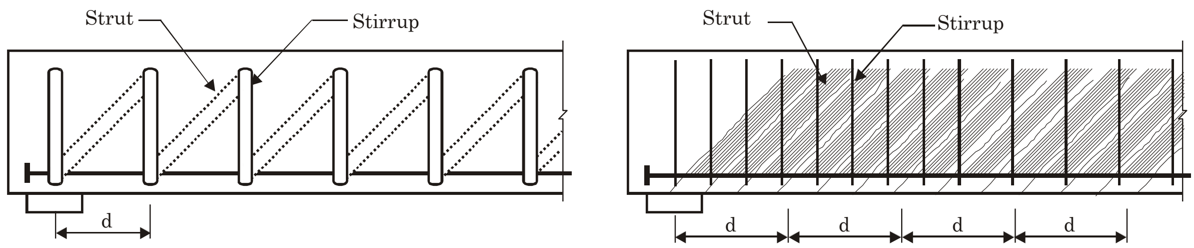

Fig. 10.1: Parallel chord truss model

Equilibrium expressions from this model, as derived from Fig. 10.2, are presented in Eqns. 10.1-10.3. As shown, the diagonal compressive in the concrete, f_2, as well as the stress in the longitudinal and vertical reinforcements, f_l and f_v, are functions of both the shear force, V, and the angle of diagonal compression from the longitudinal axis, θ. For a member subjected to a known shear force, ,V, this leads to the seemingly intractable problem of their being four unknowns (f_2, f_l, f_v, θ) but only 3 equilibrium expressions to use to solve for these unknowns.

$$f_2 = \frac{V}{b_w jd}\left(\tan\theta + \frac{1}{\tan\theta}\right); \quad f_\ell = \frac{V}{A_\ell \tan\theta}; \quad f_v = \frac{V\tan\theta \cdot s}{jd \cdot A_v} \qquad (10.1)\ (10.2)\ (10.3)$$

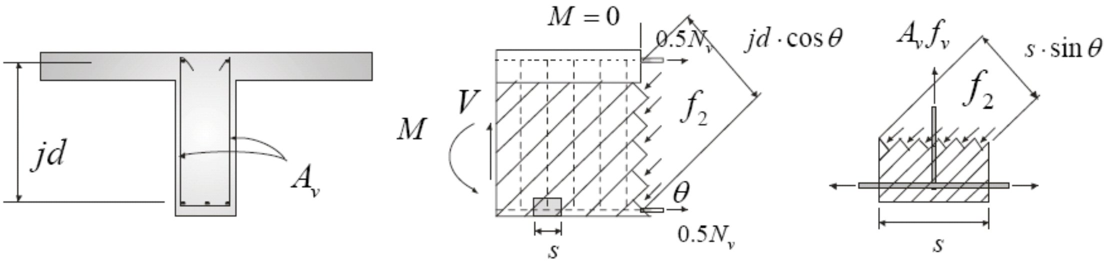

Fig. 10.2: Free body diagrams for developing equilibrium relationships

Code organizations took different approaches to shear design to address this fundamental problem. The building code provisions of the American Concrete Institute (ACI318-08) assumed that the angle of diagonal compression was 45 degrees and then limited the contribution of stirrups to guard against diagonal crushing occurring before yielding of the transverse reinforcement (stirrups). ACI318-08 also included an expression for the concrete contribution to shear resistance, V_c, that is added to the contribution from transverse reinforcement, V_s, in determining the nominal shear capacity, $V_n = V_c + V_s$. By contrast, plasticity based approaches have commonly been used in European design practice, EC2 (2002) and DIN (2001), in which the capacity is taken to be when a mechanism forms of stirrup yielding and concrete reaching its diagonal compressive strength of $f_{2,\max} \approx 0.6 f_{ck} \approx 0.6 f'_c$. A lower limit to θ of 18º in EC2 is used to evaluate the contribution of shear reinforcement by Eqn. 10.4.

$$V_s = \frac{A_v f_y jd \cot\theta}{s} \qquad (10.4)$$

The development of the Compression Field Theory (CFT) by Mitchell and Collins (1974), followed by the Modified Compression Field Theory (MCFT) by Vecchio and Collins 1986), introduced consideration of strain compatibility and provided relationships for the compressive and tensile response of cracked concrete. This made it possible to solve for the angle θ as well as to predict the complete load-deformation response of members to shear. The MCFT was used to derive the shear design provisions for the Load and Resistance Factor Design (LRFD) in the bridge design specifications of the American Association of State, Highway, and Transportation Officials (AASHTO, 2004). These specifications are herein referred to as the LRFD provisions. The contributions of V_c and V_s for members containing minimum transverse reinforcement were made a function of the shear demand and level of longitudinal strain at mid-depth of the section (or region) being designed. The Canadian Standards Association, (CSA, 2004), adopted a simplified shear design approach based on the MCFT in which the dependency on shear demand was removed.

To convey the magnitude of the differences in these methods, consider Fig. 10.3 that shows a longitudinal segment of a prestressed concrete girder. The locations of the stirrups are shown by the dotted lines. For the 45 degree truss model used in ACI318, 8 stirrups would be counted in evaluating V_S. By the LRFD specifications, in which θ was calculated to be 21 degrees, then coincidentally 21 stirrups would be counted in evaluating V_S. This is 2.5 times more stirrups than in the ACI provisions. It is noteworthy that the number of stirrups crossing a diagonal crack is 16, which is closer to the LRFD count that that of ACI.

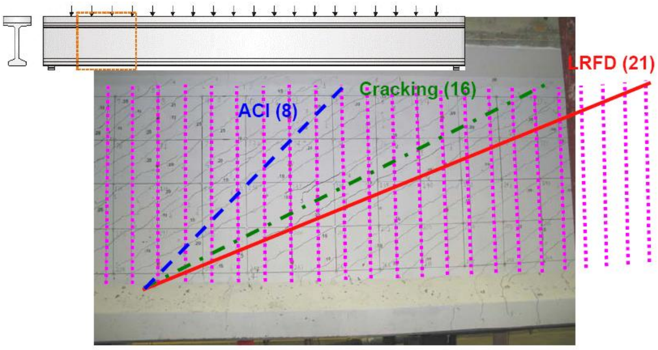

Fig. 10.3: Number of stirrups contributing to shear capacity in prestressed girders

It is also important to note that the relationship deemed appropriate for V_C depends on the relationship used to evaluate V_S. For members with shear reinforcement, the measured concrete contribution from an experiment is $V_{c,test} = V_{test} - V_s = V_{test} - A_v f_y d \cot\theta / s$. Thereby, if V_S is underestimated by using a larger than actual angle of diagonal compression, then V_C at ultimate may be overestimated; this is likely the case of the design of prestressed members using the ACI318 provisions.

The paper presents observations and findings from a research project on the shear behaviour of large prestressed concrete bridge girders that were load tested to failure. Several reports and papers have already been written about what was learned from these tests. This paper will not attempt to provide comprehensive information on any one research finding, but rather present a significant number of observations and findings; references are made when available to more comprehensive information. Part 2 of this paper describes the testing program. Part 3 presents significant observations about the response of B(beam) regions where plane sections remain plane. Part 4 provides an assessment of the measured contributions to shear resistance by stirrups as well as individual components of the "concrete" contributions. Part 5 examines the behaviour of end regions in which plane sections theory does not apply and the behaviour was observed to be dependent on geometric and design details.

10.2 Girder testing program, setup, and instrumentation

10.2.1 Test objectives

The research presented in this paper was sponsored by the US National Academy of Sciences National Cooperative Highway Research Program. The objective of this sponsored research was to determine how to extend the LRFD shear provisions to high-strength concrete (HRC) based on a review of existing test data and new data generated as part of this research project. The primary variables for the testing program were concrete strength, design shear stress level, strand anchorage and end reinforcement details. The members were designed to study different aspects of shear resistance and modes of failure, a few of which are shown as examples in Fig 10.4. Girder 5 was designed with minimum shear reinforcement such that failure was likely to be due to rupture of the stirrups. Girder 2 was designed using heavy shear reinforcement in which stirrups were expected to yield but large compressive stresses would be developed as they funnelled into the support. In Girder 6, debonding of nearly 50% of strands was used to investigate the influence of strand slip on shear response. Girder 9 was over-reinforced in shear so that stirrups were unlikely to yield prior to failure of the beam. While not shown in Fig. 10.4, tests were also completed to obtain failures away from the end region. The results from 20 tests on 10 girders were generated. Two test results were obtained for each girder and the ends were designed differently. After one end failed, that region was repaired and then the member was reloaded until failure was achieved at the other end.

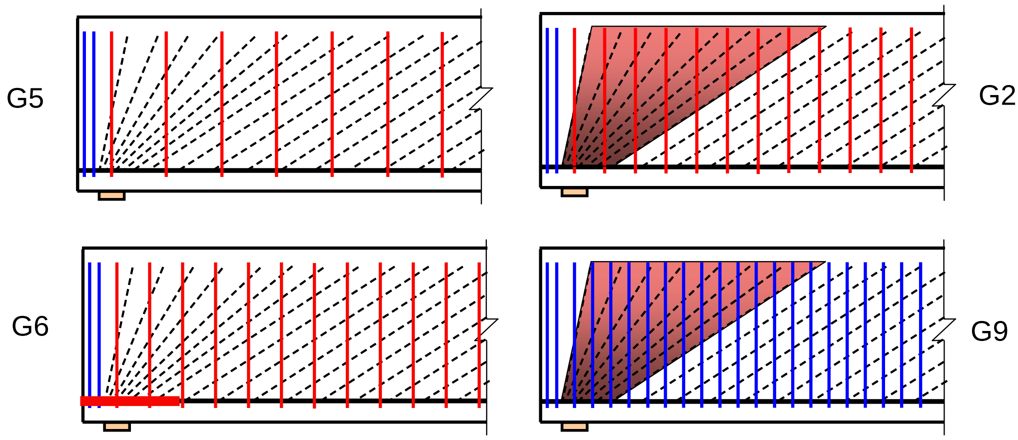

Fig. 10.4: Types of shear tests

10.2.2 Test setup and loading

All test girders were 1.63 m (63-inch) deep bulb-tees on which a 203 (8 inch) thick deck slab was cast. These girders were simply supported on a 15.2 (50 foot) span and loaded to failure under a uniformly distributed load from 44 hydraulic jacks on the centre 13.4 m (44 feet) of its span. A uniformly distributed load was selected to produce a realistic pattern of cracking through the shear regions. Displacement control was used at midspan and the same pressure was fed to the other jacks. See Fig. 10.5

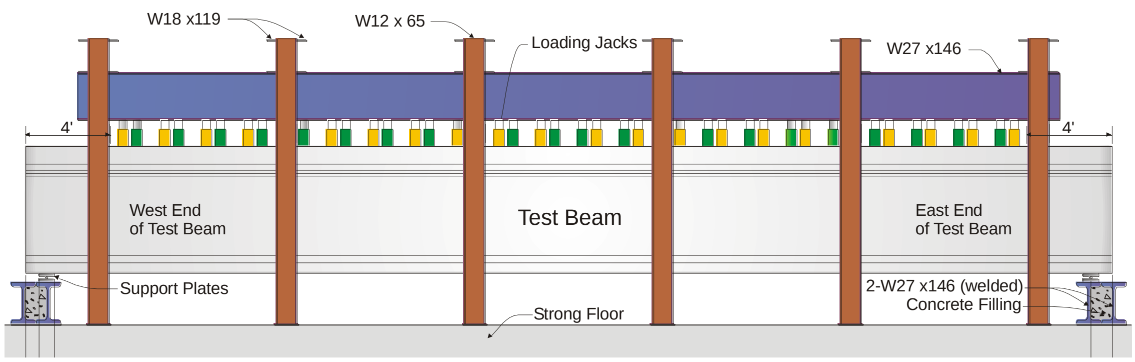

Fig. 10.5: Experimental test setup (1 ft. = 0.3048 m)

10.2.3 Instrumentation

An extensive instrumentation plan was used to collect detailed information on the response of the test girders. For each girder, about 30 displacement transducers were used to measure the deformed shape, shear deformations, and strand slip; up to 150 strain gages were attached to reinforcement and 40 long surface strain gages were attached to the concrete. The strains in the bottom bulb from the time of casting to the time of testing were recorded. A coordinate measurement machine (CMM) was used to record the deformations in 3D space of approximately 200 light emitting diode (LED) targets. Traditional portable displacement units were used to measure in-plane deformations on a regular grid over the length of each girder.

10.2.4 Crack measurement and recording method

One of the important features on this project was the creation of an automated crack recording method. From the 20-30 pictures taken at various angles over the length of the girder, image analysis methods based on the principles of close-range digital photogrammetry were used to track the measured development of cracking to an accuracy of about 3 mm. As illustrated in Fig. 10.6, the location of cracks in image coordinate space was transformed to real-world (or specimen) coordinate position. Finally, the crack images from all measurement positions were combined for each stage of measurement.

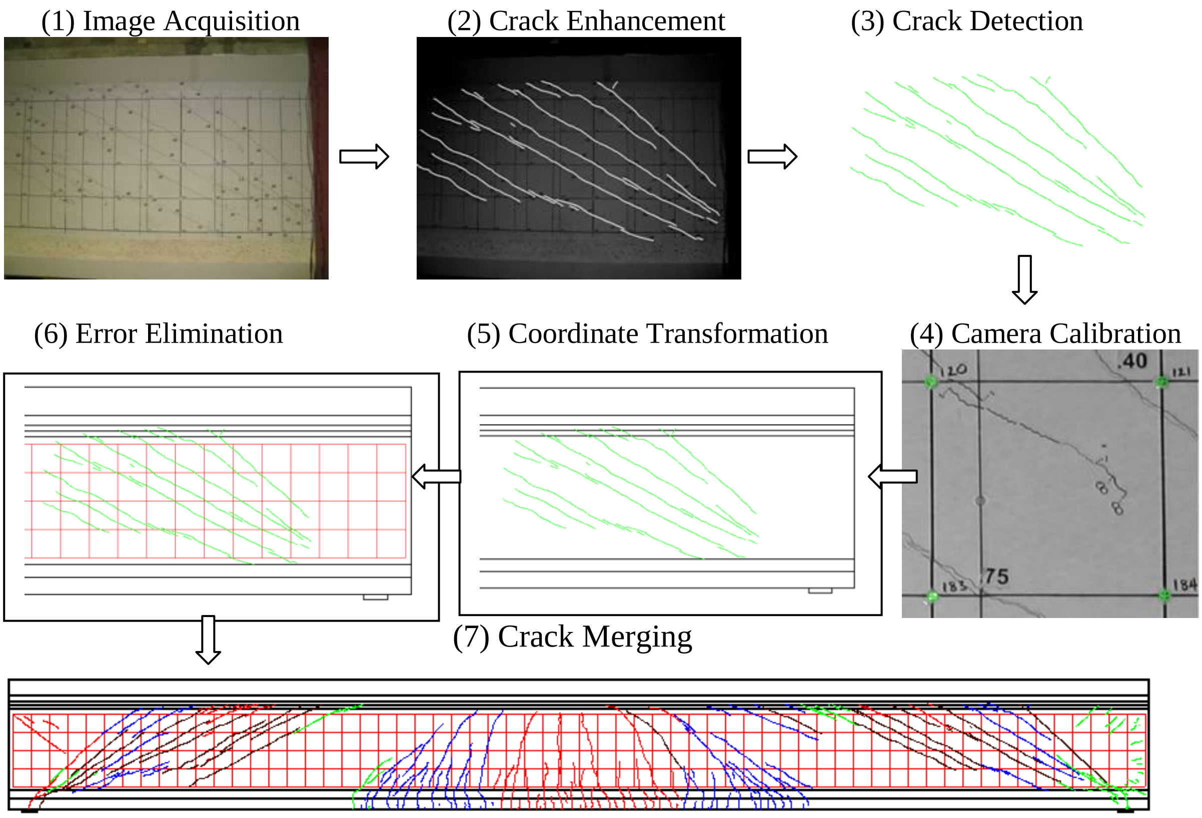

Fig. 10.6: Crack measurement and recording method as developed by Sun (2009)

10.3 B-Region response

10.3.1 Beam shear behaviour

This part of the papers examines beam shear behaviour over the part of the structure where plane sections are expected to remain plane. Fig. 17 illustrates that beam shear behaviour was achieved over a substantial length of the girder as shown by the region of parallel diagonal cracks over a length that is more than twice the depth of the member.

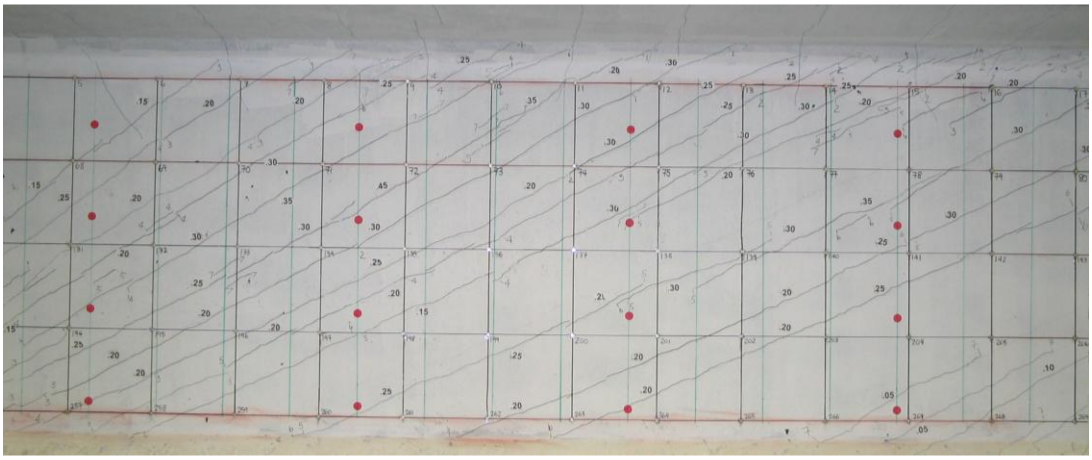

Fig. 10.7: Cracking patterns which demonstrate that beam shear behaviour was achieved

To further assess if beam shear behaviour was achieved, the shear strains in the web were calculated from the measured CMM target positions at four corner points for four different grids. As shown in Fig. 10.8a, these measurements were made over different gage lengths both adjacent to the support as well as starting at a distance equal to about the depth of the beam from the support. Fig. 10.8b shows that similar strains were measured throughout this region.

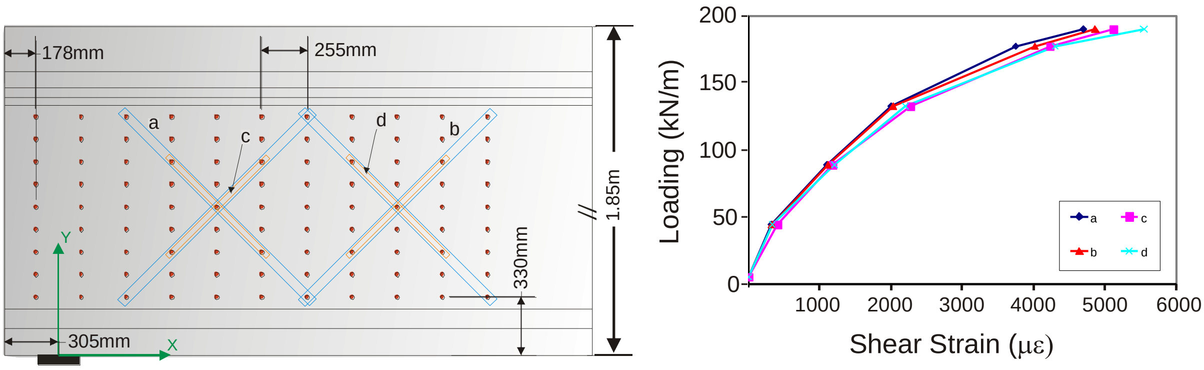

(a) Four shear strain measurement grids (b) Shear strains measured by four grids

Fig. 10.8: Shear straining measured by coordinate measurement machine

When failure due to beam shear is experienced, two of the expected modes of failure are (i) yield and rupture of the stirrup reinforcement and (ii) yield of stirrups followed by crushing of the field of diagonal compression. Both of these were observed in this testing project. An example of the first of these is presented in Fig. 10.9a and the latter in Fig. 10.9b

10.3.2 Accuracy of relationships for predicting shear strength and cracking characteristics

The ratio of measured shear strength to the nominal capacity was determined for the LRFD, CSA, R2K, and ACI methods for determining shear strength. The LRFD, CSA, and ACI methods were previously mentioned. R2K stand for Response 2000 which is a compatibility-based beam analysis program developed by Bentz (2000) which implements the MCFT and is able to predict the shear response of prestressed and non-prestressed members that are subjected to combinations of shear, moment, and axial loading. The mean strength ratio (test/code) for the LRFD, CSA, and R2K methods were essentially the same at 1.11, 1.10 and 1.10 respectively as were the coefficients of variation (COV) at 10%, 10%, and 12% respectively. This illustrates consistency in MCFT based approaches. The mean strength ratio and COV for ACI318-08 was 1.36 and 7%. All of these calculations were made with no limit placed on f'_c. No trend in strength ratios with concrete compressive strengths was observed.

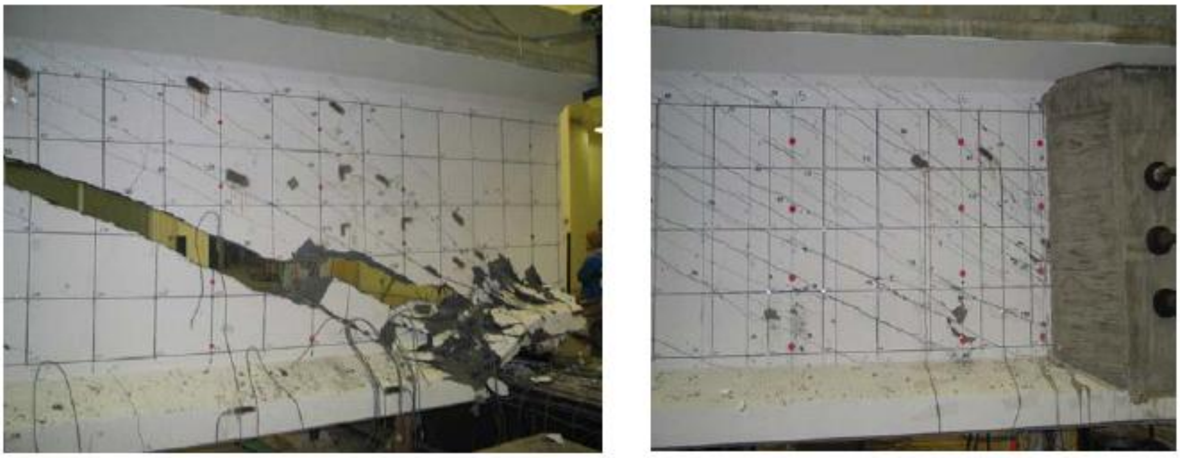

(a) Failure at East end of Girder 5 (b) Failure of diagonal compression field in Girder 8

Fig. 10.9: Failure condition on east side of girder 5

The results from the girder testing were also used to evaluate the accuracy in ACI318-08 provisions for estimating web-shear, flexure, and flexure-shear cracking strengths. The mean ratios of measured to code-calculated values were 1.21, 0.88, and 0.88 respectively and the corresponding COVs were 19%, 11%, and 6%. These methods use a modulus of rupture cracking stress of $0.625\sqrt{f'_c}$ where f'_c is in MPa units ($7.5\sqrt{f'_c}$ where f'_c is in psi units). The results from these tests suggest that the modulus of rupture stress should be changed to $0.5\sqrt{f'_c}$ where f'_c is in MPa units ($6\sqrt{f'_c}$ where f'_c is in psi units). The COVs are satisfactorily low given the variability associated with cracking loads, and justify the utility of including these types of relationships in codes of practice for assessing when cracking is expected to occur. In addition to cracking strengths, it is also useful to examine cracking angles. The angle of diagonal cracking based on Mohr's circle of stress can be estimated as $\cot\theta = \sqrt{1 + f_{pc}/f_t}$ where f_{pc} is the effective compressive stress at the centroidal axis of the member due to prestress and f_t is the cracking strength which can be taken as $0.33\sqrt{f'_c}$ when f'_c is in MPa units ($4\sqrt{f'_c}$ where f'_c is in psi units). The ratio of the measured to predicted cotangent of the critical web shear cracking angle was 1.06 indicating that a stress analysis slightly overestimates that angle of cracking. The ratio of the cotangent of the measured angle of cracking to the LRFD calculated angle for θ was 0.91 indicating that the LRFD provisions rely on a flatter angle of diagonal compression than the angle of diagonal cracking.

10.3.3 Patterns of stirrup straining and shear cracking

It is useful to examine the complexity of behaviour that models for behaviour are trying to capture. This complexity is evident through examination of the patterns of observed stirrup straining and cracking. Three of these observations are now shared and briefly discussed.

Fig. 10.10 presents the pattern of shear cracking on the West half of Girder 3 as well as the straining in two B-Region stirrups, one of these stirrups "S3" is in the web-shear region and the other stirrup "S7" is in the flexure-shear region. As shown in Fig. 10.10b for the web-shear stirrup, the strain on Gage 3 on Stirrup 3 goes from no strain to close to yield strain at the onset of shear cracking and continues to increase with loading. The observation that stirrups may yield at less than 50% of the nominal capacity raises concerns over fatigue. It is also interesting to examine the development of strain in stirrup S7 that is in the flexure shear region. As shown in Fig. 10.10c, the strains in this stirrup were also starting to increase rapidly with increasing load toward that end of the test, perhaps indicating that a shear failure was imminent in this flexure shear region even if the mechanism of failure is unclear. It is also important to note that the cracks in this flexure shear region are steep (close to and ever greater than 45º) and when coupled with the more relaxed spacing requirements in regions of lower shear stress could result in fewer than the expected number of stirrups carrying the load.

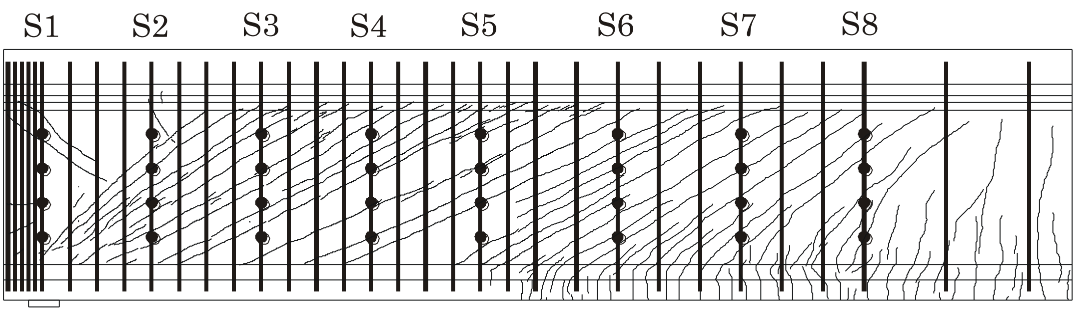

(a) Cracking patterns in West Half of Girder 3; four strain gages on each of stirrups S1 to S8 with Gage 1 being at the bottom and Gage 4 being at the top

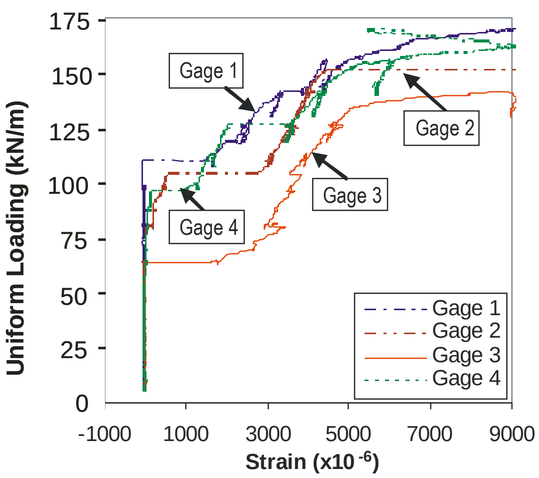

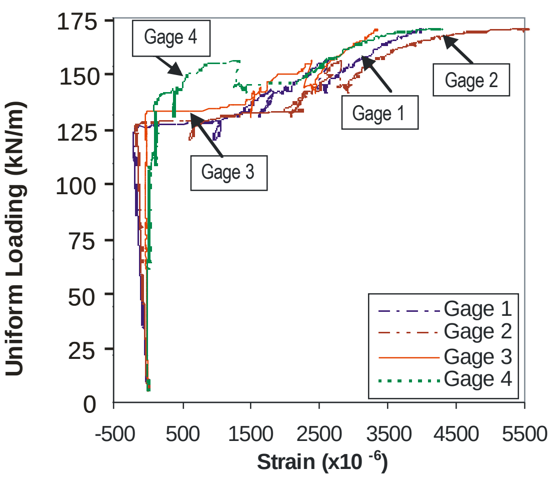

(b) Strain in S3; web-shear region

(c) Strain in S7; flexure-shear region

Fig. 10.10: Cracking patterns and stirrup straining on West half of Girder 3

Fig. 10.11 presents the pattern of shear cracking on the East half of Girder 4 at 53% of the nominal capacity as calculated using the LRFD specifications. There is a widely held belief in much of US bridge engineering practice that prestressed concrete members, particularly in shear, will not crack under regular service loads or even maximum permit load levels. The level of cracking shown in Fig. 10.11 would be unacceptable by some owners for concerns associated with durability, unsightliness, inspection assessment, and fatigue. This girder was designed to support a shear stress of 0.15 f'_c. More shear cracking would be expected to occur under service load levels in a member designed for a higher shear stress level.

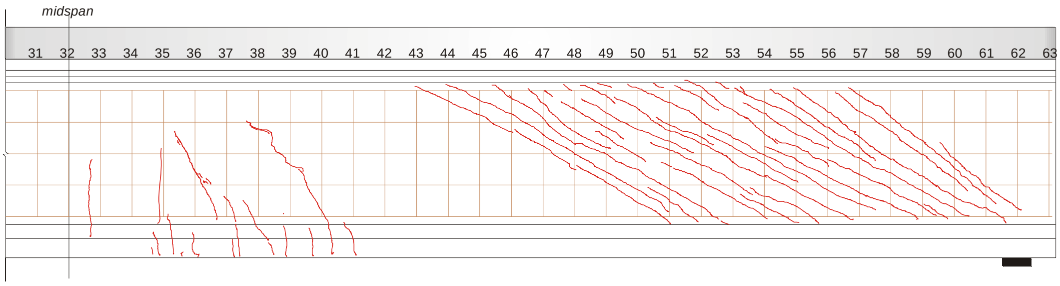

Fig. 10.11: Pattern of measured cracking at 53% of nominal design force on East half of girder 4

Another item of interest to bridge owners is the maximum expected shear crack widths. This is shown in Fig. 10.12 for all 20 test results. Not surprisingly, the crack widths became better controlled as the percentage of shear reinforcement increased. This is some consolation for the concern over cracking in members designed to resist higher shear forces.

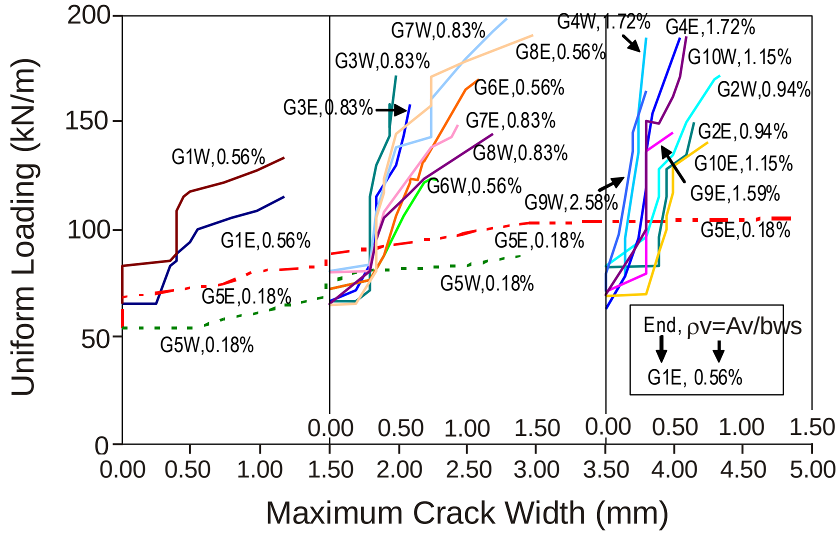

Fig. 10.12: Development of crack widths "Body text" style for all normal paragraph text

10.4 Components of shear resistance

10.4.1 Crack-based free-body diagram (CFBD)

In most codes-of-practice, shear resistance is calculated as the simple summation of a concrete and a shear reinforcement contribution, $V_n = V_c + V_s$. However, the mechanisms of shear resistance are quite complex with there being many contributing elements that are a function of the imposed loading, realized deformation, and sometimes several other factors. In most models, all of the contributions beyond that due to tension in shear reinforcement and inclined prestressing steel are lumped into the concrete contribution term, V_c. It has generally agreed the great majority of the concrete contribution to shear capacity comes from resistance to sliding along diagonal cracks as well as the shear which is transmitted in the uncracked compression zone at the top of the beam. In the case of prestressed bulb-tee girders, it may also be appropriate to consider the shear that can be transmitted in the heavily prestressed lower bulb. Fig. 10.13 presents a crack-based free-body diagram (CFBD) that identifies most of the contributors to shear resistance. This part (10.4) of the paper examines the experimentally measured components to shear resistance.

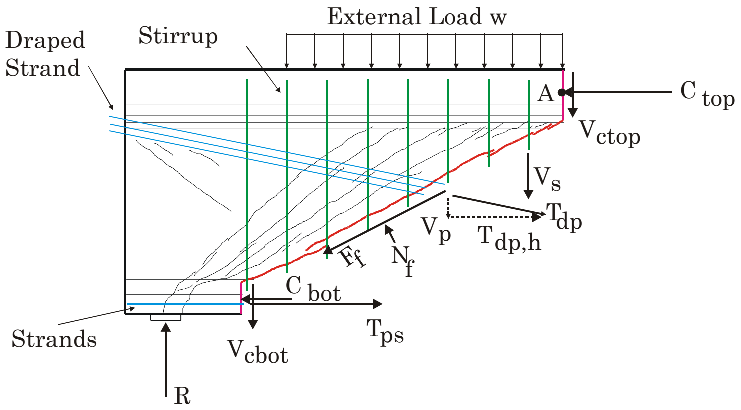

Fig. 10.13: Crack-based free-body diagram (CFBD)

10.4.2 Experimental Visualization (ExVis) software

These experiments generated a very large amount of test data from multiple types of measurement systems. Traditional methods of data analysis, such as through the use of spreadsheets or Matlab, are limited, not well correlated with image data, and do not necessarily consider the physical geometry of the test structure, load conditions, or material properties. To more fully understand and utilize the test data, a visualization and data-analysis tool was created that serves as a post-processor for experimental test data. ExVis, standing for Experimental Visualization, is a tool in which the geometry and material properties of the test structure and all aspects of the measured response are integrated in a data analysis and exploration environment. Fig. 10.14a on the next page shows the left end of a girder. Every part of the test structure and all instruments are selectable objects. The stirrups and strands are shown in blue, the strain gages on the stirrups are marked with round dots, the LVDTs are shown in orange, and the cracks are shown in red. For each instrument is available the measured response. The data-curve window is being used in Fig. 10.14a to display the developing strain in an individual strain gage, S2-1. This plot shows that there is very little strain until the time of cracking and a rapid development in straining after cracking.

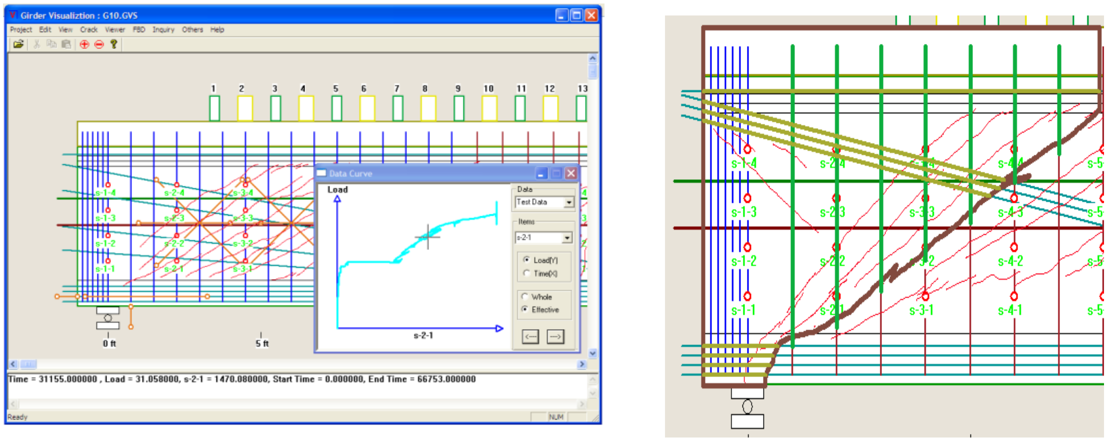

(a) ExVis screen shot (b) ExVis crack-based free-body diagram

Fig. 10.14: Interface for Experimental Visualization (ExVis) software and crack-based free body diagram

The ExVis program allows the user to build crack-based free body diagrams (CFBD), as shown in Fig. 10.14b. The user simply selects the cracls and the program builds the associated CFBD. The total shear force at any point in the loading is determined by the measured forces in the top loading jacks. The shear carried by the stirrups are evaluated from the measured strains in this stirrups and the concrete contribution, V_c, is taken as the total shear less that which is calculated to be carried by the stirrups. A significant source of potential error in this approach is that the actual strain in the reinforcement along the crack interfaces was different than that determined from the available measurements; this likely leads to an underestimation of V_s.

10.4.3 Evaluation of V_c and V_s contributions to shear resistance

The ExVis program was used to examine the concrete and shear reinforcement contributions to resistance for approximately 350 CFBDs. Fig. 10.15 provides two examples of this. The left plot is for a member with a moderately light amount of shear reinforcement. It shows that until cracking that nearly all of the loading was carried by the concrete as would be expected. At the onset of cracking, the stirrup contribution was calculated to immediately go to its yield strength while the concrete contribution dropped to very little. With additional loading the concrete contribution increased up until failure occurred. The figure on the right is for a member that contained a very large amount of shear reinforcement in this web-shear region. This plot illustrates that at cracking there is only a modest increase in V_s and that the steel reinforcement contribution increases approximately linearly with increasing loading. The concrete contribution remained relatively constant after cracking up until peak load. Through the examination of these 350 CFBDs, it was possible to characterize the load share between concrete and steel in the web-shear region as a function of the tensile strength of the concrete and the amount and yield strength of the provided shear reinforcement. See NCHRP (2007) and Sun (2007) for a full presentation of this methodology.

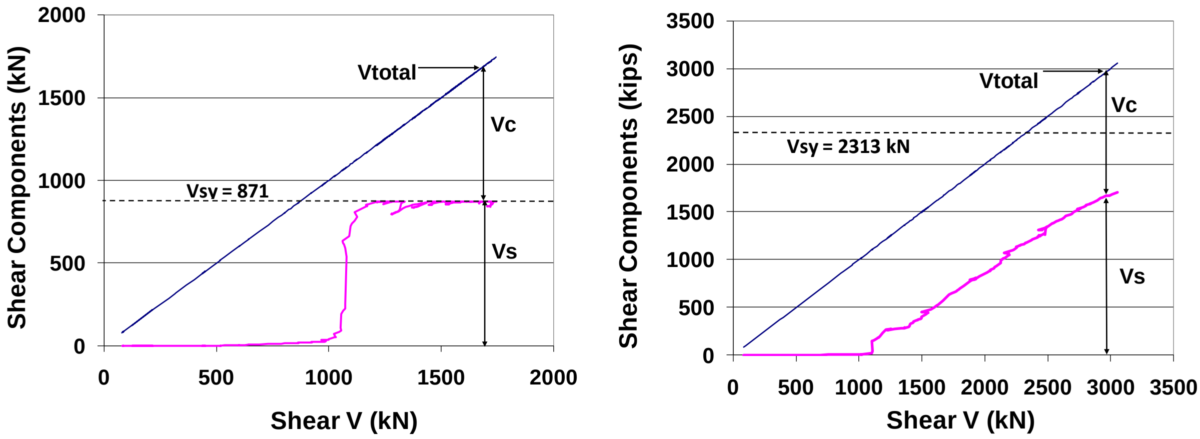

a) Girder 1 Crack G1E5 (b) Girder 4 Crack G4E7

Fig. 10.15: Determination of Vs and Vc for selected examples

10.4.4 Components of Vc

Based on elastic analysis of the gross cross-section, about 8% of the total shear would be expected to be carried by the bottom bulb in an uncracked section as shown by the solid line in Fig. 10.16b. By measuring the change in concrete strain as determined from the concrete surface strain gages, see Fig. 10.16a or through readings from the CMM, it was possible to estimate the shear force being carried in the bottom bulb. This was found to be very close to the elastic condition until the shear reinforcement yielded, after which the portion carried by the bottom bulb dramatically increased. A similar observation was made for other girders. While this was not unexpected, this example demonstrates the need and value of making the types of comprehensive measurements that make possible the quantification of such effects.

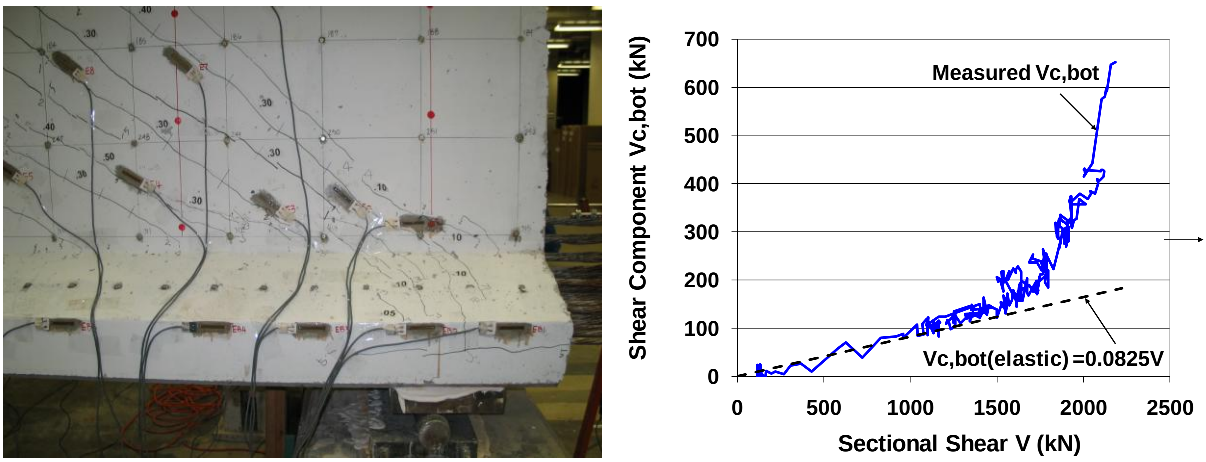

(a) Location of concrete surface strain gages (b) Contribution of bottom bulb

Fig. 10.16: Method for determining contribution of bottom bulb to shear resistance

Fig. 10.17 presents the calculated contributions to shear resistance from the main contributors to shear resistance for one CFBD on the East half of Girder 5. In this example, the portion carried by the top slab was assumed to be the portion carried of the total shear as determined from an elastic analysis. The portion of the shear that was carried by the concrete in the web was taken as the total shear less that calculated to be supported by the stirrups, bottom bulb, and top slab. Making a similar evaluation for a large number of CFBDs provided insight into how shear is carried in structural concrete. See Sun (2007) for this methodology. The capabilities of the ExVis program continue to be enhanced through funding from a US National Science Foundation's Network for Earthquake Engineering Simulation project.

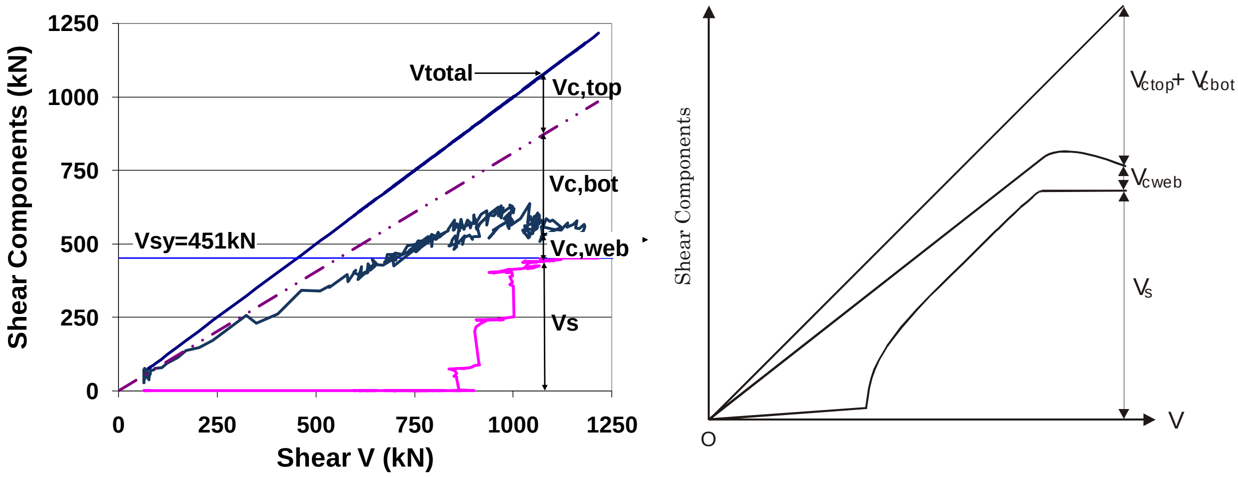

(a) Components of resistance for G5E (b) Generalization of components of resistance

Fig. 10.17: Contributions of four key contributors to shear resistance for G5E

10.5 End-Region behaviour

While the data collected in this research program provided good insight into the behaviour of B-Regions, the majority of the failures were due to breakdown of brittle mechanisms of resistance in the end (or discontinuity) regions of these girders. The three types of end region failures observed in this project were: (i) those by compressive failure of the strut just above the support, (ii) shear-compression failures at the interface between the bottom bulb and the web, and (iii) failure due to inadequate longitudinal tension capacity at the face of the support. A few observations and findings on each of these types of brittle failures are now provided.

10.5.1 Localized diagonal crushing failures

As was previously shown in Fig. 10.4, in a simply supported member the field of diagonal compression that is marching towards the support must funnel down to the support in the last compression diagonal. As shown by the pattern of diagonal cracking in Figs. 10.6, 10.7, 10.11, 10.13, 10.14, and 10.16, the diagonal compressive stress is expected to be close to double above the support relative to what it is a short distance along the length of the beam from the support. A similar observation was made from the predictions of the non-linear finite element analyses of the test girders. See Lee (2009). Consequently, diagonal crushing occurred above the support, as shown in Fig. 10.18, well in advance of crushing of the parallel diagonal compressive field away from the support.

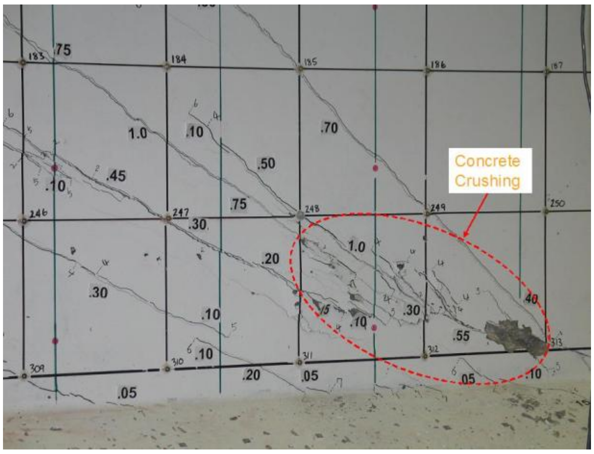

Fig. 10.18: Localized crushing in web above right support

10.5.2 Shear-compression failures at web to bulb interface

One of the common modes of failure in this testing program was a shear compression failure that developed at the base of the web just above the bulb and inside of the support. Fig. 10.19 presents the type of damage that was observed just before failure; local slip and crushing is evident. It also presents a short segment of the condition after the brittle failure that could extend over a length of up to 3-4 m.

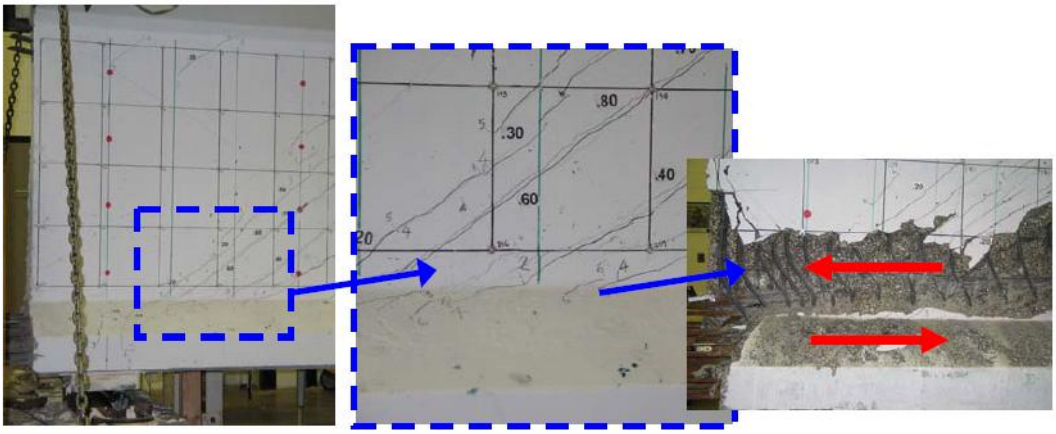

Fig. 10.19: Initiation of shear-compression failures at web to bulb interface

The heavy shear-compression demand on this region was predicted by non-linear finite element analyses. There was very acceptable agreement between the predicted and measured shear straining and vertical straining in this complex region as shown in Fig. 10.20. Based on an examination of all test results, a methodology was developed for assessing when this type of shear compression failure was likely to occur so that designers can guard against such brittle failures occurring in practice. This methodology is presented in Nagle (2008).

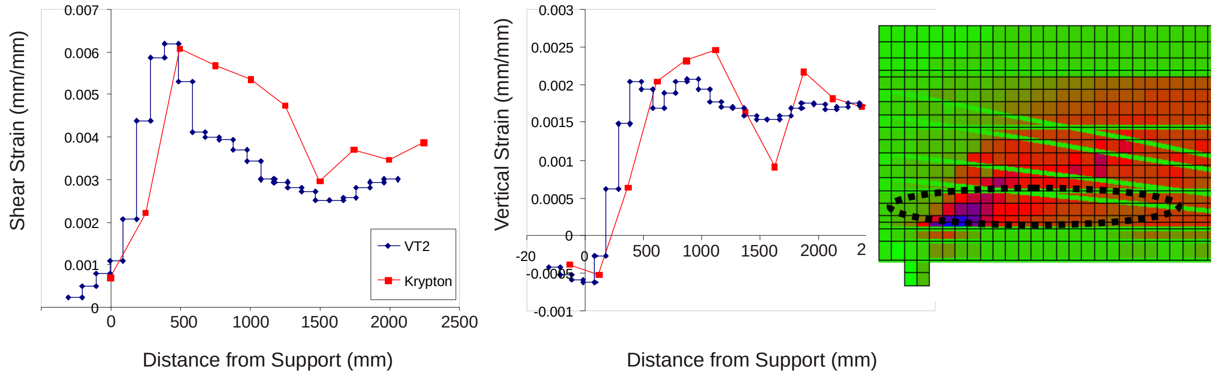

Fig. 10.20: Evaluation of state of stress that lead to shear-compression failures

10.5.3 Inadequate longitudinal tension capacity at the face of the support

The third and final type of end region driven failure that was observed in this research program was due to inadequate longitudinal tensile capacity at the inside face of the support. This type of failure was only observed in 2-3 of the 20 tests. There is some uncertainty in how to best calculate both the demand for and capacity of this reinforcement. One of the two methods for evaluating the demand is the strut-and-tie model for which the most appropriate angle of diagonal compression to use at the support is in question. The other method is to utilize a CFBD from the edge of the support (See Fig. 10.21a) in which both the angle of cracking and the role of the provided level of shear reinforcement on this demand are somewhat uncertain. See LRFD (2004) for this method. On the capacity side of the equation, it has generally been assumed that the prestressing strand is within its transfer length until the inside face of the support and thereby the higher bond stresses associated with transfer may be used. However, the results from this research indicate that it is common for shear cracking to extend down through up to a few of the layers of strands at the support as shown in Fig. 10.21b. The presence of cracking through the strands indicates that it is more appropriate to use the lower development bond stress level for part of the strand length when determining the capacity of the longitudinal tension reinforcement at the inside face of the support.

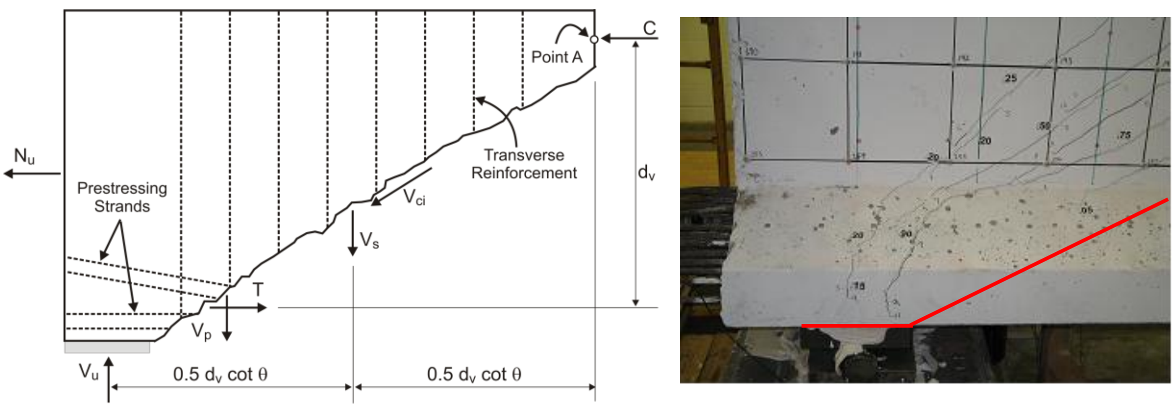

(a) LRFD FBD for evaluating demand on longitudinal reinforcement (b) Measured cracking above support

Fig. 10.21: Evaluation of state of stress that lead to shear-compression failures

10.6 Summary and discussion of key observations

This paper presented a collection of observations made during a research program in which 20 shear tests were conducted on large prestressed bulb-tee girders. A summary of the observations that are considered most significant are discussed below.

1.) The “shear” capacity of a bulb-tee girder may be limited by many aspects of the design and geometry including the capacity of the stirrups, the capacity of the field of diagonal compression, slip resistance along cracks, the compressive capacity in the web above a support, the shear/compression capacity at the base of the web that is a short distance from the support, and the available longitudinal tensile capacity at the inside face of the support. While not all of these would be considered to be classical beam shear failures, they require consideration; building and bridge code committees should provide guidance and restrictions to avoid brittle and unexpected failures in the field. The responsibility for ensuring a proper design of end regions remains vague. While some codes-of-practice properly identify this region as a discontinuity region and thereby require the use of the strut-and-tie model to either design or check the capacity of these end regions, it is unlikely that this will be done by a large percentage of design engineers. This is due to the unfortunate situation whereby all regions are typically designed by sectional approaches. This is being further solidified by the development and use of computer-based design tools that only deal with sectional approaches.

2.) In members designed to resist very high shear stresses, it is possible that shear cracking will occur under service loads. The expression in the ACI318-08 building code for web-shear cracking and flexure shear cracking provides a simple and accurate means of checking whether or not the member is likely to be cracked in shear under service loads. This is providing that the modulus of rupture is taken as $0.5\sqrt{f'_c}$ where f'_c is in MPa units ($6\sqrt{f'_c}$ where f'_c is in psi units).

3.) Once shear cracking occurs in a member, transverse reinforcing steel (stirrups) will become significantly engaged in carrying the applied shear force. The increase in stirrup bar stress due to cracking will depend on the amount of provided shear reinforcement and the tensile strength of the concrete. The larger the amount of shear reinforcement, the smaller will be the increase in bar stress upon cacking and the better will shear cracking be controlled. In the case of light or even modest amounts of shear reinforcement, this reinforcement may yield after initial shear cracking and this could lead to fatigue concerns.

4.) Advanced measurement systems are now available that can make a very detailed and comprehensive measurement of surface deformations of concrete structures. The most promising technologies include the use of coordinate measurement machines, digital image correlation, and other non-contact measurement systems. Photogrammetric methods are particularly effective for developing a complete record of the development of cracking as well as for the measurement of built geometries.

5.) In order to make effective use of the large volume of data than can now be collected from experiments, it is necessary to develop and make use of new methods for data visualization and analysis. One such tool, ExVis, was developed to function similarly as does a post-processor for predictions from numerical models but in this case for experimental test data. The data included information about the test structure and its response including the geometric details of the structure, material properties, support conditions, loadings, crack images, and all experimental measurements. The combination of this type of data-visualization and exploration tool, coupled with dense test data, has the potential to greatly increase the value of experiments for progressing both our understanding and numerical methods for predicting the response of concrete structures to complex states of stress.

10.7 References

AASHTO (2004) LRFD Bridge Design Specifications. 3rd edition, Washington, D.C., 1450 pp.

ACI or ACI318-08 (2008),Committee 318 (2008), Building Code Requirements for Structural Concrete (ACI 318-08) and Commentary (ACI 318 R-08). Farmington Hills, 521 pp.

Bentz, E. C., and Collins, M. P., (2000) "Response 2000." http://www.ecf.utoronto.ca/~bentz/r2k.htm (2000

CSA (2004) Committee A23.3, Design of Concrete Structures, CSA A23.3-04. Rexdale, Ontario, Canada, 240 pp.

DIN (2001) 1045-1, Deutsche Norm: Tragwerke aus Beton, Stahlbeton und Spannbeton - Teil 1: Bemessung und Konstruktion. S. (Concrete, reinforced and prestressed concrete strutures - Part 1: Design). Normenausschuss Bauwesen (NABau) im DIN Deutsches Institut für Normung e.V. Beuth Verl. Berlin (July 2001) pp. 1 - 148.

EC2 (2002) Commission of the European Communities, Eurocode No. 2: Design of Concrete Structures - Part 1: General Rules and Rules for Buildings. prEN 1992-1-1. draft (July 2002).

Kuchma (2008), D.A., Kim, K.S., Nagle, T., Sun, S., and Hawkins, N.M. "Shear Tests on High-Strength Prestressed Bulb-Tee Girders: Strengths and Key Observations", ACI Structural Journal, Vol. 105, No. 3, pp. 358-367, May-June 2008

Lee, H-H (2009), "Validation of Computational Models for the Behavior of Structural Concrete", PhD Thesis, University of Illinois

Mörsch, E., (1920), Der Eisenbetonbau-Seine Theorie und Anwendung (Reinforced Concrete Construction-Theory and Application). 5th edition, Wittwer, Stuttgart, Vol. 1, Part 1 (1920).

Mörsch, E., (1922), Der Eisenbetonbau-Seine Theorie und Anwendung (Reinforced Concrete Construction-Theory and Application). 5th edition, Wittwer, Stuttgart, Vol. 1, Part 2 (1922).

Mitchell, D., and Collins, M. P., (1974) "Diagonal Compression Field Theory - A Rational Model for Structural Concrete in Pure Torsion." ACI Structural Journal, Vol. 71, pp. 396-408.

NCHRP (2007) National Cooperative Highway Research Program Report 579 "Application of the LRFD Bridge Design Specifications to High-Strength Structural Concrete: Shear Provisions", http://onlinepubs.trb.org/onlinepubs/nchrp/nchrp_rpt_579.pdf , 206 pp., 2007

Nagle, T.N. (2007) "Design and Behavior of End Regions of Prestressed Concrete Girders", PhD Thesis, University of Illinois

Ritter, W., (1899), "Die Bauweise Hennebique," Schweizerische Bauzeitung, Vol. 33, No. 7, pp. 59-61.

Sun, S. (2007) "Shear Behavior and Capacity of Large Scale Prestressed Bulb-Tee Girders", PhD Thesis, University of Illinois

Sun, S., Kuchma, D.A., and Kim, K.S., (2009) "Analysis of Photographically Measured Crack Development from Shear Tests on Large Bridge Girders", Journal of the Precast Concrete Institute, Vol. 54, No. 4, pp. 81-98

Vecchio, F. J., and Collins, M. P., (1986) "The Modified Compression Field Theory for Reinforced Concrete Elements Subjected to Shear." Journal of the American Concrete Institute, Vol. 83, No. 2, pp. 219-231.

11 Thin-walled open-section P/C beams in fire: A case study

Patrick Bamonte[1], Roberto Felicetti[1], Pietro G. Gambarova[1] and Ezio Giuriani[2]

[1] Politecnico di Milano, Milan, Italy
[2] Università di Brescia, Brescia, Italy

Abstract: The assessment of fire safety in a heavy-duty pre-tensioned simply-supported beam with an inverted V section is presented in this paper. Architecturally-valuable thin-walled beams have been used in Italy for the last forty years in the roofs of large industrial or office buildings. Typically, a series of girders (= secondary beams, with interposed concrete or polycarbonate panels) are supported by other girders resting on columns (= main beams), having different sections (double-tee/inverted-V/channel sections). After several decades since their design and construction based on past code provisions and technologies, a reuse of the building and/or more severe loads often require the beams to be rechecked in fire, even more since these members frequently exhibit severe symptoms of distress, often in the form of longitudinal cracking induced by transverse bending. The beam in question, with thin and inclined webs, is checked both at the Ultimate Limit State (ULS) and in fire, with reference to bending and shear. As for shear, both the traditional truss model with variable strut inclination and a dedicated truss model are used, the former wherever the state of stress is regular (in the undisturbed zones, far from the supports) and the latter in the diffusive zones close to the supports. Reference is made to the provisions of Eurocode 2. Albeit rather peculiar for its unusual cross-section, the beam in question offers the opportunity to focus the attention on some general aspects concerning the safety verifications on thin-walled concrete members in fire conditions, and on some peculiarities of past design practice.

11.1 Introduction

The astonishing development of the Italian prefabrication industry in the sixties and seventies of the past century, and the growing interest in the same period for prestressing, favoured the design and construction of many challenging prestressed concrete members. This growth was fostered by the economic boom of the late fifties and sixties, and by the ensuing diffusion of industrial buildings, characterized by large spans and requiring the use of large-span structural members [Barazzetta (2004)].

Beside double-tee girders (I-girders) and tapered beams (deeper at mid-span), that were not very demanding from a structural view point [Taerwe et al. (2006)], new types of pioneering P/C members were developed for the roofs of office and light-industry buildings, which were characterized by thin-walled open and complex sections, small-diameter distributed reinforcement and – in general – high static efficiency (see Figure 11.1, where the main beams have an inverted-V section and the secondary beams a V-section). These prismatic beams (called wing sections in the Italian technical parlance) were a turning point in the conceptual design of roof members. The compression chord and the tension stringer were not aligned on the vertical axis of the cross-section and were not connected by a single web, but by two thin inclined wings. In the secondary beams, this design philosophy brought in larger widths and simpler connecting members (concrete, glass or plastic panels) placed between the contiguous beams. Different sections (V, U and channel sections) started to be systematically developed in the 80s, when new (and more refined) calculation methods became available to most designers, and full-scale testing allowed to shed some light on such complex phenomena as transverse bending and its interaction with longitudinal bending.

As a matter of fact, the small thickness of the inclined webs enhances the transverse deformability of the section, and makes the ensuing shape loss a very dangerous occurrence, because of the reduction of the internal lever arm, to the detriment of the bending stiffness.

Fig. 11.1: View of a prefabricated roof with external and internal inverted-V main beams resting on tapered columns

The (often) smooth, small-diameter and distributed bars used for the transverse reinforcement make these beams rather shear-sensitive (especially in the end zones, where prestressing is hardly effective) with reference to both the Ultimate Limit State in shear and the fire.

In this paper a rather stiff pre-tensioned simply-supported beam with an inverted-V section (Figure 11.2) and length 12 m (= 40 ft) is considered.

To check whether this beam has a sufficient fire resistance, its load-bearing capacity should be assessed not only in bending and shear far from the supports (where the stresses are regularly distributed), but also in the end zones, where the stress field markedly depends on the position of the supports. For instance, in the case in question the beam is in some way suspended at the extremities, where the top chord rests on the columns (Figure 11.3).

These topics are treated in the paper, where the thermal field in the concrete, in the strands and in the ordinary reinforcement, is investigated in detail, in order to work out the various contributions to fire resistance. Reference is made to the provisions of European Codes (2002, 2004).

11.2 Geometry, prestressing and reinforcement of the beam

The main roof beams considered in this paper are characterized by an inverted-V section of 1.6 m height, 2.4 m width, and a nominal span of 11.5 m (Figures 11.2 and 11.3). The section is constant and there are no end diaphragms. Each main beam supports 4 secondary beams along each side. At each extremity, the secondary beams rest on a couple of teeth protruding laterally from the wings of the main beams. (Hence, the main beams are subjected basically to the rather concentrated loads transmitted by the 4 + 4 secondary beams, Figure 11.4; each of these loads, however, is applied in the two sections containing the teeth, see Figure 11.10; note that in the following reference is made to the internal main beams, since the external beams – along the sides of the roof – support only four secondary beams).

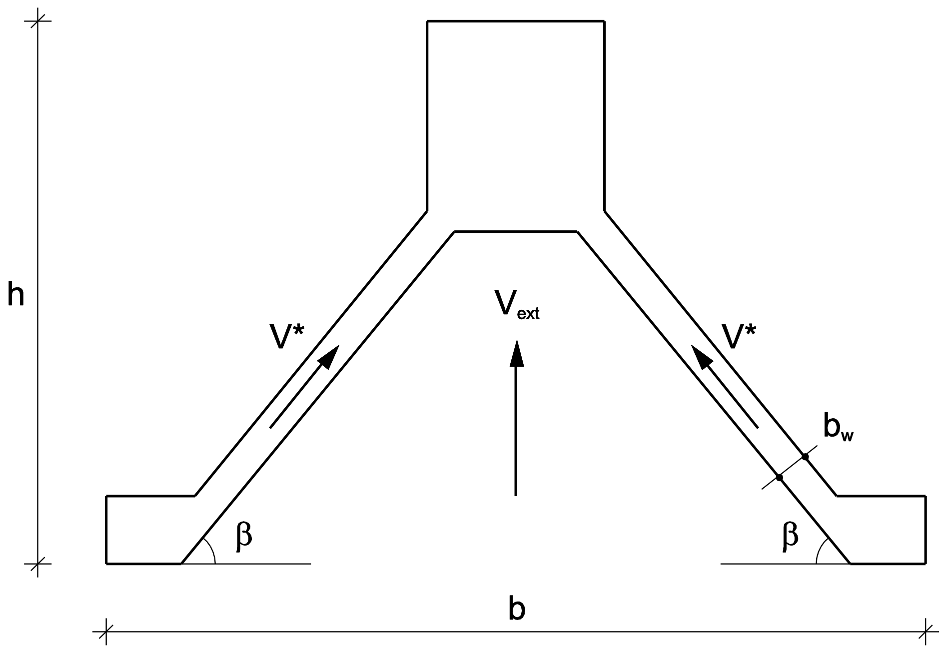

Fig. 11.2: Example of a wing-type section, with the shear force V_{ext} and its components V^* acting on the wings; and geometry of the section examined in this paper: total depth h = 1600 mm; width b = 2400 mm; thickness of the wings b_w = 90 mm; overall length L = 12 m; and β = 51°

The structural layout is that of a simply-supported beam; since this scheme is statically-determinate, all the possible variations of the internal forces ensuing from thermal gradients and prevented thermal dilations in case of fire are ruled out, something that does not occur – for instance – in monolithic slab-type roofs, that exhibit large redistributions of the internal forces in fire conditions [Bamonte et al. (2009); Buchanan (2002)].

The support system and the assembly tolerances are such that no significant membrane action in the plane of the roof is to be expected; moreover, the connection devices placed between the main beams and the top of the columns (threaded steel bolts) do not allow the transmission of significant horizontal forces to the columns.

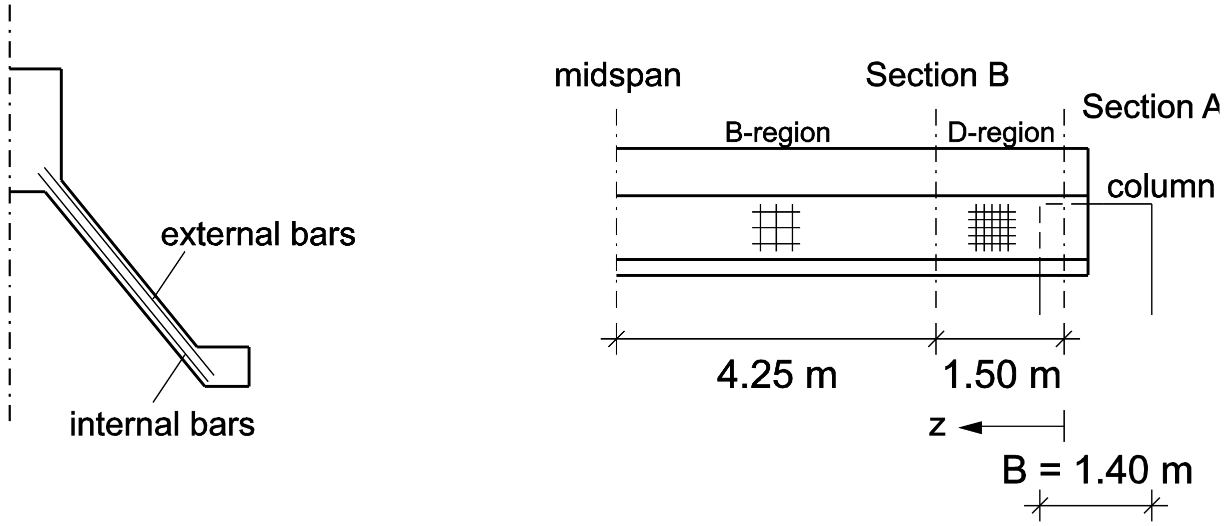

Fig. 11.3: (a) Half cross-section with the indication of the columns; and (b) lateral view, with the layout of the transverse reinforcement. Section A at z = 0; and Section B at z = 1.50 m

The teeth supporting the secondary beams are limited to a rather small portion of the beam span and will be ignored in the following, where reference will be made only to the current section.

It is worth observing that the two wings connecting the upper compression chord with the bottom tension chord (or stringer) are rather thin (90 mm).

The position of the prestressing reinforcement (26 strands; diameter = 0.5 in; number of wires in each strand = 7; diameter of each wire close to 4.2 mm; cross-sectional area of the strand = 98.7 mm^2) is given in Figure 11.5, where the boundary conditions adopted in the thermal analysis of the current section are indicated as well. The numbering of the strands was carried out on the basis of the horizontal layers, at increasing values of the coordinates x and y.

From the position of the strands it is possible to determine the effective depth d, that will be used in the following for the calculations. In a structural element that is subjected to a combination of bending and shear, the effective depth is defined as the distance between the top of the compression chord ("extrados") and the tension chord, that coincides with the centroid of the tensile reinforcement. In the case under investigation, it is reasonable to assume that strands 1 to 12 will contribute to the tension force at the ULS, while the strand 13 is located inside the compression chord.

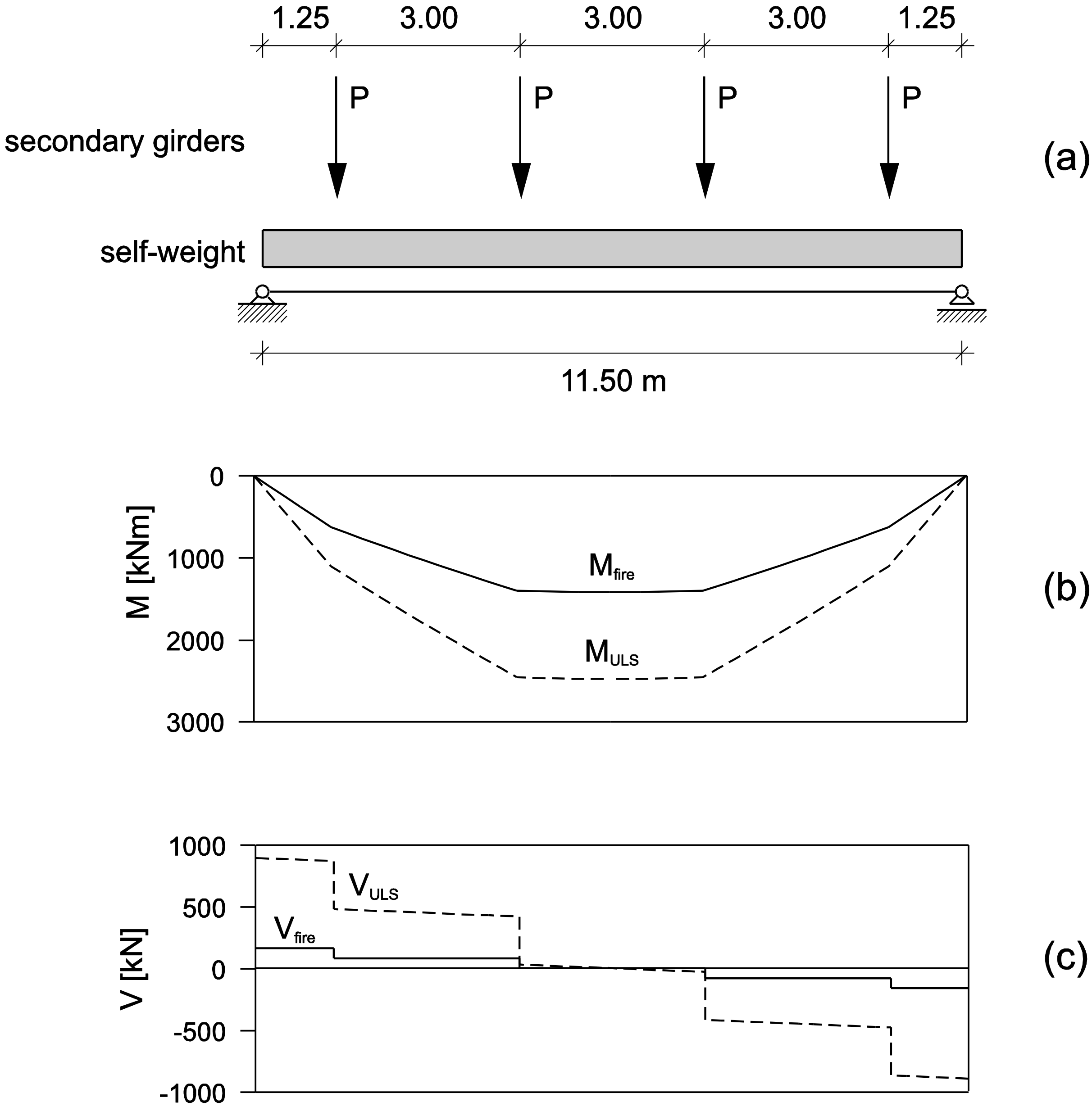

Fig. 11.4: (a) Loads acting on the beam; and (b,c) diagrams of the internal forces, at the Ultimate Limit State (dashed curves) and in fire (continuous curves). P_{fire} = 212 kN; P_{ULS} = 390 kN

Therefore, the position of the centroid of the tensile reinforcement (y_{av} = 360 mm in Figure 11.5) is determined as the weighted average of the positions of the single strands, taking into account the fact that the strands are characterized by the same cross-section; the effective depth and the internal lever arm of the section at the ULS are: $d = h - y_{av}$ = 1600 - 360 = 1240 mm; z = 0.9 d = 1116 mm; in each web or wing: $d^* = d/\sin(\beta) \approx 1600$ mm; $z^* = z/\sin(\beta) \approx 1400$ mm (Figure 11.10).

The main geometric properties of the section are:

- Cross-sectional area: $A = 6197\ cm^2$
- Distance of the centroid from the intrados (Figure 11.5): $y_G = 85$ cm
- Second moment with respect to the horizontal axis x': $I_{x}' = 16.03 \times 10^6\ cm^4$
- Second moment with respect to the vertical axis y: $I_y = 20.19 \times 10^6\ cm^4$

In Figure 11.3 the lateral view of one half of the beam shows the layout of the ordinary reinforcement in each inclined web or wing. In each web, the zone closest to the support (D-region) and that close to mid-span (B-region) are differently reinforced. In each web or wing:

- D-region: Vertical reinforcement: two-leg ∅8 mm-stirrups (spacing = 70 mm);
  Horizontal reinforcement: two layers of ∅8 mm-bars (spacing 70 mm).
- B-region: Vertical reinforcement: two-leg ∅6 mm-stirrups (spacing = 200 mm);
  Horizontal reinforcement: two layers of ∅8 mm-bars (spacing = 210 mm).

In this paper, reference will be made to both D- and B-regions, as the former is characterized by diffusive stresses and the latter by regularly-distributed stresses.

11.3 Loads and internal forces

The dead load consists of the self-weight of the main beam and of the four rather concentrated loads transmitted by the secondary beams (Figure 11.4). These loads are applied at 1.25 and 4.25 m from each support. The self-weight of the beam is determined on the basis of the previously calculated cross-sectional area (current section). As for the loads transmitted by the secondary beams, reference should be made separately to their self weight, and to their permanent and variable loads.

Assuming for each secondary beam the following values:

- Length = 18 m
- Spacing (mean plane-to-mean plane) = 3.0 m
- Sectional area = 2705 cm^2

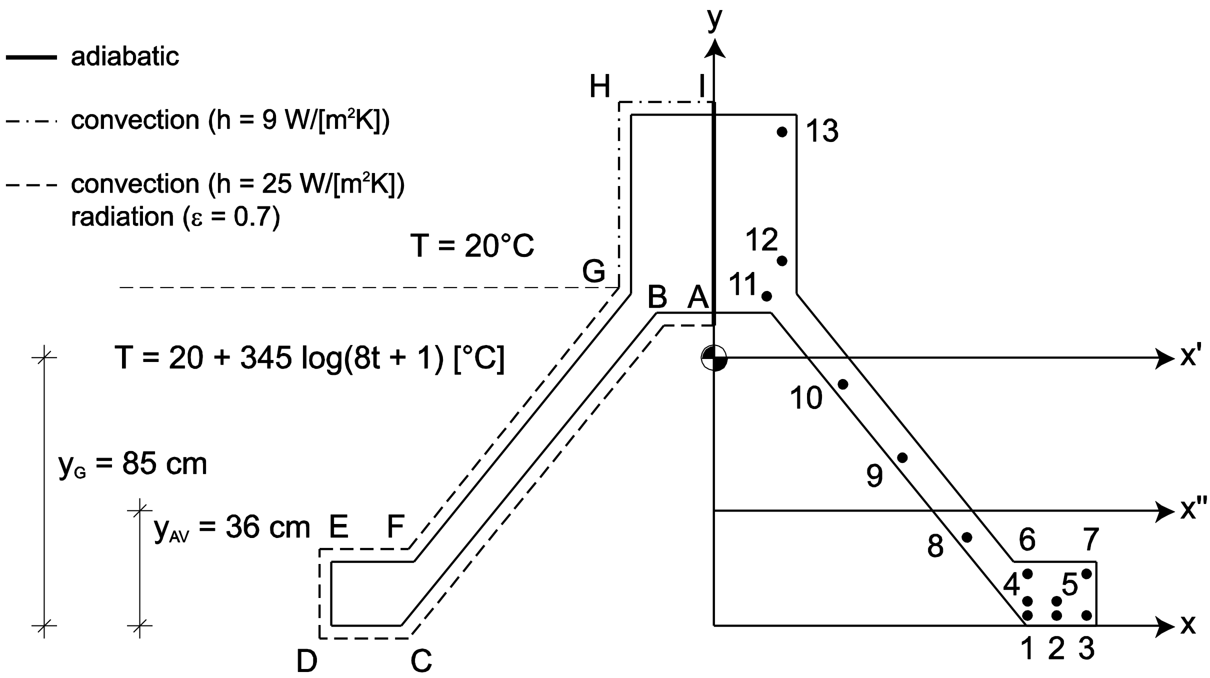

Fig. 11.5: Prestressing strands, centroid of the section, and centroid of the tension reinforcement at the ULS (Strands 1-12); and boundary conditions of the thermal problem (thick line = adiabatic; dashed line = standard fire; dash-dotted line: 20°C); t = [min]

- Area pertaining to each secondary beam = 3.0 × 18.0 = 540 m^2
- Self weight of the concrete panels covering or connecting the secondary beams = 1.0 kN/m^2
- Snow load (the only variable or live load) = 1.50 kN/m^2

The following loads should be resisted by each main beam:

- Self-weight of the main beam: g_{k1} = 15.50 kN/m
- Self-weight of the secondary beams: P_{gk1} = 121.50 kN
- Permanent loads applied to the secondary beams (including the overlapping of the panels): P_{gk2} = 73.80 kN
- Snow load transmitted by each couple of secondary beams: P_{qk1} = 81.00 kN

The applied loads and the diagrams of the internal forces (bending moment and shearing force) are indicated in Figure 11.4. Note that the diagrams refer to the Ultimate Limit State and to fire, respectively. Hence, two situations are considered:

- in ordinary conditions, following the provisions of the Italian Code (that is very similar to Eurocode 2), the Ultimate Limit State (ULS) is checked with the self-weight of the element increased by 30%, and the superimposed permanent and variable loads increased by 50%;
- in fire conditions the beam is subjected to the permanent loads at their characteristic values (i.e. the values are not increased), plus a suitable share of the variable load (for the snow on roof elements = 20%).

On the basis of the aforementioned provisions, the maximum bending moment at mid-span has the following values:

- Bending moment in fire conditions: M_{fire} = 1419 kNm
- Bending moment at the Ultimate Limit State: M_{ULS} = 2479 kNm

The same provisions are used for the maximum shear force, that occurs near the supports (D-region, Section A, z = 0, Figure 11.3):

- Shear force in Section A in fire conditions: $V_{A,fire}$ = 512 kN
- Shear force in Section A at the Ultimate Limit State: $V_{A,ULS}$ = 896 kN

Since the arrangement of the transverse reinforcement is not span-wise uniform, the shear-bearing capacity should be checked also in the B-region (Section B, z = 1.50, Figure 11.3):

- Shear force in Section B in fire conditions: $V_{B,fire}$ = 277 kN
- Shear force in Section B at the Ultimate Limit State: $V_{B,ULS}$ = 476 kN

Note that for simplicity the suffix "Sd" has not been introduced (for instance, $M_{Sd,fire}$ and $M_{Sd,ULS}$, instead of M_{fire} and M_{ULS}).

Finally, being simply supported with no axial restraints, the beam is subjected to no redistributions of the internal forces, which can be assumed to be constant during the fire.

11.4 Materials properties

The following materials properties were assumed according to the provisions of EC2:

- Characteristic cubic/cylindrical strength of the concrete R_{ck}/f_{ck} = 45/35 MPa
- Design strength at the ULS under sustained loads (uniaxial/biaxial stresses) f_{cd}/f_{cd}' = 19.8/9.9 MPa
- Design strength in fire (uniaxial/biaxial stresses) f_{cd}/f_{cd}' = 35.0/17.5 MPa
- Characteristic/design strength at yielding of the transverse reinforcement f_{yk}/f_{yd} = 500/435 MPa

For the prestressing reinforcement the following values are assumed:

- Elastic modulus of the prestressing reinforcement E_p = 195000 MPa
- Characteristic strength of the prestressing steel at failure/at yielding $f_{ptk}/f_{p0.1k}$ = 1668/1422 MPa
- Initial stress (before concreting) σ_{p0} = 1200 MPa
- Stress at the serviceability Limit State (strands with low relaxation) σ_{p1} = 1000 MPa
- Initial imposed deformation (before concreting) ε_{p0} = 6.15‰

The deformation imposed to the strands before concreting is a sort of initial “lack of compliance” between the strands and the surrounding concrete, and has to be taken into account in the calculation of the bending capacity at the ULS, after the stress redistributions ensuing from shrinkage, creep and relaxation of the prestressing strands. However, if the prestressing steel has enough ductility (which is usually the case), the bending resistance is little affected by the value of ε_{p0}.

Beside the materials properties in ordinary conditions, the properties at high temperature are to be introduced as well. In Figure 11.6 the normalized decay curves for the prestressing and ordinary steel, and for concrete are plotted as a function of the temperature (Eurocode 2, 2004).

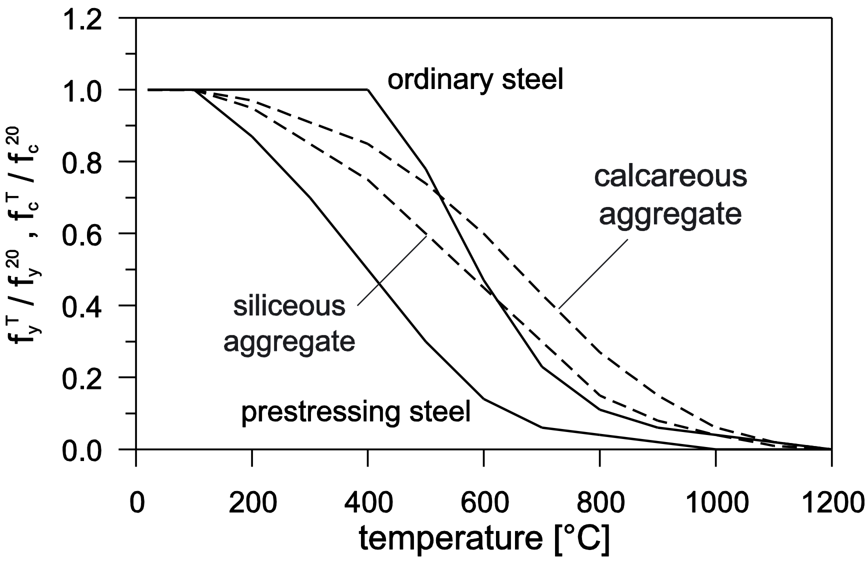

Fig. 11.6: Decay of the yield strength of the prestressing and ordinary reinforcement (continuous lines), and of concrete compressive strength (dashed lines), as a function of the temperature (EC2)

11.5 Fire analysis

11.5.1 Evaluation of the thermal field

The evaluation of the bearing capacity in fire conditions requires the preliminary thermal analysis of the cross section of the element. The aim of such analysis is to determine the temperature distribution, when the relevant boundaries are exposed to the fire.

In the following, reference is made to the standard ISO-834 temperature-time curve.

In the case under examination, the boundary conditions that are used to represent the fire are the following (Eurocode 1 (2002), Figure 11.5):

- along the sides defined by Points A-G, where the flames directly attack the surface of the beam, the ambient temperature is assumed to vary following the standard ISO834 temperature-time curve (whose expression is reported in Figure 11.5, left): the heat transfer to the structural element is governed by convection (convection coefficient = 25 W/[m^2·K]) and radiation (concrete emissivity = 0.7);

- along the sides defined by Points G-I, where the surface of the beam is directly exposed to the external environment at 20°C, the heat exchange between the beam and the environment is governed again by convection and radiation; the two phenomena, however, are lumped together, as it is usually done, by introducing convection with a suitably modified coefficient (= 9 W/[m^2·K]);

- along the side defined by points I-A there is no heat exchange (adiabatic conditions), because of symmetry.

Heat transfer inside the beam occurs by conduction, that is controlled by concrete thermal properties, namely conductivity and specific heat, and by the density. The values used in the analysis were chosen in accordance with the provisions of Eurocode 2 (2004). For the thermal conductivity, the Eurocode allows to choose between an upper curve and a lower curve; in the present case, the mean value was assumed in the analysis.

The thermal analysis was carried out by means of the finite element code ABAQUS, by setting up a two-dimensional model of the cross section, that neglects the reinforcement (as usually done in the thermal analysis of R/C and P/C members). Triangular elements with quadratic shape functions (6 nodes for each element) were adopted; the mesh consisted of 1320 elements with 2849 nodes (Figure 11.7a).

Figure 11.7b shows the thermal field for a standard-fire duration of 60 minutes. The temperature contour lines are plotted only in the area where the temperature is above 500°C. This value is usually considered as a threshold for both concrete and ordinary steel, as both materials suffer a significant strength loss above 500°C, but keep most of their strength unaffected by the thermal field below this temperature. Therefore, in the so-called simplified approach to fire analysis the 500°C isothermal line separates the area of the section that is fully effective in resisting the fire from the remaining area that is severely damaged and can be neglected (except for the reinforcement comprised in this area). In the following, the simplified approach based on the 500°C-isothermal will be used in bending, but the more refined multi-zone approach will be adopted in shear. (Note that the former approach does not require the knowledge of concrete decay at high temperature, which is required by the latter approach).

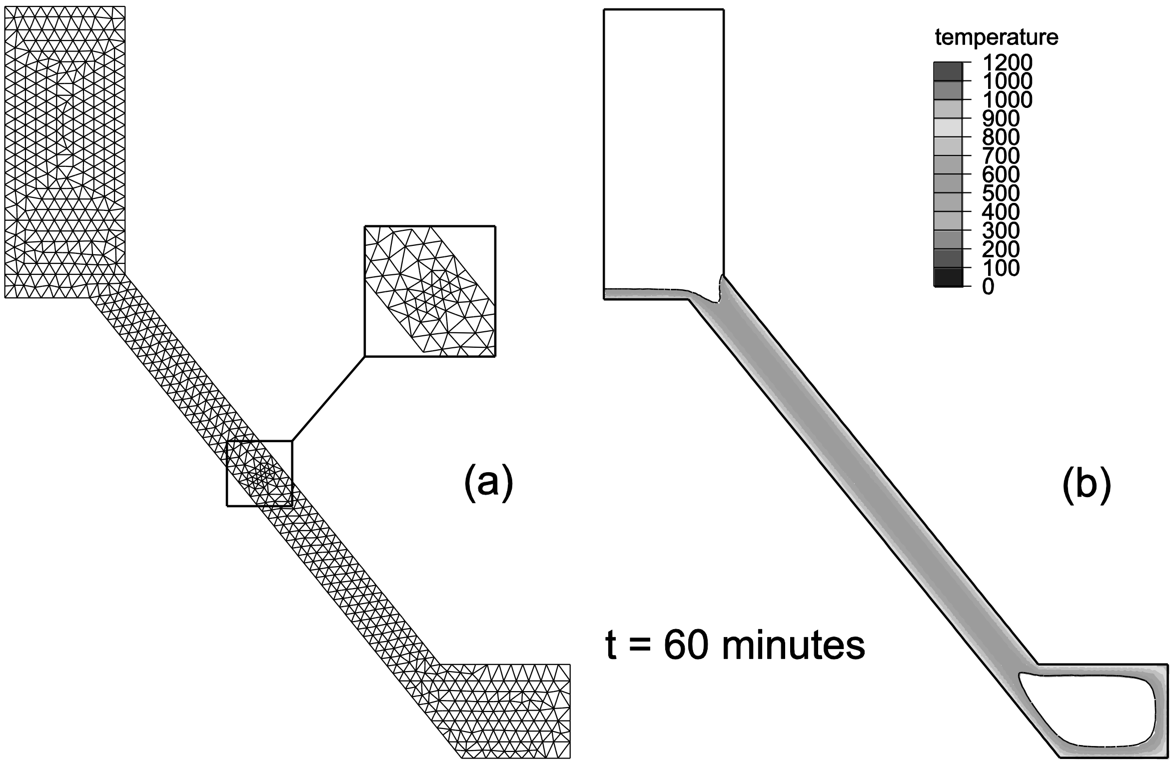

Fig. 11.7: Thermal analysis: (a) 2D modeling of half section; and (b) position of the 500°C isothermal line inside the section for t = 60 minutes (the wing is totally above 500°C)

Figure 11.8 shows the temperatures in the prestressing strands as a function of the fire duration; clearly, these values have a significant influence on the overall behavior of the beam in fire, since (a) the thermal dilations ensuing from the temperature rise bring in a very rapid and sizable prestress loss [Gales et al. 2010]; and (b) the above-mentioned thermal damage negatively affects the yield strength, thus reducing the bending capacity in fire. For instance, at t = 60 minutes, the isothermal line 500°C coincides with the mean line of the section of the wing and the effective or reduced thickness of the wing becomes zero (according to the 500°C-isothermal line approach). This is the reason why a more refined approach should be used in shear (the above-mentioned multi-zone approach), as the shearing force is mainly absorbed by the wings.

The temperatures in Figure 11.8 are the starting point for evaluating the decay of the mechanical properties of each strand. To this end, the decay curves provided by the design codes as a function of the temperature should be used (see the curves provided by EC2 in Figure 11.6). It is worth noting that beyond 1000°C, the strength of the prestressing steel becomes negligible.

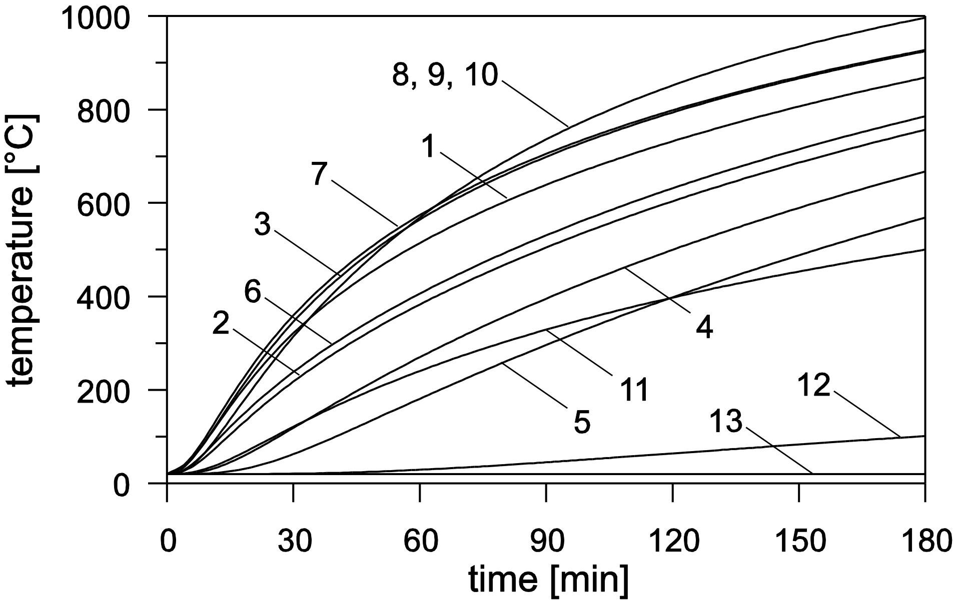

Figure 11.8: Temperatures in the prestressing strands as a function of the fire duration (ISO-834 fire)

11.5.2 Bending capacity at the ULS and in fire

The bending capacity was determined by assuming a non linear distribution of the compression stresses acting on the concrete (approximated by means of a stress block), and an elastic-perfectly plastic behaviour for the prestressing steel, with infinite ductility. The internal lever arm at 20°C turned out to be close to 0.9d.

The resisting moment M_{Rd} is ual to 3173 kNm, that is approximately 30% larger than the design moment at the Ultimate Limit State (3173/2479 = 1.28).

In underreinforced sections, the bending capacity is governed by the yielding of the reinforcing steel, in order to ensure enough ductility at the ULS. The same applies in fire conditions, where the temperature-induced decay of the reinforcing steel determines the decrease of the bending capacity. Hence, as already mentioned, knowing the decay of the yield strength for each strand is a must; the starting point is the evolution of the temperature in each strand (Figure 11.8).

The decay of the sectional bearing capacity in bending is evaluated by using the 500°C-isotherm method, which is suggested by the Eurocode 2 for any members subjected to normal stresses. The main assumptions of this simplified method are:

- concrete that has reached temperatures above 500°C is considered totally damaged, and thus not effective from a structural point of view ($f_c^T = 0$);
- concrete that has reached temperatures below 500°C is assumed to have the same mechanical properties as in virgin conditions ($f_c^T = f_c^{20} = f_c$);
- for both the prestressing and ordinary reinforcement, the mechanical decay is evaluated on the basis of the actual temperature (Figures 11.7 and 11.8).

It is worth recalling that, in fire conditions, the resistance is evaluated on the basis of the characteristic strengths of the materials, and not of the design strengths, as at the Ultimate Limit State.

The value of the bending moment in fire conditions at mid-span is $M_{Sd,fire} = M_{fire} =$ 1419 kNm.

Figure 11.9 shows the decay of the resisting bending capacity according to two different approaches:

- lower curve (●): 500°C-isotherm method;
- upper curve (◆): the decay is assumed to be ual to the average decay of the yield strength in the prestressing strands in tension (Strands 1-12); this assumption implies that the internal lever arm is constant during the fire, something that in principle is not correct.

It is worth noting that the two approaches yield results that are practically coincident; the second approach, however, tends to slightly overestimate the contribution of the strands in the web (8, 9 and 10), that are the hottest (Figure 11.8), and thus are more prone to thermal decay. The intersection between the curves (representing the decay of the bending capacity) and the horizontal line (representing the bending moment in fire) is close to 80 minutes.

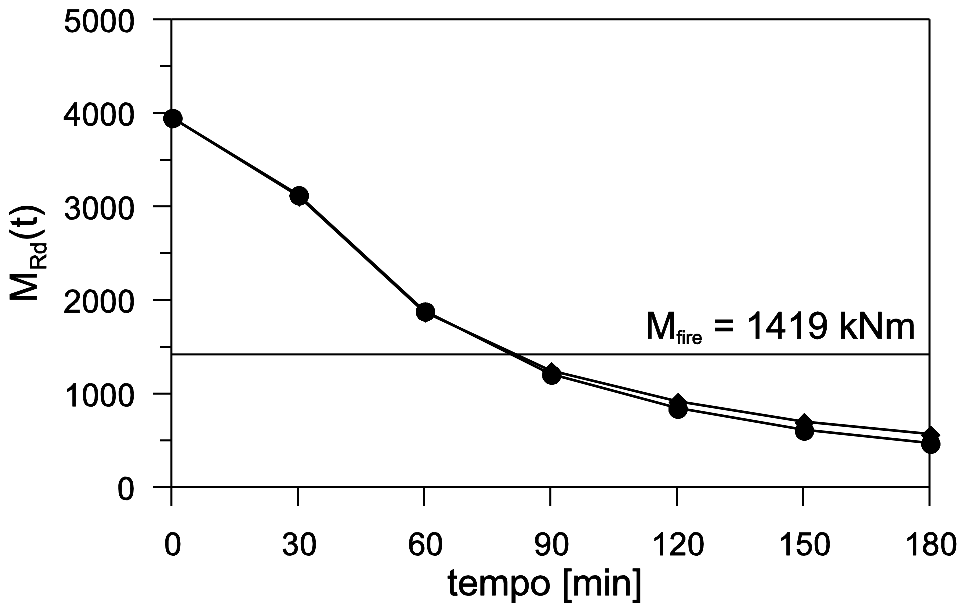

Fig. 11.9: Evaluation of the fire resistance in bending: (•) 500°C-isotherm method; and (♦) according to the average decay of the yield strength of the prestressing reinforcement

11.5.3 Shear capacity at the ULS and in fire

The evaluation of the bearing capacity in shear can be carried out by assuming that the shear force is resisted solely by the two inclined webs, as shown in Figure 11.2, where the shearing force V_{ext} (due to the external or applied loads) has two components V* acting on each wing. The angle of the wings with respect to a horizontal axis is $\beta \approx 51°$.

The forces V* and V_{ext} (the latter evaluated through structural analysis) are related by the following simple expression:

$$V^* = V_{ext}/[2\cdot\sin(\beta)] \approx 0.64V_{ext}$$

It is now possible to evaluate the maximum force acting on each single wing, on the basis of the maximum shear values in Section A (z = 0) and in Section B (z = 1.50 m):

- Shear force in Section A (in fire conditions) $V^*_{A,fire} = 329$ kN
- Shear force in Section A (at the Ultimate Limit State) $V^*_{A,ULS} = 576$ kN
- Shear force in Section B (in fire conditions) $V^*_{B,fire} = 178$ kN
- Shear force in Section B (at the Ultimate Limit State) $V^*_{B,ULS} = 306$ kN

D-region

In this D-region [Schlaich et al., 1987], the reaction exerted by the support spreads into the inclined webs, while the prestressing force – albeit rather distributed – is not totally efficient (and is neglected in the following).

The web behaviour can be modelled through a strut and tie mechanism, with the formation at the onset of collapse of compressive and tensile bands representing the concrete and the reinforcement, respectively.

The position of the struts and ties depends on the geometry, on the size of the bands and on the distribution of the reaction at the supports, see Figure 11.10, where half a beam is represented; the loads P* = V*A/4 = 144/82 kN (at the ULS/in fire, including the self-weight of the beam) act in the mean plane of each wing and are transmitted by the secondary beams in the sections containing the supporting teeth, that are 4 over 50% of the span. (Note that the nominal span in Figure 11.10 L_N = 11.10 m is slightly smaller than the span L = 11.50 m adopted in the evaluation of the internal forces – see Figure 11.4 – because the reaction has been considered as linearly-distributed at the column-beam contact, that is B/2 = 70 cm-long, as the column side is B = 140 cm, see Figure 11.3).

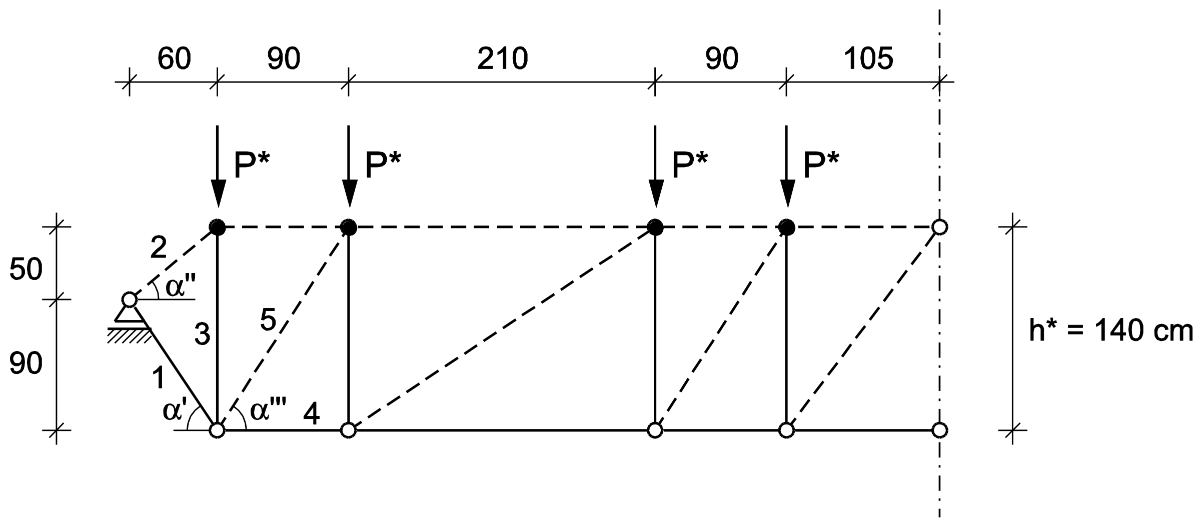

Fig. 11.10: Strut-and-tie model adopted in each web for the D-regions; the extension to the mid-span section is for the sake of completeness; the traditional variable-inclination model has been used far from the supports (in the B-regions); α' ≅ 56° ; α'' ≅ 57° ; α''' ≅ 40°

The axial forces in the truss members closest to the support are as follows:

- in fire: $N_{1,fire}$ = 253 kN; $N_{2,fire}$ = -183 kN; $N_{3,fire}$ = 35 kN; $N_{4,fire}$ = 299 kN; $N_{5,fire}$ = -292 kN

- at the ULS: $N_{1,ULS}$ = 445 kN; $N_{2,ULS}$ = -321 kN; $N_{3,ULS}$ = 62 kN; $N_{4,ULS}$ = 525 kN; $N_{5,ULS}$ = -514 kN

In order to evaluate the resisting contributions, the resisting sections should be defined. As each member represents a more or less wide "band" related to wing geometry, to the reinforcement and to the loads, among the 5 members belonging to the D-region, only the ties 1 and 4, and the strut 2 will be considered. (As a matter of fact, tie 3 is hardly loaded, and strut 5 takes advantage of the full height of the wing).

For tie 1, all the reinforcement distributed over a length h*/2 = 70 cm in both directions x and y has been considered:

- Vertical reinforcement: two-leg stirrups ∅8 mm/70 mm $\Rightarrow A_y = 1005\ mm^2$

- Horizontal reinforcement: two layers of ∅8 mm/70 mm $\Rightarrow A_x = 1005\ mm^2$

As the steel ratio in the vertical and horizontal directions are ual, the shear resistance of the reinforcement (after yielding) in any direction – and namely at α' = 56° – is the same as in the x and y directions:

$$A_1 = A_y = A_x \approx 1000\ mm^2$$

For the tie 4, the strands 1-7 have been grouped together:

$$A_4 = 691\ mm^2$$

For strut 2, the transverse side of its section is ual to the thickness of the wing (b_w = 90 mm), while the other side may be prudentially taken close to 1/5 of the effective depth of of the wing (320 mm). Hence $A_2 = 28800\ mm^2$.

Hence, the checks are satisfied both in fire (at t = 0) and at the ULS:

- $N_{1,Rd,fire} = A_1 f_{yk}$ ($N_{1,Rd,ULS} = A_1 f_{yd}$) = 500 kN (435 kN*) $\Rightarrow N_{1,fire}$ ($N_{1,ULS}$) = 253 kN (445 kN*)

- $N_{2,Rd,fire} = A_2 f_{ck}'$ ($N_{2,Rd,ULS} = A_2 f_{cd}'$) = 504 kN (286 kN*) $\Rightarrow N_{2,fire}$ ($N_{2,ULS}$) = 183 kN (321 kN*)

- $N_{4,Rd,fire} = A_4 f_{p0.1k}$ ($N_{4,Rd,ULS} = A_4 f_{pd}$) = 982 kN (855 kN) $\Rightarrow N_{4,fire}$ ($N_{4,ULS}$) = 299 kN (525 kN)

(*) As the focus is on fire resistance, this check may be considered as satisfied.

The resisting contributions $N_{4,Rd,fire}$ and $N_{4,Rd,ULS}$ should be reduced (-25% in the following) to take into account the limited anchored length of the strands, which prevents them from being fully effective in the section containing the joint among tie 2, tie 3 and strut 5.

It should be remembered that in fire (t ≥ 0) not only the reinforcement, but also the concrete exhibit a mechanical decay. Hence, the resisting contributions of the reinforcement and of the wings will be evaluated separately. (Especially in thin-walled members, the concrete of the webs may be in principle as heat-sensitive as the reinforcement, something that does not occur in solid members, where the mean temperature of the concrete is much lower than that of the reinforcement).

Assuming for the two layers of the transverse reinforcement (stirrups + longitudinal bars) a cover of 20 mm (from the heated surfaces to the axes of the bars, as usual in fire design), the temperature-time curve of the transverse reinforcement is shown in Figure 11.11, together with the decay of the normalized strength at yielding.

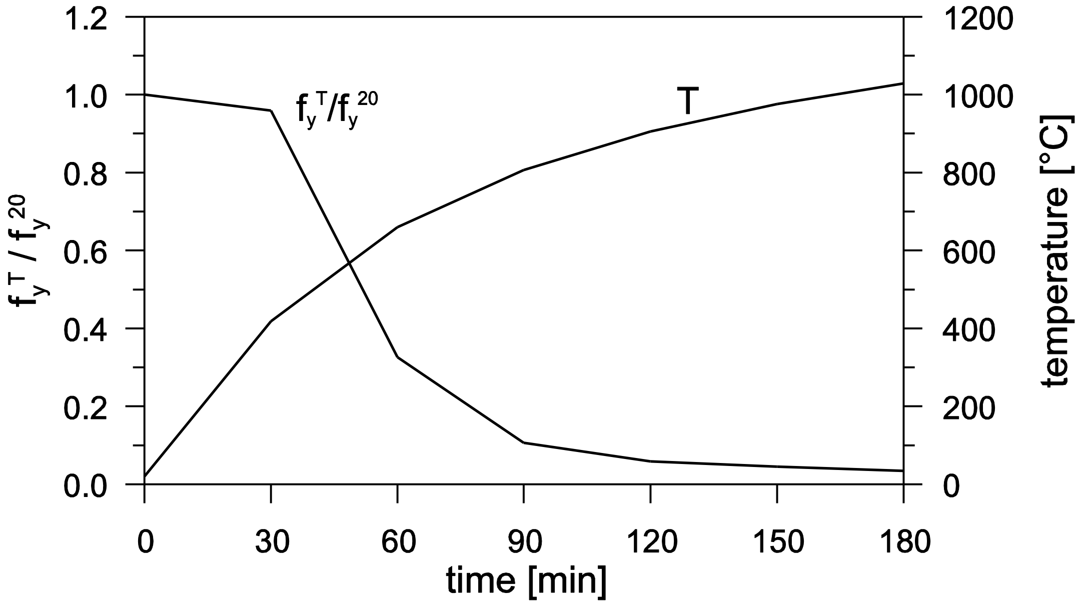

Fig. 11.11: Plots of the temperature in the transverse reinforcement and of the normalized strength at yielding (according to EC2), as a function of the fire duration

The evaluation of concrete decay under shear-compression (i.e. in the struts) has been performed with the zone method, by subdividing each wing into 8 layers (= 4 zones, Figure 11.12a), which are symmetric with respect to the mean plane. The evolution of the mean temperature in each layer – as a function of the fire duration – is shown in Figure 11.12b.

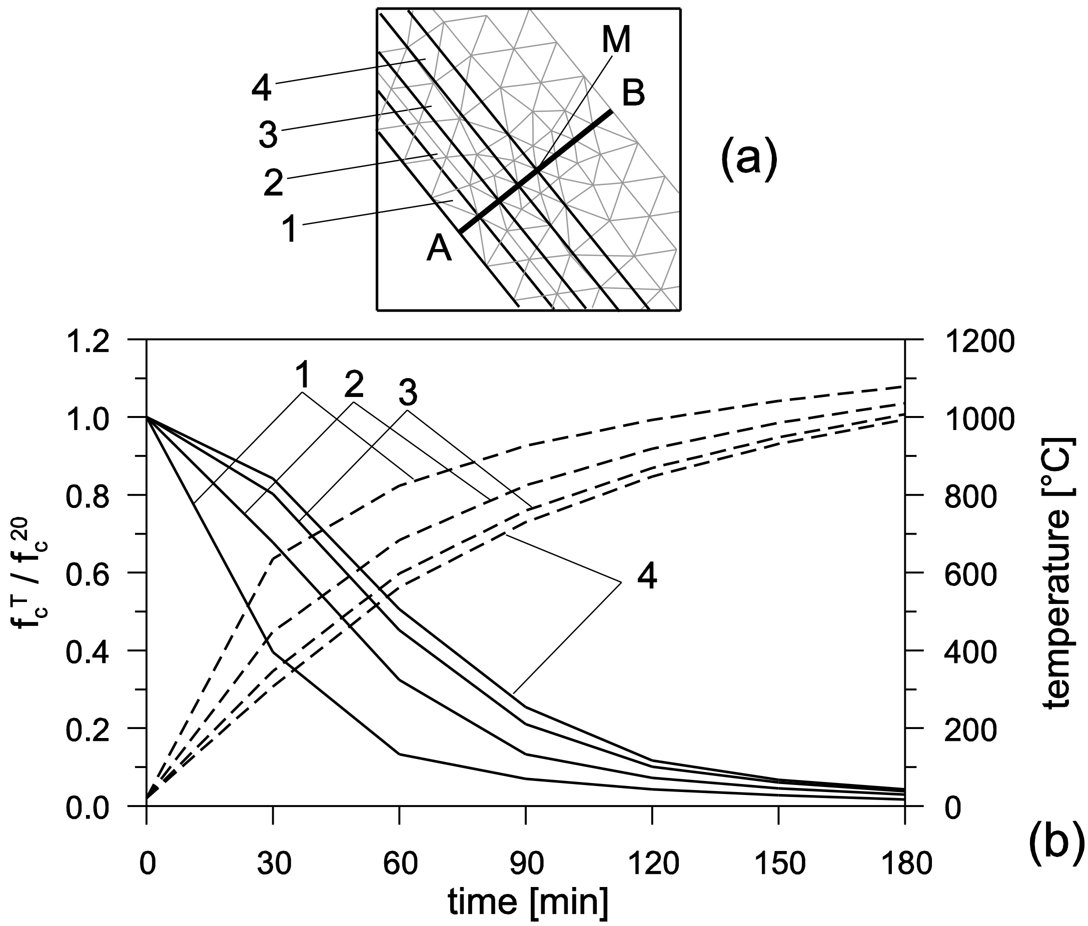

Fig. 11.12: (a) Subdivision of the wing section into 4 zones; and (b) plots of the mean temperature (dashed curves) and of the normalized concrete strength in each zone (continuous curves), as a function of fire duration

In Figure 11.13 the normalized strength decay of the concrete $k_c(M)$ in the mean plane (M along the chord AB, Figure 11.12a) and the mean normalized strength decay k_{cm} (evaluated among the four zones) are plotted, together with the temperature in the mean plane T(M), as a function of fire duration.

In the following, the expressions of k_{cm}, a_z (= thickness of the totally-damaged layer) and of b_w^R (= effective or reduced thickness) are reported, according to EC2:

$$k_{cm} = [(1 - 0.2/n)/n] \cdot \Sigma_i\, k_c(Ti) \quad (11.1)$$

$$a_z = b_w/2 \cdot [1 - k_{cm}/k_c(M)] \quad (11.2)$$

$$b_w^R = b_w - 2a_z = b_w \cdot [k_{cm}/k_c(M)] \quad (11.3)$$

where: n = number of the zones

T_i = mean temperature of the i-th zone

b_w = web or wing design thickness

It is worth noting that $k_{cm}/k_c(M)$ brings in the lack of uniformity of the thermal field.

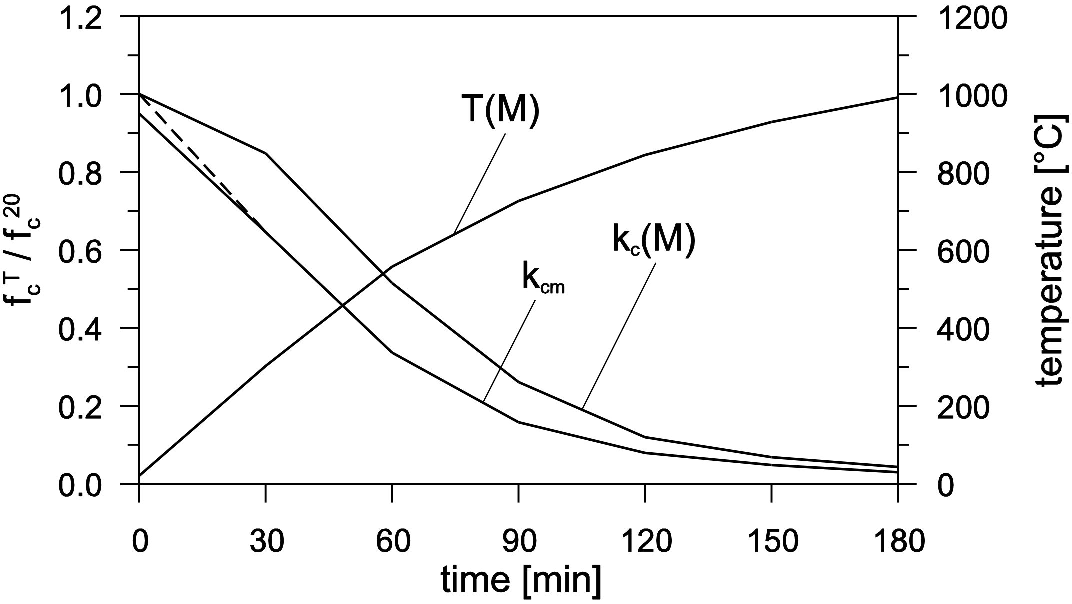

Fig. 11.13: Plots of the temperature T(M) and of the normalized-strength decay kc(M) in the mean plane of the wing, and plot of the mean decay of the normalized strength kcm: the dashed curve is in accordance with the actual temperature at the beginning of the fire (T = 20°C, ambient temperature), and the continuous curve is in accordance with Eq. (11.1)

The reduced or effective thickness b_w^R is plotted in Figure 11.14 as a function of fire duration. Note that (a) at the beginning of the fire (T = 20°C), the value of k_{cm} becomes 1 only if $n \rightarrow \infty$ [in our case, with n = 4, k_{cm} = 0.95, which means: b_w^R (20°C or t = 0) = 85.5 mm, instead of 90 mm]; and (b) the rather odd evolution of b_w^R with the fire duration has to do with the temperature-dependency of k_{cm} and k_c(M).

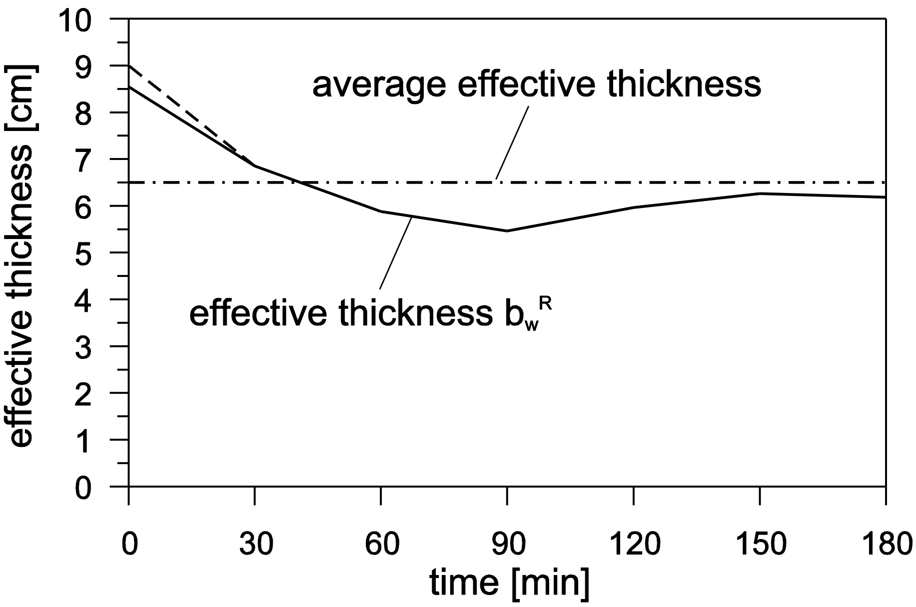

Fig. 11.14: Plot of the effective or reduced thickness bwR as a function of the fire duration: the dashed curve is in accordance with geometry (bw = 90 mm) and the continuous curve is in accordance with Eq. (11.1)

In Figure 11.15 the axial capacities of the members 1 (tie), 2 (strut) and 4 (tie) are plotted as a function of the fire duration ($N_{1,Rd,fire}$; $N_{2,Rd,fire}$; and $N_{4,Rd,fire}$, respectively), together with the corresponding values of the internal forces in fire conditions ($N_{1,fire}$; $N_{2,fire}$; and $N_{4,fire}$). Note that the axial capacity of each member is obtained by multiplying the reduced section by the strength corresponding to the temperature in the mid-plane T(M).

In the D-region, section z = 0 m, the collapse occurs at roughly 50 minutes because of steel yielding in the inclined tie No.1 (Figure 11.10), while it would occur at roughly 58 minutes in case of concrete crushing in strut No.2 and at 70 minutes in case of steel yielding in tie No.4.

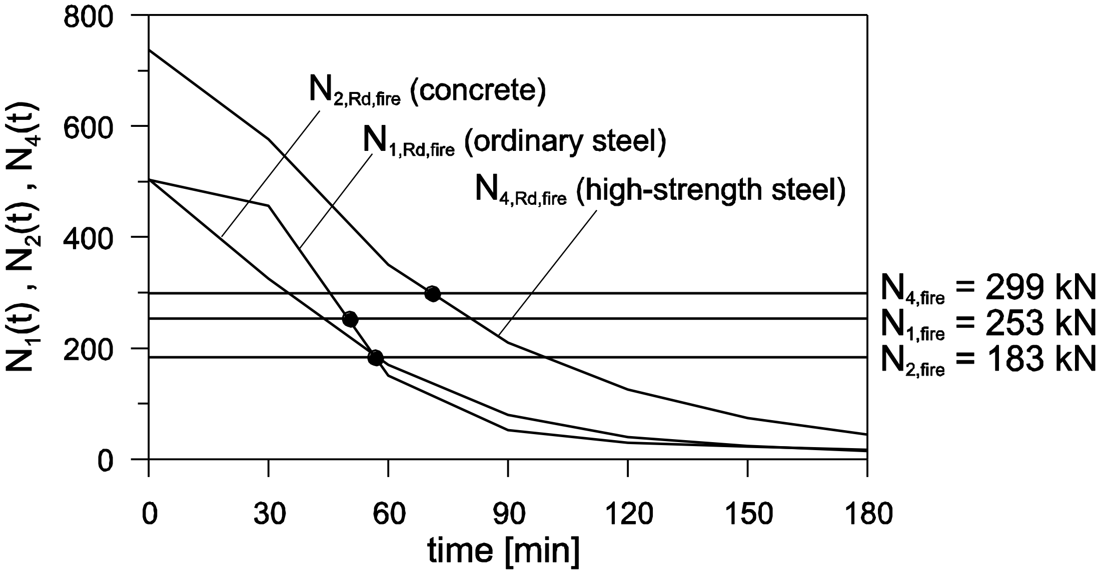

Fig. 11.15: Evaluation of the shear resistance in fire: plots of the different shear-resisting contributions, as a function of the fire duration

B-region

The bearing capacity is checked by using the traditional truss model, with variable inclination (i.e. to be established by the designer), that is a realistic representation of the mechanical behaviour of thin concrete webs subjected to prevailing shear [Leonhardt et al. (1973), Dei Poli et al. (1987), Adebar et al. (1998), Toniolo and di Prisco (2010)]. The resisting mechanism consists of transverse reinforcement, longitudinal reinforcement, concrete compression chord and inclined concrete struts (Figure 11.16).

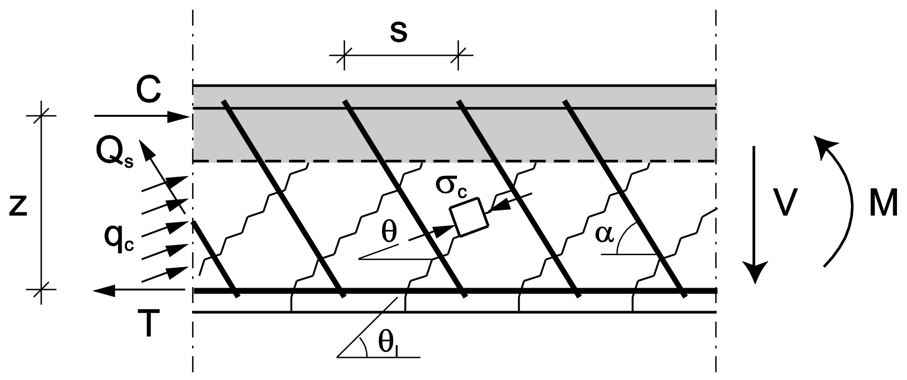

Fig. 11.16: Shear-resisting truss system (22° ≤ θ ≤ 45°); α = 90° for stirrups; and α ≠ 0 for inclined reinforcement (none in the case in question)

The transverse reinforcement consists of stirrups: two-leg ∅6mm ($A_{sw} = A_{st} = 56.5$ mm^2), with $s_{sw} = 200$ mm.

The contributions to the shear capacity of each wing are as follows (no inclined bars):

- Stirrups $V^*_{Rsd} = 0.9 \cdot A_{st} \cdot (d^*/s_{st}) \cdot f_{yd} \cdot \cot(\theta)$
- Inclined concrete struts $V^*_{Rcd} = 0.9 \cdot d^* \cdot b_w \cdot \alpha_c \cdot f_{cd}' \cdot \cot(\theta)/[1 + \cot^2(\theta)]$

where: A_{st} (stirrup area, two legs) = 56.5 mm^2; s_{st} = 200 mm

d^* (effective depth of each single wing) = $d_{AV}/\sin(\beta)$ = 1600 mm

b_w (web or wing thickness) = 90 mm

α_c (coefficient that takes care of the favourable effect of prestressing) = 1.00 - 1.25 (EC2)

By assuming that (a) the prestressing force is fully distributed on the sections at the ULS ($\alpha_c = 1 + \sigma_{cp}/f_{cd} = 1.21$) and is totally ineffective in fire ($\alpha_c = 1.00$), and (b) the mean prestressing stress acting in the strands is close to 1000 MPa, the value of θ turns out to be even less than the minimum (22°) specified by EC2. Hence, in the following θ is given the value 22°.

The following values are obtained for the shear resistances:

- $V^*_{B,Rsd}$ = 489 kN at the ULS; and 506 kN in fire (t = 0)
- $V^*_{B,Rcd}$ = 532 kN at the ULS; and 777 kN in fire (t = 0)

The above values of the resisting shear forces are higher than the acting shear forces in both ULS and fire conditions (for t = 0), as $V^*_{B,ULS}$ = 306 kN, and $V^*_{B,fire}$ = 178 kN.

In Figure 11.17 the decay of the resisting contributions of the stirrups and of the concrete are plotted as a function of the fire duration. The plots of Figure 11.17 were obtained in the same thermal conditions as those previously discussed for the transverse reinforcement in the D-region (see Figure 11.11).

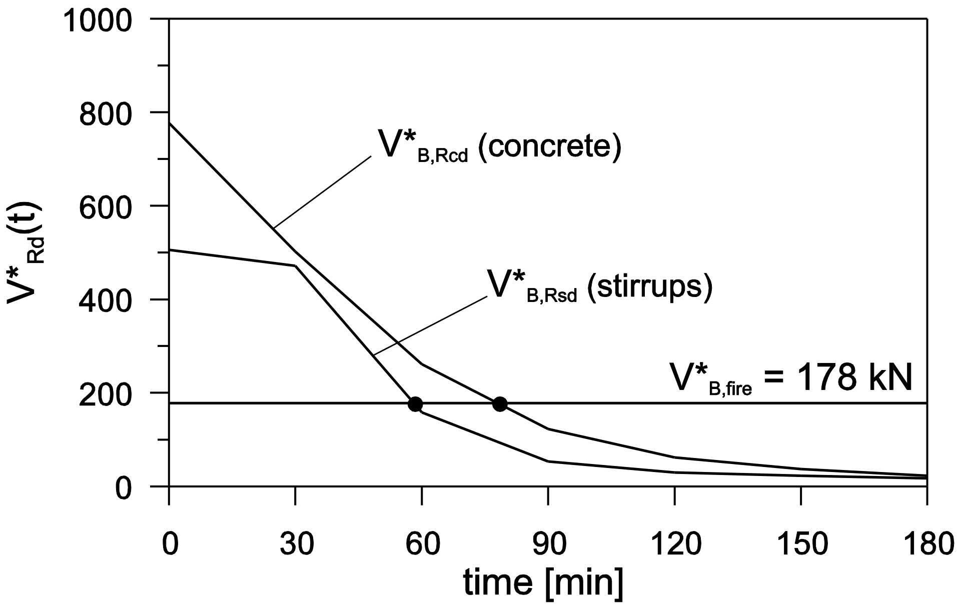

Figure 11.17: Evaluation of the fire resistance in shear, Section B with z = 1.5 m

In the B-region, section z = 1.50 m, the collapse occurs at roughly 60 minutes because of stirrups yielding, while it would occur at roughly 80 minutes in case of concrete crushing.

It is worth noting that in the previous calculations, it was implicitly assumed that in fire conditions the inclination of the concrete struts is the same as in virgin conditions at the Ultimate Limit State (i.e. $\theta = 22°$ in the B-region). The strut inclination, however, is in principle affected by concrete and steel strength decay, as well as by the stress redistribution ensuing from first cracking and from the decreasing effectiveness of prestressing at high temperature. Hence θ dependence on the thermal field should be in some way introduced, but addressing this topic – even concisely – is beyond the scope of this paper.

11.6 Concluding remarks

Thin-walled open-section P/C girders in fire conditions are among the most heat-sensitive structural members, because of their large exposed surfaces, rather small thickness, small-diameter reinforcement and limited cover, not to talk about the distributed prestressing (in pre-tensioned members), that limits the protection offered by the cover to the strands closest to the heated surfaces.

In the heavy-duty inverted-V girder investigated in this paper, the results of the analysis in standard-fire conditions show that bending is not a problem, since the fire resistance is close to 80 minutes. Such a figure (that is appropriate for a single storey, industrial or office building) is predicted by both the 500°C-isotherm method, and the method based on the average decay of the yield strength of the strands, with minimal differences.

In shear (that is definitely dangerous in thin-walled members), the results show that care should be used in modelling the end zones, where strut-and-tie models allow to understand the roles of the concrete struts (whose effective section may markedly decrease because of the heat-induced damage in the concrete) and of the steel ties (either stirrups or prestressing strands). In the case in question, the shear resistance in fire in the end zones (D-regions) turns out to be close to 50 minutes, while in the undisturbed zones (B-regions) is close to 60 minutes (in both cases the reinforcement fails first, but the fire resistance of the concrete in compression is not much larger!).

Two comments may be made with reference to the checks performed in this study: (a) in the end zones, the check at the Ultimate Limit State may be more critical than in fire conditions in spite of the heat-induced materials damage, because in the latter case materials strengths are definitely larger at the onset of fire and loads are definitely smaller; and (b) in the undisturbed zones, decreasing too much the transverse reinforcement – even if justified at the ULS – may lead to a critical situation in fire, because of the little protection offered to the stirrups by the rather small concrete cover.

Furthermore, contrary to solid sections, where concrete tends to keep its integrity in fire and a number of internal redundancies can be mobilized together or after steel yielding, in thin-walled members exposed to fire concrete may become as critical as the reinforcement in terms of resistance, as no sizable contributions coming from the redundancies of the strut-and-tie system should be expected.

11.7 References

Adebar P.E., Collins M.P., Mitchell D., Reineck K.H. and Rogowsky D.M.* (1998): "Recent Approaches to Shear Design of Structural Concrete", ASCE-ACI Committee 445 on Shear and Torsion, ASCE Journal of Structural Engineering, V.124, No.12, pp.1375-1417 (*Members of Subcommittee 445-1, who prepared this report).

Bamonte P., Felicetti R. and Gambarova P.G. (2009): "Punching Shear in Fire-Damaged Reinforced Concrete Slabs", ACI Special Publication 265 "Thomas T.C. Hsu Symposium on Shear and Torsion in Concrete Structures", pp. 345-366.

Barazzetta G. (ed., 2004): "Aldo Favini – A Life for Architecture and Engineering (in Italian), pub. by CLUP (Milan, Italy), 126 pp.

Buchanan A. (2002): "Structural Design for Fire Safety", Wiley & Sons, 436 pp.

CEN, European Committee for Standardization. EN 1991–1–2, Eurocode 1: Actions on structures – Part 1–2: General actions – Actions on structures exposed to fire, Brussels, Belgium, 2002.

CEN, European Committee for Standardization. EN 1992–1–2, Eurocode 2: Design of concrete structures – Part 1–2: General rules – Structural fire design, Brussels, Belgium, 2004.

Dei Poli S., Gambarova P.G. and Karakoç C. (1987). "Aggregate Interlock Role in R/C Thin-Webbed Beams in Shear", ASCE Journal of Structural Engineering, V. 113, No. 1, pp. 1-19.

Gales J., Bisby L. and Macdougall C. (2010): "Fire Induced Transient Creep Causing Stress Relaxation and Tendon Rupture in Unbonded Post-Tensioned Structures: Experiments and Modeling", Proceedings of the Sixth International Conference "Structures in Fire" – SIF'10, East Lansing (Michigan), June 2-4, 2010, pp. 727-734.

Leonhardt F., Koch R. and Rostasy F.S. (1973): "Schubversuche an Spannbetonträgern", Deutscher Ausschuss für Stahlbeton, V. 227, Berlin (Germany).

Schlaich J., Schäfer K. and Jennewin M. (1987): "Toward a Consistent Design of Structural Concrete", PCI Journal, Vol. 32, No. 3, pp. 74-149.

Taerwe L., Poppe, A.-M., Annerel, E. and Vandevelde, P. (2006): "Structural Assessment of a Pretensioned Concrete Girder after Fire Exposure", Proceedings of the 2nd International *fib* Congress, Napoli (Italy), 5-8 June 2006, full paper on CD.

Toniolo G. and di Prisco M. (2010): "Reinforced Concrete – Ultimate Limit State Design" (in Italian), publ. by Zanichelli, Bologna (Italy), 569 pp.

12 Design of FRC beams for shear using the VEM and the draft Model Code approach

Stephen Foster

Professor, Centre for Infrastructure Engineering and Safety
School of Civil and Environmental Engineering
The University of New South Wales, Australia

Abstract: While fibre reinforced concrete is in its fourth decade of development, it has yet to find common application in building structures and there no national standard that yet exists that treats fibre reinforced concrete in a systematic manner. This is addressed, to some extent, in the proposed *fib* Model Code 2010. In this paper, the model presented in the 2010 *fib* draft Model Code is assessed against the available test data for members failing in shear and a reasonable correlation is observed. It is noted, however, that there is an inconsistency in the approaches adopted for steel fibre reinforced concrete and for conventionally reinforced concrete members. This difference is assessed and, based on a physical model for fracture of steel fibre reinforced concrete, a revised model is proposed. In the model it is shown that the relationship between the shear provided by the concrete matrix and that of the fibres is coupled. The proposed model is tested against data collected from the literature with a good correlation observed.

12.1 Introduction

While fibre reinforced concrete (FRC) is in its fourth decade of development, it has yet to find common application in building structures. While the latest fibres, and their technological development, bear little resemblance to those first used in the current era by Romualdi and Batson (1963), the concept of the use of fibres to bridge micro and macro cracks that occur in a cementitious matrix due to various states of tensile stress and strain remains unchanged. While the use of fibres in unreinforced tunnel linings has become common practice and the use of fibres in moderating early age shrinkage cracking in large concrete pavements and precast panels has seen moderate take up, the use of the technology for providing resistance to loads as primary tensile reinforcement has been somewhat slower.

The influence of steel fibres has been shown by many researchers to increase the shear capacity of beams. For example, plotted in Figure 12.1 is the shear capacity τ against the effective depth, d, for the rectangular beams of Rosenbusch and Teutsch (2003). These beams contained either zero or one-half percent end hooked steel fibres, while other parameters such as concrete strength, shear span to depth ratio (a/d) and the longitudinal reinforcement ratio (ρ_l) remained relatively constant. Both the influence of the fibres on the performance of the sections and the size effect are clearly evident. Also plotted is the strength prediction line of the Level III model of the *fib* draft Model Code (2010) for beams and it observed that the model provides for a reasonable approximation to the Rosenbusch and Teutsch data. Note, in Figure 12.1, $\tau = V_u/(b_w.z)$ where V_u is the experimental shear failure load, b_w is the width of the web and z is the internal lever and is taken as $z = 0.9d$.

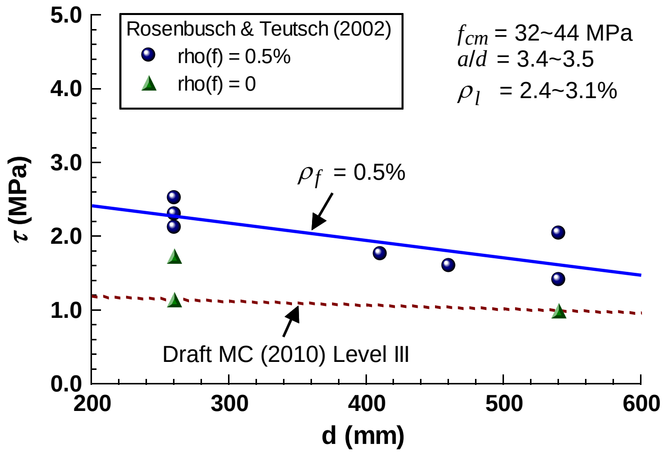

Fig. 12.1: Influence of fibres on the shear strength of SFR shear critical beams

Potentially, steel fibres can be used to replace a substantial quantity of conventional shear reinforcement in reinforced and prestressed concrete beams. While the material cost of the fibres exceeds that of relatively cheap shear steel reinforcement, significant savings can be obtained in substantially reducing on site labour costs. In this paper, and based on the design models for shear in the *fib* draft Model Code (2010), a more general lower bound modelling approach is developed for the design of fibre reinforced and prestressed concrete beams. In the model, the shear is carried by integrating of the concrete, fibre and reinforcing steel components with shear stresses above those carried by concrete and dowel action, carried with steel fibres, steel reinforcement or a combination of steel fibres and conventional shear reinforcement.

12.2 The Variable Engagement Model - VEM

In order to develop a model for calculating the tensile contribution of fibres to any beam section, the tensile strength contribution to a fibre-concrete matrix must first be determined. One such model is the variable engagement model (VEM) developed by Voo and Foster (2003, 2004) and Foster et al. (2006). Since its introduction, the VEM approach has been extended for Mode II (Lee and Foster, 2008, Foster 2009) and mixed mode fracture (Htut and Foster 2010). The Mode I model, referred to as VEMI, is discussed, in brief, in this section.

The full derivation of the VEMI is given in Voo and Foster (2003, 2004, 2009) and Foster et al. (2006). In brief, the tensile strength (f_{tf}) provided by the fibres over a plane of unit area is written as

$$f_{tf} = K_f \, \alpha_f \, \rho_f \, \tau_b \tag{12.1}$$

where $\alpha_f = l_f / d_f$ is the aspect ratio of the fibre, ρ_f is the volumetric fraction of fibres, τ_b is the bond stress between the fibres and the concrete matrix and K_f is a global orientation factor and is a function of the current crack opening displacement, w. If the the maximum stress provided by the fibres is required, K_f in Eq. (12.1) is replaced with $K_{f,max}$.

The global orientation factor can be determined by probability and is affected by the shape of the domain over which the orientation is considered. For the case where all fibres pullout from the matrix and fibres are randomly orientated in three dimensions, the global orientation factor is given by Voo and Foster (2009) as

$$K_f = \frac{1}{\pi} \tan^{-1}\left[w/\left(\alpha_{\mathrm{I}}\, l_f\right)\right] \left(1 - \frac{2w}{l_f}\right)^2 \tag{12.2}$$

where α_{I} is a fibre engagement coefficient.

In the formulation of Eq. (12.2), it is assumed that all fibres are pulled out from the matrix and there is no fibre fracture. Thus, Eq. (12.2) applies provided that

$$l_f < l_{crit} = \frac{d_f}{2} \frac{\sigma_{fu}}{\tau_b} \tag{12.3}$$

where l_{crit} is a critical fibre length for fibre fracture and σ_{fu} is the tensile strength of the fibre. If Eq. (12.3) is violated then a portion of the fibres will fracture and Eq. (12.2) does not apply. While Voo and Foster (2004, 2009) also formulated the case for inclusion of fibre fracture, as fibre fracture is an inefficient use of fibres and, thus, undesirable, only beams with fibre pullout failure are considered in this paper. That is, only beams where the maximum fibre length for all types of fibres used in the member are less than the critical length, l_{crit}.

The engagement parameter (α_{I}) has been calibrated using a uniform bond approach along the fibre length and verified against a wide range of test data, the results of which are given in Voo and Foster (2003, 2009). In the verification of the model, a good theoretical to experimental correlation was obtained. During the calibration process, it was determined that for straight and end hooked steel fibres the engagement parameter may be taken as

$$\alpha_{\mathrm{I}} = 1/\left(3.5\alpha_f\right) \tag{12.4}$$

While the VEM model adopted here is based on a uniform bond model, further detail of this approach and an alternative using a lumped bond approach, where bond is lumped into a snubbing zone and a hooked zone, is presented by Lee and Foster (2007, 2008) for the case of Mode II fracture.

For the uniform bond model, the interfacial fibre/matrix bond strength is taken as

$$\tau_b = k_b \sqrt{f_{ck}} \tag{12.5}$$

where k_b is a bond factor determined by the fibre and matrix type (taken as 0.8 for end-hooked steel fibres, 0.6 for crimped steel fibres and 0.4 for straight steel fibres in concrete) and f_{ck} is the compressive cylinder strength. To obtain the peak stress provided by the steel fibre reinforced concrete (SFRC), the value of $K_{f,max}$ may be obtained through determining the value of w that corresponds to $dK_f/dw = 0$ and solving for K_f in Eq. (12.2). However, it can be shown mathematically that no closed form solution exists for the first differential of Eq. (12.2) and the solution needs to found numerically. Alternatively, for fibres with an aspect ratio ranging from 20 to 120 and diameters from 0.15 to 0.9 mm, values for $K_{f,max}$ can be obtained with good accuracy from

$$K_{f,max} = 0.5 - \frac{0.645}{\alpha_f^{\,0.450}} \tag{12.6}$$

12.3 Plasticity approach: Crack Sliding Model

Amongst the many legitimate approaches that could be adopted, the first discussed is the plasticity approach. Based on the plasticity modelling approaches developed at the Technical University of Denmark under the direction of M.P. Nielsen, Zhang (1994, 1997) developed a model, referred to as the crack sliding model (CSM), for the shear strength of beams without web reinforcement. In 2006, Voo et al. combined the upper bound modelling approach developed by Zhang with their VEM and showed a good correlation against test data for ultra-high performance concrete beams with relatively high quantities of steel fibres.

According to the CSM, the cracking of concrete introduces a potential yield-slip line that, due to a reduced sliding resistance, forms the critical failure mechanism. For both non-prestressed and prestressed simply supported beams of rectangular cross-section and loaded with either single or two symmetrically located point loads, the ultimate shear capacity of the section can be determined by

$$V_u = \frac{1}{2} f_c^* b_v \, h \left(\sqrt{1+\left(\frac{x}{h}\right)^2} - \frac{x}{h} \right) \tag{12.7}$$

where f_c^* is the effective compressive strength of the SFRC, b_v and h are the width of the web and full depth of the section, respectively, and x is the horizontal projection of the yield line (Figure 12.2).

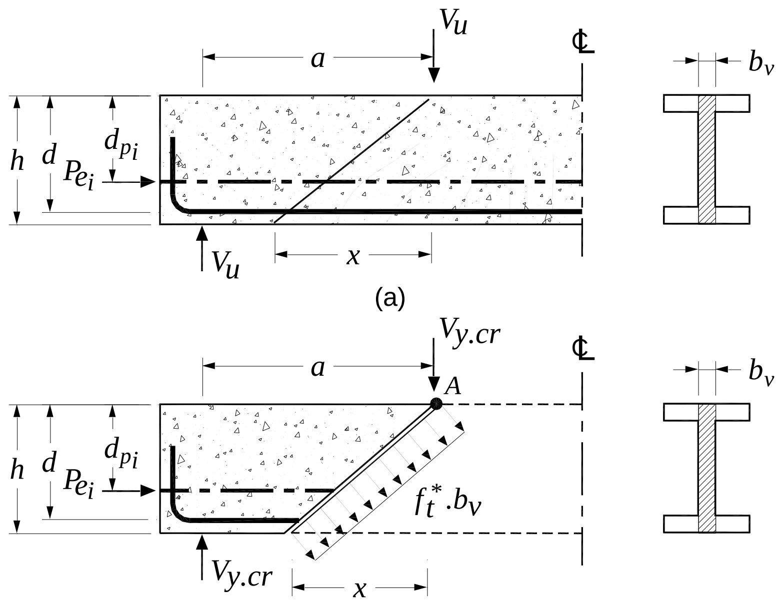

Fig. 12.2: Simply supported beam with critical diagonal crack: (a) yield line; (b) cracking load.

To determine the starting position of the critical crack, the ultimate shear (V_u) is taken as equal to the shear along at the diagonal crack yield surface ($V_{y.cr}$). For definition purposes, the diagonal crack strength ($V_{y.cr}$) is defined as the shear capacity of the beam when the diagonal crack is fully developed with a uniform effective tensile stress bridging the crack. For a simply supported beam under point loading, the diagonal crack shear is determined by taking the moment about the crack tip (marked A in Figure 12.2b) and is written as

$$V_{y.cr} = \frac{1}{2} f_t^* \, b_v \; \frac{h^2 + x^2}{a} + \frac{\sum P_{e_i} \, d_{p_i}}{a} \tag{12.8}$$

where d_{p_i} is the distance of the effective prestressing force (P_{e_i}) at the "i^{th}" level from the top surface of the beam, a is the shear span and f_t^* is the effective tensile strength of the SFRC. The solution for x is obtained by equating V_u given by Eq. (12.7) to $V_{y.cr}$ given in Eq. (12.8), giving

$$f_c^* \left(\sqrt{1 + \left(\frac{x}{h} \right)^2} - \frac{x}{h} \right) = f_t^* \frac{\left(x^2 + h^2 \right)}{ah} + \frac{2 \sum P_{e_i} d_{p_i}}{a b_v h} \quad .... \quad for \;\; 0 \le x \le a \tag{12.9}$$

with $f_t^* = \nu_t \, f_{tf}$ and $f_c^* = \nu_c \, f_{cm}$,where ν_t and ν_c are tensile and compressive strength effectiveness factors, respectively.

In modelling of their reactive powder concrete beams (RPC) with high volumes of steel fibres, Voo et al. (2006) took ν_t = 0.8 and ν_c = 0.8, which was later confirmed by Voo et al. (2010) as being appropriate for simply supported SFR-RPC beams. While the CSM-VEM model was not promoted by Voo et al. (2006) as a general model for FRC members with conventional quantities of steel fibres, it has been shown by Spinella et al. (2010) that the model can be calibrated for SFRC by empirically adapting the values for ν_t and ν_c appropriately. It needs to be noted, however, that Eq. (12.7) and, subsequently, Eq. (12.9), are only applicable for symmetrically point loaded simply supported reinforced beams and require reformulation for uniformly loaded beams (Zhang, 1997) and for continuous beams (Hoang and Nielsen, 1998). Thus, this approach is not pursued further here.

12.4 Shear in SFRC beams: 2010 draft Model Code Approach

Section 7.7, of the draft Model Code (2010) provides the following formula for the determination of the strength of SFRC beams without stirrups:

$$V_{Rd,F} = \left\{ \frac{0.18k}{\gamma_c} \left[100 \rho_l \left(1 + 7.5 \frac{f_{Ftuk}}{f_{ctk}} \right) f_{ck} \right]^{1/3} + 0.15 \sigma_{cp} \right\} b_w \, d \tag{12.10}$$

where γ_c is the partial safety factor for concrete, ρ_l is the reinforcement ratio, f_{Ftuk} is the tensile strength of the concrete assessed at the crack width w_u = 1.5 mm, f_{ck} is the compressive strength of the concrete, σ_{cp} is the average compressive stress on the section due to axial load or prestress (but taken as not greater than $0.2 f_{ck}/\gamma_c$), b_w is the width of the web, d is the effective depth of the section and k is a size effect parameter taken as

$$k = 1 + \sqrt{200/d} \le 2.0 \tag{12.11}$$

For further detail on the background of the draft Model Code shear provisions for SFRC beams without web reinforcement, the reader is referred to Minelli (2005) and Chapter 4 of this Bulletin. Eq. (12.10) is adapted from the Eurocode 2 provisions for beams that do not contain shear reinforcement and is empirical in nature. The approach of the draft Model Code considers fibres as contributing to the concrete component of the resistance of shear through a factor applied to the longitudinal reinforcement ratio. It should be noted, however, that in Eurocode 2 if the value of ρ_l exceeds 0.02, a value of ρ_l = 0.02 is entered into the equation and a similar limit should be applied to Eq. (12.10).

The predictions of Eq. (12.10) (with the limit of ρ_l = 0.02 included in Eq. (12.10)) are compared for 180 data on fibre reinforced concrete beams without stirrups collected from the literature, referred to as data Set A. For this dataset, only those beams that failed in a shear mode are included with beams failing at a load more than five percent greater than the flexural capacity predicted by AS3600 (2009) excluded. Details of the full dataset are provided in Table 1. For the cases in the literature where only concrete cube compression strengths are reported ($f_{c.cube}$), the equivalent cylinder strength is taken as $f_{ck} = 0.8 f_{c,cube}$. In the calculations, the tensile strength of the concrete at w = 1.5 mm was evaluated using the VEMI approach described above.

To provide a further assessment, a subset of 115 specimens (Set B) is considered with specimens excluded as follows: a/d <2.5, l_f/b < 2, f_{ck} > 70 MPa, non-rectangular in section. The exclusions are made to reduce scatter due to effects known to increase conservatism or for which the model was not specifically designed. That is, for a/d <2.5 arching action is significant, for l_f/b < 2 the boundary effect on fibre orientation should not be ignored and for f_{ck} > 70 MPa, cracking can be through aggregate particles lowering the concrete contribution to the shear strength.

The model predictions are plotted in Figure 12.3 for data Set A against the shear span to effective depth ratio, a/d, and against Set B for tensile stress provided by the fibres according to the VEMI for w = 1.5 mm. While the model is shown to generally perform well against the available data, it’s largely empirical development makes it inconsistent with the new approaches for shear adopted in Section 7.3.3 of the draft Model Code that look to physical models to describe behaviour. In the following section, an alternative model is proposed that is consistent with the shear design provisions of the code.

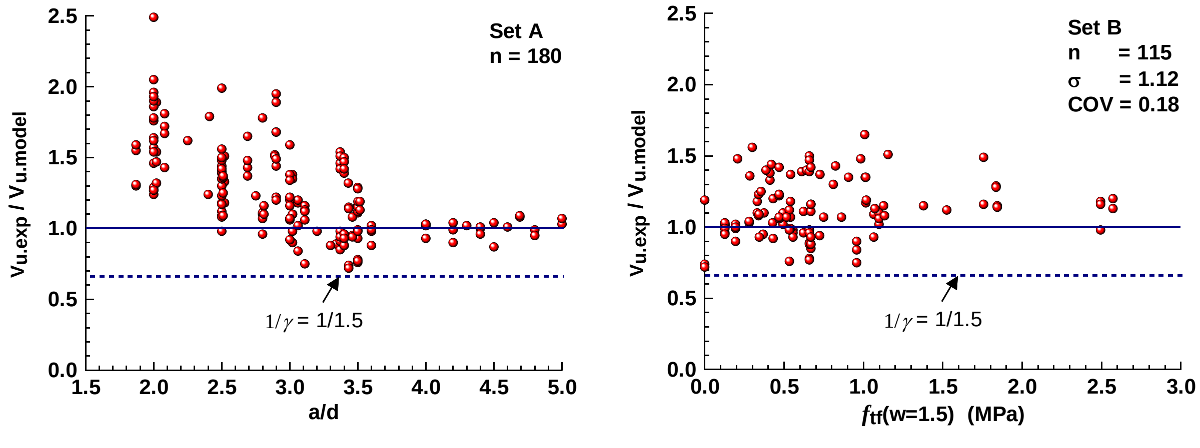

(a) (b)

Fig. 12.3: Comparison of Draft Mode Code (2010) model for SFRC beams against (a) a/d and (b) tensile stress at w = 1.5 mm.

Reference	Specimen
Batson et al. (1972)	C2, C3, D3, F2, G3, L1, L2, M1, M2, M3, N1, O1, P2, R1, R2, S1, X1, X2,
Muhidin and Regan (1977)	TLF3, TFL4
Robert and Ho (1982)	F3.0B1
Jindal (1984)	G-2.0, G-2.4, H-2.0
Swamy and Bahia (1985)	B52, B54
Uomoto et al. (1986)	ICW-0.75-B2, ICW-1.50-B2, ICW-1.50-B11, SF-0.75-B3, SF-0.75-B4, SF-0.75-B5, SF-0.75-B6, SF-0.75-B8, SF-1.50-B3
Mansur et al. (1986)	Beam B1, Beam B2, Beam B3, Beam C6, Beam E2, Beam E3
Lim et al. (1987)	2/0.5/2.5, 4/1.0/2.5, 4/1.0/3.5, 4/0.5/2.5, 4/0.5/3.5
Murty and Venkatacharyulu (1987)	A22, A23, A24, A25, B32, B33
Narayanan and Darwish (1987)	SF1, SF2, SF3, SF4, SF5, SF6, B1, B7, B9, B11, B12, B13, B16, B17, B18, B19, B20, B23, B24, B25, B26, B27, B28, B29, B30, B31
Kaushik et al. (1987)	B, C, D, E, F, G, H, I, J
Batson & Alguire (1987)	1, 2, 3
Li et al. (1992)	A-25-3-2.2-1, A-25-3-2.2-2, A-25-3-2.2-4, B-25-3-2.2-1, B-25-3-2.2-2, B-25-2-2.2 B-25-2.25-2.2, B-25-2.5-2.2, B-25-2.75-2.2, B-25-3-3.3, B-50-3
Swamy et al. (1993)	1TLF-1, 1TLF-2, 2TLF-1
Tan et al. (1993)	Beam 2, Beam 3, Beam 4, Beam 5
Imam et al. (1995)	B6, B7, B12
Casanova et al. (1997)	HSFRC1, HSFRC2
Adebar et al (1997)	FC2, FC8, FC9, FC10
Noghabai (2000)	3 Type B, 3 Type C, 4 Type C, 5 Type C – Mix, 6 Type C – Mix, 7 Type C, 8 Type C, 9 Type C, 10 Type C, 2 Type D, 3 Type D – Mix, 4 Type D
Barragan (2002)	B20x30S1, B20x30S2, B20x45S1, B20x50S2, B20x60S1, B20x60S2, T10x50S1, T10x50S2, T15x50S1, T15x50S2, T23x50S2, T15x75S1, T15x100S1
Rosenbusch & Teutsch (2002)	1.2/2, 1.2/3, 1.2/4, 2.3/2, 2.3/3, 2.4/2, 2.4/3, 2.6/2, 20x30-SFRC-1, 20x45-SFRC-1, 20x60-SFRC-1, T10x50-SFRC-1, T15x50-SFRC-1, T15x75-SFRC-1, T15x100-SFRC-1, 20x30-SFRC-2, 20x50-SFRC-2, T10x50-SFRC-2, T15x50-SFRC-2, T23x50-SFRC-2
Cucchiara et al. (2004)	B10, B11, B20
Balázs& Kovács (2004)	RC-A2
Minelli et al. (2005)	NSC1-FRC1, NSC2-FRC1, NSC3-FRC1, HSC-FRC1
Para-Montesinos et al. (2006)	Beam 4, Beam 7, Beam 9, Beam 10, Beam 11
Dinh et al. (2010)	B18-0a, B18-0b, B18-2d, B18-3a, B18-5a, B27-4b, B27-7

Table 12.1: SFR concrete beams failing in shear (and not limited by flexural strength).

It is worthy of note that at the boundary of Eq. (12.10) for $\rho_f = 0$, the model reverts to the approach of Eurocode 2. In Figure 12.4, the data set used by Bentz in Chapter 2 to assess the various models in Section 7.3.3 of the draft code is used to assess the condition of $\rho_f = 0$ in Eq. (12.10) (note that for $\rho > 0.02$, a value of 0.02 is used in Eq. (12.10)). The data set is limited to 1282 specimens with $a/d \geq 2.5$. It is observed that the model gets progressively less conservative as a/d increases. This was observed for the Eurocode 2 model by Bentz and Collins (2008). This is important in that at low fibre volumes, the data scatter for SFRC cannot be better than that of plain concrete.

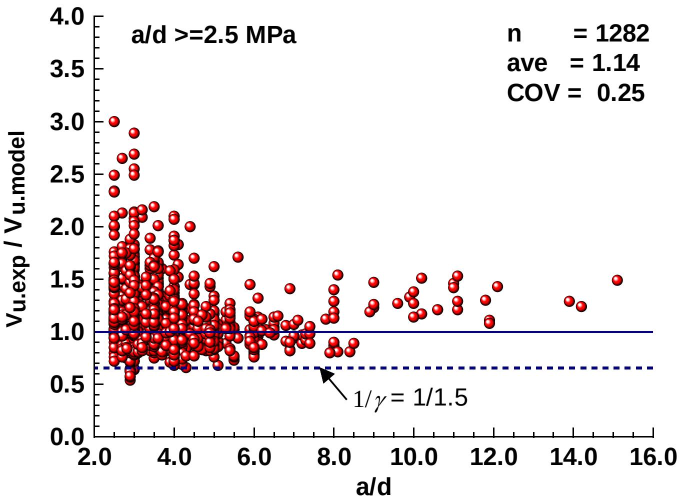

Fig. 12.4: Comparison of the Code Draft (2010) model for SFRC beams with zero fibres.

12.5 A consistent approach for design of shear in SFRC Beams

In Chapter 3, it was shown that the critical shear crack theory of Muttoni (2008), which forms the basis of the punching shear provisions of the draft Model Code, could be supplemented with the VEM to provide a physical model for design of SFRC slabs in two-way shear. A similar approach is developed here. The draft Model Code adopts a tiered approach for the design for shear, with Level III being the highest level for routine design and Levels II and I providing for increasing levels of approximation. The Level III model, based on the simplified Modified Compression Field Theory (MCFT) approach of Bentz et al. (2006), is used here together with the VEMI as the basis for the proposed model for SFRC beams and one-way slabs.

Codes of practice such as ACI-318 (2008), Eurocode 2 (2004), AS3600 (2009) and others generally adopt a semi-rational approach for the design of beams for shear. In these models, the total shear is resisted partially by a component taken by the concrete (V_{uc}) and a component taken by the reinforcing steels (V_{us}), with V_{uc} generally determined through empirical means and V_{us} obtained by a truss model. RILEM (2000) recommended that a similar approach be applied to steel fibre reinforced concrete beams with the shear resistance calculated by

$$V_{Rd} = V_{Rd,c} + V_{Rd,s} + V_{Rd,f} \geq V_{Ed} \tag{12.12}$$

where $V_{Rd,f}$ is the contribution of the fibres and the other terms are as presented in Chapter 2. An inspection of the Level III model and the VEM, however, shows that the contributions of the concrete $V_{Rd,c}$ and fibres $V_{Rd,f}$ are coupled, as each are a function of the width of the critical shear crack (Figure 12.5) and, thus, must be solved simultaneously.

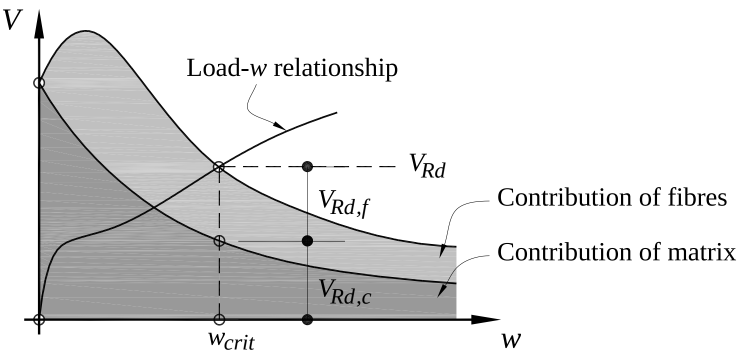

Fig. 12.5: Coupling of matrix and fibres components for determination of shear capacity.

The Level III model adopted for the draft code is described by Bentz in Chapter 2 of this Bulletin where, provided that web crushing does not control the design, the steel and concrete components are given, respectively, by

$$V_{Rd,s} = \frac{A_{sw}}{s_w} z f_{ywd} \left(\cot\theta + \cot\alpha\right)\sin\alpha \tag{12.13}$$

$$V_{Rd,c} = k_v \frac{\sqrt{f_{ck}}}{\gamma_c} b_w z \tag{12.14}$$

where A_{sw} and s_w are the cross sectional area of shear reinforcement and the spacing of the reinforcement, respectively, z is the internal moment lever arm (and is taken as z = 0.9d), f_{ywd} is the design strength of the web reinforcing steel, θ and α are the angles of the compressive strut and the reinforcing steel relative to the longitudinal axis of the member, respectively, and k_v is a parameter that determines the capacity of the web to resist the aggregate interlock stresses that provide the concrete contribution to the shear strength:

$$k_v = \frac{0.4}{(1+1500\varepsilon_x} \cdot \frac{1300}{1000+0.7k_{dg}z} \quad (\text{for } \rho_w = 0) \tag{12.15}$$

where

$$\begin{aligned} k_{dg} &= \frac{48}{16+d_g} \geq 1.15 && \text{for } f_c' \leq 70\,\text{MPa} \\ &= 3.0 && \text{for } f_c' \leq 70\,\text{MPa and for light-weight concrete} \end{aligned} \tag{12.16}$$

and d_g is the maximum size of the aggregate particles.

In the development of this model, it was shown that the crack width at the mid-height on the section may be simplified to

$$w = 0.2 + 1000\,\varepsilon_x \geq 0.125\,\text{mm} \tag{12.17}$$

where ε_x is the longitudinal strain calculated at the mid-depth of the member:

$$\varepsilon_x = \frac{M_{Ed}/z + 0.5V_{Ed}\cot\theta + 0.5N_{Ed} - A_p f_{po}}{2(E_s A_s + E_p A_p)} \tag{12.18}$$

In Eq. (12.18), M_{Ed}, V_{Ed}, and N_{Ed}, are the stress resultants determined from the factored design loads, A_s and A_p are the cross-sectional areas of the reinforcing and prestressing steels, respectively, E_s and E_p are the elastic moduli of the reinforcing and prestressing steels, respectively, and f_{p0} is the stress in the prestressing strands when the strain in the adjacent concrete is zero. The angle θ in Eqs. (12.13) and (12.18) is taken as

$$\theta = 29^{\text{o}} + 7000\,\varepsilon_x \tag{12.19}$$

In Chapter 3 of this Bulletin, Muttoni and Ruiz demonstrated that fibre component stresses may be integrated across the critical crack to determine the fibre contribution to the shear capacity. As a simplification, the average stress maybe determined and multiplied by the area of the failure surface. As such, the fibre component may be determined through the VEM with the model as described in Figure 12.6 giving

$$V_{Rd,f} = k_{fd}\,f_{tf}(w)\,b_w\,z\cot\theta \tag{12.20}$$

where k_{fd} is a fibre dispersion reduction factor, taken as k_{fe} = 0.82. This factor takes into account deviations in the crack path around fibre ends where the location of the crack is not fixed by the specimen geometry (Htut, 2010). The factor was obtained through X-ray image analysis and represents the average stress factor for a critical crack forming along the path of least resistance.

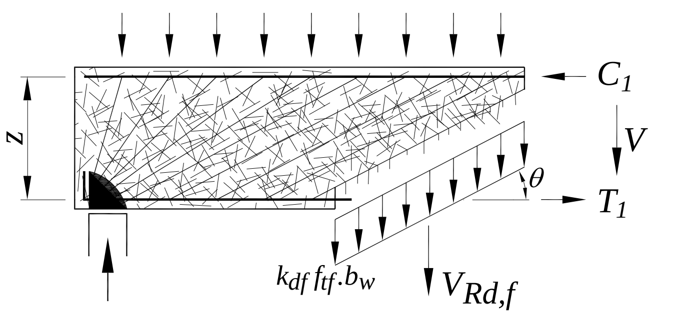

Fig. 12.6 : Fibre reinforcement component for SFR beams failing in shear.

Consistent with the Level III model, we adopt the crack width at the mid-depth of the section to determine the average fibre component stress contribution. The solution is then iterated through Eqs. (12.13) to (12.19), with the fibres component obtained from Eqs. (12.1) to (12.5).

12.6 Assessment of proposed model

The model for determining the strength of SFRC beams in shear developed in the previous section is assessed against the database outlined in Table 12.1 and the results presented in Figure 12.7. Figure 12.7(a) compares the full data set against the shear span to depth ratio and a reasonable correlation is observed, especially when compared to that of the Level III model presented in Chapter 2. In Figure 12.7(b) and (d)-(f), the results of the reduced data set (Set B described above) are compared to the overall depth of the member, the tensile strength provided by the fibres at the predicted critical crack opening displacement, the crack width corresponding to the ultimate load and the longitudinal strain measured at the specimen mid-depth, respectively. It is seen that when compared to the predictions outlined in Chapter 2 for the Level III model, the Level III model with the VEM adopted for the fibres contribution correlates well (mean of 1.07 and COV of 0.16) and without bias. In Figure 12.7(c) the data of Set B is complemented with data for high strength concrete (f_{cm} > 70 MPa) and denoted as Set C. Again a reasonable correlation is observed but it is noticed that the higher strength concrete data is biased towards the conservative side. This reflects the conservative nature of the assumption of $d_g = 0$ in Eq. (12.16) for concrete strengths exceeding 70 MPa.

12.7 Minimum shear reinforcement

ACI-318 (2008) allows for steel fibres to contribute to the minimum shear resistance of beams, replacing conventional reinforcing steel stirrups. The rules, however, are quite prescriptive, apply only to deformed fibres of $\rho_f \geq 0.75\%$ or require testing of a fibre reinforced concrete mix to establish its performance criteria. The draft Model Code, on the other hand, does not specify the fibre type or volume directly but, rather, that the minimum strength provided by the fibres at a crack width of w_u = 1.5 mm must exceed a threshold value given by

$$f_{Ftuk} \geq 0.05\sqrt{f_{ck}} \tag{12.21}$$

Adopting the VEM for the stress versus crack opening displacement relationship, then with f_{ck} = 40 MPa and 30 mm end hooked steel fibre of 0.5 mm diameter (α_f = 30/0.5 = 60, k_b = 0.8) and fibre strength of σ_{fu} = 1000 MPa, the quantity of fibres needed to satisfy Eq. (12.21) is ρ_f = 0.0067 (0.67%), slightly less than that prescribed by ACI-318. Note that a check of the critical fibre length shows that: $\tau_b = 0.8\sqrt{40}$ = 5.1 MPa, the critical fibre length for pullout is $l_{crit} = 0.5 \times 1000/(2 \times 5.1)$ = 49 mm and, therefore, the fibres proposed are satisfactory. It is also worthy of note that as the fibre-matrix bond strength in the VEMI is taken to be a function of $\sqrt{f_{ck}}$, with the VEMI Eq. (12.21) becomes a function of the fibre type (end-hooked, straight, etc.) and the fibre aspect ratio α_f .

To be consistent with of the minimum fibre volume required by Clause 7.13.5.2 of the draft Model Code, the coefficient term in Eq. (12.21) would be 0.12. In this case, the quantity of fibres required would be ρ_f = 0.016 (1.6%). Clearly, this quantity of fibres is too high and not consistent with the observations of others (Parra-Montesinos, 2006)! Looking at the Australian model for shear (AS3600, 2009), the minimum allowed steel shear reinforcement is

$$f_{Ftuk} \geq 0.06\sqrt{f_{ck}} \tag{12.22}$$

but taken as not less than 0.35 MPa. For the example considered above, this equates to a minimum volume of fibres of $\rho_f = 0.0085$ (0.85%). It is concluded that the minimum quantity of shear reinforcement as required by Clause 7.13.5.2 of the draft Model Code needs revision. Further, the minimums required by the clause on minimum shear reinforcement and Clause 7.7.3.2.4 on minimum fibre reinforcement for shear need to be made consistent.

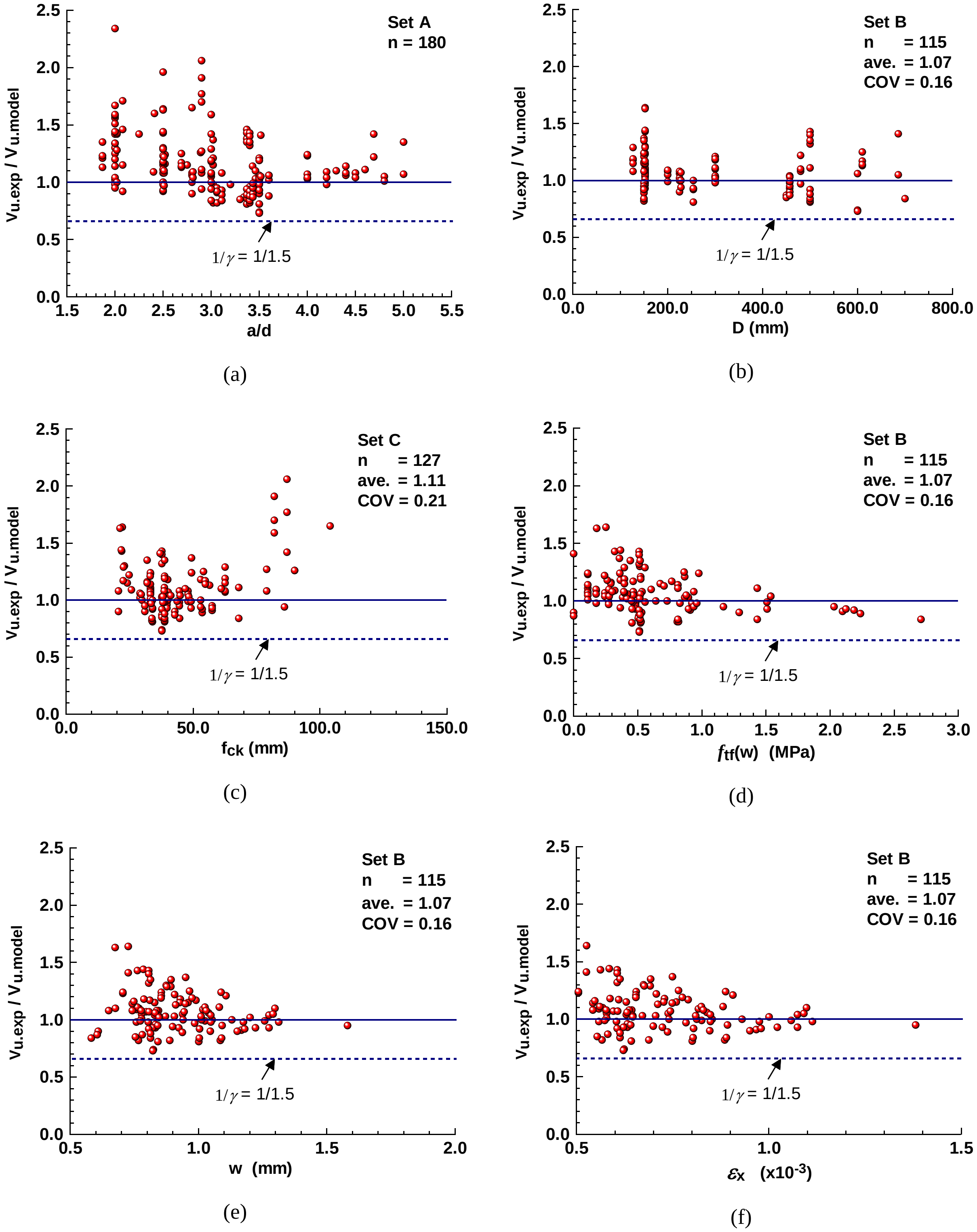

Fig. 12.7: Comparison of proposed SFRC model Draft Mode Code (2010) model for SFRC beams against (a) a/d, (b) overall depth, (c) concrete strength, (d) fibre component stress, (e) crack width at the formation of critical crack and (f) mid-depth longitudinal strain.

12.8 Conclusions

The paper presents a model for the design of steel fibre reinforced concrete beams in shear and compares the model in the draft Model Code. It is noted that the models for conventionally reinforced concrete and SFRC are inconsistent at their boundary (ie at $\rho_f = 0$) and an alternative model is proposed that is consistent with the Level III model described in the draft code for conventionally reinforced beams in shear. The fibre reinforced component is obtained using the variable engagement model approach of Voo and Foster (2003, 2004) to describe the tensile stress versus crack opening displacement of fibre reinforced concrete. A third model based on an upper-bound approach was described, but not perused in depth in this paper due to its complexity in providing of a generalised solution for routine design.

The empirically derived model presented in the draft Model Code treats the fibres as additional longitudinal reinforcement in the context of the current Eurocode 2 equation. While the model provides a reasonable correlation to the available data for SFRC beams failing in shear, for members with low volumes of fibres it can provide a correlation no better than that of the Eurocode model.

The draft Model Code adopts a tiered approach to design for shear, with higher level models generally providing for more accurate solutions. In reviewing the Level III model for shear and the behaviour of SFRC, it is shown that the concrete and fibre components are coupled by the critical crack opening displacement at the point of failure. In this case the two components cannot be treated separately and an additional equation is needed in the solution to describe the fibre contribution as a function of the critical crack width. This can either be found experimentally, as shown by Muttoni and Ruiz in Appendix A of Chapter 3 of this Bulletin, or by using an appropriate model to describe the tensile σ-w relationship of SFRC, such as the VEMI. A comparison of the data available for beams failing in shear indicates a good correlation using this approach with the data scatter not dissimilar to that indicated by Bentz in Chapter 2 for the concrete component alone. It is, thus, recommended that the approach for the design of SFRC beams be made consistent with that of the general approach for the design of beams in shear presented in Section 7.3.3 of the draft Model Code.

Finally, in this paper the minimum reinforcement requirements for SFRC and for conventionally reinforced concrete are reviewed. It is observed that there is an inconsistency with the minimum shear contribution provided by the steel or fibre steel reinforcement in the two approaches. In this context, the minimum conventional shear reinforcement and fibre reinforcement models need to be reviewed.

12.9 References

ACI-318, 2008. “Building Code Requirements for Structural Concrete and Commentary”, ACI Committee 318, 456 pp.

Adebar, P., Mindess, S., Pierre, D. S., and Olund, B., 1997. “Shear Tests of Fiber Concrete Beams without Stirrups”, ACI Structural Journal, Vol. 94, No. 1, pp: 68-76.

AS3600, 2009. “Concrete Structures”, Australian Standard, Standards Association of Australia.

Balázs, G. L., and Kovács, I., 2004. “Effect of Steel Fibres on the Cracking Behaviour of RC Members”, Proceeding of the 6th RILEM Symposium on Fibre-Reinforced Concrete (FRC) – BEFIB 2004, Varenna, Italy, September, pp: 1007-1017.

Barrangan, B. E., 2002. “Failure and Toughness of Steel Fiber Reinforced Concrete under Tension and Shear”, PhD. Thesis, Universitat Politecnica de Catalunya, March.

Batson, G. B., and Alguire, C., 1987. "Steel Fibers as Shear Reinforcement in Reinforced Concrete T-Beams", Proceedings of the International Symposium on Fibre Reinforced Concrete, Madras, India, December, pp: 1.113-1.123.

Batson, G., Jenkins, E., and Spatney, R., 1972. "Steel Fibers as Shear Reinforcement in Beams", ACI Journal, Vol. 69, No. 10, October, pp: 640-644.

Bentz, E.C., Vecchio, F.J., and Collins, M.P., 2006, "The Simplified MCFT for Calculating the Shear Strength of Reinforced Concrete Elements", ACI Structural Journal, Vol. 103, No. 4, pp: 614-624.

Bentz, E.C., and Collins, M.P., 2008, "Comparing EC2, ACI, and CSA Shear Provisions to Test Results", Proceedings of International *fib* Symposium, Taylor Made Concrete Structures – New Solutions for Our Society, Amsterdam, Netherlands, 19-22 May.

Casanova, P., Rossi, P., and Schaller, I., 1997. "Can Steel Fibers Replace Transverse Reinforcements in Reinforced Concrete Beams?" ACI Materials Journals, Vol. 94, No. 5, Sept-Oct, pp: 341-354.

Cucchiara, C., Mendola, L. L., and Papia, M., 2004. "Effectiveness of Stirrups and Steel Fibres as Shear Reinforcement", Cement & Concrete Composites, Vol. 26, pp: 777-786.

Eurocode 2, 2004 (EN 1992-1-1:2004), "Design of Concrete Structures - Part 1-1: General Rules and Rules for Buildings", European-Commission.

Dinh, H.H., Parra-Montesinos, G.J., and Wight, J.K., 2010. "Shear Behavior of Steel Fiber-Reinforced Concrete Beams without Stirrup Reinforcement", ACI Structural Journal, Vol. 107, No. 5, pp: 597-606.

fib draft Model Code, 2010. "Model Code 2010: First Complete Draft", Bulletins 55 and 56, Fédération Internationale du Béton (*fib*).

Foster S.J., 2009. "The Application of Steel-Fibres as Concrete Reinforcement in Australia: from Material to Structure", Materials and Structures, Vol. 42, No. 9, November, pp: 1209-1220.

Foster, S.J., Voo, Y.L., and Chong K.T., 2006. Chapter 5 "Analysis of Steel Fiber Reinforced Concrete Beams Failing in Shear: Variable Engagement Model", in Finite Element Analysis of Reinforced Concrete Structures, Eds. Lowes, L., and Filippou, F., ACI SP-237.

Furlan Jr., S., and de Hanai, J. B., 1997. "Shear Behaviour of Fiber Reinforced Concrete Beams", Cement and Concrete Composites, Vol. 19, pp: 359-366.

Hoang, L.C. and Nielsen, M.P., 1998. "Plasticity Approach to Shear design", Cement and Concrete Composites, Vol.20, pp: 437-453.

Htut, T.N.S., 2010. "Fracture Processes in Steel Fibre Reinforced Concrete", PhD Thesis, School of Civil and Environmental Engineering, The University of New South Wales, 389 pp.

Htut, T.N.S. and Foster S.J., 2010. "Unified Model for Mixed Mode Fracture of Steel Fibre Reinforced Concrete", Fracture Mechanics of Concrete and Concrete Structures, Fiber Reinforced Concrete, Vol. 3, B. H. Oh, et al. (eds), Proceedings of the 7th International Conference on Fracture Mechanics Concrete and Concrete Structures (FramCoS-7), Jeju, Korea, May 23-28, 2010, pp: 1469-1477.

Imam, M., Vandewalle, L., and Mortelmans, F., 1995. "Shear-Moment Analysis of Reinforced high Strength Concrete Beams Containing Steel Fibres", Canadian Journal of Civil Engineering, Vol. 22, pp: 462-470.

Jindal, R. L., 1984. "Shear and Moment Capacities of Steel Fiber Reinforced Concrete Beams", Fiber Reinforced Concrete, SP-81-1, American Concrete Institute, Detroit, pp: 1-16.

Kaushik, S. K., Gupta, V. K., and Tarafdar, N. K., 1987. "Behaviour of Fiber Reinforced Concrete Beams in Shear", Proceedings of the International Symposium on Fibre Reinforced Concrete, Madras, India, December, pp: 1.133-1.149.

Lee, G.G. and Foster, S.J., 2007. "Behaviour of Steel Fibre Reinforced Mortar III: Variable Engagement Model II", UNICIV Report R-448, The University of New South Wales, School of Civil and Environmental Engineering, Kensington, Sydney, Australia, September, ISBN: 85841 415 5, 106 pp.

Lee, G.G. and Foster, S.J., 2008. "Modelling of Shear-Fracture of Fibre-Reinforced Concrete", Proceedings of International *fib* Symposium, Taylor Made Concrete Structures – New Solutions for Our Society, Amsterdam, Netherlands, 19-22 May.

Li, V. C., Ward, R., and Hamza, A. M., 1992. "Steel and Synthetic Fibers as Shear Reinforcement" ACI Material Journal, Vol. 89, No. 5, September-October, pp: 499-508.

Lim, T. Y., Paramasivam, P., and Lee, S. L., 1987. "Shear and Moment Capacity of Reinforced Steel-Fiber-Concrete Beams", Magazine of Concrete Research, Vol. 39, No. 140, September, pp: 148-160.

Mansur, M. A., Ong, K. C., and Paramasivam, P., 1986. "Shear Strength of Fibrous Concrete Beams without Stirrups", Journal of Structural Engineering, ACSE, Vol. 112, No. 9, September, pp: 2066-2079.

Minelli, F., 2005. "Plain and Fiber Reinforced Concrete Beams under Shear Loading: Structural Behavior and Design Aspects", Ph.D. Thesis, Department of Civil Engineering, University of Brescia, February 2005, pp: 422.

Minelli, F., Balázs, G. L., Kovács, I., and Plizzari, G. A., 2005. "Design Aspects for Shear in SFRC Beams", Proceedings of *fib* Symposium "Keep Concrete Attractive", Budapest, pp: 316-321.

Muhidin, N. A., and Regan, P.E., 1977. "Chopped Steel Fibres as Shear Reinforcement in Concrete Beams", Fibre Reinforced Materials, Institution of Civil Engineers, London, pp: 149-163.

Murty, D. S. R., and Venkatacharyulu, T., 1987. "Fibre Reinforced Concrete Beams Subjected to Shear Force", Proceedings of the International Symposium on Fibre Reinforced Concrete, Madras, India, December, pp: 1.125-1.132.

Muttoni A., 2008. "Punching shear strength of reinforced concrete slabs without transverse reinforcement", ACI Structural Journal, Vol. 105, No. 4, pp: 440-450.

Narayanan, R., and Darwish, I. Y. S., 1987. "Shear in Prestressed Concrete Beams Containing Steel Fibres", The International Journal of Cement Composites and Lightweight Concrete, Vol. 9, No. 2, May, pp: 81-90.

Noghabai, K., 2000. "Beams of Fibrous Concrete in Shear and Bending: Experiment and Model", Journal of Structural Engineering, February, pp: 243-251.

Parra-Montesinos, G. J., 2006. "Shear Strength of Beams with Deformed Steel Fibers: Evaluating an Alternative to Minimum Transverse Reinforcement", Concrete International, November, pp: 57-67.

RILEM TC 162-TDF, 2000. "Test and design methods for steel fibre reinforced concrete: Recommendations, σ-ε-design method, Materials and Structures, Vo. 33, No. 226, pp. 75-81

Robert, T. M., and Ho, N. L., 1982. "Shear Failure of Deep Fiber Reinforced Concrete Beams", International Journal of Cement Composites and Lightweight Concrete (Harlow), Vol. 4, No. 3, August, pp: 145-152.

Romualdi, J.P., and Batson, G.B., 1963. "Behaviour of Reinforced Concrete Beams with Closely Spaced Reinforcement," Journal of the American Concrete Institute, Proceedings V. 60, No. 6, June, pp. 775-789.

Rosenbusch, J., and Teutsch, M., 2003. "Shear Design with σ-ε-Method", Proceedings of the RILEM TC 162-TDF Workshop: Test and Design Methods for the Steel Fibre Reinforced Concrete-Background and Experiences, Bochum, Germany, pp: 105-118.

Spinella, N., Colajanni, P., and Recupero, A., 2010, "Simple Plastic Model for Shear Critical SFRC beams", ASCE, Journal of Structural Engineering, Vol. 136, No. 4, pp. 390-400.

Swamy, R. N., and Bahia, H. M., 1985. "The Effectiveness of Steel Fibers as Shear Reinforcement", Concrete International, Vol. 7, No. 3, March, pp: 35-40.

Swamy, R. N., Jones, R., and Chiam, A. T. P., 1993. "Influence of Steel Fibers on the Shear Resistance of Lightweight Concrete I-Beams", ACI Structural Journal, Vol. 90, No. 1, January-February, pp: 103-114.

Tan, K. H., Murugappan, K., and Paramasivam, P., 1993. "Shear Behaviour of Steel Fiber Reinforced Concrete Beams", ACI Structural Journal, Vol. 89, No. 6, pp: 3-11.

Uomoto, T., Weeraratne, R. K., Furukoshi, H., and Fujino, H., 1986. "Shear Strength of Reinforced Concrete Beams with Fibre Reinforcement", RILEM Symposium on the Developments in Fibre Reinforced Cement and Concrete, July, Vol. 2, paper 8.7, pp: 10.

Voo Y.L., Poon W.K., Foster, S.J., 2010, "Shear Strength of Steel Fiber-Reinforced Ultrahigh-Performance Concrete Beams without Stirrups", ASCE, Journal of Structural Engineering, Vol. 136, No. 11, 2010, pp. 1393-1400.

Voo, J.Y.L. and Foster, S.J., 2003. "Variable Engagement Model for Fibre Reinforced Concrete in Tension", UNICIV Report R-420, School of Civil and Environmental Engineering, The University of New South Wales, Sydney, Australia, June, ISBN: 85841 387 6, 86 pp.

Voo, J.Y.L. and Foster, S.J., 2004. "Tensile Fracture of Fibre Reinforced Concrete: Variable Engagement Model", Sixth Rilem Symposium on Fibre Reinforced Concrete (FRC), Varenna, Italy, 20-22 September, pp: 875-884.

Voo Y.L. and Foster S.J., 2009. "Reactive Powder Concrete: Analysis and Design of RPC Girders", Lambert Academic Publishing, 364 pp, ISBN. 978-3-8383-2406-7.

Voo, Y.L., Foster, S.J., and Gilbert, R.I., 2006. "Shear Strength of Fibre Reinforced Reactive Powder Concrete Prestressed Girders without Stirrups", Journal of Advanced Concrete Technology, Japanese Concrete Institute, Vol. 4, No. 1, pp: 123-132.

Zhang, J.P., 1994. "Strength of Cracked Concrete: Part 1 – Shear Strength of Conventional Reinforced Concrete Beams, Deep Beams, Corbels, and Prestressed Reinforced Concrete Beams without Shear Reinforcement", Report No. 311, Technical University of Denmark, Department of Structural Engineering, Lyngby, 106 pp.

Zhang, J.P., 1997. "Diagonal Cracking and Shear Strength of Reinforced Concrete Beams", Magazine of Concrete Research, Vol. 49, No. 178, March, pp. 55-65.

13 Shear strength of FRC members with little or no shear reinforcement: a new analytical model

Fausto Minelli and Giovanni A. Plizzari

DICATA - Department of Civil, Architectural, Environmental and Land Planning Engineering
University of Brescia, Italy

Abstract: This paper firstly reports some recent results of an experimental campaign on Fiber Reinforced Concrete (FRC) beams under shear loading tested at the University of Brescia: nine full scale beams, having a height varying from 500 to 1500 mm, were tested for investigating the effect of steel fibers on key-parameters influencing the shear response of concrete members, with special emphasis on FRC toughness and size effect. All tested members contained no conventional shear reinforcement. Results show that a relatively low volume fraction of fibers can significantly increase loading capacity and ductility. The latter determines visible deflection and prior warning of impending collapse, which is not possible in plain concrete beams (without transverse reinforcement). The size effect issue is substantially limited and it is shown that, with a rather tough FRC composite, it is possible to completely eliminate this detrimental effect. In addition, an analytical model for predicting the shear strength of FRC members is derived, based on an extension of the Simplified Modified Compression Field Theory (SMCFT) to materials having a not negligible toughness, as for FRC. The enhanced toughness is modelled in terms of modification of the tension stiffening, tension softening and crack spacing, all governing the behaviour of cracked members under shear. The proposed model aims at being a useful tool for design.

13.1 Introduction

A significant change in the shear and punching shear provisions, included in the first draft of *fib* Model Code (2010), referred to in the following as MC2010, which was officially presented during the *fib* Congress in Washington D.C., can be outlined. Four different approximation levels are proposed for designing shear members, incorporating statements and models well recognized such as Modified Compression Field Theory [Vecchio and Collins (1986)] and the variable truss angle theory. The equations have been defined with a basic structure that requires two significant parameters, namely the angle of inclination of the stress field, θ, and a coefficient for a concrete contribution k_v (more often referred as β). The MC2010 first draft provides three levels of approximation to calculate these terms with the first and third based on the MCFT and the second based on a strain-modified form of plasticity. As the level of approximation increases, the quality of the predictions improves, but with more complex calculations (as extensively explained in Chapter 2 of this bulletin).

The shear workshop held in Salò on October 15-16, 2010 provided an opportunity to discuss the new approaches and verify how they meet or diverge from one another. Moreover, it is of paramount importance to foresee the implications that the new models may determine in the field and in structural design and applications. In the workshop, both the shear behaviour of reinforced concrete (RC) and fiber reinforced concrete (FRC) elements was discussed.

The behaviour and design of reinforced concrete (RC) members subjected to shear remain an area of much concern in spite of the vast number of experiments that have been conducted to assess the shear capacity of structural concrete members. Design codes are frequently changed and generally becoming more stringent, so that structures that were designed several decades ago typically do not comply with the requirements of current codes. A consensus concerning mechanisms of shear transfer and the interpretation of collapse modes for members without web reinforcement that fail in shear are still missing. It remains a pressing need to establish design and analysis methods that provide realistic assessments of the strength, stiffness and ductility of structural elements subjected to shear loading [ASCE-ACI Committee 445 (1998) and Vecchio (2000)].

Several reports published over the past 25 years confirm the effectiveness of steel fibers as shear reinforcement. Fibers are used to enhance the shear capacity of concrete or to partially or totally replace stirrups in RC structural members [Imam et al. (1997)]. This relieves reinforcement congestion at critical sections such as beam-column junctions in seismic applications. Fiber reinforcement may also significantly reduce construction time and costs, especially in areas with high labour costs, and possibly even labour shortages, since stirrups involve relatively high labour input to bend and fix in place. Fiber concrete can also be easily deployed in thin or irregularly shaped sections, such as architectural panels, where it may be very difficult to place stirrups. This is of paramount significance for many secondary structural elements in which a minimum conventional reinforcement is not required for equilibrium.

Many studies [Imam et al. (1997), Casanova et al. (1997), Khuntia et al. (1999), Swamy et al. (1993), Lim and Oh (1999), Gustafsson and Noghabai (1999), Choi et al. (2007) and Dinh et al. (2010)] produced a number of experimental researches on the shear resistance of Steel Fiber Reinforced Concrete (SFRC) and also defined new equations for predicting the ultimate shear strength of SFRC beams. Even though these studies can be certainly considered a good advancement for understanding the shear behaviour of SFRC members, many of them are characterized by tests on beams of special geometry with a limited range of crucial parameters and conditions (concrete class, fiber geometry, content and composition, size, longitudinal and transverse reinforcing ratio) being investigated. In addition, most of the experiments are characterized by a depth smaller than 500 mm.

In this respect, 9 out of more than 30 experimental tests on full-scale SFRC beams (with a height up to 1.5 m) are presented in this paper, which focus on the fiber's role in delaying shear crack localization, in mitigating the size effect and in allowing a stable crack development with associated load and ductility increases. Moreover, an extension of the SMCFT [Bentz et al. (2006)] to FRC beams undergoing shear is proposed, to the aim of defining a number of requirements useful for structural and safe shear design of FRC members. First attempts can be seen in Minelli (2005), Minelli and Plizzari (2006), in the recent Italian Standard for FRC structures DT 204 (2006) and in the first draft of the *fib* Model Code (2010). Since FRC is a concrete with higher toughness that cannot be neglected, as generally assumed in plain concrete (PC), a unique shear design approach should be pursued both for FRC (toughness considered) and PC (toughness neglected). With this assumption, a physical model will be herein proposed as an advancement of the previous well established procedures available in the literature.

13.2 Recent tests on full scale shear-critical beams: can fibers mitigate the size effect in shear?

In the following, the main results from experiments on nine full-scale beams tested under a three point loading system and a shear span-to-depth ratio a/d of 3 will be presented and discussed. Beams were made with different amounts of steel fibers: 0, 50 and 75 kg/m^3 (corresponding to a volume fraction of 0, 0.64 and around 1%, respectively) and, for each fiber content, three beams with different depths were cast: 500 mm (beams H500), 1000 mm (beams H1000) and 1500 mm (beams H1500). All beams had the same width of 250 mm and gross cover (60 mm). Different effective depths were therefore obtained: 440, 940 and 1440 mm, respectively for specimens H500, H1000 and H1500.

Fig. 13.1 illustrates the geometry of the specimens and the reinforcement details. Longitudinal reinforcement was positioned in two layers and the reinforcement ratio was approximately 1% for all test specimens. 8Φ14, 8Φ20 and 8Φ24 deformed bars were placed respectively in H500, H1000 and H1500 beams.

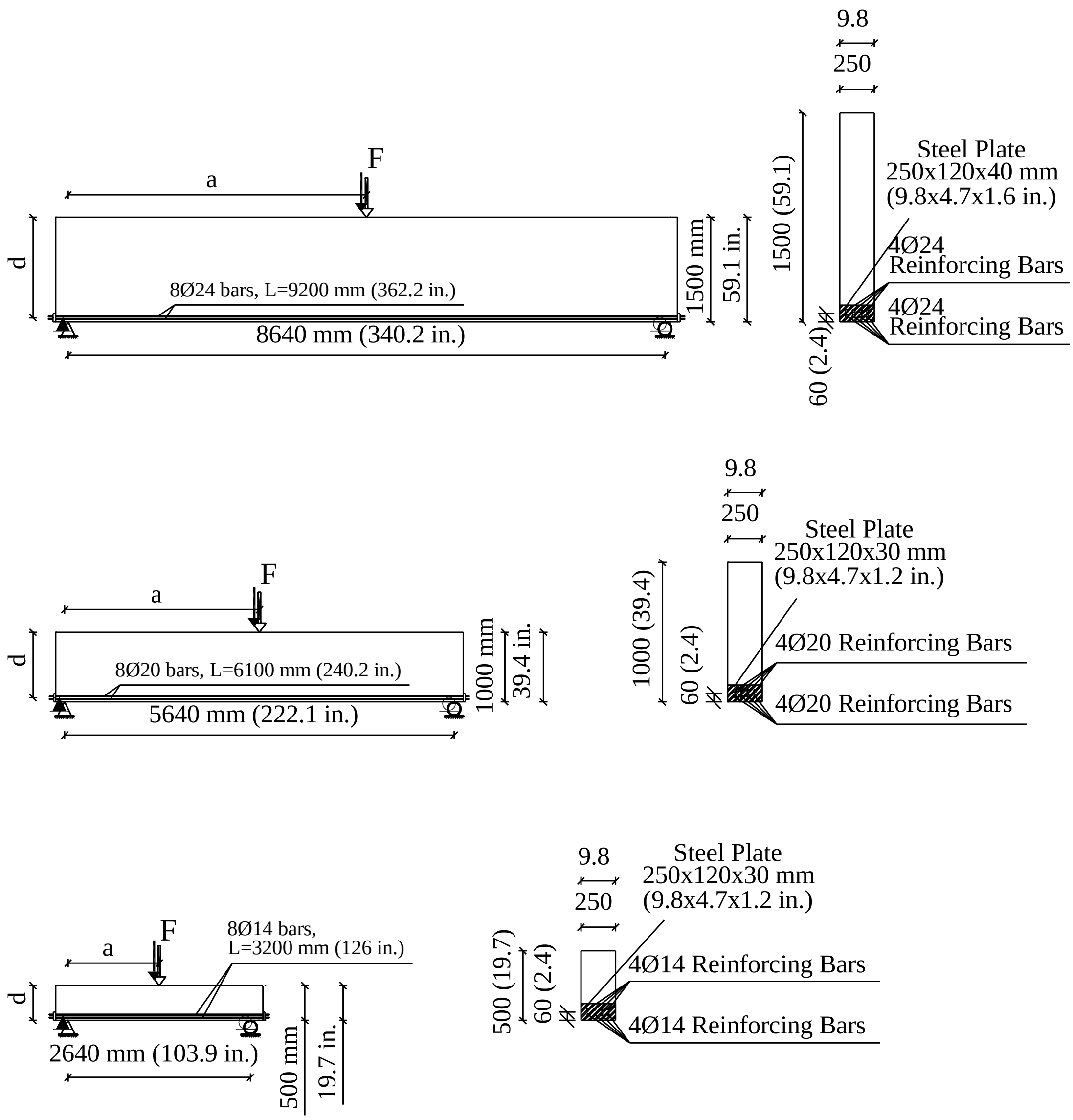

Fig. 13.1: Geometry and reinforcement details of beams

A normal strength concrete having a characteristic strength f_{ck} of about 30 MPa, provided by a concrete supplier, was utilized. The mix composition was the same for all specimens except for the amount of fibers and the quantity of plasticizer. Table 13.1 lists the mechanical properties of concrete: the concrete compressive and tensile strength, the Young's modulus of elasticity as well as the residual flexure strength values $f_{R,1}$, $f_{R,2}$ $f_{R,3}$ $f_{R,4}$, corresponding to different crack widths of 0.5, 1.5, 2.5 and 3.5 mm [EN 14651 (2005)], are listed. Hooked end steel fibers, having a length of 50 mm, a diameter of 0.8 mm (aspect ratio L/ϕ of 62.5) and a tensile strength of 1100 MPa were adopted. The yielding and tensile ultimate strength of the longitudinal rebars were: 506 MPa and 599 MPa for ϕ14 bars; 555 MPa and 651 MPa for ϕ20 bars and 518 MPa and 612 MPa for ϕ24 bars, typical for S500 steel according to the current EC2 (2005).

	Concrete Designation		
	PC	FRC50	FRC75
f_{cm} (MPa)	38.7	32.1	33.1
f_{ct} (MPa)	3.0	2.4	2.5
E_c (MPa)	33500	30800	32100
$V_{f,tot}$ (kg/m^3)	0	50	75
$f_{R,1}$ (MPa)	--	5.4	6.0
$f_{R,2}$ (MPa)	--	5.5	6.1
$f_{R,3}$ (MPa)	--	5.0	6.0
$f_{R,4}$ (MPa)	--	4.5	5.5

Table 13.1: Mechanical properties of concrete and post-cracking residual strengths according to EN 14651

The experimental results reported in Fig. 13.2 and Fig. 13.3 represent the load-midspan displacement and the shear crack width development, as a function of the external load. A shear failure was seen for all nine elements. Regarding the shallowest beams (d=440 mm), however, in both FRC beams, the maximum flexure load was reached, with clear yielding of longitudinal rebar and a rather significant ductility for beam H500 FRC50 (Fig. 13.2 (a)).

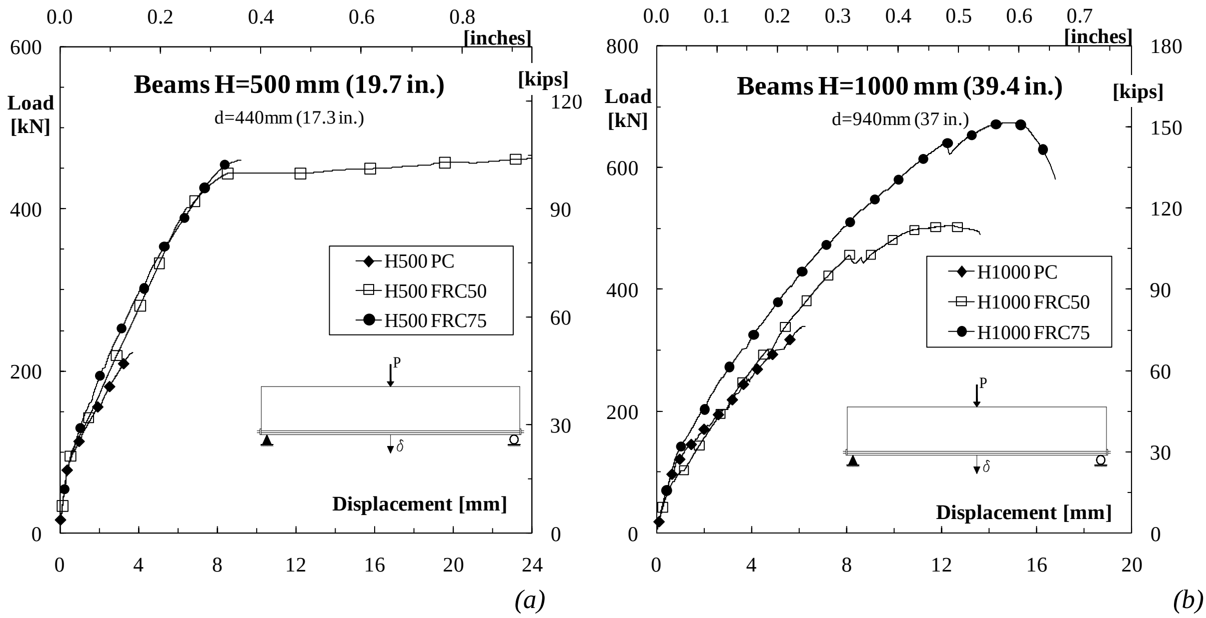

Fig. 13.2: Load-deformation experimental curves of members 440 mm deep (a) and 940 mm deep (b)

Especially from both H1000 and H1500 test series, a significant enhanced post-cracking stiffness is observed for FRC beams, due to stiffening effect, in tension, which is due to the bridging effect of fibers (non-zero tensile stress at a crack) and to the smaller crack spacing, both in flexure than in shear. This evidence, already widely discussed and observed in previous experimental campaigns [Minelli (2005)], will be the basis for the set of equations toward the modelling of the shear strength of FRC beams.

The addition of fibers promoted a stable propagation and progressive development of several shear cracks, which led to a more ductile behaviour with vertical deflections 2-3 times greater than those recorded in the reference plain concrete beams, as clearly evidenced by the experimental plots. Concerning shear cracking, Fig. 13.3 (b) reports the crack development, as a function of the load, for the H1500 series. Note that the crack width evolution is better controlled in FRC: in particular, evident shear cracking begins at 320 kN for the reference sample, whereas it occurs at 570 kN and 890 kN for the FRC50 and FRC75 beams, respectively. While the plain concrete member fails at the emergence of the first shear crack, with a maximum shear crack width of 0.2-0.25 mm, multi-cracking (in shear) was seen for the FRC samples, with single shear crack wider than 1-2 mm and, even more important, still steadily propagating.

Table 13.2 reports the failure mode, the experimental shear load, the shear stress and the ratio between the ultimate experimental moment, M_u, and the maximum flexural capacity of the member, $M_{u,fl}$. For all beams without fibers, the ultimate bending moment was calculated assuming the yielding of rebars within a classical stress-block approach according to MC2010. For the FRC beams, the material toughness was taken into account by adopting the approach included in the first draft of the MC2010, which assumes a tensile stress-block having a constant tension equal to f_{FTu}. The latter is related to the residual nominal bending strength f_{R3} as $f_{FTu}=f_{R3}/3$. As shown in Table 13.2, the value $M_u/M_{u,fl}$ is even higher than 1 in the case of H500 FRC beams (1.11 for FRC50, with a significant ductility, and 1.06 for FRC75), but not for the PC beam (with a value of 0.60). As expected, the $M_u/M_{u,fl}$ ratio decreases with increasing size for plain concrete, according to the literature, whereas, in both FRC members, the deepest elements (H1500 FRC50 and H1500 FRC75) were closer to the flexural capacity than the corresponding H1000 FRC specimens. Further research has to be performed before confirming, for FRC samples, a different trend compared to that expected. However, the peculiar and unexpected behaviour of the 1.5 m deep FRC specimens can be discussed by looking at the crack phenomena, as described in Fig. 13.4 (sample H1500 FRC50). In the case of the FRC beams, a larger number of shear cracks appears, and the collapse is not necessarily related to the first shear crack, as in plain concrete specimens. In fact, steel fibers control and stabilize the shear crack propagation: once formed, they might be able to transmit higher stresses, provided that the FRC composite is sufficiently tough. A degree of crack redistribution may be established (i.e. if the first shear crack is able to resist higher stresses, a second one might form as the external load increases) by allowing a progressive shear crack formation up to failure. Six different shear cracks formed and gradually developed in the member H1500 FRC50 (Fig. 13.4). Only shear crack # 6 appeared just prior to collapse: it had a very brittle and sudden development, bringing the member immediately up to failure. This happened, however, for load and deformation levels almost doubled compared to the reference element, ensuring sufficient warning before the failure.

As a further typical aspect of FRC elements, the evidence that the addition of fibers and the consequent enhanced toughness of the composite are able to promote a strongly stable crack formation and propagation, might involve a rather higher residual compressive strength, through inclined struts, compared to non fibrous structural elements. For the same load level, a more distributed crack pattern, with more closely spaced and smaller cracks, may reduce the detrimental factor referred to as compression softening (the strut should therefore be more efficient). However, these preliminary considerations should be confirmed by suitable experimental results.

In conclusions, from the values listed in Table 13.2, it is possible to emphasize a rather promising role of FRC in mitigating the scale effects. Nevertheless, even if provided in adequate amount, fibers are not able to completely eliminate this detrimental effect.

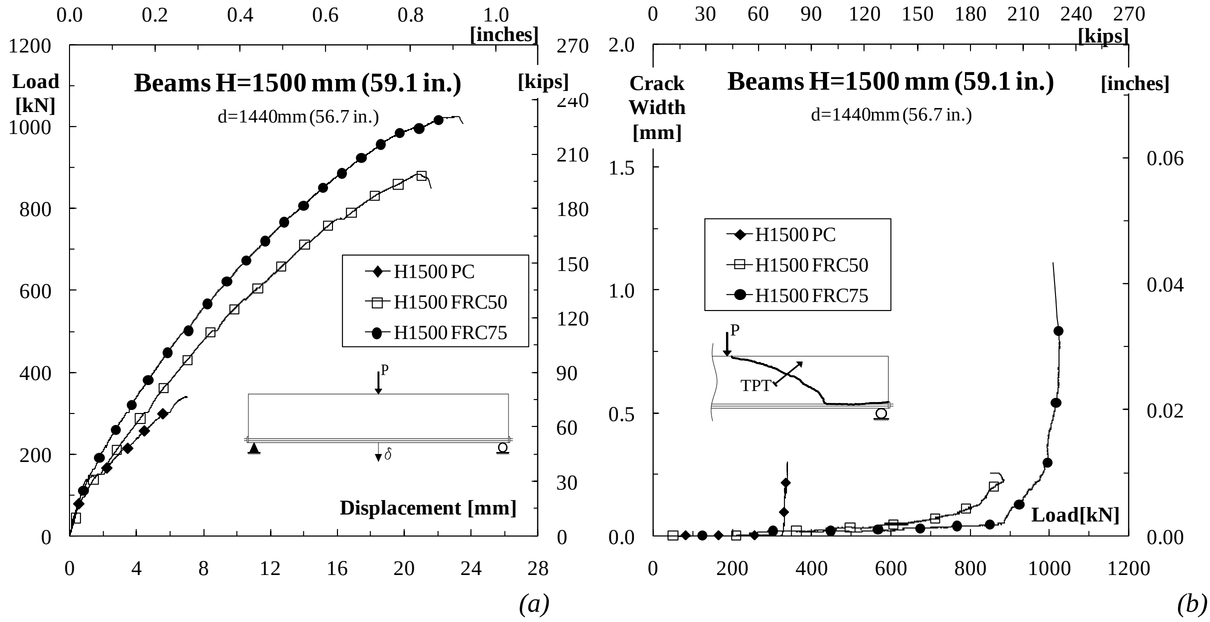

Fig. 13.3: Load-deformation experimental curves (a) and main shear crack width-load curves (b) of 1440 mm deep beams.

Specimen	Failure mode	$V_{u,exp}$ [kN]	v_u [MPa]	$v_u/(f_c)^{1/2}$ [-]	M_u [kN m]	$M_{u,fl}$ [kN m]	$M_u/M_{u,fl}$ [-]
H500 PC	Shear	116	1.05	0.17	153	254	0.60
H500 FRC50	Flexure	240	2.18	0.38	316	285	1.11
H500 FRC75	Flexure	235	2.13	0.37	310	293	1.06
H1000 PC	Shear	188	0.80	0.13	529	1210	0.44
H1000 FRC50	Shear	272	1.16	0.20	767	1325	0.58
H1000 FRC75	Shear	351	1.49	0.26	989	1356	0.73
H1500 PC	Shear	211	0.59	0.09	911	2511	0.36
H1500 FRC50	Shear	484	1.34	0.24	2089	2791	0.75
H1500 FRC75	Shear	554	1.54	0.27	2394	2864	0.84

Table 13.2: Main experimental results

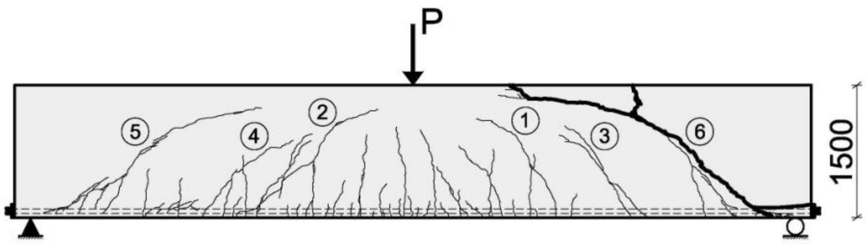

Fig. 13.4: Crack evolution for specimen H1500 FRC50

13.3 Extending the simplified MCFT to FRC (Simplified FRC-MCFT)

Fibers definitely have demonstrated the ability to increase the shear strength of members containing little or no shear reinforcement. Fibers can substitute the minimum amount of transverse reinforcement. They also significantly increase the concrete contribution to shear resistance by providing toughness to the composite.

It is therefore essential to develop analytical models and design tools allowing engineers to incorporate fibers in their design process. Analytical procedures are however better accepted if based on a reliable physical model and on a strong background.

In order to be consistent with the first draft of the MC2010, the Simplified Modified Compression Field Theory [Bentz et al. (2006)] will be pursued to come up with an analytical proposal that should not be a simple extension of an empirical formulation, but derived from a strong model based on equilibrium, compatibility and constitutive laws. Moreover, the authors strongly believe that fibers should be included within the context of the concrete contribution, since FRC is a composite characterized by a mechanical property that is generally neglected in plain concrete, namely the toughness. This approach provides a more representative modeling of the actual behaviour of FRC, which is characterized by an enhanced residual tensile stresses across the crack faces and an improved aggregate interlock (since fibers keep cracks smaller).

Since shear cracking in SFRC members proved to develop in a quite stable fashion, even for crack widths greater than 3 mm [Minelli (2005); Minelli and Plizzari (2006)], the residual post-cracking strength related to the ultimate limit state (f_{R3}), determined from EN 14651 (2005), is considered. The ability of fibers in controlling the second branch of the shear-critical crack, even for large crack widths, is due to their capability of bridging the two faces of a crack. By keeping cracks stable, the shear capacity of members considerably increases until, eventually, the full flexural capacity is attained.

An attempt to extend the SMCFT to fiber reinforced concrete materials is addressed in the following. This proposal will be identified as Simplified FRC-MCFT (referred to as FRC-MCFT in the following).

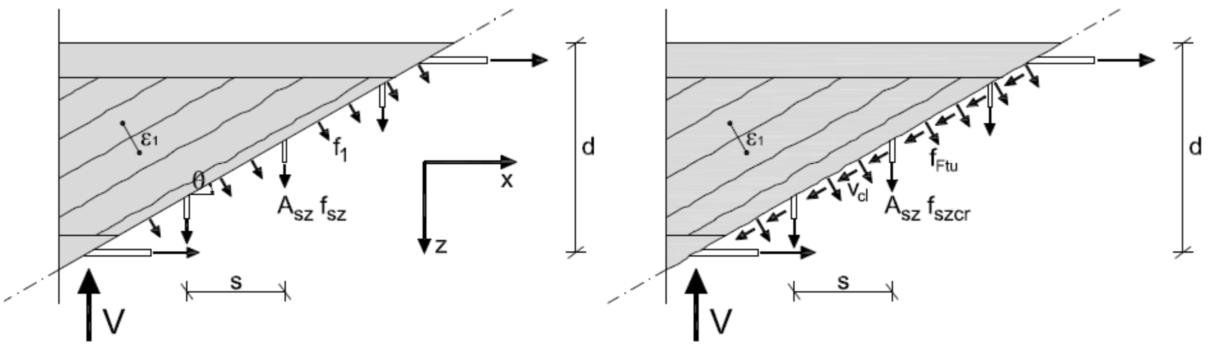

Fig. 13.5: Free body of a beam loaded in shear: (a) calculated average stresses; (b) local stresses at crack

In agreement with the SMCFT, the following assumptions are adopted:

- Clamping stresses f_z=0 are very limited, therefore negligible; this is a reasonable assumption for beams;
- FRC is considered having softening behaviour in tension, which means that after the peak load and the activation of the bridging effect between the two adjacent faces of a crack, the material is not able to exceed the peak load. A simplified rigid-plastic behaviour is assumed: the only parameter that has to be taken into account is the ultimate residual strength f_{Ftu} (MC2010), which must be lower than the concrete tensile strength f_{ct}.

From Fig. 13.5 (a), one can easily write the vertical equilibrium (z direction) along a section between cracks (average stresses), inclined as the angle of principal compressive stresses θ:

$$\mathrm{V} = A_{sz} \cdot f_{sz} \frac{d \cdot \cot \vartheta}{s} + f_1 \cdot \cot \vartheta \cdot b_w \cdot d \tag{13.1}$$

where f_1 is the average principal tensile stress in the cracked concrete.
In terms of stresses, Eq. 13.1 can be rearranged as:

$$\mathrm{v} = \left(\rho_{sz} \cdot f_{sz} + f_1\right) \cdot \cot \vartheta \tag{13.2}$$

The vertical equilibrium for conditions at a crack (Fig. 13.5 (b)) can be expressed as:

$$\mathrm{V} = A_{sz} \cdot f_{szcr} \frac{d \cdot \cot \vartheta}{s} + f_{Ftu} \cdot \cot \vartheta \cdot b_w \cdot d + v_{ci} \cdot b_w \cdot d \tag{13.3}$$

In terms of stresses, Eq. 13.3 can be rearranged as:

$$\mathrm{v} = \left(\rho_{sz} \cdot f_{szcr} + f_{Ftu}\right) \cdot \cot \vartheta + v_{ci} \tag{13.4}$$

where:
- f_{szcr} is the tensile stress in the stirrup at a crack.
- v_{ci} is the shear stress on crack, whose maximum value for plain concrete is:

$$v_{ci} = \frac{0.18 \cdot \sqrt{f_{ck}}}{0.31 + \dfrac{24 \cdot w}{a + 16}} \tag{13.5}$$

where *a* is the maximum aggregate size and *w* is the crack width. This expression was derived by Vecchio and Collins (1986) on the basis of experimental data of Walraven (1981). It is assumed that the ability of transmitting shear stress on crack is not substantially influenced by steel fibers, which do not offer significant dowel action along the two faces of a crack. This assumption, according also to the "Variable Engagement Model" by Foster (see Chapter 12 of this bulletin) is however to be more thoroughly evaluated. Future research will be done by the authors with this respect.

It is assumed that, at failure, the transverse reinforcement reaches the yielding so that:

$$f_{szcr} = f_{sz} = f_{sy} \tag{13.6}$$

The two equilibrium equations (Eq. 13.2 and 13.4) can be rearranged to give:

$$v = (\rho_{sz} \cdot f_{sy} + f_1) \cdot \cot \vartheta \tag{13.7}$$

$$v = (\rho_{sz} \cdot f_{sy} + f_{Ftu}) \cdot \cot \vartheta + v_{ci} \tag{13.8}$$

Both of these equations can be expressed, according to the classical theory, as the sum of a concrete (v_{FRC}) and a transverse reinforcement (v_S) contribution as:

$$v = v_{FRC} + v_s = k_v \cdot \sqrt{f_{ck}} + \rho_z \cdot f_{sy} \cdot \cot \vartheta \tag{13.9}$$

where k_v represents a coefficient for the concrete contribution, generally referred as β in the classical formulation of MCFT.

While defining the concrete contribution (k_v depends on the average tensile stress in the cracked concrete) it should be noticed that fibers are able to significantly increase the average tensile stress between cracks. Fibers stiffen the post-cracking response of R/C members and, in addition, result in smaller crack spacings. A number of studies have investigated this point with promising results. Minelli et al. (2010), within a research project in common with the University of Brescia (Italy) and Toronto (Canada), tested eighty-eight reinforced concrete tension prismatic members (tension ties), characterized by normal strength concrete, different cross sections, reinforcing ratios, fiber volumes and fiber typologies. The authors brought to light that FRC diffusely influences the behaviour of tension-ties at serviceability limit states, by reducing crack width and determining a crack pattern with narrower and well closely spaced cracks [Minelli et al. (2010)]. In addition, fibers stiffen the post-cracking response of R/C members, diminishing the displacement of structures. As an example, the average crack spacing values from the experimental campaign are summarized in Fig. 13.6 (a) for all tests performed. Fibers enable a noticeable increase in the number of cracks varying from 45% to almost 100% and a consequent reduction of the crack spacing varying from 25% to 55%. The experimental evidence will influence both the average tensile stress in cracked concrete (f_1) and the crack spacing.

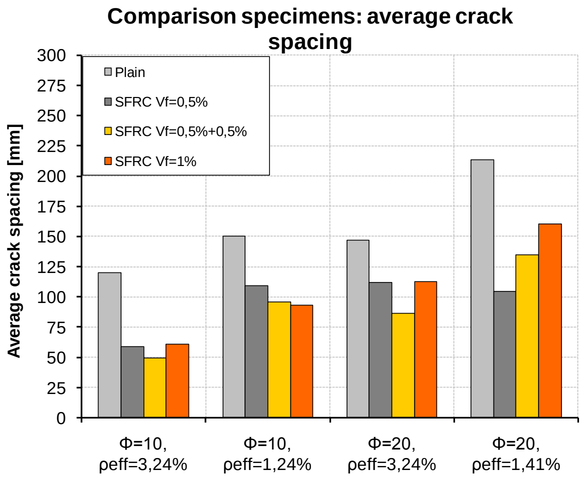

(a)

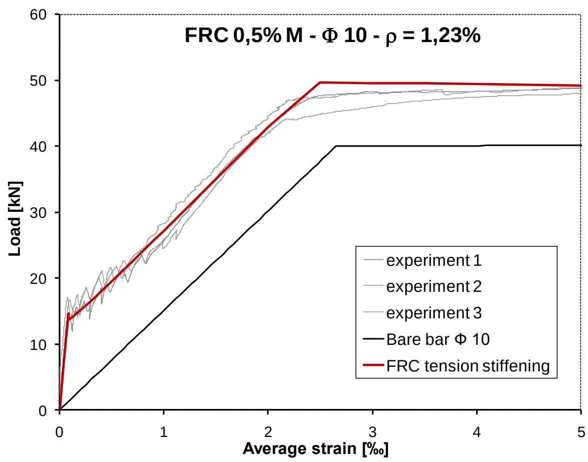

(b)

Fig. 13.6: Average experimental crack spacing at crack stabilized stage (a); comparison of Eq. 13.11 against experiments from tension ties (b)

Further studies are required for the development of an analytical formulation for crack spacing and tension stiffening effect in members with a broad variety of fiber contents, typologies and concrete matrices. A first attempt is presented herein.

The analytical model for tension stiffening describing the average principal tensile stress in cracked reinforced concrete, according to Vecchio and Collins (1986), is given by:

$$f_1 = \frac{f_{ct}}{1+\sqrt{500 \cdot \varepsilon_1}} \tag{13.10}$$

where ε_1 is the principal tensile strain and f_{ct} is the concrete tensile strength that, according to the MCFT, must be assumed equal to $0.33(f_{ck})^{1/2}$. While dealing with FRC elements, an adaptation to the expression of Eq. 13.10 is herein proposed as follows:

$$f_1 = f_{Ftu} + \frac{f_{ct} - f_{Ftu}}{1+\sqrt{500 \cdot \varepsilon_1}} \tag{13.11}$$

The two formulations are plotted in Fig. 13.7 (a) for a R/C and a FRC member with f_{FTU}=0.5f_{ct}. Fig. 13.7 (b) shows the simplified rigid-plastic constitutive law assumed for the calculation and included in the first draft of the MC 2010, expressed in terms of strain. Note that the ultimate strain of a FRC material is defined as ε_{Fu}=2% for variable strain distribution along the cross section and 1% for a constant tensile strain distribution along the cross section (the maximum crack width cannot exceed 2.5 mm). The relationship proposed adequately describes the experimental results on tension ties carried out at the University of Brescia [Minelli et al. (2010)]. It is a quite simple but effective model, even though one can argue that the combined effects of local strain at cracks, strains between cracks and bond-slip are all included together.

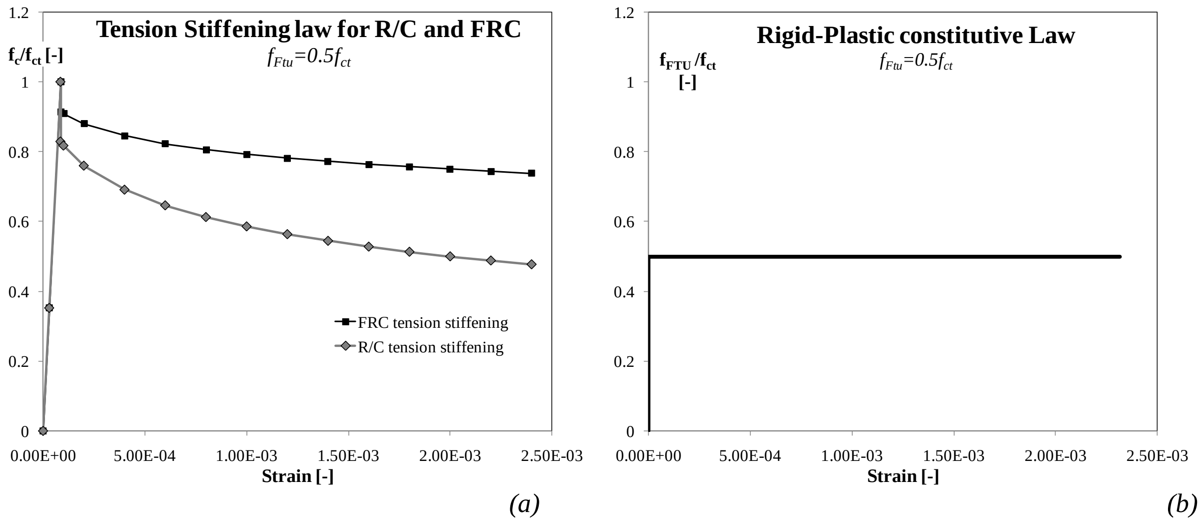

Fig. 13.7: Adaptation of the cracked concrete constitutive law in tension for FRC from the well known empirical correlation included in the MCFT theory based on Vecchio and Collins (1986). (a) Assumed rigid-plastic constitutive law according ot the first draft of fib MC (2010) (b)

Eq. 13.11 seems to be quite reasonable as, for $f_{FTU}=0$, it is consistent with the base curve for R/C elements (Eq. 13.10), while, for $f_{FTU}=f_{ct}$, the stress-strain post-peak behaviour is constantly equal to the tensile strength. Once again, one should notice that only tension softening materials are considered; therefore, f_{Ftu} must be lower than f_{ct}. Moreover, Eq. 13.11 seems to well reproduce the experimental results on tension ties, as reported in Fig. 13.6 (b).

Eq. 13.9 can be rearranged, for conditions at a crack, as follows:

$$v \leq f_{Ftu} \cdot \cot \vartheta + \frac{0.18 \cdot \sqrt{f_{ck}}}{0.31 + \dfrac{24 \cdot w}{a + 16}} + v_s \tag{13.12}$$

which means that the factor $k_{v,FRC,crack}$ is

$$k_{v,FRC,crack} \leq \frac{f_{Ftu} \cdot \cot \vartheta}{\sqrt{f_{ck}}} + \frac{0.18}{0.31 + \dfrac{24 \cdot w}{a + 16}} \tag{13.13}$$

In terms of averages stresses,

$$v = \left(f_{Ftu} + \frac{0.33 \cdot \sqrt{f_{ck}} - f_{Ftu}}{1 + \sqrt{500 \cdot \varepsilon_1}} \right) \cdot \cot \vartheta + v_s \tag{13.14}$$

The corresponding factor $k_{v,FRC,avg}$ is

$$k_{v,FRC,avg} = \left(f_{Ftu} + \frac{0.33 \cdot \sqrt{f_{ck}} - f_{Ftu}}{1 + \sqrt{500 \cdot \varepsilon_1}} \right) \cdot \frac{\cot \vartheta}{\sqrt{f_{ck}}} \tag{13.15}$$

For members not containing any transverse reinforcement, the highest value of the tension factor k_v occurs when Eq. 13.13 and Eq. 13.15 give the same value. In doing so, one can determine the angle of principal compressive stresses in the web, θ, as follows:

$$\cot \vartheta = \frac{0.18}{0.31 + \dfrac{24 \cdot w}{a + 16}} \cdot \sqrt{f_{ck}} \cdot \frac{1 + \sqrt{500 \cdot \varepsilon_1}}{0.33 \cdot \sqrt{f_{ck}} - f_{Ftu}} = \frac{v_{ci}}{f_{ct} - f_{Ftu}} \cdot \left(1 + \sqrt{500 \cdot \varepsilon_1}\right) \tag{13.16}$$

Note that θ is affected by the FRC toughness (f_{Ftu}). From compatibility, it is possible to relate the longitudinal strain ε_x to ε_1, as reported in the following equation:

$$\varepsilon_1 = \varepsilon_x \cdot \left(1 + \cot^2 \vartheta\right) + \varepsilon_2 \cdot \cot^2 \vartheta \tag{13.17}$$

The principal compressive strain ε_2 depends on f_2. In the case of beams without transverse reinforcement, where we can assume that $\rho_{sz}=f_z=0$, from equilibrium (average stresses) one can determine f_2 as:

$$f_2 = f_1 \cdot \cot^2 \vartheta \tag{13.18}$$

Furthermore, by assuming that the compressive stress in these elements (without transverse reinforcement) will be small, a linear relationship between stress and strain in compression can be assumed as follows:

$$\varepsilon_2 = \frac{f_2}{E_c} \quad \text{with} \quad E_c = 4950 \cdot \sqrt{f_{ck}} \tag{13.19}$$

as conventionally assumed in the MCFT (1986) formulation. Eq. 13.17 then becomes:

$$\varepsilon_1 = \varepsilon_x \cdot \left(1 + \cot^2 \vartheta\right) + \frac{f_1 \cdot \cot^4 \vartheta}{4950 \cdot \sqrt{f_{ck}}} = \varepsilon_x \cdot \left(1 + \cot^2 \vartheta\right) + \frac{\left(f_{Ftu} + \dfrac{f_{ct} - f_{Ftu}}{1 + \sqrt{500 \cdot \varepsilon_1}}\right) \cdot \cot^4 \vartheta}{4950 \cdot \sqrt{f_{ck}}} \tag{13.20}$$

The last parameter to be defined is the crack width *w*, which is assumed as:

$$w = s_\theta \cdot \varepsilon_1 \quad \text{with} \quad s_\theta = \frac{1}{\dfrac{\sin \vartheta}{s_x} + \dfrac{\cos \vartheta}{s_z}} \tag{13.21}$$

where s_x and s_z represent the crack spacing in the longitudinal and vertical direction, as a characteristic of the crack control properties of the longitudinal and vertical reinforcement. As a rough simplification, which is useful for design, s_x can be taken as the vertical distance between bars aligned in the x-direction while s_z is the horizontal spacing between vertical bars aligned in z-direction [Bentz et al. (2006)]. For members without transverse reinforcement, s_z equals infinity; therefore:

$$w = s_\theta \cdot \varepsilon_1 = \frac{s_x}{\sin \vartheta} \cdot \varepsilon_1 \tag{13.22}$$

As already mentioned, fibers significantly reduce the crack spacing, allowing for a rather more closely spaced crack pattern. A number of studies tried to analytically model this experimental evidence. In this paper, the crack spacing reduction factor, as proposed by Moffat (2001) was herein suitably adapted to the ultimate residual strength, f_{Ftu}, according to MC2010, as follows:

$$s_{x,FRC} = s_x \cdot \left(1 - \frac{f_{Ftu}}{f_{ct}}\right) \tag{13.23}$$

The latter equation is, once again, only applicable to strain softening materials ($f_{Ftu} < f_{ct}$).

Eq. 13.1 to Eq. 13.23 represent a complete set of equations for the prediction of the shear capacity of FRC beams. A suitable solution technique is proposed as follows:

1) Choose a tentative value of the longitudinal strain ε_x;

2) Estimate the angle principal compressive stresses in the web θ;

3) Calculate ε_1 using Eq. 13.20;

4) Calculate or assume the crack spacing s_x, then $s_{x,FRC}$ (Eq. 13.23) and s_θ. Calculate w (Eq. 13.22) and the maximum shear stress at a crack v_{ci} (Eq. 13.5);

5) Calculate θ from Eq. 13.16; if the calculation is different from the angle assumed in step 2, return to step 2 and revise estimate;

6) Calculate *v* from Eq. 13.12 and 13.14 and verify that the shear strength at crack be equal to the shear strength in the configuration of average stresses (between cracks); calculate f_1 (Eq. 13.11);

7) Check ε_x; estimate a new value of ε_x and return to Step 1 until convergence. This check can be found using the following relationship, which represents the horizontal equilibrium between cracks (Fig. 13.5 (b)):

$$\varepsilon_x = \frac{f_{sx}}{E_s} = \frac{v \cdot \cot \vartheta - f_1}{E_s \cdot \rho_s} \tag{13.24}$$

where f_{sx} is the tensile stress in the longitudinal reinforcement.

8) Check that the longitudinal reinforcement can transmit the required stresses at crack being smaller than the yield stress. From the horizontal equilibrium at crack, it results that:

$$f_{sxcr} = \frac{(v + v_{ci}) \cdot \cot \vartheta - f_{Ftu}}{\rho_x} \leq f_{sy} \tag{13.25}$$

If the relation is not verified, return to step 1 and increase the value of ε_x.

The above presented analytical procedure will be applied to a collection of FRC beams available worldwide.

As a general conclusion, the model proposed:

- is a physical model: it is not an extension of an empirical formulation but of a strong model based on equilibrium, compatibility and constitutive laws. Constitutive laws were suitably improved for including the main key-influencing factors in shear due to fibers: tension stiffening, tension softening and crack spacing;
- includes the shear contribution of fibers not as a separate addendum but as an enhancement of the concrete contribution by modifying the factor k_v (β). As it increases, k_v allows for a greater transfer of stresses; the angle of principal compressive stresses in the web θ is, as expected, also affected by fibers, whereas it would not be if fibers were included separately;
- is based on a toughness index of the composite (the ultimate residual strength, f_{Ftu}, that is related to the residual strength f_{R3}), which is more significant than both the fiber content and the fiber factor. Concrete toughness can be easily determined from standard tests (three point bending tests) on the FRC composite;
- applies only for strain-softening FRC materials.

13.4 Conclusions

In the present paper, the beneficial effects of providing steel fibers as spread shear reinforcement have been scrutinized. Fibers, even in relatively low amount, greatly influence the shear behaviour of beams, basically by delaying the occurrence of the shear failure mechanism and, eventually, by altering the collapse from shear to flexure, with enhanced bearing capacity and ductility. Fibers allow, if supplied in sufficient quantity, a well distributed crack pattern in the critical area under shear, delaying or even avoiding the formation of the single critical shear crack, which brings the member to a brittle failure. If this happens, it is associated with visible warning, cracking and deflections, unlike for plain concrete members.

A recent series of 9 experiments showing the effect of steel fibers in mitigating the size effect issue in shear was also presented. It was shown that fibers in reinforced concrete elements under shear significantly reduce the scale effect, even if provided in relatively low amounts. To fully avoid such an experimental drawback, a greater toughness is required, reachable with higher fiber contents.

Finally, an adaptation of the Simplified Modified Compression Field Theory to FRC has been proposed and identified as FRC-MCFT: opposite to other models, it includes the enhanced toughness of FRC into the concrete contribution, determining different values of the concrete factor k_v and the angle θ. A complete set of equations accounting for equilibrium, compatibility and constitutive laws have been discussed and a solution technique proposed. An enhanced tension stiffening law, a non negligible tension softening at crack and a smaller crack spacing (with respect to classical reinforced concrete structures), were taken into account in the proposed analytical procedure.

The analytical model has to be validated against experiments. Moreover, it should be simplified toward an easier utilization. Preliminary validation against experimental results carried out at the University of Brescia evidences that the proposal is rather promising.

13.5 References

ASCE-ACI Committee 445 on Shear and Torsion, “Recent Approaches to Shear Design of Structural Concrete”, *Journal of Structural Engineering*, V. 124, No. 12, 1998, pp. 1375-1417.

Bentz, E.C., Vecchio, F.J., and Collins, M.P., 2006, “The Simplified MCFT for Calculating the Shear Strength of Reinforced Concrete Elements”, *ACI Structural Journal,* V. 103, No. 4, pp.614-624

Casanova, P., Rossi, P., and Schaller, I., “Can Steel Fibers Replace Transverse Reinforcement in Reinforced Concrete Beams?”, *ACI Material Journal*, V. 94, No. 5, 1997, pp. 341-354.

Choi, K-K., Park, H-G., and Wight, J., “Shear Strength of Steel Fiber-Reinforced Concrete Beams without Web Reinforcement”, *ACI Structural Journal,* V. 104, No 1, 2007, pp. 12-22.

CNR DT 204/2006., “Guidelines for the Design, Construction and Production Control of Fibre Reinforced Concrete Structures”, National Research Council of Italy, 2006, pp. 59.

Dinh, H. H., Parra-Mointesinos, G.J., and Wight, J., “Shear Behavior of Steel Fiber-Reinforced Concrete Beams without Stirrup Reinforcement”, *ACI Structural Journal,* V. 107, No 5, 2010, pp. 597-606.

EN 14651-5: Precast Concrete Products – Test method for metallic fibre concrete – Measuring the flexural tensile strength, Europ. Standard, 2005, pp.20.

Eurocode 2 EN 1992-1-1. “Design of Concrete Structures, General rules and rules for buildings”, 2005.

fib Bulletin 55, *Model Code 2010 – First complete draft, Volume 1* (chapters 1-6), 318 pages, 2010, ISBN 978-2-88394-95-6.

fib Bulletin 56, *Model Code 2010 – First complete draft, Volume 2* (chapters 7-10), 312 pages, 2010, ISBN 978-2-88394-096-3.

Gustafsson, J., and Noghabai, K., “Steel Fibres as Shear Reinforcement in High Strength Concrete Beams”, Technical Report, Luleå University of Technology, Division of Structural Engineering, 1999, pp. 1-18.

Imam, M., Vandewalle, L., Mortelmans, F., and Van Gemert, D., “Shear Domain of Fibre-Reinforced High-Strength Concrete Beams”, *Elsevier Engineering Structures Journal*, V. 19, No. 9, 1997, pp. 738-747.

Khuntia, M., Stojadinovic, B., and Goel, S., “Shear Strength of Normal and High-Strength Fibre Reinforced Concrete Beams without Stirrups”, *ACI Structural Journal*, V. 96, No. 2, 1999, pp. 282-289.

Lim, D.H., and Oh, B.H., “Experimental and Theoretical Investigation on the Shear of Steel Fibre Reinforced Concrete Beams”, *Elsevier Engineering Structures*, V. 21, No. 10, 1999 pp. 937-944.

Minelli, F., “Plain and Fiber Reinforced Concrete Beams under Shear Loading: Structural Behavior and Design Aspects”, *Ph.D. Thesis*, Department of Civil Engineering, University of Brescia, February 2005, pp. 422.

Minelli, F., and Plizzari, G.A., “Steel Fibers as Shear Reinforcement for Beams”, Proceedings of The Second Fib Congress, Naples, Italy, 5-8 June 2006, abstract on page 282-283, full length paper available on accompanied CD, 2006, pp.12.

Minelli, F., Tiberti, G. and Plizzari, G.A., “Cracking in FRC R/C elements: a preliminary experimental study” 3rd *fib* International Congress, Washington D.C., May 29- June 2, 2010, available on CD, 12 pp.

Moffatt, K., 2001. “Analyse de Dalles de Pont avec Armature Réduite et Béton de Fibres Metalliques”,M.Sc.A. Thesis, École Polytechnique de Montréal (in French), 248 pp.

Nawy, E.G., “Fundamental of High-Performance Concrete”, 2nd Edition, John Wiley and Sons, Inc., New York, 2001

Swamy, R.N., Jones, R., and Chiam, A., “Influence of Steel Fibres on the Shear Resistance of Lightweight Concrete T-Beams”, *ACI Structural Journal*, V. 90, No. 1, 1993, pp. 103-114.

Vecchio, F.J. and Collins, M.P., 1986, “The Modified Compression Field Theory for Reinforced Concrete Elements Subjected to Shear,” *ACI Journal*, 83(2) pp. 219-231.

Vecchio, F.J., “Analysis of Shear-Critical Reinforced Concrete Beams”, *ACI Structural Journal*, V. 97, No. 1, 2000, pp. 102-110.

Walraven, J.C., 1981, “Fundamental Analysis of Aggregate Interlock,” *Journal of the Structural Division*, ASCE, 107(ST11), pp 2245-2270.

14 Effectiveness of steel fiber as minimum shear reinforcement: panel tests

J. Susetyo[1] and F. J. Vecchio[2]
[1] Engineer, Hatch Mott McDonald Ltd, Mississauga, Canada
[2] Professor, University of Toronto, Toronto, Canada

Abstract: Ten 890×890×70 mm concrete panels were tested under in-plane pure-shear monotonic loading conditions to evaluate the effectiveness of steel fibers in controlling shear cracking. The results of the tests indicate that concrete elements exhibiting ductile behavior, good shear resistance, and good crack control characteristics can be obtained with an adequate addition of steel fibers. Assessments were also made of the influence of fiber aspect ratio, fiber length, fiber tensile strength, fiber volume content, and concrete compressive strength on the shear crack control of fiber reinforced concrete (FRC). In addition, finite element (FE) analyses were performed to investigate whether currently available constitutive models can be utilized to accurately represent the behavior of the FRC panels tested. The analytical results indicate that improved constitutive models for tension response and crack spacing of FRC are required for successful finite element modeling.

14.1 Introduction

With the increasing use of high strength concrete, a general reduction in the cross-sectional area of typical concrete sections is possible due to the increased stress capacity of the material. However, the amount of the reduction realizable is sometimes limited by the minimum dimensions necessary to accommodate reinforcement or by requirements for concrete cover and reinforcement spacing. This is particularly true with respect to the shear reinforcement in thin-web members. In addition, under some conditions, design codes will require the inclusion of minimum shear reinforcement; shown in Table 14.1 are the minimum shear reinforcement ratios required by ACI [ACI Committee 318 (2008)] and CSA [CAN/CSA Standard A23.3-04 (2004)] for 50 MPa and 80 MPa concrete. Thus, if a concrete material possessing good crack control characteristics were to exist, comparable to at least that provided by the inclusion of minimum shear reinforcement, then the need for shear reinforcement could be reduced or eliminated in many instances. This would lead to the design of thinner and more efficient structures.

Previous research on fiber reinforced concrete (FRC) has shown that the addition of steel fibers to concrete significantly improves the tensile behavior and the crack control characteristics of the concrete, resulting in reduced crack widths and crack spacing [e.g. Grzybowski & Shah (1990), Shah et al. (1998), Banthia et al. (1993), Ong & Paramasivam (1989)]. It is therefore appealing to study the feasibility of FRC as a replacement for some or all shear reinforcement, in some cases, in order to obtain optimized designs of concrete structures.

f_c (MPa)	ρ_{min} (%)	
	CSA A23.3-04	ACI 318M-08
50	0.095	0.104
80	0.120	0.123

Table 14.1: Minimum shear reinforcement ratios

Numerous studies have been conducted on the shear strength of steel fiber reinforced concrete beams [e.g., Adebar et al. (1997), Tan et al. (1993), Ashour et al. (1992), Minelli and Vecchio (2006)]. Test results have definitively shown that the addition of steel fibers substantially improves the shear behaviour of the beams. Due to the bridging effects provided by the fibers, less brittle shear failures were achieved and, in some cases, the mode of failure was transformed from shear to a ductile flexural mode.

Although these previous studies are significant in that they demonstrate the effectiveness of steel fibers as a means of improving shear behaviour, they stop short of defining general constitutive models that characterize the contribution of the steel fibers to shear resistance. To provide an experimental basis for developing such models, a series of panel tests was conducted at the structural laboratories of the University of Toronto using the Panel Element Tester. The use of panel tests enables a more thorough investigation of fiber reinforced concrete behaviour under shear-dominant conditions, since they enable constant and uniform shear stress conditions to be imposed over a large specimen area without the presence of the obscuring effects of flexure. Interactions between conventional steel reinforcement and fiber reinforced concrete can thus be assessed, and various aspects of concrete behaviour such as tension stiffening, tension softening, and compression softening can be evaluated. In addition, factors that influence the effect of steel fibers on concrete shear resistance can be better assessed. These factors include fiber volume content, fiber aspect ratio, fiber length, fiber tensile strength, and concrete compressive strength.

14.2 Experimental program

Ten 890×890×70 mm panels were tested under in-plane pure-shear monotonic loading condition using the Panel Element Tester (see Fig. 14.1) to evaluate the crack control characteristics of FRC. The matrix of test parameters employed is given in Table 14.2.

Two panels served as control specimens, and as such were orthogonally reinforced with 40-D8 deformed wires in the longitudinal direction (ρ_x = 3.31 %) and with 10-D4 deformed wires in the transverse direction (ρ_y = 0.42%). Specimen reinforcement details are depicted in Fig. 14.2 a. Note that the level of transverse reinforcement provided in the control specimens was approximately four times the amount corresponding to the minimum shear reinforcement ratios required by ACI and CSA. The higher transverse reinforcement ratio was necessitated by the requirement for a symmetric reinforcement arrangement about the axis of the shear keys, which serve to transfer the load from the machine hydraulic jacks to the concrete panel, to prevent the introduction of moments at the shear keys.

The remaining eight panels, containing steel fibers, were reinforced in the longitudinal direction only with 40-D8 deformed bars (ρ_x = 3.31%). Specimen reinforcement details are depicted in Fig. 14.2 b. Three types of Dramix hooked-end steel fibers (RC80/50-BN, RC80/30-BP, and RC65/35-BN) were used to investigate the influence of fiber aspect ratio, fiber length, and fiber tensile strength on the crack control performance of FRC. In addition, three different fiber volume contents (0.5%, 1.0%, and 1.5%) and two different concrete compressive strengths (50 MPa and 80 MPa) were investigated.

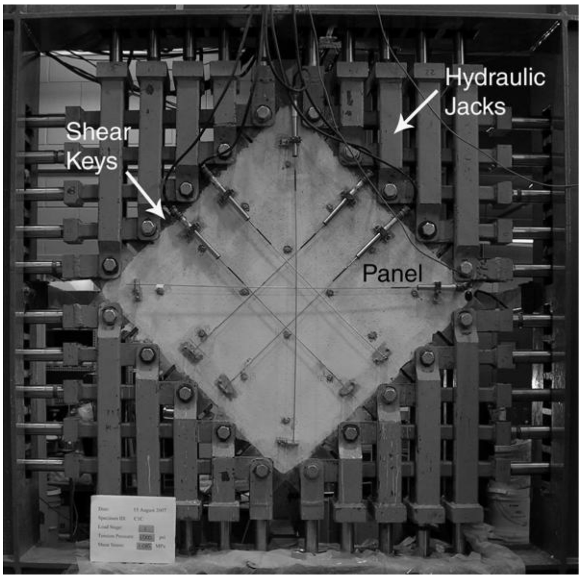

Fig. 14.1: Panel specimen shown in Panel Element Tester

ID	Specified f_c (MPa)	Fiber Content (%)	Fiber Type
C1C	50	-	-
C1F1V1	50	0.5	RC80/50-BN
C1F1V2	50	1.0	RC80/50-BN
C1F1V3	50	1.5	RC80/50-BN
C1F2V3	50	1.5	RC80/30-BP
C1F3V3	50	1.5	RC65/35-BN
C2C	80	-	-
C2F1V3	80	1.5	RC80/50-BN
C2F2V3	80	1.5	RC80/30-BP
C2F3V3	80	1.5	RC65/35-BN

Table 14.2: Test Matrix

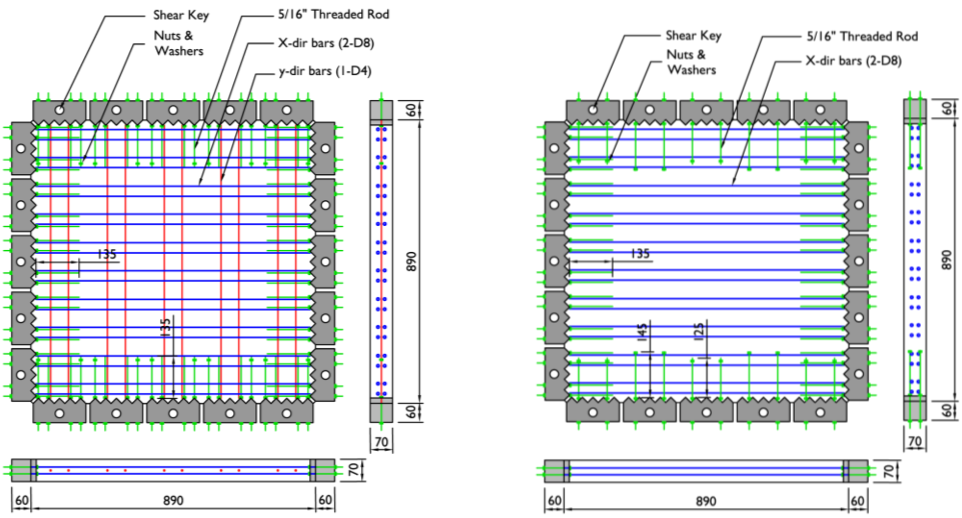

(a) (b)

Fig. 14.2: Test panel details. (a) Control panel. (b) FRC panel.

Rebar Type	$Ø_b$ (mm)	A_s (mm²)	E_s (GPa)	f_y (MPa)	ε_y (mε)	f_u (MPa)	ε_u (mε)
D4	5.72	25.81	187.2	446.9	2.41	548.9	57.6
D8	8.10	51.61	224.7	552.2	2.58	647.2	45.4

Table 14.3: Properties of conventional reinforcement

Fiber Type	l_f (mm)	$Ø_f$ (mm)	$l_f/Ø_f$	f_{fu} (MPa)
RC80/50-BN	50	0.62	81	1050
RC80/30-BP	30	0.38	79	2300
RC65/35-BN	35	0.55	64	1100

Table 14.4: Properties of fibers [Bekaert (2003)]

Details of concrete mix properties and construction methods can be found in Susetyo (2009). The properties of the conventional reinforcement and the fibers used in the panels are listed in Table 14.3 and Table 14.4, respectively. Due to the cold-forming of the deformed wires, the yield plateau could not be determined; the yield strength and the yield strain were thus determined from the proportionality limit of the wire steel.

Instrumentation of the panels consisted of Linear Variable Displacement Transducers (LVDTs) mounted on the surface of the concrete, displacement transducers (Zurich gauges) used in conjunction with fixed targets mounted on the surface of the concrete, and electrical resistance strain gauges of 5 mm gauge length mounted on the surface of the reinforcing steel. The LVDTs were used to monitor the overall deformation of the panels. The Zurich gauges were used to obtain more detailed definitions of local deformations. The electrical resistance strain gauges on the reinforcing steel provided continuous measurement of local strains in the reinforcement. Pressure transducers on the Tester's hydraulic control system and load cells placed on several load actuators provided a continuous monitoring of the loads applied to the specimens.

The tests were conducted by loading the panels under monotonically increasing in-plane pure shear load. Prior to loading, initial Zurich gauge readings were taken to determine the undeformed state of a test panel. Load was then applied until the first crack was detected, at which point readings corresponding to the first load stage were taken. Loading then continued, in stages, until the panel reached its maximum load carrying capacity, entered post-peak response and eventually failed. Between the first-cracking and failure, typically 10 to 15 load stages were employed. At each load stage, Zurich gauge readings were taken, crack patterns were marked and photographed, crack widths were measured, and surface conditions were carefully surveyed.

14.3 Experimental results

14.3.1 Failure mode

The results of the panel tests are summarized in Table 14.5. As indicated in the table, all of the FRC panels failed due to aggregate interlock failure. A typical FRC panel at failure is shown in Fig. 14.3. Data on reinforcement stresses indicate that at the onset of failure, the conventional longitudinal reinforcement provided within the FRC panels had not yielded and the concrete had not reached its ultimate compressive strength. The failures of the control panels, on the other hand, were initiated by yielding or rupturing of the transverse reinforcement. Note, however, that the stresses in the longitudinal reinforcement of the control panels remained at levels comparable to those in the FRC panels, and did not reach the reinforcement yield strength at the onset of panel failure.

ID	f_{cm} (MPa)	τ_r (MPa)	γ_r (mε)	τ_u (MPa)	γ_u (mε)	w_m (mm)	$s_{r,m}$ (mm)	σ_{sx} (MPa)	σ_{sy} (MPa)	Failure Mode
C1C	65.7	2.01	0.086	5.77	6.01	0.55	57.2	250	501	y-bar yield
C1F1V1	51.4	2.09	0.197	3.53	2.77	0.55	114.4	148	-	Shear Slip
C1F1V2	53.4	2.65	0.139	5.17	5.27	0.45	54.7	201	-	Shear Slip
C1F1V3	49.7	1.83	0.055	5.37	5.10	0.45	57.2	204	-	Shear slip
C1F2V3	59.7	1.85	0.070	6.68	6.20	0.45	38.1	256	-	Shear Slip
C1F3V3	45.5	2.24	0.118	5.59	4.27	0.50	57.2	213	-	Shear slip
C2C	90.5	2.57	0.099	6.40	7.00	0.50	66.2	341	512	y-bar yield
C2F1V3	79.0	2.17	0.131	6.90	5.25	0.70	36.0	315	-	Shear slip
C2F2V3	76.5	1.59	0.110	6.31	4.35	0.65	46.6	224	-	Shear slip
C2F3V3	62.0	2.10	0.222	5.57	4.97	0.60	40.6	238	-	Shear slip

Table 14.5: Summary of panel tests

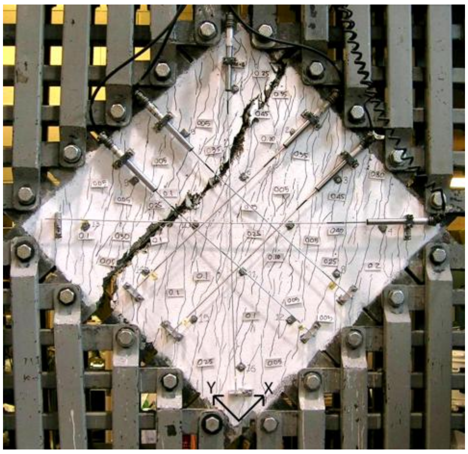

Fig. 14.3: FRC Panel C1F2V3 at failure

14.3.2 Maximum shear resistance

All fiber reinforced concrete panels, except for Panel C1F1V1, managed to withstand at least 87% of the maximum shear stresses sustained by the control panels (see Table 14.5). Panel C1F2V3, with 1.5% RC80/30-BP fibers, surpassed the strength of the control panels by a factor of 1.16. Panel C1F1V1, having a low 0.5% fiber volume content, was able to sustain only 61% of the ultimate shear resistance of Panel C1C, its respective control panel. It is evident that this low fiber content was not sufficient to guarantee equivalent shear resistance. Nevertheless, good shear behaviour of the concrete panels without transverse reinforcement was achievable with a moderate to a high fiber addition, especially given that the control panels contained approximately three to four times the code-prescribed minimum shear reinforcement amounts.

ID	f_{cm} (MPa)	$\tau_{u\text{-}exp}$ (MPa)	ACI318M-08			CSA A23.3-04		
			$A_{sw}/(b\times s_{sw})$* (%)	τ_R (MPa)	$\frac{\tau_{u\text{-}exp}}{t_R}$	$A_{sw}/(b\times s_{sw})$* (%)	τ_R (MPa)	$\frac{\tau_{u\text{-}exp}}{\tau_R}$
C1C	65.7	5.77	0.120**	2.80	2.06	0.109**	2.87	2.01
C1F1V1	51.4	3.53	0.106	2.48	1.42	0.096	2.61	1.35
C1F1V2	53.4	5.17	0.108	2.53	2.05	0.098	2.65	1.95
C1F1V3	49.7	5.37	0.104	2.44	2.20	0.095	2.57	2.09
C1F2V3	59.7	6.68	0.114	2.67	2.50	0.104	2.78	2.41
C1F3V3	45.5	5.59	0.100	2.33	2.40	0.091	2.47	2.26
C2C	90.5	6.40	0.123**	2.87	2.23	0.128**	2.97	2.15
C2F1V3	79.0	6.90	0.123	2.87	2.40	0.119	2.92	2.36
C2F2V3	76.5	6.31	0.123	2.87	2.20	0.117	2.91	2.17
C2F3V3	62.0	5.57	0.116	2.72	2.05	0.106	2.82	1.98

** code-prescribed minimum shear reinforcement ratio; ** actual 0.42%*

Table 14.6: Shear resistance of concrete panels containing minimum shear reinforcement as predicted by ACI 318M-08 and CSA A23.3-04

Table 14.6 compares the nominal shear resistances calculated using ACI 318M-08 [ACI Committee 318 (2008)] and CSA A23.3-04 [CAN/CSA Standard A23.3-04 (2004)], for concrete panels containing minimum shear reinforcement, to the resistances observed experimentally. For these calculations, the capacity reduction factor (ACI) and the material resistance factors (CSA) were set to 1.0. Longitudinal reinforcement and concrete compressive strength were taken as equal to those of the test panels. The results summarized in Table 14.6 again suggest that steel fibers are a viable means of replacing minimum to low amounts of shear reinforcement. Even with a low fiber volume content of 0.5%, the shear resistance of the fiber reinforced panel C1F1V1 was 42% greater than the shear resistance calculated for minimum shear reinforcement in accordance with ACI 318M and 35% greater than the shear resistance calculated for minimum shear reinforcement in accordance with CSA A23.3. Increasing the fiber volume content to 1.0% and 1.5% resulted in shear resistances that were at least double the values calculated using ACI 318M and CSA A23.3.

14.3.3 Ductility

The shear stress-shear strain responses of the test panels are compared in Fig. 14.4. All fiber reinforced panels, except Panel C1F1V1, performed reasonably well in terms of the maximum shear strain attained at failure. With the exception of Panel C1F1V1, all fiber reinforced panels were able to undergo a maximum shear deformation of at least 62% of that of the control panels. Although not exceptional, this was remarkably good performance considering the absence of transverse reinforcement in the panels. Once again, Panel C1F2V3 was able to match Panel C1C in terms of maximum shear deformation. In contrast, Panel C1F1V1, with its low fiber volume content of 0.5%, was only able to deform to 46% of the maximum shear deformation exhibited by the control panel. This further suggests that to ensure good shear behaviour in the absence of transverse reinforcement, a fiber volume addition of greater than 0.5% is required.

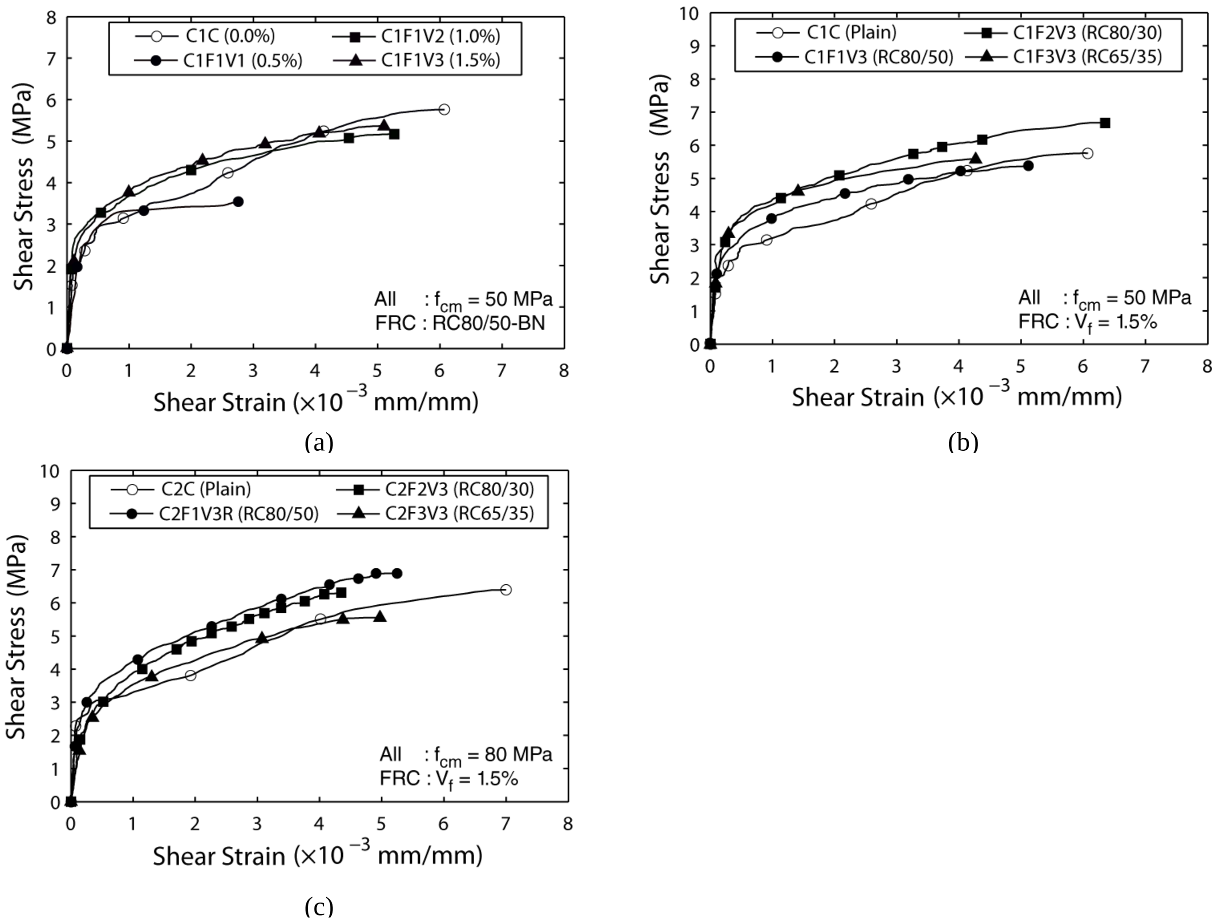

Fig. 14.4: Load-deformation response of test panels

14.4 Discussion

14.4.1 Crack control characteristics

An important property of FRC is its ability to control crack propagation. In conventionally reinforced concrete (RC), crack control is provided by the bonded steel reinforcement. Without it, the concrete exhibits a brittle behavior. In FRC, the fibers act as crack controllers and, therefore, the behavior of the concrete is significantly improved.

Fig. 14.5 compares the maximum crack width of all panels. It can be observed that for normal strength concrete panels, the FRC panels exhibited smaller crack widths than did the control panel under the same shear stress. This exemplifies the ability of fibers to control crack propagation. Due to the smaller crack widths, high stresses could still be transmitted across the crack and, thus, the integrity of the cracked panels could be maintained. An exception was Panel C1F1V1. Although it initially exhibited smaller crack widths than did the control panel, it was incapable of controlling the cracks at later load stages. The large crack widths limited the magnitude of shear stress that could be transmitted across the cracks, and hence led to the relatively poor performance of Panel C1F1V1.

The influence of fiber volume content on the crack control characteristics can be observed in Fig. 14.5 a. A fiber volume of 0.5% was deemed too low to guarantee adequate crack control, as illustrated by the wide cracks of Panel C1F1V1. Increasing the fiber content to 1.0% significantly reduced the crack widths by a factor of 3. However, not much additional improvement was obtained in increasing the fiber content from 1.0% to 1.5%.

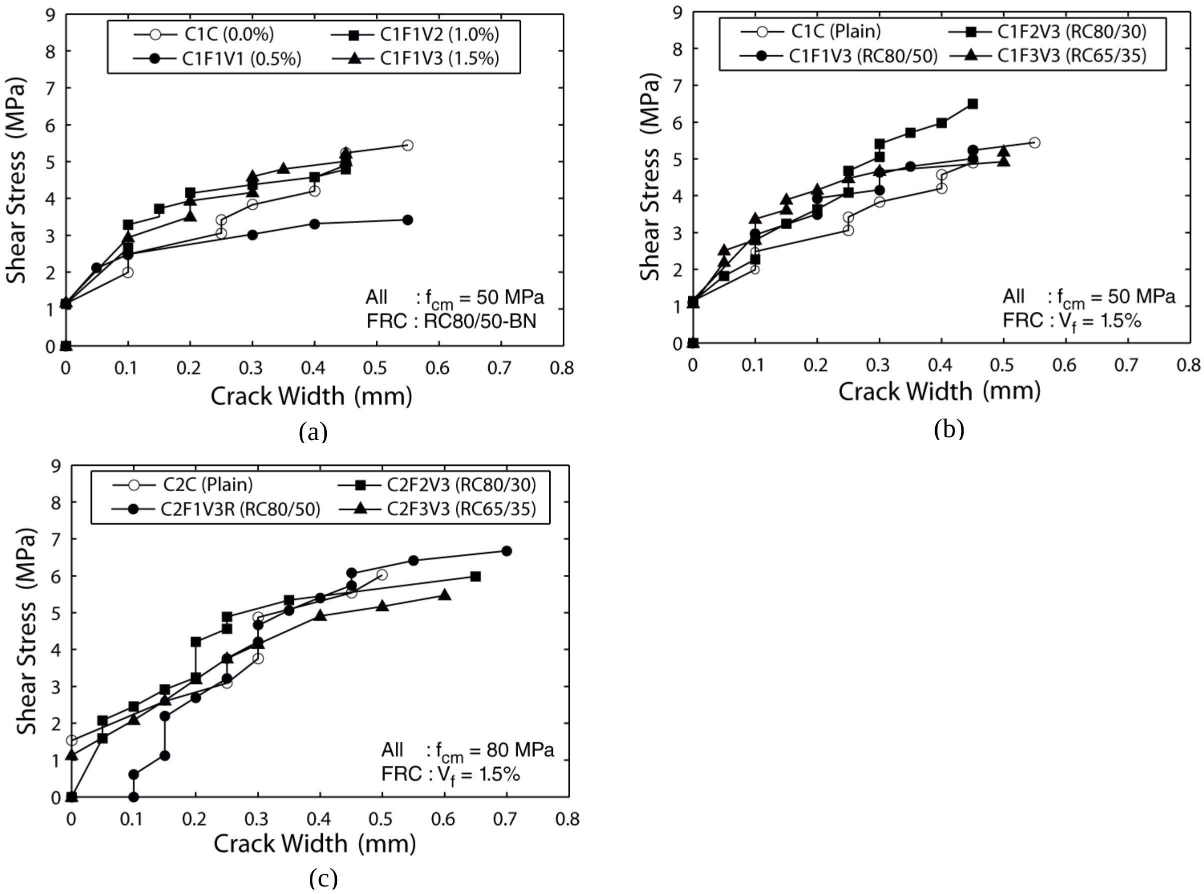

Fig. 14.5: Crack widths measured in test panels

The influence of the fiber type on the crack control characteristics is also illustrated in Fig. 14.5 b and Fig. 14.5 c. As indicated in the figures, the panels containing high aspect ratio fibers exhibited smaller crack widths than did panels containing low aspect ratio fibers.

The effectiveness of the fibers to control the crack width was less pronounced in high strength concrete panels than in normal strength concrete panels. Although the fibers in the FRC panels still exhibited a remarkable crack control ability, there was no indication of a significant improvement in their crack control characteristics over those of the conventional RC panel, as indicated in Fig. 14.5.

14.4.2 Influence of fiber content

Fig. 14.4 a shows the responses of panels having similar concrete strengths and fiber type, but different amounts of fiber. Panel C1C was the control panel with zero fiber content, whereas Panel C1F1V1, Panel C1F1V2, and Panel C1F1V3 contained 0.5%, 1.0%, and 1.5% by volume of RC80/50-BN Dramix® steel fibers, respectively.

A comparison of the shear stress-shear strain responses depicted in Fig. 14.4 a indicates a strong similarity in behavior prior to cracking. However, the similarity diminished as the panels were subjected to higher shear stresses. All FRC panels except Panel C1F1V1 exhibited a gradual softening in the response until failure occurred. The control panel C1C also exhibited softening in the response, but at a lower stiffness. Panel C1F1V1, having only 0.5% of fibers by volume, exhibited a plateau in the response soon after the first crack appeared. Its response remained flat until the panel failed at a considerably lower shear resistance and ductility level than those of the control panel.

It is evident that an increase in the fiber content led to an improvement in concrete performance. Doubling the fiber volume content from 0.5% to 1.0% resulted in a 46% increase in the shear resistance and a 94% increase in the maximum attainable shear deformation. However, less than 4% added improvement in performance was obtained from increasing the fiber volume content from 1.0% to 1.5%. It is suspected that the optimum fiber addition threshold for this particular concrete mix might have been exceeded with the 1.5% fiber addition, as suggested by Rossi (1998), leading to the minor improvement.

Examination of the principal tensile stress-principal tensile strain responses of the panels further clarified the influence of the fiber content on the behavior of FRC. For example, consider the tensile responses of the panels constructed with 50 MPa concrete and containing variable amounts of RC80/50-BN fibre, shown in Fig. 14.6 a. Although the response of Panel C1F1V1 demonstrated improvement over the response of the control panel, it still exhibited a strain softening behavior immediately after the maximum principal tensile stress was attained soon after cracking. By increasing the fiber volume content to at least 1.0%, substantial improvements in the concrete tensile behavior were observed, as indicated by the plateau in the principal tensile stress responses and by the high residual post-cracking tensile strengths. Again, only a marginal increase in the tensile stresses that could be transmitted across the cracks was obtained from increasing the fiber content from 1.0% to 1.5%, leading to the minor performance improvement of Panel C1F1V3 relative to Panel C1F1V2.

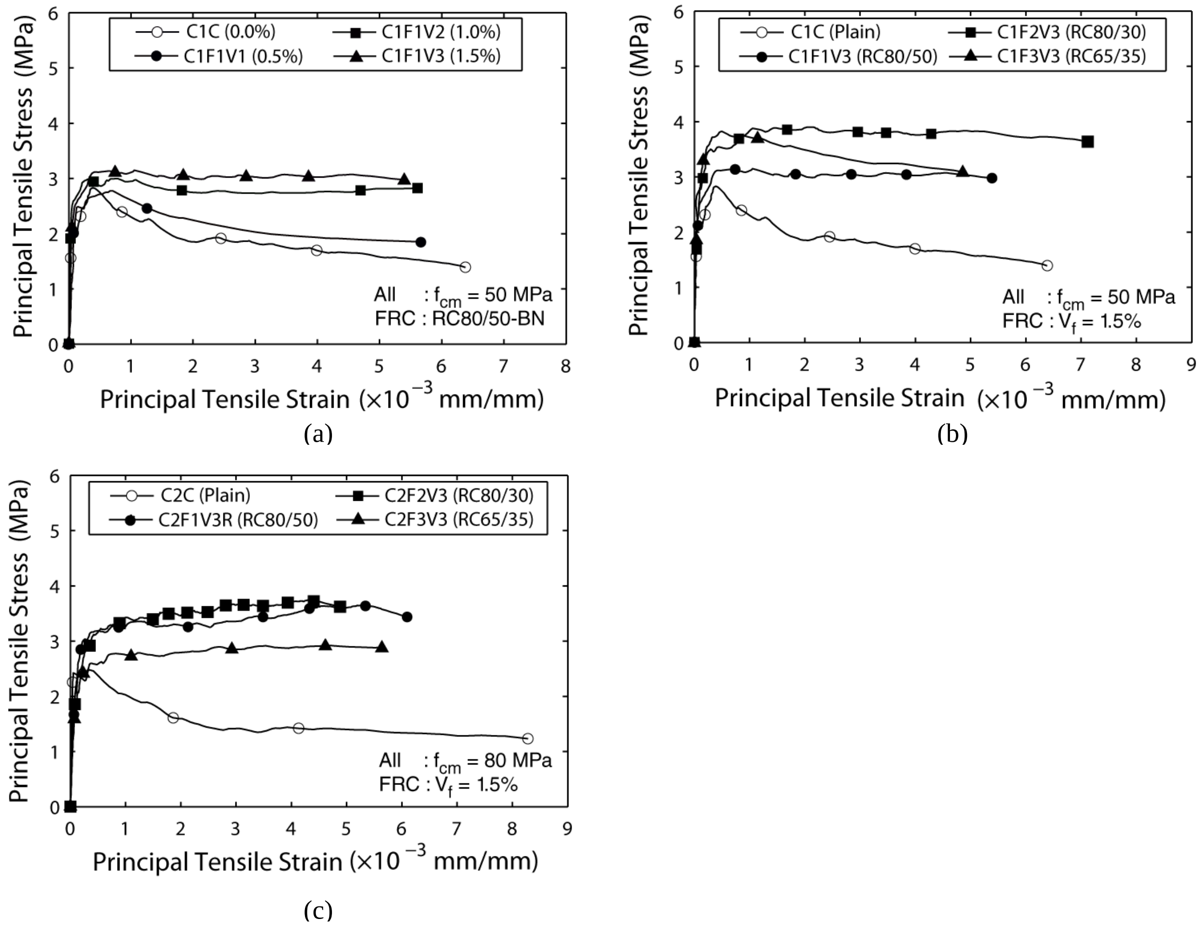

Fig. 14.6: Principal tensile stress-strain response of panels

14.4.3 Influence of fiber type

Fig. 14.4 b compares the load-deformation responses for panels having a 50 MPa nominal concrete strength and containing 1.5% of fibers by volume but varying in the type of fiber used; Fig. 14.4 c does the same for panels with an 80 MPa nominal concrete strength. It is evident from the plots that varying the type of fibers used noticeably altered the response of the panels, with the fibre length and fibre aspect ratio being significant influencing factors.

Panels containing short fibers (C1F2V3) typically exhibited a higher shear resistance than panels containing long fibers with a similar aspect ratio (C1F1V3). An examination of the principal tensile stress responses, shown in Fig. 14.6 b and 14.6 c, also suggested a similar conclusion. It is presumed that this is due to the actual number of fibers present in the panels. Despite the same fiber content, the number of individual fibers was larger for short fibers than for long fibers due to the shorter length and the smaller diameter, leading to an increased possibility of the fibers intersecting microcracks. The development of microcracks into macrocracks could then be well controlled, and the concrete performance would be improved.

Further examination of the responses plotted in Fig. 14.4 reveals the influence of the fiber aspect ratio on the panel responses. High aspect ratio fibers appear to be more effective than low aspect ratio fibers in improving the behavior of the concrete. The shear stress responses of Panel C1F1V3 and Panel C1F2V3, which contained fibers with aspect ratios of 81 and 79, respectively, showed better post-cracking ductility than did Panel C1F3V3, which contained fibers with an aspect ratio of 64. Furthermore, the principal tensile stress responses of Panel C1F1V3 and Panel C1F2V3 (Fig. 14.6 b) indicated a plateau after the maximum principal tensile stresses had been attained, whereas the response of Panel C1F3V3 showed a strain softening behavior. These findings emphasize the important influence of the fiber aspect ratio, more than the fiber length, on the effectiveness of fiber reinforcing, and agree well with the conclusions drawn by Johnston & Skarendahl (1992).

The fiber tensile strength did not seem to have a significant influence on the responses of the FRC panels tested in this research program. It appeared that the tensile stresses that were developed in the fibers were lower than the fiber ultimate tensile strength since no fiber fracture was observed. All activated fibers appeared to experience ductile fiber slippage instead of brittle fiber fracture, accounting for the ductile behavior of the FRC panels. Note that the tensile strength of the fibers does influence the moment capacity of the fibers, which affects the required force to straighten the hooks and pull the fibers out from the concrete.

14.4.4 Influence of concrete matrix strength

Concrete strength did not seem to have a substantial influence on the shear stress response of the panels, as no significant correlation was discernable from the observed behaviors depicted in Fig. 14.4. In the case of panels containing the RC80/50-BN fibers, a higher concrete strength resulted in a higher shear resistance. However, in panels containing the RC65/35-BN fibers, the opposite was observed: a higher concrete strength resulted in a lower shear resistance. It appeared that the type of fibers used in the panel was more influential than the strength of the concrete matrix.

Another indication that the concrete strength did not significantly influence the FRC behavior was given by the principal tensile stress responses, plotted in Fig. 14.6. The influence of concrete strength on the panel behavior varies with the type of fibers used. Nevertheless, it is evident that the FRC panels substantially outperformed conventionally reinforced concrete panels in terms of concrete tensile behavior, as indicated by the high residual post-cracking tensile stress.

14.5 Modeling of panels

Nonlinear finite element (FE) modeling of the panels was performed using program VecTor2 to investigate whether currently available constitutive models can accurately simulate the behavior of the FRC panels. Consider the FE modeling performed for Panel C1F1V3. The panel was modeled as one four-node plane stress rectangular concrete element with a dimension of 890×890×70 mm, as indicated in Fig. 14.7. The element was restrained against movements in the x- and y-directions at the lower left corner, and against movements in the y-direction at the lower right corner. The element was loaded in pure shear, with the load applied as monotonically increasing nodal forces at the corners of the element. The bonded conventional reinforcement was modeled as smeared reinforcement embedded within the concrete element.

Two tension softening constitutive models for FRC are available in VecTor2: custom tension softening model, in which four points representing the tension softening curve are provided as input to the program; and the Variable Engagement Model (VEM) [Voo & Foster (2003)].

The FE analysis results for Panel C1F1V3 using the custom tension softening curve and the VEM are given in Table 14.7. The shear stress-strain and principal tensile stress-strain responses are plotted in Fig. 14.8. It is evident from the results that the FE analysis could not accurately capture the behavior of the FRC panel using the currently available constitutive models. Although it managed to reasonably predict the responses of the panels up to the failure stresses obtained from the experiments, the FE analysis significantly overestimated the strength and the deformation capacity of the FRC panels.

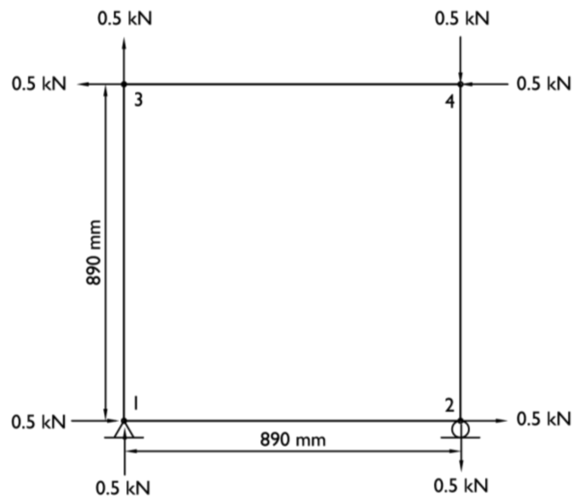

Fig. 14.7: Finite element modeling of the panels

	Experiment	Custom Tension Softening	VEM
τ_u (MPa)	5.37	7.77	6.10
γ_u (me)	5.10	20.70	18.85
Max σ_{c1} (MPa)	3.13	4.31	2.38
Max σ_{c2} (MPa)	-9.70	-19.20	-16.20
Max σ_{sx} (MPa)	204	501	439
w_m (mm)	0.45	1.63	2.19
$s_{r,m}$ (mm)	57.2	57.2	78.1

Table 14.7: FE results of Panel C1F1V3

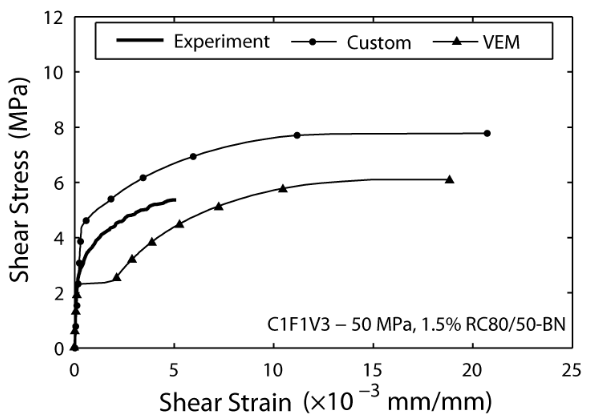

Fig. 14.8: Predicted shear response of Panel C1F1V3

A closer inspection of the FE analysis results reveals a possible explanation for the overestimation in the predicted response. In the formulation of the Modified Compression Field Theory (MCFT) [Vecchio & Collins (1986)] and the Disturbed Stress Field Model (DSFM) [Vecchio (2000)], on which VecTor2 is based, the concrete average post-cracking tensile stress is determined as the maximum of the stress calculated using the tension stiffening model and that calculated using the tension softening model. Whereas the concrete principal tensile stress due to tension stiffening is assumed to be zero at the crack, the concrete principal tensile stress due to tension softening is assumed to continue to exist at the crack. In an FRC member, the addition of the fibers significantly increases the post-cracking tensile stresses and ductility of the concrete. Thus, the concrete principal tensile stresses due to tension softening remain consistently higher than those due to tension stiffening throughout the loading history. As a consequence, the average tensile stresses in FRC elements can typically be transmitted across the cracks without any increase in the local reinforcement stresses. This results in no local shear stresses arising at the cracks and, hence, no crack shear slip. The panels will continue to carry the applied load until another failure mechanism, either crushing of the concrete or yielding of the x-direction reinforcement, takes place. Improvements to the DSFM with respect to FRC are currently being developed.

Additional FE analyses were performed using various crack spacings to investigate the influence of the crack spacing on the predictions. Average crack spacing is used to correlate the average concrete principal tensile strain required by the constitutive models to the crack width used in the VEM and in custom tension softening curve.

The analysis results are plotted in Fig. 14.9. As the results indicate, larger crack spacings resulted in wider crack widths. With the custom tension softening curve, a wider crack width caused the concrete principal tensile stress to degrade at a faster rate. With the VEM, a wider crack width resulted in fibers being engaged sooner in carrying the tensile stress, leading to an early strength gain in the panels. In both cases, reductions in the strength and deformation capacity of the panel were observed.

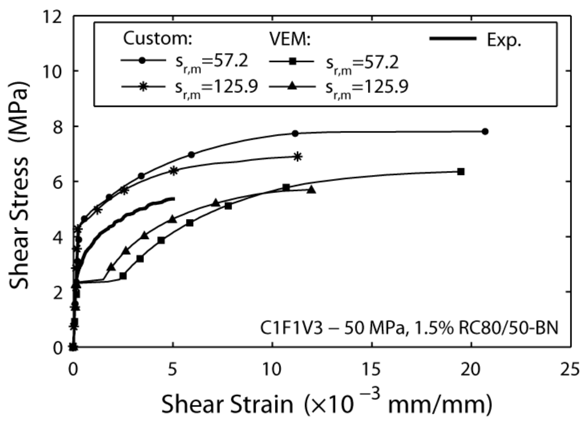

Fig. 14.9: Influence of crack spacing on prediction results

14.6 Conclusions

The results obtained from a series of panel tests indicate that the FRC panels containing a fiber volume content of at least 1.0% managed to withstand at least 87% of the maximum shear stresses sustained by the conventionally reinforced concrete panels, and were able to undergo at least 62% of the maximum shear deformations of the conventionally reinforced concrete panels. A fiber volume addition of 0.5% was found to be insufficient to guarantee adequate shear resistance and shear deformation of the panel.

The amount of fiber addition significantly influenced the behavior of the panels. A fiber volume content of 0.5% was too low to control crack propagation. Increasing the fiber content to 1.0% resulted in a 46% increase in the shear resistance, a 94% increase in the maximum shear deformation, and a reduction in the crack widths by a factor of 3. However, only a minor improvement was obtained by increasing the fiber volume content from 1.0% to 1.5%, possibly due to fiber saturation.

The concrete compressive strength was not found to significantly influence the shear response of the FRC panels. The fiber type was found to be more influential than the concrete compressive strength. The use of fibers with a high aspect ratio resulted in much improved post-cracking deformation capacities and crack control characteristics compared to when fibers with a low aspect ratio were used. The panels containing short fibers were found to exhibit a higher shear resistance and a higher maximum concrete principal tensile stress than the panels containing long fibers with a similar aspect ratio due to the presumably larger number of fibers for the same fiber volume content.

Significant overestimations of the shear strength and the deformation capacity of all FRC panels were obtained from nonlinear finite element analyses using the available constitutive models. They are believed to be the result of the failure to properly recognize the correct tension stiffening behavior and the aggregate interlock mechanism. In addition, crack spacing was found to significantly influence the analysis results.

14.7 References

ACI Committee 318, 2008. "Building Code Requirements for Structural Concrete and Commentary - ACI 318M-08", *American Concrete Institute*, 436p.

Adebar, P., Mindess, S., St.-Pierre, D., and Olund, B., 1997. "Shear Tests of Fiber Concrete Beams Without Stirrups", *ACI Structural Journal*, Vol. 94, No. 1, January-February 1997, pp. 68-76.

Ashour, S.A., Hasanain, G.S., and Wafa, F.F., 1992. "Shear Behavior of High-Strength Fiber Reinforced Concrete Beams", *ACI Structural Journal*, Vol. 89, No. 2, March-April 1992, pp. 176-184.

Banthia, N., Azabi, M., & Pigeon, M. 1993. Restrained Shrinkage Cracking in Fiber-Reinforced Cementitious Composites. *Materials and Structures* 26(7): 405-413.

Bekaert 2003. Product Data Sheet for Dramix Fibers. http://www.bekaert.com/building.

CAN/CSA Standard S6-06, 2006. *Canadian Highway Bridge Design Code*. Canada: Canadian Standards Association.

Grzybowski, M. & Shah, S.P. 1990. Shrinkage Cracking on Fiber Reinforced Concrete. *ACI Materials Journal* 87(2): 138-148.

Johnston, C.D. & Skarendahl, A. 1992. Comparative Flexural Performance Evaluation of Steel Fiber-Reinforced Concretes According to ASTM C1018 Shows Importance of Fiber Parameters. *Materials and Structures* 25(4): 191-200.

Minelli, F. and Vecchio, F.J., 2006. "Compression Field Modelling of Fiber-Reinforced Concrete Members Under Shear Loading", *ACI Structural Journal*, Vol. 103, No. 2, March-April 2006, pp. 244-252.

Ong, K.C.G. & Paramasivam, P. 1989. Cracking of Steel Fiber Reinforced Mortar due to Restrained Shrinkage. In R.N. Swamy and B. Barr (eds), *Fiber Reinforced Cements and Concretes: Recent Developments*: 179-187. London: Elsevier Science Publishers Ltd.

Rossi, P. 1998. *Les Bétons de Fibers Métalliques*. Paris: Presses de l'École Nationale des Ponts et Chaussées.

Susetyo, J. 2009. *Fiber Reinforcement for Shrinkage Crack Control in Prestressed, Precast Segmental Bridges*. PhD. Thesis. University of Toronto. Canada.

Shah, S.P., Weiss, J., & Yang, W. 1998. Shrinkage Cracking - Can It Be Prevented?. *Concrete International* 20(4): 51-55.

Tan, K.H., Murugappan, K., Paramasivam, P., 1993. "Shear Behavior of Steel Fiber Reinforced Concrete Beams", *ACI Structural Journal*, Vol. 90, No. 1, January-February 1993, pp. 3-11.

Vecchio, F.J. & Collins, M.P. 1986. The Modified Compression Field Theory for Reinforced Concrete Elements Subject to Shear. *ACI Journal* 83(2): 219-231.

Vecchio, F.J. 2000. Disturbed Stress Field Model for Reinforced Concrete: Formulation. *ASCE Journal of Structural Engineering* 126(9): 1071-1077.

Voo, J.Y.L. & Foster, S.J. 2003. Variable Engagement Model for Fiber Reinforced Concrete in Tension. *UNICIV Report No. R-420 June 2003*. Sydney: The University of New South Wales.

Notations

A_s	area of reinforcement
A_{sw}	area of shear reinforcement
E_s	modulus of elasticity of steel
V_f	volume content of steel fiber
b	width
f_c	cylinder compressive strength of concrete
f_{cm}	mean value of compressive strength f_c at an age of 28 days
f_{fu}	tensile strength of steel fiber at maximum load
f_y	tension yield stress of non-prestressing reinforcement
f_u	tensile strength of reinforcing bar at maximum load
l_f	length of steel fiber
s_{sw}	spacing of shear reinforcement
$s_{r,m}$	mean spacing between cracks
w_m	mean crack width
ε_y	yield strain of reinforcing steel
ε_u	total elongation of reinforcing bar at maximum load
γ_r	shear strain at the onset of cracking
γ_u	shear strain at ultimate shear stress
ρ_{min}	minimum ratio of reinforcement
ρ_x	ratio of reinforcement in the x-direction (longitudinal direction)
ρ_y	ratio of reinforcement in the y-direction (transverse direction)
σ_{c1}	principal tensile stress of concrete
σ_{c2}	principal compression stress of concrete
σ_{sx}	steel stress in the x-direction (longitudinal direction)
σ_{sy}	steel stress in the y-direction (transverse direction)
τ_r	shear stress at the onset of cracking
τ_R	resistance to shear stress
τ_u	ultimate shear stress
Ø_b	nominal diameter of reinforcing steel bar
Ø_f	diameter of steel fiber

15 Use of steel fibre reinforcement for shear resistance in beams and slab-column connections

Gustavo J. Parra-Montesinos[1], James K. Wight[2], Hai H. Dinh[3] and Min-Yuan Cheng[4]

[1]Associate Professor, University of Michigan, Ann Arbor, USA
[2]Frank E. Richart, Jr. Collegiate Professor, University of Michigan, Ann Arbor, USA
[3]Engineer, Moffatt and Nichol, San Francisco, USA
[4]Assistant Professor, National Taiwan University of Science and Technology, Taipei, Taiwan

Abstract: Steel fibres are known to increase the shear strength of reinforced concrete flexural members by providing diagonal tension resistance and controlling the opening of diagonal cracks, which increases aggregate interlock. It is therefore of interest to determine in which cases steel fibre reinforcement can be used as replacement of traditional shear reinforcement in concrete members. Two applications were investigated in this study: 1) beams under gravity-type loading; and 2) slab-column connections under both gravity-type and earthquake-type loading. The results from experimental research presented herein indicate that hooked steel fibres in volume fractions greater than or equal to 0.75% are effective in ensuring multiple diagonal cracking and substantially increasing shear strength. The shear strength of all steel fibre reinforced concrete (SFRC) beams tested in this investigation exceeded $0.3\sqrt{f_c}$ (MPa). Compared to a beam with stirrup reinforcement satisfying the minimum requirements in the 2008 ACI Building Code, the SFRC beams exhibited higher shear strength and enhanced cracking pattern, indicating that hooked steel fibres in a 0.75% volume fraction can be used in lieu of minimum stirrup reinforcement in beams. Fibres were also found effective in increasing punching shear strength and ductility in slab-column connections under monotonically-increased loading, as well as under combined gravity load and lateral displacement reversals. Drift capacities exceeding 3% were observed in two SFRC large-scale connections with a 1.5% hooked fibre volume fraction, subjected to a gravity shear ratio of approximately 0.4 [gravity shear stress of $0.13\sqrt{f_c}$ (MPa)] in combination with bi-axial lateral displacements. In contrast, a nominally identical regular concrete connection with shear stud reinforcement failed at 1.6% drift.

15.1 Introduction

Steel fibre reinforcement has long been recognized to increase shear resistance in reinforced concrete flexural members [Batson, Jenkins and Spatney (1972); Swamy and Bahia (1985); Schantz (1993); Adebar et al. (1997); Noghabai (2000); Rosenbusch and Teutsch (2002); Kwak et al. 2002); Parra-Montesinos (2006)]. The contribution of fibre reinforcement to shear resistance can be attributed to the ability of fibres to: 1) transfer stresses across diagonal cracks; and 2) control the spacing and widening of diagonal cracks, which increases aggregate interlock. From a practical viewpoint, however, the use of steel fibres is most attractive in cases where they can completely replace bar-type shear reinforcement. As the test results described herein will show, this is possible in beams requiring minimum shear reinforcement and in connections between slabs and columns.

15.2 Shear tests of steel fibre reinforced concrete beams

A survey of tests conducted by the first author [Parra-Montesinos (2006)] on steel fibre reinforced concrete (SFRC) beams without stirrup reinforcement revealed two main conclusions: 1) when used in a volume fraction greater than or equal to 0.75%, a stress $\frac{V}{bd} = 0.3\sqrt{f_c}$ (MPa) represented a lower bound to the beam shear strength; and 2) most of the available test data corresponded to beams of relatively small depth ($h_b \leq 300$ mm). In that survey, only beams with deformed steel fibres (i.e., hooked or crimped) were considered, given their improved pullout response due to mechanical anchorage compared to straight steel fibres. Fig. 15.1 shows a plot of average shear stress versus beam effective depth d for beams with shear span-to-effective depth ratio (a/d) greater than or equal to 2.8 [for information on test data, see Parra-Montesinos (2006)]. Different markers are used to indentify ranges in fibre volume content. As can be seen, the majority of the data correspond to effective depths d of approximately 280 mm or less and fibre volume fractions V_f less than or equal to 1%, with very few data points corresponding to beams with more realistic depths (e.g., $d \geq 350$ mm).

The limited shear test data for deeper beams have prevented researchers from evaluating whether: 1) the efficiency of fibre reinforcement to contribute to shear resistance remains relatively unchanged in deeper beams; and 2) fibre reinforcement can effectively reduce shear size effect. In order to generate data that could help answer these questions, a comprehensive experimental program was recently conducted at the University of Michigan [Dinh, Parra-Montesinos, and Wight (2010)].

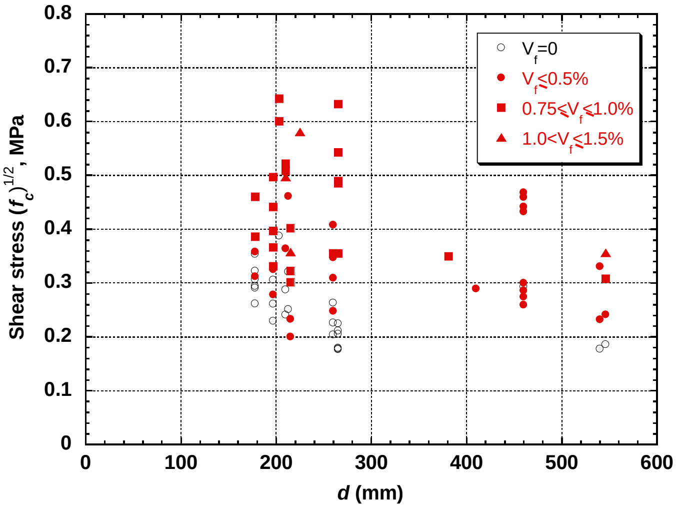

Fig. 15.1: Shear strength versus effective depth for SFRC slender beams (a/d ≥ 2.8)

A total of 28 simply supported beams were tested under monotonically increased concentrated force. Test variables were: 1) beam depth; 2) fibre type and content; and 3) longitudinal reinforcement ratio. Table 15.1 lists the main features of the test specimens.

Beams with overall depths of either 455 mm (Series B18) or 685 mm (Series B27) were tested to evaluate the effect of beam depth on diagonal cracking distribution and shear strength. All fibres evaluated had hooks at their ends. However, fibres of various lengths and diameters, as well as tensile strength, were evaluated in volume fractions ranging between 0.75% and 1.5%. Table 15.2 lists the main properties for the three types of fibres used. The change in tension longitudinal reinforcement ratio ρ, which varied between 1.6% and 2.7%, was meant to allow the evaluation of shear behaviour in SFRC beams prior to and after flexural yielding has occurred.

Fig. 15.2 shows the reinforcement details for the test beams. All test beams had a shear span-to-effective depth ratio (a/d) of approximately 3.5 in order to reduce the effect of arch action on beam behaviour. In general, the beams were tested in pairs to increase the reliability of the data. For comparison purposes, two regular concrete beams were tested in both Series B18 and Series B27. In Series B18, these two beams did not contain stirrup reinforcement, while in Series B27, one of the two regular concrete beams was reinforced with stirrup reinforcement satisfying the minimum requirements in the 2008 ACI Building Code [ACI Committee 318 (2008)]. Concrete for all beams had a specified concrete strength of 41 MPa, while course aggregate consisted of crushed limestone with a maximum size of 6 mm.

15.2.1 Material properties

Standard material tests were conducted to determine: 1) concrete compressive strength; 2) flexural behaviour of the SFRCs investigated; and 3) stress-strain response of the steel reinforcing bars. Concrete compressive strength was determined from tests of 100x200 mm cylinders. Results from concrete cylinder tests are listed in Table 15.1. SFRC flexural behaviour, on the other hand, was evaluated through ASTM 1609 third-point bending tests [ASTM 1609-06 (2006)]. These tests were conducted on 150x150x510 mm (460 mm span) unnotched beams. The average response obtained from ASTM beams made out of the SFRC used in several of the test specimens is shown in Fig. 15.3. Steel bar properties were determined through direct tensile tests of representative bar samples. Yield strength values are listed at the bottom of Fig. 15.2.

Beam	b (mm)	d (mm)	a/d	ρ (%)	Fiber type	V_f (%)	f_c MPa	P_u (kN)	v_u (MPa)	$\frac{v_u}{\sqrt{f_c}}$
B18-0a	152	381	3.43	2.7	-	-	42.8	168	1.1	0.17
B18-0b	152	381	3.43	2.7	-	-	42.8	162	1.1	0.17
B18-1a	152	381	3.43	2.0	1	0.75	44.8	441	2.9	0.44*
B18-1b	152	381	3.43	2.0	1	0.75	44.8	413	2.8	0.41*
B18-2a	152	381	3.50	2.0	1	1.00	38.1	437	3.0	0.49*
B18-2b	152	381	3.50	2.0	1	1.00	38.1	445	3.1	0.50*
B18-2c	152	381	3.50	2.7	1	1.00	38.1	503	3.5	0.57*
B18-2d	152	381	3.50	2.7	1	1.00	38.1	367	2.6	0.41
B18-3a	152	381	3.43	2.7	1	1.50	31.0	384	2.6	0.46
B18-3b	152	381	3.43	2.7	1	1.50	31.0	507	3.4	0.61
B18-3c	152	381	3.43	2.7	1	1.50	44.9	494	3.3	0.49
B18-3d	152	381	3.43	2.7	1	1.50	44.9	490	3.3	0.49
B18-5a	152	610	3.43	2.7	2	1.00	49.2	445	3.0	0.43
B18-5b	152	610	3.43	2.7	2	1.00	49.2	565	3.8	0.54
B18-7a	152	610	3.43	2.0	3	0.75	43.3	498	3.3	0.50*
B18-7b	152	610	3.43	2.0	3	0.75	43.3	490	3.3	0.50*
B27-1a	203	610	3.50	2.0	1	0.75	50.8	908	2.9	0.41
B27-1b	203	610	3.50	2.0	1	0.75	50.8	837	2.7	0.38
B27-2a	203	610	3.50	2.0	2	0.75	28.7	872	2.8	0.53
B27-2b	203	610	3.50	2.0	2	0.75	28.7	854	2.8	0.52
B27-3a	203	610	3.50	1.6	1	0.75	42.3	846	2.7	0.42*
B27-3b	203	610	3.50	1.6	1	0.75	42.3	863	2.8	0.43*
B27-4a	203	610	3.50	1.6	2	0.75	29.6	663	2.1	0.40
B27-4b	203	610	3.50	1.6	2	0.75	29.6	556	1.8	0.33
B27-5	203	610	3.50	2.1	1	1.50	44.4	1081	3.5	0.53*
B27-6	203	610	3.50	2.1	2	1.50	42.8	1046	3.4	0.52*
B27-7	203	610	3.50	1.6	-	-	37.0	402	1.3	0.21
B27-8	203	610	3.50	1.6	-	Min. Stirrups	37.0	570	1.8	0.30

*Reinforcement yielded. All beams failed in shear except for Beam B27-3a, which failed in flexure.

Table 15.1: Summary of SFRC test beams

Fibre type	Length (mm)	Diameter (mm)	Aspect ratio	Strength (MPa)
1	30	0.55	55	1100
2	60	0.75	80	1050
3	30	0.38	80	2300

Table 15.2: Steel fibre properties

15.2.2 Shear behaviour of SFRC test beams

15.2.2.1 Cracking Pattern

The behaviour of the SFRC beams was distinctly different compared to that of regular concrete beams without stirrup reinforcement. While the regular concrete beams without shear reinforcement failed soon after the first diagonal crack developed, multiple diagonal cracks were observed in all SFRC beams. In the regular concrete beam with minimum stirrup reinforcement, the cracking pattern could be considered somewhere in between that of the regular concrete beams unreinforced in shear and the multiple cracking observed in the SFRC beams. Fig. 15.4 shows a comparison of the cracking pattern for beams with no stirrups, minimum stirrup reinforcement, and Type 1 fibre reinforcement in a 0.75% volume fraction.

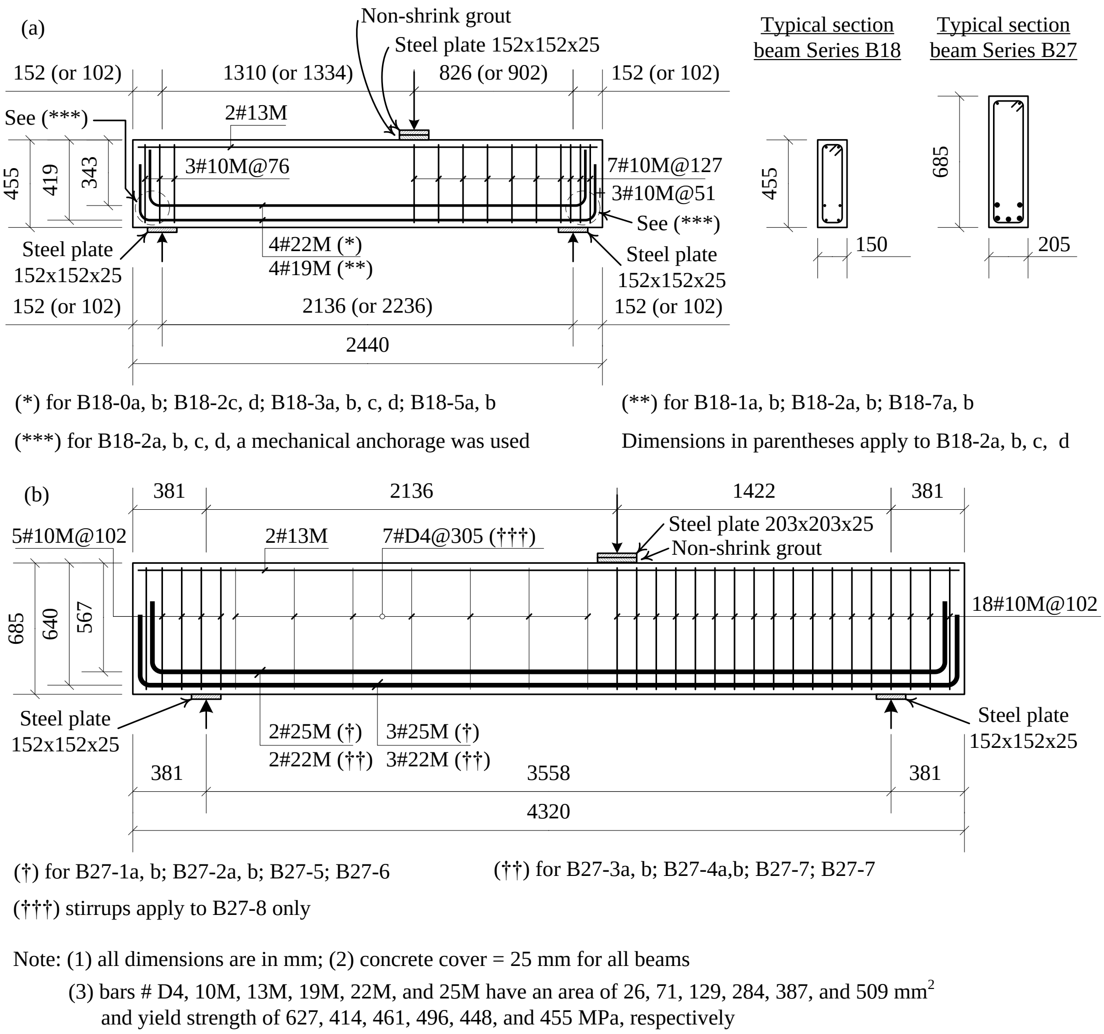

Fig. 15.2: Reinforcement details for SFRC test beams

Cracking spacing was evaluated by determining the average horizontal crack spacing at beam mid-depth. Horizontal rather than perpendicular spacing between cracks was measured due to the fact that inclined cracks are generally not parallel to each other and tend to change direction as they propagate to the beam compression zone. Horizontal crack spacing, however, can be easily converted into a perpendicular crack spacing by assuming an average crack angle. Even though multiple cracking developed in all SFRC beams regardless of their depth, the average crack spacing increased with beam depth. A horizontal crack spacing equal to 0.4*d* seems to capture well the observed dependency of crack spacing with beam depth for the two beam depths considered.

Crack widths were monitored through manual measurements, as well as the use of a non-contact infrared-based tracking system (Optotrak). While manual measurements could be taken at several load levels, the Optotrak system allowed the estimation of crack widths close to failure, which permitted the determination of a critical crack width at which failure of the SFRC beams occurred. This critical crack width was found to depend on fibre length, being on the order of 5% of the length of the fibre used (i.e., 1.5 mm and 3 mm for the beams with Type 1 and 3, and Type 2 fibres, respectively).

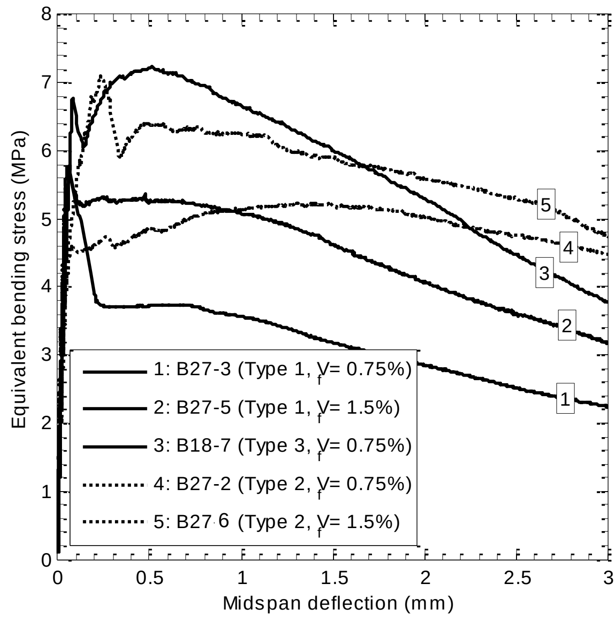

Fig. 15.3: Results from ASTM 1609 four-point bending tests

15.2.2.2 Load versus deflection response

All beams constructed with regular concrete exhibited a linear behaviour up to shear failure, which even for the beam with minimum stirrup reinforcement occurred in a rather brittle manner. The load versus displacement response of the SFRC test beams was influenced by the amount of flexural reinforcement and fibre content, which determined whether shear failure occurred prior to or after flexural yielding. The beams that exhibited flexural yielding prior to shear failure are identified in Table 15.1. For SFRC beams that failed in shear prior to flexural yielding, the response was approximately linear up to failure. However, the presence of fibres allowed the development of multiple diagonal cracks and the widening of at least one of them prior to a shear failure, which provided some warning about the imminence of failure. Ultimate failure in these beams, however, was rather sudden.

For cases in which flexural yielding preceded a shear failure, the shear stress versus displacement response exhibited a well defined yield plateau. However, because the shear force demand associated with flexural yielding was close to the beam shear capacity when behaving in the elastic range (prior to flexural yielding), the degree of yielding often varied, even within the same pair of beams. Fig. 15.5 shows representative responses for the regular concrete beams (with and without stirrups), as well as for the SFRC beams that failed prior to or after flexural yielding.

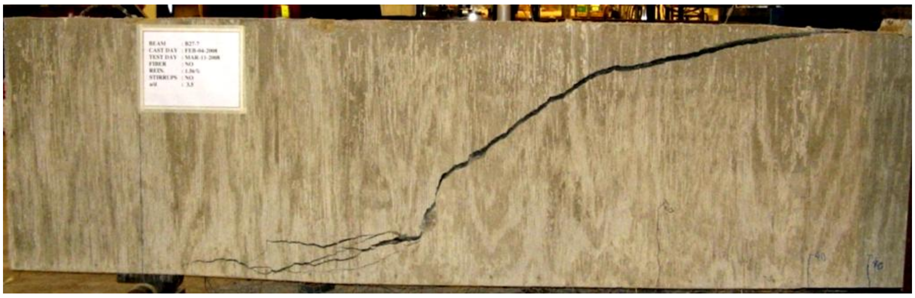

a) Regular concrete Beam B27-7 without stirrups

b) Regular concrete Beam B27-8 with minimum stirrup reinforcement

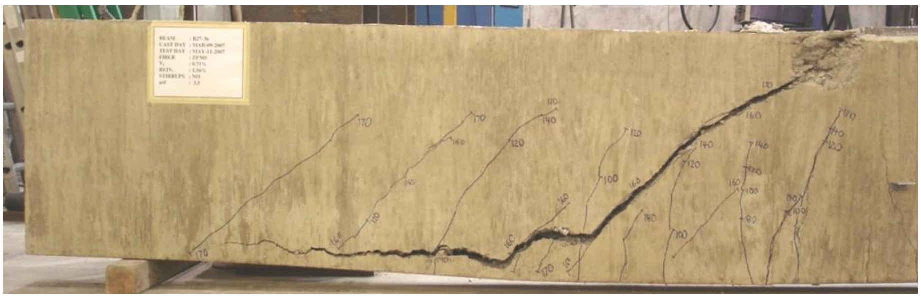

b) SFRC Beam B27-3b with a 0.75% volume fraction of Type 1 fibres

Fig. 15.4: Cracking pattern in regular concrete and SFRC beams

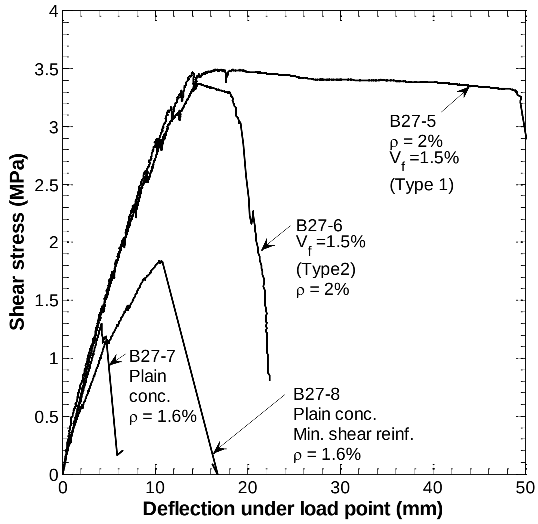

Fig. 15.5: Load versus displacement behaviour of selected test specimens

All SFRC beams except for Beam B27-3a ultimately failed in shear, either in shear compression or diagonal tension. In some cases, a splitting crack along the longitudinal reinforcement was also observed, caused by bond degradation attributed to either lumping of fibres along the top layer of tension reinforcement or voids created during concrete casting, or both. Beam B27-3a was the only test beam that failed in flexure due to crushing of the compression zone after extensive flexural yielding had taken place. As mentioned earlier, shear failure of the SFRC beams occurred after one of the diagonal cracks reached a width on the order of 5% of the fibre length.

15.2.2.3 Shear strength

All SFRC beams exhibited a shear strength between $0.33\sqrt{f_c}$ and $0.61\sqrt{f_c}$ (MPa), while the shear strength of the regular concrete beams without stirrups was $0.17\sqrt{f_c}$ and $0.21\sqrt{f_c}$ (MPa) for the beams with 455 and 685 mm of depth, respectively. The beam with stirrup reinforcement satisfying the minimum requirements in the 2008 ACI Code exhibited a nearly 50% increase in shear strength ($0.30\sqrt{f_c}$, MPa) compared to the regular concrete beam.

In order to evaluate the effect of fibre content on the shear strength of the SFRC beams, Fig. 15.6 shows a plot of average shear stress versus fibre volume ratio for all three fibre types investigated. All SFRC beams shown in Fig. 15.6 contained a longitudinal reinforcement ratio ρ approximately equal to 2.0%, while ρ was equal to 2.7% and 1.6% in the RC beams (fibre volume fraction = 0 in Fig. 15.6) with overall depth of 455 and 685 mm, respectively. As shown in the figure, fibres were most effective at a 0.75% volume fraction. On average, adding fibres in a 0.75% volume fraction led to a more than double increase in shear strength compared to the beams without shear reinforcement. Increasing the fibre volume ratio from 0.75% to either 1% or 1.5% led to a further increase in strength, but at a lower rate.

15.3 Estimation of shear strength of steel fibre reinforced concrete beams

From observations made during the beam tests described above, a simple model has been proposed [Dinh (2009)] for estimating the shear strength of beams with deformed steel fibres. The model is based on the assumption that at failure, beam shear strength can be calculated as the summation of shear due to diagonal tension resisted by fibres, and shear carried in the compression zone. Fibre contribution through diagonal tension is not independent of aggregate interlock. As mentioned earlier, fibres control the growth of diagonal cracks, which increases aggregate interlock. For simplicity, however, the entire contribution from stresses at a crack is assumed to come from diagonal tension resisted by the fibre reinforcement.

Fig. 15.7 shows the assumed shear failure mode for SFRC beams. At failure, the beam is assumed to rotate about point *P*. A diagonal crack with a horizontal projection at the level of the tension reinforcement of (d-c) (i.e., α = 45 degrees in Fig. 15.7), where c represents the neutral axis depth, is assumed at this stage. Consistent with the measured crack widths at failure, the width of the critical crack at the level of the longitudinal tension steel is taken equal to $0.05L_f$, where L_f is the fibre length. The beam shear strength is then calculated as the summation of the vertical component of the resultant tension force across the critical diagonal crack, $V_{FRC} = T_f\ cos(\alpha)$, and the shear carried by the beam compression zone, V_{cc}. The determination of V_{FRC} and V_{cc} is discussed next.

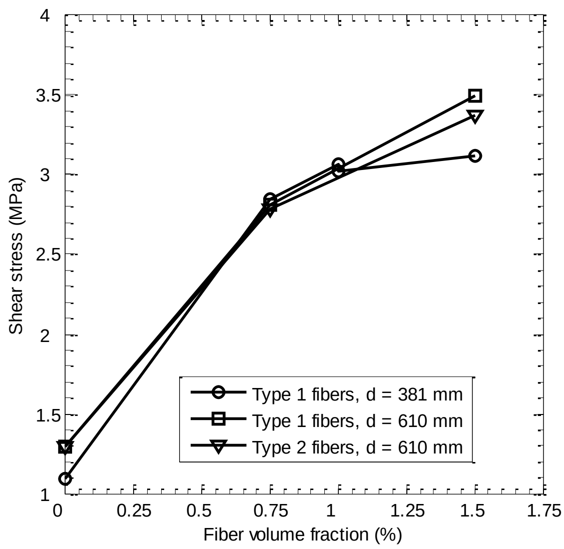

Fig. 15.6: Effect of fibre volume fraction on shear strength

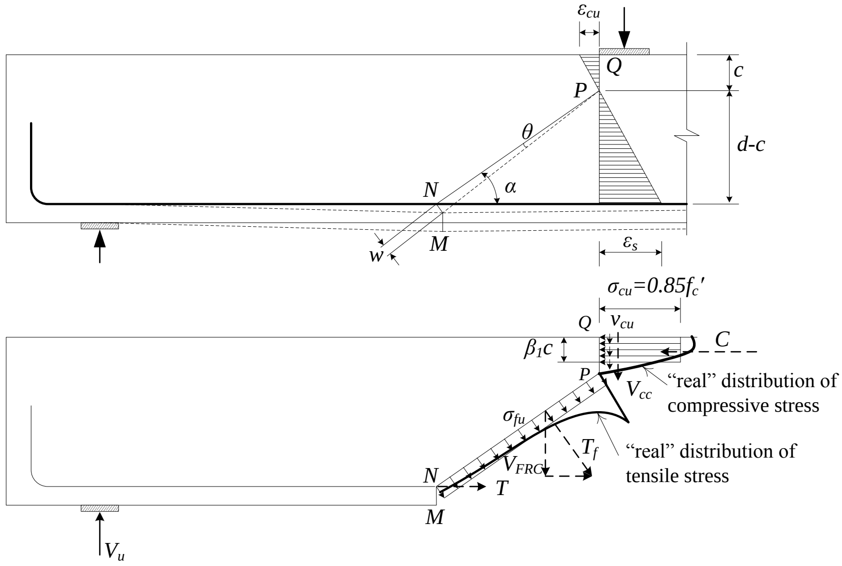

Fig. 15.7: Assumed critical diagonal crack and stresses at failure

15.3.1 Fibre contribution to beam shear strength, V_{FRC}

The fibre contribution to beam shear strength requires the estimation of the tensile stresses across the critical diagonal crack. For this purpose, an analogy is made between the critical diagonal crack in an actual beam, which is assumed to increase in width as the distance from the neutral axis increases, and the flexural crack that forms in the middle third of an ASTM 1609 beam. Assuming that the average tensile stress perpendicular to these two cracks is equal at a given maximum crack width, the problem could be simplified by looking at the average tensile stress in the ASTM 1609 beam at a crack width corresponding to the critical crack width, which based on test results is taken equal to $0.05L_f$. It is worth mentioning that if more than one flexural crack develops in the ASTM beam, the procedure outlined next is not applicable. Such a case, however, is rare in SFRC materials with fibre contents not exceeding 1% by volume.

For design purposes, the specification of a mid-span deflection at which the average tensile stress in an ASTM 1609 beam is to be calculated is more attractive than the use of a target crack width. This requires the determination of a relationship between the two variables, which can be done based on Fig. 15.8. Assuming that ASTM beam deflections are entirely due to the opening of a single crack in the middle third of the beam, located at a distance βL from the closest support, the mid-span deflection at the critical crack width w_{cr}, δ_{cr}, can be calculated as follows,

$$\delta_{cr} = \frac{w_{cr}\beta L}{2(h-c)} \tag{15.1}$$

where $w_{cr} = 0.05L_f$, h is the beam height, c is the neutral axis depth, and βL ranges between 1/3 and 1/2 of the span length L. Given the randomness of the crack location, βL is conservatively taken as $0.5L$. The neutral axis depth at the critical crack width can be calculated assuming a uniform compressive stress of $0.85f_c$ over the entire compression zone . It should be mentioned, however, that any error incurred in the estimation of the neutral axis depth has a small effect on the determination of the average tensile stress, given the fact that it represents a very small percentage of the total beam depth. Because of this and based on test observations, the use of $c = 0.1h$ is recommended. Taking $\beta L = 0.5L$ and $c = 0.1h$, and considering the fact that in ASTM 1609 beams $L = 3h$, Eq. (15.1) can be simplified as follows,

$$\delta_{cr} \cong \frac{0.05L_f(0.5L)}{2(0.9h)} = \frac{L_f(3h)}{72h} = \frac{L_f}{24} \tag{15.2}$$

The average tensile stress at the critical crack width (σ_{fu} in Fig. 15.7), can then be calculated based on the applied moment at a mid-span deflection δ_{cr} as follows,

$$\sigma_{fu} = \frac{2(M)_{\delta=\delta_{cr}}}{0.9bh^2} \tag{15.3}$$

In order to account for potential differences between the behaviour of SFRC in ASTM 1609 beams and that in the actual beam (e.g. due to fibre distribution, specimen size), it is recommended that a strength reduction factor, arbitrarily selected as 0.8, be applied to the average tensile stress in Eq. (15.3) for use in the calculation of V_{FRC}.

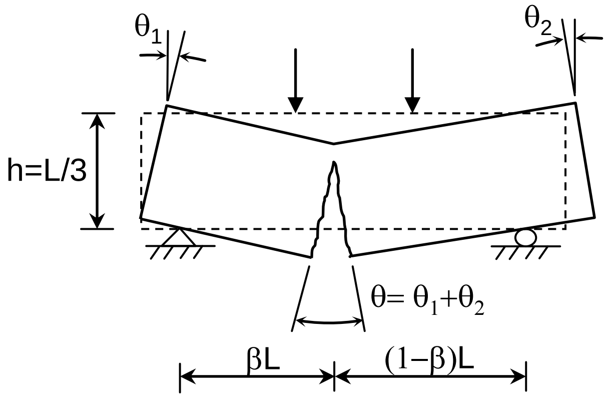

Fig. 15.8: Assumed deformations in ASTM 1609 beam

15.3.2 Shear carried by beam compression zone, V_{cc}

The shear carried by the beam compression zone is determined based on the failure criterion developed by Bresler and Pister (1958) for concrete subjected to combined shear and compression stresses. This failure criterion is defined by Eq. (15.4) as follows,

$$\frac{v_{cu}}{f_c} = 0.1\left[0.62 + 7.86\left(\frac{\sigma_{cu}}{f_c}\right) - 8.46\left(\frac{\sigma_{cu}}{f_c}\right)^2\right]^{1/2} \tag{15.4}$$

where v_{cu} and σ_{cu} are the acting shear stress and normal compressive stress at failure, respectively. It has been shown [Dinh (2009)] that rather than calculating v_{cu} based on a nonlinear compressive stress distribution over the beam compression zone, the use of Whitney's stress block, as defined in the ACI Building Code [ACI Committee 318 (2008)], leads to conservative estimations of the shear carried in the compression zone. In this case,

σ_{cu} = 0.85f_c and v_u = 0.11f_c over a depth a = $\beta_1 c$, where β_1 = 0.85 for $f_c \leq$ 28 MPa and β_1 = 0.65 for $f_c \geq$ 55 MPa. Linear variation in β_1 is assumed for 28 MPa < f_c < 55 MPa. The shear carried by the beam compression zone is thus calculated as,

$$V_{cc} = 0.11 f_c \beta_1 cb = 0.11 \frac{T_s}{0.85} = 0.13 A_s f_y \tag{15.5}$$

where A_s is the area of tension steel and f_y is the yield strength of the tension reinforcement. In Eq. (15.5), the neutral axis depth is calculated at yielding of the tension steel, assuming the beam is under-reinforced, as required for design.

The proposed model was evaluated by comparing shear strength predictions with experimental results for a total of 59 SFRC beams reported in the literature [Mansur, Ong, and Paramasivam (1986); Narayanan and Darwish (1987); Lim, Paramasivam, and Lee (1987); Li, Ward, and Hamza (1992); Tan, Murugappan, and Paramasivam (1993); Casanova and Rossi (1999); Noghabai (2000); Rosenbusch, and Teutsch (2002); Kwak et al. (2002); and Cucchiara, La Mendola, and Papia (2004)], in addition to the 25 SFRC beams tested in this investigation. The beams considered satisfied the following conditions:

1) shear span-to-depth ratio $a/d \geq 2.5$
2) beam depth h between 230 mm and 685 mm
3) longitudinal tension reinforcement ratio ρ between 1.2% and 4.5%
4) concrete cylinder strength f_c between 20.7 MPa and 104 MPa
5) hooked steel fibres in volume fractions ranging between 0.5% (39 kg/m^3) and 2% (157 kg/m^3)
6) fibre tensile strength $\geq$ 1030 MPa
7) fibre length-to-diameter ratio between 55 and 100.

Because no data were available with regard to flexural performance of the SFRC materials except for the beams tested in this investigation, the following expression was used to evaluate σ_{fu} (in MPa), based on results from ASTM 1609 tests performed on the materials used in this research.

$$\sigma_{fu} = 0.8\ x\ 1.5 (\frac{V_f}{0.0075})^{\frac{1}{4}} \tag{15.6}$$

where 0.8 is a strength reduction factor to account for differences in material behaviour in small ASTM 1609 beams and larger scale beams, as explained earlier.

A plot of the ratio between predicted and experimental shear strength versus fibre volume fraction V_f is shown in Fig. 15.9. As can be seen, the proposed model predicted reasonably well the shear strength of the SFRC beams. The mean value and standard deviation of the predicted versus experimental strength ratio was 0.79 and 0.12, respectively. The predictions were consistent for the range of fibre volume fractions considered. It should be mentioned that shear strength was over-predicted in only 4% of the cases and the percentage of over-prediction did not exceed 6% in any case.

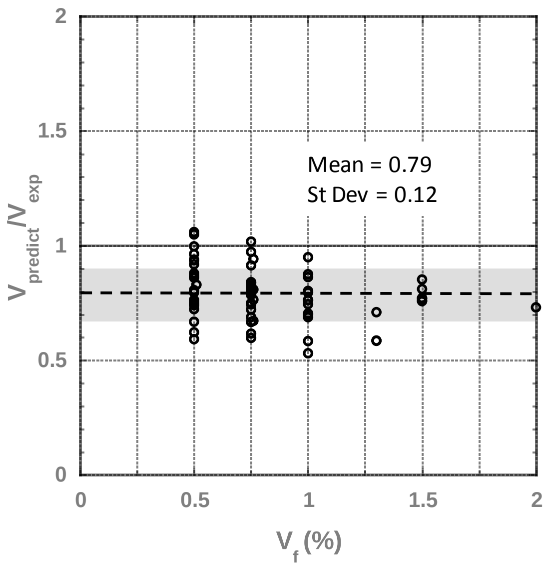

Fig. 15.9: Predicted versus experimental shear strength of SFRC beams

15.4 Fibre reinforcement for punching shear resistance in slab-column connections

A natural application of fibre reinforcement for shear resistance is slab-column or slab-pile connections. These connections are particularly susceptible to punching shear failures because loads applied on the slabs are transferred directly to the columns. The 2008 ACI Building Code [ACI Committee 318 (2008)] specifies the following nominal punching shear strength for slabs unreinforced in shear and supported by square columns,

$$v_n = \frac{1}{3}\sqrt{f_{ck}} \tag{15.7}$$

where v_n (MPa) is calculated assuming a critical perimeter located at a distance $d/2$ from the column faces. It should be mentioned that in Eq. (15.7), the specified concrete strength according to the ACI Code, f_c', has been replaced by the characteristic concrete strength f_{ck} for consistency with European notation. In many cases, this shear strength is not sufficient to satisfy the shear demand and thus, shear reinforcement is required in the slab in the vicinity of the column. In the United States, headed shear studs [Dilger and Ghali (1981)] are the preferred option for shear reinforcement in slab-column connections.

In earthquake-prone regions, punching shear in slab-column connections becomes even more critical [Moehle (1996)]. This is because even when not designed to contribute to lateral strength and stiffness, the connections in slab-column frames must be capable of transferring shear while undergoing earthquake-induced deformations. In this case, the design of the connection requires a check of lateral displacement capacity under the expected gravity load such that a punching failure becomes unlikely during a design level earthquake. Typically, this check is performed through the use of a drift versus gravity shear ratio chart, developed based on results from laboratory tests. Gravity shear ratio is defined as the connection shear due to gravity loads divided by the nominal shear strength [often calculated from Eq. (15.7)], while drift represents the difference in lateral displacement between two adjacent stories divided by the story height. The drift versus gravity shear ratio interaction assumed in the ACI Building Code [ACI Committee 318 (2008)], along with data obtained from tests of slab-column connections under lateral displacement reversals, is shown in Fig. 15.10. In practice, it is often the case that the calculated drift capacity for the expected gravity shear ratio is less than the design drift, which leads to the use of shear reinforcement, typically in the form of shear studs. Fig. 15.11 shows a photo of a slab-column connection with shear stud reinforcement in a building located on the United States west coast.

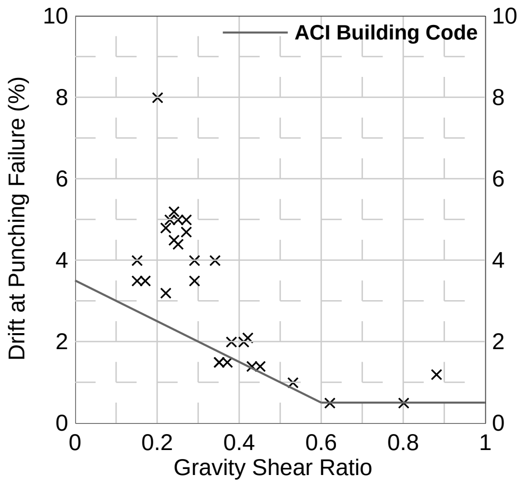

Fig.15.10: Comparison of drift versus gravity shear ratio interaction in 2008 ACI Code and experimental data [Cheng, Parra-Montesinos, and Shield (2010)]

Fig. 15.11: Shear stud reinforcement in slab-column connection (courtesy of E. Miranda)

The use of fibre reinforcement to increase punching shear resistance in slab-column connections has several potential advantages compared to the use of shear studs, including: 1) fibres are uniformly dispersed around the connection as opposed to being located at discrete locations; 2) fibres do not require on-site installation, which reduces labour; and 3) potential interference of shear reinforcement with slab flexural reinforcement is eliminated with the use of fibres. In order to evaluate the potential of fibre reinforcement to increase shear resistance and ductility in slab-column connections, particularly when subjected to earthquake loading, an investigation was recently conducted at the University of Michigan and the University of Minnesota [Cheng and Parra-Montesinos (2009); Cheng, Parra-Montesinos, and Shield (2010)]. This experimental program, along with the main findings, is discussed next.

15.4.1 Behaviour of steel fibre reinforced concrete slab-column connections

15.4.1.1 Slab-column connections under gravity-type loading

The behaviour of slab-column connections subjected to gravity-type loading has been extensively studied in the past [e.g. Swamy and Ali (1982); Alexander and Simmonds (1992); Shaaban and Gesund (1994); Harajli, Maalouf, and Khatib (1995); McHarg et al. (2000); Cheng and Parra-Montesinos (2010)]. A common conclusion from these investigations is that steel fibres are effective in increasing punching shear resistance and ductility, and in some cases [Swamy and Ali (1982); Harajli, Maalouf, and Khatib (1995)], the use of fibre reinforcement has been reported to lead to an enlargement of the punching shear surface.

For illustration purposes, the behaviour of three slab-column connections tested by Cheng and Parra-Montesinos (2010) are shown in Fig. 15.12b. These responses were obtained from tests of 152 mm thick, 1520 mm square slabs simply supported around their perimeter and subjected to a monotonically-increased concentrated force through a 152 mm square column stub in the middle of the slab (Fig. 15.12a). The slabs were reinforced with a grid of bottom reinforcement consisting of 13 mm bars at 152 mm spacing for a tension reinforcement ratio in each direction ρ, based on the overall slab thickness, of 0.56%.

Two of the slabs whose responses are shown in Fig. 15.12b were reinforced with a 1.5% volume fraction of either Type 1 or Type 3 fibres (Table 15.2), while the other slab was unreinforced in shear. Shear stress in Fig. 15.12b was calculated as the applied shear V divided by the critical perimeter length, b_o, and the slab effective depth d. As mentioned earlier, the critical perimeter in the ACI Building Code [ACI Committee 318 (2008)] is assumed to be located at $d/2$ from each column face. In order to account for differences in concrete strength between the test specimens, the shear stress in Fig. 15.12b is expressed as a function $\sqrt{f_c}$. The applicable ACI Code design stress of $0.33\sqrt{f_c}$ (MPa) is also shown in the figure.

As shown in Fig. 15.12b, the slab with regular concrete failed at an average punching shear stress slightly higher than the ACI Code value and after limited flexural yielding had taken place. The specimen with 1.5% volume fraction of Type 3 fibres, on the other hand, exhibited a normalized shear stress and deflection approximately 20% and 70% greater than those in the specimen without fibres, respectively. This specimen exhibited substantial flexural yielding prior to failing in punching shear. The slab with a 1.5% volume fraction of Type 1 fibres, on the other hand, failed at a deflection only 20% larger than that in the regular concrete slab, but with a 50% greater normalized shear stress at failure. The ultimate load in the two SFRC slabs was nearly the same and governed by their flexural capacity. Different concrete compressive strengths, however, were the main reason for the difference in normalized shear stress at failure. The results from these tests, which are consistent with results reported in the literature, further confirm that steel fibres are effective as punching shear reinforcement in slabs subjected to gravity loading and could lead to a change in failure mode from brittle punching shear failure to ductile flexural yielding.

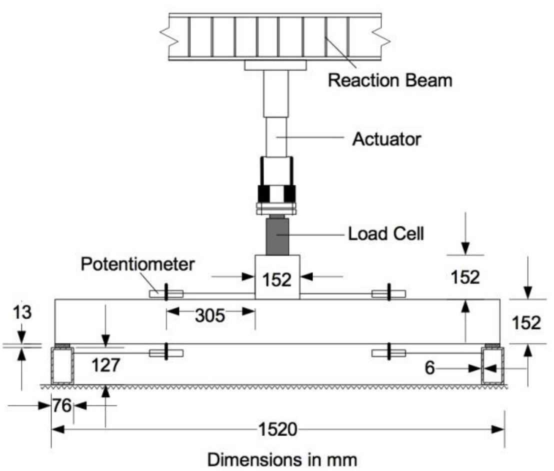

a) Test setup for slabs subjected to monotonically-increased punching shear

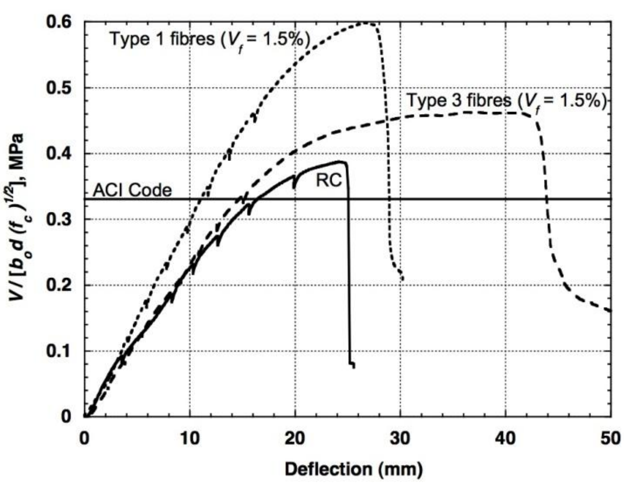

b) Normalized punching shear stress versus deflection response for RC and SFRC slabs

Fig. 15.12: Test setup and behaviour of slabs under monotonically-increased punching shear

15.4.1.2 Slab-column connections under earthquake-type loading

Most research studies on the use of fibre reinforcement in slab-column connections have been limited to gravity-type loading and thus, the ability of fibre reinforcement to increase punching shear strength and ductility in slab-column connections subjected to earthquake-type loading is not well known. In order the address the lack of experimental data on this subject, an experimental investigation that included the tests of three large-scale slab-column connections under combined gravity load and bi-axial lateral displacements was recently completed at the University of Michigan and the University of Minnesota [Cheng and Parra-Montesinos (2009); Cheng, Parra-Montesinos, and Shield (2010)].

Fig. 15.13 shows a photo of one of the test connection subassemblies at the University of Minnesota NEES-MAST Laboratory. Each specimen represented a first story interior connection. A 406 mm square column was fixed connected to a base block and extended one full story below and approximately a half-story above the slab. Lateral displacements were applied at the top of the column through a "rigid" steel crosshead. The slab was approximately 5.2 m square in plan and 152 mm thick. Each corner of the slab was supported by a hydraulic actuator such as to prevent vertical displacements while allowing horizontal displacements and rotations. Gravity load was simulated, in addition to the slab self-weight, through four hydraulic jacks. A gravity shear ratio of approximately 0.5 was targeted during the tests. Once the gravity load was applied, lateral displacements were applied at the top of the column to various drift levels (lateral displacement divided by distance from top of column to top of base block). Each loading cycle followed a clover-leaf pattern (Fig. 15.14).

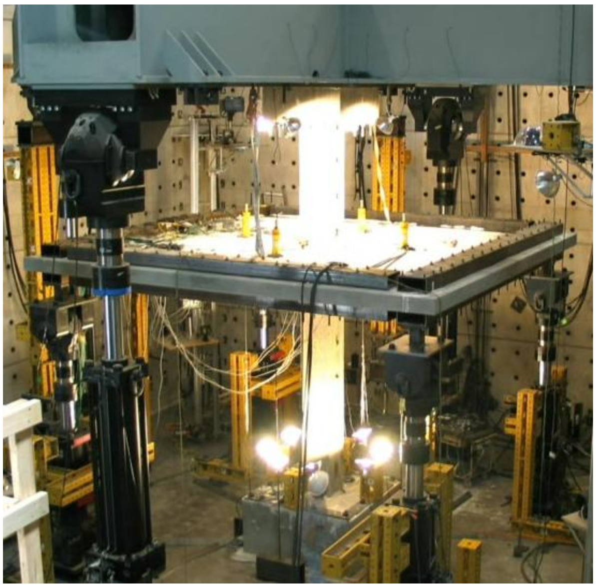

Fig. 15.13: Slab-column subassembly at NEES-MAST Laboratory

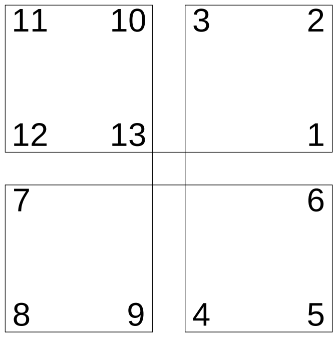

Fig. 15.14: Bi-axial displacement pattern per cycle

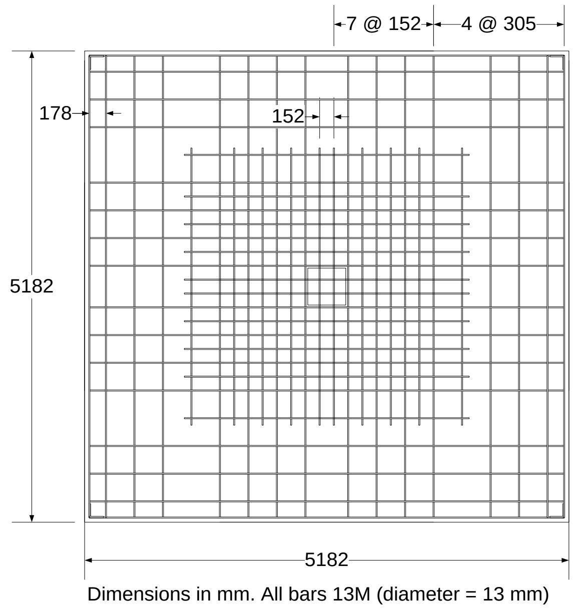

Fig. 15.15: Slab top reinforcement

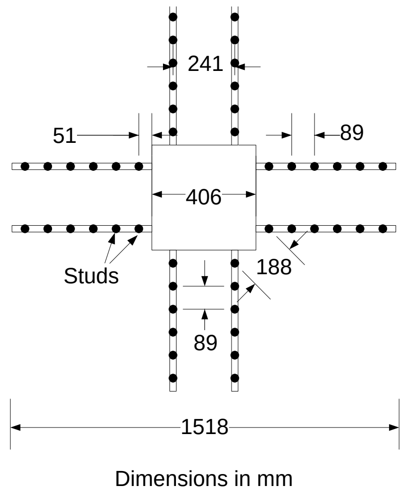

Fig. 15.16: Shear stud layout in Specimen 3

All three specimens were nominally identical, except for the shear reinforcement in the connection. The design flexural reinforcement at the top of the slab is shown in *Fig*. 15.15. The reinforcement at the bottom of the slab consisted of a grid of 13 mm diameter bars uniformly spaced at 305 mm. The connection of Specimens 1 and 2, within a square area defined by a distance of four times the slab thickness from each column face, was reinforced with a 1.5% volume fraction of Type 1 and Type 3 fibres (Table 15.2), respectively. The connection of Specimen 3, on the other hand, was reinforced with shear stud reinforcement, as shown in Fig. 15.16.

Regular and fibre reinforced concretes were supplied by a local ready-mix concrete company. In both cases, the specified concrete compressive strength, maximum aggregate size, and minimum slump were 28 MPa, 13 mm, and 150 mm, respectively. Results from cylinder tests indicated a compressive strength at the test day of 36.9 and 30.8 MPa for the fibre reinforced concrete used in Specimens 1 and 2, respectively, while the regular concrete used in the connection of Specimen 3 had a compressive strength of 44.4 MPa.

The lateral load versus drift response for both North-South and East-West directions for Specimens 1 and 3 is shown in Fig. 15.17. The behaviour of Specimens 1 and 2 was similar and thus, only that of Specimen 1 is shown. As can be seen, Specimen 1 exhibited a far superior drift capacity compared to Specimen 3 with shear stud reinforcement. Punching shear-related damage in Specimen 1 was first noticed during the cycle at 2.3% in each direction (3.2% total drift for diagonal loading direction; points 2, 5, 8 & 11 in Fig. 15.14), as indicated by a circle in the figure, while a complete punching failure developed when the specimen was displaced to 2.75% drift (3.9% total drift). In Specimen 2, on the other hand, a complete punching shear failure developed by the end of the cycle at 2.3% drift (3.2% total drift). Specimen 3, with shear stud reinforcement, failed during the cycle at 1.15% in each direction (1.6% total drift). Measured gravity shear at failure was approximately 0.4 for all three specimens.

From the drift versus gravity shear ratio chart shown in Fig. 15.10, a drift of 1.5% is estimated for a connection subjected to a gravity shear ratio of 0.4. While Specimens 1 and 2 with fibre reinforced concrete exhibited a drift capacity more than twice the value specified in the ACI Building Code, Specimen 3 with shear stud reinforcement exhibited a drift capacity close to the specified value, suggesting little contribution from this type of shear reinforcement to connection ductility.

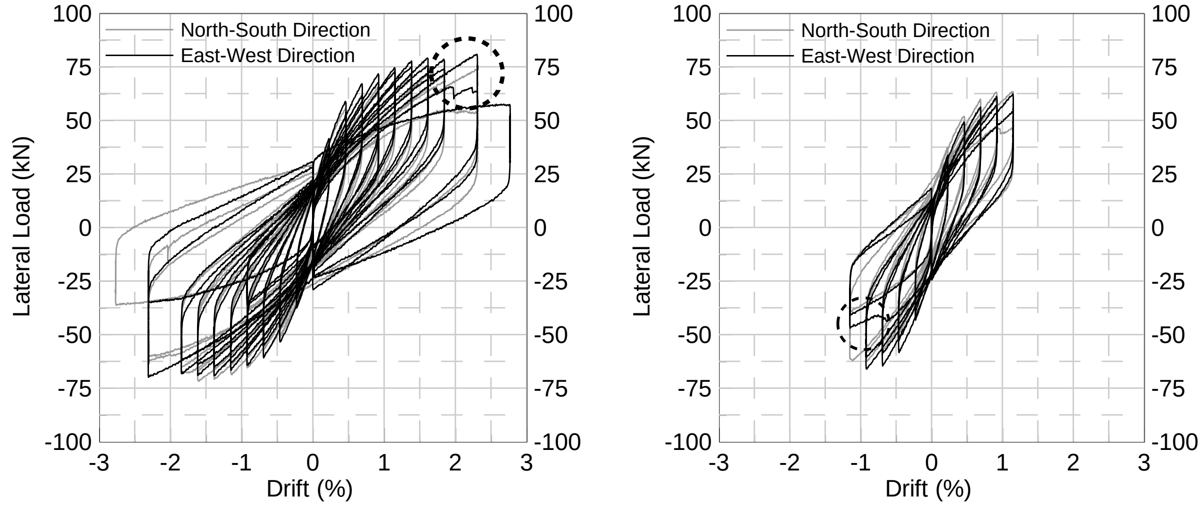

a) Specimen 1(SFRC) *b) Specimen 3(RC)*

Fig. 15.17: Hysteresis behaviour of slab-column connection subassemblies

In addition to superior drift capacity, the use of SFRC in slab-column connections led to enhanced damage tolerance. For example, only minor damage was observed in the connection of Specimen 1 at 2.8% total drift, as shown in Fig. 15.18a. In contrast, the regular concrete connection (Specimen 3) had already exhibited a punching shear failure at 1.6% total drift (Fig. 15.18b).

In summary, the results from these three tests demonstrate that fibre reinforcement is effective in contributing to punching shear resistance and deformation capacity of slab-column connections subjected to earthquake-induced deformations and has therefore the potential for use in lieu of more traditional types of shear reinforcement, such as shear studs.

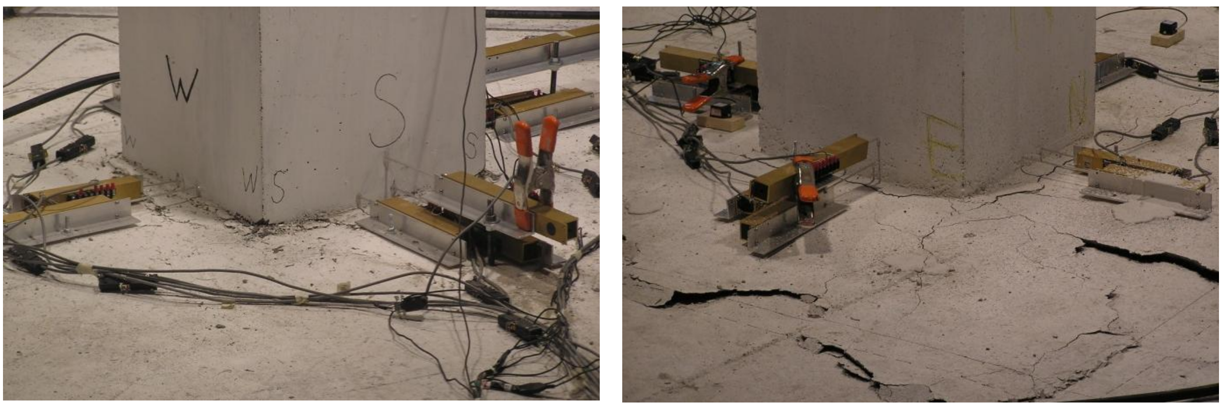

a) Specimen 1 (SFRC) at 2.8% total drift *b) Specimen 3 (RC) at 1.6% total drift*

Fig. 15.18: Damage in SFRC versus RC slab-column connections

15.5 Conclusions

Results from experimental research on the use of hooked steel fibres for shear resistance in beams and slab-column connections are presented. The following conclusions can be drawn from the results presented:

- Hooked steel fibres in volume fractions greater than or equal to 0.75% are effective in ensuring multiple diagonal cracking and substantially increasing shear strength in beams without stirrup reinforcement. The shear strength of all steel fibre reinforced concrete (SFRC) beams tested in this investigation exceeded that $[0.3\sqrt{f_c}$ (MPa] of a beam with stirrup reinforcement satisfying the minimum requirements in the 2008 ACI Building Code, indicating that hooked steel fibres in a 0.75% volume fraction can be used in lieu of minimum stirrup reinforcement in beams.
- The shear strength of SFRC beams without stirrup reinforcement can be estimated with reasonable accuracy as the summation of shear resistance contributed by fibre tensile stresses across diagonal cracks and shear carried in the beam compression zone. Average tension stresses across a critical diagonal crack can be estimated from standard ASTM 1609 four-point bending tests, while the shear carried in the beam compression zone is determined from a failure criterion for concrete subjected to combined compressive and shear stresses.
- Hooked steel fibres in a 1.5% volume fraction were found to be effective in increasing punching shear strength and ductility in slab-column connections under monotonically-increased loading, as well as under combined gravity load and lateral displacement reversals. Drift capacities exceeding 3% were observed in two SFRC large-scale connections subjected to a gravity shear ratio of approximately 0.4 [gravity shear stress of $0.13\sqrt{f_c}$ (MPa)] in combination with bi-axial lateral displacements. In contrast, a nominally identical regular concrete connection with shear stud reinforcement failed at 1.6% drift.

15.6 Acknowledgements

The research on the use of fibre reinforcement in slab-column connections was sponsored by the US National Science Foundation, as part of the Network for Earthquake Engineering Simulation (NEES) Program, under Grant No. CMMI 0421180. The support of Bekaert Corporation, which donated the fibres used in this investigation, is greatly appreciated. The opinions expressed in this paper are those of the writers and do not necessarily represent the views of the sponsors.

15.7 References

ACI Committee 318 (2008). "Building code requirements for structural concrete and commentary (ACI 318-08)," American Concrete Institute, Farmington Hills, Michigan.

Adebar, P., Mindess, S., St.-Pierre, D., and Olund, B. (1997). "Shear tests of fiber concrete beams without stirrups," *ACI Structural Journal*, Vol. 94, No. 1, pp. 68-76.

Alexander, S.D.B., and Simmonds, S.H. (1992). "Punching shear tests of concrete slab-column joints containing fiber reinforcement," *ACI Structural Journal*, Vol. 89, No. 4, pp. 425-432.

Ashour, S. A., Hasanain, G.S., and Wafa, F.F. (1992). "Shear behavior of high-strength fiber reinforced concrete beams," *ACI Structural Journal*, Vol. 89, No. 2, pp.176-184.

ASTM International (2006). “C 1609/C 1609M-06, Standard test method for flexural performance of fiber-reinforced concrete (using beam with third-point loading), 8 pp.

Batson, G., Jenkins, E., and Spatney, R. (1972). “Steel fibers as shear reinforcement in beams,” *ACI Journal*, Vol. 69, No. 10, pp. 640-644.

Bresler, B., and Pister, K.S. (1958). “Strength of concrete under combined Stresses,” *ACI Journal Proceedings*, Vol. 55, No. 9, pp. 321-345.

Casanova, P., and Rossi, P. (1999). “High-strength concrete beams submitted to shear: steel fibers versus stirrups,” *Structural Applications of Fiber Reinforced Concrete (SP-182)*, American Concrete Institute, Farmington Hills, MI, pp. 53-68.

Cheng, M.-Y., and Parra-Montesinos, G.J. (2009). “Punching shear strength and deformation capacity of fiber reinforced slab-column connections under earthquake-type loading,” *Report UMCEE 09-01*, Department of Civil and Environmental Engineering, University of Michigan, Ann Arbor, MI, 334 pp.

Cheng, M.-Y., and Parra-Montesinos, G.J. (2010). “Evaluation of steel fiber reinforcement for punching shear resistance in slab-column connections. Part I: monotonically increased load,” *ACI Structural Journal*, Vol. 107, No. 1, pp. 101-109.

Cheng, M.-Y., Parra-Montesinos, G.J., and Shield, C.K. (2010). “Shear strength and drift capacity of fiber reinforced concrete slab-column connections subjected to bi-axial displacements,” *Journal of Structural Engineering*, ASCE, Vol. 136, No. 9, pp.1078-1088.

Cucchiara, C., La Mendola, L., and Papia, M. (2004). “Effectiveness of stirrups and steel fibres as shear reinforcement,” *Cement and Concrete Composites*, Vol. 26, No. 7, pp. 777-786.

Dilger, W.H., and Ghali, A. (1981). “Shear reinforcement for concrete slabs,” *Journal of the Structural Division*, Proceedings of the American Society of Civil Engineers, Vol. 107, No. ST12, pp. 2403-2420.

Dinh, H.H. (2009). “Shear behavior of steel fiber reinforced concrete beams without stirrup reinforcement,” *Doctoral Dissertation*, Department of Civil and Environmental Engineering, University of Michigan, Ann Arbor, MI, pp. 285.

Dinh, H.H., Parra-Montesinos, G.J., and Wight, J.K. (2010). “Shear strength of steel fiber reinforced concrete beams without stirrup reinforcement,” *ACI Structural Journal*, Vol. 107, No. 5, pp. 597-606.

Harajli, M.H., Maalouf, D., and Khatib, H. (1995). “Effect of fibers on the punching shear strength of slab-column connections,” *Cement & Concrete Composites*, Vol. 17, No. 2, pp. 161-170.

Kwak, Y.-K., Eberhard, M.O., Kim, W.-S., and Kim, J. (2002). “Shear Sstrength of steel fiber-reinforced concrete beams without stirrups,” *ACI Structural Journal*, V. 99, No. 4, pp. 530-538.

Li, V.C., Ward, R., and Hamza, A.M. (1992). “Steel and synthetic fibers as shear reinforcement,” *ACI Materials Journal*, Vol. 89, No. 5, pp. 499-508.

Lim, T.Y., Paramasivam, P., and Lee, S.L. (1987). “Shear and moment capacity of reinforced steel-fibre-concrete beams,” *Magazine of Concrete Research*, Vol. 39, No. 140, pp. 148-160.

Mansur, M.A., Ong, K.C.G., and Paramasivam, P. (1986). “Shear strength of fibrous concrete beams without stirrups,” *ASCE Journal of Structural Engineering*, Vol. 112, No. 9, pp. 2066-2079.

McHarg, P. J., Cook, W. D., Mitchell, D., and Yoon, Y.-S. (2000). "Benefits of concentrated slab reinforcement and steel fibers on performance of slab-column connections," *ACI Structural Journal*, Vol. 97, No. 2, pp. 225-234.

Moehle, J.P. (1996). "Seismic design considerations for flat-plate construction," *ACI Special Publication 162*, Farmington Hills, MI, pp. 1-34.

Narayanan, R., and Darwish, I.Y.S. (1987). "Use of steel fibers as shear reinforcement," *ACI Structural Journal*, Vol. 84, No. 3, pp. 216-227.

Noghabai, K. (2000). "Beams of fibrous concrete in shear and bending: experiment and model," *Journal of Structural Engineering*, Vol. 126, No. 2, pp. 243-251.

Parra-Montesinos, G.J. (2006). "Shear strength of beams with deformed steel fibers," *Concrete International*, Vol. 28, No. 11, pp. 57-66.

Rosenbusch, J., and Teutsch, M. (2002). "Trial beams in shear," *Brite/Euram Project 97-4163*, Final Report, Sub Task 4.2, Technical University of Braunschweig.

Shaaban, A. M., and Gesund, H. (1994). "Punching shear strength of steel fiber-reinforced concrete flat plates," *ACI Structural Journal*, Vol. 91, No. 4, pp. 406-414.

Shantz, B.A. (1993). "The effect of shear stress on full scale steel fiber reinforced concrete beams," *Master of Science Thesis*, Department of Civil and Environmental Engineering, Clarkson University, Potsdam, NY, 86 pp.

Swamy, R.N., and Ali, S.A.R. (1982). "Punching shear behavior of reinforced slab-column connections made with steel fiber concrete," *ACI Journal*, Vol. 79, No. 5, pp. 392-406.

Swamy, R.N., and Bahia, H.M. (1985). "The effectiveness of steel fibers as shear reinforcement," *Concrete International*, Vol. 7, No. 3, pp. 35-40.

Tan, K.H., Murugappan, K., and Paramasivam, P. (1993). "Shear behavior of steel fiber reinforced concrete Beams," *ACI Structural Journal*, Vol. 90, No. 1, pp. 3-11.

*fib – fédération internationale du béton – the International Federation for Structural Concrete – is grateful for the invaluable support of the following National Member Groups and Sponsoring Members, which contributes to the publication of **fib** technical bulletins, the Structural Concrete Journal, and **fib**-news.*

National Member Groups

AAHES - Asociación Argentina del Hormigón Estructural, Argentina
CIA - Concrete Institute of Australia
ÖVBB - Österr. Vereinigung Für Beton und Bautechnik, Austria
GBB - Groupement Belge du Béton, Belgium
ABCIC - Associação Brasileira da Construção Industrializada de Concreto, Brazil
ABECE - Associação Brasileira de Engenharia e Consultoria Estrutural, Brazil
fib Group of Canada
CCES - China Civil Engineering Society
Hrvatska Ogranak ***fib***-a (HOFIB) - Croatian Group of ***fib***
Cyprus University of Technology
Ceska betonarska spolecnost, Czech Republic
Dansk Betonforening DBF - Danish Concrete Society
Suomen Betoniyhdistys r.y. - Concrete Association of Finland
AFGC - Association Française de Génie Civil, France
Deutscher Ausschuss für Stahlbeton, Germany
Deutscher Beton- und Bautechnik-Verein e.V. – dbv, Germany
Technical Chamber of Greece
Hungarian Group of ***fib***, Budapest Univ. of Tech. & Economics
The Institution of Engineers (India)
Management and Planning Organization, Iran
IACIE - Israeli Association of Construction and Infrastructure Engineers
Consiglio Nazionale delle Ricerche, Italy
JCI - Japan Concrete Institute
PCEA - Prestressed Concrete Engineering Association, Japan
Administration des Ponts et Chaussées, Luxembourg
Betonvereniging - ***fib*** Netherlands
New Zealand Concrete Society
Norsk Betongforening - Norwegian Concrete Association
Chancellery of the Polish Academy of Sciences
Committee of Civil Engineering, Concrete Structures Section, Poland
GPBE - Grupo Portugês de Betão Estrutural, Portugal
Society For Concrete and Prefab Units of Romania
Technical University of Civil Engineering, Romania
Association for Structural Concrete (ASC), Russia

Association of Structural Engineers, Serbia
Slovak Union of Civil Engineers
Slovenian Society of Structural Engineers
ACHE - Asociacion Cientifico-Técnica del Hormigon Estructural, Spain
Svenska Betongföreningen, Sweden
Délégation nationale suisse de la ***fib***, IS-BETON, EPFL, Switzerland
ITU - Istanbul Technical University, Turkey
Research Inst. of Build. Constructions, Ukraine
fib UK Group
ASBI - American Segmental Bridge Institute, USA
PCI - Precast/Prestress. Concrete Institute, USA
PTI - Post Tensioning Institute, USA

Sponsoring Members

Preconco Limited, Barbados
Liuzhou OVM Machinery Co., Ltd., China
Consolis Technology Oy Ab, Finland
Fachverband Beton- u. F. B.-W. e. V., Germany
FIREP Rebar Technology GmbH, Germany
MKT Metall-Kunststoff-Technik GmbH, Germany
Larsen & Toubro Ltd., ECC Division, India
Sireg S.P.A., Italy
Fuji P. S. Corporation Ltd., Japan
Obayashi Corporation, Japan
Oriental Construction Co. Ltd., Japan
P. S. Mitsubishi Construction Co., Ltd., Japan
PC Bridge Company Ltd., Japan
SE Corporation, Japan
Sumitomo Mitsui Construct. Co. Ltd., Japan
BBR VT International Ltd., Switzerland
SIKA Services AG, Switzerland
VSL International Ltd, Switzerland
PBL Group Ltd., Thailand
CCL Stressing Systems Ltd., United Kingdom
Strongforce Engineering PLC, United Kingdom

fib Bulletins published since 1998

N°	Title
1	Structural Concrete – Textbook on Behaviour, Design and Performance; Vol. 1: Introduction - Design Process – Materials Manual - textbook (244 pages, ISBN 978-2-88394-041-3, July 1999)
2	Structural Concrete – Textbook on Behaviour, Design and Performance Vol. 2: Basis of Design Manual - textbook (324 pages, ISBN 978-2-88394-042-0, July 1999)
3	Structural Concrete – Textbook on Behaviour, Design and Performance Vol. 3: Durability - Design for Fire Resistance - Member Design - Maintenance, Assessment and Repair - Practical aspects Manual - textbook (292 pages, ISBN 978-2-88394-043-7, December 1999)
4	Lightweight aggregate concrete: Extracts from codes and standards State-of-the-art report (46 pages, ISBN 978-2-88394-044-4, August 1999)
5	Protective systems against hazards: Nature and extent of the problem Technical report (64 pages, ISBN 978-2-88394-045-1, October 1999)
6	Special design considerations for precast prestressed hollow core floors Guide to good practice (180 pages, ISBN 978-2-88394-046-8, January 2000)
7	Corrugated plastic ducts for internal bonded post-tensioning Technical report (50 pages, ISBN 978-2-88394-047-5, January 2000)
8	Lightweight aggregate concrete: Part 1 (guide) – Recommended extensions to Model Code 90; Part 2 (technical report) – Identification of research needs; Part 3 (state-of-art report) – Application of lightweight aggregate concrete (118 pages, ISBN 978-2-88394-048-2, May 2000)
9	Guidance for good bridge design: Part 1 – Introduction, Part 2 – Design and construction aspects. Guide to good practice (190 pages, ISBN 978-2-88394-049-9, July 2000)
10	Bond of reinforcement in concrete State-of-art report (434 pages, ISBN 978-2-88394-050-5, August 2000)
11	Factory applied corrosion protection of prestressing steel State-of-art report (20 pages, ISBN 978-2-88394-051-2, January 2001)
12	Punching of structural concrete slabs Technical report (314 pages, ISBN 978-2-88394-052-9, August 2001)
13	Nuclear containments State-of-art report (130 pages, 1 CD, ISBN 978-2-88394-053-6, September 2001)
14	Externally bonded FRP reinforcement for RC structures Technical report (138 pages, ISBN 978-2-88394-054-3, October 2001)
15	Durability of post-tensioning tendons Technical report (284 pages, ISBN 978-2-88394-055-0, November 2001)
16	Design Examples for the 1996 FIP recommendations *Practical design of structural concrete* Technical report (198 pages, ISBN 978-2-88394-056-7, January 2002)
17	Management, maintenance and strengthening of concrete structures Technical report (180 pages, ISBN 978-2-88394-057-4, April 2002)

N°	Title
18	Recycling of offshore concrete structures State-of-art report (33 pages, ISBN 978-2-88394-058-1, April 2002)
19	Precast concrete in mixed construction State-of-art report (68 pages, ISBN 978-2-88394-059-8, April 2002)
20	Grouting of tendons in prestressed concrete Guide to good practice (52 pages, ISBN 978-2-88394-060-4, July 2002)
21	Environmental issues in prefabrication State-of-art report (56 pages, ISBN 978-2-88394-061-1, March 2003)
22	Monitoring and safety evaluation of existing concrete structures State-of-art report (304 pages, ISBN 978-2-88394-062-8, May 2003)
23	Environmental effects of concrete State-of-art report (68 pages, ISBN 978-2-88394-063-5, June 2003)
24	Seismic assessment and retrofit of reinforced concrete buildings State-of-art report (312 pages, ISBN 978-2-88394-064-2, August 2003)
25	Displacement-based seismic design of reinforced concrete buildings State-of-art report (196 pages, ISBN 978-2-88394-065-9, August 2003)
26	Influence of material and processing on stress corrosion cracking of prestressing steel – case studies. Technical report (44 pages, ISBN 978-2-88394-066-6, October 2003)
27	Seismic design of precast concrete building structures State-of-art report (262 pages, ISBN 978-2-88394-067-3, January 2004)
28	Environmental design State-of-art report (86 pages, ISBN 978-2-88394-068-0, February 2004)
29	Precast concrete bridges State-of-art report (83 pages, ISBN 978-2-88394-069-7, November 2004)
30	Acceptance of stay cable systems using prestressing steels Recommendation (80 pages, ISBN 978-2-88394-070-3, January 2005)
31	Post-tensioning in buildings Technical report (116 pages, ISBN 978-2-88394-071-0, February 2005)
32	Guidelines for the design of footbridges Guide to good practice (160 pages, ISBN 978-2-88394-072-7, November 2005)
33	Durability of post-tensioning tendons Recommendation (74 pages, ISBN 978-2-88394-073-4, December 2005)
34	Model Code for Service Life Design Model Code (116 pages, ISBN 978-2-88394-074-1, February 2006)
35	Retrofitting of concrete structures by externally bonded FRPs. Technical Report (224 pages, ISBN 978-2-88394-075-8, April 2006)
36	2006 *fib* Awards for Outstanding Concrete Structures Bulletin (40 pages, ISBN 978-2-88394-076-5, May 2006)
37	Precast concrete railway track systems State-of-art report (38 pages, ISBN 978-2-88394-077-2, September 2006)
38	Fire design of concrete structures – materials, structures and modelling State-of-art report (106 pages, ISBN 978-2-88394-078-9, April 2007)

N°	Title
39	Seismic bridge design and retrofit – structural solutions State-of-art report (300 pages, ISBN 978-2-88394-079-6, May 2007)
40	FRP reinforcement in RC structures Technical report (160 pages, ISBN 978-2-88394-080-2, September 2007)
41	Treatment of imperfections in precast structural elements State-of-art report (74 pages, ISBN 978-2-88394-081-9, November 2007)
42	Constitutive modelling of high strength / high performance concrete State-of-art report (130 pages, ISBN 978-2-88394-082-6, January 2008)
43	Structural connections for precast concrete buildings Guide to good practice (370 pages, ISBN 978-2-88394-083-3, February 2008)
44	Concrete structure management: Guide to ownership and good practice Guide to good practice (208 pages, ISBN 978-2-88394-084-0, February 2008)
45	Practitioners' guide to finite element modelling of reinforced concrete structures State-of-art report (344 pages, ISBN 978-2-88394-085-7, June 2008)
46	Fire design of concrete structures —structural behaviour and assessment State-of-art report (214 pages, ISBN 978-2-88394-086-4, July 2008)
47	Environmental design of concrete structures – general principles Technical report (48 pages, ISBN 978-2-88394-087-1, August 2008)
48	Formwork and falsework for heavy construction Guide to good practice (96 pages, ISBN 978-2-88394-088-8, January 2009)
49	Corrosion protection for reinforcing steels Technical report (122 pages, ISBN 978-2-88394-089-5, February 2009)
50	Concrete structures for oil and gas fields in hostile marine environments State-of-art report (36 pages, IBSN 978-2-88394-090-1, October 2009)
51	Structural Concrete – Textbook on behaviour, design and performance, vol. 1 Manual – textbook (304 pages, ISBN 978-2-88394-091-8, November 2009)
52	Structural Concrete – Textbook on behaviour, design and performance, vol. 2 Manual – textbook (350 pages, ISBN 978-2-88394-092-5, January 2010)
53	Structural Concrete – Textbook on behaviour, design and performance, vol. 3 Manual – textbook (390 pages, ISBN 978-2-88394-093-2, December 2009)
54	Structural Concrete – Textbook on behaviour, design and performance, vol. 4 Manual – textbook (196 pages, ISBN 978-2-88394-094-9, October 2010)
55	*fib* Model Code 2010, First complete draft – Volume 1 Draft Model Code (318 pages, ISBN 978-2-88394-095-6, March 2010)
56	*fib* Model Code 2010, First complete draft – Volume 2 Draft Model Code (312 pages, ISBN 978-2-88394-096-3, April 2010)
57	Shear and punching shear in RC and FRC elements Workshop proceedings. Technical report (268 pages, ISBN 978-2-88394-097-0, October 2010)

Abstracts for *fib* Bulletins, lists of available CEB Bulletins and FIP Reports, and an order form are available on the *fib* website at www.fib-international.org/publications.